Towards Polyyne Rotaxanes and Catenanes

Connor W. Patrick

St. Cross College

University of Oxford

A thesis submitted for the degree of

Doctor of Philosophy

Hilary 2022

Acknowledgements

First and foremost, I would like to thank my supervisor, Professor Harry L. Anderson, for providing me with the opportunity to carry out my DPhil and for the invaluable discussions, ideas, support and guidance during my time in Oxford. The time that Harry dedicates to every group member is significant and deserved recognition. I would also like to thank all the talented PostDocs who have taught me much throughout time in the group. In particular, Dr Steffen Woltering for his patience in showing me the ropes and supporting me during my first two years – you have been the centre of many unforgettable moments, food challenges and entertainment that have made my time in Oxford so special! I would also like to express my appreciation to Dr Amber Thompson and Dr Kirsten Christensen for their help with many (challenging) crystal structures. The NMR service, particularly Dr Nader Amin and Professor Tim Claridge, have provided me with enormous support and instrument time, for which I am very grateful. Another special thanks must go to Dr Steffen Woltering, Dr Przemyslaw Gawel, Dr Andrew Frawley, Dr Jeff Van Raden and Dr Yueze Gao for proofreading parts of this thesis.

I would like to thank all members of the group, both past and present, who make the group a supportive and fun place to work: Ali, Andrew, Bart, Bobby, Boom, He, Henrik, Iago, Isa, Isaac, Jake, James, Janko, Jeff, Josh, Kate, Keith, Kenny, Lara, Lorel, Marcin, Martin, Michael, Michel, Pernille, Prakhar, Przemek, Qiang, Steffen, Théa, Virginia, Wenjun, Will, Wojtek and Yueze. My sincerest thanks go to my friends, who were a constant source of support and encouragement during my time in Oxford. In particular: Joey Feld, for the excellent lockdown entertainment and innumerable memories over the past four years in Oxford and; Dr Lorel Scriven, for her support and friendship throughout my DPhil and for the much-needed pub trips and cycling breaks.

A final thanks must go to my family, for their continued love, support and encouragement; none of this would be possible without you. I am incredibly grateful to He. Your unbridled love and support helped me finish my DPhil and have made the last years truly unforgettable.

Abstract

This thesis summarises attempts towards polyyne [*n*]rotaxanes and cyclocarbon [*n*]catenanes. Carbon allotropes built purely from *sp* carbon atoms have long fascinated chemists but have yet to be isolated or characterised due to their high reactivity. This thesis documents work towards isolating both linear and cyclic *sp* carbon chains.

Chapter 1 reviews the history of carbon allotropes, focussing on cyclic and linear forms of *sp* carbon. Synthetic strategies towards preparing acetylene-rich molecules, rotaxanes and catenanes are discussed**.**

Chapter 2 discusses development of a novel masked alkyne equivalent (MAE) with intrinsic metal binding abilities. A simple masked triyne can be synthesised in only three steps, but photochemical unmasking of this group could not be realised due to a competing dimerisation process.

Chapter 3 details new strategies for synthesising polyyne [3]rotaxanes with two macrocycles on the same polyyne thread. An active metal template route using dicobalt-masked precursors was developed to prepare two polyyne [3]rotaxanes. The thermal stabilities of the two rotaxanes were evaluated relative to the naked polyyne dumbbell and were found to be significantly more stable in decalin at 80 °C.

Chapter 4 presents a novel approach to cyclocarbon [*n*]catenanes and polyyne [*n*]rotaxanes. The coupling of a [2]rotaxane bearing two temporary bulky MAE stoppers provides access to precursors of cyclocarbon [*n*]catenanes and polyyne [*n*]rotaxanes. Early unmasking experiments have successfully afforded a polyyne bearing 24 contiguous acetylene units and indicate that larger polyynes should be viable using this route.

Chapter 5 summarises key results in this thesis and highlights potentials avenues for this chemistry in the future.

Supplement to Statement of Authorship

Chapter 3 details the first preparation of a polyyne [3]rotaxane. Initial synthetic work, including the preparation of compounds **3.22·M4**, **3.23·M4**, **3.24·(M4)**$_2$, and **3.22·(M4)**$_2$, and crystallisation of **3.22·M4**, was carried out by former Part II student Mr Joseph Woods, with guidance from Dr Przemyslaw Gawel. Subsequently, the author repeated and optimised all steps, prepared the **M5** rotaxanes and all other compounds in this chapter, and investigated the thermal stability of these compounds. Claire E. Otteson and Professor Ramesh Jasti provided initial samples of nanohoop **M5**. Dr Amber L. Thompson determined the crystal structure of **3.22·M4**. Professor Tim D. W. Claridge provided help and advice with NMR spectroscopy.

Chapter 4 details a synthetic approach to dicobalt-masked polyyne [*n*]rotaxanes and cyclocarbon [*n*]catenanes. The author planned all synthetic routes detailed in this chapter and carried out the synthesis of all compounds except for **3.23·M6**, **4.8·M6**, **4.11·M6**, **4.12·M6**, **4.16·(M6)**$_3$ and **4.17·(M6)**$_4$, which were carried out by Dr Yueze Gao. Optimisation of the (*m*CPBA) dicobalt unmasking conditions were made by Dr Yueze Gao and Mr Prakhar Gupta. Dr Amber L. Thompson determined the crystal structures of **4.9**, **4.1·M4**, **4.13·(M4)**$_2$ and **4.1·M6**. Attempts towards brominating dicobalt-masked acetylenes were made by former Part II student Mr Joseph Woods. Professor Tony Parker provided help and advice with Raman spectroscopy.

Contents

List of Publications

1 H. L. Anderson, C. W. Patrick, L. M. Scriven and S. L. Woltering, *Bull. Chem. Soc. Jpn.*, 2021, **94**, 798–811.

2 C. W. Patrick, J. F. Woods, P. Gawel, C. E. Otteson, A. L. Thompson, T. D. W. Claridge, R. Jasti and H. L. Anderson, *Angew. Chem. Int. Ed.* 2022, **61**, e202116897; *Angew. Chem.* 2022, **134**, e202116897.

List of Abbreviations

Abbreviations

AMT	Active Metal Template
Ar	Aryl
BAA	Bond Angle Alternation
BLA	Bond Length Alternation
br	Broad
CCDC	Cambridge Crystallographic Data Centre
CNT	Carbon Nanotube
DAP	Diaryl phenanthroline
DBU	1,8-Diazabicyclo[5.4.0]undec-7-ene
dcpm	Bis(dicyclohexylphosphino)-methane
DFT	Density Functional Theory
DIPEA	*N*,*N*-Diisopropylethylamine
DMAP	4-Dimethylaminopyridine
DMF	*N*,*N*-Dimethylformamide
dmpm	Bis(dimethylphosphino)methane
dppm	Bis(diphenylphosphino)methane
DSC	Differential Scanning Calorimetry
DWCNT	Double-Walled Carbon Nanotube
eq.	Equivalents
ESI	Electrospray Ionisation
FBW	Fritsch-Buttenberg-Wiechell
FET	Field-Effect Transistor
FTIR	Fourier Transform Infra-Red
GPC	Gel Permeation Chromatography
HRMS	High-Resolution Mass Spectrometry
HRTEM	High-Resolution Transmission Electron Microscopy
LD-TOF	Laser-Desorption Time-Of-Flight
MAE	Masked Alkyne Equivalent
MALDI	Matrix-Assisted Laser Desorption/Ionisation
*m*CPBA	*meta*-Chloroperoxybenzoic acid
MS	Mass Spectrometry
MWCNT	Multi-Walled Carbon Nanotube
NBS	*N*-Bromosuccinimide
n-BuLi	*n*-Butyllithium
NIS	*N*-Iodosuccinimide
NMR	Nuclear Magnetic Resonance
PCC	Pyridinium chlorochromate
PMT	Passive Metal Template
p-^{t}Bu	*para*-*tert*-Butyl [tris(4-*tert*-butylphenyl)methyl]
SEC	Size Exclusion Chromatography
STEM	Scanning Tunneling Electron Microscopy
SWCNT	Single-Walled Carbon Nanotube
TBAF	Tetrabutylammonium fluoride
TBAI	Tetrabutylammonium iodide
TBS	*tert*-Butyldimethylsilyl
TES	Triethylsilyl
THF	Tetrahydrofuran
TIPS	Triisopropylsilyl
TLC	Thin Layer Chromatography
TMEDA	*N*,*N*,*N*',*N*'-Tetramethylethylene-diamine
TMS	Trimethylsilyl
Tr*	Supertrityl [tris(3,5-di-*tert*-butylphenyl)methyl]
Ts	Tosyl, toluenesulfonyl
UV-vis	Ultraviolet-visible
VT-NMR	Variable Temperature Nuclear Magnetic Resonance

1

Introduction

Contents

Chapter 1 - Introduction

1.1 Allotropes of Carbon and Carbon-Rich Materials

Carbon forms more compounds than any other element, except hydrogen.[1] Carbonaceous compounds are the basis for life on Earth and they are crucial in many artificial materials. They play an ever-growing role in various technological fields with a vast array of applications in chemistry and physics.[2] The prevalence of carbon-based compounds is the direct result of the chemical behaviour and physical properties of carbon. Possessing four valence electrons in its outer shell gives carbon impressive bonding diversity, capable not only of forming strong bonds with itself, but also to nearly all other elements in almost limitless variety.

Elemental carbon naturally exists in two allotropes: diamond and graphite – both of which have been known for thousands of years. Both exhibit impressive stability – the origin of their high natural abundance, especially for graphite, is likely the reason these two allotropes were discovered so long ago. Differing hybridisation states of carbon gives each allotrope unique properties. For example, diamond (sp^3) is the hardest natural material known, while graphite (sp^2) is a highly conductive material.

Conceptually, there are many theoretical ways to construct other carbon allotropes from solely *sp*, sp^2 and sp^3 carbon atoms (or combinations thereof), although these are less thermodynamically stable and so are not typically found in nature.[3,4] Despite the long-standing knowledge of diamond and graphite, only in the last 35 years has the discovery of new sp^2-hybridised carbon allotropes – zero-dimensional fullerenes,[5] one-dimensional carbon nanotubes[6] and two-dimensional graphene[7] and biphenylene networks[8] – strengthened interest into further research of carbon-rich materials (Figure 1.1). Of these, however, the only molecules consisting entirely of carbon that have been isolated and properly characterised are the fullerenes (C_{60}, C_{70}, etc.).[9] Despite their structurally-simplistic nature, there still remains simple, theoretical allotropes of carbon that continue to elude us.[10]

Pioneering work by Kroto *et al.* subject graphite to laser vaporisation, then utilised time-of-flight mass spectrometry to allow fleeting observations of a C_{60} cluster to be made for first time.[9] Through careful tuning of the conditions, clustering could be optimised to favour the formation of C_{60}. It was not until five years later when Huffman *et al.* published their

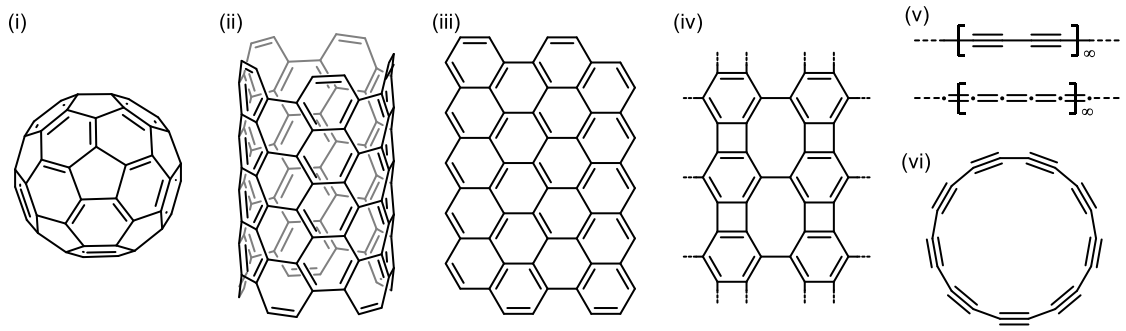

Figure 1.1: Recent allotropes of carbon: (i) buckminsterfullerene, C_{60};[9] (ii) (5,5)-armchair single-walled carbon nanotube;[12] (iii) graphene sheet;[13] (iv) planar nonbenzenoid biphenylene network;[8] (v) (*top*) polyynic and (*bottom*) cumulenic forms of carbyne (proposed, yet to be realised) and; (vi) cyclo[18]carbon.[14,15]

breakthrough work on isolating C_{60} in macroscopic quantities.[11] It was this work that led to the realisation that functionalisation of fullerenes was the key to unlocking their full potential. The release of strain stored in the spherical carbon framework provides the driving force of these exohedral functionalisations. This was only part of the ground-breaking research that landed Curl, Kroto and Smalley the 1996 Nobel Prize in Chemistry.[9]

The exohedral covalent binding of organic donor molecules, such as porphyrins to fullerenes, can be used to transform light into chemical energy. The porphyrin-C_{60} donor-acceptor dyad (compound **1.1a**, Figure 1.2) can undergo photoinduced electron transfer from the porphyrin to C_{60}, acting as a sensitiser and makes possible the prospect of organic solar cells using these compounds. Only recently have non-fullerene molecules surpassed the long-standing reign of fullerenes as high-efficiency acceptors in photovoltaic devices.[16,17] Additionally, compound **1.1b** (phenyl-C_{61}-butyric acid methyl ester, PCBM) serves as an *n*-type conductor in highly inexpensive and comparatively efficient plastic solar cells.[16] Compounds **1.1c** and **1.1d** are both water-soluble adducts that exhibit remarkable biological properties regarding anti-HIV activity[18] and metal-free superoxide dismutation,[19] respectively. Fullerenes are also used in the fields of liquid crystals[20] and their salts, such as K_3C_{60} or $(TDAE)C_{60}$, are superconductors[21] and ferromagnets, respectively.[22]

A patent filed in 1889 first proposed the idea of growing filaments of carbon through methane deposition although it was not until 1993, over 100 years later, when Ichihashi *et al.* (using a similar technique to that Kroto *et al.* used for the C_{60} clusters) grew the first carbon filament – a single walled carbon nanotube (SWCNT).[12] SWCNTs can be considered as an intermediate between fullerene cages and flat graphene sheets, where a graphene sheet is rolled along one of the Bravais lattice vectors to form a hollow cylinder. As such, CNTs are networks

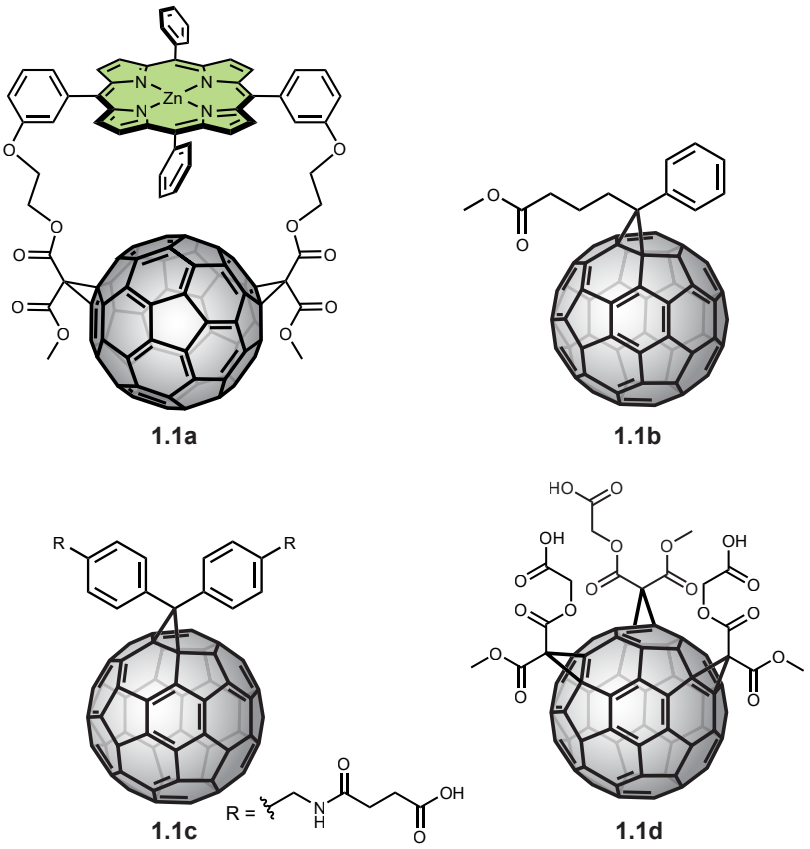

Figure 1.2: Examples of substituted fullerene derivatives with outstanding materials or biological properties.[16,18,19]

of sp^2-hybridised carbon atoms. More recent syntheses of CNTs are typically made via chemical-vapour deposition methods, where careful control over of preparation conditions can allow for both single-walled and multi-walled carbon nanotubes (MWCNTs) to be formed.[23,24] Unlike fullerenes, the lower stability and poor solubility of CNTs makes their functionalisation difficult. While various methods for purification and functionalisation have been reported, structural changes during functionalisation, coupled with the lack of control over aggregation both pose major problems.[25]

Surprisingly, the second most recent allotrope to be discovered, graphene, was done so using the simplest technique. In 2004, important work by Novoselov *et al.* demonstrated that single layers of graphene could be removed from a graphite sheet via mechanical exfoliation using Scotch tape,[13] before going on to manufacture atomically-thick graphene sheets into field-effect transistors (FETs). The discovery and characterisation of graphene awarded Novoselov and Geim with the 2010 Nobel Prize in Physics. With its high thermal stability, electrical conductivity and near-transparent nature, graphene is one of the most recent technologically-important materials, and is rapidly finding its way into countless new technologies. Since its

discovery in 2004, a SciFinder search reveals the literature has exploded and over 180,000 articles involving graphene have been published in peer-reviewed journals.

Fullerenes, nanotubes and graphene have all found uses in various applications as novel energy harvesting and storage materials. Furthermore, organo-electronic materials derived from these compounds have made their way into real-world devices that are currently being produced.[13,26] These materials are even being incorporated into fabrics; coating cotton threads with conductive nanotubes forms a lightweight thread that can be easily woven into fabrics to add strength and electrical conductivity.[27]

While it is clear that there has been a recent explosion in sp^2 allotropes of carbon, little has been reported regarding *sp* allotropes. Carbon allotropes consisting of purely *sp* carbon atoms are claimed[28] (and separately disputed[29]) to exist in interstellar dust and meteorites, yet allotropes comprising of exclusively *sp* carbon atoms – carbyne and cyclo[*n*]carbons – have never been isolated by researchers; only fleeting gas-phase observations,[30,31] or on-surface studies have been successful.[14] Carbyne can be viewed either as an infinitely long polyyne chain $(-C\equiv C-)_\infty$ with alternating single and triple bonds, or as an infinite cumulene chain $(=C=C=)_\infty$ where all bond lengths are equal. There are many questions regarding these allotropes that remain unanswered, such as: what is the ground state structure of carbyne and cyclocarbons – are they cumulenic (consecutive double bonds), or are they polyynic (alternating single-triple bonds)?; and do these molecules exhibit bond length alternation (BLA)? Finding the answer to these questions is of both keen academic interest and technological importance. The strong, directional bonding of linear carbon is expected to display exceptionally high tensile strength and Young's modulus (40 times that of diamond),[32,33] making it useful in mechanical applications. Meanwhile, the presence or absence of BLA strongly affects the electronic properties of compounds, and is known to directly affect the band gap in molecules. As such, the usefulness of these materials for electronic applications (e.g. molecular wires and extremely small FETs) is determined by these effects.[33,34]

1.2 Polyynes and Carbyne

Polyynes are linear (one-dimensional) chains of alternating single and triple carbon-carbon bonds. Arising from their two orthogonal π-systems and heavily restricted bond rotation,

polyynes suffer little-to-no loss in conjugation due to conformation effects and, as such, are highly conjugated systems. Consequently, it is predicted that polyyne-rich materials will display remarkable conductance properties[35,36] and that carbyne should exhibit either metallic or semiconductor behaviour,[37] often leading to extended polyynes being termed 'molecular wires'. Other than applications in molecular electronics, polyynes may also find uses in optical applications; the molar absorptivity of polyynes steadily increases with increasing chain length. For example, a ^{t}Bu-stoppered decayne possesses a significant molar extinction coefficient of 753,000 $dm^3\ mol^{-1}\ cm^{-1}$ at its absorption maximum.[38] Despite these applications for polyynes, a large majority of research is focussed on preparing stable derivatives as model compounds for carbyne.

1.2.1 Synthetic Approaches to Polyynes

Pioneering work by Entwistle in 1951[39] and Bohlmann in 1953[40] gave researchers their first insights into the nature of linear carbon when they prepared short acetylenic oligomers – methyl end-capped oligoynes Me–$(C{\equiv}C)_n$–Me (n = 2–6) and ^{t}Bu analogues (n = 2–7), respectively. In 1972 Walton and co-workers reported a series of triethylsilyl end-capped oligoynes, Et_3Si–$(C{\equiv}C)_n$–$SiEt_3$ (n = 4–10, 12 and 16), which could be desilylated to return both singly- and doubly-deprotected oligoynes, including the dodecayne H–$(C{\equiv}C)_{12}$–H.[41,42] The largest hurdle to overcome when synthesising long chains of *sp*-hybridised carbon atoms is the large thermodynamic instability that increases rapidly with increasing length of the polyyne. For example, butadiyne rapidly polymerises above 0 °C, while hexatriyne has been reported to be explosive;[43] there have been other reports of carbon-rich compounds exploding from simply touching a glass ampoule.[33] The crosslinking of polyynes to give amorphous carbon, or graphite, is a highly exothermic process.[4,44] Despite this, there exist multiple approaches in stabilising extended linear carbon systems. The main examples of which will be discussed later.

Since these seminal reports, the use and enlargement of bulky stoppering groups has been employed to prepare a variety of acetylene-rich compounds of increasing length. For example, Hirsch *et al.* utilised nitrile capping groups to prepare octayne **1.2** (Figure 1.3).[45] By using bulkier *tert*-butyl capping groups Bohlmann,[40] and later Walton *et al.*,[41] isolated oligoynes up to 12 acetylene units in length (**1.3**). Both trialkylsilane-capped oligoynes up to 10 and 16 acetylene units have been prepared using isopropyl (**1.4a**) and ethyl (**1.4b**) alkyl groups,

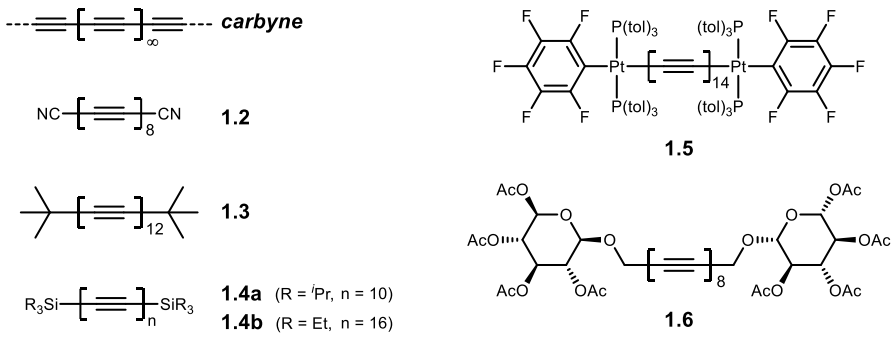

Figure 1.3: The structure of carbyne and various attempts towards the synthesis of oligo-/polyynes: nitrile-capped octayne **1.2** reported by Hirsch *et al.*;[45] *tert*-butyl capped dodecayne **1.3** reported by Bohlmann and Walton *et al.*;[40,41] triisopropylsilyl-capped decayne **1.4a** reported by Tykwinski *et al.*;[48] triethylsilyl-protected oligoyne **1.4b** reported by Walton *et al.*;[41,42] platinum-terminated polyyne **1.5** reported by Gladysz *et al.* and;[46] a glycosylated octayne **1.6** prepared by Frauenrath *et al.*[47]

respectively. In one noteworthy synthetic achievement, Zheng and Gladysz successfully prepared a stable platinum-capped polyyne bearing 14 triple bonds (compound **1.5**, Figure 1.3), suggesting the possibility of using metals as terminating groups.[46] One other interesting example was reported by Frauenrath *et al.* who employed a copper-free Negishi-like heterocoupling protocol to prepare symmetrical diglycosylated oligoynes up to 8 acetylenes in length (compound **1.6**, Figure 1.3).[47] Extrapolation of trends for these reported compounds is being used to give us our first glimpse into the physical properties and chemical nature of carbyne.

In an alternative approach, single-walled (SW), double-walled (DW) and multi-walled (MW) carbon nanotubes have found uses as confining nanoreactors to produce and stabilise one-dimensional materials, including ultra-narrow graphene ribbons[49] and short polyynes.[50] In 2003, Zhao *et al.* reported the use of MWCNTs as hosts for one-dimensional carbon nanowires of approximately 100 atoms, formed using hydrogen arc discharge evaporation of carbon rods.[51] More recent work by Shi *et al.* employed a high temperature and high vacuum procedure to generate DWCNT-shielded carbyne chains of more than 6,000 carbon atoms in length.[52] These nanotube-protected carbyne species could be directly observed using both high-resolution transmission electron microscopy (HRTEM) and scanning tunneling electron microscopy (STEM). In addition, resonance Raman spectroscopy was used to characterise the shielded polyyne, displaying a very intense band with a fine structure between 1,850 and 1,880 cm^{-1}. While this work provided an early glimpse into the physical properties of carbyne, characterisation by means of NMR would be impractical due to solubility issues with these

compounds, and UV-vis spectroscopy would be additionally restricted by the absorption of the DWCNT host.

Other approaches worth highlighting include stabilisation of oligoynes through co-crystallisation with metal complexes,[53] or through stabilisation by helical wrapping of polyynes.[54] For the former, the interaction of trimeric (perfluoro-*o*-phenylene)mercury with α,ω-diphenylpolyynes (containing 4-12 *sp*-hybridised atoms) leads to the formation of metal-polyyne adducts (**1.7**, Scheme 1.1a) whereby the polyynes are stabilised through their entrapment and physical separation in a supramolecular lattice. In the solid state, the α,ω-diphenylpolyynes lie approximately planar, sandwiched between two mercury-containing species and stabilised via secondary Hg-π interactions. Infra-red spectroscopy on this species revealed essentially identical spectra to that of the free polyyne, suggesting that the supramolecular forces are relatively weak and do not significantly affect either the structure or the electronics of the encapsulated polyynes. In another approach, Gladysz *et al.* reported a series platinum-capped *sp* carbon chains of 6 acetylene units in length, encapsulated by an sp^3 carbon double helix.[54] By using long, flexible aryl phosphine ligand bridging between the two metal termini, the ligands intertwine and generate a double-helical structure (**1.8**, Scheme 1.1b). The helix should act as a shield for the acetylene, preventing any reactive species from being in close proximity to it. Unfortunately, the authors did not comment on the stability benefits brought by such an approach.

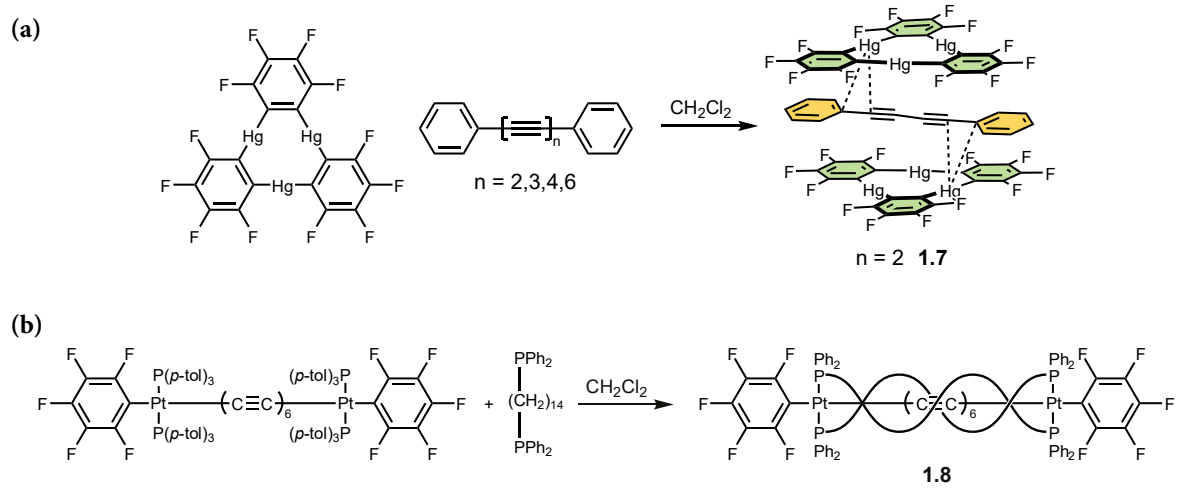

Scheme 1.1: Synthesis of a (a) acetylene·$Hg_3(C_6F_4)_3$ complex **1.7**;[53] (b) double-helical complex **1.8** by ligand substitution under high dilution conditions.[54]

In 2010, important work by Tykwinski *et al.* prepared a series of oligo-/polyynes, with the largest consisting of 44 *sp*-hybridised carbon atoms (22 contiguous acetylene units).[6] The key to isolating polyynes of such length was the use of bulky supertrityl (tris(3,5-di-*tert*-butylphenyl)methyl, **Tr***) stoppering groups (compound **1.9**, Figure 1.4), capping both ends of the polyynic chain. It is possible that polyynes beyond 44 *sp* carbon atoms were unstable, both to prepare (due to reactivity of the precursors), and to isolate. It is expected that a limit to end group protection of polyynes would be reached, restricting the protection of the *sp* carbon chain. While the supertrityl stoppers are very bulky, much of this bulk was localised at the terminus of the polyyne and does not extend far over the chain. Since this milestone publication, the Tykwinski group has continued to refine this chemistry to successfully prepare the longest polyyne reported to date – one bearing 48 *sp* carbon atoms, or 24 contiguous acetylenes.[55] In this report, a pyridyl-based (**Py***) stopper was developed (compound **1.10**, Figure 1.4), where the bulky substituents are directed over the acetylene chain, such that the stoppers can better shield the polyyne, despite the steric bulk being less than the original supertrityl stopper.

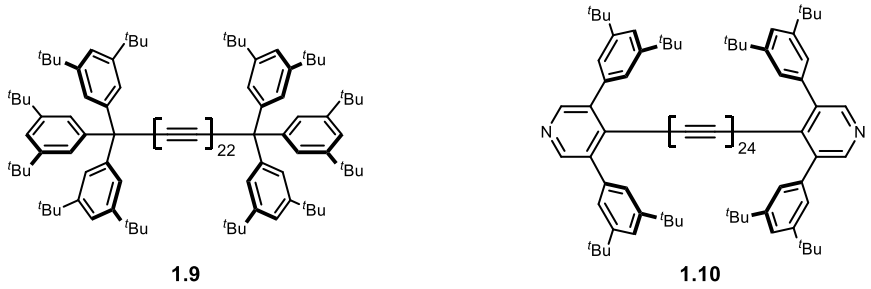

Figure 1.4: Tykwinski's efforts towards improving polyyne stability using bulky **1.9** supertyityl-[6] and **1.10** pyridyl-based[55] stoppering groups.

Two useful methods exist for assessing steric impact of a given group: (i) by calculating percent buried volume (%V_{bur}), which provides a convenient single number that can be compared between systems and; (ii) by calculating steric maps, which provide a graphical representation of the steric profile of a given group represented by contour plots.[56] In the case of the former, the percent buried volume is defined as the percentage of a sphere around a central atom that is occupied by a given functional group. Increased bulk around the central atom is reflected by a higher %V_{bur} (and lower percentage free volume, %V_{free}). The percentage buried volume was calculated for both the supertrityl- and pyridyl-capped oligoynes at each *sp* carbon along the chain, until %V_{bur} reached a constant value – the point at which the bulk of the stopper offers little steric protection to the thread.[57] Molecular geometries were taken from

solid state structures obtained from the Cambridge Crystallographic Data Centre (CCDC) (identifiers GAGYUK and MAKNAR for supertrityl- and pyridyl-capped oligoynes, respectively)[6,55] for both series of molecules. Plotting %V_{bur} vs carbon position along the chain (Figure 1.5) demonstrates that while supertrityl offers the highest bulk around C0 and C1, the protection falls off more rapidly with distance away from the stopper. For the supertrityl series, no interactions with the stopper are observed at C5 and beyond (see contour plots in Figure 1.6 and Section 1.6), meanwhile this point is reached at C7 for the pyridyl stopper – two atoms further along the *sp* carbon chain. Even though these predict little stopper influence beyond C5 or C7 for the supertrityl and pyridyl series, respectively, previous studies have demonstrated that even oligoynes much longer than this are stable under ambient conditions. These calculations simply represent one method of quantifying bulk but are highly dependent on the parameters used (e.g. sphere radius). They also do not take into account the flexibility of the polyyne thread, nor the rapid rotation of the ^{t}Bu groups on the stopper – both of which would likely offer greater protection than predicted. Even so, these provide a relatively simple way to evaluate end group protection for these capped oligoynes.

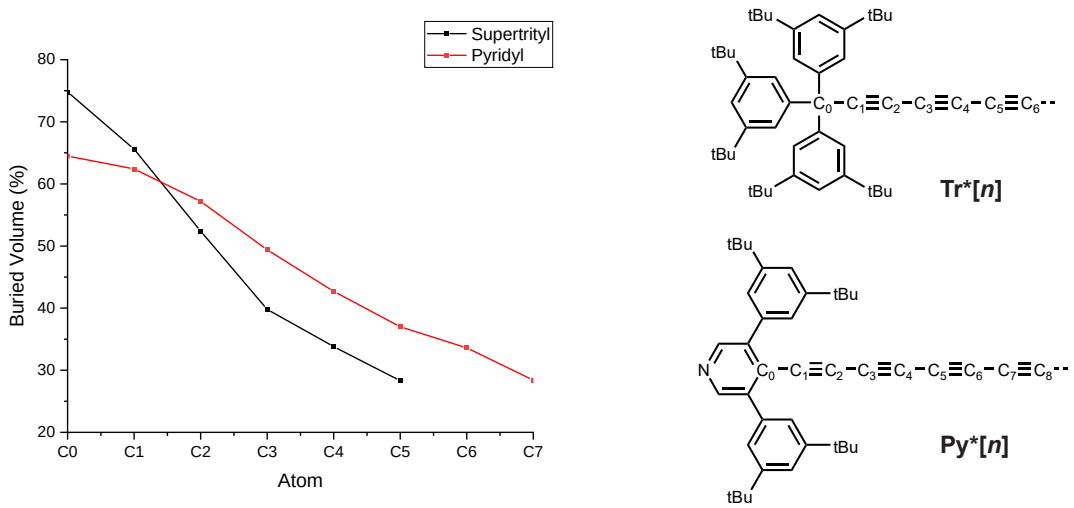

Figure 1.5: The percent buried volume (%V_{bur}) was calculated using Samb*V*ca (version 2.1)[57] for each *sp* carbon along the stoppered oligoyne chain until no interaction with the stopper was observed (corresponding to C5 and C7 for the (black) supertrityl- and (red) pyridyl-capped series, respectively). Solid state geometries were obtained from the CCDC (identifiers GAGYUK and MAKNAR for supertrityl- and pyridyl-capped oligoynes, respectively).[6,55] Sphere radius, r = 4.0 Å, mesh spacing = 0.10 Å, hydrogen atoms included, bond radii = ×1.17 as recommended by Cavallo *et al.*[58]

Tykwinski's work also nicely demonstrates the various effects these end groups may have on the physical properties of the polyyne. It was found that for shorter oligoynes, the end groups can have a marked effect on their physical properties, observable by NMR, Raman and UV-vis spectroscopy. However, these influences begin to diminish as the length increases until

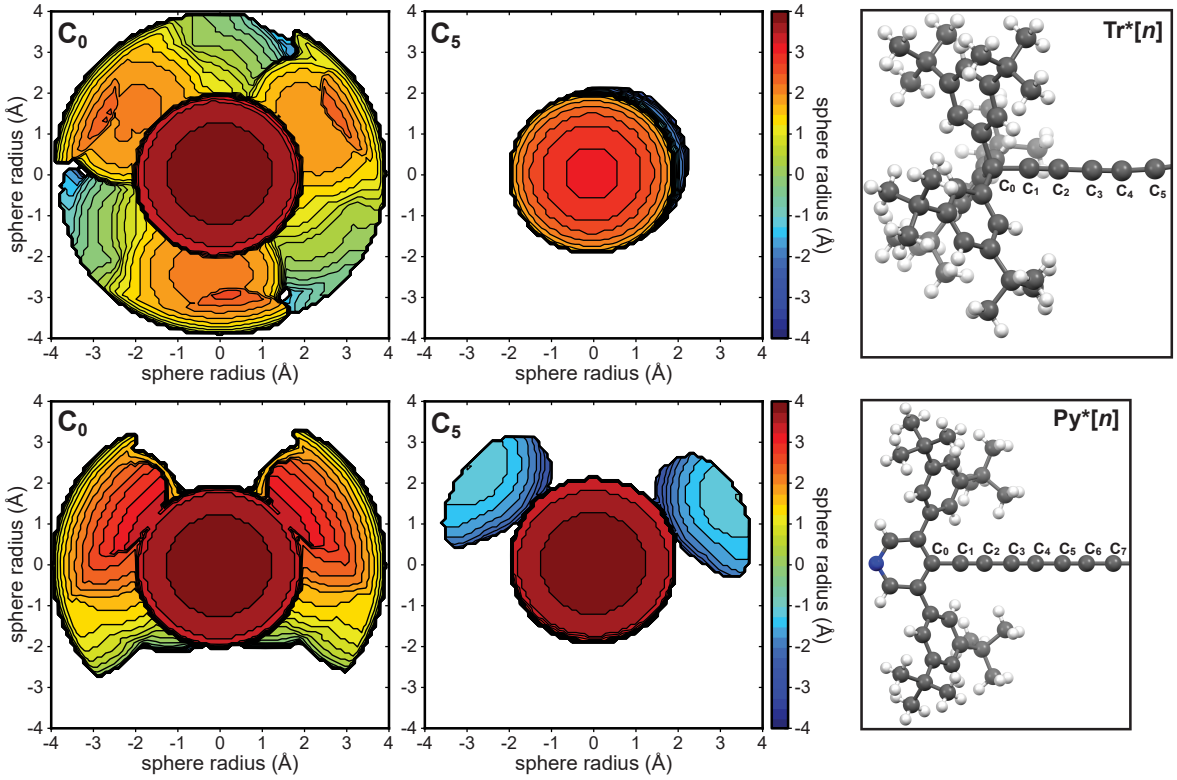

Figure 1.6: Two steric contour maps at C0 and C5 for (*top*) supertrityl-capped oligoynes **Tr*[*n*]** and (*bottom*) pyridyl-capped oligoynes **Py*[*n*]** calculated using Samb*V*ca (version 2.1)[57] using solid state geometries obtained from the CCDC (identifiers GAGYUK and MAKNAR for supertrityl- and pyridyl-capped oligoynes, respectively).[6,55] Full contour maps for C0-6 for **Tr*[*n*]** or C0-7 and **Py*[*n*]** can be found in Figures S1.1 and S1.2, Section 1.6.

C≡C carbon atoms can be considered free from end group effects – a point termed the polyyne-carbyne limit. Extrapolation of data from the series of pyridyl-capped polyynes predicts that carbyne will be a polyynic (rather than cumulenic) material, possessing a finite bandgap at 2.01 eV (617 nm). Meanwhile, ^{13}C NMR studies suggest that as the oligoyne approaches the polyyne-carbyne limit, resonances begin to converge towards a value of 63.4 ppm; matching well to that predicted by the supertrityl-capped[6] and *tert*-butyl capped[59] polyynes (both 63.7 ppm). Despite these end groups being chemically very different – supertrityl and *tert*-butyl groups being capped by sp^3 centres, while pyridyl groups being capped by sp^2 centres – the fact that these series of polyynes converge towards near-identical values strongly suggests the effects of the end groups are no longer present. It was then predicted through convergence of experimental values obtained from the aforementioned spectroscopic techniques, and corroborated by BLA data (obtained via X-ray crystallography), that the carbyne limit will be reached by $n \approx$ 34-37 acetylene units. While we still have a way to go before reaching this limit, research over the last 70 years suggests that this will soon be possible.

1.2.2 UV-vis Studies on Polyynes

UV-vis spectroscopy is a useful tool for the characterisation of extended oligo-/polyynes due to typically well-resolved spectra.[45] It is worth taking some time to highlight various features in the UV-vis spectra of polyynes that make this technique such a useful tool for their characterisation. There have been a large number of polyynes reported, prepared either using bulky terminal substituents, or by supramolecular encapsulation, and characterised by UV-vis spectroscopy.[6,48,61–64] The vast majority of these investigations have either had little comment on the UV spectra of polyynes, or only presented superficial analysis regarding the most intense optical bands (λ_{main}) in the spectra. With the occasional exception,[55,65] little attention has been turned to investigating the weak bands (λ_{weak}), which are often observed at higher wavelengths from the λ_{main} bands (Figure 1.7). In a number of cases where these have been noticed, the origins have been dismissed by the authors as the result of impurities,[66] or arising from orbital mixing with the terminal stoppering groups.[46,61] There exist two systems, a series of H-capped oligoynes **H**[***n***] and a series of diaryl oligoynes, that have been studied in detail. For the former, the unique characteristic spectra arise from the lack of terminal substituents and its $D_{\infty h}$ symmetry,[67–69] while end-groups effects complicate analysis of the latter due to conjugation and symmetry considerations that arise.

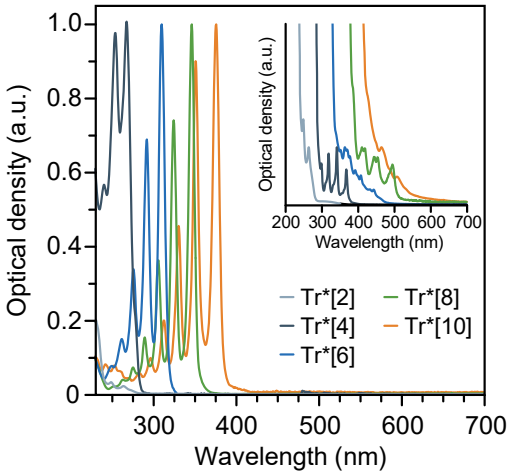

Figure 1.7: UV-vis spectra of the **Tr***[***n***] oligoyne series.[60] λ_{main} transitions dominate the spectrum, λ_{weak} transitions are shown in the insert.

The presence of terminal substituents in oligoynes R–(C≡C)$_n$–R (**R**[***n***]) perturbs the energy profile compared to the terminal oligoynes **H**[***n***] through conjugation while also altering the symmetry of the molecules. Taking the supertrityl-capped oligoyne series **Tr***[***n***] from earlier, the end groups lower the overall symmetry of the molecule. Computational analyses of this series show the point group D_3 with frontier orbitals of E symmetry. A transition between these frontier orbitals will result in a splitting of the excitation energy levels into three distinct electronic states: one degenerate state with E symmetry and two non-degenerate states with respective A_1 and A_2 symmetry. Of these, only the A_2 and E states are dipole-allowed

representations (a consequence of the D_3 symmetry), while the A_1 state remains symmetry-forbidden. Differing from carbyne, where both the $S_0 \rightarrow S_1$ and $S_0 \rightarrow S_{2/3}$ remain symmetry-forbidden ($D_{\infty h}$), transitions to the degenerate $S_{2/3}$ state (E) now become weakly allowed due to the lower symmetry.[60] This manifests itself as a series of weak absorption bands in the UV-vis spectra at lower energies – i.e. λ_{weak} (see insert, Figure 1.7). Such bands are expected to disappear as chain lengths approach the carbyne limit, where end group effects are no longer present (and hence the symmetry once again approaches $D_{\infty h}$). Experimentally, however, this may not be the case as even small deviations from the idealised linear conformation will render them weakly allowed, although their negligible absorption coefficients may make them difficult to detect by UV-vis spectroscopy.[65]

Recent work by Tykwinski and Frauenrath *et al.* detailed in-depth steady-state UV-vis studies of two oligoyne series, the supertrityl-capped and glycosylated oligoynes **Tr*[*n*]** and **Glu[*n*]**, respectively (Figure 1.8).[60] As expected, both show a red-shift with increasing number of triple bonds *n* and display the characteristic vibronic fine structure for lengths of $n > 4$. In all cases, the longest wavelength absorption λ_{main} exhibits the largest molar absorption coefficient (i.e. is most strongly absorbing). For both series, λ_{main} shifts to longer wavelengths (from 240 nm to 390 nm for **Glu[4]** and **Glu[12]** respectively), while the molar absorption coefficient ε_{main} increases significantly with increasing *n*, reflecting the larger degree of conjugation in longer oligoynes. The **Tr*[*n*]** series appears slightly red-shifted by 10-30 nm in comparison to the **Glu[*n*]** series, which the authors attributed to a combination of hyperconjugation and additional solvatochromic effects of the supertrityl stopper. Closer inspection of the UV-vis spectra of both series reveals additional absorption bands (λ_{weak}), with the lowest energy transition being over 100 nm more red-shifted than λ_{main}. One possible origin of the λ_{weak} bands could arise from aggregation (e.g. due to π-π interactions) of the oligoynes. Aggregation effects would be expected to show temperature dependence, but since no significant change in the

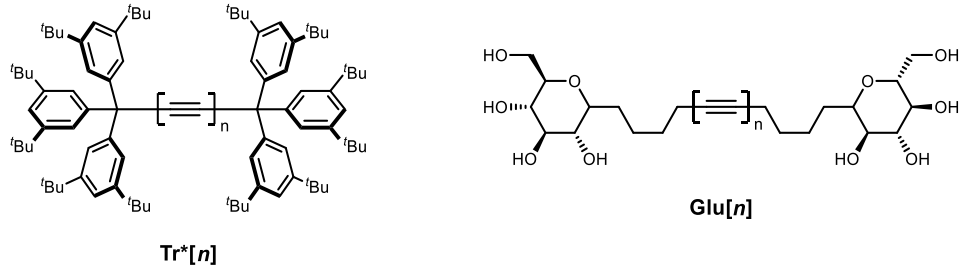

Figure 1.8: The structures of the supertrityl-capped oligoyne **Tr*[*n*]** and glycosylated oligoyne **Glu[*n*]** series.

spectral form was observed upon varying temperature, these can be discredited from the origins of λ_{weak}.

The authors concluded that in both cases, the S_1 state remains unpopulated due to the dipole-forbidden $S_0 \rightarrow S_1$ transition, and so are absent from experimental UV-vis spectra; this is in good agreement with previous computational analyses.[70] The 'weak signals' were therefore attributed to the weakly-allowed $S_0 \rightarrow S_{2/3}$ transition to the degenerate state E. In accordance with the weakly-allowed nature of this transition, the amplitudes of λ_{weak} are a few orders of magnitude lower than those of λ_{main}, which can therefore be attributed to a higher, symmetry-allowed $S_0 \rightarrow S_n$ transition. Such assignments were in good agreement with computational analysis performed on the same series of compounds (CAM-B3LYP). Experimentally- and computationally-determined energies for the $S_0 \rightarrow S_1$ and $S_0 \rightarrow S_{2/3}$ transitions were plotted against $1/n$ (Figure 1.9). For both **Tr*[*n*]** and **Glu[*n*]**, the energies were found to converge at near-identical saturation values for the optical energy gap (E_{opt}) – the lowest energy transition observed corresponding to the vertical excitation energy from the ground state to the first dipole-allowed excited state – tabulated in Table 1.1.

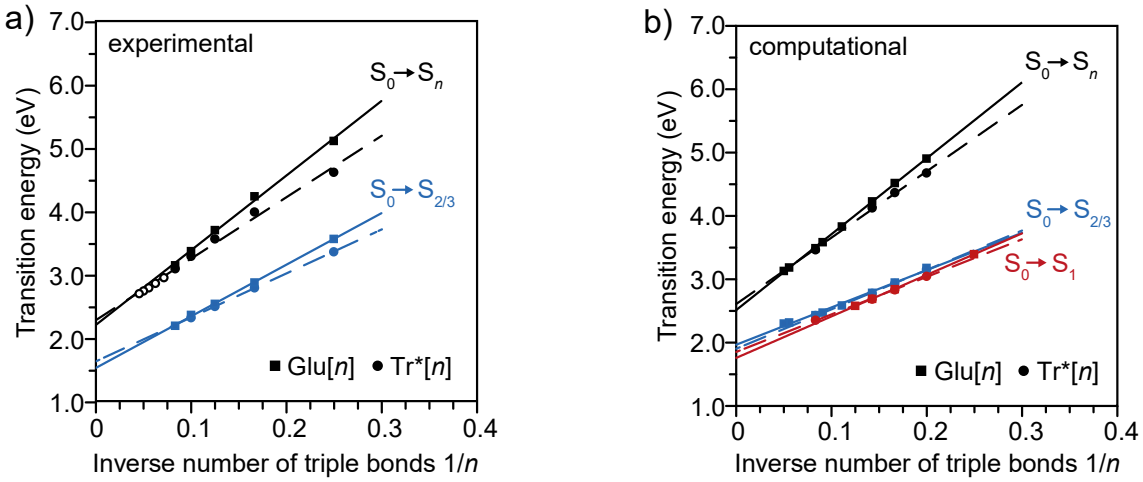

Figure 1.9: (a) Plot of the energies of the experimentally determined $S_0 \rightarrow S_n$ (main) transitions and the $S_0 \rightarrow S_{2/3}$ (weak) transitions against the inverse number of carbon-carbon triple bonds $1/n$ for **Glu[*n*]** in CH_2Cl_2 and **Tr*[*n*]** in *n*-hexane (open symbols represent data obtained for the **Tr*[*n*]** series from the literature).[6] (b) Plot of the energies of the computationally determined $S_0 \rightarrow S_n$ (main), $S_0 \rightarrow S_{2/3}$ (weak), as well as $S_0 \rightarrow S_1$ (forbidden) transitions against the inverse number of carbon-carbon triple bonds $1/n$ for **Glu[*n*]** in CH_2Cl_2 and **Tr*[*n*]** in *n*-hexane. In both cases, the saturation values have been determined by linear extrapolation.[60]

While all trends and differences are fully reproduced via computational methods, the calculated energies are slightly overestimated. This was attributed to the CAM-B3LYP functional having a tendency to over-localise electron density distribution[71,72] and thus transition energies, especially when the effects of vibronic coupling are neglected.[73]

Table 1.1: Tabulated experimentally and computationally determined values for the optical gap for the **Tr*[*n*]** and **Glu[*n*]** series of oligoynes.[60]

Transition	Experimental				Computational			
	Tr*[*n*]		**Glu[*n*]**		**Tr*[*n*]**		**Glu[*n*]**	
	E_{opt} / eV	λ_{opt} / nm	E_{opt} / eV	λ_{opt} / nm	E_{opt} / eV	λ_{opt} / nm	E_{opt} / eV	λ_{opt} / nm
$S_0 \rightarrow S_n$	2.28	543	2.21	561	2.59	478	2.50	496
$S_0 \rightarrow S_{2/3}$	1.64	756	1.53	810	1.96	634	1.89	656

Furthermore, minor deviations from a linear extrapolation approach between the experimentally-determined **Tr*[*n*]** and **Glu[*n*]** series may be attributed to hyperconjugation to the Tr* stoppering groups for that series. Despite this, the generally good agreement between experimental and computational results for both series, and both the $S_0 \rightarrow S_n$ (main) and $S_0 \rightarrow S_{2/3}$ (weak) transitions is important as it gives confidence in the ability to computationally predict the $S_0 \rightarrow S_1$ transitions that could not otherwise be measured experimentally.

To summarise this work in more simplistic terms; for shorter oligoynes, the end groups reduce the symmetry of the molecule, which manifests itself as a series of low-intensity electronic absorptions (λ_{weak}) in UV-vis spectra. As the length of the oligoyne increases, the higher pseudo-symmetry that results gradually leads to these absorptions becoming forbidden, and ultimately disappearing, as the polyyne-carbyne limit is approached. Importantly, these studies have reassessed the estimates for both the optical and fundamental gap of carbyne to (E_{opt} = 1.5–1.6 eV), which is approximately 0.6–0.7 eV smaller than those previously estimated based on analysis of λ_{main} UV-vis bands alone. It could be argued that an approach based on these weak transitions may not be applicable as polyynes approach the carbyne limit because that would result in the disappearance of such weak transitions. However, even minor deviations from the idealised linear geometry would render these transitions partially allowed, and thus make this approach better suited to describing E_{opt} than others previously reported.

1.3 Cyclo[*n*]carbons

Cyclo[*n*]carbons are monocyclic molecules composed entirely of *sp*-hybridised carbon atoms, where *n* defines the number of constituent atoms bound to make up the ring. In 1966, Hoffmann reported extended Hückel calculations on linear and cyclic C_n for *n* = 4–18 and

concluded that, due to two orthogonal $(4n+2)\pi$ electron systems, some cyclo[n]carbons, such as cyclo[18]carbon, would benefit from additional stabilisation, when compared to their linear analogues.[74] This theory was supported by semi-empirical calculations using Modified Neglect of Diatomic Overlap (MNDO) theory in 1986.[75] During the last decades there have been several theoretical studies on finite-sized oligoynes,[76–79] cyclo[n]carbons[77,80–83] and carbyne.[81,84–87]

Bond length alternation (BLA) is an important parameter when describing π-conjugated molecules.[88] High levels of BLA indicate weak conjugation, while lack of BLA is a characteristic signature for aromatic molecules, such as benzene. Based on this, doubly aromatic C_n molecules (with $n = 4k + 2$) would be expected to favour regular cumulenic D_{nh} geometries (i.e. no BLA). In contrast, Jahn-Teller distortions in antiaromatic molecules (with $n = 4k$), should give rise to alternating C–C single and C≡C triple bonds (i.e BLA ≠ 0) with polyynic $D_{(n/2)h}$ geometry.[82] Virtually all calculations on large C_n systems suggest the presence of Peierls distortion – the distortion of a periodic lattice of a one-dimensional crystal arising from the oscillation of atoms within the chain. As a result, the perfect order in a one-dimensional crystal is broken and the overall symmetry of the system is lowered – i.e. the chain is polyynic, even when $n = 4k + 2$.[89] This preference for a polyynic structure relates to the fact that polyynes are generally more stable than cumulenes.[90] Due to Peierls distortion, the polyynic form of cyclo[18]carbon would be favoured over a cumulenic from. The symmetry of C_{18} is therefore expected to be D_{9h} (structure **B**, Figure 1.10) rather than the higher-symmetry D_{18h} cumulenic form (structure **A**), as would be predicted based on aromaticity rules alone.

When predicting the geometries of cyclo[n]carbons (where n is an even number), there are four geometries that must be considered (illustrated for C_{18} in Figure 1.10): **A**, D_{nh} cumulene (BLA = 0; BAA = 0): **B**, $D_{(n/2)h}$ polyyne (BLA ≠ 0; BAA = 0); **C**, $D_{(n/2)h}$ cumulene (BLA = 0; BAA ≠ 0) and; **D**, $C_{(n/2)h}$ polyyne (BLA ≠ 0; BAA ≠ 0). The predictions of the lowest energy

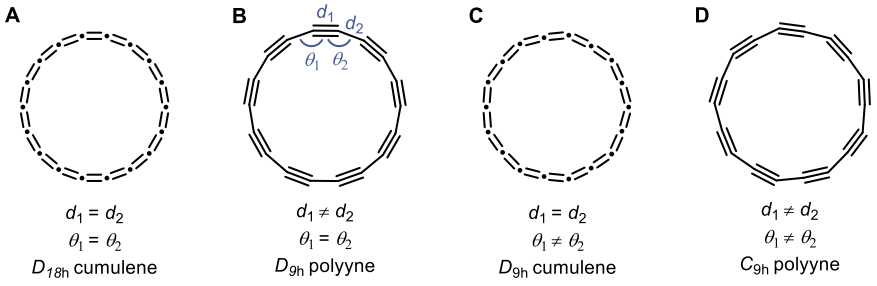

Figure 1.10: Four possible structures of a cyclo[18]carbon. Bond length alternation is defined as BLA = $d_1 - d_2$ and bond angle alternation is defined as BAA = $\theta_1 - \theta_2$.

geometries for C_n systems (where n = 6–24) have been the subject of many computational studies. A survey of these three results leads to three generalisations: (i) small aromatic rings ($n = 4k + 2$) with $n \leq 10$ have structure **C** (BLA = 0; BAA ≠ 0); small antiaromatic rings ($n = 4k$) with $n \leq 16$ have structure **D** (BLA ≠ 0; BAA ≠ 0) and; large rings ($n \geq 24$) have polyyne structures **D** or **B** (BLA ≠ 0).

The structures of intermediate rings ($16 < n < 24$) are difficult to calculate and, not surprisingly, the results depends strongly on the computational method used. For example, Hartree-Fock (HF),[80] quantum Monte Carlo (MC)[83] and coupled cluster[91] methods predict that the ground state of C_{18} to be polyynic (structures **B** or **D**). In contrast, most density functional theory (DFT)[77,82,92–95] and second-order Møller-Plesset (MP2)[96,97] calculations predict a cumulenic ground state (structures **A** or **C**). In general, pure DFT theory tends to underestimate the BLA of polyacetylenes, while the HF method typically overestimates it.[98] Hybrid density functionals exist that include enough exchange correlation also correctly predict a polyyne structure for the larger rings, producing intermediate results between those of Hartree-Fock and pure DFT theory. These are generally in good agreement with high level coupled cluster and quantum Monte Carlo calculations,[77,82,83] and with recent experimental results for C_{18} (*vide infra* Section 1.4.2).

1.4 Synthesis of Acetylene-Rich Systems

The significant decrease in the stability of polyynes as they become longer is the main hurdle in the synthesis of such molecules. There have been many previous attempts towards the synthesis of polyynes and cyclocarbons,[80,99–103] yet the instability of extended polyynic systems have made all attempts thus far unsuccessful in isolating cyclocarbons in solution. As discussed previously, polyynes tend to undergo detrimental crosslinking reactions and are susceptible to nucleophilic attack. Despite this, there exist two main strategies for increasing the stability of polyynes: (i) bulky terminal substituents (described in Section 1.2.1) and; (ii) supramolecular encapsulation whereby the polyyne chain is encapsulated and thus shielded by a chemically-inert macrocycle. Regarding the latter, work by both our group and the Tykwinski group has demonstrated the effects to polyyne stability brought about by rotaxane formation; supramolecular encapsulation improves the thermal stability of the polyynes.[62,104]

1.4.1 General Synthetic Methods

The synthesis of polyynes in the laboratory heavily relies on a number of methods involving the homo- and heterocoupling of terminal acetylenic precursors.[80,105,106] Alternative approaches can be used in combination to aid preparation of more challenging targets, such as the elimination[107,108] or extrusion[31,109] of functional subunits assist in assembling the framework of linear or cyclic polyynes. The ease of deprotonation of the terminal proton under mild conditions plays an important role in the rich chemistry of acetylenes. Combining this with the ability of terminal acetylenes to undergo metalation is crucial in several coupling reactions.

In 1869, Carl Glaser discovered one of the most important reactions to be used in the synthesis of acetylenes. His work demonstrated the oxidative dimerisation of Cu(I) phenylacetylide in the presence of O_2 to yield diphenylbutadiyne, Scheme 1.2.[110] This discovery has since sparked interest in C_{sp}-C_{sp} couplings, and many variations on the traditional Glaser homocoupling have since been developed. To summarise, in 1956 Eglinton and Galbraith reported an oxidative homocoupling of alkynes using a stoichiometric Cu(II) source ($Cu(OAc)_2$) in the presence of pyridine.[111,112] Following that, in 1962 Hay reported conditions using catalytic quantities of CuCl in the presence of a *N*,*N*,*N*',*N*'-tetramethylethylenediamine (TMEDA) ligand, using O_2 as the oxidant.[113] The TMEDA acts to improve solubility of the Cu(I) catalyst in common organic solvents, such as acetone and dichloromethane, thereby accelerating the rate of reaction. Further modifications to the original Glaser reaction have employed the use of Pd catalysts, which can promote the homocoupling when traditional Cu(I)/Cu(II)-promoted ones prove ineffective.[114,115]

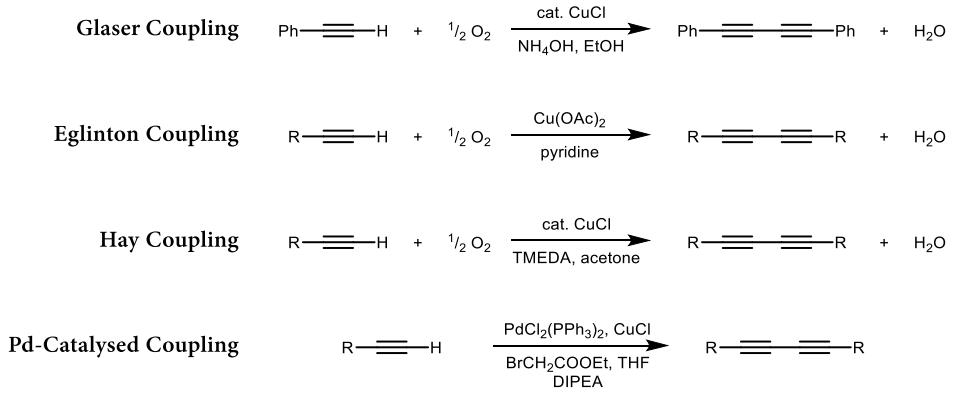

Scheme 1.2: The original Cu(I)-catalysed Glaser acetylene coupling, and variations thereof.

While these homocoupling reactions typically work efficiently in generating symmetrical polyynes, they are often unsuitable for preparing their asymmetric counterparts.

Of the reactions discussed thus far, none are selective in cross coupling to give asymmetric polyynes. While cross coupling can be achieved by such approaches, it must be done so statistically and by using a large excess of one reagent over the other. This changed in 1955 when Paul Cadiot and Wladyslav Chodkiewicz developed a protocol for the cross coupling of a halo-acetylene with a terminal acetylene.[116] Unlike the Glaser coupling, and many of its variations, the Cadiot-Chodkiewicz cross coupling is performed under an inert atmosphere, where the halo-acetylene adds to the Cu(I)-acetylide species in an oxidative addition step, and itself acts as the oxidant necessary for the coupling reaction to proceed.[117] Due to this, the Cadiot-Chodkiewicz reaction affords good selectivity for the cross-coupled, asymmetric product. Even so, some homocoupling between reagents is usually inevitable, particularly when the alkynes are bulky or when the electronic properties of the reactants are similar.[118] Typical coupling partners for these reactions are bromoacetylenes, although the use of iodoacetylenes has also been reported.[119–122] Chloroacetylenes have little practical importance as they are generally not sufficiently reactive to undergo such a reaction and tend to undergo homocoupling.[106]

Negishi *et al.* and later Dvořák *et al*. have reported cross-couplings of Zn-acetylides (prepared *in situ*) with bromoacetylenes to afford asymmetric oligoynes.[118,123,124] The Zn-acetylides are formed first by lithiation of silyl-protected alkynes (or unprotected, terminal alkynes), then subsequent transmetallation with $ZnBr_2$. The high selectivity of this reaction allows it to be employed for the cross-coupling of alkynes where a statistical Glaser or Cadiot-Chodkiewicz cross coupling proves ineffective or unsuitable. The preparation of alkadiynyl (trialkyl)silanes (Scheme 1.3) are usually prepared under standard Cadiot-Chodkiewicz coupling conditions, but only with robust silyl protecting groups (TES, TBS, TIPS).[125] However, the instability of the TMS group under the reaction conditions makes such an approach unsuitable, and instead milder Pd co-catalysed cross-coupling with zinc acetylides should be selected.[123]

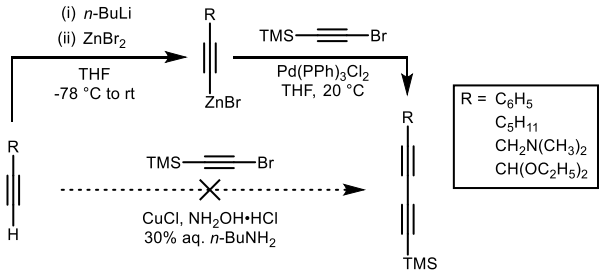

Scheme 1.3: Preparation of alkadiynyl(trimethyl)silanes from a Negishi coupling of a terminal acetylene with bromoethynyl(trimethyl)silane.[123]

1.4.2 Masked Alkyne Equivalents (MAEs)

While the developments in C_{sp}-C_{sp} couplings have been pivotal in forming longer polyynic systems, the instability of the products remain a barrier to their synthesis. As oligoynes get longer and longer, the shielding effect of stopper groups becomes weaker. One approach taken to overcome this is to break the conjugation with a motif ('masking' the polyyne) that, upon application of a suitable stimulus, can be removed without trace ('unmasking') to yield the intact polyyne. Such masking groups for acetylenes are termed 'masked alkyne equivalents' (MAEs). Thus far, all attempts towards the synthesis of cyclocarbon have incorporated a MAE into a cyclic precursor designed to unmask and generate cyclocarbon when the MAE is removed (Figure 1.11).[14,15,80,101,103,126] The unmasking chemistry varies depending on the MAE, but generally unmasking proceeds through a retro-Diels Alder,[80] an oxidation/decomplexation,[99] a cheletropic fragmentation[31] or a photochemical process.[101]

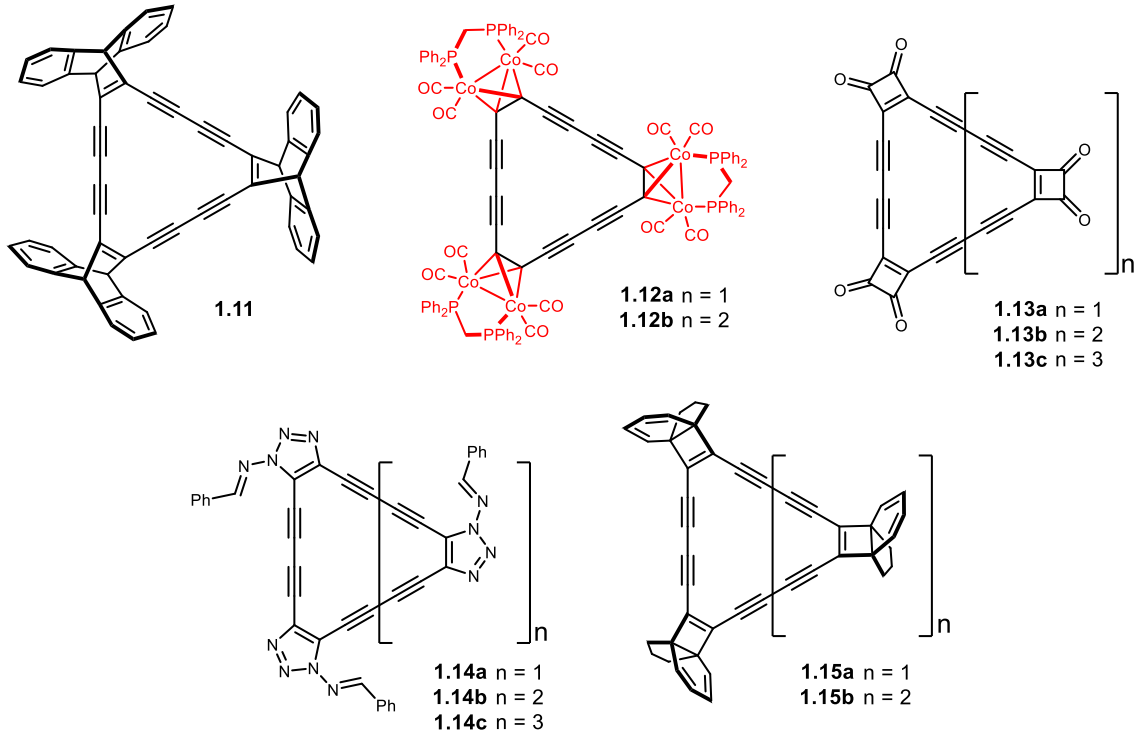

Figure 1.11: Synthetic attempts towards the synthesis of cyclocarbons. (**1.11**) F. Diederich, *et al.*[80]; (**1.12**) F. Diederich, *et al.*[99]; (**1.13**) F. Diederich, *et al.*[126,127]; (**1.14**) C. W. Rees, *et al.*[103]; (**1.15**) Y. Tobe, *et al.*[101] and related structures.[31,100]

In 1989, pioneering work by Diederich *et al.* captured researchers' interest with their efforts towards synthesising cyclocarbons.[80] This was the first synthesis towards cyclocarbons employing the use of MAEs; in this case, well-established anthracene moieties were used. These MAEs are known to undergo retro-Diels-Alder reactions to generate strained acetylenes.[128] Using a TMS-protected bis-acetylene anthracene species, the compound was successfully

deprotected to afford the terminal alkyne and subsequently oxidatively coupled under Eglinton-Glaser conditions to construct the dodecahydro[18]annulene **1.11** – a precursor to cyclo[18]carbon. Unfortunately, the expected three-fold [4+2] retro-Diels-Alder to eliminate anthracene and return C_{18} was unsuccessful; only in the gas phase after heating to 800 K was the desired cyclo[18]carbon observed by laser-desorption time-of-flight (LD-TOF) mass spectroscopy. Further attempts towards unmasking by flash vacuum pyrolysis of **1.11** yielded only anthracene and a polymeric carbonaceous material. The limited success of these attempts is perhaps unsurprising. It is likely that when cyclo[*n*]carbon molecules come together, they probably react to generate a cross-linked polymer or C_{60} clusters, in a similar manner to long linear polyynes.[44]

Following on from this, Diederich *et al.* shifted focus towards using a dicobalt carbonyl-based MAE[99] in which a dicobalt carbonyl species can reversibly complex a C≡C bond to give compounds stable under ambient conditions (Scheme 1.4). Diederich and co-workers modified the carbonyl complex through substitution of a bidentate bis(diphenylphosphino)methane (dppm) ligand in place of two CO ligands to improve the stability of the resulting protected oligoynes. This dicobalt carbonyl MAE is of particular interest as it acts to stabilise polyacetylenes in two ways: (i) in breaking conjugation of the polyyne by changing the hybridisation state of the carbon atoms from *sp* to sp^3 and; (ii) by providing substantial steric bulk that acts to prevent close contacts between two masked polyynes. One additional advantage of these dicobalt-masked acetylenes is that the masking process introduces a significant bend between the two attached groups, aiding the formation of curved and cyclic structures.[99,129] Using similar conditions to the anthracene MAEs previously, an oxidative Eglinton-Glaser coupling successfully afforded compounds **1.12a** and **1.12b** as highly-stable crystalline solids that could be characterised by X-ray crystallography. Oxidative

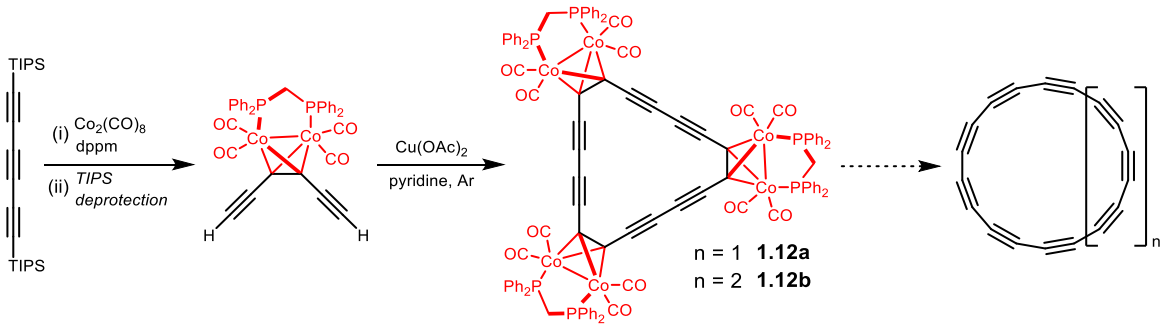

Scheme 1.4: Synthetic attempts to cyclo[*n*]carbons using dicobalt carbonyl masking groups.[30,99]

decomplexation of **1.12a** would be expected to generate cyclo[18]carbon,[130] but the authors found no suitable conditions to successfully remove the dicobalt MAE. It is worth highlighting that since this seminal publication, there have been a few conditions reported that are successful in unmasking this MAE.[129,131]

In their most recent attempt, Diederich *et al.* employed cyclobutadienone-based masking groups towards preparing cyclocarbons (Scheme 1.5).[126,127] The reactive nature of conjugated ketones made this synthesis more complex than for the previous MAEs. Compounds **1.13a**, **1.13b** and **1.13c** were prepared first by masking the ketones as ketals then unmasking later in the synthesis. Laser desorption mass spectra of carbon oxide **1.13a** revealed the successive loss of CO molecules to give cyclo[18]carbon, in both positive and negative modes.[126] Subjecting the larger carbon oxides, **1.13b** and **1.13c**, to the same conditions generated cyclo[24]- and cyclo[30]carbons. The mass spectra from the unmasking of these compounds have provided insights into the mechanism of fullerene formation.[132–134] Previously, it was thought that fullerenes were formed directly from small carbon fragments, such as C_2, from vaporisation of graphite.[135] However, this work found that C_{30}^+ coalesces exclusively into C_{60}^+, while C_{18}^+ and C_{24}^+ form mainly C_{70}^+, and suggests that cyclocarbons are intermediates in the conversion of C_2 to C_{60} and C_{70}. Attempts were then made to isolate cyclo[18]carbon by irradiation of **1.13a** in a matrix of solid 1,2-dichloroethane at 15 K. Infra-red (IR) spectroscopy was used to follow the appearance of a ketene signal and a disappearance of the carbonyl band in the starting material, but unfortunately no spectroscopic signature of C_{18} could be detected under these conditions.[30]

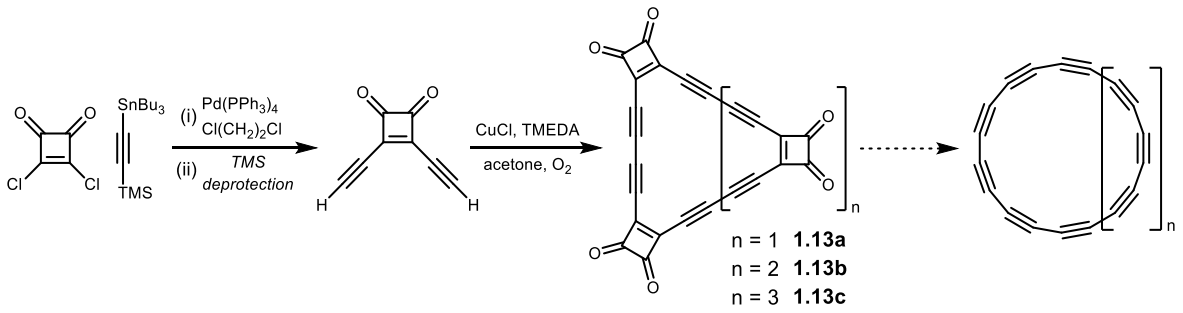

Scheme 1.5: Synthetic attempts to cyclo[*n*]carbons using cyclobutadienone masking groups.[126,127]

Following on from Diederich's work, in 1996 Rees *et al.* prepared a new class of masked cyclic trimers, tetramers and pentamers based on a 1-amino-1,2,3-triazole MAE (compound **1.14**, Figure 1.11).[103] The authors claimed that one advantage of this MAE is that the especially

mild conditions ($Pb(OAc)_4$, CH_2Cl_2, −78 °C) required to deprotect the MAE should afford the desired cyclo[*n*]carbon cleanly and with minimal side reaction. Even so, the authors were unable to unmask the aminotriazole-substituted dehydroannulenes to liberate the desired cyclocarbon.

In the same year, Tobe *et al.* developed an alternative MAE based on propellane-annulated dehydroannulenes. Using diethynyl[4.3.2]-propellatriene as a precursor, the $Cu(OAc)_2$-mediated oxidative homocoupling of which provided a reliable and efficient route to the corresponding cyclic trimer and tetramer, both precursors for cyclo[18]- and cyclo[24]carbons, respectively. Irradiation of dodecadehydro[18]-annulene (compound **1.15**, Figure 1.11) in furan with a low-pressure mercury lamp (254 nm) quickly resulted in the loss of at least one of the indane units by a [2+2] cycloreversion process to yield highly-reactive tetradecadehydro[18]-annulene intermediates. Repeating this reaction in THF once again resulted in the liberation of indane, but this time an uncharacterised polymeric material was also observed. As with the many prior approaches, is possible that cyclo[18]carbon was obtained, but reacted so rapidly that it could not be characterised.

In 2003, the Tobe group reported a new masked alkyne equivalent, in which they use the cheletropic fragmentation of radialenes as a method for unmasking the MAE (Scheme 1.6).[31] In a series of test reactions, the radialenes, composed of bicyclo[4.3.1]deca-1,3,5-triene moieties (**1.16a**), were demonstrated to yield oligoynes in up to 45% yield upon irradiation of the MAE with UV light. It was noted that that unmasking does not proceed cleanly and an isomerisation product (**1.16b**) of the starting material was obtained in 30% isolated yield. By using an oxidative Eglinton cyclisation reaction, Tobe and co-workers were able to reliably generate the cyclic trimer, tetramer, pentamer and hexamer in varying yield as precursors to corresponding cyclo[18/24/30/36]carbons. The target cyclo[*n*]carbon was observed as a fragment in LD-TOF

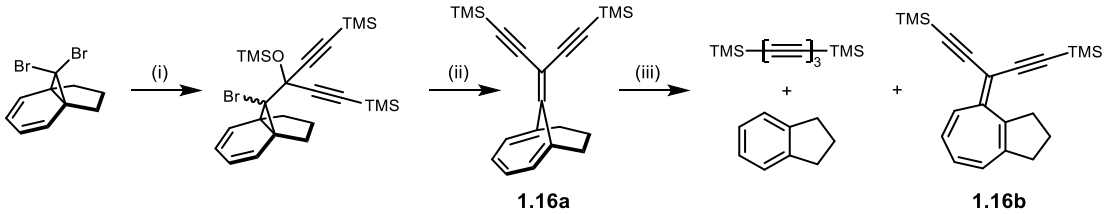

Scheme 1.6: Preparation of radialene **1.16a** and its subsequent light-promoted unmasking to bis-TMS triyne and competing isomerisation product **1.16b**. (i) *n*−BuLi, −100 °C *then* $(TMS\text{-}C{\equiv}C)_2C{=}O$, −70 °C *then* TMSCl, THF; (ii) *t*−BuLi, pentane, −110 °C *then* TMSCl; (iii) hν (254 nm), *n*−hexane.

for all ring sizes yet, as with all other attempts, the authors were unable to isolate the final cyclocarbons.

Since this work, our group has demonstrated the successful unmasking of cyclocarbon oxide **1.13a** using atom manipulation on a bilayer of NaCl on Cu(III) at 5 K.[14] Scanning-tunneling microscopy-atomic force microscopy (STM-AFM) was successfully employed to sequentially remove masking CO groups from the precursor upon application of a targeted voltage pulse from the STM tip. Not only could each MAE be removed individually, AFM images and, most importantly, the final cyclo[18]carbon could be obtained at each step (Figure 1.12). This ground-breaking work has given researchers the first insights into some of the

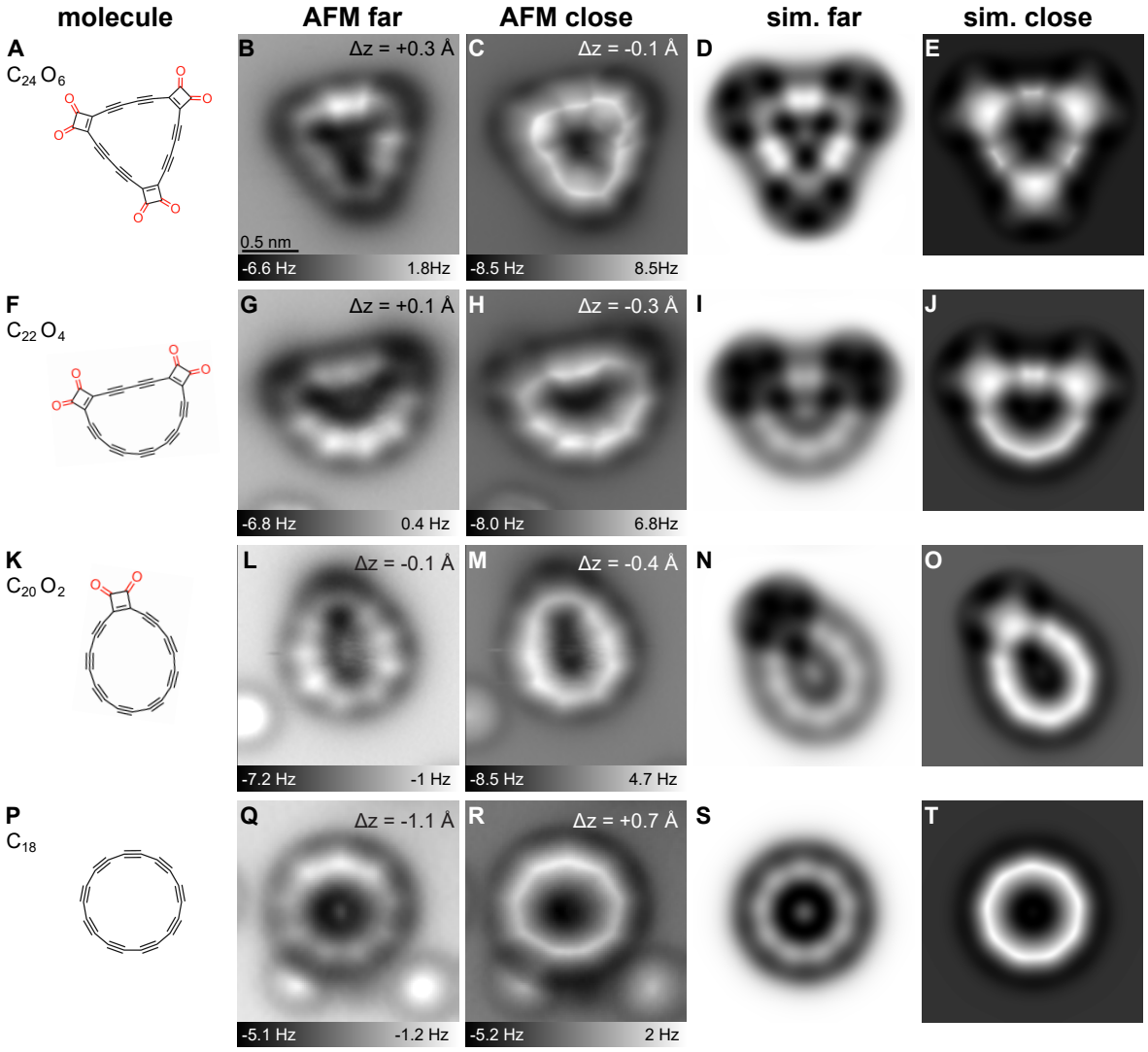

Figure 1.12: AFM images (columns 2 and 3), corresponding to structures shown in column 1, were recorded with a CO-functionalised tip at different tip offsets Δz, with respect to an STM set point (I = 0.5 pA, V = 0.2 V) above the NaCl surface. Images **A-E**, **F-J**, **K-O** and **P-T** correspond to the starting material, mono-unmasked intermediate, bis-unmasked intermediate and final compound C_{18}, respectively.[14] Bright features in the lower part of images **L**, **M**, **Q**, and **R** correspond to individual CO molecules. Columns 4 and 5 show simulated AFM images based on gas-phase DFT-calculated geometries, with the distances "far" and "close" corresponding to the respective AFM distances. From K. Kaiser *et al.*, *Science*, 2019, **365**, 1299–1301. Reprinted with permission from AAAS.

properties of cyclo[18]carbon. Most notable of which was the observation that the molecules possessed D_{9h} symmetry, thereby confirming C_{18} adopts a polyynic, rather than cumulenic, structure with defined positions of alternating triple and single bonds, at least on a NaCl/Cu bilayer. Arising from the high reactivity of cyclocarbon oxide **1.13a** it was possible to induce covalent coupling between molecules by atom manipulation. This interesting finding could potentially allow for covalent coupling involving cyclocarbon to be employed in the synthesis of other carbon allotropes and carbonaceous materials.

It is evident from previous attempts towards cyclo[*n*]carbons that the synthesis of pristine cyclocarbon is extremely challenging. It is likely that in many of the previous attempts to synthesise cyclocarbon, unmasking of the precursors does form the target, but the high reactivity means that detrimental side reactions occur too quickly to isolate cyclocarbon itself. While these exciting reports have furthered interest into cyclocarbon, for the highest chance of isolating and characterising cyclocarbons, a conceptually quite different approach is likely required.

1.5 Mechanically Interlocked Materials

The stability of polyynes still remains a large problem and is restricting their study. Bulky stoppering groups can be used to stabilise polyynes, but there remain other methods to stabilise *sp*-carbon chains without functionalisation. In 1994, it was first proposed that polyynes could be stabilised by mechanical insulation.[10] In threading the chain through the cavity of a macrocycle to form rotaxanes and pseudorotaxanes, the shielding effect of the macrocycle should prevent polyynes chains from coming into close contact with one another.[136] Since then, this stability enhancement has been periodically acknowledged by a number of chemists[107,137] before being definitively proven in 2015 by Frauenrath,[64] and one year later by work published by our group in conjunction with Twkwinski.[62]

The important distinguishing feature in mechanically interlocked molecules is that they are topologically linked; they are often referred to as possessing a 'mechanical bond', rather than a covalent one.[138] What differs from other supramolecular assemblies is that while these assemblies can often be deconstructed by different stimuli, mechanically interlocked structures require the breaking of one or more covalent bonds to separate each component.[139] When two

rings are interlinked, the resulting architecture is referred to as a catenane (Figure 1.13). Meanwhile the threading of an axle through a ring generates a pseudorotaxane (the axle can still slip out from the ring), the stoppering of which generates a rotaxane.[140] The mechanical bond, and molecular machines that soon followed, were recognised by the Nobel Prize in Chemistry in 2016.

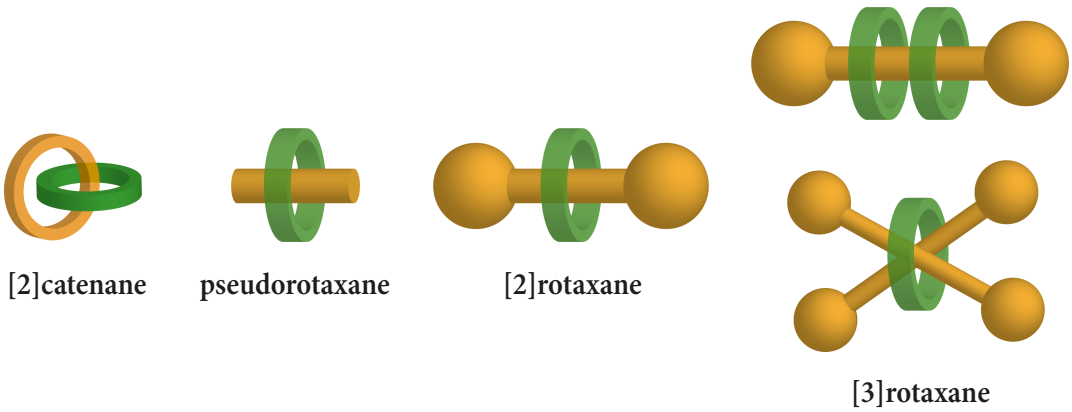

Figure 1.13: Pictorial representation illustrating some types of mechanically interlocked structures.

There are, in general, two synthetic approaches towards rotaxanes: statistical synthesis and template-directed synthesis. In 1967, Harrison *et al.* reported the first synthesis of a rotaxane using a procedure that relied on the likelihood that two halves of a dumbbell-shaped molecule would react through the cavity of the macrocycle – a statistically unlikely occurance.[141] The macrocycle was bound to a solid-support resin and then both halves of the dumbbell passed over the resin 70 times to return the rotaxane in an, at that time, reasonable 6% yield. Of course, since this report progress has improved significantly, and a plethora of creative syntheses have been devised. Excellent yields have been obtained through preorganisation of the components using hydrogen bonding,[142] anionic,[143,144] and hydrophobic interactions,[145] as well as through metal coordination.

1.5.1 Metal-Templated Synthesis

In forming mechanically interlocked molecules, two or more components must be held in such a conformation that the two components cross over each other (generating a 'crossing point'). Should no crossing points be formed, a non-interlocked species will result. Coordination of components to metal ions can be used to preorganise them in positions determined by the preferred coordination geometry of a given metal ion and, in doing so, generate the necessary crossing points. Two variations of metal-templated synthesis of interlocked materials exist:

passive metal template (PMT) and active metal template (AMT). While the former was developed first, the latter has become more popular in recent years.[146]

The passive metal template approach was first envisaged by Jean-Pierre Sauvage in 1983 as a route to synthesising catenanes. In this work Sauvage, recognising the preference of Cu(I) ions to adopt a tetrahedral geometry, used a Cu(I) complex with two bidentate ligands, which adopt geometries orthogonal to each other. By using components with sufficient rigidity and lateral extension, he was able to generate the required crossing points for catenane formation. These theories were later confirmed in 1986 when a diphenol phenanthroline motif was used to effectively coordinate Cu(I), which could then be interlocked by treating with a diiodo polyethyleneglycol chain in a Williamson ether synthesis-type reaction (Scheme 1.7).[147] In this breakthrough work, Sauvage managed to obtain the [2]catenane **1.17** in an impressive 27% yield; other approaches at the time typically required 6-20 steps and obtained the desired catenane in sub-1% yields.

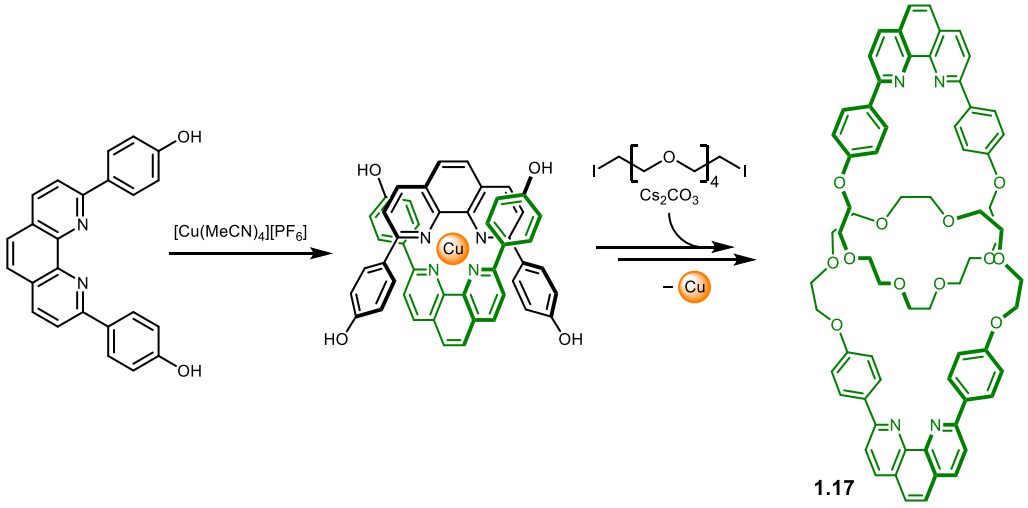

Scheme 1.7: Preparation of a [2]catenane **1.17** via a Cu(I)-promoted passive metal template approach.[147]

All systems utilising a PMT approach share two features: (i) each component must possess permanent coordination sites in order to assemble the structure and; (ii) a stoichiometric amount of metal is required as a minimum.[148] Since this work, a number of other PMT systems have been reported that exploit alternative metal coordination geometries, such as octahedral,[149,150] square planar[151,152] and linear sites.[153] Using a PMT strategy, a plethora of mechanically interlocked molecules have been reported: most importantly for our group, rotaxanes and catenanes,[154] but other ingenious designs such as the molecular shuttle reported by Sauvage *et al.*,[155] as well as his and Leigh's molecular knots.[156,157]

Even though a passive metal template approach has been key in developing chemistry to create such interesting molecules, the full potential of metal ions is not being utilised. An active metal template (AMT) approach can be considered an extension to the passive one, whereby the metal not only acts as a template, holding each component in the correct conformation to favour mechanical interlocking, but also plays an additional "active" role in catalysing covalent bond formation, locking the components together. There are several attractive features to an active template approach: (i) no requirement for permanent recognition groups on each component, affording improved structural diversity; (ii) catalytic (sub-stoichiometric) quantities of metals can be used in some cases; (iii) inherent efficiency and flexibility benefit in the metal playing a dual-role and; (iv) the strategy may prove applicable to a wide range of well-known transition metal-catalysed reactions.

Leigh *et al*. first pioneered such an approach in 2006 where they reported an active metal templated copper(I)-catalysed terminal alkyne-azide 1,3-cyclocaddition (CuAAC) to assemble [2]rotaxane **1.18**, Scheme 1.8.[158] The mild conditions and high-yielding nature of this reaction made it an ideal candidate to which an AMT approach could be applied. In this one-pot reaction, an equimolar quantity of pyridine-containing macrocycle **1.19**, alkyne **1.20**, azide **1.21** and Cu(I) source were stirred at room temperature to return the [2]rotaxane **1.18** in 57% yield, after demetallation with KCN. Both the alkyne and azide components contained sufficiently bulky stoppering groups (trityl) to prevent the macrocycle from slipping off the thread. Through systematic variation of the reaction conditions, Leigh found that in using sub-stoichiometric amounts of Cu(I) and addition of pyridine (to prevent the multidentate [2]rotaxane sequestering the copper) it was possible to isolate the [2]rotaxane in an impressive 84% yield using this approach. In later work, the authors discovered that using a high ratio of macrocycle:Cu(I) can result in the formation of a double-threaded [3]rotaxane, as illustrated in Scheme 1.9.[159]

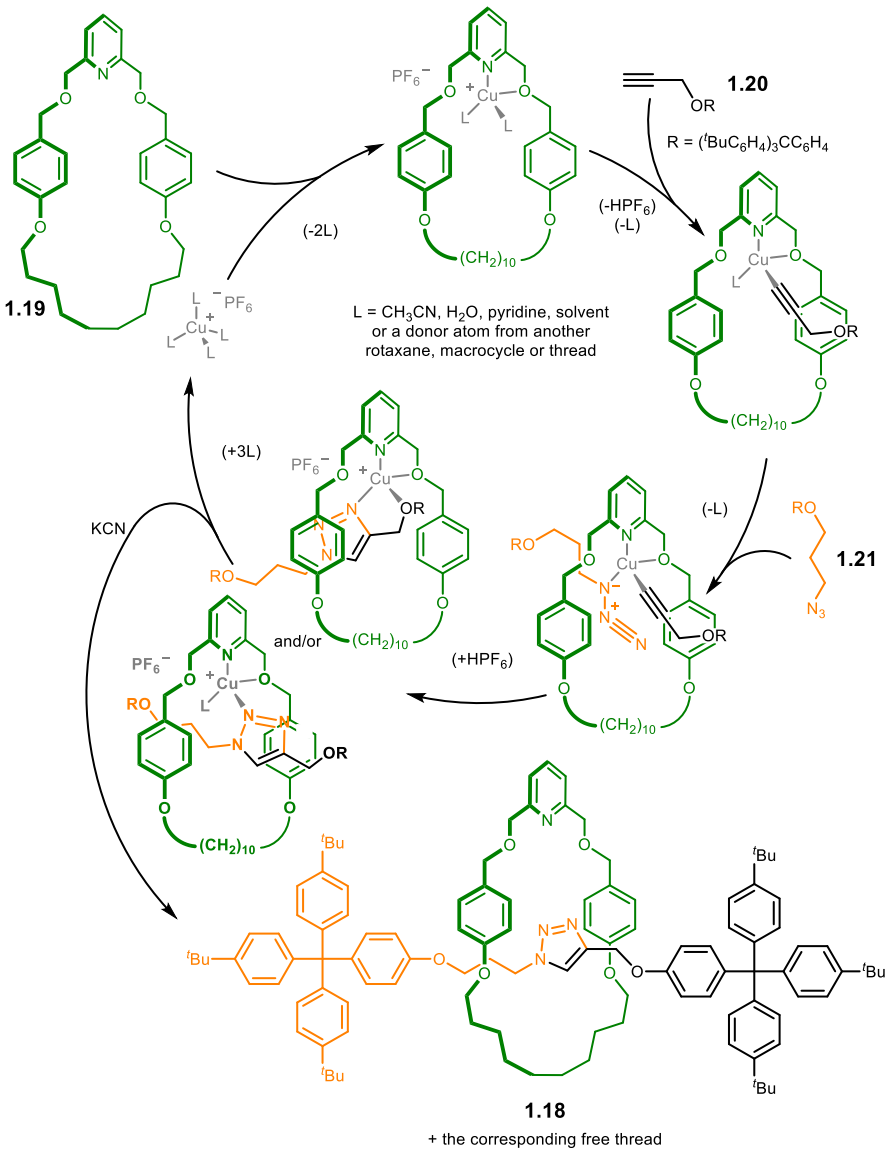

Scheme 1.8: Proposed catalytic cycle for the Cu(I) active metal template synthesis of [2]rotaxane **1.18** from a pyridine-based macrocycle **1.19**, a terminal alkyne **1.20**, and an azide **1.21**.[158] R = tris(4-*tert*-butylphenyl)methyl.

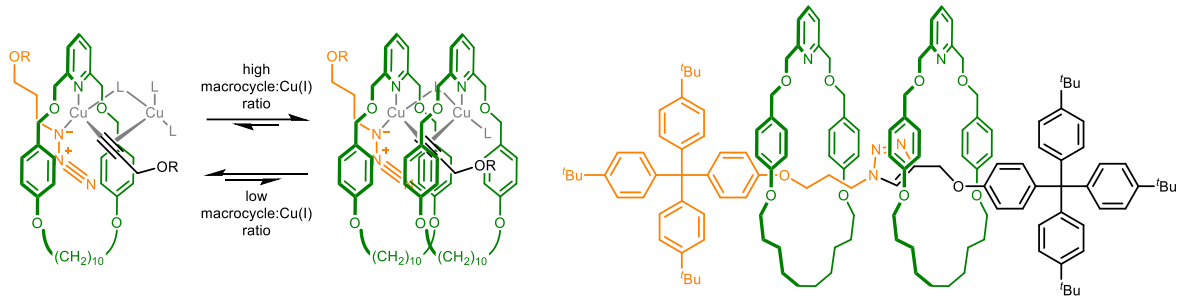

Scheme 1.9: The proposed mechanism of formation of [3]rotaxane from a bimetallic intermediate in the active-metal template CuAAC reaction.[159]

Only eight months later, Saito *et al.* reported the second example using an AMT approach – an alkyne coupling.[160] The authors successfully synthesised [2]rotaxane **1.22** (Scheme 1.10) via an AMT copper-catalysed Glaser homocoupling through the cavity of a

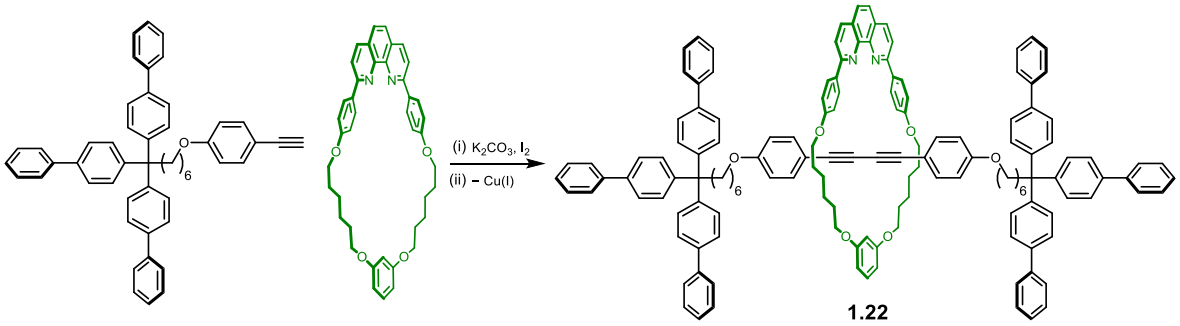

Scheme 1.10: Synthesis of [2]rotaxane **1.22** via an active-metal template Glaser coupling reported by Saito *et al.*[160]

phenanthroline-based macrocycle. In phenanthroline coordinating the Cu(I) ion, the catalytic site resides inside the cavity of the macrocycle. The binding of two alkynes to the two vacant sites of Cu(I) is orthogonal to the plane of the macrocycle such that, when the two are extruded via a reductive elimination process, they are linked through the cavity of the macrocycle. In using only a small excess of acetylene-bearing substrate, the desired [2]rotaxane **1.22** could be synthesised in 72% yield.

As mentioned briefly, one advantage to an AMT approach is that it is likely other transition metals can be utilised to generate interlocked compounds. Analogously to the Saito system, in 2007 Leigh *et al.* developed an AMT synthesis in which catalytic quantities of Pd(II) were used to template and catalyse the homocoupling of alkynes under relatively mild conditions.[161] Due to a preference of Pd(II) cations for square planar geometries, a monodentate, pyridine-based macrocycle was used to ensure the geometry was set up such that the [2]rotaxane (compound **1.23**, Scheme 1.11) was the prevailing product. Using 5-10 mol% of Pd(II) and iodine, to oxidise Pd(0) back to Pd(II), the [2]rotaxane could be afforded in 90% yield – higher than when using stoichiometric quantities of Pd(II) (43-61%). The mechanism proposed by the authors suggest that first a transmetallation step occurs between a copper acetylide species and the macrocycle-Pd(II) complex. From there *trans-cis* isomerisation takes

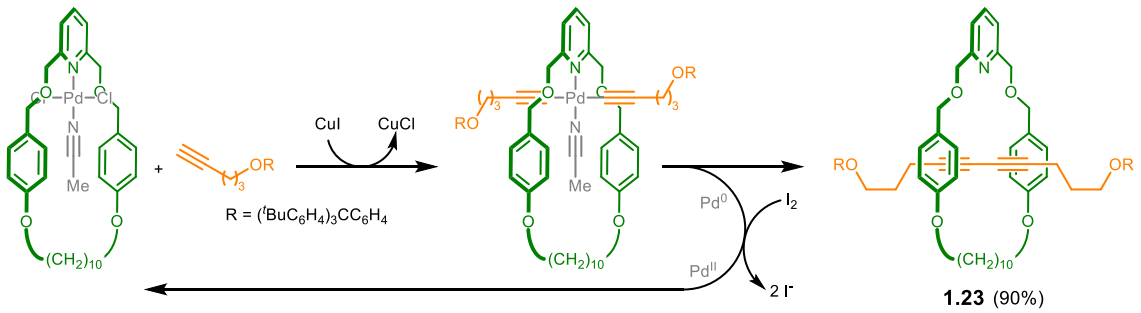

Scheme 1.11: Pd(II)-catalysed active-metal template Glaser homocoupling developed by Leigh *et al.* The addition of I_2 allows regeneration of the Pd catalyst.[161]

place (the acetylenes remain attached to the Pd(II) centre at all times), before undergoing reductive elimination to form the key C-C bond and generate the rotaxane. The Pd(0) is then recycled back to Pd(II) using an excess of I_2 present in the reaction mixture.

In 2012, a collaboration between our group and the Tykwinski group used an AMT approach, similar to that developed by Saito *et al.*, in which we reported the first synthesis of polyyne [2]rotaxanes of up to 10 acetylenes in length (**1.24**, Figure 1.14).[104] Simultaneous work by Gladysz *et al.* employed a similar approach to prepare Pt-capped polyyne [2]rotaxane **1.25** containing four acetylenes in *ca.* 9% yield.[63]

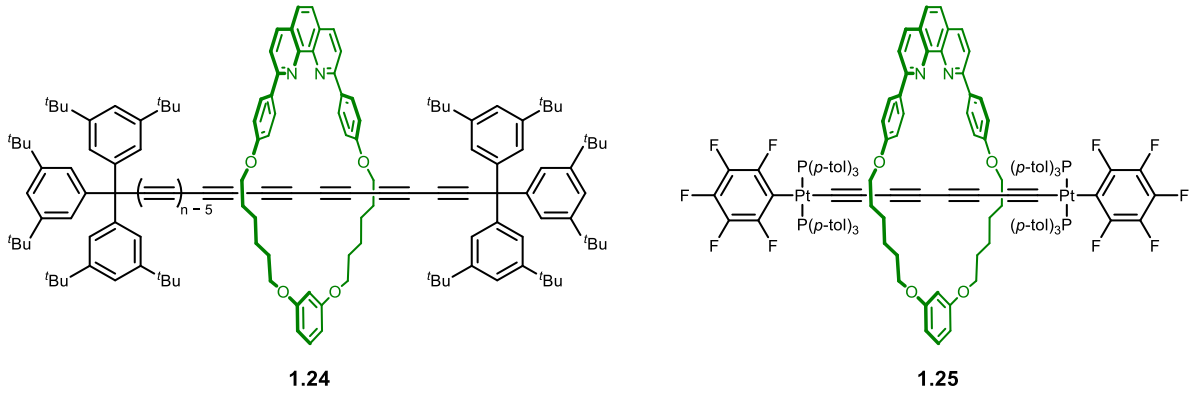

1.24 **1.25**

Figure 1.14: The first two polyyne [2]rotaxanes reported: a decayne **1.24** and a platinum-capped tetrayne **1.25** reported by Anderson *et al.*[104] and Gladysz *et al.*,[63] respectively.

A second collaborative project between the Anderson and Tykwinski groups in 2015 prepared a [9]cumulene [2]rotaxane **1.26** (Scheme 1.12) and presented the first evidence that supramolecular encapsulation provides a method of stabilising highly-reactive *sp*-carbon chains, and other reactive π-systems.[162] Due to the higher reactivity of [*n*]cumulenes compared to [*n*]polyynes, the use of sterically bulky end groups reaches a practical limit much quicker than polyynes,[163] with the [9]cumulene (9 *sp*-carbons) being the longest cumulene, reported

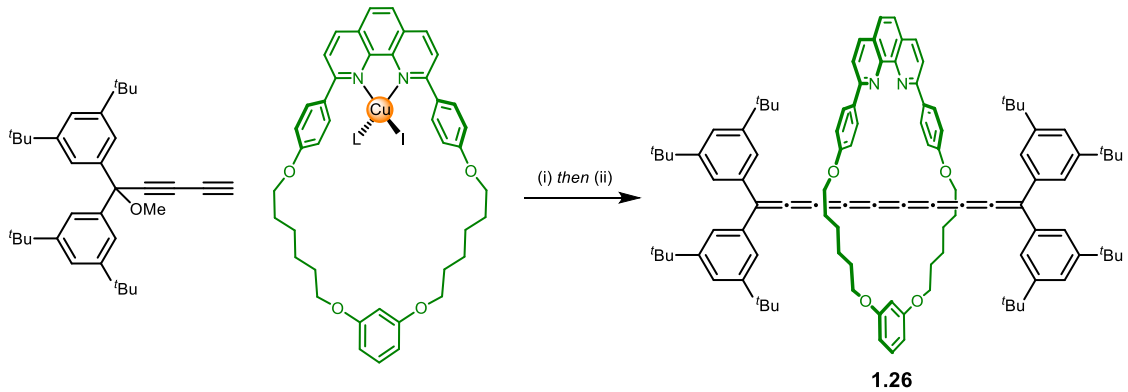

1.26

Scheme 1.12: Preparation of [9]cumulene rotaxane **1.26**.[162] (i) K_2CO_3, I_2, THF, 60 °C (67%); (ii) $SnCl_2$ (anhydrous), HCl (1 M in Et_2O), Et_2O, Ar, 25 °C (33%).

only 5 times to date.[164–167] By employing supramolecular encapsulation strategies, and the kinetic stabilisation benefits it offers, it is expected that [*n*]cumulenes with $n > 9$ could be synthesised and stabilised by this approach. This would give an interesting contrast to polyynes as the two approach the carbyne limit.

A study into the effects of polyyne length and macrocycle cavity size upon the yield and stability of polyyne rotaxanes was conducted by our group and the Tykwinski group in 2016.[62] A series of polyynes, up to 12 acetylene units in length, were threaded through a variety of macrocycles (**1.27a**-**d**, Figure 1.15) and the stability examined by differential scanning calorimetry (DSC). For longer polyynes ($n = 8$, 9 and 12 acetylene units), DSC revealed that the rotaxanes decomposed at higher temperatures when compared to the corresponding unthreaded axles, and that the stability enhancement improves as the polyyne becomes longer. The highest yields were obtained for systems using macrocycles of intermediate size, as well as when a Cadiot-Chodkiewicz cross coupling was used over a homocoupling reaction. This study also reported [3]rotaxane **1.28** (Figure 1.16), formed from two polyynes threaded through a single macrocycle. The steric bulk of the supertrityl end groups, coupled with the steric constraints imposed on the system by the macrocycle, meant that the polyyne chains could not adopt the required geometry to undergo any degradation processes. This finding effectively highlights the ability for supramolecular encapsulation to provide mechanical insulation of polyynes.

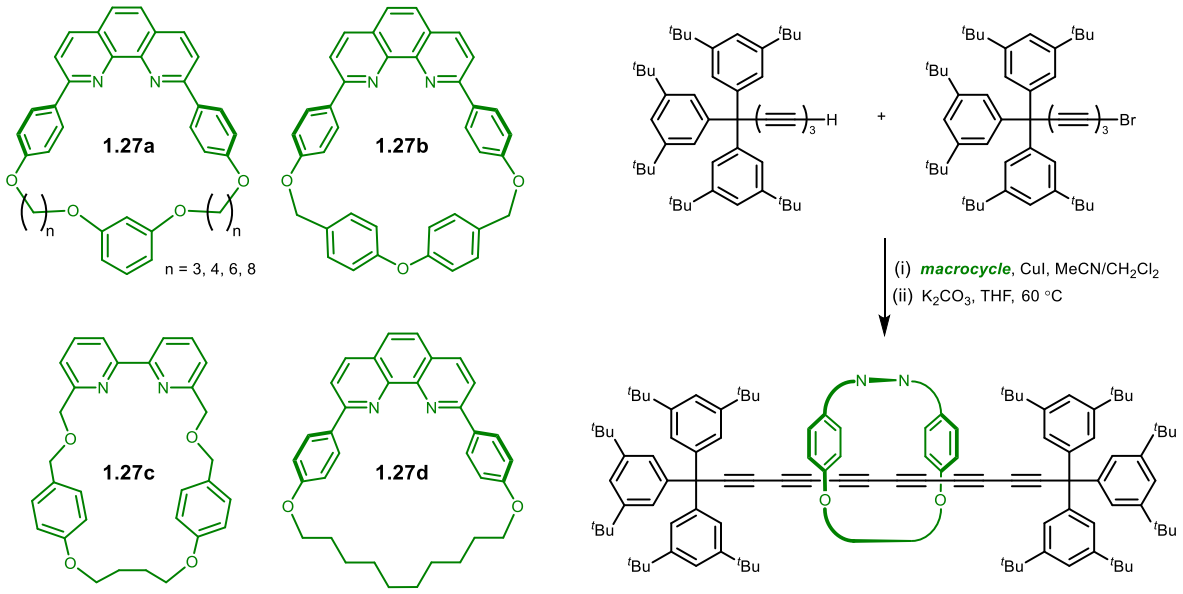

Figure 1.15: The various macrocycles used by Anderson *et al.* in the preparation of a polyyne [2]rotaxane.[62]

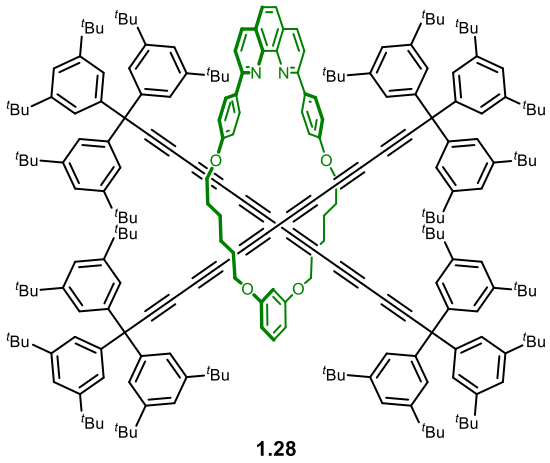

1.28

Figure 1.16: Steric requirements imposed on the system by the macrocycle in this [3]rotaxane enforces the diagonal arrangement of polyyne axles and prevents their crosslinking.[62]

Polyynes have a rich chemistry with an attractive potential for eagerly anticipated applications in topics such as organic field effect transistors,[168] solar cells,[169] and nanomechanical systems,[170] all of which remain essentially unexplored. While some efforts have been focussing on stabilising polyynes with bulky stoppering groups, it is becoming clear that this approach is reaching its limit and alternatives should be sought after if we want to isolate chains many times longer than currently possible. Based on recent research, there is a clear and marked benefit in stability to be had when threading fragile *sp*-carbon threads through the cavities of macrocycles. It is therefore hoped that π-systems, such as cyclocarbons, could be stabilised by supramolecular encapsulation to give catenanes. It is also conceivable that the threading multiple macrocycles along a long polyyne could be used as a method of stabilising polymers of *sp*-carbon atoms, thereby providing a method of stabilising models for carbyne. Both of these aspects will be discussed in later chapters.

1.6 Appendix

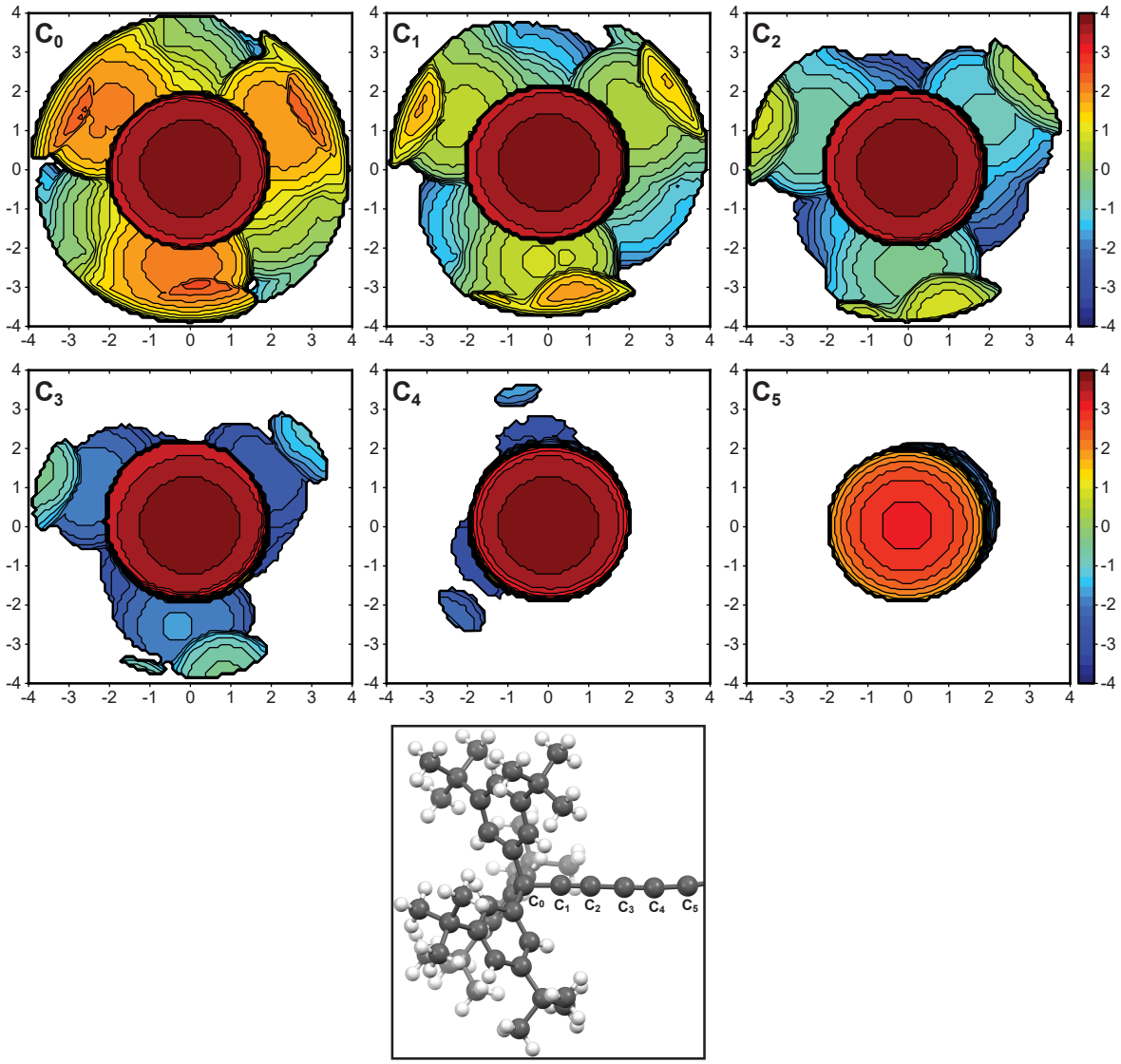

Figure S1.1: Steric maps of supertrityl-capped oligoynes **Tr*[*n*]** calculated using Samb*V*ca (version 2.1)[57] using a solid state geometry obtained from the CCDC (identifier GAGYUK).[6]

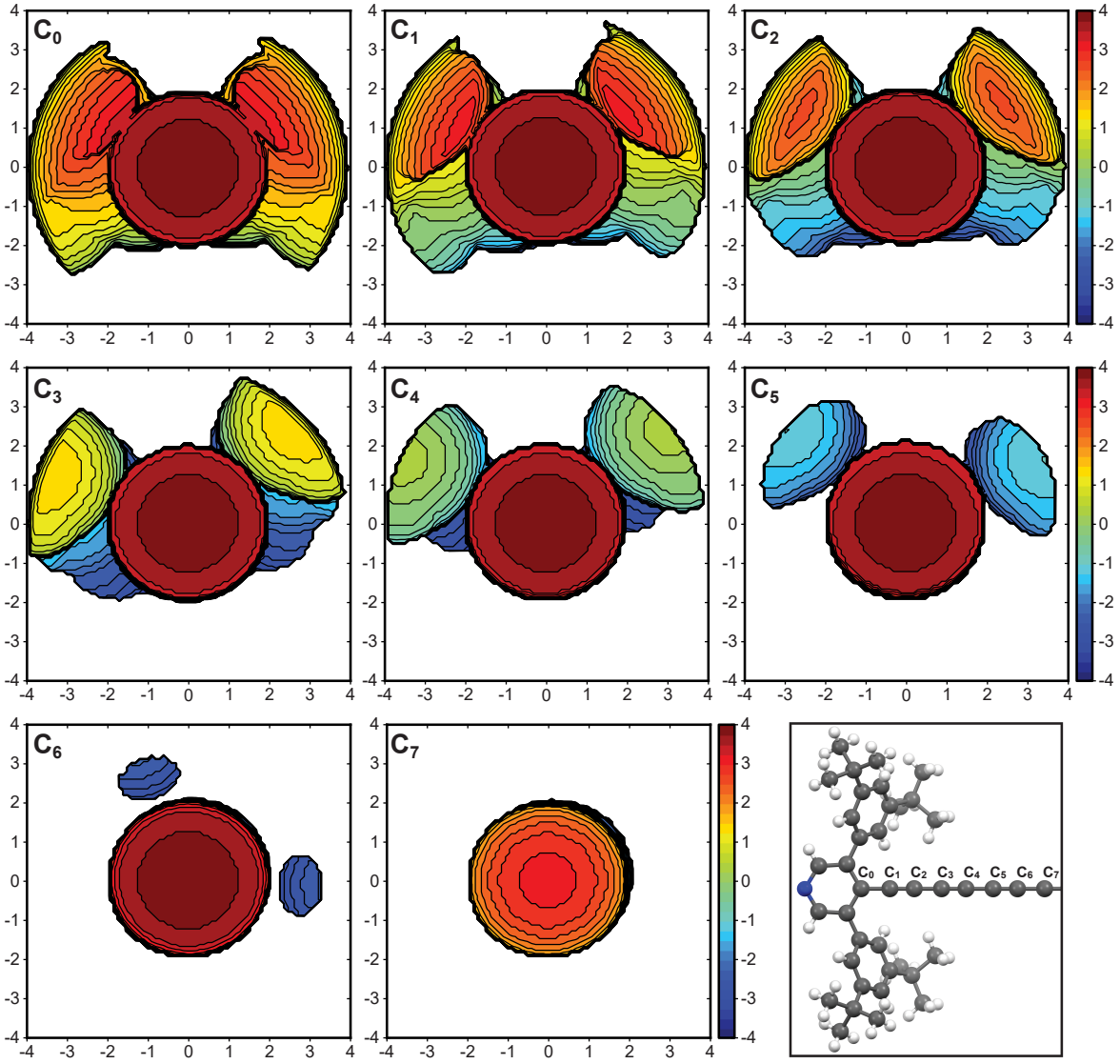

Figure S1.2: Steric maps of pyridyl-capped oligoynes **Py*[*n*]** calculated using Samb*V*ca (version 2.1)[57] using a solid state geometry obtained from the CCDC (identifier MAKNAR).[55]

1.7 References

1 D. R. Lide, Ed., *CRC Handbook of Chemistry and Physics*, CRC Press/Taylor and Francis, Boca Raton, FL, 89th edn., 2009.

2 A. Hirsch, *Nat. Mater.*, 2010, **9**, 868–871.

3 F. Diederich and Y. Rubin, *Angew. Chem. Int. Ed.*, 1992, **31**, 1101–1123.

4 C. Ross, K. Scherlach, F. Kloss and C. Hertweck, *Angew. Chem. Int. Ed.*, 2014, **53**, 7794–7798.

5 P. Manini, W. Amrein, V. Gramlich and F. Diederich, *Angew. Chem. Int. Ed.*, 2002, **41**, 4339–4343.

6 W. A. Chalifoux and R. R. Tykwinski, *Nat. Chem.*, 2010, **2**, 967–971.

7 R. F. Curl and R. E. Smalley, *Science*, 1988, **242**, 1017–1022.

8 Q. Fan, L. Yan, M. W. Tripp, O. Krejčí, S. Dimosthenous, S. R. Kachel, M. Chen, A. S. Foster, U. Koert, P. Liljeroth and J. M. Gottfried, *Science*, 2021, **372**, 852–856.

9 H. W. Kroto, J. R. Heath, S. C. O'Brien, R. F. Curl, R. E. Smalley, S. C. O'Brien, R. F. Curl and R. E. Smalley, *Nature*, 1985, **318**, 162–163.

10 F. Diederich, *Nature*, 1994, **369**, 199–207.

11 W. Krätschmer, L. D. Lamb, K. Fostiropoulos and D. R. Huffman, *Nature*, 1990, **347**, 354–358.

12 S. Iijima and T. Ichihashi, *Nature*, 1993, **363**, 603–605.

13 K. S. Novoselov, A. K. Geim, S. V. Morozov, D. Jiang, Y. Zhang, S. V. Dubonos, I. V. Grigorieva and A. A. Firsov, *Science*, 2004, **306**, 666–669.

14 K. Kaiser, L. M. Scriven, F. Schulz, P. Gawel, L. Gross and H. L. Anderson, *Science*, 2019, **365**, 1299–1301.

15 L. M. Scriven, K. Kaiser, F. Schulz, A. J. Sterling, S. L. Woltering, P. Gawel, K. E. Christensen, H. L. Anderson and L. Gross, *J. Am. Chem. Soc.*, 2020, **142**, 12921–12924.

16 G. Dennler, M. C. Scharber and C. J. Brabec, *Adv. Mater.*, 2009, **21**, 1323–1338.

17 C. Yan, S. Barlow, Z. Wang, H. Yan, A. K. Y. Jen, S. R. Marder and X. Zhan, *Nat. Rev. Mater.*, 2018, **3**, 18003.

18 S. H. Friedman, D. L. DeCamp, R. P. Sijbesma, G. Srdanov, F. Wudl and G. L. Kenyon, *J. Am. Chem. Soc.*, 1993, **115**, 6506–6509.

19 G.-F. Liu, M. Filipović, I. Ivanović-Burmazović, F. Beuerle, P. Witte and A. Hirsch, *Angew. Chem. Int. Ed.*, 2008, **47**, 3991–3994.

20 S. Campidelli, T. Brandmüller, A. Hirsch, I. M. Saez, J. W. Goodby and R. Deschenaux, *Chem. Commun.*, 2006, 4282–4284.

21 K. Holczer, O. Klein, S.-M. Huang, R. B. Kaner, K.-J. Fu, R. L. Whetten and F. Diederich, *Science*, 1991, **252**, 1154–1157.

22 P.-M. Allemand, K. C. Khemani, A. Koch, F. Wudl, K. Holczer, S. Donovan, G. Gruner and J. D. Thompson, *Science*, 1991, **253**, 301–302.

23 H. Omachi, T. Nakayama, E. Takahashi, Y. Segawa and K. Itami, *Nat. Chem.*, 2013, **5**, 572–576.

24 T. J. Sisto, L. N. Zakharov, B. M. White and R. Jasti, *Chem. Sci.*, 2016, **7**, 3681–3688.

25 A. Hirsch, *Angew. Chem. Int. Ed.*, 2002, **41**, 1853.

26 S. Bae, H. Kim, Y. Lee, X. Xu, J.-S. Park, Y. Zheng, J. Balakrishnan, T. Lei, H. Ri Kim, Y. Il Song, Y.-J. Kim, K. S. Kim, B. Özyilmaz, J.-H. Ahn, B. H. Hong and S. Iijima, *Nat. Nanotechnol.*, 2010, **5**, 574–578.

27 B. S. Shim, W. Chen, C. Doty, C. Xu and N. A. Kotov, *Nano Lett.*, 2008, **8**, 4151–4157.

28 R. Hayatsu, R. G. Scott, M. H. Studier, R. S. Lewis and E. Anders, *Science*, 1980, **209**, 1515–1518.

29 P. P. K. Smith and P. R. Buseck, *Science*, 1982, **216**, 984–986.

30 F. Diederich, Y. Rubin, O. L. Chapman and N. S. Goroff, *Helv. Chim. Acta*, 1994, **77**, 1441–1457.

31 Y. Tobe, R. Umeda, N. Iwasa and M. Sonoda, *Chem. Eur. J.*, 2003, **9**, 5549–5559.

32 L. Itzhaki, E. Altus, H. Basch and S. Hoz, *Angew. Chem. Int. Ed.*, 2005, **44**, 7432–7435.

33 R. H. Baughman, *Science*, 2006, **312**, 1009–1110.

34 B. Akdim and R. Pachter, *ACS Nano*, 2011, **5**, 1769–1774.

35 N. D. Lang and P. Avouris, *Phys. Rev. Lett.*, 2000, **84**, 358–361.

36 N. D. Lang and P. Avouris, *Phys. Rev. Lett.*, 1998, **81**, 3515–3518.

37 S. Tongay, R. T. Senger, S. Dag and S. Ciraci, *Phys. Rev. Lett.*, 2004, **93**, 136404.

38 R. R. Tykwinski, W. Chalifoux, S. Eisler, A. Lucotti, M. Tommasini, D. Fazzi, M. Del Zoppo and G. Zerbi, *Pure Appl. Chem.*, 2010, **82**, 891–904.

39 E. R. H. Jones, M. C. Whiting, J. B. Armitage, C. L. Cook and N. Entwistle, *Nature*, 1951, **168**, 900–903.

40 F. Bohlmann, *Angew. Chem.*, 1953, **65**, 385–389.

41 T. R. Johnson and D. R. M. Walton, *Tetrahedron*, 1972, **28**, 5221–5236.

42 R. Eastmond and D. R. M. Walton, *Tetrahedron*, 1972, **28**, 4591–4599.

43 J. B. Armitage, N. Entwistle, E. R. H. Jones and M. C. Whiting, *J. Chem. Soc.*, 1954, **147**, 147.

44 T. R. Hoye, B. Baire, D. Niu, P. H. Willoughby and B. P. Woods, *Nature*, 2012, **490**, 208–212.

45 G. Schermann, T. Grösser, F. Hampel and A. Hirsch, *Chem. Eur. J.*, 1997, **3**, 1105–1112.

46 Q. Zheng, J. C. Bohling, T. B. Peters, A. C. Frisch, F. Hampel and J. A. Gladysz, *Chem.*

Eur. J., 2006, **12**, 6486–6505.

47 T. N. Hoheisel and H. Frauenrath, *Org. Lett.*, 2008, **10**, 4525–4528.

48 S. Eisler, A. D. Slepkov, E. Elliott, T. Luu, R. McDonald, F. A. Hegmann and R. R. Tykwinski, *J. Am. Chem. Soc.*, 2005, **127**, 2666–2676.

49 A. Chuvilin, E. Bichoutskaia, M. C. Gimenez-Lopez, T. W. Chamberlain, G. A. Rance, N. Kuganathan, J. Biskupek, U. Kaiser and A. N. Khlobystov, *Nat. Mater.*, 2011, **10**, 687–692.

50 D. Nishide, H. Dohi, T. Wakabayashi, E. Nishibori, S. Aoyagi, M. Ishida, S. Kikuchi, R. Kitaura, T. Sugai, M. Sakata and H. Shinohara, *Chem. Phys. Lett.*, 2006, **428**, 356–360.

51 X. Zhao, Y. Ando, Y. Liu, M. Jinno and T. Suzuki, *Phys. Rev. Lett.*, 2003, **90**, 187401.

52 L. Shi, P. Rohringer, K. Suenaga, Y. Niimi, J. Kotakoski, J. C. Meyer, H. Peterlik, M. Wanko, S. Cahangirov, A. Rubio, Z. J. Lapin, L. Novotny, P. Ayala and T. Pichler, *Nat. Mater.*, 2016, **15**, 634–639.

53 T. J. Taylor and F. P. Gabbaï, *Organometallics*, 2006, **25**, 2143–2147.

54 J. Stahl, J. C. Bohling, E. B. Bauer, T. B. Peters, W. Mohr, J. M. Martín-Alvarez, F. Hampel and J. A. Gladysz, *Angew. Chem. Int. Ed.*, 2002, **41**, 1871.

55 Y. Gao, Y. Hou, F. Gordillo Gámez, M. J. Ferguson, J. Casado and R. R. Tykwinski, *Nat. Chem.*, 2020, **12**, 1143–1149.

56 A. Gómez-Suárez, D. J. Nelson and S. P. Nolan, *Chem. Commun.*, 2017, **53**, 2650–2660.

57 L. Falivene, Z. Cao, A. Petta, L. Serra, A. Poater, R. Oliva, V. Scarano and L. Cavallo, *Nat. Chem.*, 2019, **11**, 872–879.

58 A. Poater, B. Cosenza, A. Correa, S. Giudice, F. Ragone, V. Scarano and L. Cavallo, *Eur. J. Inorg. Chem.*, 2009, **2009**, 1759–1766.

59 W. A. Chalifoux, R. McDonald, M. J. Ferguson and R. R. Tykwinski, *Angew. Chem. Int. Ed.*, 2009, **48**, 7915–7919.

60 J. Zirzlmeier, S. Schrettl, J. C. Brauer, E. Contal, L. Vannay, É. Brémond, E. Jahnke, D. M. Guldi, C. Corminboeuf, R. R. Tykwinski and H. Frauenrath, *Nat. Commun.*, 2020, **11**, 4797.

61 T. Gibtner, F. Hampel, J.-P. Gisselbrecht and A. Hirsch, *Chem. Eur. J.*, 2002, **8**, 408–432.

62 L. D. Movsisyan, M. Franz, F. Hampel, A. L. Thompson, R. R. Tykwinski and H. L. Anderson, *J. Am. Chem. Soc.*, 2016, **138**, 1366–1376.

63 N. Weisbach, Z. Baranová, S. Gauthier, J. H. Reibenspies and J. A. Gladysz, *Chem. Commun.*, 2012, **48**, 7562.

64 S. Schrettl, E. Contal, T. N. Hoheisel, M. Fritzsche, S. Balog, R. Szilluweit and H. Frauenrath, *Chem. Sci.*, 2015, **6**, 564–574.

65 A. Spantulescu, T. Luu, Y. Zhao, R. McDonald and R. R. Tykwinski, *Org. Lett.*, 2008, **10**, 609–612.

66 W. Mohr, J. Stahl, F. Hampel and J. A. Gladysz, *Chem. Eur. J.*, 2003, **9**, 3324–3340.

67 T. Wakabayashi, Y. Wada, N. Iwahara and T. Sato, *J. Phys. Conf. Ser.*, 2013, **428**, 012004.

68 R. Gleiter and D. B. Werz, *Chem. Rev.*, 2010, **110**, 4447–4488.

69 E. Kloster-Jensen, H.-J. Haink and H. Christen, *Helv. Chim. Acta*, 1974, **57**, 1731–1744.

70 L. D. Movsisyan, M. D. Peeks, G. M. Greetham, M. Towrie, A. L. Thompson, A. W. Parker and H. L. Anderson, *J. Am. Chem. Soc.*, 2014, **136**, 17996–18008.

71 M. Renz, M. Kess, M. Diedenhofen, A. Klamt and M. Kaupp, *J. Chem. Theory Comput.*, 2012, **8**, 4189–4203.

72 D. Jacquemin, E. A. Perpète, G. E. Scuseria, I. Ciofini and C. Adamo, *J. Chem. Theory Comput.*, 2008, **4**, 123–135.

73 M. Dierksen and S. Grimme, *J. Chem. Phys.*, 2004, **120**, 3544–3554.

74 R. Hoffmann, *Tetrahedron*, 1966, **22**, 521–538.

75 J. Bernholc and J. C. Phillips, *J. Chem. Phys.*, 1986, **85**, 3258–3267.

76 C. Zhang, Z. Cao, H. Wu and Q. Zhang, *Int. J. Quantum Chem.*, 2004, **98**, 299–308.

77 J. M.L. Martin, J. El-Yazal and J.-P. François, *Chem. Phys. Lett.*, 1995, **242**, 570–579.

78 M. Weimer, W. Hieringer, F. Della Sala and A. Görling, *Chem. Phys.*, 2005, **309**, 77–87.

79 U. Mölder, P. Burk and I. A. Koppel, *J. Mol. Struct. THEOCHEM*, 2004, **712**, 81–89.

80 F. Diederich, Y. Rubin, C. B. Knobler, R. L. Whetten, K. E. Schriver, K. N. Houk and Y. Li, *Science*, 1989, **245**, 1088–1090.

81 E. J. Bylaska, J. H. Weare and R. Kawai, *Phys. Rev. B*, 1998, **58**, R7488–R7491.

82 M. Saito and Y. Okamoto, *Phys. Rev. B*, 1999, **60**, 8939–8942.

83 T. Torelli and L. Mitas, *Phys. Rev. Lett.*, 2000, **85**, 1702–1705.

84 M. Kertesz, J. Koller and A. Aman, *J. Chem. Phys.*, 1978, **68**, 2779.

85 N. A. Popov and E. M. Shustorovich, *J. Struct. Chem.*, 1966, **6**, 566–569.

86 S. Tongay, S. Dag, E. Durgun, R. T. Senger and S. Ciraci, *J. Phys. Condens. Matter*, 2005, **17**, 3823–3836.

87 T. D. Poulsen, K. V. Mikkelsen, J. G. Fripiat, D. Jacquemin and B. Champagne, *J. Chem. Phys.*, 2001, **114**, 5917–5922.

88 S. R. Marder, L.-T. Cheng, B. G. Tiemann, A. C. Friedli, M. Blanchard-Desce, J. W. Perry and J. Skindhoj, *Science*, 1994, **263**, 511–514.

89 E. J. Bylaska, R. Kawai and J. H. Weare, *J. Chem. Phys.*, 2000, **113**, 6096–6106.

90 D. Wendinger and R. R. Tykwinski, *Acc. Chem. Res.*, 2017, **50**, 1468–1479.

91 G. V. Baryshnikov, R. R. Valiev, A. V. Kuklin, D. Sundholm and H. Ågren, *J. Phys. Chem. Lett.*, 2019, **10**, 6701–6705.

92 D. A. Plattner and K. N. Houk, *J. Am. Chem. Soc.*, 1995, **117**, 4405–4406.

93 A. E. Boguslavskiy, H. Ding and J. P. Maier, *J. Chem. Phys.*, 2005, **123**, 034305.

94 P. W. Fowler, N. Mizoguchi, D. E. Bean and R. W. A. Havenith, *Chem. Eur. J.*, 2009, **15**, 6964–6972.

95 K. Remya and C. H. Suresh, *RSC Adv.*, 2016, **6**, 44261–44271.

96 V. Parasuk, J. Almlof and M. W. Feyereisen, *J. Am. Chem. Soc.*, 1991, **113**, 1049–1050.

97 M. Feyereisen, M. Gutowski, J. Simons and J. Almlöf, *J. Chem. Phys.*, 1992, **96**, 2926–2932.

98 S. Yang and M. Kertesz, *J. Phys. Chem. A*, 2006, **110**, 9771–9774.

99 Y. Rubin, C. B. Knobler and F. Diederich, *J. Am. Chem. Soc.*, 1990, **112**, 4966–4968.

100 Y. Tobe, H. Matsumoto, K. Naemura, Y. Achiba and T. Wakabayashi, *Angew. Chem. Int. Ed.*, 1996, **35**, 1800–1802.

101 Y. Tobe, T. Fujii, H. Matsumoto, K. Naemura, Y. Achiba and T. Wakabayashi, *J. Am. Chem. Soc.*, 1996, **118**, 2758–2759.

102 Y. Tobe, T. Fujii and K. Naemura, *J. Org. Chem.*, 1994, **59**, 1236–1237.

103 G. A. Adamson and C. W. Rees, *J. Chem. Soc. Perkin Trans. 1*, 1996, **2**, 1535–1543.

104 L. D. Movsisyan, D. V. Kondratuk, M. Franz, A. L. Thompson, R. R. Tykwinski and H. L. Anderson, *Org. Lett.*, 2012, **14**, 3424–3426.

105 Y. Rubin and F. Diederich, *J. Am. Chem. Soc.*, 1989, **111**, 6870–6871.

106 P. Siemsen, R. C. Livingston and F. Diederich, *Angew. Chem. Int. Ed.*, 2000, **39**, 2632–2657.

107 M. D. Weller and L. R. Cox, *Compt. Rend. Chim.*, 2009, **12**, 366–377.

108 A. Orita and J. Otera, *Chem. Rev.*, 2006, **106**, 5387–5412.

109 P. Bäuerle, M. Ammann, M. Wilde, G. Götz, E. Mena-Osteritz, A. Rang and C. A. Schalley, *Angew. Chem. Int. Ed.*, 2007, **46**, 363–368.

110 C. Glaser, *Ber. Dtsch. Chem. Ges.*, 1869, **2**, 422–424.

111 G. Eglinton and R. Galbraith, A., *Chem. Ind. (London)*, 1956, 737.

112 G. Eglinton and A. R. Galbraith, *J. Chem. Soc.*, 1959, 889.

113 A. S. Hay, *J. Org. Chem.*, 1962, **27**, 3320–3321.

114 J. A. Marsden, J. J. Miller and M. M. Haley, *Angew. Chem. Int. Ed.*, 2004, **43**, 1694–1697.

115 A. Lei, M. Srivastava and X. Zhang, *J. Org. Chem.*, 2002, **67**, 1969–1971.

116 P. Cadiot and W. Chodkiewicz, *Comptes rendus l'Académie des Sci.*, 1955, **241**, 1055–1057.

117 J. Berná, S. M. Goldup, A.-L. Lee, D. A. Leigh, M. D. Symes, G. Teobaldi and F. Zerbetto, *Angew. Chem. Int. Ed.*, 2008, **47**, 4392–4396.

118 E. Negishi and L. Anastasia, *Chem. Rev.*, 2003, **103**, 1979–2018.

119 H. M. Barentsen, M. van Dijk, H. Zuilhof and E. J. R. Sudhölter, *Macromolecules*, 2000, **33**, 775–780.

120 J. S. S. Neto, B. A. Iglesias, D. F. Back and G. Zeni, *Adv. Synth. Catal.*, 2016, **358**, 3572–3585.

121 F. Cataldo, L. Ravagnan, E. Cinquanta, I. E. Castelli, N. Manini, G. Onida and P. Milani, *J. Phys. Chem. B*, 2010, **114**, 14834–14841.

122 P. García-Domínguez, R. Alvarez and Á. R. de Lera, *Eur. J. Org. Chem.*, 2012, **2012**, 4762–4782.

123 M. Křováček and D. Dvořák, *J. Heterocycl. Chem.*, 2015, **52**, 40–47.

124 E. Negishi, M. Hata and C. Xu, *Org. Lett.*, 2000, **2**, 3687–3689.

125 J. P. Marino and H. N. Nguyen, *J. Org. Chem.*, 2002, **67**, 6841–6844.

126 Y. Rubin, M. Kahr, C. B. Knobler, F. Diederich and C. L. Wilkins, *J. Am. Chem. Soc.*, 1991, **113**, 495–500.

127 Y. Li, Y. Rubin, F. Diederich and K. N. Houk, *J. Am. Chem. Soc.*, 1990, **112**, 1618–1623.

128 M.-C. Lasne and J.-L. Ripoll, *Synthesis (Stuttg).*, 1985, **1985**, 121–143.

129 M. M. Haley and B. L. Langsdorf, *Chem. Commun.*, 1997, **2**, 1121–1122.

130 Y. Shvo and E. Hazum, *J. Chem. Soc. Chem. Commun.*, 1974, 336.

131 J. Lewis, B. Lin, M. S. Khan, M. R. A. Al-Mandhary and P. R. Raithby, *J. Organomet. Chem.*, 1994, **484**, 161–167.

132 S. W. McElvany, M. M. Ross, N. S. Goroff and F. Diederich, *Science*, 1993, **259**, 1594–1596.

133 J. Hunter, J. Fye and M. F. Jarrold, *Science*, 1993, **260**, 784–786.

134 N. S. Goroff, *Acc. Chem. Res.*, 1996, **29**, 77–83.

135 T. M. Chang, A. Naim, S. N. Ahmed, G. Goodloe and P. B. Shevlin, *J. Am. Chem. Soc.*, 1992, **114**, 7603–7604.

136 J. Huuskonen, J. E. H. Buston, N. D. Scotchmer and H. L. Anderson, *New J. Chem.*, 1999, **23**, 1245–1252.

137 I. Ben Shir, S. Sasmal, T. Mejuch, M. K. Sinha, M. Kapon and E. Keinan, *J. Org. Chem.*, 2008, **73**, 8772–8779.

138 J. F. Stoddart, *Chem. Soc. Rev.*, 2009, **38**, 1802–1820.

139 L. Fang, M. A. Olson, D. Benítez, E. Tkatchouk, W. A. Goddard III and J. F. Stoddart, *Chem. Soc. Rev.*, 2010, **39**, 17–29.

140 J. E. Beves, B. A. Blight, C. J. Campbell, D. A. Leigh and R. T. McBurney, *Angew. Chem. Int. Ed.*, 2011, **50**, 9260–9327.

141 I. T. Harrison and S. Harrison, *J. Am. Chem. Soc.*, 1967, **89**, 5723–5724.

142 D. A. Leigh, A. Murphy, J. P. Smart and A. M. Z. Slawin, *Angew. Chem. Int. Ed.*, 1997, **36**, 728–732.

143 J. A. Wisner, P. D. Beer, M. G. B. Drew and M. R. Sambrook, *J. Am. Chem. Soc.*, 2002, **124**, 12469–12476.

144 G. T. Spence and P. D. Beer, *Acc. Chem. Res.*, 2013, **46**, 571–586.

145 H. Ogino, *J. Am. Chem. Soc.*, 1981, **103**, 1303–1304.

146 M. Denis and S. M. Goldup, *Nat. Rev. Chem.*, 2017, **1**, 0061.

147 C. O. Dietrich-Buchecker, J.-P. Sauvage and J. M. Kern, *J. Am. Chem. Soc.*, 1984, **106**, 3043–3045.

148 J. D. Crowley, S. M. Goldup, A.-L. Lee, D. A. Leigh and R. T. McBurney, *Chem. Soc. Rev.*, 2009, **38**, 1530.

149 N. Belfrekh, C. Dietrich-Buchecker and J.-P. Sauvage, *Inorg. Chem.*, 2000, **39**, 5169–5172.

150 D. A. Leigh, P. J. Lusby, S. J. Teat, A. J. Wilson and J. K. Y. Wong, *Angew. Chem. Int. Ed.*, 2001, **40**, 1538–1543.

151 A.-M. Fuller, D. A. Leigh, P. J. Lusby, I. D. H. Oswald, S. Parsons and D. B. Walker, *Angew. Chem. Int. Ed.*, 2004, **43**, 3914–3918.

152 A.-M. L. Fuller, D. A. Leigh and P. J. Lusby, *Angew. Chem. Int. Ed.*, 2007, **46**, 5015–5019.

153 S. M. Goldup, D. A. Leigh, P. J. Lusby, R. T. McBurney and A. M. Z. Slawin, *Angew. Chem. Int. Ed.*, 2008, **47**, 6999–7003.

154 N. Solladié, J.-C. Chambron and J.-P. Sauvage, *J. Am. Chem. Soc.*, 1999, **121**, 3684–3692.

155 P. Gaviña and J.-P. Sauvage, *Tetrahedron Lett.*, 1997, **38**, 3521–3524.

156 C. O. Dietrich-Buchecker and J.-P. Sauvage, *Angew. Chem. Int. Ed.*, 1989, **28**, 189–192.

157 D. A. Leigh, R. G. Pritchard and A. J. Stephens, *Nat. Chem.*, 2014, **6**, 978–982.

158 V. Aucagne, K. D. Hänni, D. A. Leigh, P. J. Lusby and D. B. Walker, *J. Am. Chem. Soc.*, 2006, **128**, 2186–2187.

159 V. Aucagne, J. Berná, J. D. Crowley, S. M. Goldup, K. D. Hänni, D. A. Leigh, P. J. Lusby, V. E. Ronaldson, A. M. Z. Slawin, A. Viterisi and D. B. Walker, *J. Am. Chem. Soc.*, 2007, **129**, 11950–11963.

160 S. Saito, E. Takahashi and K. Nakazono, *Org. Lett.*, 2006, **8**, 5133–5136.

161 J. Berná, J. D. Crowley, S. M. Goldup, K. D. Hänni, A.-L. Lee and D. A. Leigh, *Angew. Chem. Int. Ed.*, 2007, **46**, 5709–5713.

162 M. Franz, J. A. Januszewski, D. Wendinger, C. Neiss, L. D. Movsisyan, F. Hampel, H. L. Anderson, A. Görling and R. R. Tykwinski, *Angew. Chem. Int. Ed.*, 2015, **54**, 6645–6649.

163 J. A. Januszewski and R. R. Tykwinski, *Chem. Soc. Rev.*, 2014, **43**, 3184–3203.

164 W. Ried, W. Schlegelmilch and S. Piesch, *Chem. Ber.*, 1963, **96**, 1221–1228.

165 J. A. Januszewski, D. Wendinger, C. D. Methfessel, F. Hampel and R. R. Tykwinski,

Angew. Chem. Int. Ed., 2013, **52**, 1817–1821.

166 F. Bohlmann and K. Kieslich, *Chem. Ber.*, 1954, **87**, 1363–1372.

167 F. Bohlmann and K. Kieslich, *Abh. Braunschw. Wiss. Ges.*, 1957, **9**, 147–166.

168 A. D. Scaccabarozzi, A. Milani, S. Peggiani, S. Pecorario, B. Sun, R. R. Tykwinski, M. Caironi and C. S. Casari, *J. Phys. Chem. Lett.*, 2020, **11**, 1970–1974.

169 B. J. Eckstein, F. S. Melkonyan, N. Zhou, E. F. Manley, J. Smith, A. Timalsina, R. P. H. Chang, L. X. Chen, A. Facchetti and T. J. Marks, *Macromolecules*, 2017, **50**, 1430–1441.

170 Y. Han, J. Zhou, H. Wang, L. Gao, S. Feng, K. Cao, Z. Xu and Y. Lu, *Appl. Nanosci.*, 2021, **11**, 1075–1091.

2

Phenanthroline-Based MAE

Contents

Chapter 2 - Phenanthroline-Based MAE

2.1 Introduction

Since Carl Glaser's seminal work on C_{sp}-C_{sp} coupling reactions in 1869, the number of extended acetylenic systems reported in literature has grown rapidly. While there is no doubt that such reactions have been key in forming acetylene-rich systems, a new problem now presents itself: the stability of these compounds, which falls off significantly with an increasing number of constituent C≡C triple bonds. While there have been many previous attempts towards the synthesis of linear acetylenes and cyclocarbons,[1–6] the instability of these acetylene-rich systems has prevented isolating these species in solution. This tendency to undergo degradation further complicates the synthesis of linear acetylenes, and there is now a stronger requirement than ever to find approaches for improving their stability.

Chapter 1 highlighted multiple strategies to overcome these alkyne stability issues. Rotaxanes with polyyne axles have been previously prepared and have demonstrated enhanced stability of the thread versus the non-interlocked dumbbell.[7–13] Taking this further, temporary alkyne masking groups can be used to aid preparation of longer polyynes. As discussed in Chapter 1, Section 1.4.2, many masked alkyne equivalents (MAEs) have been developed, particularly for the synthesis of cyclo[*n*]carbons, that can be transformed into alkynes by activation with light,[3–5,14–17] heat,[1,2,18–20] or chemical reagents.[2,6,21–25] Photolabile MAEs are an interesting target as they generally show good stability during a range of chemical transformations. With regard to their use in preparing polyyne rotaxanes, there are four factors worth considering: (i) the MAE must be chemically stable under the conditions of rotaxane formation; (ii) it should be sufficiently bulky to act as a temporary stopper and prevent dethreading of the rotaxane; (iii) successful and clean unmasking of the MAE must be possible when part of mechanically-interlocked systems and; (iv) the MAE should be easy to synthesise.

Recently, our group has shown that a cyclobutene-fused phenanthrene system **2.1a** (Scheme 2.1) can act as an effective alkyne masking group, protecting long polyynes during synthesis, and then can be removed without trace upon irradiation of UV light.[10] The synthesis of these cyclobutene-fused phenanthrene systems proceeds first via a [2+2] photochemical cycloaddition between phenanthrene and trichloroethylene. Ultra-violet irradiation (350 nm)

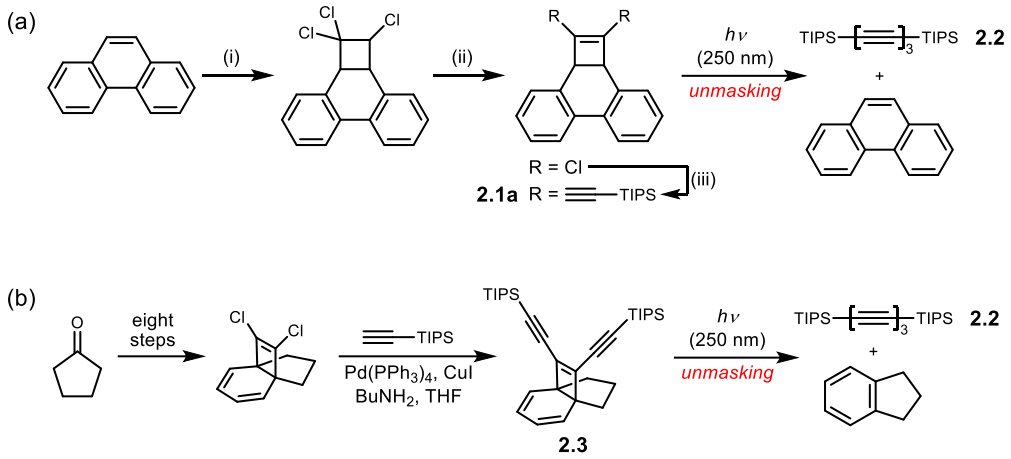

Scheme 2.1: Photochemical masking of (a) a cyclobutene-fused phenanthrene **2.1a**, and its subsequent unmasking. (i) trichloroethylene, *hv* (350 nm); (ii) NaOH, EtOH, *reflux*; (iii) TIPS-acetylene, $Pd(PPh_3)_4$, CuI, *n*-$BuNH_2$, THF; (b) an indane-masked triyne **2.3**. Note the phenanthrene masking group requires six fewer steps to reach masked triyne **2.1a** (compared to **2.3**).

of the mixture over 3-4 days readily affords the trichloro-phenanthrene, which eliminates HCl after treatment with NaOH to give the dichlorocyclobutene. A Sonogashira cross-coupling was employed to install TIPS-acetylene groups in place of the chlorides to give a 'masked' bis-TIPS triyne **2.1a**. This masked compound then went on to be used as a simple model system in subsequent unmasking studies. A key benefit brought by this particular MAE was the significantly shorter synthesis compared to those previously reported; it only takes three steps to reach a masked triyne such as **2.1a**, whereas the indane masking groups developed by Tobe *et al*. required 9 steps to reach the same point (**2.3**, Scheme 2.1b).

Studies were then made to evaluate the unmasking of phenanthrene-masked triyne **2.1a**. Irradiation of this compound in $CDCl_3$ with UV light (250 nm) for 21 hours led to the liberation of phenanthrene in 80% yield, determined by ^{1}H NMR. The generation of bis-TIPS triyne **2.2** was also confirmed by ^{1}H NMR, albeit in an unexpectedly low 20% yield, together with a complex mixture of other products. Reference experiments established that triyne **2.2** was stable to UV irradiation at 250 nm, meaning that any side reactions or decomposition of the triyne under the unmasking conditions could be ruled out. Repeating the unmasking using UV light of longer wavelength (350 nm) provided further insight into the unmasking process. Under these conditions, no phenanthrene was detected, but instead a [2+2] dimer – [3]-ladderane **2.1b**, (formed by two molecules of **2.1a**) – was generated quantitatively, as identified by ^{1}H NMR then confirmed by its X-ray crystal structure. Irradiation of **2.1b** with higher energy UV light (250 nm) then triggered a [2+2] photochemically-induced cycloreversion to liberate one

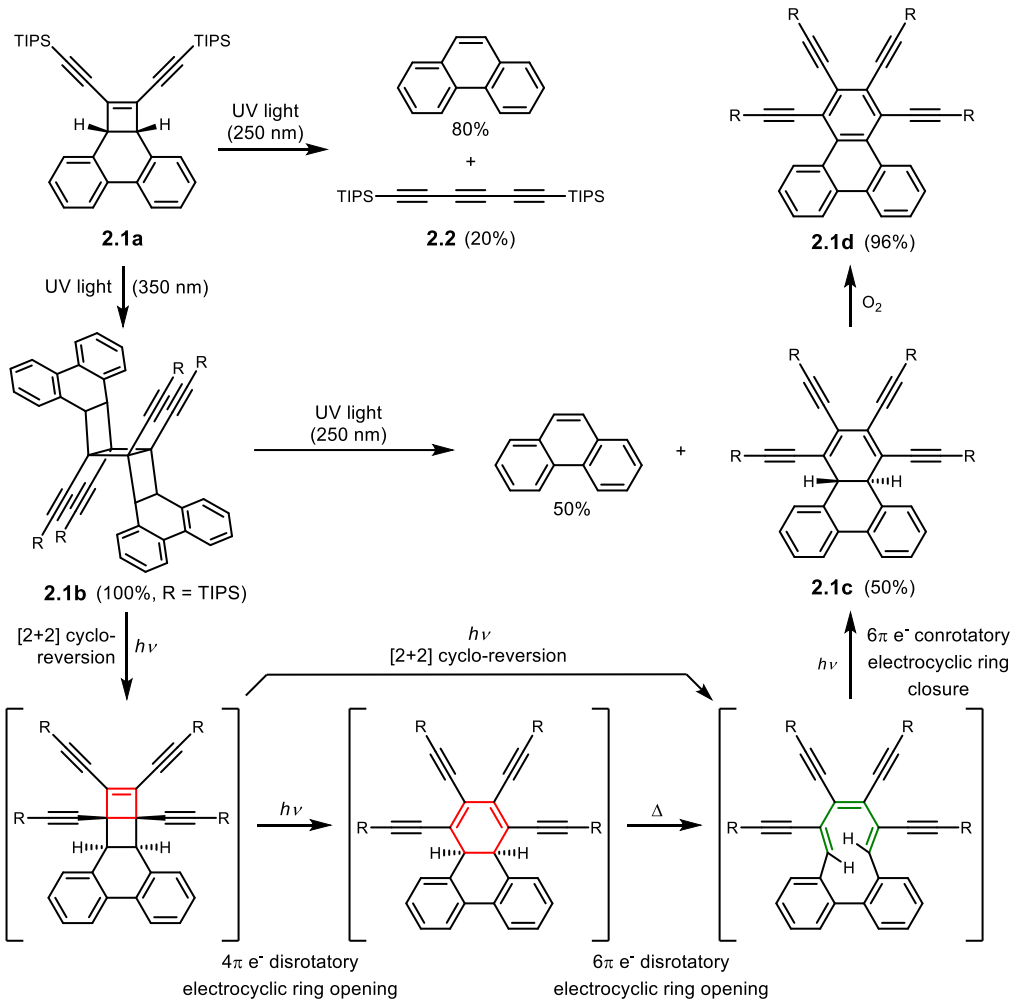

Scheme 2.2: Reactivity of phenanthrene MAE **2.1a**. The various products and their respective distributions are shown following irradiation of **2.1a** with UV light at 250 nm or 350 nm, as well as irradiation of dimer **2.1b** at 250 nm. A possible mechanism for the formation of dihydrotriphenylene is also shown (R = TIPS).

unit of phenanthrene and returned dihydrotriphenylene **2.1c**, which slowly oxidised in air to give triphenylene **2.1d**. This compound was also formed as a minor product (~10%) from the direct irradiation of **2.1a** with light of 250 nm wavelength. To summarise: only when phenanthroline **2.1a** was irradiated with high energy light (250 nm) directly, was the unmasking process observed as expected and; when irradiating **2.1a** at 350 nm, the dimer is formed exclusively, which then prevents the possibility for successful unmasking, even after subsequent irradiation at 250 nm.

A [2]rotaxane employing this phenanthrene MAE was later prepared from asymmetric phenanthrene **2.4** in an active metal template alkyne homocoupling reaction (Scheme 2.3). Bulky tris(4-*tert*-butylphenyl)methyl (*p*-^{t}Bu) alkyne-capping groups were added to prevent the macrocycle from later slipping off the dumbbell after formation.[26] The synthesis of a phenanthrene [2]rotaxane **2.5** was achieved using a copper-mediated oxidative homocoupling

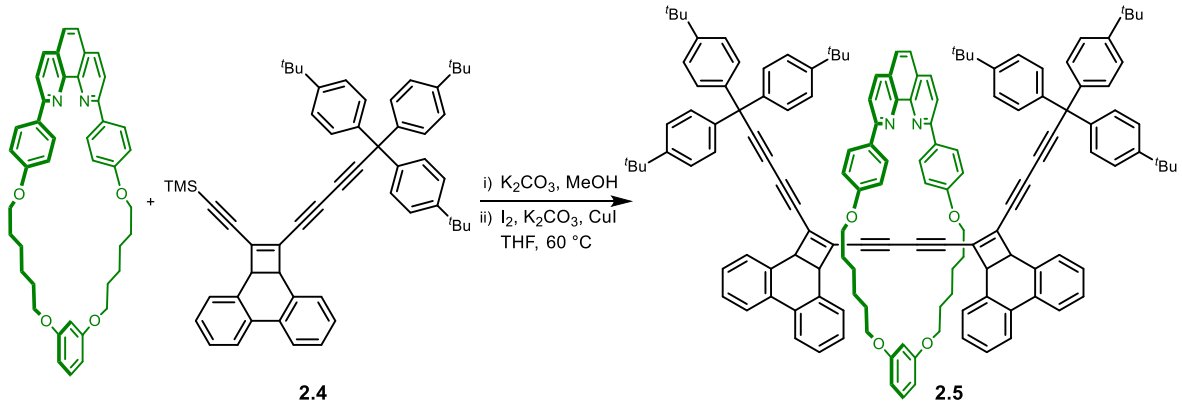

Scheme 2.3: Synthesis of a phenanthrene-masked octayne [2]rotaxane **2.5** via an active metal template oxidative alkyne homocoupling reaction.

in 56% yield. Subsequent unmasking experiments for this rotaxane were noted to proceed significantly less efficiently than for the model compound. While **2.1a** can be unmasked in a range of solvents ($CDCl_3$, THF-d_8, benzene-d_6), the only suitable solvent that did not lead to degradation of the rotaxanes was cyclohexane-d_{12}. The rotaxanes successfully expelled both phenanthrene masking groups, albeit markedly slower than for indane masking groups in an analogous [2]rotaxane, under the same unmasking conditions. Similar to that observed in the model system, longer wavelengths led to undesirable side reactions and prevented successful unmasking. Nevertheless, octayne [2]rotaxane **2.5** could be successfully prepared in 34% yield from the masked [2]rotaxane, clearly demonstrating the unmaking ability of the phenanthrene-based masking group.

The aim of the work in this chapter is to further extend this chemistry by developing a novel alkyne masking group, related to this phenanthrene system, but with intrinsic metal-binding abilities. We expect that this MAE would have a similar ability to stabilise polyynes during their synthesis as those previously reported, and also be able to participate in passive metal template approaches to forming mechanically interlocked molecules. The benefits of metal template approaches have been discussed extensively in Section 1.5.1 of Chapter 1. As an example application for such an MAE, one could envisage macrocycle-MAE complexes when a suitable metal ion is present, to form an air-stable pre-catenane or pre-rotaxane complex (Figure 2.1). Such a complex should generate the required molecular crossover points to aid formation of interlocked compounds – both rotaxanes and catenanes depending on whether a stoppering or cyclisation reaction is used. An unmasking step at late stages of the synthesis could then be utilised to return the acetylene chain.

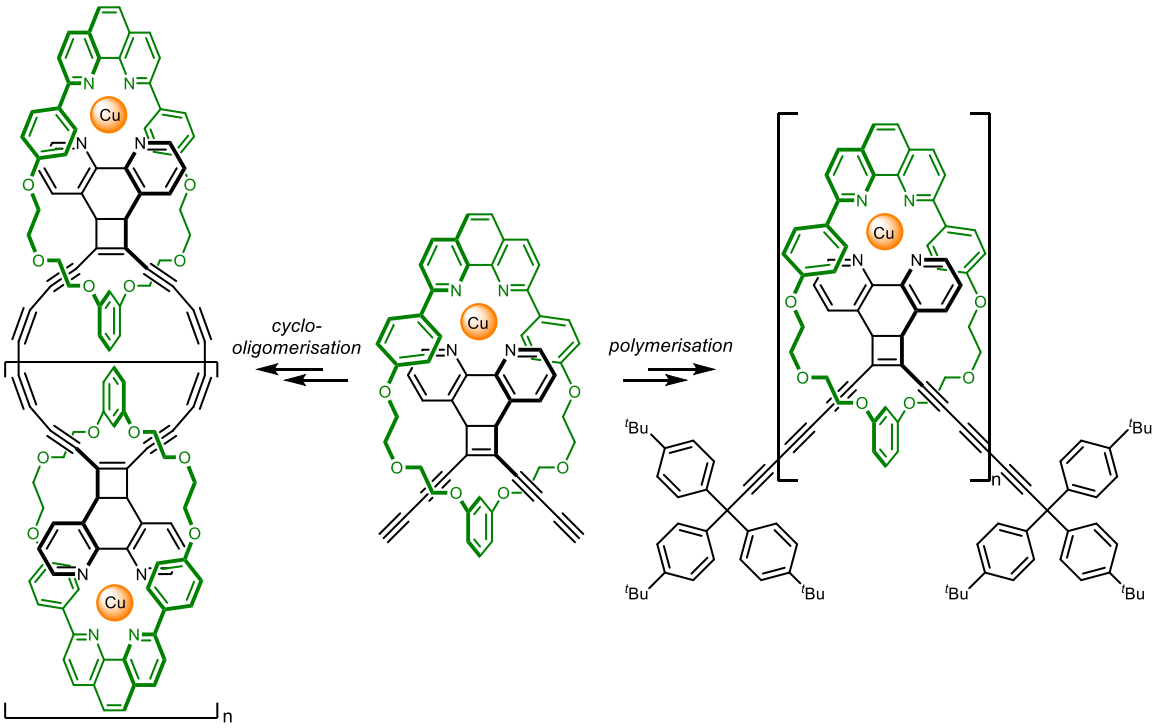

Figure 2.1: Both catenanes and rotaxanes can be prepared using a pre-formed MAE-macrocycle complex.

2.2 MAE Development

An overarching goal of this thesis is to employ metal templates in building carbon-rich interlocked molecules. Metal templates have a well-established history in improving yields of mechanically interlocked compounds by holding the precursors in well-defined geometries, before a subsequent reaction can be used to capture the interlocked products.[27–35] This idea can be taken further where the metal not only pre-organises the components, but also plays an additional bond-forming role.[36] Use of such 'active' metal templates is becoming more popular as an elegant, single-step approach to preparing interlocked molecules. One problem with active template approaches, however, is that their success can be extremely capricious and challenging to predict. Sometimes only seemingly small changes to reagents or macrocycles involved in the coupling can completely prevent the formation of interlocked products with no apparent explanation.[10]

In this project, we aim to explore a passive metal template (PMT) approach. Both MAE and macrocyclic components will bear intrinsic metal-binding motifs that will allow for their preorganisation by coordination to a suitable metal ion. A separate bond-forming reaction, either with other units of the same complex (to generate cyclic species), or separate stoppering units (to generate linear species) can then be employed to lock the threaded components

together. Inspired by the success of the phenanthrene masking group discussed earlier, we decided to explore a related system based on 1,10-phenanthroline (Figure 2.1). We expected that preparation of the MAE component would proceed akin to the phenanthrene system, requiring only a few steps before the unmasking ability of the MAE could be evaluated first on a model system, then being used to prepare rotaxanes and catenanes.

2.2.1 Synthesis of a Model MAE System

Starting from 1,10-phenanthroline, initial attempts were made to prepare the trichloro cyclobutane-fused phenanthroline **2.6** (Scheme 2.4). In a similar vein to the phenanthrene system, subjecting a solution of 1,10-phenanthroline in neat trichloroethylene to UV irradiation at 350 nm was successful in affording the [2+2] cycloaddition product.[10,37] The reaction proceeds somewhat slower than for the phenanthrene system. To address this, optimisations were made to the reaction setup. As may be expected for light-promoted reactions, the rate of reaction was found to vary significantly with the diameter of the reaction tube in the photoreactor. Initial experiments were made in standard test tubes (15 mm, borosilicate glass), but upon switching to much narrower (5 mm) NMR tubes, significantly improved reaction rates were observed – albeit still slower than for the phenanthrene system. With this new setup, trichlorophenanthroline **2.6** can be generated in 63% yield after 7 days of irradiation (determined by ^{1}H NMR) on a ~2 g scale. Attempting to push the yield higher with further irradiation was found to be detrimental, presumably due to competing light-induced degradation processes. Unlike with the analogous phenanthrene, the strong stacking affinity exhibited by these molecules (suggested by highly concentration-dependent ^{1}H NMR phenanthroline resonances) led to challenging purification by standard normal phase silica techniques. Fortunately, using reverse phase chromatography (C_{18}, H_2O/MeOH eluent system) was found to successfully separate both isomers of **2.6** (*syn* and *anti*, in an approximate 3:17 ratio) from any decomposition products and unreacted starting material.

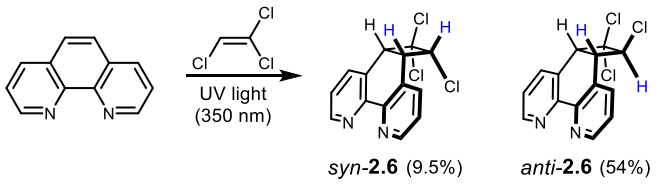

Scheme 2.4: [2+2] Photoinduced cycloaddition of 1,10-phenanthroline with trichloroethylene to prepare trichlorophenanthroline **2.6**. Both *syn* and *anti* isomers are formed in an approximate 3:17 ratio, respectively.

The base-promoted elimination of HCl to give dichloro cyclobutene-fused phenanthroline **2.7** was then investigated (Scheme 2.5). To our surprise, and in stark contrast to the analogous elimination on trichlorophenanthrene, simply treating trichloro **2.6** with NaOH (in EtOH at reflux) did not return the expected compound. Instead, it appears that complete substitution of the chlorine atoms had instead occurred to give the dihydroxy cyclobutene phenanthroline (see box, Scheme 2.5). Reducing the temperature of the reaction to 40 °C significantly slowed the reaction of **2.6**, but still resulted in substitution of the chlorine atoms by hydroxide. To overcome this, a host of different base and solvent combinations were trialled, the most notable of which are summarised in Table 2.1.

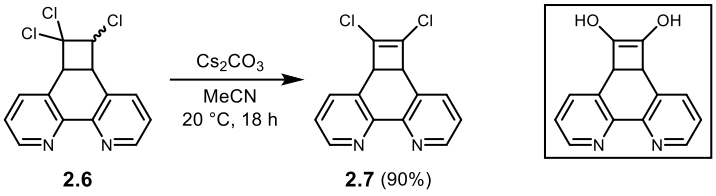

2.6 **2.7** (90%)

Scheme 2.5: Preparation of dichloro cyclobutene-fused phenanthroline **2.7** from the base-promoted elimination of **2.6**. Using established conditions for the analogous phenanthrene (NaOH/EtOH),[10] complete substitution of the chloride groups was observed, see box.

Table 2.1: Attempted conditions for the elimination of HCl from trichlorophenanthroline **2.6**, indicating the observed outcome.

Entry	Base	Conditions	Outcome
1	NaOH	EtOH, 80 °C, 3 h	Elimination successful, but complete Cl substitution by OH
2	^{t}BuOK	EtOH, 60 °C, 3 h	Elimination successful, some desired product obtained, some Cl substitution by OEt
3	^{t}BuOK	^{t}BuOH, 60 °C, 3 h	Starting material recovered
4	^{t}BuOK	THF, 60 °C, 3 h	Decomposition observed
5	^{t}BuOK	THF, 0 °C, 1 h	Unidentified product obtained
6	DBU	CH_2Cl_2, 20 °C, 2 d	Some desired product obtained, reaction did not reach completion and some decomposition evident
7	Cs_2CO_3	MeCN, 20 °C, 18 h	Desired product obtained, reaction slow but complete overnight

We had hoped that the lower nucleophilicity and high bulk of ^{t}BuOK would prove beneficial to this elimination yet, unfortunately, while some desired product could be observed

by ESI-MS after treating phenanthroline **2.6** with ^{t}BuOK in EtOH (entry **2**), we also noticed chloride substitution by ethoxide. ^{t}BuOK in ^{t}BuOH (entry **3**) was found ineffective at promoting elimination, and the trichloro species was fully recovered. Switching to an aprotic solvent (THF) resulted in complete and rapid decomposition of the phenanthroline species at 60 °C (entry **4**), while at reduced temperatures (0 °C) a single, unidentified by-product was formed (entry **5**). High resolution ESI-MS analysis presented an isotope pattern indicative of a compound with no chlorine atoms present. As it was looking likely that this was not the expected elimination product, no further efforts were made to establish its identity.

A non-nucleophilic organic base, 1,8-diazabicyclo[5.4.0]undec-7-ene (DBU), was then investigated for this elimination (entry **5**). Initial observations were promising, with ESI-MS showing a signal for the expected product, but despite leaving the reaction for 2 days it never reached completion and decomposition gradually became more apparent. Fortunately, it was found that treating **2.6** with Cs_2CO_3 in dry MeCN (entry **7**) appeared more promising. Stirring a room temperature mixture of base and trichlorophenanthroline for 18 hours returned the expected dichloro elimination product **2.7** in ~85% yield, without any evidence of decomposition or chloride substitution.

With reliable routes developed to both trichloro- and dichlorophenanthrolines **2.6** and **2.7**, respectively, efforts turned to the Sonogashira coupling with TIPS-acetylene used to prepare a masked triyne reference compound (**2.8**, Scheme 2.6). Following in the same theme of the previous steps, this coupling proved more difficult than expected. Treating dichloro **2.7** to conditions that showed prior success with the phenanthrene system (CuI, $Pd(PPh_3)_4$, *n*-$BuNH_2$, THF)[10] gave no indication of successful coupling, and only starting material could be recovered. It is known that Sonogashira couplings are heavily influenced by the reactivity of sp^2 halide coupling partner, with vinyl iodides and bromides both showing higher reactivity than vinyl chlorides.[38] Even so, it is still surprising that simply changing from a phenanthrene to

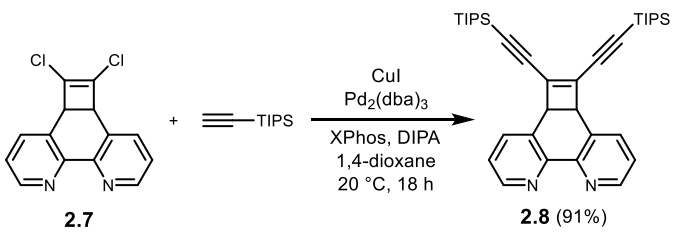

2.7 **2.8** (91%)

Scheme 2.6: Sonogashira coupling between dichlorophenanthroline **2.7** and TIPS-acetylene.

phenanthroline core was sufficient to completely shut down the coupling reaction. A number of alternative conditions were screened, varying the Pd source, Pd ligand, base, solvent and temperature, and are summarised in Table 2.2.

Table 2.2: Summary of selected conditions for the Sonogashira coupling of dichloride **2.7** with TIPS-acetylene. All entries used catalyst and CuI loadings of 5 mol% and 15 mol%, respectively.

Entry	Pd Source	Pd Ligand	Conditions	Yield
1[10]	$Pd(PPh_3)_4$	-	*n*-$BuNH_2$, THF, 50 °C	0%
2[14]	$Pd(PPh_3)_4$	-	Et_3N, THF, 50 °C	0%
3[39]	$Pd(PPh_3)_4$	-	DIPA, THF, 50 °C	0%
4[40]	$Pd(PPh_3)_4$	-	piperidine, 60 °C	~5%
5[41]	$Pd(PPh_3)_2Cl_2$	-	toluene/DIPA 1:2, 50 °C	0%
6[42]	Na_2PdCl_4	[^{t}Bu$_3$PH][BF_4]	Na_2CO_3, THF, 50 °C	0%
7[43]	$Pd(dppf)Cl_2$	PPh_3 (10 mol%)	$ZnBr_2$, DIPEA/DMF, 70 °C	0%
8[44]	$Pd_2(dba)_3$	[^{t}Bu$_3$PH][BF_4]	DIPA, dioxane, 80 °C	0%
9[45]	$Pd_2(dba)_3$	SPhos	DIPA, dioxane, 80 °C	0%
10	$Pd_2(dba)_3$	XPhos	DIPA, dioxane, 80 °C	91%

Despite the many variations of coupling conditions trialled, virtually all formed none, or just trace amounts, of the desired product. Use of an active $Pd(PPh_3)_4$ palladium source (entries **1**-**4**), or activating palladium ligands (SPhos, entry **9**, Figure 2.2 left) proved ineffective in the preparation of **2.8**. After rigorous optimisation, successful coupling was eventually achieved after switching to $Pd_2(dba)_3$ (5 mol%) with an activating phosphine ligand (XPhos, 15 mol%, Figure 2.2 right) for the catalyst system, and using DIPA and dioxane as the respective base and solvent. This reaction appears to be scalable and has been successful in preparing the TIPS-protected model compound **2.8** in isolated yields of up to 91%. Due to a significant shift in polarity between the dichloro and TIPS-protected compounds, purification becomes significantly more facile; routine (normal phase) silica gel chromatography proved effective for these compounds and avoided the requirement for costly and time-consuming reverse phase chromatography.

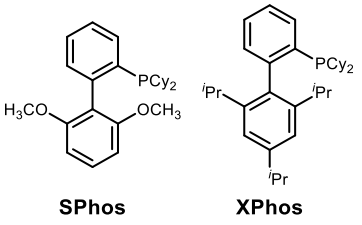

Figure 2.2: Structures of (*left*) SPhos and (*right*) XPhos ligands.

2.2.2 Evaluating MAE Performance

With the TIPS-protected phenanthroline **2.8** in hand, investigations were then made into the unmasking ability of this model compound. Phenanthroline **2.8** was subject to the same unmasking procedures optimised on the previously reported phenanthrene **2.1a**, since this would allow the unmasking ability between the two to be directly compared. Based on detailed studies on the phenanthrene system, it appears crucial that oxygen is absent during unmasking process, so as to prevent undesired side-reactions from dominating.[10] A sample of phenanthroline **2.8** was dissolved in $CDCl_3$, then thoroughly degassed (via four freeze-pump-thaw cycles then backflushing with Ar) before irradiation. Phenanthroline **2.8** was irradiated with UV light (250 nm) in 10-minute intervals and the conversion followed by ^1H NMR.

A ^1H NMR stack plot of over the course of 1 hour of irradiation is presented in Figure 2.3. After only 10 minutes it is evident that a new species is being formed, although rather curiously, none of the new resonances appeared to correspond with any of those expected for the either of the expected products – 1,10-phenanthroline or bis-TIPS triyne **2.2**. More rigorous analysis the reaction after a 20 hour irradiation period appeared to suggest that, rather than

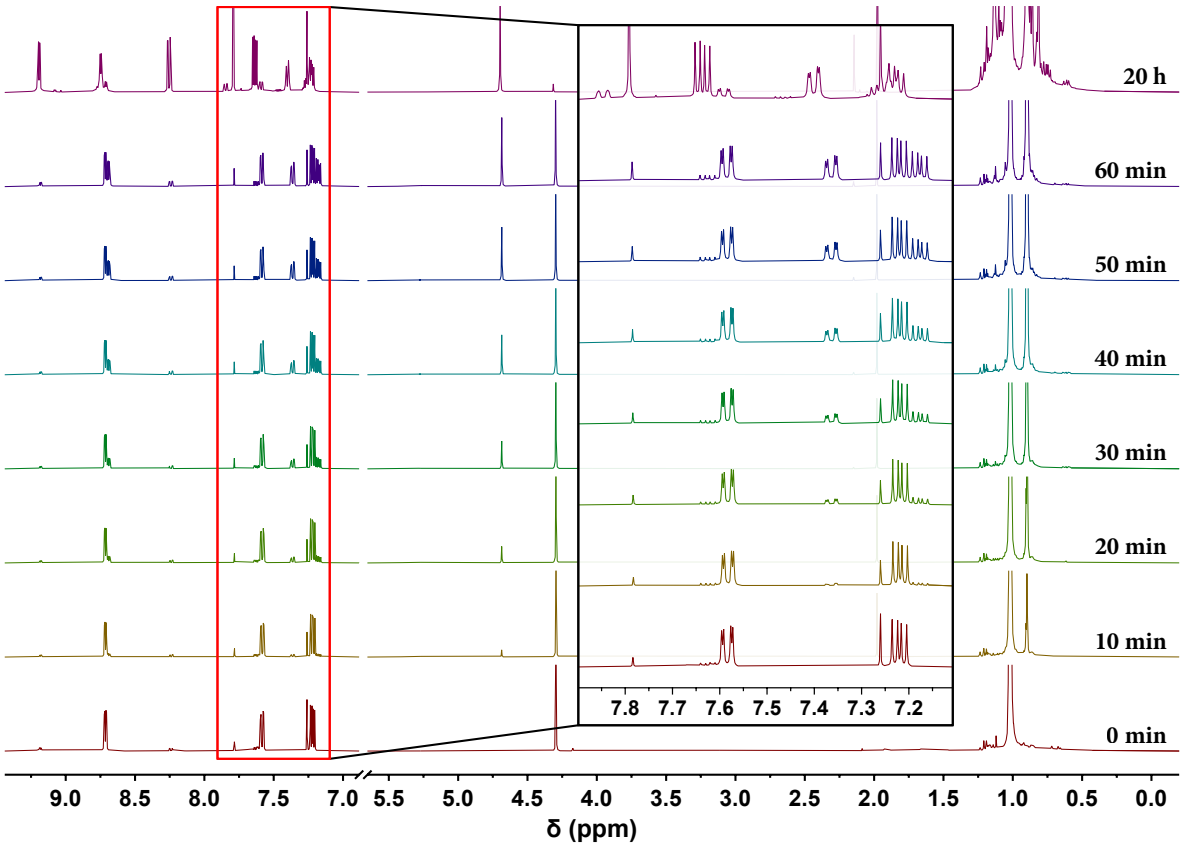

Figure 2.3: Progress of the unmasking of phenanthroline **2.8** was followed by ^1H NMR after 10-minute intervals of UV irradiation at 250 nm ($CDCl_3$, 400 MHz, 298 K).

undergoing the expected [2+2] cycloreversion, a dimer is instead formed in a [2+2] cycloaddition between two molecules of **2.8**. ESI-MS analysis of this mixture corroborated this theory, displaying a strong signal at m/z = 1133.6, corresponding to the $[M+H]^+$ ion for dimer **2.9** (Scheme 2.7). Subjecting this sample to further irradiation at 250 nm resulted in the formation two additional species; one identified as 1,10-phenanthroline and a second species **2.10** containing both a phenanthroline core and TIPS protecting groups.

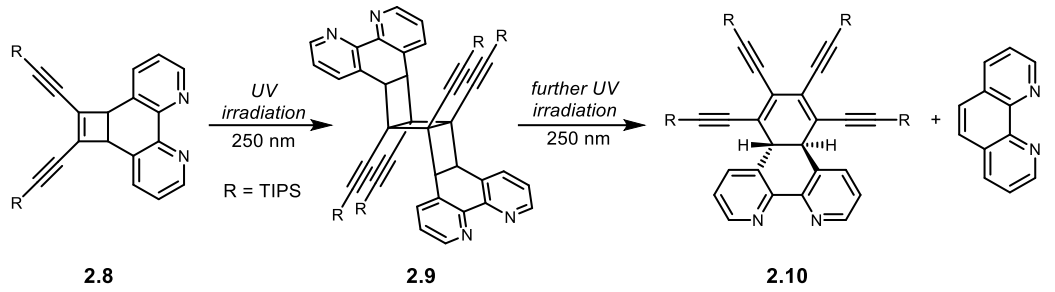

Scheme 2.7: Suspected reaction pathway during irradiation of **2.8** at 250 nm. Stereochemistry of **2.10** is presumed from studies on the analogous phenanthrene system.[10]

Curiously, the ^{1}H NMR integration ratio between the phenanthroline core and TIPS groups do not match with what would be expected for the desired product. Based on this NMR evidence, and further supported by ESI-MS, which displayed a strong signal for the $[M+H]^+$ ion at m/z = 953.6, we believe that the cyclobutane ring in the [3]-ladderane has opened, releasing one molecule of 1,10-phenanthroline in the process. While a similar observation has been made on the phenanthrene system (**2.1c**, Scheme 2.2), in that case the dimer was obtained by irradiation first at 350 nm (not at 250 nm as in this example), before opening of the cyclobutane ring by further irradiation at 250 nm. For the phenanthrene system this issue was mitigated by directly irradiating the TIPS-protected phenanthrene with UV at 250 nm to afford clean and rapid unmasking. In this system, however, irradiation of our sample with higher energy UV (i.e. < 250 nm) is impractical and would have required more specialist equipment before this could be investigated.

2.3 Overcoming Dimerisation

It was quickly becoming apparent that dimerisation of these phenanthroline MAEs could not be easily mitigated without significant and costly modifications to our current photoreactor setup. We instead envisaged an alternative approach to supress dimerisation. In simply forming a mechanically interlocked molecule with the MAE, we hoped that the macrocycle would act to

'shield' the MAE from itself, preventing two units from coming into contact and undergoing the detrimental [2+2] cycloaddition. With the pathway to the [3]-ladderane effectively shut down, we expected that MAE unmasking would now prevail over any other competing processes. We envisaged a simple [2]rotaxane could be formed by stoppering the MAE component through the cavity of a macrocycle and should act as a good model system to evaluate this theory. Multiple approaches exist towards preparing [2]rotaxanes. We initially expected to form the target [2]rotaxane in a 'threading then stoppering' approach (Figure 2.4, left), in which a thread is formed through the cavity of a macrocycle. Alternatively, we also anticipate that an alternative "clipping" approach (Figure 2.4, right), in which a macrocyclic precursor could be cyclised around a pre-formed thread, should also prove successful.

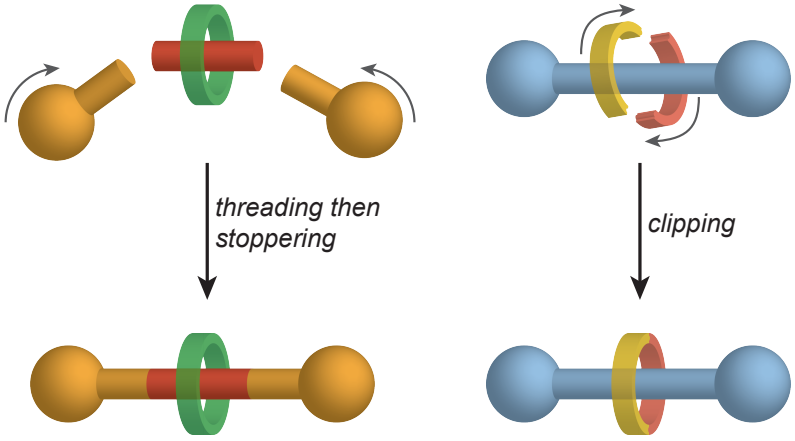

Figure 2.4: Pictorial representation of two common approaches to synthesis of mechanically interlocked compounds: (*left*) threading of a pre-formed macrocycle, then stoppering and (*right*) clipping of macrocyclic components around a pre-formed thread.

2.3.1 "Threading then Stoppering" Approach

In a threading then stoppering approach, the MAE and macrocycle must first be preorganised such that the MAE is held inside the macrocyclic cavity. Phenanthroline motifs present in both MAE and macrocyclic components are ideally suited to form tetrahedral complexes with Cu(I) cations, in a passive template approach. Mixing these two components with a Cu(I) source should thread the MAE through the macrocyclic cavity to generate a pseudorotaxane in which the two components are held orthogonal to each other. A subsequent stoppering reaction with a bulky stopper will prevent the macrocycle from dethreading and lock the components together to give the [2]rotaxane. This approach requires the synthesis of two key components: a macrocycle and a stopper with sufficient bulk to trap the interlocked components.

2.3.1.1 Macrocycle Synthesis

Macrocycles incorporating phenanthroline units are commonplace and are perfect candidates in forming interlocked compounds using passive metal templates.[27,46–48] Macrocycle **M1** utilises a diaryl phenanthroline core and was chosen due to its well-documented affinity for Cu(I) ions, relative ease of synthesis, modest cavity size and high flexibility offered by the ethylene glycol strap.[47,49] Mechanically interlocked compounds involving **M1** have been previously reported,[50–52] and offered reassurance that our target [2]rotaxane should be prepared with ease. Synthesis of macrocycle **M1** (summarised in Scheme 2.8) first involves the lithiation of 4-bromoanisole then later attack on 1,10-phenanthroline to give dianisyl phenanthroline **2.11**, then subsequent pyridine/HCl hydrolysis of which returns diphenol phenanthroline **2.12**. Diol **2.13** was prepared by treatment of phenanthroline **2.12** with 2-(2-chloroethoxy)ethanol, then converted to ditosylate **2.14**. Reaction of the ditosylate with resorcinol under high-dilution conditions returned macrocycle **M1** in 60% yield.

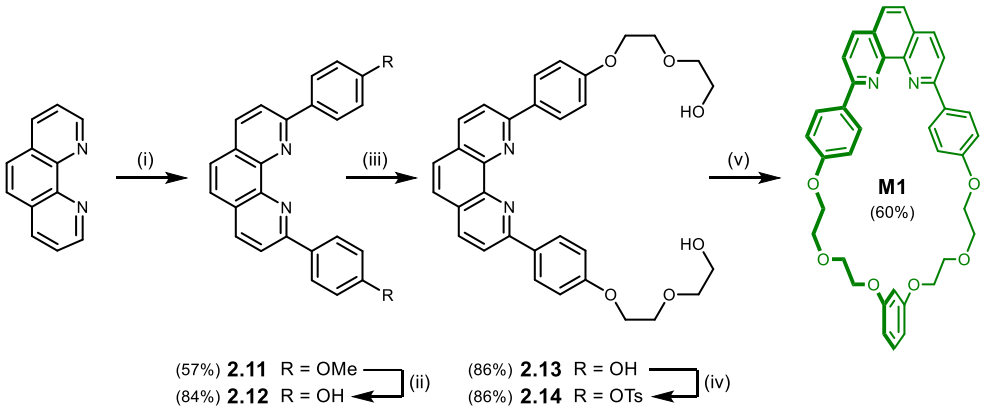

Scheme 2.8: Preparation of macrocycle **M1**.[50,52,53] (i) 4-bromoanisole, *n*-BuLi, THF, −78 °C, 3 h, Ar then 1,10-phenanthroline, toluene, −78 °C to 20 °C, 20 h, Ar then MnO_2, CH_2Cl_2, 20 °C, 30 min (ii) pyridine, HCl, 200 °C, 3 h, Ar; (iii) 2-(2-chloroethoxy)ethanol, Cs_2CO_3, DMF, 90 °C, 18 h, Ar; (iv) tosyl chloride, DMAP, Et_3N, CH_2Cl_2, 0 °C to 20 °C, 22 h, Ar; (v) resorcinol, Cs_2CO_3, DMF, 60 °C 24 h, Ar.

2.3.1.2 *para*-^{t}Bu Trityl Stopper Synthesis

With regard to the stoppering group, a suitably large stopper is necessary to prevent dethreading. CPK and space-filling computational models both suggest that a *para*-^{t}Bu trityl-based stopper would provide sufficient bulk to prevent dethreading (Figure 2.5), while also being expected to show good thermal and chemical stability with respect to a variety of chemical transformations. Stopper **2.18** is readily prepared from 1-bromo-4-*tert*-butylbenzene by first treating with Mg metal to give corresponding magnesium bromide,[26] then addition of diethyl

carbonate to return *para*-^{t}Bu-based alcohol **2.15** (Scheme 2.9). Conversion of alcohol **2.15** to chloride **2.16**, then addition of ethynyl magnesium bromide successfully affords the terminal acetylene **2.17**. The corresponding bromoacetylene **2.18** could then be prepared by treating **2.17** with NBS/$AgNO_3$.[10]

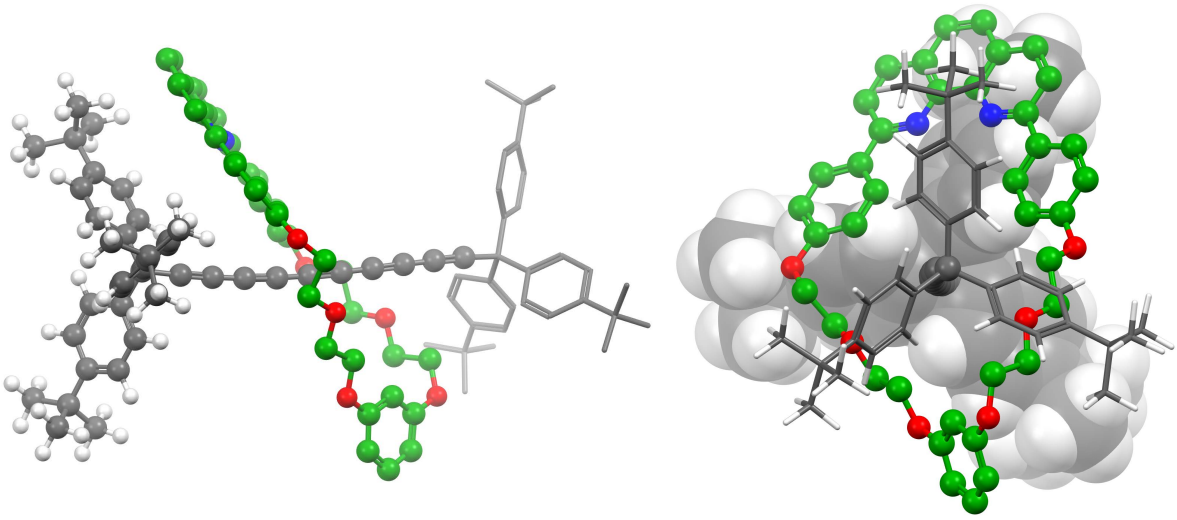

Figure 2.5: Optimised geometry of a *para*-^{t}Bu stoppered hexayne [2]rotaxane (MM+). Installation of *tert*-butyl groups on a trityl stopper will provide sufficient bulk to prevent **M1** from dethreading.

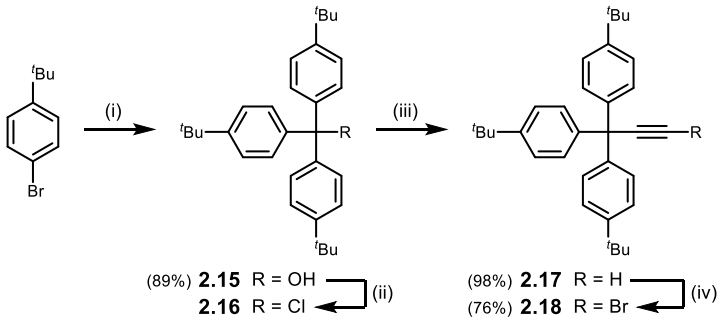

Scheme 2.9: Synthesis of stoppers **2.17** and **2.18**.[10,26] (i) Mg, THF, 40 °C, 2 h, Ar then diethyl carbonate, THF, 40 °C 3 h, Ar; (ii) oxalyl chloride, THF, 20 °C, 4 h, Ar; (iii) ethynylmagnesium bromide, THF, 20 °C, 3 d, Ar; (iv) NBS, $AgNO_3$ (10 mol%), acetone, 20 °C, 2 h, Ar.

2.3.1.3 Attempted Rotaxane Synthesis

The cross-coupling reaction between MAE and stoppering components was first tested on the free thread **2.20** before applying the chemistry to prepare rotaxanes. TIPS groups on MAE **2.8** were first removed by TBAF in wet THF to give deprotected MAE **2.19**. The coupling between MAE **2.19** and stopper **2.17** was first investigated by a statistical Glaser cross-coupling reaction (Scheme 2.10, top) using an excess of stopper. To our surprise, and despite trialling a variety of CuCl/TMEDA/stopper concentrations and reaction temperatures, we were unable to observe formation of the desired cross-coupled product, nor were we able to detect traces of the singly

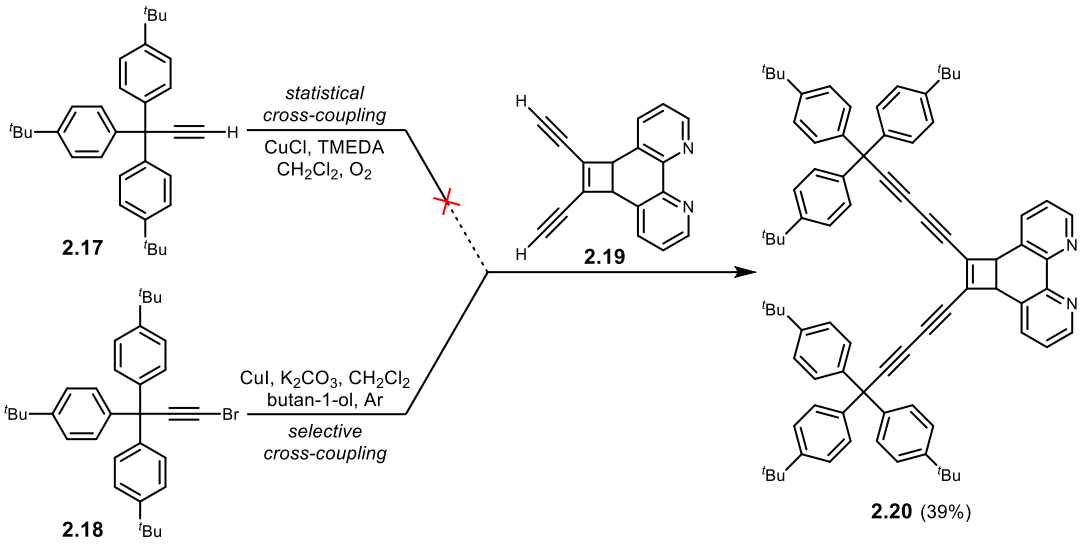

Scheme 2.10: Dumbbell **2.20** could be prepared through either a (*top*) statistical Glaser-Hay or (*bottom*) Cadiot-Chodkiewicz cross-coupling reaction.

coupled product. Only homocoupled stopper and unreacted MAE **2.19** could be isolated from the reaction. It is suspected that the reactivity of the stopper with itself is significantly greater than for the MAE component, giving it a much higher propensity to undergo homocoupling than cross-coupling with the MAE. Even when using a larger excess of the stopper in the reaction mixture, we were unable to isolate the stoppered [2]rotaxane.

To overcome the detrimental homocoupling reaction, and to improve selectivity for the cross-coupled product, we instead switched to a Cadiot-Chodkiewicz approach (Scheme 2.10, bottom). Unlike with an (unselective) Glaser-type homocoupling approach, which requires oxygen as an oxidant to drive the coupling, the Cadiot-Chodkiewicz reaction is performed under degassed conditions. The selectivity for the cross-coupled product instead comes from the reaction between an alkyne and a haloalkyne, the latter being the necessary oxidant in the reaction. Typically bromoalkynes give the highest yields for the cross-coupled product of all haloalkyne coupling partners; iodides tend to give larger quantities of homocoupled products and chlorides are generally unreactive.[54] Literature precedence of **2.18** led us to select this component as the brominated coupling partner. Subjecting MAE **2.19** and brominated stopper **2.18** to the Cadiot-Chodkiewicz conditions (CuI with K_2CO_3 in 1:1 CH_2Cl_2/butan-1-ol) was successful in affording the stoppered MAE **2.20** in 39% yield.

With the stoppering reaction now working on the thread, the reaction was then applied to prepare [2]rotaxane **2.20·M1** (Scheme 2.11). The pseudorotaxane was generated by

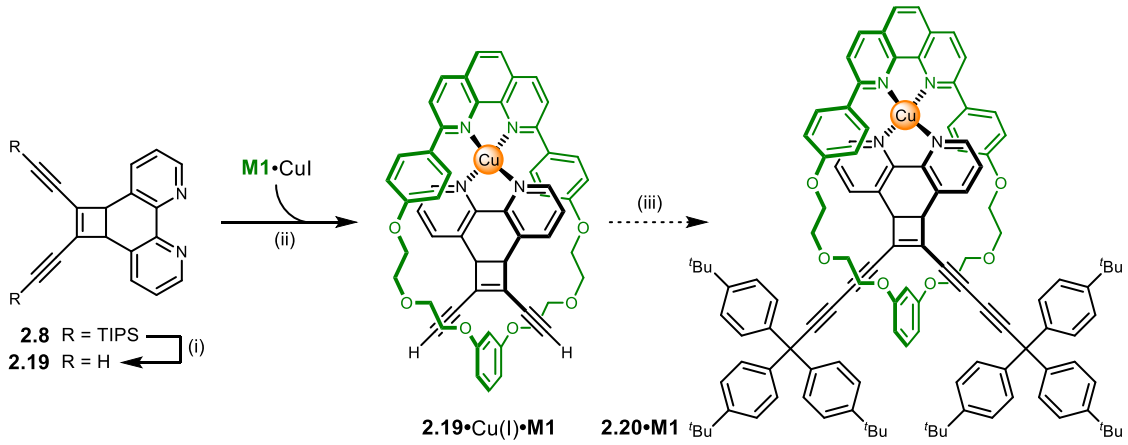

Scheme 2.11: Proposed synthesis of [2]rotaxane **2.20·M1** via a threading (step ii), then stoppering (step iii) approach. (i) TBAF, THF/H_2O (1% v/v). 20 °C, 30 min, Ar; (ii) *sonication*, CH_2Cl_2, 20 °C, 10 min, air.

sonicating a 1:1 mixture of deprotected MAE **2.19** and macrocycle-copper complex **M1**·CuI in CH_2Cl_2. Formation of the **2.19**·Cu(I)·**M1** complex was identified by ESI-MS, which displayed the expected signal at m/z = 931. The complex was then subjected to the Cadiot-Chodkiewicz stoppering reaction. We quickly observed that even after running the reaction for much longer than for the thread (24 h vs 8 h), we were unable to detect evidence of the stoppered product. The only new species was a small quantity of homocoupled stopper; MAE **2.19**, macrocycle **M1** and most of the brominated stopper **2.18** were all recovered from the reaction. It is surprising that the reaction is so unsuccessful on the complex, as the macrocycle should not alter the chemical reactivity of the MAE or stopper. We suspect that steric clashes between the macrocycle and stoppering groups may be occurring, thereby making stoppering unfavourable.

The same rotaxane-forming step reaction was also tested using an alternative macrocycle (**M2**, Scheme 2.12). The ethylene glycol chain on macrocycle **M2** should offer improved flexibility compared to **M1**, and it was hoped that this would be sufficient in reducing steric congestion around the reaction centre. **M2** was prepared following reported procedures by directly treating diphenol phenanthroline with pentaethylene glycol ditosylate and Cs_2CO_3 under high-dilution conditions (Scheme 2.12).[55] Rotaxane synthesis was then investigated using the Cadiot-Chodkiewicz coupling stoppering reaction. Unfortunately, and despite observing successful formation of the [**2.19**·Cu(I)·**M2**]$^+$ complex by ESI-MS, we were unable to detect even traces of the target [2]rotaxane. Analysis of the reaction mixture revealed a small amount of homocoupled stopper, but the bulk appeared to be predominantly starting materials.

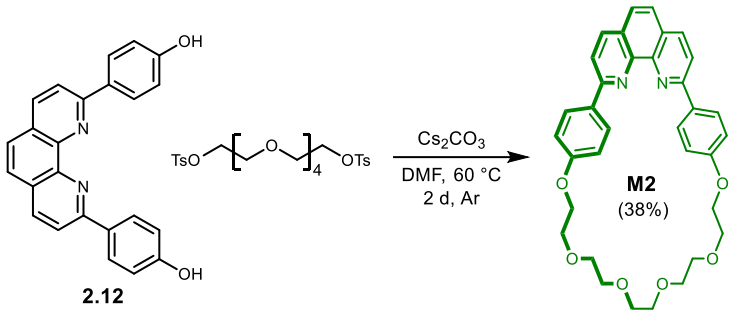

Scheme 2.12: Synthesis of a diaryl phenanthroline macrocycle **M2** with a flexible ethylene glycol strap.[55]

While it should be possible to extend the MAE by one or two acetylene units, we feared that the resulting diyne (or triyne) may suffer from low stability once the silyl protecting group had been removed, making its handling more challenging. Additionally, extension reactions to this MAE would likely be made via a statistical Glaser-Hay coupling with TMS-acetylene, yet our previous experience with MAE **2.19** suggests that poor yields of the extension product may be expected on account of the generally poor reactivity of this compound. With these factors in mind, we thought it best to explore an alternative approach towards preparing a [2]rotaxanes with an MAE thread.

2.4 "Clipping" Approach

We previously noted the difficulties in constructing the dumbbell through the macrocyclic cavity. While successful coupling between MAE and stopper was achieved on the free thread, when applying this to the complex there was no apparent reactivity. Knowing that the dumbbell can be prepared, we instead opted to investigate a "clipping" approach towards a MAE-based [2]rotaxane (Figure 2.4, right). In this approach, the dumbbell component recognises and binds the macrocyclic precursors, templating the formation of the macrocycle around this site. These recognition sites may be intrinsic to the dumbbell and macrocycle, or they may be aided by third parties, such as complexation of components to a metal ion. For this work, the phenanthroline units on both macrocyclic precursor and MAE are perfectly poised to interact with Cu(I) ions, which hold the two molecular fragments in place before the final macrocyclisation reaction.

There are many possible ways in which the clipping reaction can take place. Stoddart *et al.* pioneered the use of dialdehyde and diamine macrocyclic precursors, templated around dialkylammonium sites, demonstrating the first thermodynamically-controlled preparation of

imine-containing [2]rotaxanes (**2.21**, Figure 2.6a).[56] Subsequent reduction of these imine groups to amines then yielded a kinetically stable interlocked molecule. Related methods have since been adopted by others in preparation of interlocked molecules.[57–60] Another interesting clipping approach is one involving olefin metathesis. Grubbs *et al.* prepared a diaryl phenanthroline-based macrocyclic precursor **2.22** bearing two terminal olefinic units, which were designed to coordinate around a copper atom in a tetrahedral arrangement (Figure 2.6b).[61] Treating the pre-catenane complex with a ruthenium catalyst saw a ring-closing metathesis reaction to entrap the two, generating [2]catenane **2.23** in exceptional yields of up to 92%. Similar Ru-catalysed reversible ring opening and closing reactions have since been used to successfully prepare other catenanes and rotaxanes in good yield.[62–64]

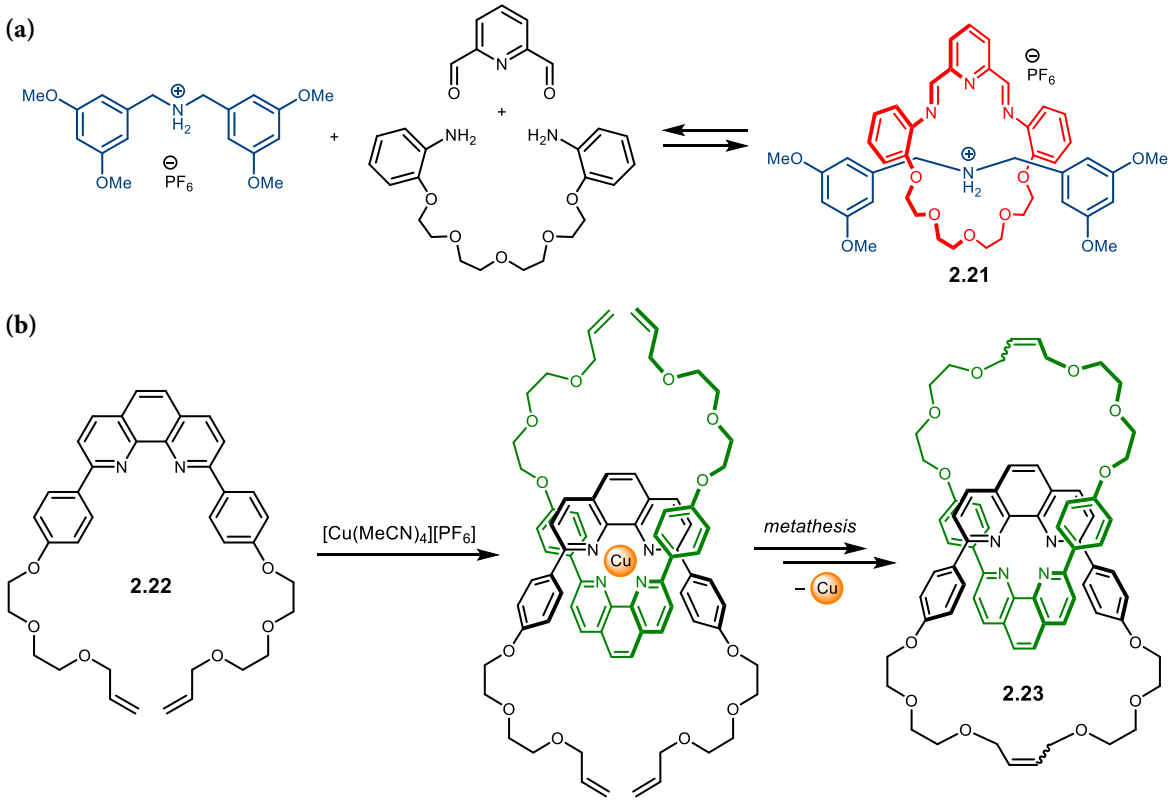

Figure 2.6: Approaches to mechanically interlocked compounds: (a) [2]rotaxane **2.21** by clipping of dialdehyde and diamine macrocyclic precursors around a dialkylammonium thread[56] and; (b) [2]catenane **2.23** by Ru-catalysed ring-closing metathesis of two Cu(I)-templated diolefin macrocyclic precursors **2.22**.[65]

The mild reaction conditions and relative ease of clipping made these metathesis reactions appealing. Strong literature precedence for use of these olefin-containing macrocycles to prepare rotaxanes and catenanes through a passive template approach provided reassurance that it should prove a viable route to our [2]rotaxane. An additional benefit is the structural similarity between the diolefin diphenylphenanthroline macrocycles compared to **M1** and **M2**,

making it quick and facile to prepare the diolefin macrocycle using precursors to those already available.

2.4.1 Macrocycle Synthesis

Macrocycle **M3** was selected due to its similarity to **M1** and **M2**, in both size and geometry. Literature precedence for **M3** suggests that synthesis would be very straightforward, requiring only a single step when starting from ethylene glycol diol **2.13**. Treating **2.13** with sodium hydride, then allyl bromide successfully afforded the terminal olefin-containing macrocycle precursor **2.22** in 33% yield (Scheme 2.13). Treating diolefin **2.22** to Grubbs G1 or G2 Ru-based catalysts at 20 °C should catalyse the reversible ring opening and closing reaction to return **M3** as a mixture of *cis* and *trans* isomers.

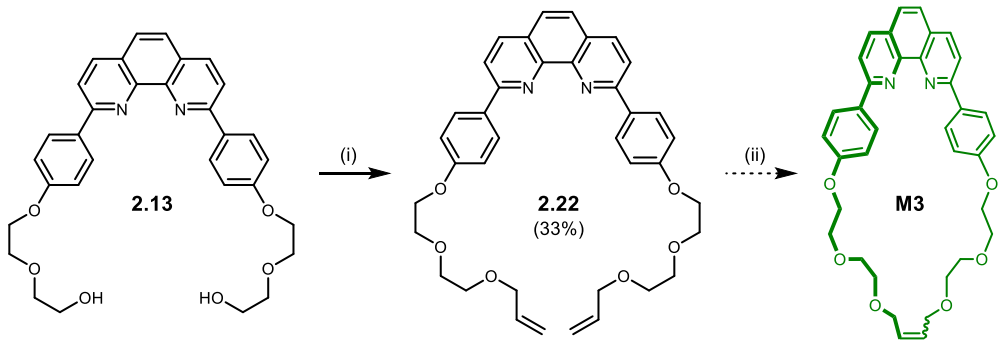

Scheme 2.13: Preparation of olefin macrocycle **M3**. (i) NaH, allyl bromide, DMF, 80 °C, 6 h, Ar; (ii) CH_2Cl_2, Grubbs G1, 20 °C, 6 h, Ar.

2.4.2 Dumbbell Synthesis

With consideration to observations made during the previous threading-then-stoppering approach, we noted the possibility that the previous dumbbell was perhaps too sterically crowded to successfully template rotaxane synthesis. To improve the likelihood of successful rotaxane formation, a modified dumbbell was instead designed (**2.27**, Scheme 2.14). Flexible alkyl linkers were employed to shift the bulky stoppering groups further away from the reaction (clipping) centre and to ensure an unhindered reaction site. Semi-empirical (PM7 level of theory with D2 dispersion corrections) space-filling computational models (Figure 2.7) suggest that dumbbell **2.27** offers sufficient special extension such that the stoppering groups would not interfere with the MAE-macrocycle complex. Extended thread **2.27** can be obtained in three steps from trityl-based alcohol **2.15**. Treating **2.15** with phenol and HCl afforded phenol **2.24**,

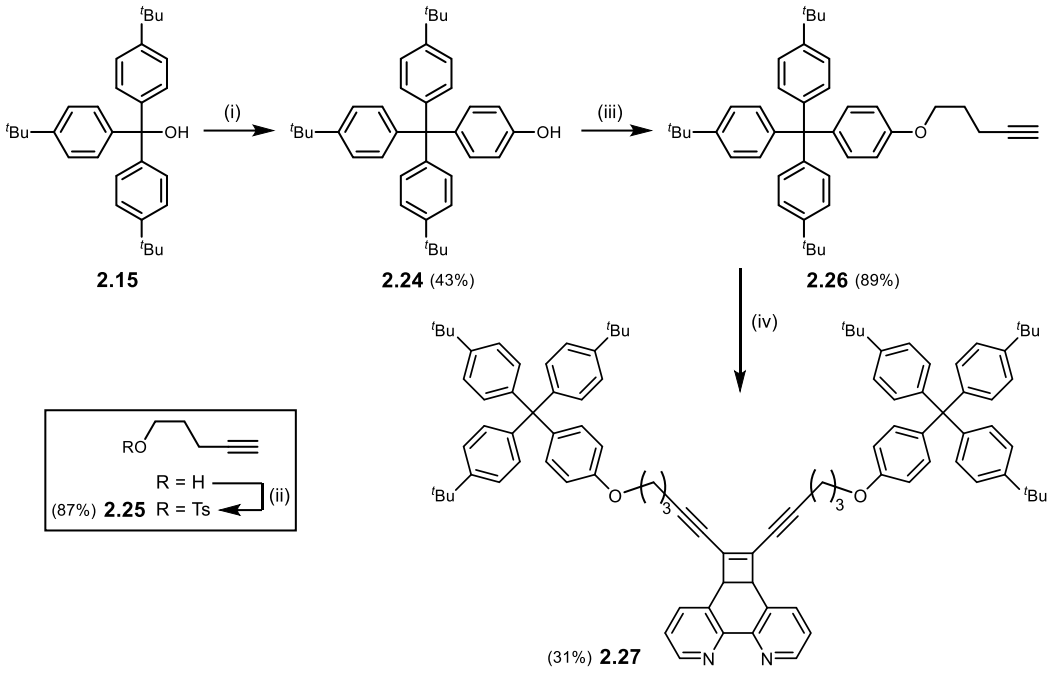

Scheme 2.14: Synthesis of extended stopper **2.27**. (i) phenol, HCl, *reflux*, 24 h, Ar; (ii) *p*-toluenesulfonyl chloride, Et_3N, CH_2Cl_2, 20 °C, 18 h, Ar; (iii) **2.25**, K_2CO_3, 18-crown-6, butanone, *reflux*, 18 h, Ar; (iv) dichlorophenanthroline **2.7**, $Pd_2(dba)_3$, CuI, XPhos, DIPA, 1,4-dioxane, 85 °C, 18 h, Ar.

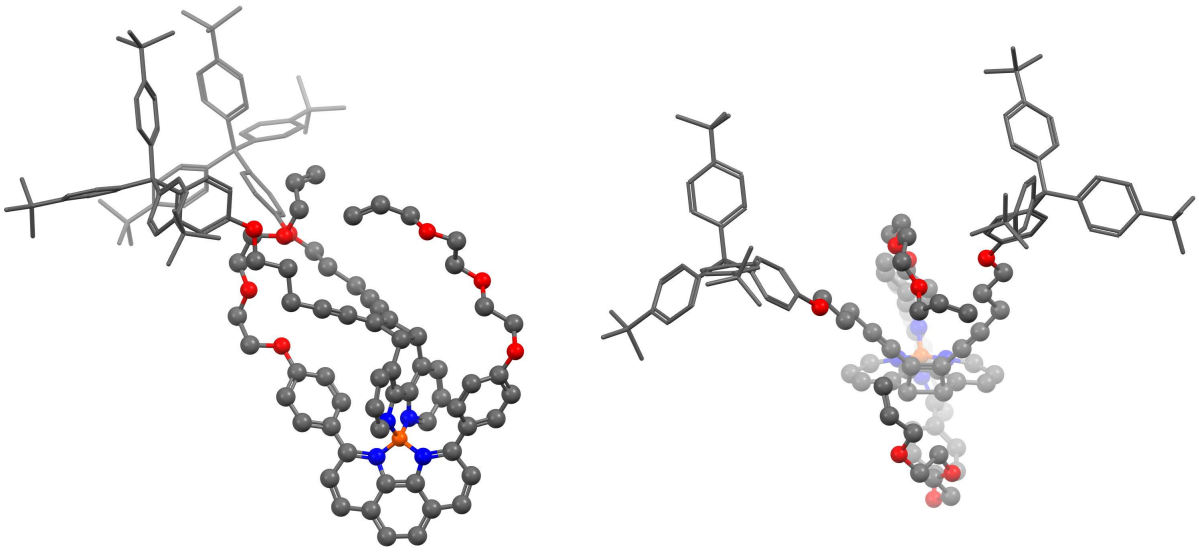

Figure 2.7: Optimised geometry of extended [**2.22**·Cu·**2.27**]$^+$ complex (semi-empirical, PM7 level of theory with D2 dispersion corrections). The diolefin strap crosses over the thread and are poised to undergo alkene metathesis.

which after treating with tosylate **2.25**, returned the extended stopper **2.26**. The stopper was installed directly onto dichlorophenanthroline **2.7** through a Sonogashira coupling to return the dumbbell **2.27** in 31% yield.

2.4.3 Attempted Rotaxane Synthesis

With both dumbbell and macrocyclic precursors in hand, attempts were then made to prepare the [2]rotaxane. Treating dumbbell **2.27** and diolefin **2.22** with a Cu(I) ion source soluble in organic solvents, $[Cu(MeCN)_4][PF_6]$, resulted in a rapid colour change from a colourless to dark brown solution, indicative of successful copper complexation. However, to our surprise ESI-MS displayed only two intense signals at m/z = 1303 and 2749, neither corresponding to the expected complex. These signals instead appear to correlate with the mass ions of two homoleptic complexes formed either from two diolefin complexes $[(\mathbf{2.22})_2{\cdot}Cu]^+$ or two dumbbell units $[(\mathbf{2.27})_2{\cdot}Cu]^+$ (Figure 2.8). Statistically we would expect formation of the heteroleptic complex to prevail, but we were unable to detect even traces of the desired heteroleptic complex $[\mathbf{2.22}{\cdot}Cu{\cdot}\mathbf{2.27}]^+$ by either mass spectrometry or NMR spectroscopy. This very unexpected and highly problematic result quickly rendered this approach unsuitable. There is little that can be done to alter the propensity for these systems to exclusively form homoleptic complexes. Without a way to prepare a MAE dumbbell/pre-macrocycle complex it will not be possible to construct the target [2]rotaxane.

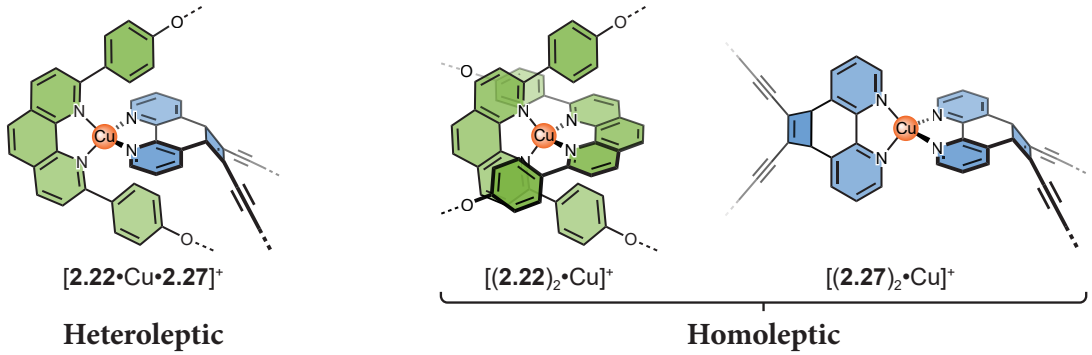

Figure 2.8: (*left*) expected heteroleptic complex $[\mathbf{2.22}{\cdot}Cu{\cdot}\mathbf{2.27}]^+$ and (*right*) the two observed homoleptic complexes $[(\mathbf{2.22})_2{\cdot}Cu]^+$ and $[(\mathbf{2.27})_2{\cdot}Cu]^+$, respectively.

It is surprising that the formation of homoleptic complexes in the clipping approach dominates the reaction outcome. When investigating a threading-then-stoppering approach, the $[\mathbf{M1}{\cdot}Cu{\cdot}\mathbf{2.19}]^+$ complex was formed exclusively, without trace of the homoleptic complexes $[(\mathbf{2.19})_2{\cdot}Cu]^+$ or $[(\mathbf{M1})_2Cu]^+$. We suspect that in this case, the fully cyclised **M1** macrocycle makes it unable to form homoleptic complexes due steric constraints imposed by the macrocyclic strap. Thus with the possibility of forming $[(\mathbf{M1})_2Cu]^+$ complex shut down, exclusive formation of the heteroleptic species is observed. In contrast, the diolefin macrocyclic

precursor **2.22** bears two independent (unlinked) olefin-terminated chains, allowing the two arms thread around each other when forming a homoleptic copper complex. We expected that these homoleptic complexes were always likely to form to some extent – just as in Sauvage's seminal literature report for preparing the [2]catenanes.[61] However, it was reasonable to expect a statistical mixture of the two homo- and one heteroleptic complexes, and not such strong selectivity for the former two. Nevertheless, these results strongly imply that a clipping approach is not viable, at least with the current system.

2.5 Conclusions

This chapter documents attempts towards building a masked alkyne equivalent with intrinsic metal coordination abilities. We have demonstrated the successful preparation of a dichloro cyclobutene-fused phenanthroline unit, which can be readily functionalised via Sonogashira coupling reactions. Unlike the closely related cyclobutene-fused phenanthrene systems, the unmasking of a phenanthroline-masked triyne was found problematic. Rather than returning the expected triyne, a [3]-ladderane was formed exclusively in a [2+2] cycloaddition between two MAE components, trapping the molecule in a state in which unmasking was no longer possible. We documented attempts to prepare [2]rotaxanes using this MAE via a passive metal template approach. Despite achieving successful stoppering on the free thread, when applying this chemistry to prepare [2]rotaxanes (via a threading-then-stoppering approach), we were unable to detect any successful stoppering, and thus [2]rotaxane. Brief investigations were made into preparing a [2]rotaxane via clipping approaches, but we soon encountered unexpected selectivity for homoleptic complexes between two MAE or macrocycle units, and not the desired heteroleptic complex, rendering such an approach unsuitable.

The formation of solely heteroleptic complexes in a clipping approach made it unsuitable in preparing [2]rotaxanes with an MAE-based thread. It is likely that by screening a host of MAE derivatives, stoppers and macrocycles, a variation of the [2]rotaxanes discussed in this chapter could be prepared. However, even should this [2]rotaxane be realised, it still remains uncertain whether the later unmasking of the phenanthroline MAE will proceed successfully. While is likely that the encapsulation offered by the threaded macrocycle will shut down the detrimental MAE dimerisation process, unmasking may simply not take place in this system, or there are still other processes that may instead occur.[10] Rather than intensifying

efforts on this system with too many variables and unknowns, it was deemed sensible to explore polyyne rotaxanes that could be prepared using existing and well documented masked alkyne equivalents instead.

2.6 References

1 F. Diederich, Y. Rubin, C. B. Knobler, R. L. Whetten, K. E. Schriver, K. N. Houk and Y. Li, *Science*, 1989, **245**, 1088–1090.

2 Y. Rubin, C. B. Knobler and F. Diederich, *J. Am. Chem. Soc.*, 1990, **112**, 4966–4968.

3 Y. Tobe, H. Matsumoto, K. Naemura, Y. Achiba and T. Wakabayashi, *Angew. Chem. Int. Ed.*, 1996, **35**, 1800–1802.

4 Y. Tobe, T. Fujii, H. Matsumoto, K. Naemura, Y. Achiba and T. Wakabayashi, *J. Am. Chem. Soc.*, 1996, **118**, 2758–2759.

5 Y. Tobe, T. Fujii and K. Naemura, *J. Org. Chem.*, 1994, **59**, 1236–1237.

6 G. A. Adamson and C. W. Rees, *J. Chem. Soc. Perkin Trans. 1*, 1996, **2**, 1535–1543.

7 L. D. Movsisyan, D. V. Kondratuk, M. Franz, A. L. Thompson, R. R. Tykwinski and H. L. Anderson, *Org. Lett.*, 2012, **14**, 3424–3426.

8 N. Weisbach, Z. Baranová, S. Gauthier, J. H. Reibenspies and J. A. Gladysz, *Chem. Commun.*, 2012, **48**, 7562.

9 L. D. Movsisyan, M. Franz, F. Hampel, A. L. Thompson, R. R. Tykwinski and H. L. Anderson, *J. Am. Chem. Soc.*, 2016, **138**, 1366–1376.

10 S. L. Woltering, P. Gawel, K. E. Christensen, A. L. Thompson and H. L. Anderson, *J. Am. Chem. Soc.*, 2020, **142**, 13523–13532.

11 P. Gawel, S. L. Woltering, Y. Xiong, K. E. Christensen and H. L. Anderson, *Angew. Chem. Int. Ed.*, 2021, **60**, 5941–5947.

12 J. M. Van Raden, B. M. White, L. N. Zakharov and R. Jasti, *Angew. Chem. Int. Ed.*, 2019, **58**, 7341–7345.

13 S. Schrettl, E. Contal, T. N. Hoheisel, M. Fritzsche, S. Balog, R. Szilluweit and H. Frauenrath, *Chem. Sci.*, 2015, **6**, 564–574.

14 Y. Tobe, T. Fujii, H. Matsumoto, K. Tsumuraya, D. Noguchi, N. Nakagawa, M. Sonoda, K. Naemura, Y. Achiba and T. Wakabayashi, *J. Am. Chem. Soc.*, 2000, **122**, 1762–1775.

15 Y. Tobe, J. Kishi, I. Ohki and M. Sonoda, *J. Org. Chem.*, 2003, **68**, 3330–3332.

16 Y. Tobe, R. Umeda, N. Iwasa and M. Sonoda, *Chem. Eur. J.*, 2003, **9**, 5549–5559.

17 D. C. Zecher and R. West, *J. Am. Chem. Soc.*, 1967, **89**, 153–155.

18 Y. Rubin and F. Diederich, *J. Am. Chem. Soc.*, 1989, **111**, 6870–6871.

19 Y. Rubin, M. Kahr, C. B. Knobler, F. Diederich and C. L. Wilkins, *J. Am. Chem. Soc.*, 1991, **113**, 495–500.

20 K. Kaiser, L. M. Scriven, F. Schulz, P. Gawel, L. Gross and H. L. Anderson, *Science*, 2019, **365**, 1299–1301.

21 J. Lewis, B. Lin, M. S. Khan, M. R. A. Al-Mandhary and P. R. Raithby, *J. Organomet. Chem.*, 1994, **484**, 161–167.

22 M. M. Haley and B. L. Langsdorf, *Chem. Commun.*, 1997, **2**, 1121–1122.

23 D. R. Kohn, P. Gawel, Y. Xiong, K. E. Christensen and H. L. Anderson, *J. Org. Chem.*, 2018, **83**, 2077–2086.

24 S. Eisler and R. R. Tykwinski, *J. Am. Chem. Soc.*, 2000, **122**, 10736–10737.

25 T. Luu, Y. Morisaki, N. Cunningham and R. R. Tykwinski, *J. Org. Chem.*, 2007, **72**, 9622–9629.

26 P. R. Ashton, R. Ballardini, V. Balzani, M. Bělohradský, M. T. Gandolfi, D. Philp, L. Prodi, F. M. Raymo, M. V. Reddington, N. Spencer, J. F. Stoddart, M. Venturi and D. J. Williams, *J. Am. Chem. Soc.*, 1996, **118**, 4931–4951.

27 C. O. Dietrich-Buchecker and J.-P. Sauvage, *Tetrahedron Lett.*, 1983, **24**, 5091–5094.

28 R. H. Grubbs, S. J. Miller and G. C. Fu, *Acc. Chem. Res.*, 1995, **28**, 446–452.

29 V. V. Rostovtsev, L. G. Green, V. V. Fokin and K. B. Sharpless, *Angew. Chem. Int. Ed.*, 2002, **41**, 2596–2599.

30 F. Bitsch, C. O. Dietrich-Buchecker, A. K. Khemiss, J.-P. Sauvage and A. Van Dorsselaer, *J. Am. Chem. Soc.*, 1991, **113**, 4023–4025.

31 N. Solladié, J.-C. Chambron and J.-P. Sauvage, *J. Am. Chem. Soc.*, 1999, **121**, 3684–3692.

32 C. O. Dietrich-Buchecker and J.-P. Sauvage, *Angew. Chem. Int. Ed.*, 1989, **28**, 189–192.

33 N. Belfrekh, C. Dietrich-Buchecker and J.-P. Sauvage, *Inorg. Chem.*, 2000, **39**, 5169–5172.

34 A.-M. Fuller, D. A. Leigh, P. J. Lusby, I. D. H. Oswald, S. Parsons and D. B. Walker, *Angew. Chem. Int. Ed.*, 2004, **43**, 3914–3918.

35 A.-M. L. Fuller, D. A. Leigh, P. J. Lusby, A. M. Z. Slawin and D. B. Walker, *J. Am. Chem. Soc.*, 2005, **127**, 12612–12619.

36 D. B. Amabilino and J. F. Stoddart, *Chem. Rev.*, 1995, **95**, 2725–2828.

37 N. P. Hacker and J. F. W. McOmie, *Tetrahedron*, 1984, **40**, 5249–5254.

38 R. Chinchilla and C. Nájera, *Chem. Rev.*, 2007, **107**, 874–922.

39 Y. Tobe, H. Nakanishi, M. Sonoda, T. Wakabayashi and Y. Achiba, *Chem. Commun.*, 1999, 1625–1626.

40 M. Alami, S. Gueugnot, E. Domingues and G. Linstrumelle, *Tetrahedron*, 1995, **51**, 1209–1220.

41 A. Matsuda, M. Shinozaki, T. Yamaguchi, H. Homma, R. Nomoto, T. Miyasaka, Y. Watanabe and T. Abiru, *J. Med. Chem.*, 1992, **35**, 241–252.

42 A. Mori, S. Fukuoka, T. Naito, H. Sekiguchi and T. Somete, *Heterocycles*, 2008, **76**, 819.

43 R. Jana, T. P. Pathak and M. S. Sigman, *Chem. Rev.*, 2011, **111**, 1417–1492.

44 Y. Morisaki, M. Gon, T. Sasamori, N. Tokitoh and Y. Chujo, *J. Am. Chem. Soc.*, 2014, **136**, 3350–3353.

45 M. Movassaghi, G. Piizzi, D. S. Siegel and G. Piersanti, *Angew. Chem. Int. Ed.*, 2006, **45**,

5859–5863.

46 C. O. Dietrich-Buchecker, A. Khemiss and J.-P. Sauvage, *J. Chem. Soc. Chem. Commun.*, 1986, 1376.

47 C. Dietrich-Buchecker and J.-P. Sauvage, *Tetrahedron*, 1990, **46**, 503–512.

48 J.-C. Chambron, V. Heitz and J.-P. Sauvage, *J. Chem. Soc. Chem. Commun.*, 1992, 1131.

49 A. I. Share, K. Parimal and A. H. Flood, *J. Am. Chem. Soc.*, 2010, **132**, 1665–1675.

50 D. B. Amabilino and J.-P. Sauvage, *Chem. Commun.*, 1996, 2441.

51 M. C. Jimenez-Molero, C. Dietrich-Buchecker and J.-P. Sauvage, *Chem. Eur. J.*, 2002, **8**, 1456–1466.

52 C. Roche, *PhD Thesis*, Université de Strasbourg & University of Sydney, 2012.

53 C. Roche, A. Sour, F. Niess, V. Heitz and J.-P. Sauvage, *Eur. J. Org. Chem.*, 2009, **2009**, 2795–2800.

54 M. Alami and F. Ferri, *Tetrahedron Lett.*, 1996, **37**, 2763–2766.

55 N.-K. Kim, H. Sogawa and T. Takata, *Tetrahedron Lett.*, 2020, **61**, 151966.

56 P. T. Glink, A. I. Oliva, J. F. Stoddart, A. J. P. White and D. J. Williams, *Angew. Chem. Int. Ed.*, 2001, **40**, 1870–1875.

57 M. Narita, I. Yoon, M. Aoyagi, M. Goto, T. Shimizu and M. Asakawa, *Eur. J. Inorg. Chem.*, 2007, **2007**, 4229–4237.

58 A. Pun, D. A. Hanifi, G. Kiel, E. O'Brien and Y. Liu, *Angew. Chem. Int. Ed.*, 2012, **51**, 13119–13122.

59 I. Yoon, M. Narita, M. Goto, T. Shimizu and M. Asakawa, *Org. Lett.*, 2006, **8**, 2341–2344.

60 W. Zhou, J. Li, X. He, C. Li, J. Lv, Y. Li, S. Wang, H. Liu and D. Zhu, *Chem. Eur. J.*, 2008, **14**, 754–763.

61 M. Weck, B. Mohr, J.-P. Sauvage and R. H. Grubbs, *J. Org. Chem.*, 1999, **64**, 5463–5471.

62 L. Wang, M. O. Vysotsky, A. Bogdan, M. Bolte and V. Böhmer, *Science*, 2004, **304**, 1312–1314.

63 F. Arico, P. Mobian, J.-M. Kern and J.-P. Sauvage, *Org. Lett.*, 2003, **5**, 1887–1890.

64 T. J. Kidd, D. A. Leigh and A. J. Wilson, *J. Am. Chem. Soc.*, 1999, **121**, 1599–1600.

65 B. Mohr, J.-P. Sauvage, R. H. Grubbs and M. Weck, *Angew. Chem. Int. Ed.*, 1997, **36**, 1308–1310.

2.7 Experimental

Contents

General Methods

Commercially available reagents were used as received. Dry solvents (THF, CH_2Cl_2, toluene, DMF) for reactions were purified by a MBraun MB-SPS-5 bench-top SPS system under nitrogen (H_2O content < 20 ppm). All other solvents used were HPLC grade and dried over appropriate drying agents when required. Petroleum ether (petrol) had a boiling point range of 40–60 °C. *N,N,N′,N′*-Tetramethylethylenediamine (TMEDA) was dried with 3 Å molecular sieves (Linde-type) and then distilled over KOH under an Ar atmosphere prior to each use. EDTA/NH_3 solution was prepared by saturating a 1:1 solution of water/aqueous 35% NH_3 solution with tetrasodium EDTA. All solutions used during workups (NH_4Cl, $Na_2S_2O_3$ and brine) were saturated aqueous solutions, unless otherwise specified. Copper(I) chloride was freshly prepared.[1]

Reactions, unless otherwise stated, were carried out in oven-dried glassware under an Ar or N_2 atmosphere. Thin layer chromatography (TLC) was carried out on aluminum-backed silica gel plates with 0.2 mm thick silica gel 60 F254 (Merck) and visualised by UV irradiation at either 254 nm or 366 nm. Preparative flash column chromatography was either carried out using flash silica gel 60 (230-400 mesh) obtained from Sigma-Aldrich, or on a Biotage Isolera One with a 200–400 nm UV detector. Size-exclusion chromatography (SEC) was carried out using Bio-Beads S-X3, 40-80 μm (BioRad). Evaporation of solvents was performed at 20–50 °C and 5–1010 mbar. Reported yields refer to pure compounds dried under high vacuum (< 0.1 mbar).

^1H and ^{13}C nuclear magnetic resonance (NMR) spectra were recorded on Bruker Avance NEO 400, AVIII HD 500 and Bruker AVIII HD 600 (Prodigy broadband cryoprobe) spectrometers at 400 MHz, 500 MHz and 600 MHz (^1H) and 101 MHz, 126 MHz and 151 MHz (^{13}C), respectively at 298 K unless stated otherwise. NMR chemical shifts were reported in ppm relative to $SiMe_4$ ($\delta = 0$) and were referenced internally with respect to residual solvent protons using the reported values. Coupling constants are reported in Hz and ^1H multiplicities are reported in accordance with the following: br = broad; s = singlet; d = doublet; t = triplet; q = quartet; and m = multiplet. ^1H assignments were made using 2D NMR methods (COSY, NOESY, HSQC, HMBC).

Electrospray mass spectrometry was carried out on a Waters Micromass LCT Premier XE spectrometer using 90:10 MeOH:H_2O (+0.1% formic acid) as the mobile phase. High-resolution ESI mass spectrometry (HR-MS) measurements were performed by the mass spectrometry service at the University of Oxford on a Waters GTC classic.

UV-vis spectra were recorded in solution on a Perkin-Elmer Lambda 20 or Perkin-Elmer Lambda 25 spectrometer at 25 °C (unless otherwise noted), in fused silica cuvettes with a pathlength of 1 cm.

Synthesis of Known Compounds

2,9-Dianisyl-1,10-phenanthroline 2.11[2,3]

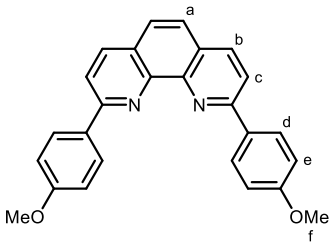

A solution of 4-bromoanisole (11 mL, 88 mmol) in dry THF (110 mL) was degassed with Ar and cooled to −78 °C. *n*-BuLi (1.6 M in hexanes, 100 mL, 0.16 mol) was added dropwise. The reaction mixture was stirred at −78 °C under Ar for 3 h. It was allowed to warm to 0 °C before transferring, by cannula, to a solution of pre-dried 1,10-phenanthroline (5.7 g, 32 mmol) in dry, degassed toluene (150 mL). The reaction was allowed to warm to 20 °C and stirred for a further 20 h under Ar. Water (50 mL) was added to hydrolyse the solution before evaporation of the solvent. The remaining solid was dissolved in CH_2Cl_2 (250 mL) and washed with water (3 × 250 mL). The organic layer was re-aromatised by addition of MnO_2 (*ca*. 60 g, 0.69 mol), dried over $MgSO_4$ and then filtered through Celite. The solvent was evaporated and the solid recrystallised from hot toluene to yield dianisyl phenanthroline **2.11** (7.1g, 18 mmol, 57%) as a pale yellow solid.

^{1}H NMR (400 MHz, $CDCl_3$) δ_H 8.45 (d, J = 8.9 Hz, 4H, H_d), 8.26 (d, J = 8.5 Hz, 2H, H_c), 8.09 (d, J = 8.5 Hz, 2H, H_b), 7.75 (s, 2H, H_a), 7.12 (d, J = 8.9 Hz, 4H, H_e), 3.93 (s, 6H, H_f).

Analytical data as in lit.[2,3]

2,9-Diphenol-1,10-phenanthroline (DPP) 2.12[2,3]

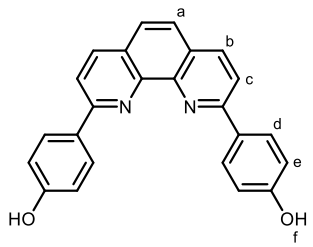

Pyridine (10.2 mL) and concentrated hydrochloric acid (11.2 mL) were combined in a flask equipped for distillation. Water was distilled from the mixture until the internal temperature rose to 205 °C. After cooling to 140 °C, dianisyl phenanthroline **2.11** (4.00 g, 10.2 mmol) was added to the reaction flask. The flask was fitted with a reflux condenser connected to an Ar source, and the mixture refluxed for 3 h at 200 °C. The mixture was allowed to cool to 120 °C, diluted with warm water (15 mL), then poured into warm water (75 mL) and the resulting suspension was refrigerated overnight. The solid was filtered and then suspended in an EtOH/H_2O mixture (75 mL/50 mL) and neutralised with dilute NaOH solution to pH = 7. The solution was diluted with hot water (300 mL), then the precipitate was filtered off and dried overnight to yield diphenol phenanthroline **2.12** (3.12 g, 8.57 mmol, 84%), as a red solid that was used in the next step without further purification.

^{1}H NMR (400 MHz, DMSO-d_6) δ_H 9.92 (br s, 2H, NH^+), 8.50 (d, J = 8.5 Hz, 2H, H_c), 8.36 (d, J = 8.8 Hz, 4H, H_d), 8.29 (d, J = 8.5 Hz, 2H, H_b), 7.93 (s, 2H_a), 7.01 (d, J = 8.7 Hz, 4H, H_e).

Analytical data as in lit.[2,3]

Diphenylphenanthroline diol 2.13[3,4]

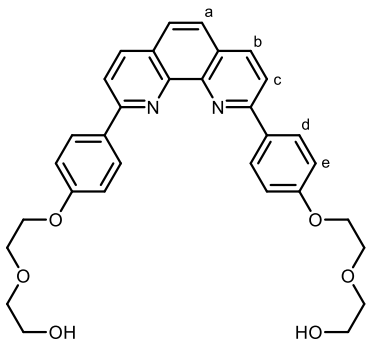

DMF (220 mL) was added to DPP **2.12** (2.20 g, 6.04 mmol) and Cs_2CO_3 (5.90, 18.1 mmol) and the mixture was stirred under N_2. 2-(2-Chloroethoxy)ethanol (3.9 mL, 36 mmol) was added,

and the mixture stirred at 90 °C under N_2 for 24 h. After filtration and subsequent evaporation of the solvent, the remaining solid was dissolved in CH_2Cl_2/MeOH (1:1, 500 mL). The solution was washed with H_2O and brine (99:1, 3 × 500 mL). The organic layer was dried over Na_2SO_4 and the solvent removed under reduced pressure. The product was purified by SiO_2 column chromatography (CH_2Cl_2/MeOH, gradient elution from 1:0 to 19:1) to yield the diphenylphenanthroline diol **2.13** as a yellow solid (2.80 g, 5.19 mmol, 86%).

^{1}H NMR (400 MHz, $CDCl_3$) δ_H 8.44 (d, J = 8.9 Hz, 4H, H_d), 8.27 (d, J = 8.4 Hz, 2H, H_c), 8.09 (d, J = 8.5 Hz, 2H, H_b), 7.75 (s, 2H, H_a), 7.14 (d, J = 8.9 Hz, 4H, H_e), 4.28 (m, 4H, CH_2), 3.95 (m, 4H, CH_2), 3.80 (m, 4H, CH_2), 3.73 (m, 4H, CH_2).

Analytical data as in lit.[3,4]

Diphenylphenanthroline ditosylate 2.14[3,4]

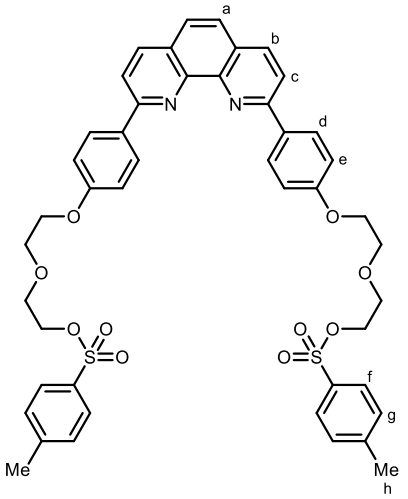

Diol **2.13** (2.8 g, 5.2 mmol) was suspended in dry CH_2Cl_2 (200 mL) and cooled to 0 °C under N_2. Triethylamine (4.4 mL, 31 mmol) and DMAP (4-dimethylaminopyridine) (50 mg, 0.41 mmol) were added to the cooled mixture before slow addition of tosyl chloride (5.3 g, 28 mmol). The mixture was under N_2 for 2 h at 0 °C, then 36 h at 20 °C. The solution was poured onto a mixture of ice (200 g) and HCl (1% aq., 50 mL). The aqueous layer was neutralised (pH = 7) with aqueous NaOH solution. The organic layer was separated, and the aqueous layer washed with CH_2Cl_2 (2 × 250 mL). The organic layers were combined and washed with water (200 mL) and dried over Na_2SO_4 before removal of the solvent under reduced pressure. The

resulting brown oil was subjected to SiO_2 column chromatography (CH_2Cl_2/MeOH, gradient elution from 99:1, then 9:1) to yield ditosylate **2.14** as a pale brown solid (3.8 g, 4.4 mmol, 86%).

^{1}H NMR (400 MHz, $CDCl_3$) δ_H 8.43 (d, J = 8.9 Hz, 4H, H_d), 8.26 (d, J = 8.4 Hz, 2H, H_c), 8.08 (d, J = 8.4 Hz, 2H, H_b), 7.81 (d, J = 8.4 Hz, 4H, H_f), 7.74 (s, 2H, H_a), 7.31 (d, J = 7.7 Hz, 4H, H_g), 7.09 (d, J = 8.9 Hz, 4H, H_e), 4.24 (m, 4H, CH_2), 4.14 (m, 4H, CH_2), 3.86 (m, 4H, CH_2), 3.89 (m, 4H, CH_2), 2.39 (s, 6H, H_h).

Analytical data as in lit.[3,4]

Macrocycle M1[3]

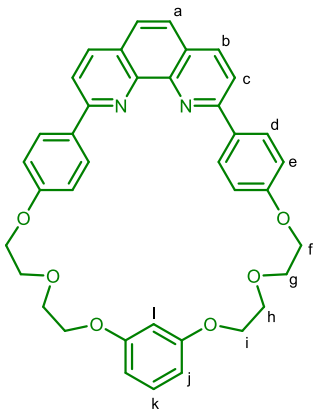

A solution of ditosylate **2.14** (3.80 g, 4.5 mmol), *m*-dihydroxybenzene (493 mg, 4.5 mmol) and dry DMF (400 mL) was degassed with N_2. The degassed mixture was transferred to a dropping funnel and added dropwise to a stirred suspension of Cs_2CO_3 (7.30 g, 22.4 mmol) in dry, degassed DMF (600 mL) over a period of 6 h, under N_2 at 20 °C. 2 h into the addition, the temperature of the reaction was increased to 60 °C. The mixture was left stirring for a further 24 h. The mixture was allowed to cool and the solvent removed under reduced pressure. The crude solid was dissolved in CH_2Cl_2 (250 mL) and washed with brine (3 × 250 mL). The organic layer was dried over Na_2SO_4 and the solvent removed under reduced pressure. The crude material was purified first via a SiO_2 plug (CH_2Cl_2 eluent), then by SiO_2 column chromatography (isocratic EtOAc, then gradient of CH_2Cl_2/MeOH from 1:0 to 9:1, all with a 2% Et_3N additive) to yield macrocycle **M1** (1.66 g, 2.7 mmol, 60%) as a white solid; R_f (CH_2Cl_2/MeOH, 99/1) = 0.84.

^{1}H NMR (400 MHz, $CDCl_3$) δ_H 8.42 (d, J = 8.8 Hz, 4H, H_d), 8.25 (d, J = 8.4 Hz, 2H, H_b), 8.07 (d, J = 8.4 Hz, 2H, H_c), 7.73 (s, 2H, H_a), 7.19 – 7.11 (m, 5H, $H_{e,k}$), 6.65 (t, J = 2.4 Hz, 1H, H_l), 6.55 (dd, J = 8.2, 2.4 Hz, 2H, H_j), 4.33 (dd, J = 6.0, 4.7 Hz, 4H, H_f), 4.22 – 4.14 (m, 4H, H_i), 3.94 (ddd, J = 6.0, 5.1, 4.0 Hz, 8H, $H_{g,h}$).

^{13}C NMR (101 MHz, $CDCl_3$) δ_C 160.2 (C_e-C-O/C_j-C-O), 160.1 (C_j-C-O/C_e-C-O), 156.4 (C_c-C-N), 146.1 (C_a-C-C_b), 136.8 (C_b), 132.8 (N-C-C-C_d), 130.1 (C_k), 129.1 (C_d), 127.6 (N-C-C-N), 125.7 (C_a), 119.3 (C_c), 115.6 (C_e), 106.9 (C_j), 102.8 (C_l), 70.2 ($C_{g/h}$), 69.7 ($C_{h/g}$), 67.9 (C_f), 67.6 (C_i).

HRMS$^+$ m/z = 615.24866 $[M+H]^+$ ($C_{38}H_{35}O_6N_2^+$ requires 615.24896).

Analytical data as in lit.[3]

Macrocycle M2[2]

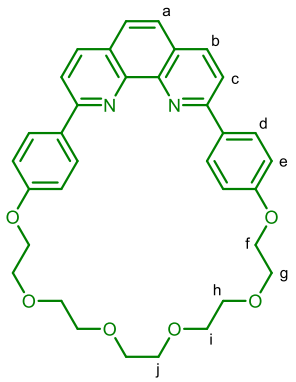

DPP **2.12** (300 mg, 80 μmol) was dissolved in dry DMF (120 mL) to which a solution of pentaethylene glycol di(*p*-toluenesulfonate) (450 mg, 80 μmol) in dry DMF (5 mL) was added. The mixture was degassed with N_2 before dropping into a stirred suspension of Cs_2CO_3 (0.79 g, 4.1 mmol) in dry, degassed DMF (100 mL), over a period of 4 h. The mixture was left stirring at 60 °C under N_2 for 2 d, then allowed to cool and the solvent removed under reduced pressure. The solid was dissolved in CH_2Cl_2 (50 mL) and washed with H_2O (2 × 50 mL), then brine (50 mL). The organic layer was dried over Na_2SO_4 before removing the solvent under reduced pressure. The crude material was purified by SiO_2 column chromatography (isocratic EtOAc, then gradient of CH_2Cl_2/MeOH from 1:0 to 9:1, all with a 2% Et_3N additive) to yield macrocycle **M2** (0.17 g, 30 μmol, 38%) as an off-white solid; R_f (CH_2Cl_2/MeOH, 99/1) = 0.36; m.p. 159-161 °C.

^{1}H NMR (400 MHz, $CDCl_3$) δ_H 8.42 (d, *J* = 8.8 Hz, 4H, H_d), 8.27 (d, *J* = 8.4 Hz, 2H, H_b), 8.07 (d, *J* = 8.4 Hz, 2H, H_c), 7.75 (s, 2H, H_a), 7.19 (d, *J* = 8.8 Hz, 4H, H_e), 4.35 (t, *J* = 5.3 Hz, 4H, H_f), 3.86 (t, *J* = 5.3 Hz, 4H, H_g), 3.76 (s, 4H, H_j), 3.76 – 3.67 (m, 8H, $H_{h,i}$).

^{13}C NMR (101 MHz, $CDCl_3$) δ_C 160.2 (C_e-C-O), 156.6 (C_c-C-N), 146.0 (C_a-C-C_b), 136.7 (C_b), 132.7 (N-C-C-C_d), 129.0 (C_d), 127.4 (N-C-C-N), 125.6 (C_a), 119.2 (C_c), 115.7 (C_e), 71.3 (C_j), 70.8 ($C_{h/i}$), 70.6 ($C_{i/h}$), 69.6 (C_g), 67.9 (C_f).

HRMS$^+$ m/z = 567.24927 $[M+H]^+$ ($C_{34}H_{35}N_2O_6^+$ requires 567.24896).

Analytical data as in lit.[2]

Diolefin macrocyclic precursor 2.22[5]

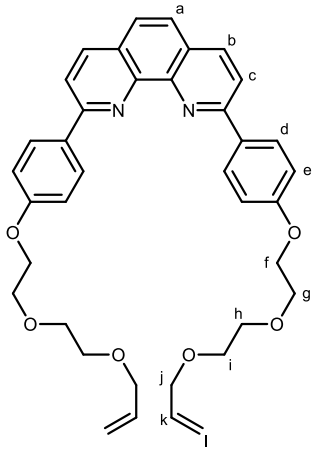

NaH (60% w/w in paraffin, 56 mg, 2.3 mmol) was added to a solution of diphenylphenanthroline diol **2.13** (0.25 g, 93 μmol) in dry DMF (20 mL). Allyl bromide (0.70 mL, 2.1 mmol) was added to the stirred solution, then heated to 80 °C for 6 h under N_2. After allowing to cool, the solvent was removed under reduced pressure, and the solid dissolved in CH_2Cl_2 (20 mL). The solution was washed with water (3 × 20 mL), dried over Na_2SO_4 and the solvent removed under reduced pressure. Purification by SiO_2 chromatography (CH_2Cl_2/MeOH, gradient elution from 1:0 to 9:1) then C_{18} chromatography (pet. ether/CH_2Cl_2 then CH_2Cl_2/MeOH, gradient elution 0:1 to 1:0 then 0:1 to 1:0) yielded diolefin precursor **2.22** (95 mg, 31 μmol, 33%).

^{1}H NMR (500 MHz, $CDCl_3$) δ_H 8.41 (d, *J* = 8.8 Hz, 4H, H_d), 8.21 (d, *J* = 8.4 Hz, 2H, H_b), 8.04 (d, *J* = 8.4 Hz, 2H, H_c), 7.69 (s, 2H, H_a), 7.11 (d, *J* = 8.8 Hz, 4H, H_e), 5.93 (ddt, *J* = 17.3, 10.4, 5.7 Hz,

2H, H_k), 5.38 – 5.09 (m, 4H, H_l), 4.29 – 4.21 (m, 4H, H_f), 4.05 (dt, J = 5.7, 1.4 Hz, 4H, H_j), 3.94 – 3.87 (m, 4H, H_g), 3.79 – 3.73 (m, 4H, H_h), 3.68 – 3.61 (m, 4H, H_i).

^{13}C NMR (126 MHz, $CDCl_3$) δ_C 160.1 (C_e-C-O), 156.3 (C_c-C-C-C_d), 146.0 (C_a-C-C_b), 136.8 (C_b), 134.8 (C_k), 132.3 (C_c-C-C-C_d), 129.0 (C_d), 127.5 (N-C-C-N), 125.6 (C_a), 119.3 (C_c), 117.2 (C_l), 114.9 (C_e), 72.3 (C_j), 71.0 (C_h), 69.8 (C_g), 69.5 (C_i), 67.6 (C_f).

Analytical data as in lit.[5]

***p*-^{t}Bu alcohol 2.15[6]**

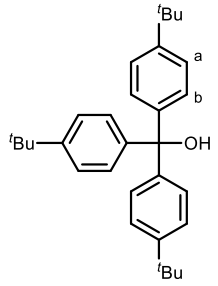

Magnesium turnings (1.43 g, 59.1 mmol) was suspended in dry THF (90 mL) and cooled to 0 °C. 1-bromo-4-*tert*-butylbenzene (12.0 g, 56.3 mmol) was added slowly and the mixture was allowed to gradually warm to 40 °C, where initiation was observed and was left stirring for 2 h. Diethyl carbonate (2.02 g, 17.1 mmol) in dry THF (40 mL) was added dropwise and the mixture stirred for a further 3 h at 40 °C. The reaction was quenched by addition of MeOH (5 mL). A saturated solution of aqueous NH_4Cl (100 mL) was added and the layers separated. The aqueous layer was further extracted with CH_2Cl_2 (3 × 100 mL) before the organic layers were combined and washed with saturated brine solution (100 mL). The organic layer was dried over Na_2SO_4, filtered and solvent removed under reduced pressure. The crude material was purified by SiO_2 chromatography (pet. ether/CH_2Cl_2, gradient elution from 1:0 to 0:1) to yield *p*-^{t}Bu alcohol **2.15** (6.51 g, 52.6 mmol, 89%) as a white solid.

^{1}H NMR (400 MHz, $CDCl_3$) δ_H 7.31 (d, J = 8.8 Hz, 6H, H_b), 7.19 (d, J = 8.8 Hz, 6H, H_a), 2.71 (s, 1H, OH), 1.31 (s, 27H, ^{t}Bu).

Analytical data as in lit.[6]

***p*-^{t}Bu phenol 2.24**[7]

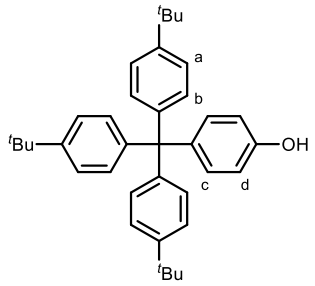

p-^{t}Bu alcohol **2.15** (10 g, 23 mmol, 1.0 eq.) and phenol (45 g, 48 mmol, 21 eq.) were gently warmed to dissolve. Concentrated HCl solution (1.0 mL, 37%) was added and the red-brown solution mixture heated to reflux for 24 h under N_2. After cooling, toluene (150 mL) and NaOH solution (150 mL, 2M) was added and the mixture separated. The organic layer was washed with additional NaOH solution (3 × 150 mL), then water (100 mL) before drying over Na_2SO_4 and removal of solvent under reduced pressure. The crude material was dissolved in CH_2Cl_2 (150 mL) and activated carbon (~15 g) was added. After filtration through a Celite plug, and removal of solvent under reduced pressure, the solid was refluxed in hexane (200 mL) for 30 min. The solid was isolated by filtration and recrystallised in toluene/hexane to yield *p*-^{t}Bu phenol **2.24** (5.2 g, 10 mmol, 43%).

^{1}H NMR (400 MHz, $CDCl_3$) δ_H 7.23 (d, J = 8.7 Hz, 6H, H_b), 7.08 (d, J = 8.8 Hz, 6H, H_a), 7.05 (d, J = 8.9 Hz, 2H, H_c), 6.70 (d, J = 8.9 Hz, 2H, H_d), 4.55 (s, 1H, O<u>H</u>), 1.30 (s, 27H, ^{t}Bu).

Analytical data as in lit.[7]

Pent-4-ynyl tosylate 2.25[8]

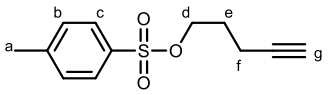

A solution of 4-pentyn-1-ol (5.96 g, 70.9 mmol, 1 eq.) and anhydrous Et_3N (20 mL, 138 mmol, 1.95 eq.) in anhydrous CH_2Cl_2 (200 mL) was cooled to 0 °C. *p*-Toluenesulfonyl chloride (14.3 g, 75.2 mmol, 1.06 eq.) was added and the solution stirred under N_2 at 20 °C for 18 h. The reaction was quenched by addition of H_2O (100 mL) and the organic layer separated. The aqueous layer was extracted with CH_2Cl_2 (30 mL), organic layers combined, dried over Na_2SO_4 and solvent removed under reduced pressure. The resulting crude oil was purified by SiO_2 chromatography

(pet. ether/CH_2Cl_2, gradient elution from 1:0 to 0:1) to yield tosylate **2.25** (14.7 g, 61.7 mmol, 87%) as a colourless oil.

^{1}H NMR (400 MHz, $CDCl_3$) δ_H 7.79 (d, J = 8.3 Hz, 2H, H_c), 7.34 (d, J = 8.3 Hz, 2H, H_b), 4.14 (t, J = 6.1 Hz, 2H, H_e), 2.44 (s, 3H, H_a), 2.25 (td, J = 6.9, 2.7 Hz, 2H, H_f), 1.88 (t, J = 2.7 Hz, 1H, H_g), 1.87 – 1.81 (m, 2H, H_e).

Analytical data as in lit.[8]

Extended *p*-^{t}Bu stopper 2.26[8]

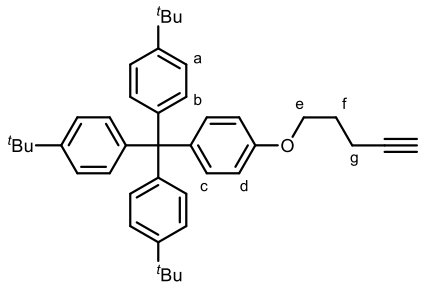

A solution of *p*-^{t}Bu phenol **2.24** (1.00 g, 1.98 mmol, 1 eq.) and pent-4-ynyl tosylate **2.25** (750 mg, 3.15 mmol, 1.59 eq.) in butanone (20 mL) containing K_2CO_3 (1.25 g, 9.91 mmol, 5 eq.) and 18-crown-6 (15 mg, catalytic amount) was heated under reflux for 18 h. After cooling to room temperature, the reaction mixture was filtered through Celite and the solid washed with CH_2Cl_2 (10 mL). The combined organic layers were concentrated under reduced pressure, and the solid dissolved in CH_2Cl_2 (15 mL). The solution was washed with water (10 mL), then brine (10 mL), dried over Na_2SO_4 and solvent removed under reduced pressure. The crude material was purified by SiO_2 chromatography (pet. ether/CH_2Cl_2, gradient elution from 1:0 to 0:1) to yield extended *p*-^{t}Bu stopper **2.26** (1.01 g, 1.76 mmol, 89%) as a white solid.

^{1}H NMR (400 MHz, $CDCl_3$) δ_H 7.23 (d, J = 8.8 Hz, 6H, H_b), 7.10 – 7.06 (m, 8H, $H_{a,c}$), 6.77 (d, J = 9.0 Hz, 2H, H_d), 4.04 (t, J = 6.1 Hz, 2H, H_e), 2.40 (td, J = 7.0, 2.7 Hz, 2H, H_g), 2.03 – 1.97 (m, 2H, H_f), 1.96 (t, J = 2.6 Hz, 1H, C≡C<u>H</u>), 1.30 (s, 27H, ^{t}Bu).

Analytical data as in lit.[8]

Synthesis of Novel Compounds

p-^{t}Bu monoyne 2.17

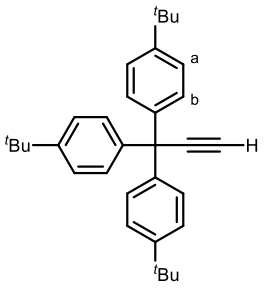

p-^{t}Bu alcohol **2.15** (1.30 g, 3.00 mmol) was dissolved in dry THF (12 mL) and oxalyl chloride (1.4 mL, 16.6 mmol) was added slowly. The mixture was allowed to stir under N_2 at 20 °C for 4 h. The solvents were removed under reduced pressure, and the remaining solid suspended in dry THF (6 mL). Ethynyl magnesium bromide (0.5 M solution in THF, 30 mL, 15.0 mmol) was added and the mixture allowed to stir under N_2 at 20 °C for a further 3 d. The mixture was cooled to 0 °C before addition of a saturated solution of aqueous NH_4Cl (10 mL). Et_2O (20 mL) was added and the organic layer separated, then the aqueous layer washed with CH_2Cl_2 (2 × 10 mL). The combined organic layers were dried over Na_2SO_4 and the solvent removed under reduced pressure. The crude material was purified by SiO_2 chromatography (pet. ether/CH_2Cl_2, gradient elution from 1:0 to 0:1) to yield *p*-^{t}Bu monoyne **2.17** (1.30 g, 2.94 mmol, 98%) as a white solid; R_f (petroleum ether) = 0.19.

^{1}H NMR (500 MHz, $CDCl_3$) δ_H 7.31 (d, J = 8.7 Hz, 6H, H_b), 7.19 (d, J = 8.5 Hz, 6H, H_a), 2.68 (s, 1H, C≡C<u>H</u>), 1.32 (s, 27H, ^{t}Bu).

^{13}C NMR (126 MHz, $CDCl_3$) δ_C 149.61 (C_a-<u>C</u>), 142.19 (C_b-<u>C</u>), 128.76 (C_a), 124.96 (C_b), 90.54 (C≡C), 72.91 (C≡C), 54.46 (C-Ar_3), 34.55 (<u>C</u>-$(CH_3)_3$), 31.52 (C-(<u>C</u>$H_3)_3$).

HRMS$^+$ m/z = 436.3129 $[M+H]^+$ ($C_{33}H_{40}^+$ requires 436.3125).

p-^{t}Bu monoyne bromide 2.18

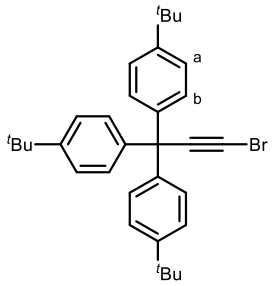

p-^{t}Bu monoyne **2.17** (200 mg, 458 μmol), *N*-bromosuccinimide (163 mg, 916 μmol) and silver nitrate (24.9 mg, 147 μmol) were dissolved in acetone (1.5 mL) and stirred at 20 °C for 2 h. The solvent was removed under reduced pressure and the crude solid material purified by SiO_2 chromatography (pet. ether/CH_2Cl_2, gradient elution from 1:0 to 0:1) to yield *p*-^{t}Bu monoyne bromide **2.18** (179 mg, 348 μmol, 76%) as an off-white solid.

^{1}H NMR (500 MHz, $CDCl_3$) δ_H 7.33 (d, J = 8.6 Hz, 6H, H_b), 7.18 (d, J = 8.6 Hz, 6H, H_a), 1.36 (s, 27H, ^{t}Bu).

^{13}C NMR (126 MHz, $CDCl_3$) δ_C 149.7 (C_a-C), 142.0 (C_b-C), 128.8 (C_a), 125.0 (C_b), 86.3 (C≡CBr), 55.7 (C-Ar_3), 43.5 (C-C≡CBr), 34.6 (C-$(CH_3)_3$), 31.5 (C-$(CH_3)_3$).

Trichlorophenanthroline 2.6

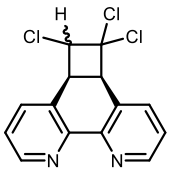

1,10-Phenanthroline (2.20 g, 12.2 mmol) and benzophenone (220 mg, 1.21 mmol) was dissolved in trichloroethylene (32 mL, 355 mmol). The mixture was divided into 16 NMR tubes and subject to UV irradiation at 350 nm for 7 d. The contents of the tubes were combined and the solvent removed under reduced pressure. The crude product was purified by reverse phase (C18) chromatography (gradient elution of H_2O/MeOH from 1:0 to 0:1) to yield both *syn*-trichlorophenanthroline **2.6** (0.36 g, 1.5 mmol, 9.5%) and *anti*-trichlorophenanthroline **2.6** (2.0 g, 6.5 mmol, 54%) as white solids.

HRMS$^+$ m/z = 310.99048 $[M+H]^+$ ($C_{14}H_{10}N_2{}^{35}Cl_3^+$ requires 310.99041).

^{1}H NMR (400 MHz, $CDCl_3$) δ_H 8.80 (dd, *J* = 4.7, 1.7 Hz, 1H, H_i), 8.72 (dd, *J* = 4.6, 1.7 Hz, 1H, H_a), 7.56 (dd, *J* = 7.8, 1.7 Hz, 1H, H_g), 7.48 (dd, *J* = 7.8, 1.7 Hz, 1H, H_c), 7.29 (dd, *J* = 7.9, 4.7 Hz, 1H, H_h), 7.25 (dd, *J* = 7.8, 4.6 Hz, 1H, H_b), 5.44 (dd, *J* = 9.4 Hz, 1H, H_2), 4.50 (d, *J* = 9.4 Hz, 1H, H_f), 4.32 (t, *J* = 9.4 Hz, 1H, H_d).

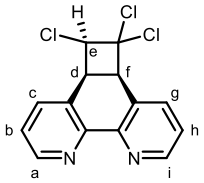

^{13}C NMR (101 MHz, $CDCl_3$) δ_C 150.9 (C_i), 150.9 (C_i-N-C), 149.9 (C_a-N-C), 149.8 (C_a), 138.6 (C_c), 136.7 (C_g), 126.3 (C_c-C-C_d), 125.3 (C_f-C-C_g), 124.2 (C_h), 123.3 (C_b), 90.5 (C_e-CCl_2), 68.9 (C_e), 51.5 (C_f), 38.5 (C_d).

m.p. 236-238 °C.

^{1}H NMR (400 MHz, $CDCl_3$) δ_H 8.66 (dd, *J* = 4.6, 1.0 Hz, 1H, H_a), 8.63 (dd, *J* = 4.7, 1.7 Hz, 1H, H_i), 7.56 (ddd, 1H, *J* = 7.8, 1.0 Hz, H_c), 7.38 (dd, *J* = 7.6, 1.7 Hz, 1H, H_g), 7.21 (dd, *J* = 7.8, 4.6 Hz, 1H, H_b), 7.13 (dd, *J* = 7.6, 4.7 Hz, 1H, H_h), 4.46 (d, *J* = 9.5 Hz, 1H, H_f), 4.40 (d, *J* = 9.5 Hz, 1H, H_e), 3.84 (t, *J* = 9.5 Hz, 1H, H_d).

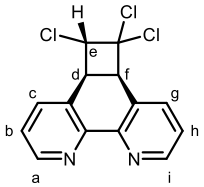

^{13}C NMR (101 MHz, $CDCl_3$) δ_C 150.4 (C_a), 150.2 (C_i), 148.6 (C_a-N-C), 148.3 (C_i-N-C), 139.7 (C_c), 135.5 (C_g), 127.6 (C_f-C-C_g), 126.0 (C_c-C-C_d), 124.1 (C_h), 123.5 (C_b), 89.4 (C_e-CCl_2), 70.4 (C_e), 52.6 (C_f), 42.1 (C_d).

m.p. 209-210 °C.

Dichlorophenanthroline 2.7

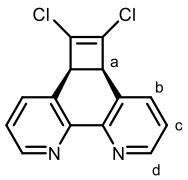

Trichlorophenanthroline **2.6** (2.39 g, 7.66 mmol) and Cs_2CO_3 (19.5 g, 59.8 mmol) were dissolved in dry MeCN (150 mL) and the mixture was stirred under N_2 at 20 °C for 24 h. The solid was removed by filtration through Celite, and then the solvent removed under reduced pressure. The crude material was purified by reverse phase (C18) chromatography (H_2O/MeOH, gradient elution from 1:0 to 0:1) to yield dichlorophenanthroline **2.7** (1.88 g, 6.82 mmol, 89%) as a white solid.

^{1}H NMR (400 MHz, $CDCl_3$) δ_H 8.72 (dd, *J* = 4.6, 1.7 Hz, 2H, H_d), 7.53 (dd, *J* = 7.7, 1.8 Hz, 2H, H_c), 7.24 (dd, *J* = 7.7, 4.7 Hz, 2H, H_b), 4.32 (s, 2H, H_a).

^{13}C NMR (101 MHz, $CDCl_3$) δ_C 149.9 (C_d), 148.6 (N-C-C-N), 136.9 (C_b), 128.8 (C_a-C-C_b), 127.5 (CCl_2-C_a), 124.0 (C_c), 46.0 (C_a).

HRMS$^+$ m/z = 275.01364 $[M+H]^+$ ($C_{14}H_9N_2{}^{35}Cl_2^+$ requires 275.01373).

TIPS-protected phenanthroline-masked triyne 2.8

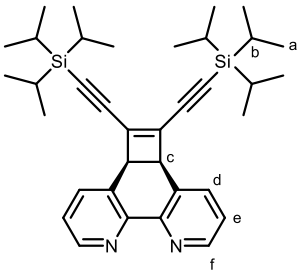

Method A: Dichlorophenanthroline **2.7** (200 mg, 0.72 mmol), $Pd(PPh_3)_4$ (50 mg, 0.04 mmol) and CuI (22 mg, 0.12 mmol) were combined in a Schlenk flask and thoroughly degassed. Piperidine (4 mL) was dried over KOH, distilled and thoroughly degassed before adding to the mixture, along with (triisopropylsilyl)acetylene-acetylene (0.80 mL, 3.8 mmol). The mixture was stirred at under N_2 at 50 °C for 2 d. The mixture was allowed to cool and the solvent evaporated under reduced pressure. The solid was dissolved in CH_2Cl_2 (25 mL) and washed with EDTA/NH_3 solution (2 × 50 mL) then brine (25 mL) before drying over Na_2SO_4 and evaporating solvent under reduced pressure. The crude material was purified by SiO_2 chromatography (pet. ether/EtOAc, gradient elution from 1:0 to 0:1) to yield TIPS-protected masked triyne **2.8** as a brown solid (106 mg, 0.21 mmol, 29%).

Method B: Dichlorophenanthroline **2.7** (200 mg, 0.72 mmol), $Pd_2(dba)_3$ (33.3 mg, 36.4 μmol), XPhos (52.0 mg, 109 μmol) and CuI (22.8 mg, 116 μmol) were combined in a Schlenk tube and thoroughly degassed. TIPS-acetylene (0.8 mL, 3.56 mmol), freshly-distilled diisopropylamine (0.92 mL, 6.54 mmol) and dry 1,4-dioxane (4.0 mL) were combined in a second Schlenk tube and thoroughly degassed. The solution was transferred via cannula to the solids, then the mixture stirred under N_2 at 80 °C for 18 h. The solvent was removed under reduced pressure and the residual solid dissolved in CH_2Cl_2 (15 mL). EDTA/NH_3 solution (15 mL) was added and the organic layer extracted. The aqueous layer was further washed with

CH_2Cl_2 (2 × 15 mL) and the combined organic extracts dried over Na_2SO_4 before removing the solvent under reduced pressure. The crude material was purified by SiO_2 chromatography (CH_2Cl_2/MeOH, gradient elution from 1:0 to 9:1) to yield TIPS-protected masked triyne **2.8** as a brown solid (377 mg, 0.66 mmol, 91%); m.p. 204-207 °C.

^{1}H NMR (400 MHz, $CDCl_3$) δ_H 8.71 (dd, *J* = 4.6, 1.8 Hz, 2H, H_f), 7.58 (dd, *J* = 7.7, 1.8 Hz, 2H, H_d), 7.22 (dd, *J* = 7.7, 4.6 Hz, 2H, H_e), 4.30 (s, 2H, H_c), 1.04 – 1.00 (m, 42H, $H_{a.b}$).

^{13}C NMR (101 MHz, $CDCl_3$) δ_C 149.42 (C_f), 149.03 (N-C-C-N), 136.89 (C_d), 134.62 (C_c-C=C), 130.88 (C_c-C-C_d), 123.91 (C_e), 100.83 (Si-C≡C), 98.86 (Si-C≡C), 44.04 (C_c), 18.63 (C_a), 11.18 (C_b).

HRMS$^+$ m/z = 567.35773 $[M+H]^+$ ($C_{36}H_{51}N_2{}^{28}Si_2^+$ requires 567.35853).

TES-protected phenanthroline-masked triyne

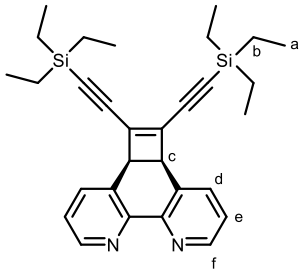

Dichlorophenanthroline **2.7** (50 mg, 0.18 mmol), $Pd(PPh_3)_4$ (13 mg, 11 μmol) and CuI (5.5 mg, 29 μmol) were combined in a Schlenk flask and were thoroughly degassed. Piperidine (1 mL) was dried over KOH and freshly distilled before adding to the solids, followed by addition of TES-acetylene (0.15 mL, 818 μmol). The mixture was warmed to 50 °C and left to stir under N_2 for 2 d. The mixture was allowed to cool and the solvent evaporated under reduced pressure. The solid was dissolved in CH_2Cl_2 (15 mL) and washed with EDTA/NH_3 solution (15 mL) then before drying over Na_2SO_4 and evaporating solvent under reduced pressure. The crude material was purified by SiO_2 chromatography (pet. ether/EtOAc, gradient elution from 1:0 to 0:1) to yield TES-protected phenanthroline-masked triyne as a brown solid (12 mg, 25 μmol 14%).

^{1}H NMR (500 MHz, $CDCl_3$) δ_H 8.73 (dd, *J* = 4.7, 1.7 Hz, 2H, H_f), 7.60 (dd, *J* = 7.6, 1.7 Hz, 2H, H_d), 7.25 (dd, *J* = 7.6, 4.7 Hz, 2H, H_e), 4.31 (s, 2H, H_c), 0.96 (t, *J* = 7.9 Hz, 18H, H_a), 0.59 (q, *J* = 7.9 Hz, 12H, H_b).

^{13}C NMR (126 MHz, $CDCl_3$) δ_C 149.5 (C_f), 149.1 (N-<u>C</u>-<u>N</u>-N), 136.8 (C_d), 134.7 (C_c-<u>C</u>=<u>C</u>), 130.8 (C_c-<u>C</u>-C_d), 123.9 (C_e), 102.0 (Si-<u>C</u>≡C), 98.2 (Si-C≡<u>C</u>), 44.1 (C_c), 7.52 (C_a), 4.33 (C_b).

HRMS$^+$ m/z = 483.26450 $[M+H]^+$ ($C_{30}H_{39}N_2{}^{28}Si_2{}^+$ requires 483.26463).

TMS-protected phenanthroline-masked triyne

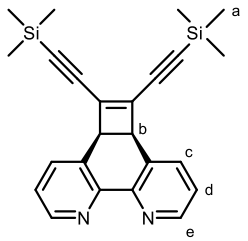

Dichlorophenanthroline **2.7** (200 mg, 0.72 μmol), $Pd_2(dba)_3$ (33 mg, 36 μmol), XPhos (52 mg, 110 μmol) and CuI (22 mg, 120 μmol) were combined in a Schlenk tube and thoroughly degassed. TMS-acetylene (0.49 mL, 3.6 mmol), dry diisopropylamine (0.92 mL, 6.5 mmol) and dry 1,4-dioxane (4.0 mL) were combined in a second Schlenk tube and thoroughly degassed. The solution was transferred via cannula to the solids, then the mixture stirred under N_2 at 80 °C for 18 h. The solvent was removed under reduced pressure and the residual solid dissolved in CH_2Cl_2 (15 mL). EDTA/NH_3 solution (15 mL) was added and the organic layer extracted. The aqueous layer was further washed with CH_2Cl_2 (2 × 15 mL) and the combined organic extracts dried over Na_2SO_4 before removing the solvent under reduced pressure. The crude material was purified by SiO_2 chromatography (CH_2Cl_2/MeOH, gradient elution from 1:0 to 9:1) to yield TMS-protected phenanthroline-masked triyne as a brown solid (210 mg, 0.52 mmol, 72%).

^{1}H NMR (400 MHz, $CDCl_3$) δ_H 8.71 (dd, *J* = 4.6, 1.8 Hz, 2H, H_e), 7.56 (dd, *J* = 7.7, 1.8 Hz, 2H, H_c), 7.24 (dd, *J* = 7.7, 4.6 Hz, 2H, H_d), 4.26 (s, 2H, H_b), 0.16 (s, 18H, H_a).

^{13}C NMR (101 MHz, $CDCl_3$) δ_C 149.4 (C_e), 149.0 (N-<u>C</u>-<u>C</u>-N), 136.7 (C_c), 134.2 (C_b-<u>C</u>=<u>C</u>), 130.6 (C_b-C-C_c), 123.9 (C_d), 104.5 (Si-<u>C</u>≡C), 96.9 (Si-C≡<u>C</u>), 44.1 (C_b), -0.2 (C_a).

HRMS$^+$ m/z = 399.17068 $[M+H]^+$ ($C_{24}H_{27}N_2{}^{28}Si_2{}^+$ requires 399.17073).

Deprotected phenanthroline-masked triyne 2.19

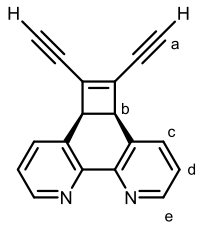

TIPS-protected phenanthroline **2.8** (50 mg, 88 μmol) was degassed with N_2. Dry THF (5 mL), H_2O (50 μL, 1% v/v) and tetrabutylammonium fluoride (1.0 M solution in THF, 88 μL, 88 μmol) were combined, then added to the phenanthroline. The mixture was allowed to stir at under N_2 at 20 °C for 10 minutes. Saturated NH_4Cl solution (5 mL) then CH_2Cl_2 (10 mL) was added, and the organic layer separated. The aqueous layer was washed with CH_2Cl_2 (2 × 5 mL). The combined organic layers were dried over Na_2SO_4 and the solvent removed under reduced pressure. The material was purified by SiO_2 chromatography (CH_2Cl_2/MeOH, gradient elution from 1:0 to 9:1) to yield deprotected masked triyne **2.19** as a white solid (21 mg, 81 μmol, 92%).

^{1}H NMR (500 MHz, $CDCl_3$) δ_H 8.76 (dd, *J* = 4.6, 1.7 Hz, 2H, H_e), 7.63 (dd, *J* = 7.7, 1.7 Hz, 2H, H_c), 7.30 (dd, *J* = 7.7, 4.6 Hz, 2H, H_d), 4.36 (s, 2H, H_b), 3.37 (s, 2H, H_a).

^{13}C NMR (126 MHz, $CDCl_3$) δ_C 149.7 (C_e), 149.0 (N-C-C-N), 136.9 (C_c), 135.1 (C_b-C=C), 130.3 (C_b-C-C_c), 124.2 (C_d), 85.7 (C_a), 75.9 (C_a≡C), 44.2 (C_b).

HRMS$^+$ m/z = 255.09189 $[M+H]^+$ ($C_{18}H_{11}N_2^+$ requires 255.09167).

Phenanthroline thread 2.20

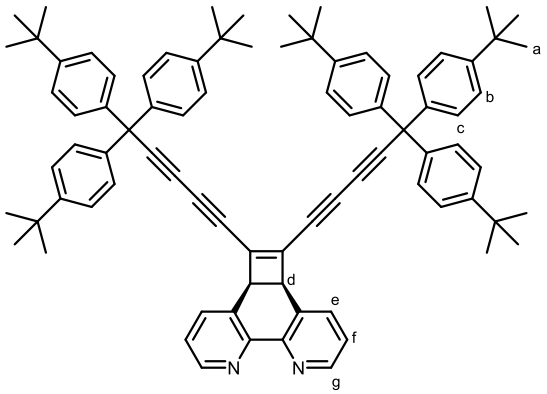

TIPS-protected phenanthroline **2.8** (50 mg, 88 μmol) was degassed and dissolved in dry, degassed THF (5 mL). Degassed H_2O (50 μL, 1% v/v) was added to the mixture before slow

addition of tetrabutylammonium fluoride (1.0 M solution in THF, 88 μL, 88 μmol). The mixture was allowed to stir at under N_2 at 20 °C for 30 minutes. Saturated NH_4Cl solution (10 mL) was added, and the organic layer extracted with CH_2Cl_2 (3 × 5 mL). The combined organic layers were dried over Na_2SO_4 and the solvent removed under reduced pressure. The material was purified by SiO_2 chromatography (CH_2Cl_2/MeOH, gradient elution from 100:0 to 90:10). Fractions containing deprotected phenanthroline **2.19** were dried. Brominated stopper **2.18** (98 mg, 0.19 mmol), anhydrous K_2CO_3 (48 mg, 0.35 mmol) and CuI (3.3 mg, 17 μmol) were added to the dried phenanthroline. CH_2Cl_2 (1 mL) and butan-1-ol (1 mL) were added and the mixture stirred under N_2 at 30 °C for 20 h. Saturated EDTA/NH_3 solution (10 mL) and CH_2Cl_2 (10 mL) were added to the mixture, and the organic layer extracted. The aqueous layer was washed with CH_2Cl_2 (2 × 5 mL), the organic extracts combined and dried over Na_2SO_4 and the solvent removed under reduced pressure. The crude material was purified first by SiO_2 chromatography (CH_2Cl_2/MeOH, gradient elution from 1:0 to 9:1), then by C18 chromatography (petrol ether/CH_2Cl_2 then CH_2Cl_2/MeOH, gradient elution from 1:0 to 0:1) to yield stoppered phenanthroline thread **2.20** as a pale brown solid (38 mg, 34 μmol, 39%).

^{1}H NMR (500 MHz, $CDCl_3$) δ_H 8.76 (dd, *J* = 4.7, 1.7 Hz, 2H, H_g), 7.64 (dd, *J* = 7.8, 1.7 Hz, 2H, H_e), 7.33 (dd, *J* = 7.8, 4.7 Hz, 2H, H_f), 7.30 (d, *J* = 8.6 Hz, 12H, H_b), 7.11 (d, *J* = 8.6 Hz, 12H, H_c), 4.36 (s, 2H, H_d), 1.30 (s, 54H, H_a).

^{13}C NMR (126 MHz, $CDCl_3$) δ_C 150.0 (C_b-C-$C(C_a)_3$), 149.7 (C_g), 149.0 (N-C-C-N), 141.2 (C_c-C$(Ar)_3$), 137.0 (C_e), 136.0 (C_d-C=C), 130.3 (C_d-C-C_e), 128.8 (C_c), 125.1 (C_b), 124.5 (C_f), 94.0 ($C(Ar)_3$-C≡C), 83.2 ($C(Ar)_3$-C≡C/C=C-C≡C), 70.2 (C=C-C≡C), 69.0 (C=C-C≡C/$C(Ar)_3$-C≡C), 55.7 (C$(Ar)_3$), 44.6 (C_d), 34.6 (C_a-C), 31.9 (C_a).

HRMS$^+$ m/z = 1123.68347 $[M+H]^+$ ($C_{84}H_{88}N_2^+$ requires 1123.68638).

UV-Vis (CH_2Cl_2): λ_{max} / nm (ε / mol^{-1} dm^3 cm^{-1}) 358 (34100), 333 (18800), 319 (18300), 309 (22500), 275 (16000), 255 (23000), 229 (64000)

Extended phenanthroline thread 2.27

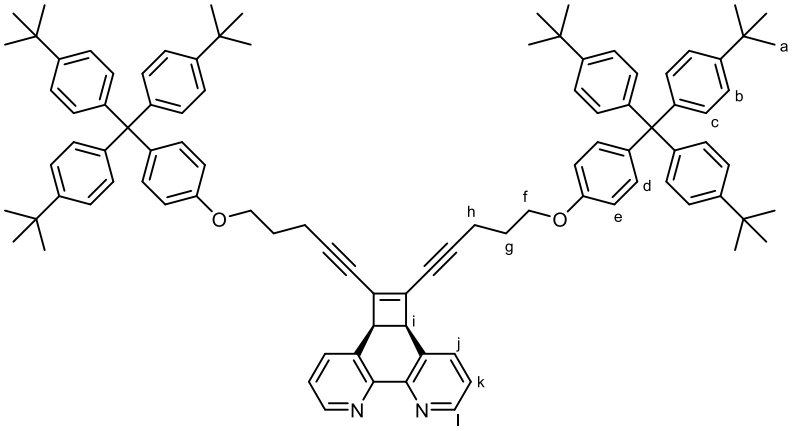

Dichlorophenanthroline **2.7** (25 mg, 91 μmol), extended stopper **2.26** (254 mg, 0.45 mmol), $Pd_2(dba)_3$ (4.2 mg, 4.5 μmol), XPhos (6.5 mg, 14 μmol) and CuI (2.8 mg, 15 μmol) were combined in a dry Schlenk tube and degassed with N_2. Separately, freshly-distilled diisopropyl amine (0.11 mL, 818 μmol) and dry 1,4-dioxane (1 mL) were combined and thorough degassed with N_2, then added to the solids. The mixture was stirred at 85 °C under N_2 for 18 h. The reaction mixture was allowed to cool before addition of CH_2Cl_2 (10 mL) and saturated EDTA/NH_3 solution (10 mL). The mixture was extracted and the aqueous layer washed with CH_2Cl_2 (2 × 10 mL), and the combined extracts dried over Na_2SO_4 and the solvent removed under reduced pressure. The crude solid was purified first by SiO_2 chromatography (CH_2Cl_2/MeOH, gradient elution from 1:0 to 9:1), then by size-exclusion chromatography (Bio Rad S-X3, $CHCl_3$) to yield stoppered phenanthroline **2.27** (38 mg, 28 μmol, 31%) as a pale-yellow solid.

^{1}H NMR (400 MHz, $CDCl_3$) δ_H 8.66 (dd, *J* = 4.6, 1.7 Hz, 2H, H_l), 7.49 (dd, *J* = 7.7, 1.7 Hz, 2H, H_j), 7.23 (d, *J* = 8.6 Hz, 12H, H_b), 7.14 – 7.03 (m, 20H, $H_{c,d,k}$), 6.75 (d, *J* = 8.9 Hz, 4H, H_e), 4.21 (s, 2H, H_i), 4.02 – 3.91 (m, 4H, H_f), 2.56 (t, *J* = 6.7 Hz, 4H, H_h), 1.95 (p, *J* = 6.7 Hz, 4H, H_g), 1.30 (s, 54H, H_a).

^{13}C NMR (101 MHz, $CDCl_3$) δ_C 156.8 ($\underline{C}Ar_4$), 149.3 (C_l), 149.0 (N-$\underline{C}$-$\underline{C}$-N), 148.4 (C_b-$\underline{C}$-$C(CH_3)_3$), 144.2 (C_c-$\underline{C}$-CAr_4), 139.9 (C_e-$\underline{C}$-O), 136.7 (C_j), 133.4 (C_i-$\underline{C}$-C≡C), 132.4 (C_d), 131.2 (C_i-$\underline{C}$-C_j), 130.8 (C_c), 124.2 (C_b), 124.0 (C_k), 113.1 (C_e), 97.5 (C_h-$\underline{C}$≡C), 74.6 (C_h-C≡$\underline{C}$), 65.9 (C_f), 63.2 (CAr_4-$\underline{C}$-C_c), 44.0 (C_i), 34.4 (C_b-C-$\underline{C}$-$C(CH_3)_3$), 31.5 (C_a), 28.7 (C_g), 16.6 (C_h).

HRMS$^+$ m/z = 1343.8367 $[M+H]^+$ ($C_{98}H_{107}N_2O_2^+$ requires 1343.8327).

TIPS-protected extended phenanthroline

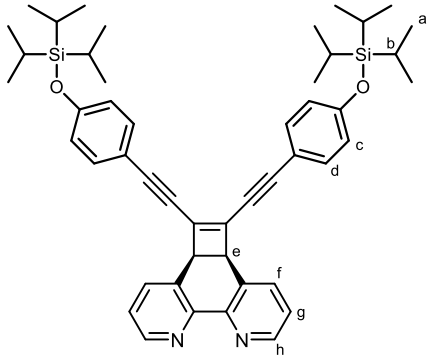

Dichlorophenanthroline **2.7** (100 mg, 36.6 μmol), (4-ethynylphenoxy)triisopropylsilane (489 mg, 1.78 mmol), $Pd_2(dba)_3$ (16.6 mg, 18.2 μmol), XPhos (26.0 mg, 54.5 μmol) and CuI (11.1 mg, 58.2 μmol) were combined in a dry Schlenk tube and thoroughly degassed. A degassed solution of dry 1,4-dioxane (3 mL) and freshly-distilled diisopropylamine (0.46 mL, 3.3 mmol) were added and the mixture stirred at 85 °C under N_2 for 2.5 h. CH_2Cl_2 (15 mL) and EDTA/NH_3 solution (15 mL) were added to the cooled solution and the organic layer extracted. The aqueous layer was washed with CH_2Cl_2 (2 × 10 mL), combined, and dried over Na_2SO_4 before removing the solvent under reduced pressure. The crude material was purified by SiO_2 chromatography (CH_2Cl_2/MeOH, gradient elution from 1:0 to 9:1) to yield TIPS-protected extended phenanthroline **2.7** (230 mg, 30.7 μmol, 84%) as a yellow solid.

^{1}H NMR (500 MHz, $CDCl_3$) δ_H 8.75 (dd, *J* = 4.7, 1.7 Hz, 2H, H_h), 7.69 (dd, *J* = 7.7, 1.8 Hz, 2H, H_f), 7.33 (d, *J* = 8.6 Hz, 4H, H_d), 7.30 (dd, *J* = 7.7, 3.0 Hz, 2H, H_g), 6.82 (d, *J* = 8.6 Hz, 4H, H_c), 4.43 (s, 2H, H_e), 1.28 – 1.22 (m, 6H, H_b), 1.09 (d, *J* = 7.4 Hz, 36H, H_a).

^{13}C NMR (126 MHz, $CDCl_3$) δ_C 157.3 (C_d-C-C≡C), 149.5 (C_h), 149.2 (N-C-C-N), 136.8 (C_f), 133.6 (C_d), 133.1 (C_e-C-C≡C), 131.3 (C_e-C-C_f), 124.1 (C_g), 120.2 (C_c), 114.7 (C_c-C-O), 97.8 (C_d-C-C≡C), 81.7 (C_d-C-C≡C), 44.4 (C_e), 18.0 (C_a), 12.8 (C_b).

HRMS$^+$ m/z = 751.4102 $[M+H]^+$ ($C_{48}H_{59}N_2O_2Si_2^+$ requires 751.4110).

Extended phenanthroline

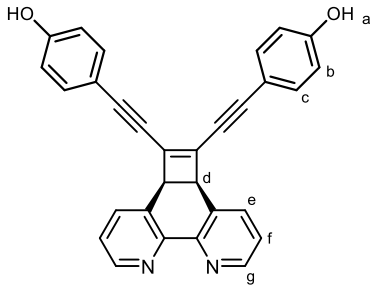

TBAF (0.14 mL, 0.14 mmol, 1.0 M in THF) was added to a solution of TIPS-protected extended phenanthroline (50 mg, 67 μmol) in dry CH_2Cl_2 (4 mL). The mixture was stirred at 20 °C under N_2 for 10 min. The reaction was quenched by addition of saturated NH_4Cl solution (2 mL), then passed through a SiO_2 plug and washed with MeOH. The solvent was removed under reduced pressure to yield a crude yellow solid. Reverse phase C18 chromatography (H_2O/MeOH, gradient elution from 1:0 to 0:1) yield extended phenanthroline (21 mg, 48 μmol, 72%) as a yellow solid.

^{1}H NMR (500 MHz, MeOD) δ_H 8.61 (dd, *J* = 4.7, 1.7 Hz, 2H, H_g), 7.81 (dd, *J* = 7.8, 1.7 Hz, 2H, H_e), 7.42 (dd, *J* = 7.8, 4.7 Hz, 2H, H_f), 7.30 (d, *J* = 8.7 Hz, 4H, H_c), 6.76 (d, *J* = 8.7 Hz, 4H, H_b), 4.43 (s, 2H, H_d).

^{13}C NMR (126 MHz, MeOD) δ_C 160.02 (C_c-C-C≡C), 149.56 (N-C-C-N), 149.26 (C_g), 138.74 (C_e), 134.58 (C_c), 133.9 (C_d-C-C≡C), 133.3 (C_d-C-C_e), 125.7 (C_f), 116.7 (C_b), 114.0 (C_b-C-O), 99.1 (C_c-C-C≡C), 81.7 (C_c-C-C≡C), 49.5, 45.4 (C_d).

HRMS$^+$ m/z = 439.1441[M+H]$^+$ ($C_{30}H_{19}N_2O_2^+$ requires 439.1441).

Selected NMR Spectra

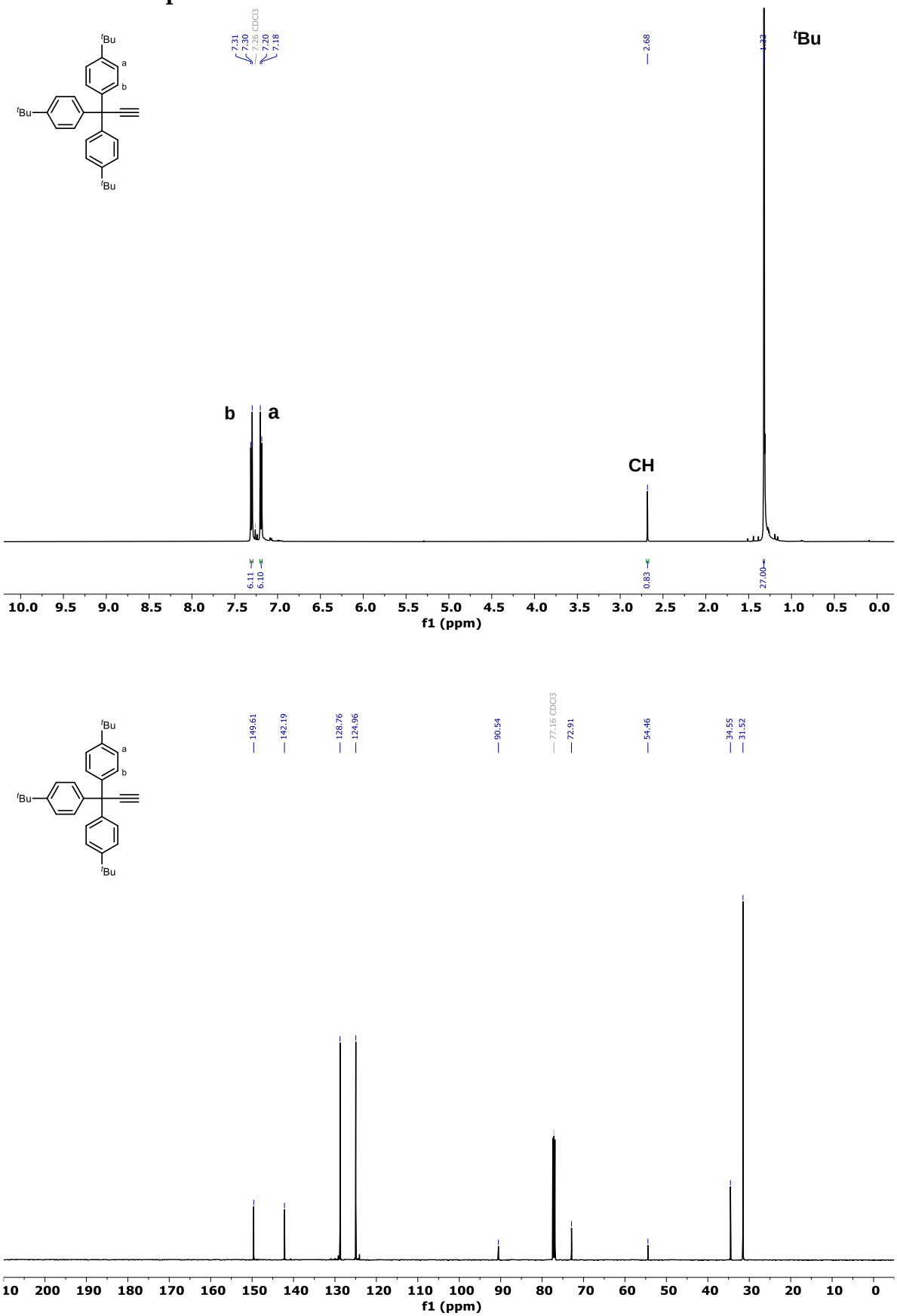

Figure S2.1: (top) ^{1}H NMR (500 MHz) and (bottom) ^{13}C NMR (126 MHz) spectra of *p*-^{t}Bu monoyne **2.17** ($CDCl_3$, 298 K).

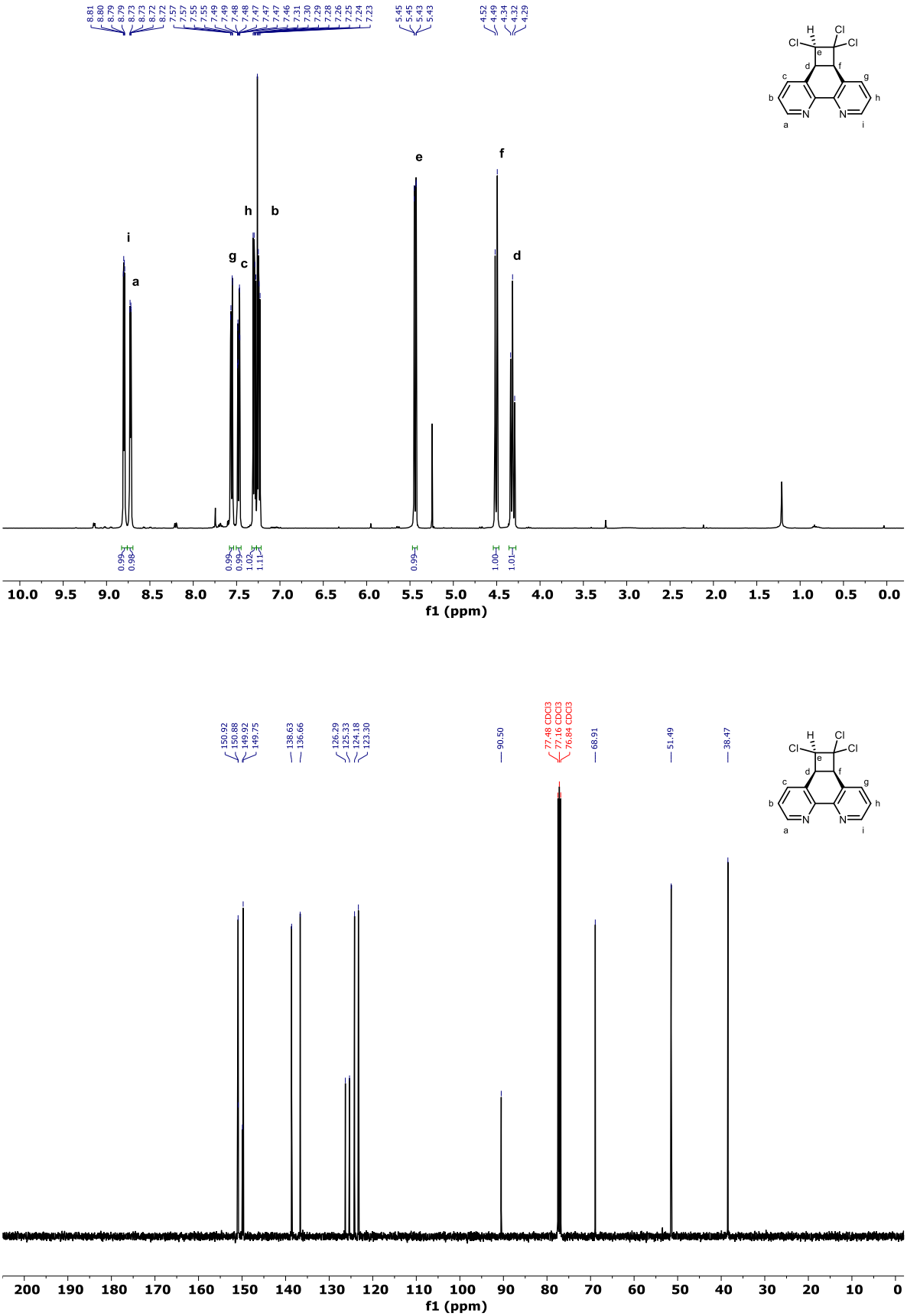

Figure S2.2: (top) ^{1}H NMR (400 MHz) and (bottom) ^{13}C NMR (101 MHz) spectra of *syn*-trichloride **2.6** ($CDCl_3$, 298 K).

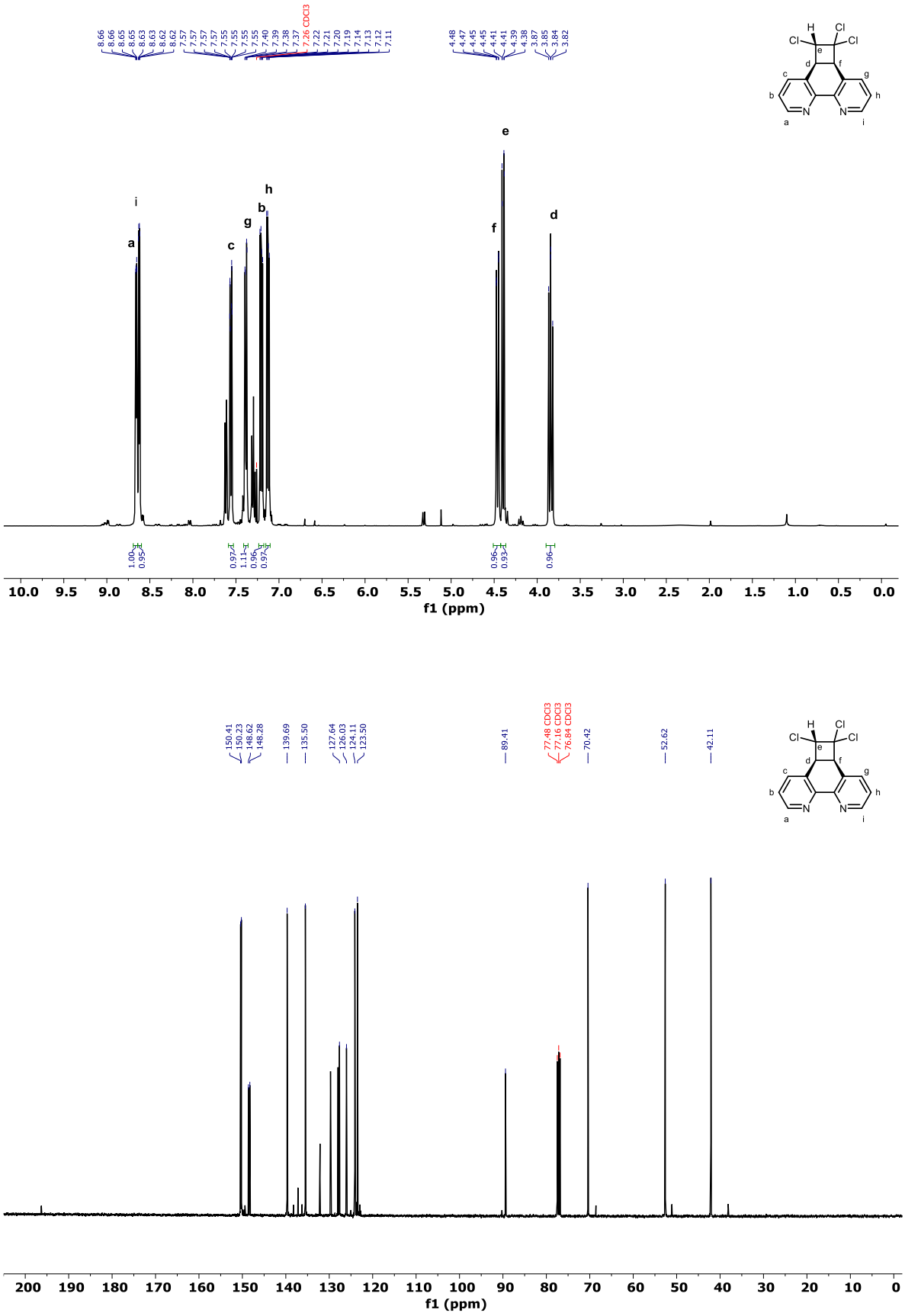

Figure S2.3: (top) ^{1}H NMR (400 MHz) and (bottom) ^{13}C NMR (101 MHz) spectra of *anti*-trichloride **2.6** ($CDCl_3$, 298 K).

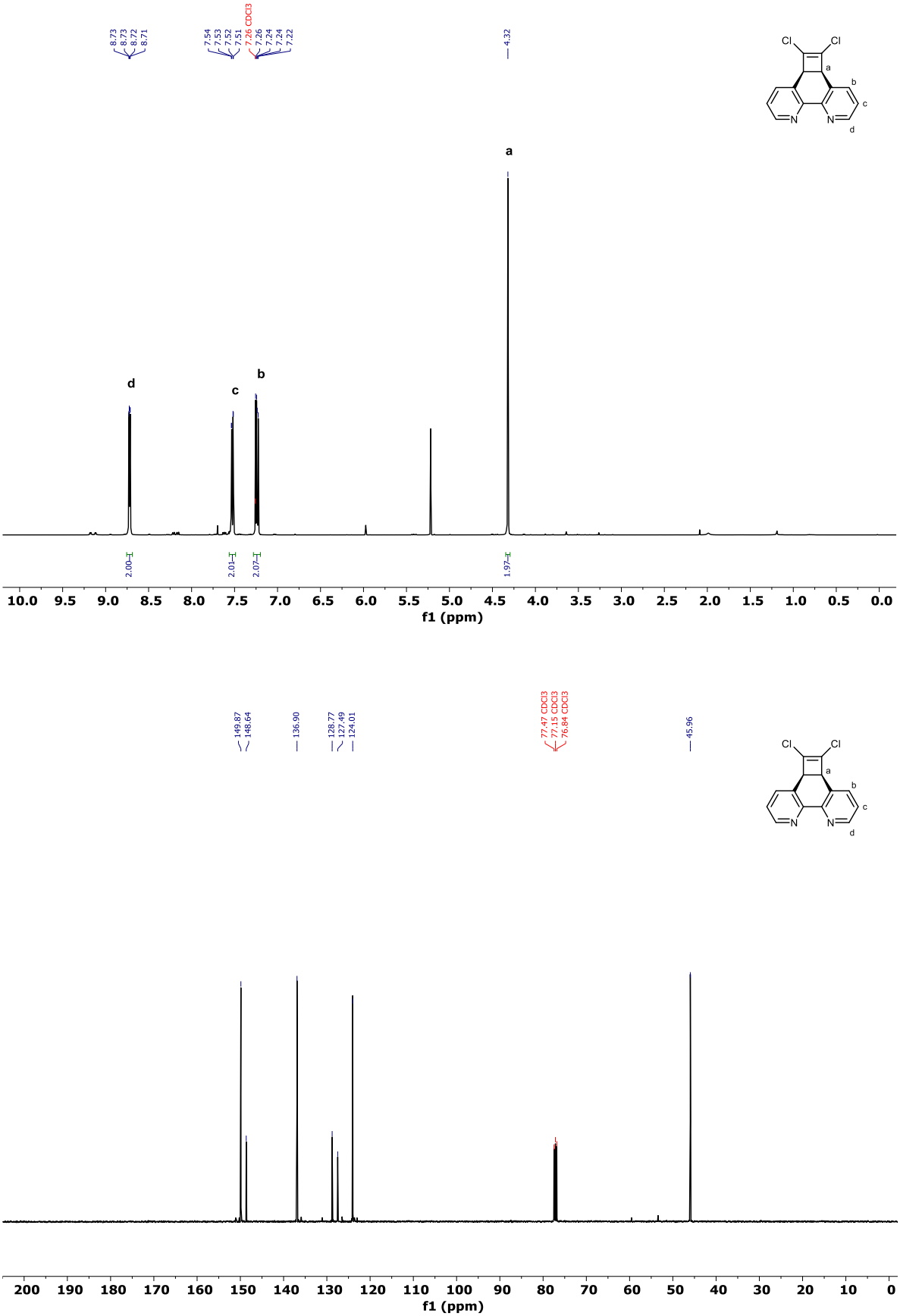

Figure S2.4: (top) ^{1}H NMR (400 MHz) and (bottom) ^{13}C NMR (101 MHz) spectra of dichloride **2.7** ($CDCl_3$, 298 K).

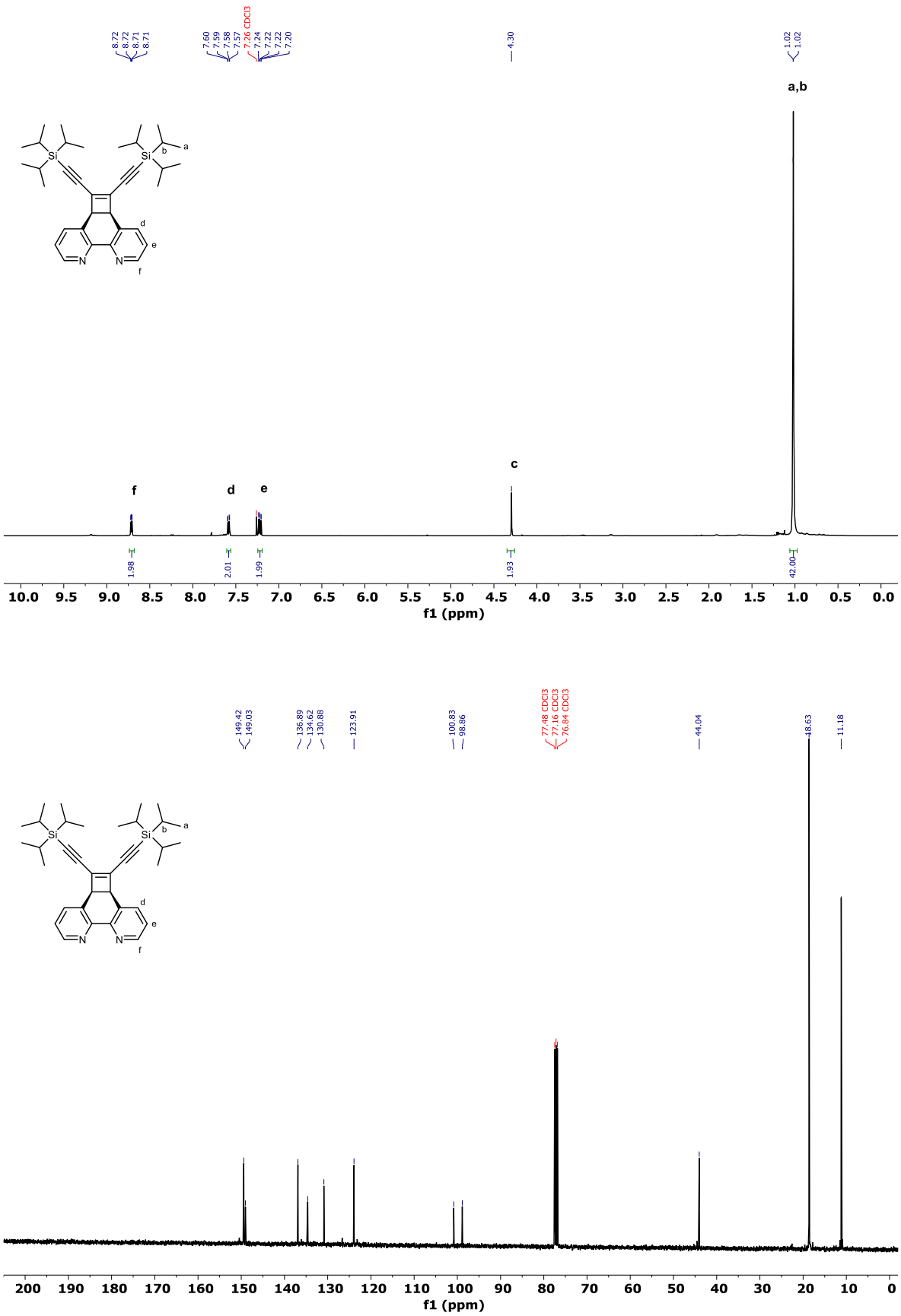

Figure S2.5: (top) ^{1}H NMR (400 MHz) and (bottom) ^{13}C NMR (101 MHz) spectra of TIPS-protected compound **2.8** ($CDCl_3$, 298 K).

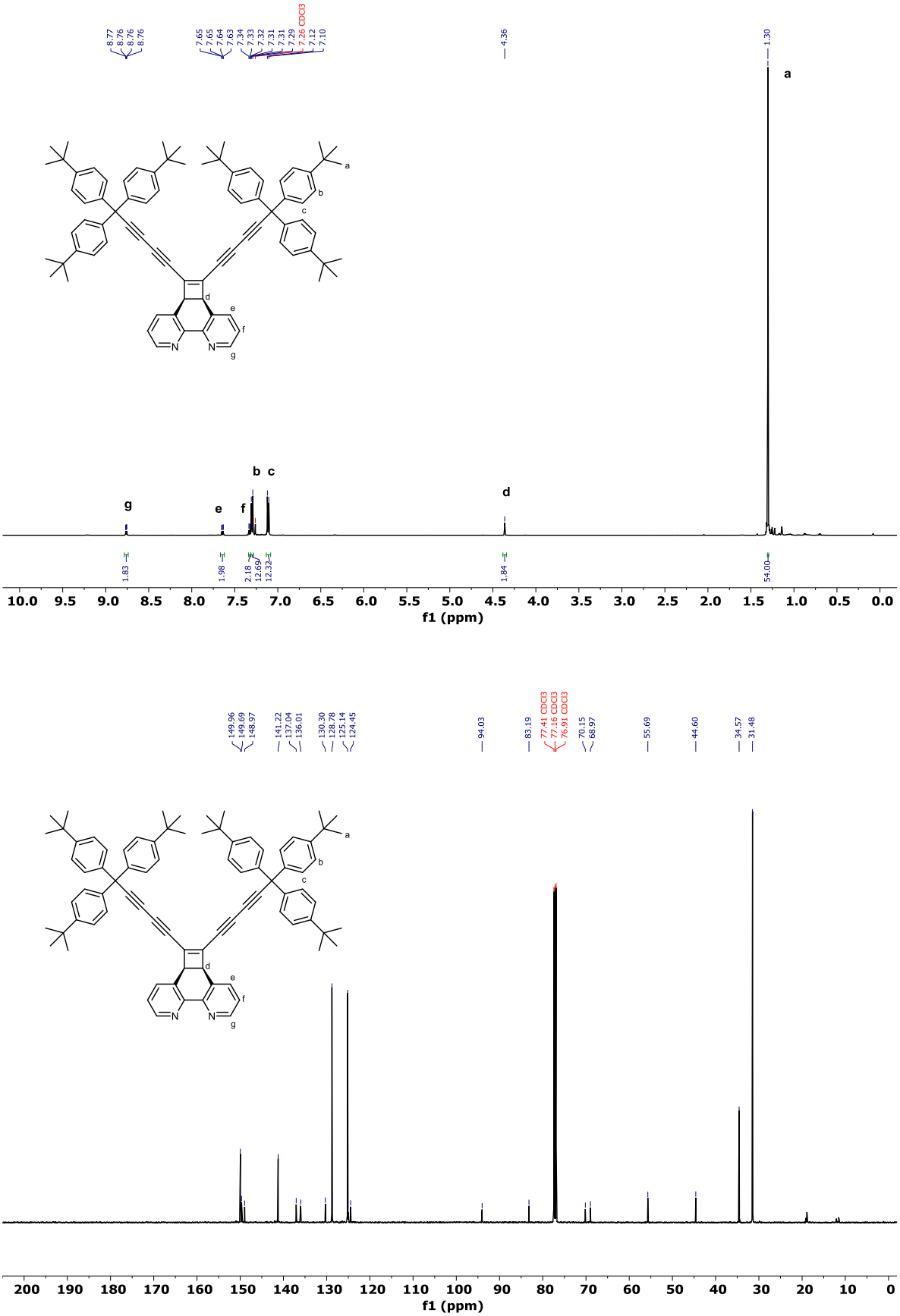

Figure S2.6: (top) ^{1}H NMR (500 MHz) and (bottom) ^{13}C NMR (126 MHz) spectra of deprotected phenanthroline **2.20** ($CDCl_3$, 298 K).

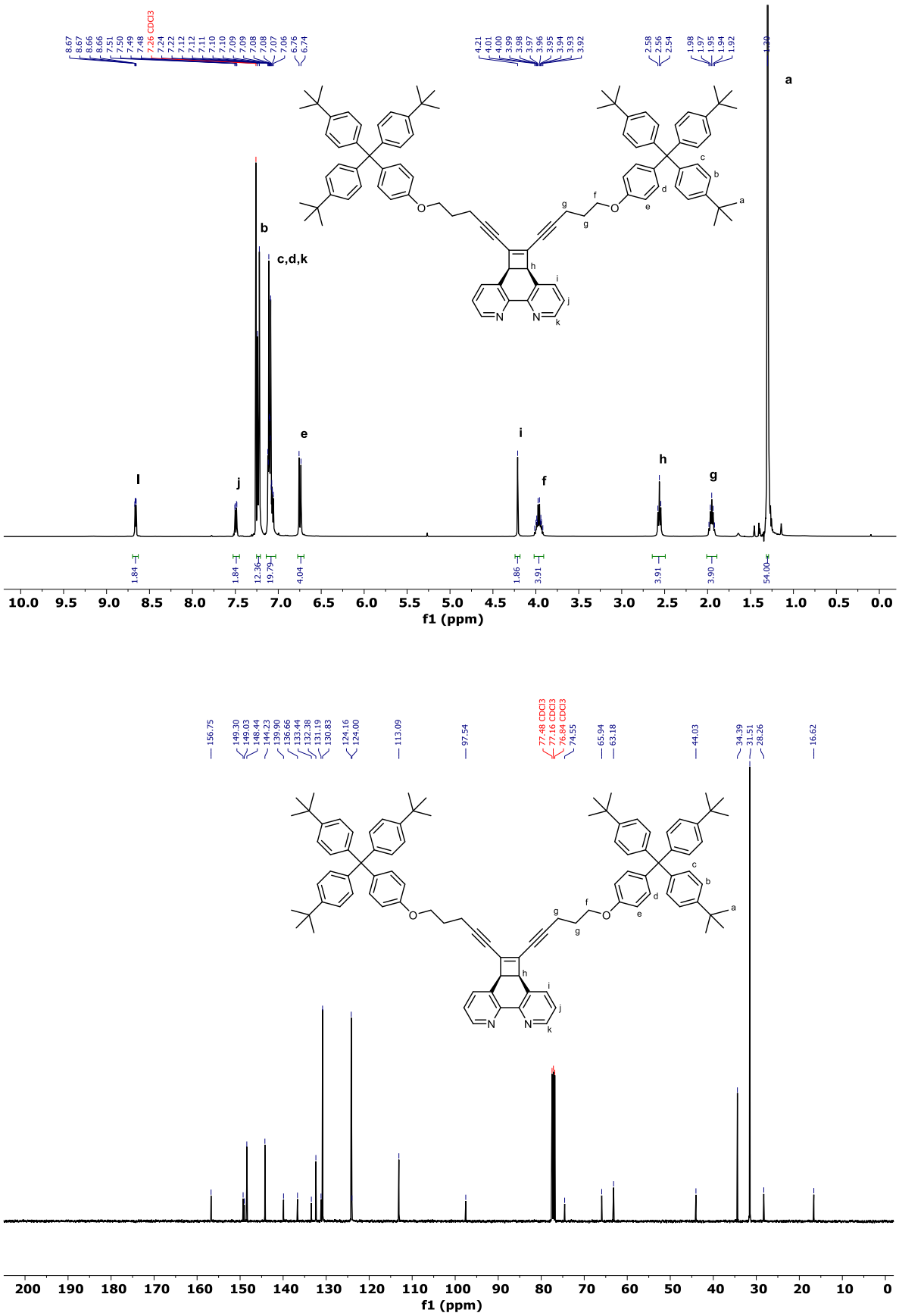

Figure S2.7: (top) ^{1}H NMR (400 MHz) and (bottom) ^{13}C NMR (101 MHz) spectra of stoppered phenanthroline **2.27** ($CDCl_3$, 298 K).

Selected Mass Spectra

(a)

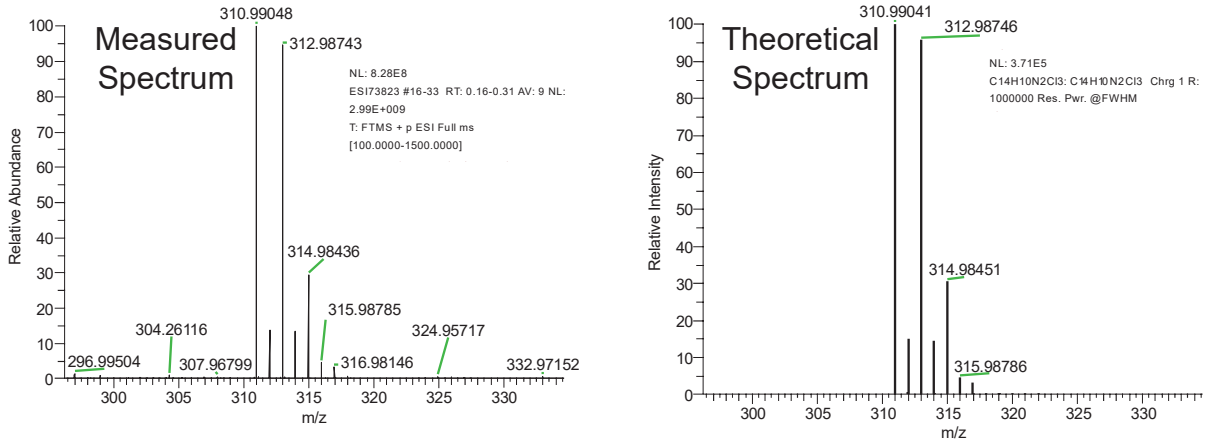

(b)

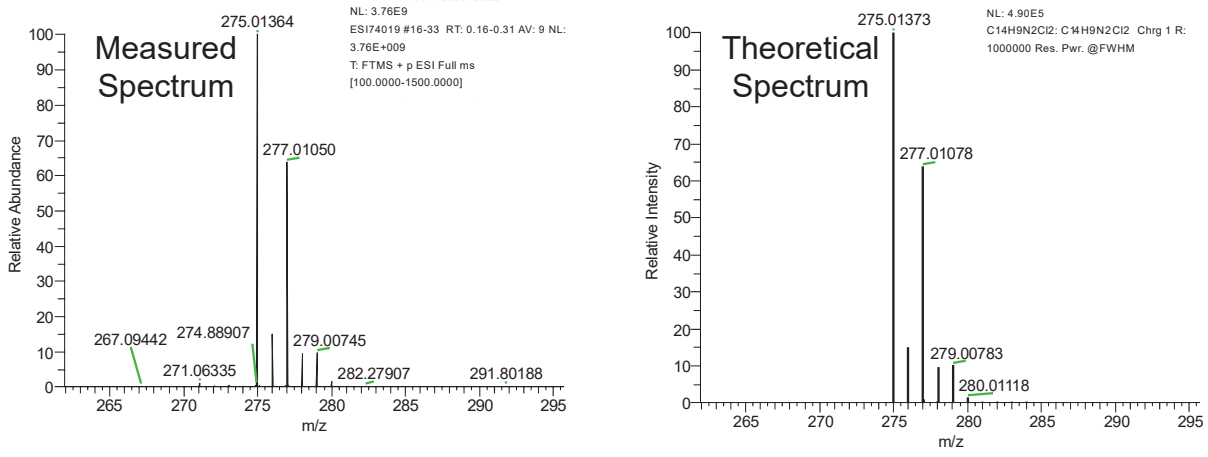

(c)

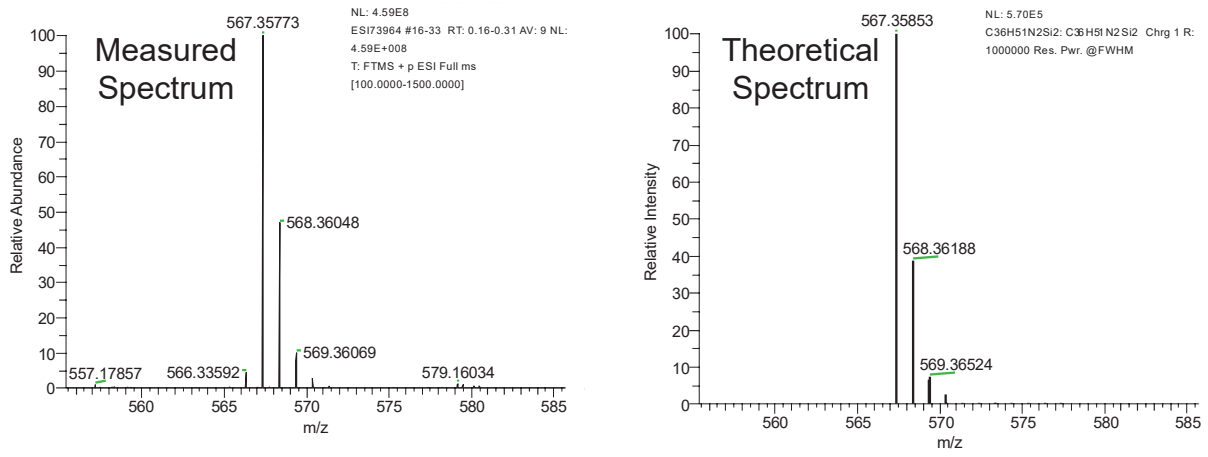

Figure S2.8: High-resolution mass spectra of (a) trichlorophenanthroline **2.6**, (b) dichlorophenanthroline **2.7** and (c) TIPS-protected phenanthroline-masked triyne **2.8**.

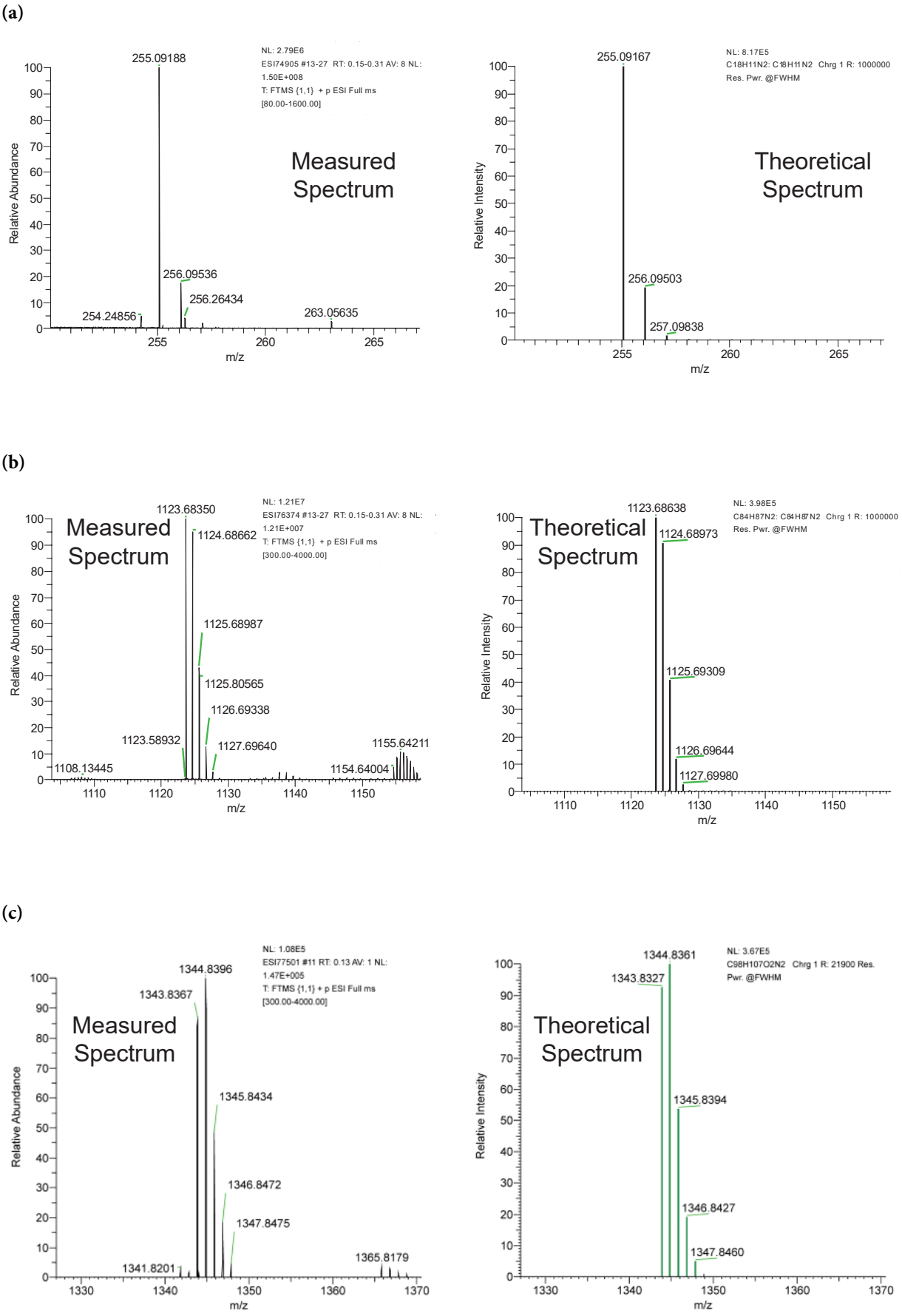

Figure S2.9: High-resolution mass spectra of (a) deprotected phenanthroline-masked triyne **2.19**, (b) phenanthroline thread **2.20** and (c) extended phenanthroline thread **2.27**

Selected UV-vis Spectra

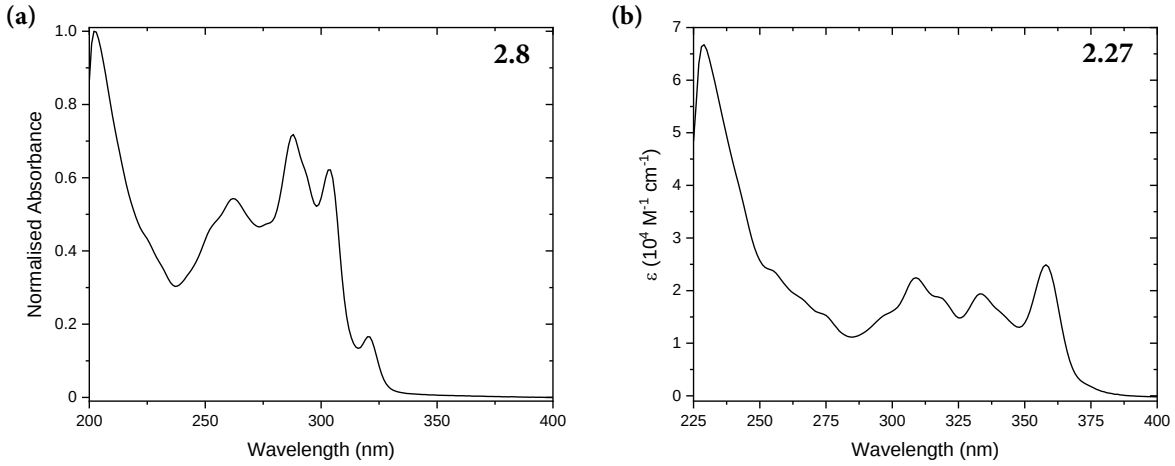

Figure S2.10: UV-vis spectra of (a) TIPS-protected phenanthroline **2.8** (MeOH) and (b) stoppered phenanthroline **2.27** (CH_2Cl_2). All solutions at 25 °C.

References

1 R. N. Keller and H. D. Wycoff, in *Inorg. Synth.*, 1946, pp. 1–4.

2 C. O. Dietrich-Buchecker and J.-P. Sauvage, *Tetrahedron Lett.*, 1983, **24**, 5091–5094.

3 C. Roche, Université de Strasbourg & University of Sydney, 2012.

4 D. B. Amabilino and J.-P. Sauvage, *Chem. Commun.*, 1996, 2441.

5 M. Weck, B. Mohr, J.-P. Sauvage and R. H. Grubbs, *J. Org. Chem.*, 1999, **64**, 5463–5471.

6 P. R. Ashton, R. Ballardini, V. Balzani, M. Bělohradský, M. T. Gandolfi, D. Philp, L. Prodi, F. M. Raymo, M. V. Reddington, N. Spencer, J. F. Stoddart, M. Venturi and D. J. Williams, *J. Am. Chem. Soc.*, 1996, **118**, 4931–4951.

7 H. W. Gibson, S. H. Lee, P. T. Engen, P. Lecavalier, J. Sze, Y. X. Shen and M. Bheda, *J. Org. Chem.*, 1993, **58**, 3748–3756.

8 V. Aucagne, J. Berná, J. D. Crowley, S. M. Goldup, K. D. Hänni, D. A. Leigh, P. J. Lusby, V. E. Ronaldson, A. M. Z. Slawin, A. Viterisi and D. B. Walker, *J. Am. Chem. Soc.*, 2007, **129**, 11950–11963.

3

Dicobalt-Masked Polyyne Rotaxanes

Contents

Chapter 3 - Dicobalt-Masked Polyyne Rotaxanes

3.1 Introduction

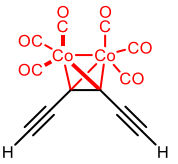

Figure 3.1: Structure of a dicobalt-masked triyne.

Dicobalt octacarbonyl complex contains two metal centres bearing six terminal carbonyl groups and bridged by two carbonyls in between. They from butterfly-like complexes with alkynes whereby two bridging carbonyls are replaced by a new Co-C bond to each acetylenic carbon (Figure 3.1).[1] Cobalt(0) complexes have found many uses in wider chemistry, such as a catalyst in the Nicholas reaction[2] and as electrochemical probes in acetylenic molecular wires,[3–6] to highlight just a few. Importantly for this work, the complexation with alkynes is a reversible process, giving these alkyne-dicobalt moieties potential use as a masked alkyne equivalent (MAE).[7,8]

The dicobalt carbonyl MAE group is particularly interesting for preparing acetylene-based structures because it can stabilise alkynes in two ways. First, the large steric bulk prevents close contacts between *sp*-chains, shutting down any detrimental cross-linking reactions.[9] Second, it breaks the conjugation of the polyyne by changing the hybridisation of the carbon atoms from *sp* to sp^3. An important feature of the dicobalt masking group is the angle (between the coordinated alkyne and its adjacent carbons) that it imparts on the polyyne while masking it. The bend that is consequentially induces in the carbon chain can be exploited to aid formation of curved structures. The $Co_2(CO)_6$ group itself can be removed in a variety of ways (alkyne-ligand exchange,[10] flash vacuum pyrolysis[11] or by oxidation[12]), but is often too unstable to perform useful chemical reactions on the complex. Substitution of two terminal carbonyls with a bidentate bridging phosphine ligand (e.g. bis(diphenylphosphino)methane, dppm) confers a significant improvement in the stability of these complexes towards desilylation and coupling reactions, but at the expense unmasking ease.[13,14]

Indeed, such complexes have already been the subject of investigation. Work by Diederich and Rubin in the early 1990s demonstrated the masking of bis-TIPS triyne with dicobalt carbonyl (Figure 3.2a).[15] Ligand exchange with dppm permitted a later cyclisation reaction to prepare macrocycles bearing three (**1.12a**) or four (**1.12b**) dicobalt masking groups – precursors to cyclo[18]- and cyclo[24]carbons, respectively (Figure 3.2b).[15,16] However, the

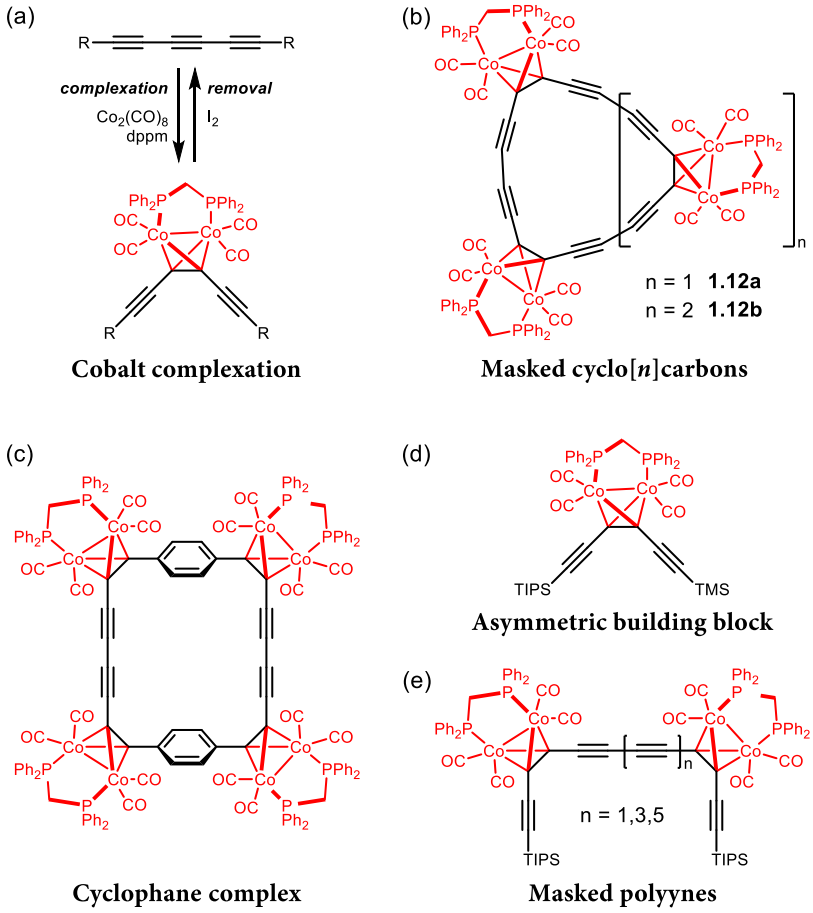

Figure 3.2: (a) Dicobalt complexation of an alkyne and its subsequent removal,[15,17] (b) C_{18} hexacobalt- and C_{24} octacobalt-masked precursors to cyclo[*n*]carbons,[15,16] (c) [8,8]paracyclophaneoctayne octacobalt complex,[17] (d) a dicobalt-masked asymmetric triyne and (e) tetracobalt-masked TIPS-capped oligoynes.[18]

dppm-stabilised dicobalt group brought challenges with the unmasking of these compounds and, coupled with the high instability of the unmasked products, meant that the target cyclocarbons were not successfully isolated. Haley *et al.* also prepared an octacobalt complex of a cyclophane with a curved tetrayne bridges, (Figure 3.2c).[17] Successful unmasking of the dicobalt carbonyl group was achieved by mild oxidation from excess I_2 in model compounds, but this could not be reproduced on the octacobalt cyclophane complex.

Research efforts in our group also focussed on these cobalt carbonyl MAEs, this time to prepare oligoynes and short polyynes with up to 10 contiguous acetylene units.[18] The key building block in this work was an asymmetric masked triyne bearing TIPS and TMS protecting groups at the termini (Figure 3.2d). The orthogonal protection of the two groups enabled removing the TMS group selectively under mild, basic conditions (K_2CO_3 in THF/MeOH) to give the mono deprotected compound. Through multiple deprotection and extension reaction sequences, cobalt-masked oligoynes of varying length (Figure 3.2e) were successfully prepared. Oxidative (Eglinton) homocoupling conditions were used to prepare these masked tetracobalt

oligoynes of varying size. Despite encountering an unusual "alkyne hopping" migration of the dicobalt group during the coupling reaction, the oligoynes could be cleanly isolated. Successful unmasking of the dicobalt MAEs was then achieved under mild conditions with elemental iodine at room temperature to afford TIPS-protected polyynes with up to 20 contiguous *sp*-hybridised carbon atoms. While is unlikely that significantly longer TIPS-capped polyynes could be prepared due to the limited protection offered by the capping groups, systems involving much bulkier and more robust end-capping groups could be envisaged, such as the supertrityl (Tr*) and pyridyl (Py*) stoppers (**1.9** and **1.10** from Chapter 1). Even then, a limit to the protection offered by these was eventually reached (22 and 24 acetylene units, respectively) as longer systems were prepared.[19,20]

This project aims to demonstrate that by incorporating multiple strategies it will be possible to prepare long polyynes. It was expected that by combining the steric protection of bulky end groups with the enhanced stability brought about by supramolecular encapsulation, long polyyne rotaxanes stable under ambient conditions could be isolated. The synthesis employed bulky dicobalt MAEs to stabilise intermediate compounds, which were then unmasked in the final step to release the polyyne rotaxane. Two polyyne rotaxanes, both with the same C_{28} polyyne dumbbell component, were prepared with different macrocycles – a larger phenanthroline-based macrocycle and a smaller cycloparaphenylene-based one – so that the stability enhancement of different macrocycles could be assessed.

3.2 Synthesis of Phenanthroline-Protected Rotaxanes

We have already mentioned the importance of adding dppm to the dicobalt MAE to improve the stability of the complex, but it additionally provides enhanced steric bulk to the masking group. Importantly for this project, this allows the MAE to serve an additional function – a temporary mechanical stopper. It should be possible to generate [2]rotaxanes through an active metal template (AMT) cross-coupling approach between a permanent stopping group and the MAE (Figure 3.3). Further coupling of this [2]rotaxane could then generate larger acetylene-based structures. To achieve good yields of the cross-coupled product (and minimise formation of undesirable homocoupled products), a reliable Cadiot-Chodkiewicz AMT coupling could be employed. As discussed in Chapter 2, the selectivity for the cross-coupled product comes from the reaction between an alkyne and a haloalkyne, the latter being the oxidant in the reaction.

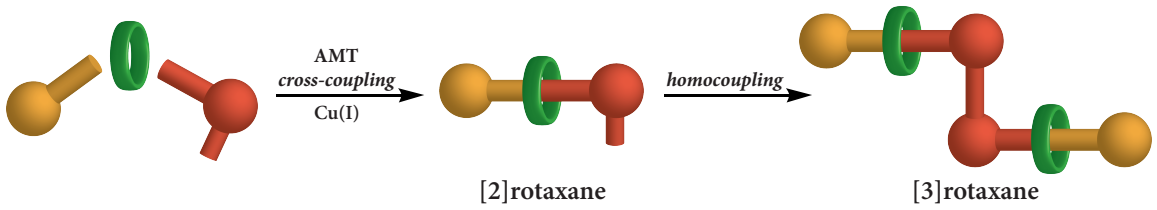

Figure 3.3: Pictorial scheme to preparing a masked [3]rotaxane. Orange represents a permanent stopper, red represents a bulky (dicobalt) masking group and green represents a macrocycle.

This project aims to prepare polyyne [3]rotaxanes and assess their stabilities relative to that of the unthreaded polyyne. We therefore decided to aim for a previously-reported polyyne that we know to be isolable under ambient conditions – a supertrityl-capped tetradecayne, first synthesised by Tykwinski *et al.*[19] The synthetic efforts can be divided into three key components: a supertrityl end-capping and sterically protecting group, a bulky MAE-based stopper and a chemically-inert macrocycle. Consideration was made into whether the dicobalt MAE part or the supertrityl stopper part should be brominated. Earlier work in our group by Dr Daniel Kohn and Mr Joseph Woods had documented many unsuccessful attempts at brominating the cobalt masking group.[21,22] Many of these attempts either left the acetylene unchanged or were sufficiently oxidising such that the masking group was removed in the process. Due to these obvious difficulties, it was sensible to prepare the supertrityl triyne bromide component, as this should be readily achievable using standard brominating agents and conditions.

3.2.1 Stopper Synthesis

The supertrityl stopper is prepared through a series of simple, high-yielding and scalable steps, first reported by Tykwinski *et al.* (Scheme 3.1).[19] Starting from the triple Friedel-Craft alkylation of benzene with ^{t}BuCl (**3.1**), then subsequent treatment with neat Br_2 afforded bromo-di-^{t}Bu benzene **3.2**.[23] Treating **3.2** with magnesium metal formed the corresponding Grignard reagent, to which diethyl carbonate was added to give supertrityl alcohol **3.3**.[19] Treatment of **3.3** with oxalyl chloride, and subsequent addition of ethynylmagnesium bromide gave the corresponding acetylene **3.4**.[19] From this, deprotonation with *n*-BuLi and attack onto TIPS propargyl aldehyde cleanly returned alcohol **3.5**, which is readily oxidised to the ketone **3.6** by either pyridinium chlorochromate (PCC) or MnO_2.[19] Synthesis of the dibromo olefin **3.7**, followed by its *n*-BuLi-promoted Fritsch–Buttenberg–Wiechell (FBW) rearrangement was

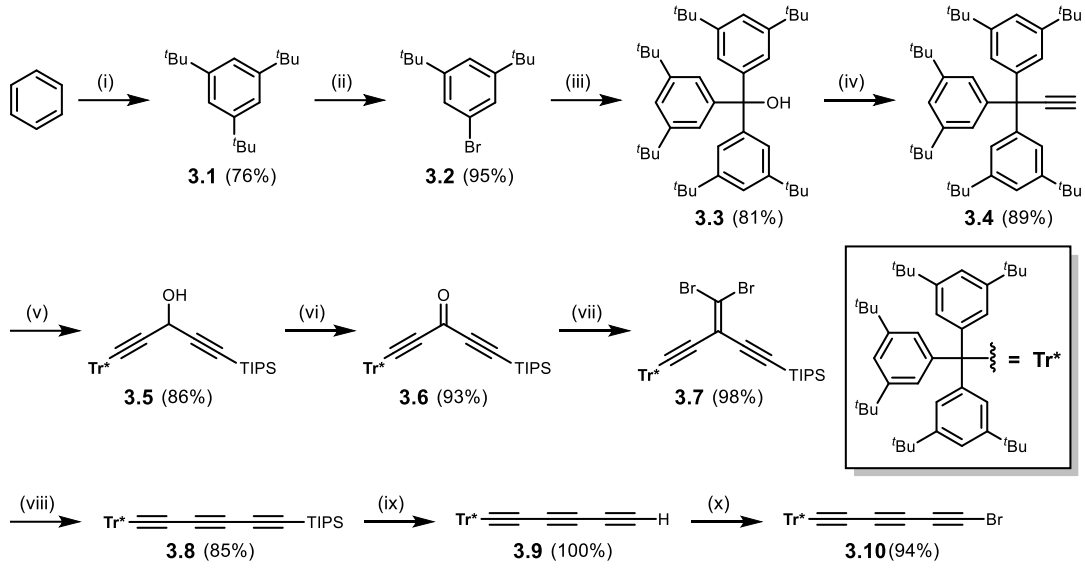

Scheme 3.1: Synthetic scheme towards brominated supertrityl triyne **3.10**.[19,23] (i) ^{t}BuCl, $AlCl_3$, −20 °C, 2 h; (ii) Br_2, Fe, $CHCl_3$, 0 °C, 4 h; (iii) Mg, THF, reflux, 18 h, Ar, then $CO(OEt)_2$, THF, 20 °C, 2 d; (iv) $(COCl)_2$, THF, 20 °C, 4 h, Ar, then ethynylmagnesium bromide, THF, 20 °C, 3 d, Ar; (v) *n*-BuLi, THF, −78 °C, 15 min, Ar, then (triisopropylsilyl)-propiolaldehyde , 20 °C, 1 h, Ar; (vi) PCC or MnO_2, CH_2Cl_2, 20 °C, 24 h, Ar; (vii) CBr_4, PPh_3, CH_2Cl_2, 20 °C, 1 h, Ar then **3.6**, CH_2Cl_2, 20 °C, 24 h, Ar; (viii) *n*-BuLi, pentane, −78 °C to 20 °C, 1 h, Ar; (ix) TBAF, THF/1% H_2O v/v, 20 °C, 15 min, Ar; (x) NBS, $AgNO_3$ (10 mol%), acetone; 20 °C, 5 h, Ar.

used to prepare the TIPS-protected Tr* triyne **3.8**.[19] Desilylation with TBAF in wet THF gave terminal triyne **3.9** before bromination by NBS, to return the brominated stopper **3.10**.[24]

3.2.2 MAE Synthesis

In this project, we first targeted construction of a [2]rotaxane, which could then be homocoupled to yield a [3]rotaxane (Figure 3.3). It was therefore crucial that we were able to carry out chemical transformations selectively at each end of the masked oligoyne at any time. While the preparation of a symmetric (bis-TIPS) variant is high-yielding,[15] the selective mono TIPS deprotection is very challenging, with only an approximate 10% yield being attainable after careful, portionwise addition of TBAF.[21] We aimed to instead use an asymmetric (TIPS-TMS) cobalt masking group **3.19**, which offers orthogonal deprotection of the two ends of the masked triyne building block. Preparation of this starts from the deprotonation of TMS acetylene, then treating with TIPS propargyl aldehyde (**3.11**) to give TIPS-TMS propargyl alcohol **3.12** (Scheme 3.2).[25] The subsequent oxidation to ketone **3.13**, conversion to dibromo olefin **3.14** and FBW rearrangement to triyne **3.15** are akin to those for the stopper **3.8**.[25] Masking TIPS-TMS triyne **3.15** with dicobalt octacarbonyl then subsequent treatment with dppm afforded two regioisomers (**3.16** and **3.17**) that were separable by silica column

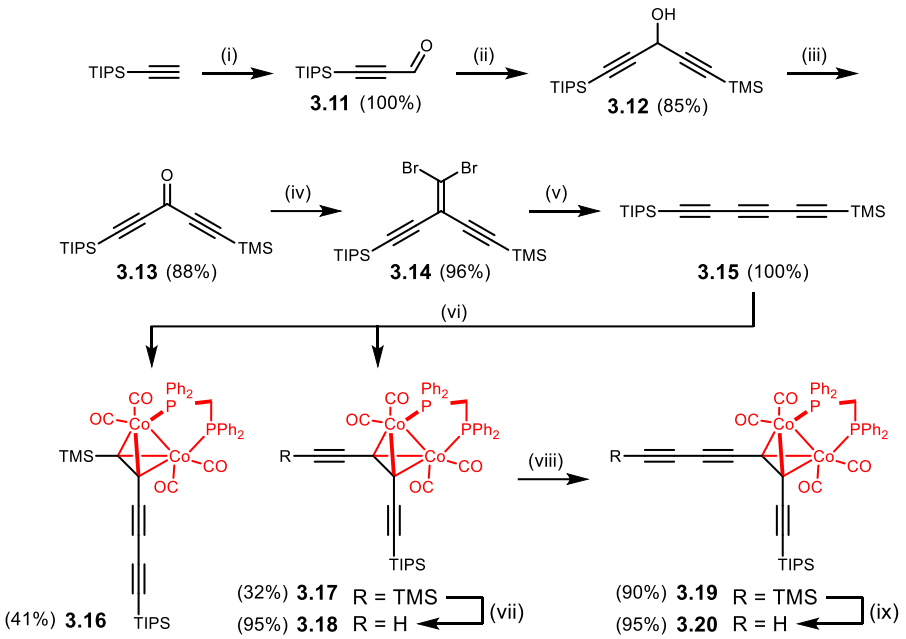

Scheme 3.2: Synthetic scheme towards dicobalt diyne **3.20**.[18,25] (i) *n*-BuLi, Et_2O, 0 °C, 30 min, Ar then DMF, −78 °C, 3 h, Ar; (ii) TMS-acetylene, *n*-BuLi, Et_2O, −40 °C, 10 min, Ar then **3.12**, −78 °C, 3 h, Ar; (iii) PCC or MnO_2, CH_2Cl_2, 20 °C, 24 h, Ar; (iv) CBr_4, PPh_3, CH_2Cl_2, 20 °C, 1 h, Ar then **3.13**, CH_2Cl_2, 20 °C, 24 h, Ar; (v) *n*-BuLi, pentane, −78 °C to 20 °C, 1 h, Ar; (vi) $Co_2(CO)_8$, pentane, 20 °C, 18 h, Ar then dppm, toluene, reflux, 30 min, Ar; (vii) K_2CO_3, THF/MeOH (1:1), 20 °C, 30 min; (viii) TMS-acetylene, CuCl, TMEDA, CH_2Cl_2, 20 °C, 30 min, O_2; (ix) K_2CO_3, THF/MeOH (1:1), 20 °C, 30 min.

chromatography.[18] The observation of two isomers in this system (*c.f.* only one isomer is generally observed in the masking of bis-TIPS triyne) can be attributed to the reduced bulk of TMS compared to TIPS. The major product (41%) was determined to be the undesired isomer with the dicobalt group adjacent to the TMS group (**3.16**), and the minor product (32%) carrying the dicobalt group on the central acetylene (**3.17**). Even though there is a large quantity of the undesired regioisomer produced, this route is still notably more efficient in obtaining terminal acetylene **3.18** than via a statistical deprotection approach of a symmetric triyne (e.g. bis-TMS or bis-TIPS). Additionally, the undesired isomer can be readily recycled back to triyne **3.15** through unmasking with I_2 in roughly 70% yield.

After TMS deprotection of **3.17** with K_2CO_3 in methanolic THF the acetylene was extended by one unit in a statistical Glaser-Hay cross coupling reaction with an excess of TMS acetylene.[18] TMS deprotection of **3.19** with K_2CO_3 in methanolic THF cleanly afforded terminal diyne **3.20**. It was noted that the deprotection of diyne **3.19** progressed quicker than for the TMS monoyne **3.17**, likely due to a combination of reduced steric hindrance from the MAE unit and the different electronics of the diyne. As oligoynes become larger, they also become more electron deficient and thus stabilise the anionic charge better.

3.2.2.1 NMR Dynamics of the Dicobalt Masking Group

It was noticed that these compounds displayed simpler NMR spectra than might be predicted based on their solid-state structures. The structure of $Co_2(CO)_8$ derivatives can be compared to those of $Fe_2(CO)_9$, in that both possess both terminal and bridging CO molecules. The structure of $Co_2(CO)_8$ can be easily visualised by removing one of the bridging carbonyls from the structure of $Fe_2(CO)_9$.[26] When contrasting the structures of these two, one can imagine the cobalt structure possesses a "vacant" bridging site.[14] It is expected that by using this "vacant" bridging site, these dicobalt-masked compounds can dynamically interconvert between two different isomers on the NMR timescale at room temperature (Figure 3.4). The fluxional motion effectively generates a mirror plane on the NMR time scale that contains the cobalt-cobalt bond to give what appears to be a species of higher symmetry than expected.

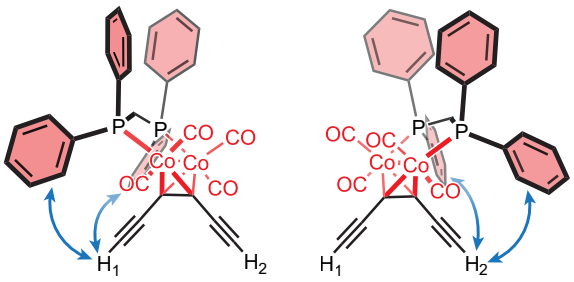

Figure 3.4: Fluxional motion of the dppm ligand at 298 K makes H_1 = H_2 (chemically equivalent) on the NMR timescale. At lower temperatures this fluxional process is halted such that $H_1 \neq H_2$ (chemically non-equivalent).

The fluxional behaviour of dicobalt-masked hexatriyne was studied by variable temperature NMR (VT-NMR) experiments. ^1H and ^{31}P spectra were recorded between 193 K and 298 K. Upon cooling, an obvious splitting to the P-CH_2 bridge protons was observed in the ^1H NMR spectrum (Figure 3.5). The sharp triplet (298 K) displays significant broadening around 253 K, before separating into two very broad, overlapping signals at 243 K, presumably as the rate of interconversion between the two conformations is reduced and the process now occurs slower than the NMR timescale. These signals begin to sharpen as the temperature is reduced further to 193 K – the limit of the NMR probe. A similar effect was observed for the terminal acetylene resonance, which at room temperature appears as a barely-resolved triplet, but when cooling to 223 K, undergoes significant broadening before separating into two chemical environments below this. Upon cooling, the ^{31}P spectrum showed a progressive sharpening of the single phosphorus resonance. While the ^{13}C spectrum was not measured, it would also be expected that two carbonyl environments would be observed as the interconversion between the two isomers is inhibited at low temperatures.

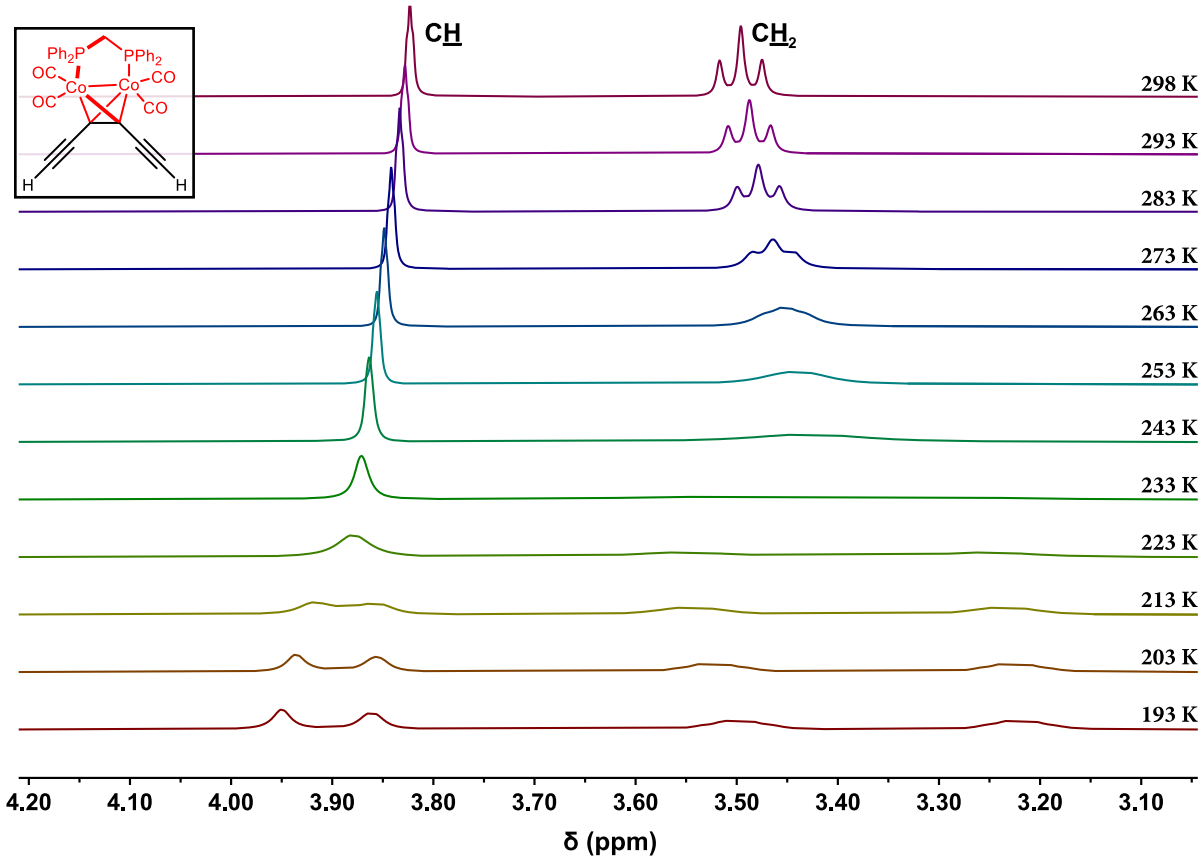

Figure 3.5: ^{1}H VT-NMR spectrum of dicobalt-masked triyne between 298-193 K (500 MHz, CD_2Cl_2).

Rate constants k at each temperature T were determined using line shape analysis of the terminal acetylene resonance. Plotting $\ln(k/T)$ *vs* T^{-1} was used to prepare an Eyring plot (Figure 3.6), to which a linear function could be fitted, allowing the enthalpy $\Delta H^{\ddagger}$ and entropy $\Delta S^{\ddagger}$ for this fluxional motion to be extracted. From these, the Gibbs free energy of this process at 298 K ($\Delta G^{\ddagger}_{298\ K}$) can be estimated to be 37 ± 5 kJ mol^{-1}, corresponding to a rate constant of *ca.* 10^6.

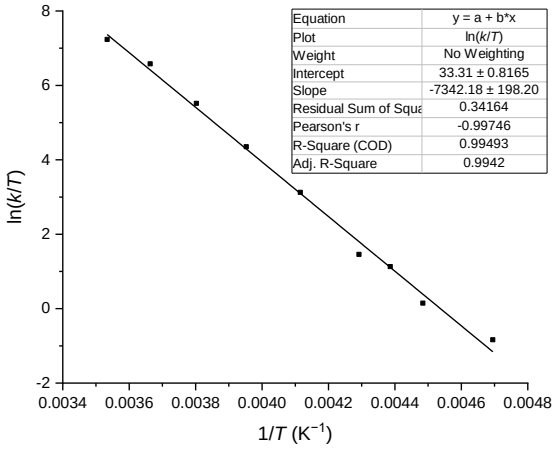

Figure 3.6: Eyring plot used to determine $\Delta H^{\ddagger}$, $\Delta S^{\ddagger}$ and $\Delta G^{\ddagger}$ for the fluxional motion of a dicobalt-masked hexatriyne in CD_2Cl_2 (further details provided in Experimental Section 3.7).

3.2.3 Macrocycle Synthesis

Active metal template approaches to rotaxanes have been successfully demonstrated with a variety of macrocycles employing different metal-binding motifs.[27] Since we were aiming for a Cu-catalysed Cadiot-Chodkiewicz coupling, we planned to use a phenanthroline-bearing macrocycle, as this motif binds Cu(I) cations strongly. Additionally, the high stability of many

reported macrocycles containing a diaryl phenanthroline (DAP) core is also an important consideration. We anticipate that chemically inert macrocycles are key to effective protection of the polyyne. An added benefit of the DAP motif is that these macrocycles can also be pre-complexed with Cu(I) cations to give a complex that is stable under ambient conditions and can be easily handled prior to their use in the AMT coupling reactions.

Reports of DAP-based macrocycles are plentiful in literature, so rather than designing a novel macrocycle we settled on one first developed by Saito *et al.* and previously used in the group.[24,28,29] This macrocycle features a DAP core and flexible hexyl linking straps connected to a resorcinol unit at the bottom (**M4**, Scheme 3.3). The high rigidity of the DAP core ensures the macrocyclic cavity remains open and unhindered, which promotes a coupling reaction through the cavity of the macrocycle to give the interlocked products. Various [2]rotaxanes combining macrocycle **M4** with oligoyne threads have been reported.[24,29–35] Crystal structure analysis for reported rotaxanes with macrocycle **M4** suggest that the macrocyclic cavity is much larger than required for a simple polyyne thread, with vertical and horizonal distances of approximately 12.0 Å and 10.5 Å, respectively.[24] Nevertheless, **M4**-bearing rotaxanes have previously been prepared with supertrityl stoppering groups.[24] Space-filling (CPK) and computational models provided further reassurance that the high bulk of the dicobalt-based MAE would be sufficient to prevent the macrocycle from slipping off the dumbbell. Through similar chemistry, we expect that rotaxanes with the same dumbbells could then be prepared using a smaller macrocycle and would allow for us to evaluate stability enhancement brought about by the macrocycle. One potential drawback of 2,9-diarylphenanthrolines is their high propensity to form stacked

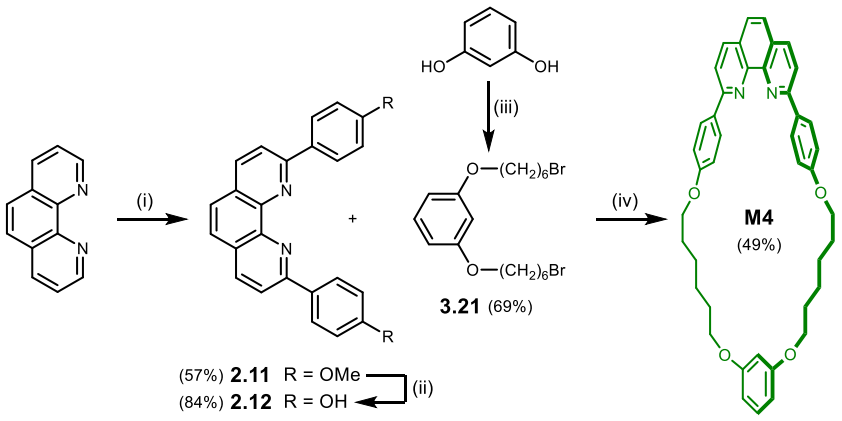

Scheme 3.3: Synthesis of phenanthroline macrocycle **M4**.[28,29] (i) 4-bromoanisole, *n*-BuLi, THF, −78 °C, 3 h, Ar then 1,10-phenanthroline, toluene, −78 °C to 20 °C, 20 h, Ar then MnO_2, CH_2Cl_2, 20 °C, 30 min (ii) pyridine, HCl, 200 °C, 3 h, Ar; (iii) 1,6-dibromohexane, K_2CO_3, acetone, 70 °C, 3 d, Ar; (iv) K_2CO_3, DMF, 60 °C, 5 h, Ar.

aggregates.[30] Should this occur, it may reduce the ability of the macrocycle to protect the polyyne thread when multiple macrocycles are present.

Synthesis of macrocycle **M4** (summarised in Scheme 3.3) first involves the lithiation of 4-bromoanisole then subsequent attack on 1,10-phenanthroline to give dianisyl phenanthroline **2.11**.[36,37] Demethylation returns diphenol phenanthroline **2.12** that in a high-dilution S_N2 macrocyclisation reaction with the dibromo strap **3.21** returns macrocycle **M4** in 49% yield.[28] Stirring **M4** with copper(I) iodide in MeCN/CH_2Cl_2 yielded the air-stable macrocycle-Cu(I) complex **M4**·CuI.

3.2.4 Rotaxane Synthesis

With all of the required components now available, attention was turned to preparing the initial stoppered [2]rotaxane. The active metal template Cadiot-Chodkiewicz cross-coupling of terminal diyne **3.20** with supertrityl bromotriyne **3.10** in the presence of macrocycle-Cu(I) complex **M4**·CuI and K_2CO_3 was successful in generating [2]rotaxane **3.22·M4** in 35% isolated yield (Scheme 3.4).

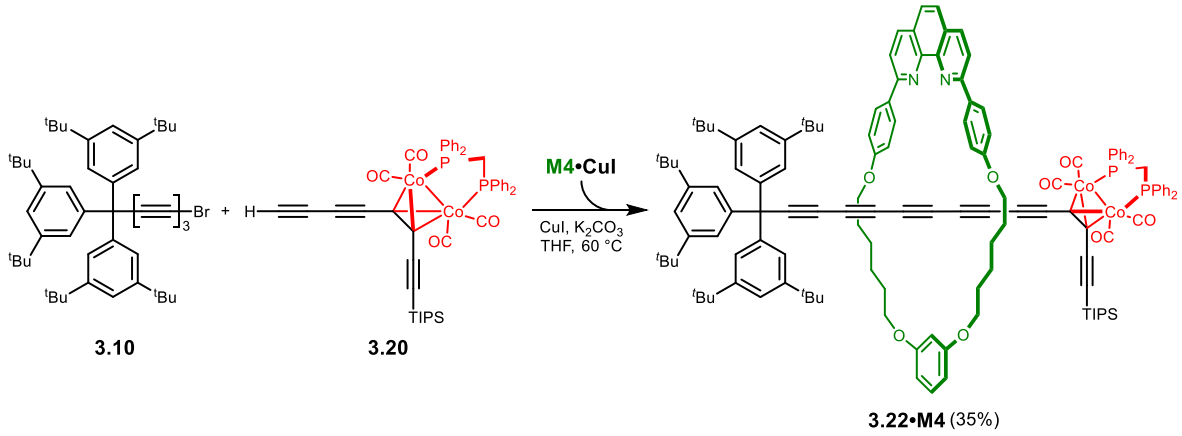

Scheme 3.4: Active metal template Cadiot-Chodkiewicz approach to dicobalt-masked [2]rotaxane **3.22·M4**.

Thorough optimisation of the reaction conditions was key to obtaining the interlocked product. For example, it was critical to use the Cu(I)·**M4** complex rather than adding the macrocycle and CuI separately. It was suspected that this was due to poor solubility of CuI in the reaction solvent (THF), but even when changing to a Cu(I) source soluble in organic solvents, such as $[Cu(MeCN)_4][PF_6]$ or $[Cu(MeCN)_4][BF_4]$, no trace of the interlocked compound could be observed – only the dumbbell and homocoupled side products were isolated. Another point of focus was the solvent system. Using conditions reported by Saito *et*

al. (toluene, K_2CO_3) necessitated high reaction temperatures (110 °C) to promote successful coupling. Running the reaction in these conditions did not yield any desired product, and identification of non-interlocked products was rendered difficult by the presumed decomposition of these under the reaction conditions. Reducing the temperature to 60 °C also failed to yield either interlocked or non-interlocked species, possibly due to the solubility issues with K_2CO_3. According to literature, related compounds were synthesised by using a THF/K_2CO_3 combination (which should improve base solubility) and lower temperatures.[24,34,38] Indeed, upon switching to THF and running the reaction at 60 °C we were successful in isolating the target [2]rotaxane **3.22·M4** in a 35% yield.

Crystals of **3.22·M4** suitable for single-crystal X-ray diffraction were grown by layered addition of methanol to its solution in dichloromethane, followed by slow evaporation of solvents. The structure (Figure 3.7) has four **3.22·M4** rotaxane moieties in the asymmetric unit and, in combination with significant disorder, contribute to an absence of high-resolution data. To ensure sensible displacement parameters, and that the local geometry remained feasible, the imposition of restraints were required. On initial refinement, many of the terminal atoms were found to display prolate displacement ellipsoids thought to be caused by disorder; these were

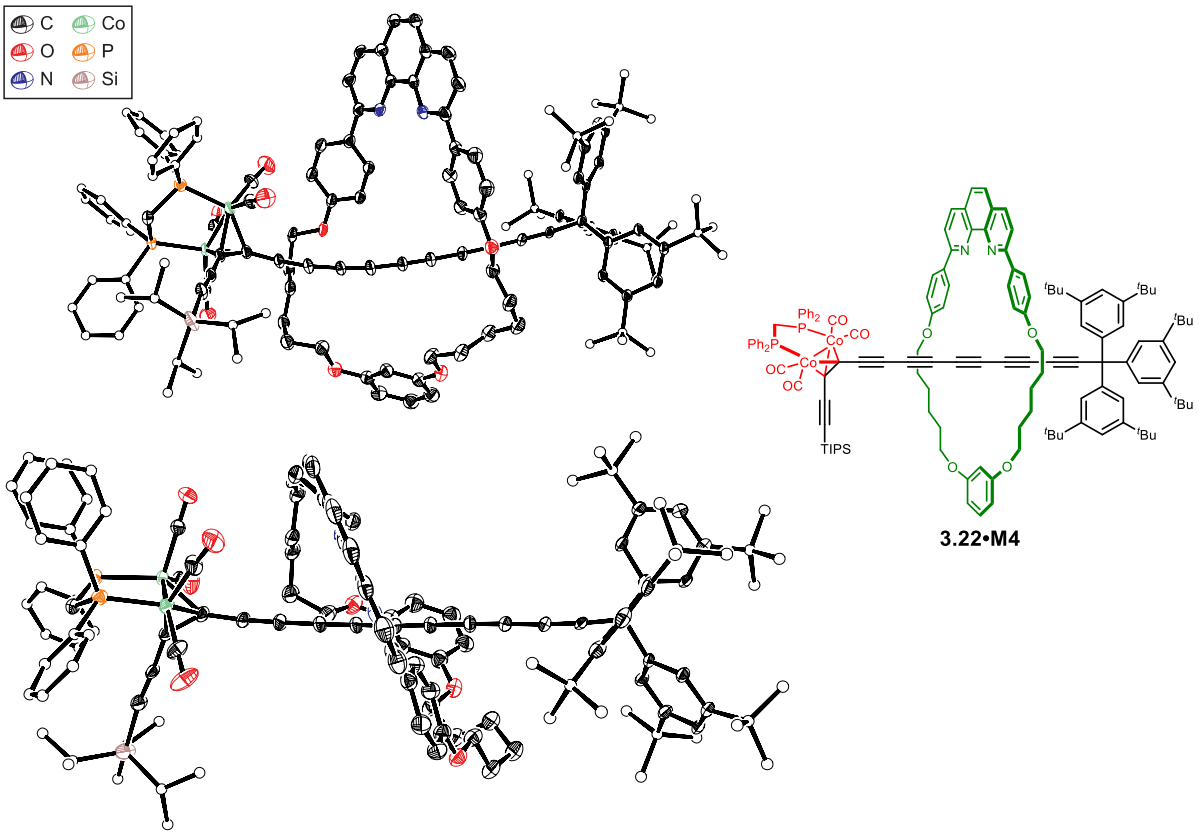

Figure 3.7: Crystal and molecular structure of [2]rotaxane **3.22·M4**. (One of the four molecules in the asymmetric unit. (displacement ellipsoids at 30% probability, hydrogen atoms and minor component of disorder omitted for clarity)

treated with a split site model, but the poor signal to noise ratio and lack of high angle data meant restraints were needed. It was therefore not possible to compare derived parameters in detail. Despite this, it is clear that all four molecules have similar geometries, with the dppm ligand oriented towards the TIPS group and away from the polyyne, so that the macrocycle is buttressed by four carbonyl groups at one face and by the three ^{t}Bu groups of a supertrityl stopper at the other face.

Cleavage of the TIPS group was achieved cleanly using TBAF in wet THF (THF/H_2O 1% v/v). In the absence of water, the reaction proceeded at a significantly reduced rate and was often accompanied by a small amount of decomposition to unidentified products. The terminal alkyne **3.23·M4** was then subjected to Cu-catalysed oxidative homocoupling using standard Glaser-Hay conditions (CuCl, TMEDA, CH_2Cl_2, O_2) to cleanly prepare the [3]rotaxane **3.24·(M4)**$_2$ in 90% yield (Scheme 3.5).

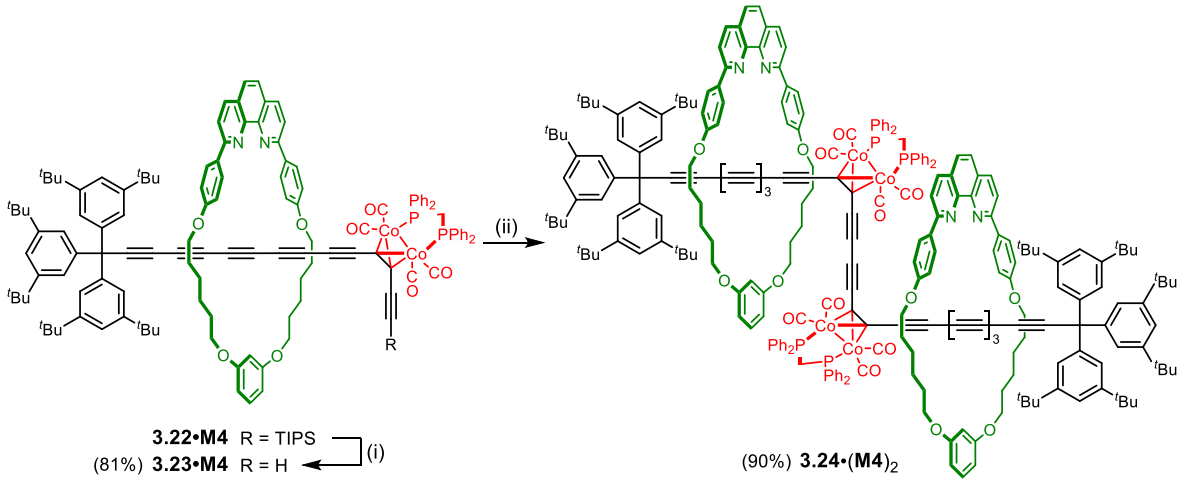

Scheme 3.5: Preparation of dicobalt-masked [3]rotaxane **3.24·(M4)**$_2$. (i) TBAF, THF/H_2O (1% v/v), 20 °C 30 min, Ar; (ii) CuCl, TMEDA, CH_2Cl_2, 20 °C, 30 min, O_2.

3.2.5 Unmasking to a Polyyne [3]Rotaxane

The unmasking of [3]rotaxane **3.24·(M4)**$_2$ to the target polyyne [3]rotaxane **3.25·(M4)**$_2$ was initially tested by treatment with I_2 (20 eq.) in THF to induce oxidative decomplexation of the dicobalt masking group (Scheme 3.6). Unfortunately, the unmasking proved extremely capricious; out of approximately 30 attempts using the aforementioned conditions, only three proved successful at obtaining polyyne [3]rotaxane **3.25·(M4)**$_2$ in yields of 20–36%. This is in stark contrast to the unmasking of dumbbell **3.24** (see Experimental Section 3.7 for further details), which reliably unmasked to give polyyne **3.25**, albeit in a 7.3% yield under the same

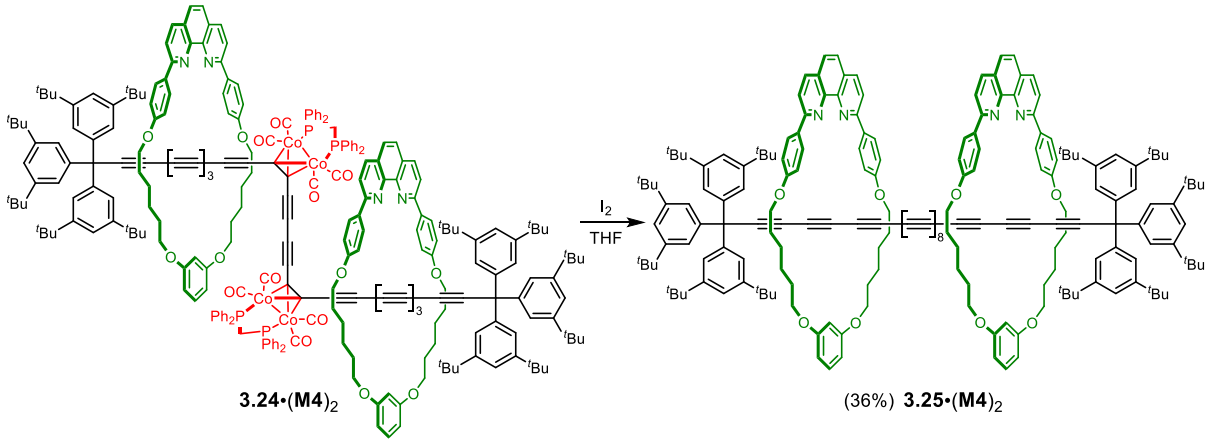

Scheme 3.6: Iodine mediated unmasking of **3.24**·(**M4**)$_2$ to give tetradecayne [3]rotaxane **3.25**·(**M4**)$_2$ through oxidative decomplexation (unmasking) of two dicobalt alkyne masking groups.

conditions. In all cases where unmasking was unsuccessful, we were unable to identify the decomposition product. A variety of conditions were screened, including solvent (and solvent mixtures), using both rigorously-degassed and oxygen-rich atmospheres and varying iodine equivalents, yet most had little effect on the outcome of the reaction. Even when the reaction did appear successful, the limited (~5 mg) scale of the reaction meant that the crude product was only ever obtained in sub-milligram quantities and further purification was required to achieve purity acceptable for characterisation by ^{1}H NMR and UV-vis spectroscopy and ESI mass spectrometry. Unfortunately, the problematic unmasking of this compound meant that the polyyne [3]rotaxane **3.25**·(**M4**)$_2$ could not be characterised by ^{13}C NMR spectroscopy.

To address the challenging unmasking step, alternative unmasking conditions were explored. So as to preserve stocks of the precious masked [3]rotaxane **3.24**·(**M4**)$_2$, initial unmasking attempts were made on the masked triyne **3.16**, then only the most promising conditions were applied to the final system. A summary of the masking conditions investigated are given in Table 3.1.

With regard to solvent selection, only the unmasking reactions in THF, CH_2Cl_2, DMF, MeCN and acetone appeared to successfully return triyne **3.15** (entries **2**-**6**, respectively). While CH_2Cl_2 and acetone initially seemed to be a promising alternative to THF, it was soon apparent that they were accompanied by significant decomposition and thus reduced yield of triyne. The unmasking reaction in MeCN appeared similar to that in THF, returning the triyne in an acceptable yield (70% or higher) with minimal decomposition. However, when applied to the masked [3]rotaxane, unexpected signals were observed in the high-resolution ESI mass

Table 3.1: Summary of selected conditions investigated for the unmasking of dicobalt-masked trine **3.16**. All reactions were performed on a 15 μmol scale (relative to **3.16**) at 20 °C under Ar, with the exception of entry **7**, which was performed under air. Where possible, unstabilised solvents were used.

Entry	Oxidant	Solvent	Outcome
1	I_2	THF	Higher [I_2], faster reaction, no visible decomposition
2	I_2 (10 eq.)	THF	Complete reaction after 15 min
3	I_2 (10 eq.)	CH_2Cl_2	Reaction fast, some decomposition observed
4	I_2 (10 eq.)	DMF	Incomplete after 30 min, decomposition observed
5	I_2 (10 eq.)	MeCN	Complete reaction after 15 min
6	I_2 (10 eq.)	Acetone	Reaction fast, some decomposition observed
7	I_2 (10 eq.)	THF	Complete reaction after 15 min
8	$Fe(NO)_3$ (10 eq.)	THF	Complete reaction after 15 min
9	NIS (10 eq.)	THF	Complete reaction after 4 hour
10	NBS (10 eq.)	THF	Complete reaction after 15 min
11	PIFA (10 eq.)	THF	Complete reaction after 15 min
12	Sulfur (10 eq.)	THF	No unmasking observed, decomposition visible
13	H_2O_2 (10 eq.)	THF	No reaction
14	Ph_2S_2 (10 eq.)	THF	No reaction
15	Ph_2Se_2 (10 eq.)	THF	No reaction

spectrum separated by approximate 63 mass units, in addition to the expected signal at m/z = 1387 for $[M+2H]^{2+}$ (Figure 3.8). These signals appear to correspond to the half-mass of a compound where I_2 is being added – likely across one of the triple bonds in the polyyne.

Flynn *et al.* previously documented the elimination of I_2 from diiodoalkenes can be promoted tetrabutylammonium iodide (TBAI).[39] The products of this unmasking reaction were treated with an excess of TBAI (20 eq.) in CH_2Cl_2 (Scheme 3.7), which after 4 hours returned the target polyyne [3]rotaxane **3.25**·(**M4**)$_2$ relatively cleanly (confirmed by UV-vis spectroscopy), albeit contaminated with tetrabutyl ammonium salts. Despite this success, it is obviously preferable to avoid the iodination of the polyyne in the first place, so exploration of alternative approaches continued.

Lewis *et al.* prepared tetracobalt tetrayne complexes employing the same ($Co_2(CO)_4$dppm) masking group and used ferric nitrate to unmask this dicobalt unit for the first time.[40] Treating masked triyne **3.16** to these conditions resulted in the swift oxidative

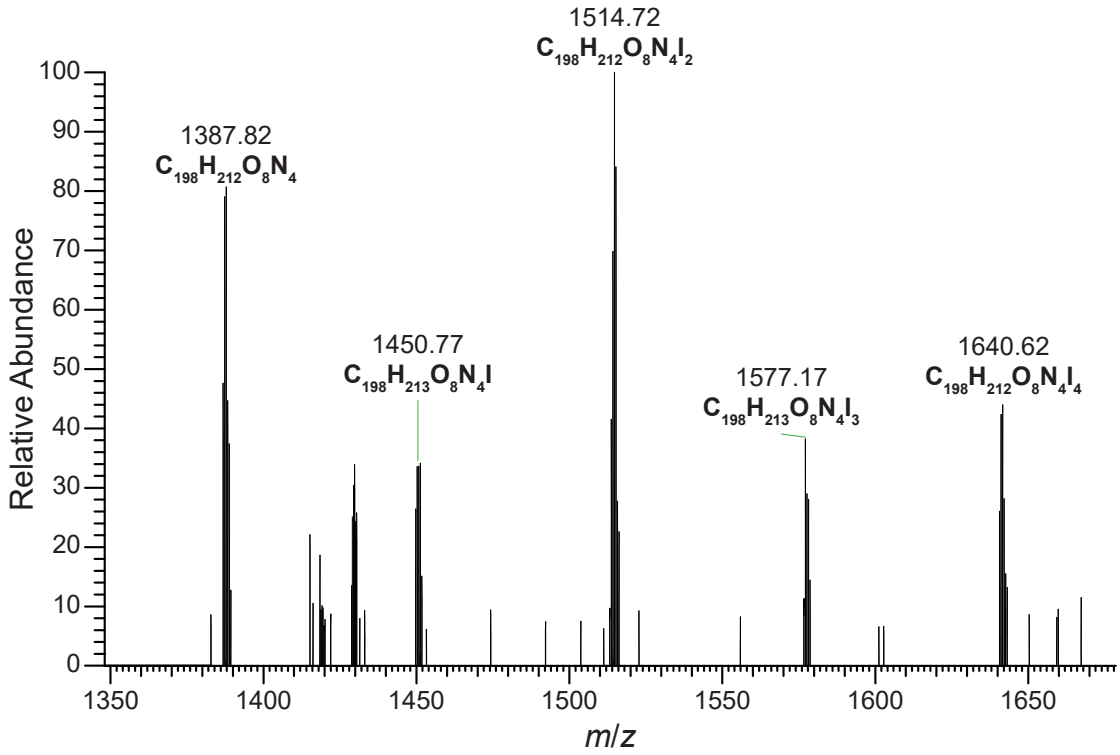

Figure 3.8: High resolution ESI mass spectrum of material isolated from unmasking dicobalt-masked [3]rotaxane **3.24**·(**M4**)$_2$ by I_2 in MeCN. Note the formation of multiple iodine-containg species ($[M+2H]^{2+}$ ions are labelled).

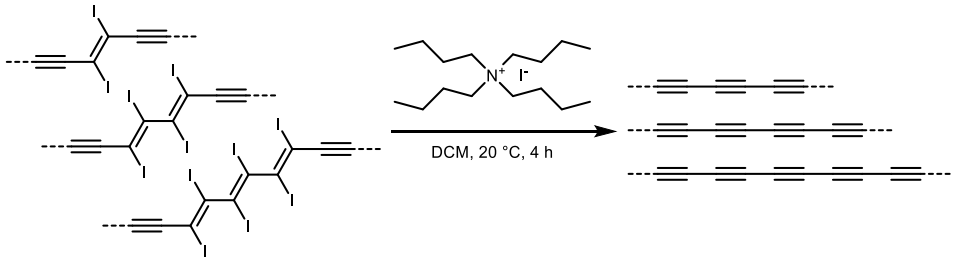

Scheme 3.7: Tetrabutylammonium iodide-promoted elimination of I_2 from diiodoacetylenes.[39]

decomplexation of the dicobalt group to return TIPS-TMS triyne (Table 3.1, entry **8**). Unfortunately, when applied to the masked [3]rotaxane **3.24**·(**M4**)$_2$, ESI-MS data appeared to suggest that only one of the dicobalt groups was removed, despite using 20 equivalents of $Fe(NO_3)_3$. While the ^{1}H NMR spectrum of a semi-purified material appeared to support this, the aromatic region corresponding to dppm resonances of the cobalt complex was more complicated than would be expected from loss of symmetry alone. We therefore suspect that some other reaction was also occurring at the cobalt complex.

N-Iodosuccinimide (NIS, Table 3.1, entry **9**) and *N*-bromosuccinimide (NBS, entry **10**) initially appeared more promising, particularly so for the latter, which displayed rapid oxidative decomplexation of the dicobalt masking group to cleanly return the triyne. Unfortunately, when

applying these conditions to the [3]rotaxane, both rapidly consumed the starting material (apparent by TLC), but no indication of product formation could be observed, nor were there any fractions obtained that displayed the distinctive UV-vis spectrum for the polyyne. Other potential oxidants tested were hydrogen peroxide (entry **13**), diphenyl disulfide (entry **14**) and diphenyl diselenide (entry **15**) although no reaction was observed for either, and the masked triyne was returned. While there are many possible oxidants and solvent combinations that could be postulated, it was becoming apparent that the macrocycle appears to be influencing the unmasking ability to a greater extent than we could have expected. Contrasting this to the masked 14-yne dumbbell **3.25** (prepared using an analogous procedure on non-interlocked precursors), which reliably gave rapid unmasking to the final 14-yne thread, albeit in low yields of approximately 10%.

3.3 Synthesis of Nanohoop-Protected Rotaxanes

To investigate the influence a macrocycle may have on the shielding of the polyyne in these [3]rotaxanes, and to test hypothesis of the effect on the macrocycle may have on the unmasking ability of the [3]rotaxane, alternative macrocycles were considered. We wanted to aim for a macrocycle that is significantly different from the phenanthroline macrocycle **M4** used previously. Cycloparaphenylenes are an interesting class of macrocyclic compounds than can be considered as a ring made up of 1,4-linked phenyl rings. These have attracted much interest of recent, particularly for their potential use in organic electronic applications due to: (i) their decreasing HOMO-LUMO gap with a decreasing number of constituent benzene units[41] – in stark contrast to linear conjugated materials, including their linear poly(*para*-phenylene) counterparts which have a narrowing HOMO-LUMO energy as molecules increase in size;[42] (ii) their size-dependent fluorescence and; (iii) their ability to form host-guest interactions that aid formation of inclusion complexes.[43,44]

Jasti *et al.* have pioneered the development of CPPs and functionalised variants, made by replacing one benzene unit in the hoop with a functionalised variant. Many CPP-based hoops (nanohoops) have been developed with variations to the linkage of constituent rings (e.g. by introducing *ortho*- or *meta*-linked rings), or through incorporation of metal-binding motifs, such as pyridine, bipyridine and phenanthroline units. Recently, Jasti *et al.* developed two 2,6-

pyridine-functionalised CPPs (Figure 3.9) with endotopic binding sites that have been shown to be good candidates in forming mechanically interlocked molecules via a Cadiot-Chodkiewicz AMT coupling reaction.[45] The geometry of the *meta*-linked pyridine is aptly positioned to direct bond-formation to the interior of the macrocyclic cavity (predicted by DFT and later confirmed by X-ray crystallography) and is key to the success of the AMT reaction.

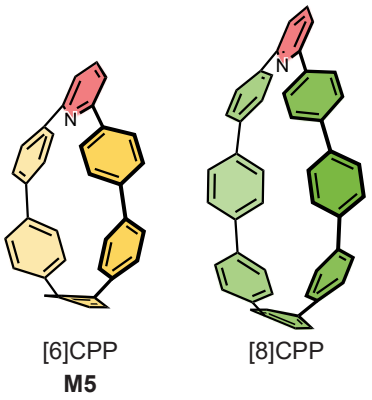

Figure 3.9: Two 2,6-pyridyl nanohoops, indicating endotopic binding sites (coloured red).

The smallest of these nanohoops – the 6-ring **M5** – was of particular interest for this project. While the fact that this is the most strained of the nanohoop series, and may risk undesirable reactions with the thread, it should also offer the best shielding of the final polyyne. An additional advantage of the nanohoops over the phenanthroline-based macrocycles are the absence of any strong interactions that may cause the hoops to stack in the final polyyne [3]rotaxane. As mentioned previously, having the two macrocycles able to move independently on the thread should provide the best protection of the thread and thus offer the highest stability to the final polyyne.

3.3.1 Nanohoop Synthesis

Initial studies towards preparing **M5**-based rotaxanes were made on a sample of nanohoop **M5** generously provided by Jasti *et al.*, then later synthesised following their reported procedures (summarised in Scheme 3.8).[45–48] One of the key components in the synthesis is the TES-protected chloroketone **3.28**, prepared from lithiation of 1-bromo-4-chlorobenzene, attack onto **3.26**, then TES protection of **3.27**. Mono-lithiation of 1,4-dibromobenzene, then subsequent attack onto the chloroketone and later TES protection of alcohol **3.29** yields the cyclohexadiene compound **3.30**. The cyclohexadiene unit acts as a 'masked' benzene group that can later undergo reductive aromatisation to return the phenyl ring. Importantly, the presence of the two sp^3 centres on the cyclohexadiene ring of these intermediates generates an out-of-plane bend that assists the formation of curved structures. In fact, this approach works so well that the macrocyclisation reaction of di-BPin **3.33** (step (ix), Scheme 3.8) to give TES-protected macrocycle **3.34** can occur in an impressive 76% yield – exceeding the yields obtained by most

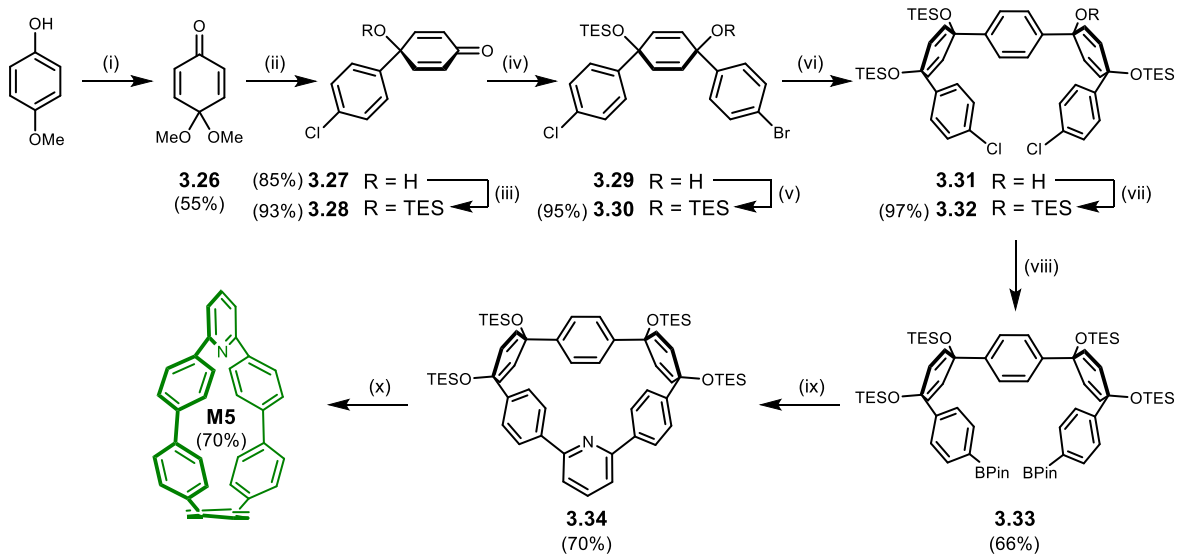

Scheme 3.8: Synthetic scheme towards 2,6-pyridiyl [6]CPP **M5**.[45–48] (i) (diacetoxyiodo)benzene, methanol, 20 °C, 18 h, Ar; (ii) 1-bromo-4-chlorobenzene, *n*-BuLi, THF, −78 °C, 30 min, Ar then **3.26**, −78 °C, 90 min, Ar then AcOH/H_2O (10%); (iii) imidazole, TESCl, DMF, 50 °C, 90 min, Ar; (iv) 1,4-dibromobenzene, *n*-BuLi, THF, −78 °C, 1 h, Ar then **3.28**, −78 °C, 1 h, Ar; (v) imidazole, TESCl, DMF, 45 °C, 18 h, Ar; (vi) *n*-BuLi, THF, −78 °C, 30 min, Ar then **3.28**, −78 °C, 1 h, Ar; (vii) imidazole, TESCl, DMF, 45 °C, 18 h, Ar; (viii) B_2Pin_2, $Pd(OAc)_2$ (5 mol%), SPhos, K_3PO_4, 1,4-dioxane; 90 °C, 2 d, Ar; (ix) 2,6-dibromopyridine, Pd SPhos G2 (10 mol%), K_3PO_4, 1,4-dioxane, 80 °C, 15 min, Ar; (x) TBAF, THF, 20 °C, 1 h, Ar then H_2SnCl_4, THF, 20 °C, 1 h, Ar then NaOH.

traditional high-dilution macrocyclisation approaches. With the cyclic structure now formed, TBAF was used to cleave the TES groups before reductive aromatisation by H_2SnCl_4 to 'unmask' the two phenyl rings and return nanohoop **M5**.

3.3.2 Nanohoop [2]Rotaxane Synthesis

With the nanohoop in hand, attempts were then made to prepare a Tr*-stoppered dicobalt-masked [2]rotaxane using nanohoop **M5** (Scheme 3.9). Due to the prior success with the THF/K_2CO_3 conditions, we first explored rotaxane synthesis under these conditions, only changing the Cu(I) source. The weaker binding of **M5** with copper(I) cations means that the **M5**·CuI complex cannot be pre-formed in the same way as for the phenanthroline-based macrocycle **M4**, so a Cu(I) source soluble in organic solvents, $[Cu(MeCN)_4][PF_6]$, was used instead. After a few attempts, we quickly found that running this reaction under these

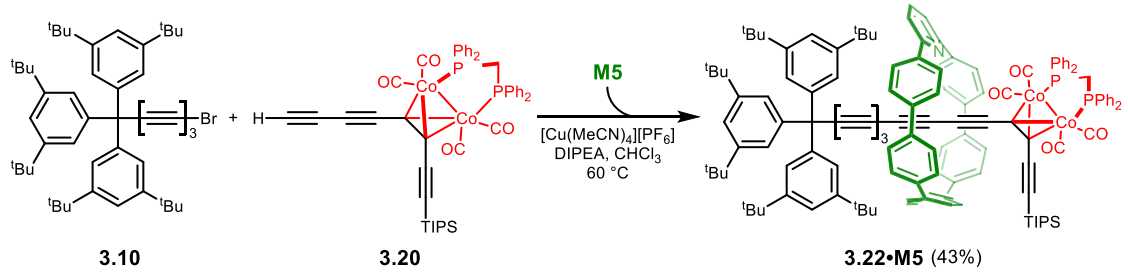

Scheme 3.9: Active metal template Cadiot-Chodkiewicz approach to dicobalt-masked [2]rotaxane **3.22·M5**.

conditions was unlikely to yield the interlocked product and only the cross- and homocoupled dumbbells were isolated instead. It is suspected that the absence of any interlocked compounds may be due to weak binding of Cu(I) ions exhibited by the nanohoop. Running the reaction in even mildly coordinating solvents, such as THF and dioxane, could result in competition between the nanohoop and solvent for Cu(I) cations. With the metal being taken away from the cavity of the macrocycle it would make sense that only the non-interlocked components are observed. Indeed, upon switching to non-coordinating solvents, such as $CHCl_3$ or toluene, and when using a more soluble base (*N*,*N*-diisopropylethylamine, DIPEA)[45,49] we were successful in isolating the nanohoop [2]rotaxane **3.22·M5** in up to 43% yield. $CHCl_3$ appeared to give marginally higher yields of the rotaxane than toluene, so this was used in subsequent reactions.

[2]Rotaxane **3.22·M5** was characterised by a suite of spectroscopic techniques. Surprisingly, ^{13}C NMR, and to a lesser extent ^{1}H NMR, spectra displayed more resonances than were initially expected – the former clearly displaying 5 additional Ar-C nanohoop resonances than expected. These resonances have been attributed to the phenylene C-H carbons of the nanohoop that, due to restricted rotation of the phenyl rings in the interlocked molecule, now become asymmetric. More detailed analysis on this observation was made on the polyyne [3]rotaxane (*vide infra* Section 3.3.4).

3.3.3 Nanohoop [3]Rotaxane Synthesis

With a robust procedure to the nanohoop [2]rotaxane **3.22·M5** now developed, the TIPS deprotection and oxidative homocoupling to the masked [3]rotaxane were then investigated (Scheme 3.10). As with the analogous **M4**-protected compound (**3.22·M4**), TBAF in wet THF proved highly successful at cleaving the TIPS group in good yield and with minimal

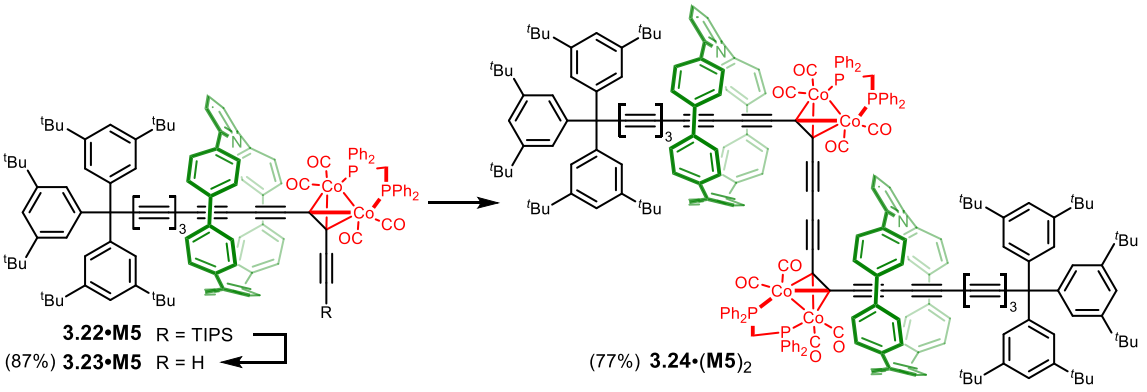

Scheme 3.10: Oxidative homocoupling scheme to prepare dicobalt-masked nanohoop [3]rotxane **3.24·(M5)**$_2$. Successful coupling was achieved using modified Glaser conditions described in Section 3.3.3.2.

decomposition. Subjecting deprotected [2]rotaxane **3.23·M5** to the same Glaser-Hay conditions as before (CuCl, TMEDA, O_2) resulted in a rapid conversion to a species of higher polarity and larger size (confirmed by TLC and analytical GPC, respectively), but with surprisingly complicated ^{1}H and ^{13}C NMR spectra. The aromatic region was most diagnostic with apparent splitting to the nanohoop resonances, suggesting that some undesirable reaction was occurring on the hoop. As it was difficult to pinpoint whether or not successful coupling was achieved, the product of this reaction was subjected to the subsequent unmasking conditions (I_2/THF). After brief purification, a species was observed with a similar UV-vis spectrum to that of the polyyne dumbbell (previously reported).[19] This suggests that the acetylene coupling is in fact working and that the polyyne is unaffected by this side reaction on the macrocycle. However, complicated ^{1}H and ^{13}C NMR spectra hint towards instability of the nanohoop with respect to these Glaser-Hay conditions.

Further verification of the nanohoop instability to these reaction conditions came from treating TIPS-protected nanohoop [2]rotaxane **3.22·M5** to the same conditions (CuCl, TMEDA, O_2, entry **1**, Table 3.2). As this molecule bears no terminal acetylene, we would not expect any coupling reaction to take place, and that only starting material would be recovered. However, we instead observed the conversion of **3.22·M5** to an unknown species displaying a similarly complicated ^{1}H NMR spectrum to that obtained in the aforementioned Glaser approach. No easily identifiable signals for starting material or suspected product could be

Table 3.2: List of nanohoop-protected [2]rotaxane **3.22·M5** coupling conditions and their respective outcomes.

Entry	Conditions	Outcome
1[50]	CuCl, TMEDA, CH_2Cl_2, O_2	Complicated NMR spectra, splitting of macrocyclic resonances suggest decomposition
2[51,52]	$Cu(OAc)_2$, pyridine, Ar	Very slow reaction, mainly staring material recovered
3[53]	CuCl, pyridine, air	Decomposition observed
4[54,55]	CuI, $Pd(PPh_3)_2Cl_2$, DIPA, $CHCl_3$, 1,4-benzoquinone, air	Complicated NMR spectra, splitting of macrocyclic resonances suggest decomposition
5[56]	CuI, $NiCl_2(H_2O)_6$, TMEDA, THF, air	Broadened and complicated NMR spectra suggest decomposition
6[57]	CuI, ethyl 2,2-dibromo-3-oxobutanoate, CH_2Cl_2, Et_3N, air	Complicated NMR spectra, splitting of macrocyclic resonances suggest decomposition

deciphered in the ESI-MS spectrum. Since TMEDA is a somewhat nucleophilic base, it is not too surprising that side reactions may occur with the strained **M5** nanohoop in this rotaxane. Curiously, when treating nanohoop **M5** alone with the Glaser-Hay conditions, it exhibits perfect stability and can be recovered unchanged. This suggests that simply **M5** being part of a rotaxane is altering the reactivity of the nanohoop.

The stability of [2]rotaxane **3.22·M5** was also evaluated with respect to variations in copper-catalysed alkyne homocoupling conditions (Table 3.2). Some of the most notable being: (i) Eglinton (entry **2**); (ii) CuCl, pyridine, air[53] (a less active but longer-lived catalyst system, entry **3**) and; (iii) Pd co-catalysed alkyne homocoupling conditions (entry **4**), under which good stability of the nanohoop [2]rotaxane was observed for all. While the stability of **M5** was no longer a concern, when attempting to convert [2]rotaxane **3.23·M5** to [3]rotaxane **3.24·(M5)**$_2$, either no coupling was observed, in the case of (i) and (ii), or the starting material, product, or both were found unstable to the conditions, as was the case for (i). Two less common coupling conditions were also attempted (entries **5** and **6**)[56,57] but the coupling reaction is both cases was unfortunately not successful.

3.3.3.1 Coupling via Mercurial Acetylides

The continued problems encountered with these copper-catalysed oxidative homocoupling reactions prompted exploration into alternative, copper-free approaches. Mercury and its ions find use in a wide array of organometallic chemistry. Most helpful to the aims of this project are its complexes with acetylenes. There have been numerous reports of Hg-acetylene linked complexes, in which two acetylenes are bridged by a Hg(II) ion.[58–61] Bruce *et al.* documented the use of these organomercurials as a bridge between two acetylenes bearing the same dicobalt carbonyl groups used in this chemistry, suggesting that the chemistry should at least be compatible with [2]rotaxane **3.23·M5**.[62] Formation of these organomercurials was achieved under mild conditions ($Hg(OAc)_2$ in THF/MeOH in the presence of a base to deprotonate the acetylene), which would be advantageous to our, apparently, reactive system. Thermal decomposition of the molecules could then be induced, in which the mercury ion is extruded, and the two bridged acetylenes are coupled together, albeit in a relatively low yield of 20%.

Preparing a Model Dicobalt-Masked Mercurial Acetylide

To gain a better understanding into the formation and extrusion of these dicobalt-capped mercurial acetylides, initial work focussed on a model system, first forming the tetracobalt mercurial acetylide **3.35** (Scheme 3.11), then testing the subsequent mercury extrusion step to give the butadiyne-linked tetracobalt species **3.36**. Target **3.36** was selected for two main reasons: (i) the relative ease with which it can be prepared and its good synthetic availability and; (ii) TMS deprotection would leave a terminal monoyne that should show somewhat similar reactivity to that of deprotected [2]rotaxane **3.23·M5** and thus should be a good model for the final target. An additional benefit of this compound is that since conditions for TMS deprotection and mercurial formation are similar (K_2CO_3 in THF/MeOH), we could explore the *in situ* TMS deprotection and mercurial formation.

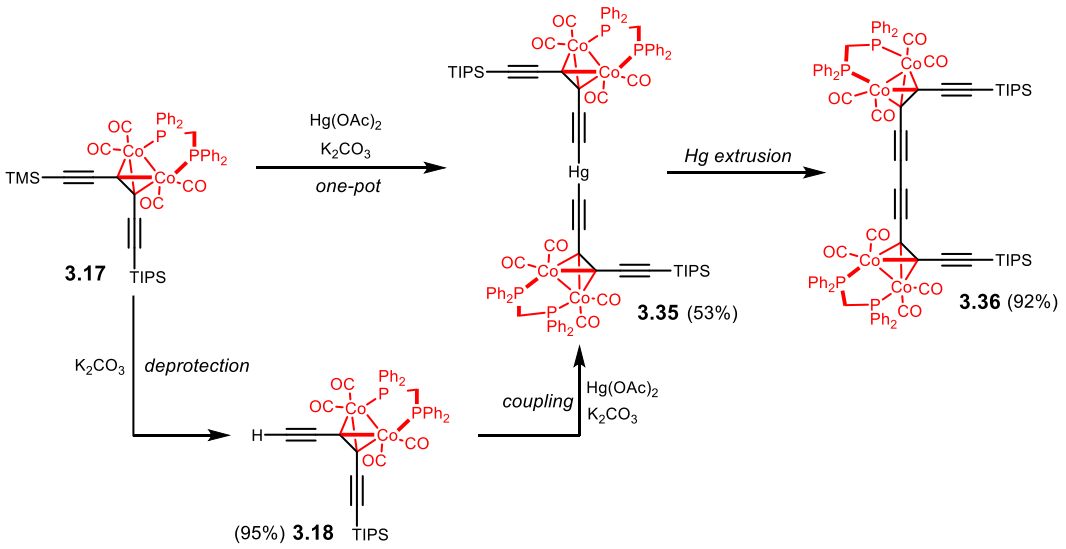

Scheme 3.11: Two approaches to dicobalt-capped mercurial acetylide **3.35**.

Treating dicobalt-masked TIPS-TMS triyne **3.17** with K_2CO_3 and $Hg(OAc)_2$ in methanolic THF resulted in the expected mercurial **3.35** being formed in an acceptable 53% isolated yield. While it was not possible to obtain mass spectrometry evidence of the mercurial, we were able to obtain good quality ^{1}H and ^{13}C NMR spectra (Figure 3.10a and b), the latter being particularly useful as a reference for when applying this to the [3]rotaxane. Additionally, we were also successful in obtaining a ^{199}Hg NMR spectrum of this compound (Figure 3.10c), displaying a resonance at 828.32 ppm that is roughly in the range that would be expected for similar mercurial acetylides. It would be interesting to look for ^{199}Hg-X correlations (e.g. in a $^{13}C/^{199}Hg$ HSQC experiment), which could give us more information about the carbon adjacent

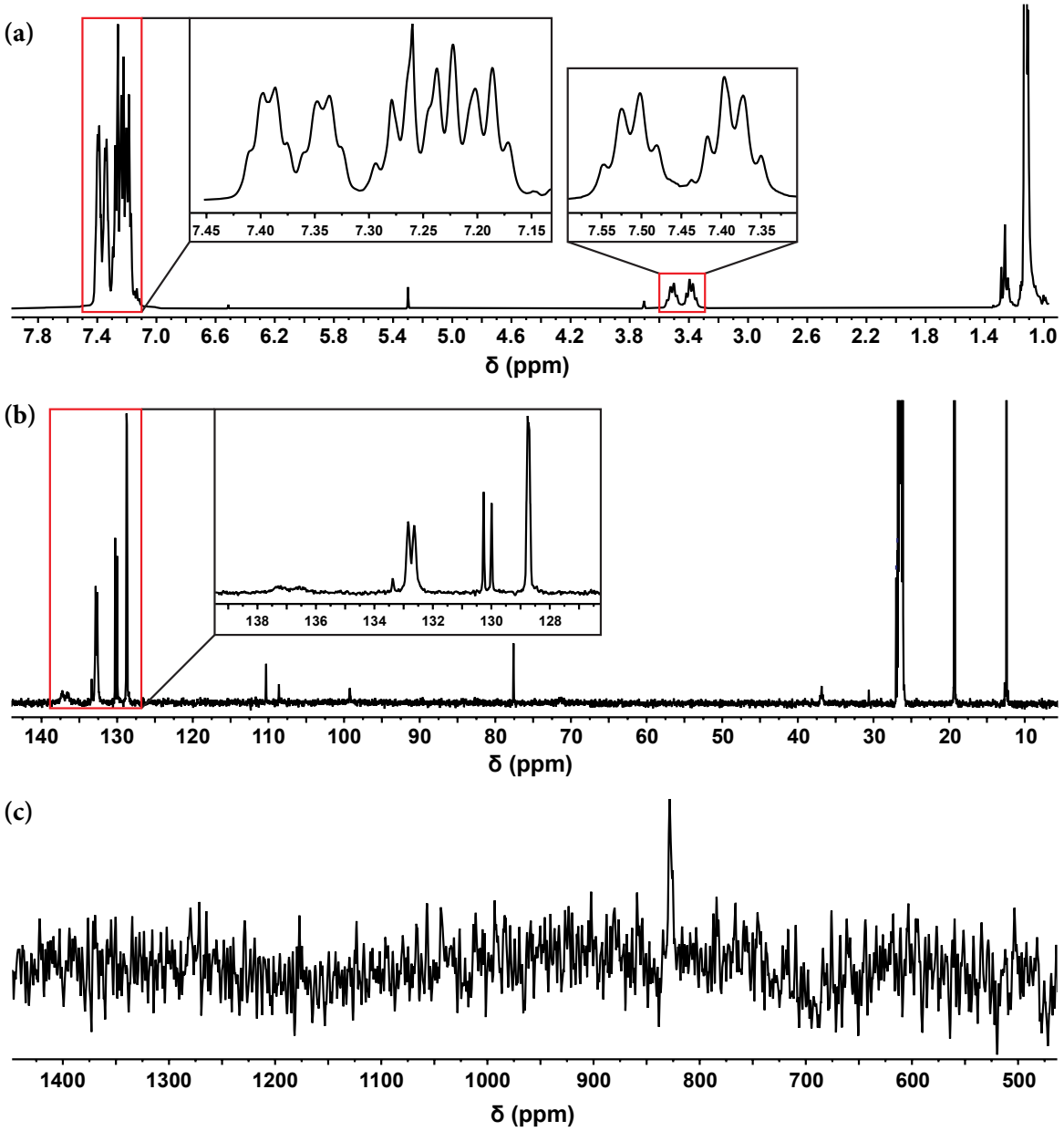

Figure 3.10: (a) ^{1}H (600 MHz, C_6D_6), (b) ^{13}C (126 MHz, C_6D_6) and (c) ^{199}Hg (89 MHz, $CDCl_3$) NMR spectra of the model dicobalt-masked mercurial acetylide **3.35**. All spectra recorded at 298 K.

to the Hg atom, but unfortunately we were unable to run such NMR experiments due to limitations in the NMR probe. Assignment of this carbon resonance was rendered more difficult due to the low sensitivity of ^{13}C, coupled with the low natural abundance of ^{199}Hg. We would expect to see satellites due to the coupling to spin-½ ^{199}Hg, which is only ~17% abundant. Combining this with the low natural abundance of ^{13}C, means we are looking at satellites for which are 17% of 1% (i.e. 0.17% abundant).

With a route to model mercurial **3.35** developed, the subsequent extrusion to give the butadiyne-linked tetracobalt compound **3.36** was investigated. The thermal extrusion procedure documented by Bruce *et al.* was first studied by elevated temperature ^{1}H NMR

experiments (Figure 3.11). The mercurial acetylide was dissolved in tetrachloroethane-d_2, thoroughly degassed by three freeze-pump-thaw cycles, then subject to ^{1}H NMR experiments at 10 minute intervals for 3 hours at 333 K (60 °C). Unfortunately, even after the 3 hour period, there was no apparent change in spectral form (Figure 3.11), other than peak broadening due to a drift in shim. This was an obvious indication that thermal extrusion was not looking like a viable option. It may be possible to induce extrusion by heating above 60 °C, but this is not practical when applying this to prepare the final [3]rotaxane. Additionally, when considering the low yield (20-30%) obtained in literature for this thermal extrusion step, it seemed best to search for alternative conditions.

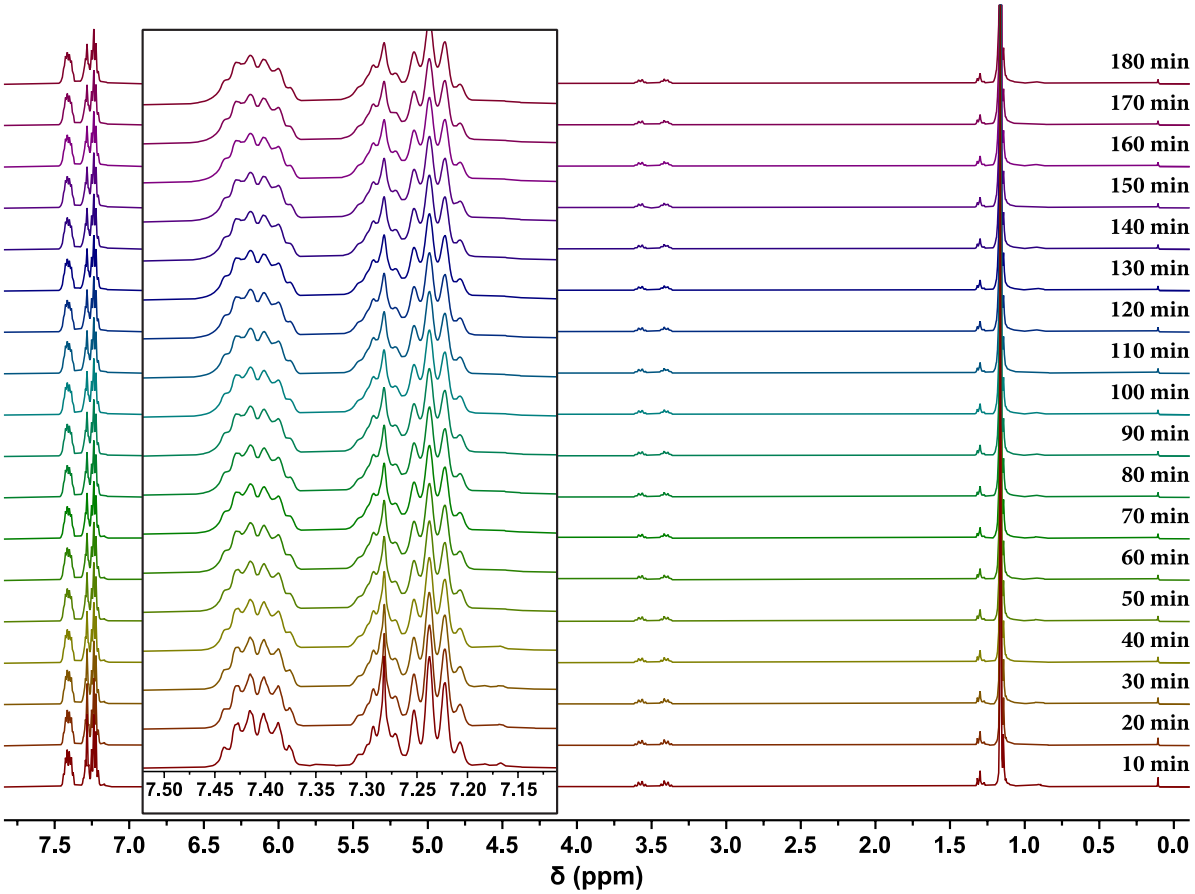

Figure 3.11: Thermal extrusion of mercury from the model mercurial acetylide **3.35** was followed by fixed time ^{1}H NMR experiments at 10 minute intervals for a total time of 3 hours (500 MHz, $Cl_2CDCDCl_2$ 333 K).

More recently, Hill *et al.* reported the extrusion of Hg from mercurial acetylides promoted by a Rh catalyst (Scheme 3.12).[58] The authors demonstrated the synthesis of tungsten-capped oligoynes, and their subsequent Rh-catalysed extrusion to yield the homocoupled product. Simply stirring a thoroughly-degassed solution of mercurial acetylide and $[Rh(PPh_3)_2(CO)Cl]$ catalyst in CH_2Cl_2 resulted in conversion to the product over a period of

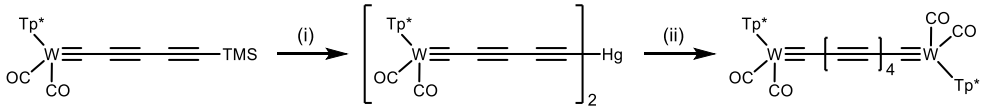

Scheme 3.12: Synthesis of ditungsten dodecahexayne via a tungsten-capped organomercurial.[58] (i) TBAF then $HgCl_2$; (ii) cat. $[RhCl(CO)(PPh_3)_2]$. Tp* = hydrotris(dimethylpyrazolyl)borate.

approximately 18 h at 40 °C. The mild nature of these conditions was promising that they would leave the dicobalt carbonyl masking group intact.

The Rh-catalysed extrusion was first tested on the model mercurial **3.35** and followed by timed ^{1}H NMR experiments at elevated temperatures (298 K, 313 K and 333 K). The degree of conversion was assessed by comparison to the butadiyne-linked tetracobalt product **3.36** (synthesised separately through a Glaser-Hay coupling approach). At 298 K, there was no observable reaction, with only starting materials being recovered after a 24 h period. Upon raising the temperature to 313 K there were signs of conversion to the reference product, with all starting material being consumed after 24 h. The final temperature on trial, 333 K was most promising, with complete conversion of the starting material to the desired product being observed after 10 h (Figure 3.12). As before, a drift in shim resulted in broadening of the signals

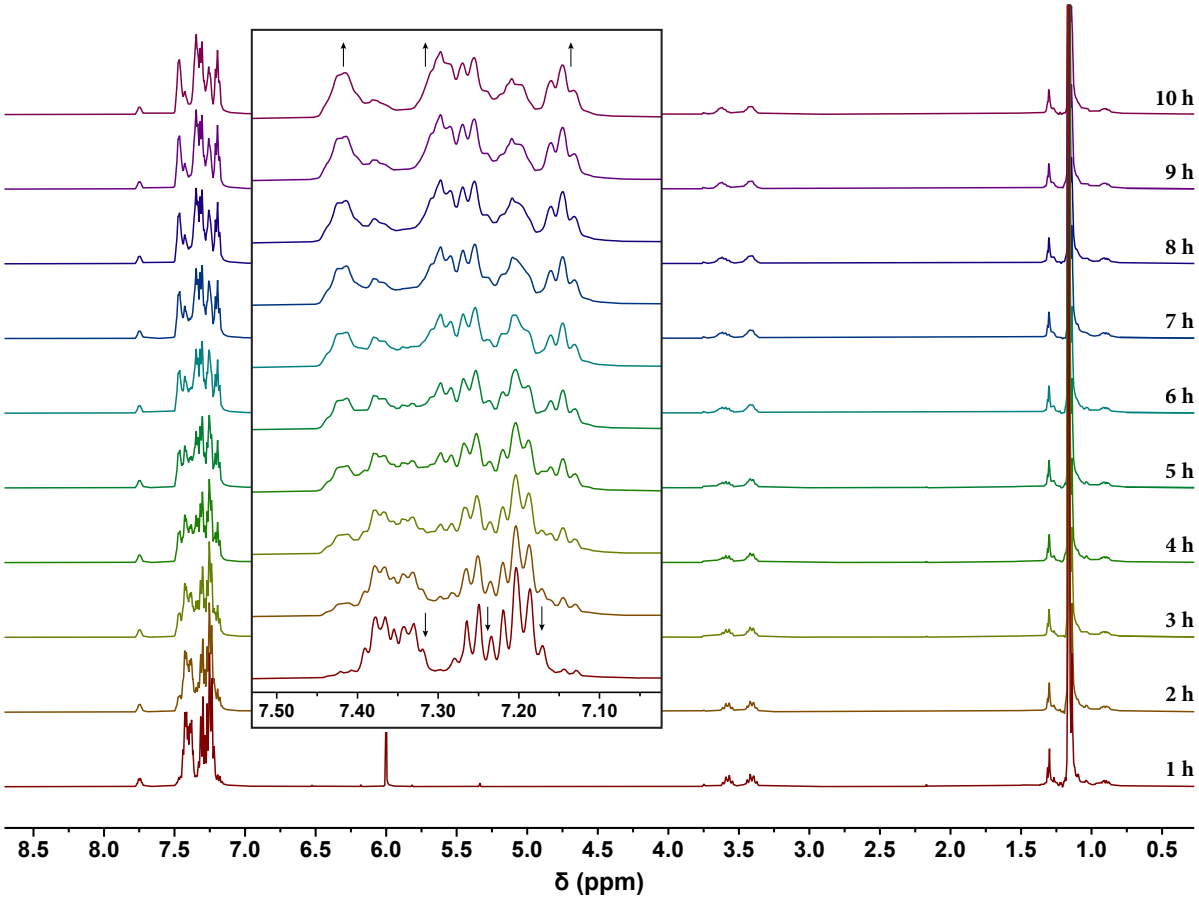

Figure 3.12: Rh-catalysed extrusion of mercury from the model mercurial acetylide **3.35** was followed by fixed time ^{1}H NMR experiments (500 MHz, $Cl_2CDCDCl_2$ 333 K) and deemed complete after 10 h. Peak broadeing is due to a drift in shim.

over the course of the experiment but shimming again after the 10 h period returned a sharpened spectrum displaying signals that match well with reference material (Figure 3.13). After purification by a short silica column, the butadiyne-linked product was obtained in a 92% isolated yield – to our surprise, higher than that reported in literature.

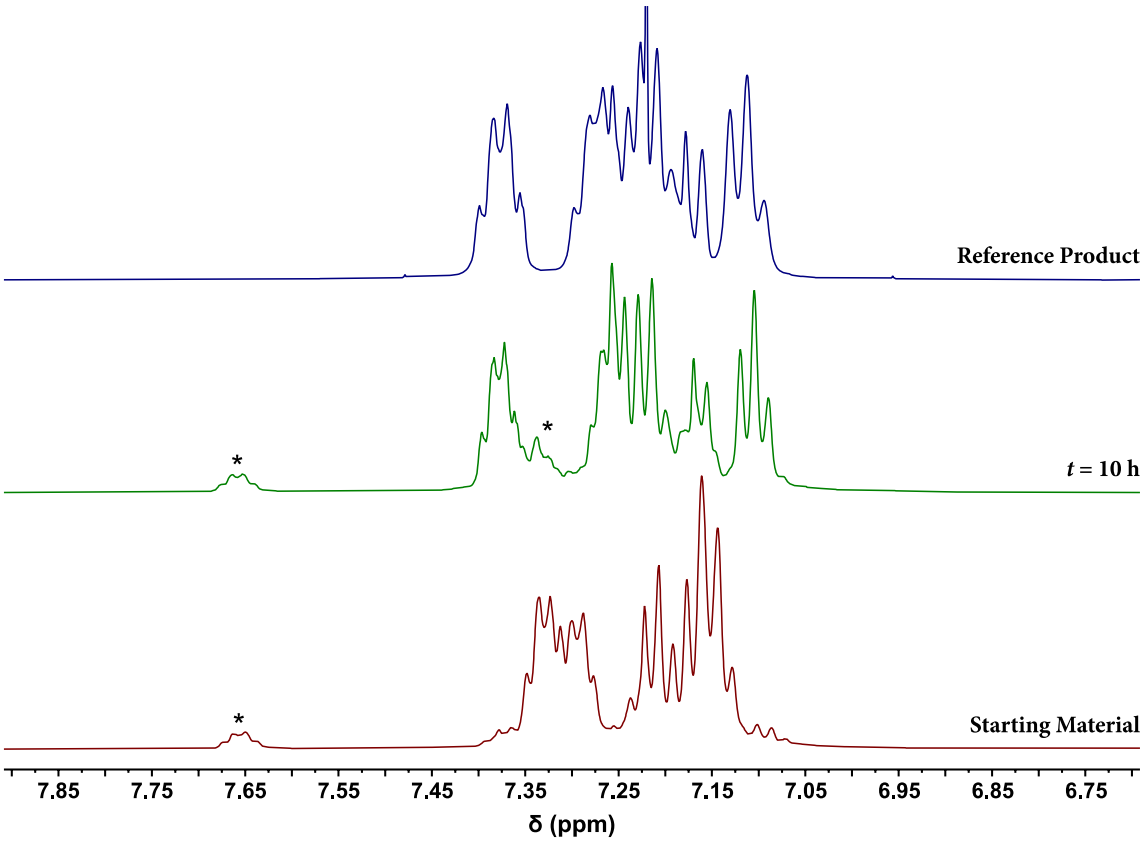

Figure 3.13: NMR (500 MHz, $Cl_2CDCDCl_2$ 298 K) comparison of the Rh-catalysed mercury extrusion of mercurial **3.35** initially and after 10 h to a reference material obtained by a Glaser approach. (* decontes Rh PPh_3 ligand resonances)

Applying Mercury Chemistry to the Nanohoop [3]Rotaxane

Following the successful formation of, and subsequent Hg-extrusion from, mercurial **3.35**, the same chemistry was then applied to the coupling of nanohoop [2]rotaxane **3.23·M5**. Unlike with the model system, the TIPS group in [2]rotaxane **3.23·M5** are stable to the mercurial formation conditions and therefore required cleavage with TBAF in wet THF. Following this, treatment with $Hg(OAc)_2$ and K_2CO_3 in THF/MeOH (Scheme 3.13) resulted in a distinct new species (detected by TLC) that was the presumed mercurial. Analytical GPC (Figure 3.14) provided further insight, displaying a major peak of similar size to the masked **M4**-protected [3]rotaxane **3.24·(M4)**$_2$ reference, and only a small peak of similar size to the [2]rotaxane – likely trace amounts of starting material. Unfortunately, there was no signal for the mercurial by

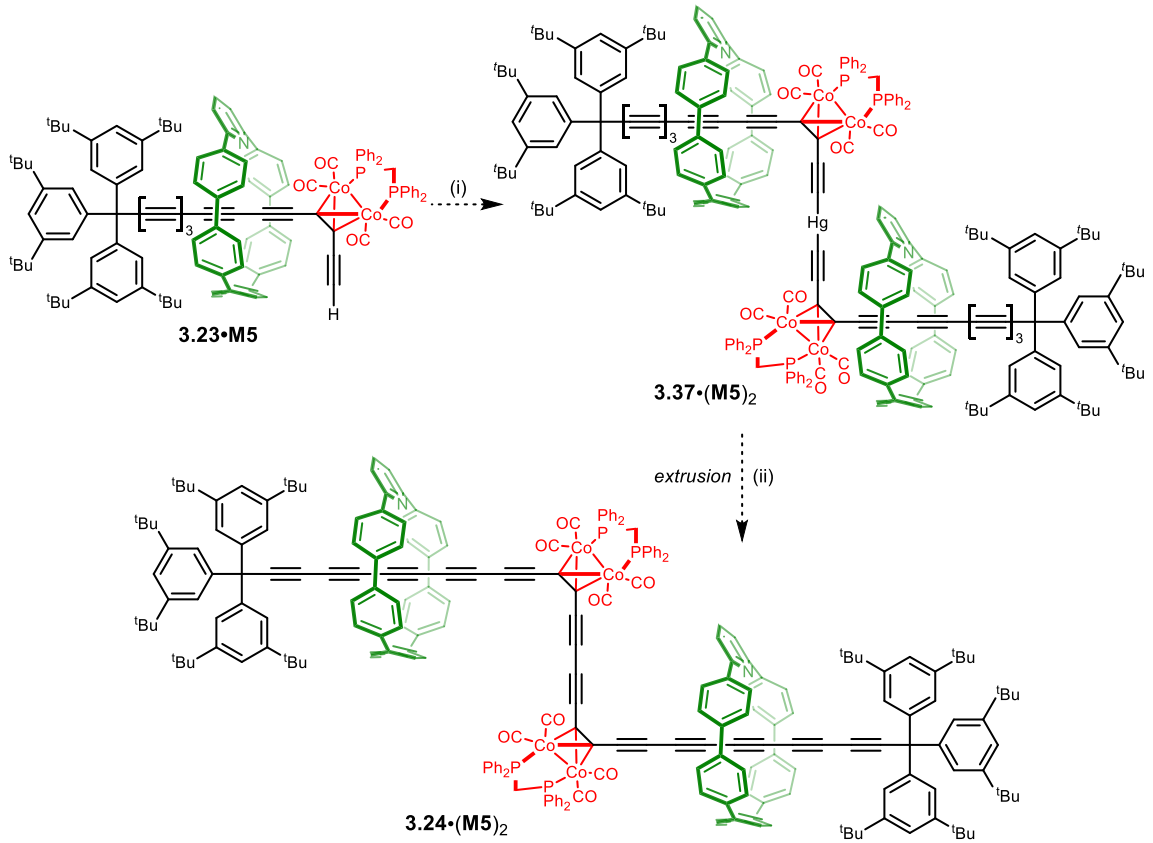

Scheme 3.13: Proposed scheme to generating dicobalt-masked nanohoop [3]rotaxane **3.24**·(**M5**)$_2$ via a mercurial acetylide **3.37**·(**M5**)$_2$. (i) $HgCl_2$, K_2CO_3, THF/MeOH; (ii) heat *or* [$Rh(PPh_3)_2(CO)Cl$], CH_2Cl_2.

either ESI- or MALDI-TOF MS methods, making characterisation of the mercurial challenging. Concerned with the potential instability of this compound, only minimal purification (silica chromatography) was performed before the subsequent extrusion step. Mercurial **3.37**·(**M5**)$_2$ was then subject to Rh-catalysed extrusion in dry, degassed $CHCl_3$ at 40 °C for 24 h. As with the model system, the near-identical polarity similar general size of both mercurial and the butadiyne-linked species made it difficult to follow the course of the reaction by TLC or GPC techniques. Compounding this was the absence of any signals in the mass spectrum, rendering mass spectrometry equally unsuitable for following the reaction. Based on our experience with the model system, the reaction was assumed complete after a 24 hour time period.

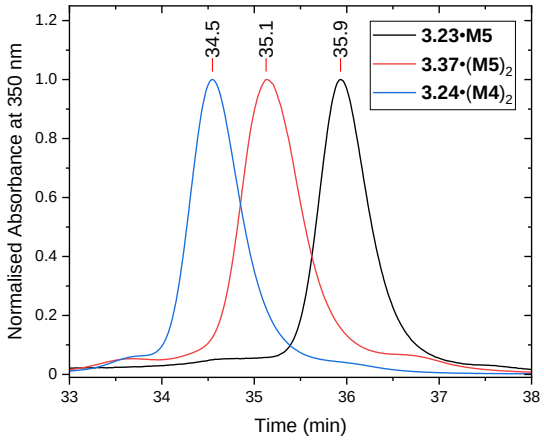

Figure 3.14: Normalised analytical GPC traces of (black) nanohoop-protected [2]rotaxane **3.23**·**M5**, (red) mercurial [3]rotaxane **3.37**·(**M5**)$_2$ and (blue) phenanthroline-protected [3]rotaxane **3.24**·(**M4**)$_2$. An intermediate retention time for **3.37**·(**M5**)$_2$ provided evidence for its successful formation.

Unfortunately, after silica and size-exclusion chromatography (to remove any [2]rotaxane starting material and Rh-catalyst), NMR spectroscopy revealed a rather complicated spectrum. The absence of the terminal acetylene resonance gave initial promise that extrusion had been successful but, as with many of the copper-catalysed couplings described previously, noticeable splitting in the ^{t}Bu and Tr* aromatic region, and complicated nanohoop signals brought cause for concern. Similarly to the previous approaches, it appeared that the molecule underwent undesired reaction to form an unidentifiable product.

With difficulties in determining whether the extrusion had been successful, the material was taken through to the final unmasking step, as this would confirm whether or not successful coupling of the polyyne thread had been achieved. Treatment of the suspected [3]rotaxane **3.24**·(**M5**)$_2$ with dicobalt unmasking conditions (I_2, THF) resulted in rapid conversion to a new species (detected by TLC) of significantly lower polarity and with the characteristic yellow/orange colour of the 14-yne. All starting material was consumed after 5 minutes, and the reaction mixture purified by silica and size-exclusion chromatography. UV-vis analysis of the suspected product pleasingly revealed the characteristic spectrum of the 14-yne (Figure 3.15), confirming that, despite a still-complicated NMR spectra, the organomercurial formation and subsequent extrusion had both been successful. That being said, the apparent splitting of the Tr* and nanohoop resonances suggest that an undesired side reaction in the extrusion step was preventing isolation of the desired material. While this work had not proved successful on the rotaxanes, the promising results from the model system means it may find use in other cases when copper-based conditions are not suitable.

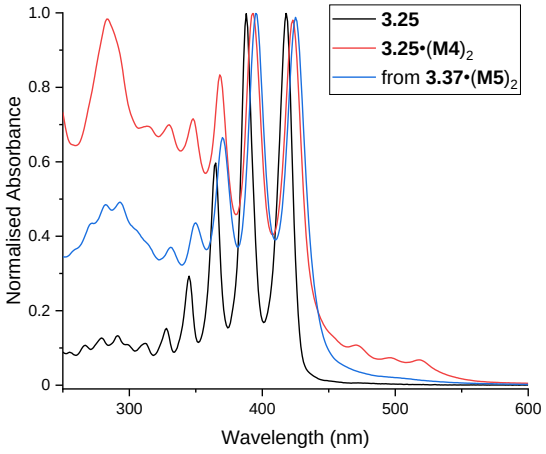

Figure 3.15: UV-vis spectrum of the suspected nanohoop [3]rotaxane (blue) obtained from Hg-extrusion of mercurial acetylide **3.37**·(**M5**)$_2$. The characterisitc vibronic band matches well with that of the **M4**-protected 14-yne [3]rotaxane **3.25**·(**M4**)$_2$ (red) and 14-yne thread **3.25** (black). All solutions in *n*-hexane at 25 °C.

3.3.3.2 Coupling via Bipyridine/Cu(I) Conditions

As alkyne homocouplings involving mercurial acetylides was proving challenging, work returned to the copper-catalysed couplings. It was noted that during the previous Glaser-Hay attempts, side reactions dominated the reaction outcome; even subjecting TIPS-protected nanohoop [2]rotaxane **3.22·M5** to Glaser-Hay conditions led to the formation of a new species. Since a similar decomposition was not observed in other copper-based couplings, we suspected that TMEDA is the cause of this undesired reaction. Alternative ligands for Cu(I) that should be less reactive than TMEDA were investigated. Bipyridines are known to chelate Cu(I) cations similarly to TMEDA but were hoped to be less reactive towards these rotaxanes. Substituted bipyridines may prove more useful due to their enhanced solubility in common organic solvents compared to their unsubstituted counterparts. 4,4'-Di-*tert*-butyl-2,2'-bipyridine (**3.38**) has previously been reported as a suitable ligand for Cu(I) in a Glaser-type reaction of oligo- and polyynes[20] and provided a promising starting point.

Deprotected nanohoop [2]rotaxane **3.23·M5** was treated with CuCl and bipyridine **3.38** (both 0.1 eq.) in CH_2Cl_2. The reaction was vigorously stirred in air at 20 °C for 24 hours. Over this time there was a slow appearance of a single new species, visualised by TLC. After a 24 hour period the reaction was stopped even though some starting material remained, so as to minimise any potential side-reactions that were seen previously with the other Cu-catalysed homocouplings. After purification to remove any remaining [2]rotaxane **3.23·M5** and bipyridine, ^{1}H and ^{13}C NMR made it instantly apparent that the reaction had been successful and masked nanohoop [3]rotaxane **3.24·(M5)**$_2$ was returned without any unwanted side reactions, albeit in a low 11% yield. Further analysis of ^{1}H spectrum revealed the absence of both the terminal acetylene and TIPS resonances (Figure 3.16). The ^{13}C NMR spectrum was also in line with our expectations, displaying the correct number of resonances. Unfortunately, and despite out best efforts, we were unable to obtain the mass spectrum of **3.24·(M5)**$_2$ by any mass spectrometry methods.

Scrupulous optimisation of this coupling reaction was made to improve the coupling efficiency. Different Cu(I) and bipyridine equivalences were screened, as well as different solvent and temperature combinations. Optimal conditions were determined to be using 10 eq. and 12 eq. of the respective bipyridine ligand **3.38** and CuCl in dry CH_2Cl_2. Heating the reaction

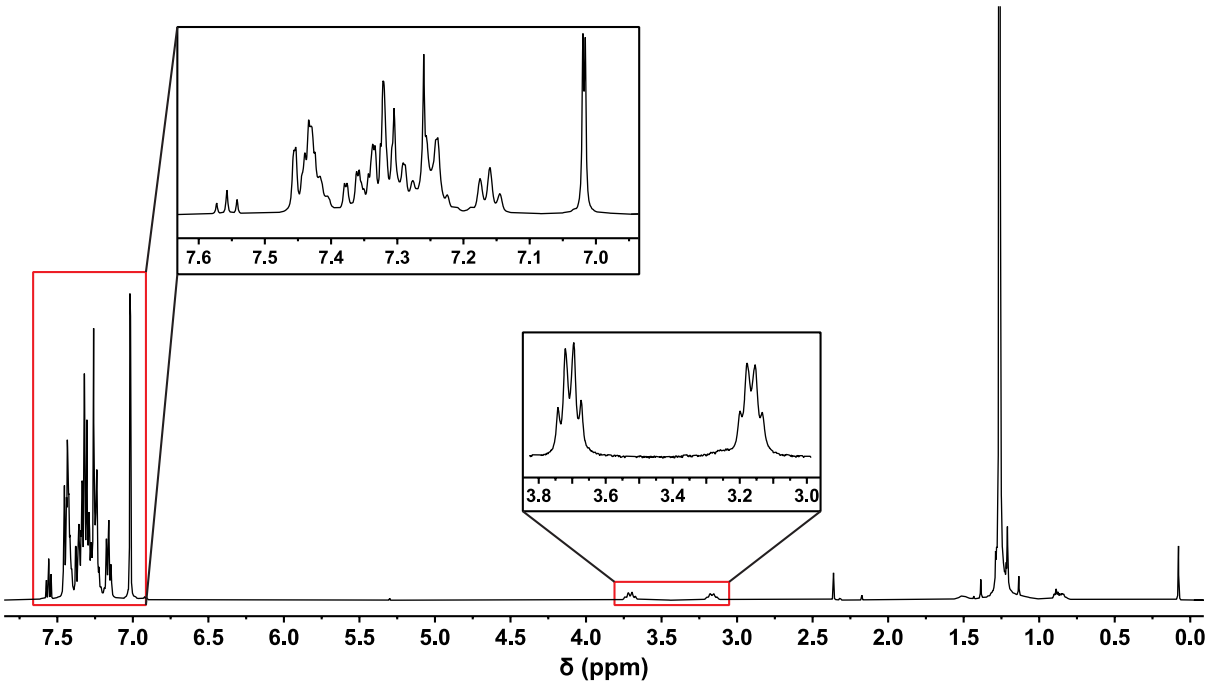

Figure 3.16: ^{1}H NMR ($CDCl_3$, 600 MHz, 298K) spectrum of the masked nanohoop [3]rotaxane **3.24**·(**M5**)$_2$ obtained through CuCl/4,4'-di-*tert*-butyl-2,2'-bipyridine Glaser-like approach.

to 40 °C appeared to result in the formation of difficult to separate by-products. Fortunately, gently warming the reaction to only 30 °C significantly accelerated the reaction, compared with coupling at 20 °C (although it is still markedly slower than with TMEDA), without forming any by-products and the masked nanohoop [3]rotaxane **3.24**·(**M5**)$_2$ was isolated in 77% yield after 20 hours.

3.3.4 Unmasking to Nanohoop Polyyne [3]Rotaxane

With a reliable procedure to masked [3]rotaxane **3.24**·(**M5**)$_2$ available, the final unmasking step to give the nanohoop polyyne [3]rotaxane was investigated. Treating **3.24**·(**M5**)$_2$ with the most optimal unmasking conditions found previously (I_2 (20 eq.) in THF) resulted in the formation of a yellow-orange species displaying the characteristic UV-vis spectrum of the 14-yne, albeit in a very low yield (~1-5%). Despite the low yield, this was a promising result. In contrast to the unmasking of the analogous **M4**-protected [3]rotaxane **3.25**·(**M4**)$_2$ (Scheme 3.6), this reaction proved reliable in generating the polyyne [3]rotaxane with every attempt. Further optimisations were attempted for this unmasking reaction on the nanohoop system and it was found that using a 1:1 THF:MeCN solvent system with the same 20 equivalents of I_2 proved the most effective for removing the dicobalt masking groups, while leaving the rest of the molecule intact.

It does, however, seem that the unmasking reaction does not proceed as cleanly as hoped. While [3]rotaxane **3.25**·(**M5**)$_2$ can be obtained every time, it was often accompanied by 1-2 additional products all bearing an intact tetradecayne thread (confirmed by UV-vis), suggesting a mild instability of either the masked or unmasked nanohoop rotaxanes to these conditions. Careful purification by preparative TLC (petroleum ether/EtOAc, 6%), was successful in affording the polyyne [3]rotaxane **3.25**·(**M5**)$_2$ in 32% isolated yield. This procedure could be reliably used to provide sufficient material for complete characterisation of polyyne [3]rotaxane **3.25**·(**M5**)$_2$ and allow for following studies into the stability of the molecule to be made. Importantly, and unlike for the **M4**-protected polyyne [3]rotaxane, sufficient material was obtained to allow for acquisition of a good quality ^{13}C spectrum, which clearly displayed all expected resonances for the chain of *sp* carbons (Figure 3.17).

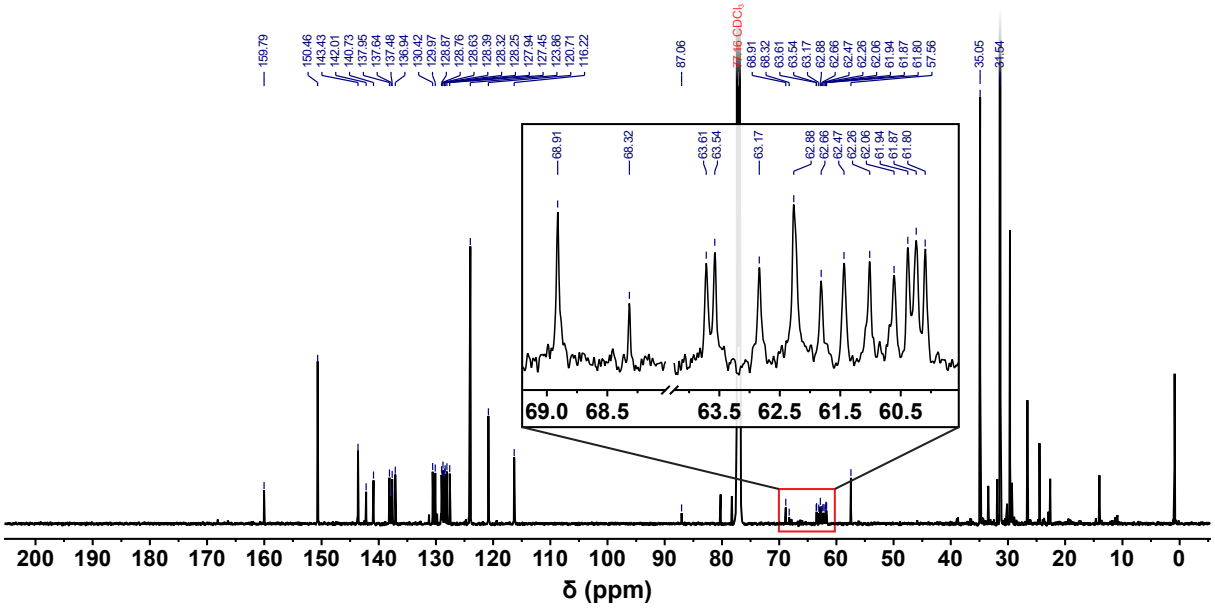

Figure 3.17: ^{13}C NMR spectrum of the nanohoop-protected polyyne [3]rotaxane **3.25**·(**M5**)$_2$ ($CDCl_3$, 151 MHz, 298 K). The acetylenic resonances have been enhanced for clarity.

As may be expected, the ^{1}H and ^{13}C NMR spectra of the [3]rotaxane **3.25**·(**M5**)$_2$ were similar to the sum of the spectra of their components (**3.25** + **M5**, see Figure S3.10 in Section 3.7), indicating the absence of any strong interactions between the polyyne dumbbell and the macrocycles. ^{1}H NOE experiments were made on [3]rotaxane **3.25**·(**M5**)$_2$ to identify whether the macrocycle is located in the vicinity of the supertrityl stoppering groups. In all experiments we were unable to detect NOEs between the ^{t}Bu and Ar-H resonances for the stopper and nanohoop. It is, however, difficult to draw any conclusions from these experiments since NOEs tend towards zero intensity at around the molecular weight of **3.25**·(**M5**)$_2$. Instead, a rotating

frame NOE experiment (e.g. ROESY), which would have non-zero NOE intensity around this mass range, would be better suited to probing any stopper-macrocycle interactions.

The NMR spectra of the nanohoop-protected rotaxanes were more complicated than expected. NMR spectra of the nanohoop polyyne [3]rotaxane **3.25**·(**M5**)$_2$ highlight this most clearly and reveals that rotation of the *para*-phenylene units of the threaded nanohoop **M5** is slow on the NMR timescale, thereby making the two faces of the nanohoop chemically non-equivalent. As a result, 10 distinct *para*-phenylene C-H environments are observed. In the ^{13}C spectrum, this manifests itself as 5 additional Ar-C resonances between 127-131 ppm, while in the ^{1}H spectrum the coupling between these now inequivalent protons manifests itself as what appears to be a series of doublet of doublets. The effects of these chemically non-equivalent environments of **3.25**·(**M5**)$_2$ are perhaps best observed by high-resolution HSQC experiments (Figure 3.18). Whereas the free nanohoop **M5** gives only 5 *para*-phenylene C-H signals, 10 *para*-phenylene C-H resonances are observed for the [3]rotaxane. Interestingly, the **M4**-

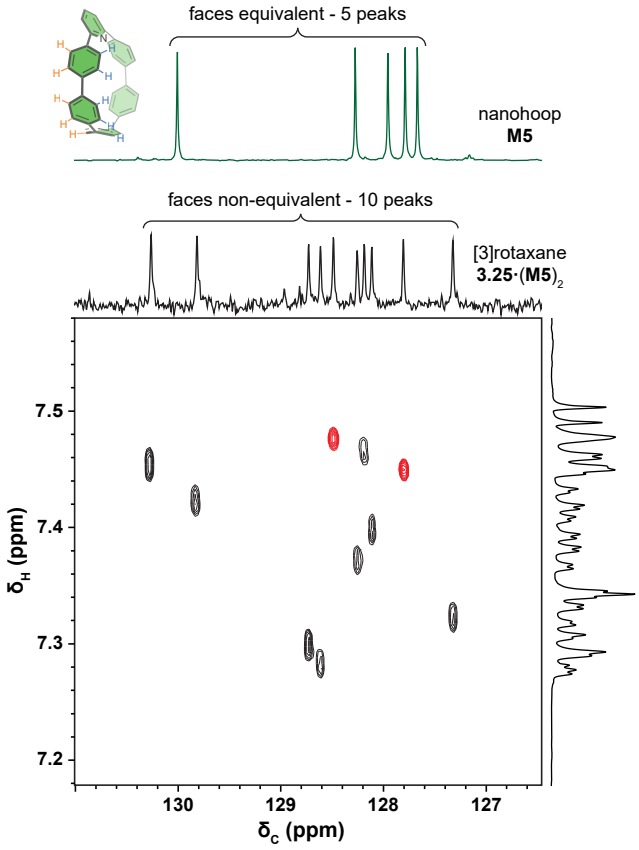

Figure 3.18: (top) Partial ^{13}C NMR spectra of (green) the free nanohoop **M5** and (black) the **M5**-protected polyyne [3]rotaxane **3.25**·(**M5**)$_2$. (bottom) High-resolution HSQC spectrum showing C-H correlation for the chemically non-equivalent *para*-phenylene C-H signals. Cross peaks arising from the middle *para*-phenylene, furthest away from the pyridine unit, have been coloured red. The ^{1}H reference spectrum has been diffusion edited to attenuate the overlapping $CHCl_3$ resonance ($CDCl_3$, 298 K, 700 MHz ^{1}H frequency).

protected polyyne [3]rotaxane did not show any such chemical non-equivalence. Unlike nanohoop **M5**, the diaryl phenanthroline unit in **M4** lies perpendicular to the polyyne, making these resonance pseudosymmetric and thus splitting is not observed.

3.4 Optical Spectroscopy and Decomposition Studies

3.4.1 UV-vis and Fluorescence Studies

The UV-vis absorption spectra of shielded polyyne [3]rotaxanes **3.25**·(**M4**)$_2$ and **3.25**·(**M5**)$_2$ (Figure 3.19a) closely resemble that of the 14-yne dumbbell **3.25**. Of note is a slight bathochromic shift in the spectra of the [3]rotaxanes (5 nm for **M4** and 7 nm for **M5**), which can be attributed to the different solvation environments in the [3]rotaxanes compared to the thread. This result is not unexpected as similar shifts in the UV-vis spectra of other polyyne rotaxanes have also been reported previously.[24] Studies were then made into the fluorescence of **M5**-protected polyyne [3]rotaxane. While free nanohoop **M5** is known to be highly fluorescent in solution,[45,49] its fluorescence is totally quenched when incorporated into [3]rotaxane **3.25**·(**M5**)$_2$ (Figure 3.19b), possibly due to energy transfer to dark states of the polyyne.[33,63,64] This suggests that although the absorption spectra show only a minimal interaction between the macrocycle and the polyyne in the ground state, there is a significant interaction in the excited state.

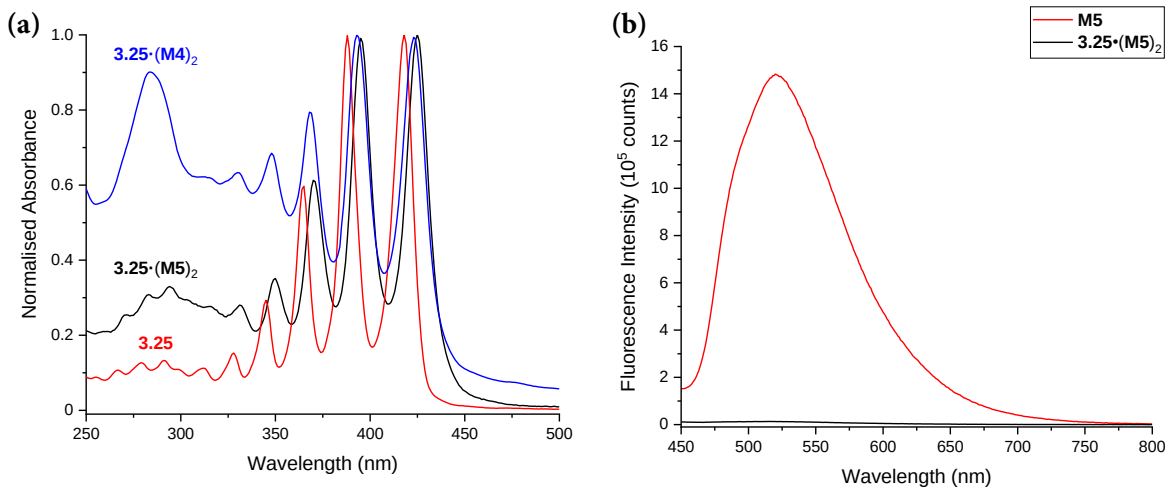

Figure 3.19: (a) Normalised UV-vis absorption spectra of polyyne **3.25** (red), phenanthroline [3]rotaxane **3.25**·(**M4**)$_2$ (blue) and nanohoop [3]rotaxane **3.25**·(**M5**)$_2$ (black), all as solutions in *n*-hexane at 25 °C. (b) Emission spectra of (red) nanohoop **M5** and (black) nanohoop-shielded polyyne [3]rotaxane **3.25**·(**M5**)$_2$ (CH_2Cl_2, 298 K, λ_{ex} 320 nm, λ_{em} 520 nm). Sample concentrations of 4.31×10^{-7} M and 8.61×10^{-7} M for nanohoop **M5** and rotaxane **3.25**·(**M5**)$_2$, respectively.

3.4.2 Decomposition Studies

One of the overarching aims of this project was to demonstrate the stability enhancement of polyynes brought about by supramolecular encapsulation. The stabilities of the polyyne [3]rotaxanes were assessed both in the solid state and in solution, then compared to the 14-yne dumbbell **3.25**. Previously, differential scanning calorimetry (DSC) has been used to demonstrate a stability enhancement in some polyyne rotaxanes.[24] DSC was used to compare the nanohoop-protected polyyne [3]rotaxane **3.25**·(**M5**)$_2$ to the 14-yne thread **3.25**. Both thread and [3]rotaxane were found to decompose at similar temperatures (155 °C and 149 °C, respectively) (Figure 3.20), suggesting no significant stability difference in the solid state between the two. One problem with studying solid-state stability is that it is influenced by unpredictable crystal packing effects. We attributed the nominal difference in stability to the threaded macrocycles lowering the symmetry of the polyyne, thereby disrupting crystal-packing interactions and thus the thermal stability compared to the thread alone.

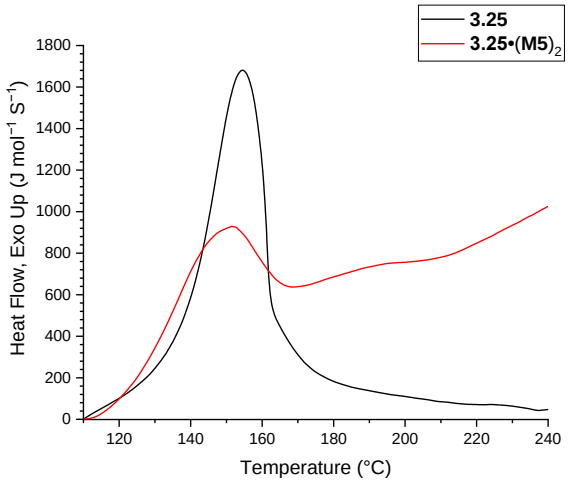

Figure 3.20: Overlaid traces of 14-yne thread **3.25** (black) and the corresponding nanohoop [3]rotaxane **3.25**·(**M5**)$_2$ (red). Traces have been baseline-corrected at T = 110 °C.

Following on from the solid state studies, we also investigated the stability of these compounds in solution. We envisaged that UV-vis spectroscopy would prove to be a useful tool to monitor these solution-based studies for two main reasons: (i) the low (~1 μM) concentrations required for UV-vis experiments mean that molecules are rarely in close proximity to each other and so decomposition should be intramolecular (first order kinetics would be expected) and; (ii) the low concentrations mean that only small quantities of sample are required (*c.f.* DSC generally requires 1-2 mg of sample per experiment), allowing the stability of even the synthetically-challenging phenanthroline-protected polyyne [3]rotaxane

3.25·(**M4**)$_2$ to be assessed. A high-boiling solvent (decalin) was chosen so that any evaporation of solvent could be considered negligible, as this may otherwise led to erroneous rate data.

Initial experiments (*method 1*) involved charging a flask with dry, degassed decalin (49.5 mL), then allowing it to reach thermal equilibrium at 80 °C over a 2 hour period. Heating was carried out using a large oil bath and an insulating jacket was placed over the flask, both in attempts to minimise thermal fluctuations during the experiment. A stock solution† of sample (0.50 mL) was then added to the flask. Aliquots (1.5 mL) were taken at timed intervals from the initial addition (the t = 0 was taken immediately after addition), then immediately cooled to 25 °C using a water bath to prevent any further reaction. UV-vis spectra were then recorded for each aliquot and baseline drift of the spectrometer was corrected for by using an average of data points from 600-700 nm, where there is no absorption from the sample. The sharp UV bands of the polyyne were found to decay exponentially and the absorption maxima of the highest intensity signal (418 and 425 nm for the thread **3.25** and nanohoop-protected [3]rotaxane **3.25**·(**M5**)$_2$, respectively) were plotted against time to reveal a decay consistent with first-order rection kinetics (Figure 3.21). Fitting these data gave apparent first-order rate constants of 0.11 s^{-1} and 0.015 s^{-1} for the dumbbell **3.25** and nanohoop [3]rotaxane **3.25**·(**M5**)$_2$, respectively.

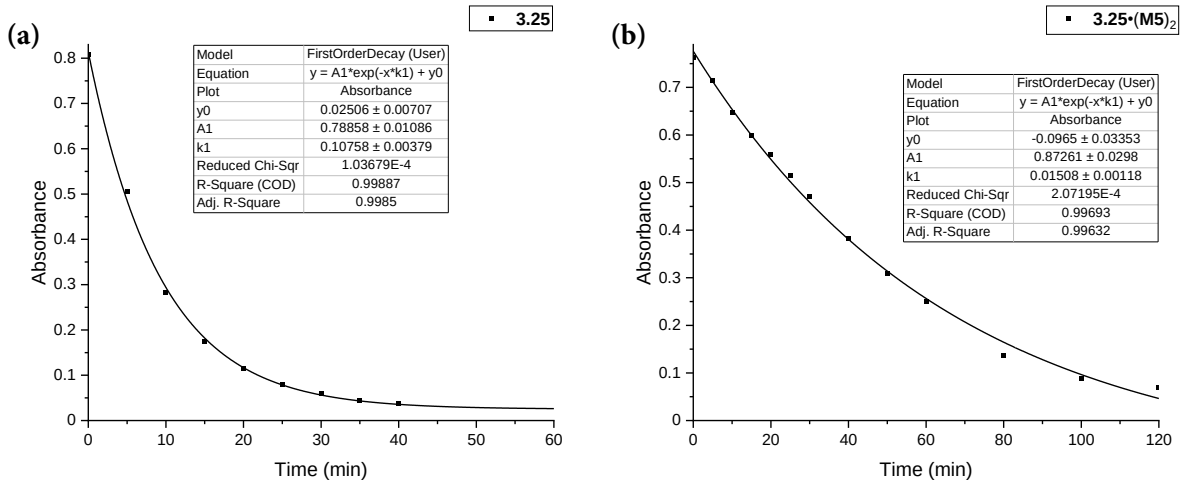

Figure 3.21: UV-vis decomposition studies following Method 1 (above) of (a) dumbbell **3.25** and (b) nanohoop polyyne [3]rotaxane **3.25**·(**M5**)$_2$. The absorbance of the lowest energy band was followed in each case. Data are fitted to a first order exponential decay, $A = (A_0 - A_f)\exp(-kt) + A_f$, where A, A_0 and A_f are the absorbance at time t, absorbance at t = 0 and absorbance at $t = \infty$, respectively, and k is the rate constant.

† A stock solution of both thread and rotaxane was prepared such that the initial absorption equals 0.7. This was to ensure that sufficient data points could be obtained before the signal is lost.

One problem with this method is that the time-critical nature of the experiment makes it highly susceptible to human error in taking the measurements. In addition, the relatively lengthy process of taking the aliquot, cooling the sample and then finally acquiring the UV-vis spectrum limits the frequency with which measurements can be taken. To address these issues, a revised method (*method 2*) was developed. In this, a UV-vis spectrometer with a Peltier-equipped cuvette holder was used and allowed gentle stirring and heating of the sample up to 100 °C inside the instrument. For these experiments a thoroughly-degassed solution of dry decalin (4 mL) and sufficient stock solution† of sample was prepared. A portion (2.0 mL) of this solution was transferred to a dry Schlenk cuvette equipped with a PTFE stirrer bar under an Ar atmosphere. The cuvette was placed into the UV-vis spectrometer and pre-heated to 80 °C in the cuvette holder. Once the temperature of the cuvette had equilibrated (approximately 30 seconds), measurements were acquired at fixed time intervals (Figure 3.22). The data was processed using the procedure described previously. Using this method, the thermal stability of the thread **3.25** and both **M4**- and **M5**-protected polyyne rotaxanes (**3.25**·(**M5**)$_2$ and **3.25**·(**M5**)$_2$, respectively) were successfully evaluated.

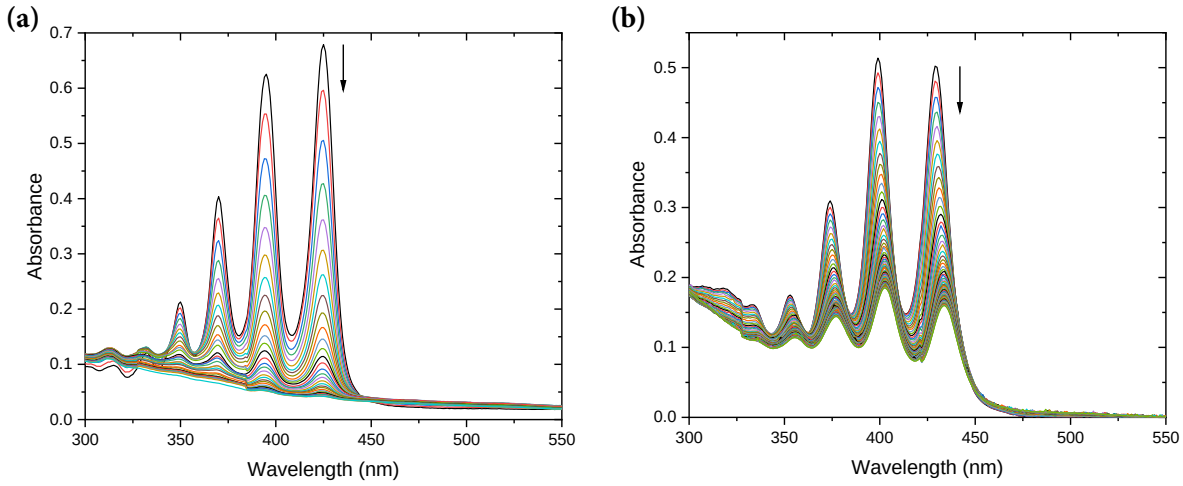

Figure 3.22: UV-vis spectra (decalin, 80 °C) during the decomposition reaction following Method 2 (above) of (a) dumbbell **3.25** over a total period of 60 minutes, and (b) nanohoop polyyne [3]rotaxane **3.25**·(**M5**)$_2$ over a total period of 240 minutes. For (a) each line is separated by a 2-minute time interval, while for (b) spectra are shown for 4-minute intervals.

Similar plots of the relative absorbance of the lowest energy band against time once again reveal an exponential decay consistent with first order reaction kinetics (Figure 3.23a-c). Fitting these data gave apparent first-order rate constants of 0.092 s^{-1}, 0.080 s^{-1} and 0.021 s^{-1} for the dumbbell **3.25**, the phenanthroline [3]rotaxane **3.25**·(**M4**)$_2$ and nanohoop [3]rotaxane **3.25**·(**M5**)$_2$, respectively. Experimental uncertainties associated with these measurements were

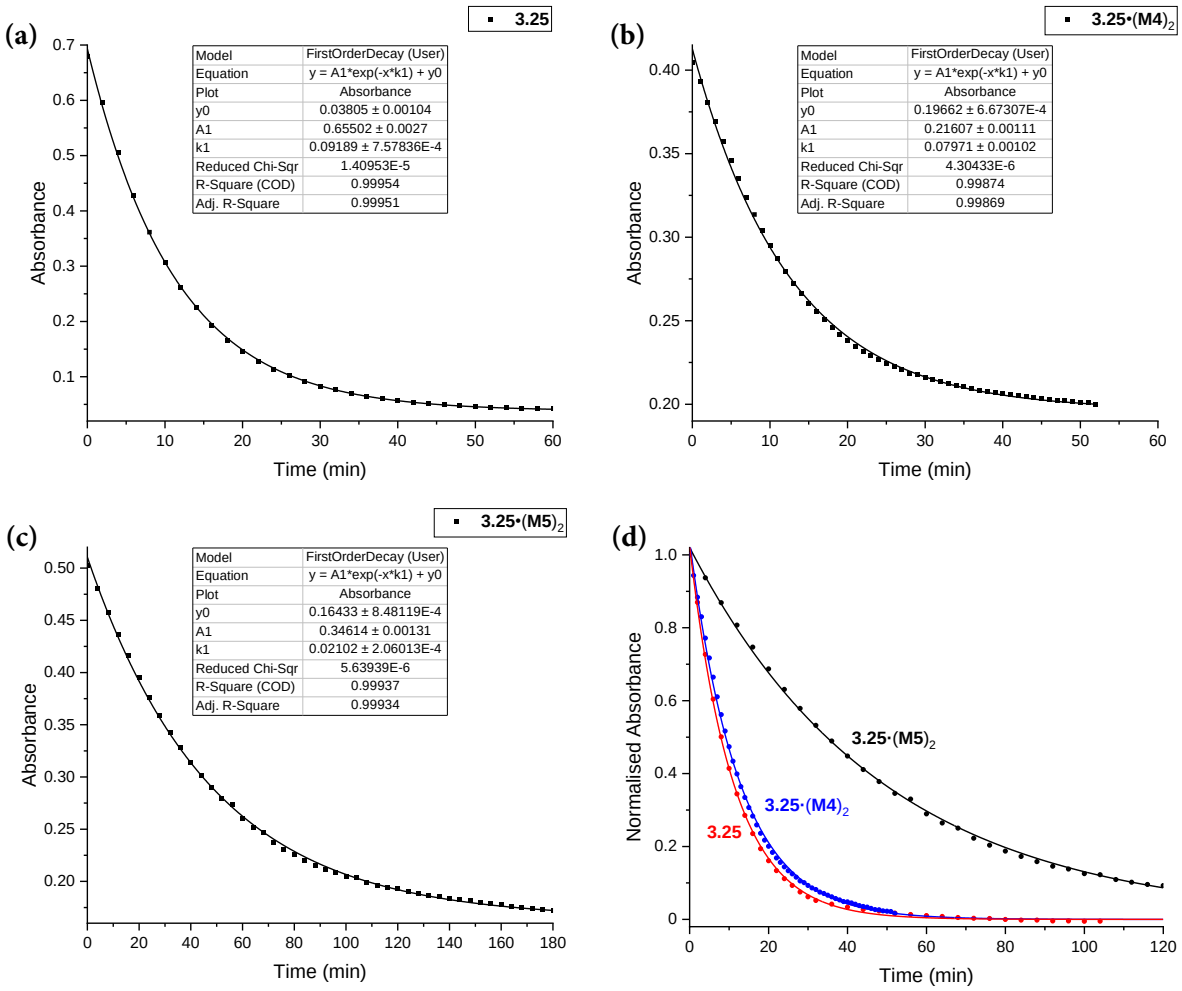

Figure 3.23: UV-vis decomposition studies following Method 2 (above) of (a) dumbbell **3.25**, (b) **M4**-protected polyyne [3]rotaxane **3.25**·(**M4**)$_2$, (c) **M5**-protected polyyne [3]rotaxane **3.25**·(**M5**)$_2$ and (d) overlaid spectra of (red) 14-yne dumbbell **3.25**, (blue) Saito [3]rotaxane **3.25**·(**M4**)$_2$, (black) nanohoop [3]rotaxane **3.25**·(**M5**)$_2$. The absorbance of the lowest energy band was followed in each case. Data are fitted to a first order exponential decay, $A = (A_0 - A_f)\exp(-kt) + A_f$, where A, A_0 and A_f are the absorbance at time t, absorbance at $t = 0$ and absorbance at $t = \infty$, respectively, and k is the rate constant.

estimated from repeat experiments at approximately 10%. Data obtained from both methods were found to give comparable kinetics, suggesting both are viable approaches to evaluating decomposition of these molecules. These data suggest that while the **M4**-protected polyyne rotaxane exhibits only a minor improvement in stability (~1.2 times), the nanohoop-protected analogue shows an approximate 4.5 fold stability enhancement in solution (Figure 3.23d). The nominal stability enhancement for **3.25**·(**M4**)$_2$ was somewhat unexpected but could be rationalised by considering the greater size and flexibility of the phenanthroline macrocycle, which may not shield the polyyne as effectively as the nanohoop. We also mentioned the **M4** macrocycles have a tendency to form stacked aggregates. Should this be occurring in **3.25**·(**M4**)$_2$, this may also help to explain the slight stability enhancement compared to the thread.

During these investigations it was noted that scrupulous degassing was important in obtaining reliable data that displayed the expected exponential decay associated with first-order decomposition kinetics. For example, running the reaction without any particular degassing step resulted in the appearance of a 'slow', almost linear, period that was then followed by a second exponential-like decay (Figure 3.24). Pre-saturating the solution with O_2 (by freeze-pump-thaw then flushing with O_2) before the measurements resulted in prolonging the 'slow' process. Thorough degassing completely eliminated the 'slow' period, and the expected exponential decay was seen without any onset. These observations imply that oxygen is somehow influencing the decay process. Perhaps it acts to quench a reactive species that would otherwise result in the decomposition of the polyyne. This ('slow' period) may continue to occur until all oxygen is consumed, after which the decay continues as the normal – the exponential, 'fast' period. This is, however, simply speculative and the exact mechanism by which this occurs remains unknown.

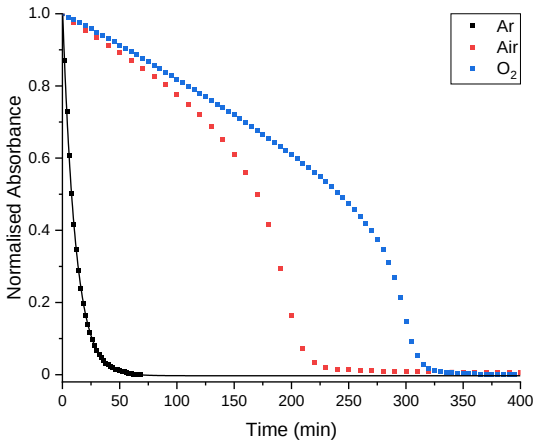

Figure 3.24: UV-vis decomposition studies of 14-yne thread **3.25**, heated using a Peltier-equipped cuvette holder of (black) Ar-degassed (red) non-degassed and (blue) O_2-saturated solutions. Note that the presence of oxygen appears to prolong the 'slow' period of decay. Intensity of the lowest energy band was followed in each case. Data have been normalised between 1 and 0 to aid comparison. All solutions in decalin at 80 °C.

A brief investigation was made to help elucidate the nature of the decomposition mechanism. A common free-radical inhibitor (2,6-di-*tert*-butyl-4-methylphenol, BHT) was added to the mixture in known quantities to assess whether decomposition may occur via a free-radical type process or by other means. It was apparent that BHT virtually shuts down the decomposition process, resulting in only a very minor decrease in absorbance intensity over time (Figure 3.25a). Once the inhibitor appeared to have been consumed, a decay similar to those seen previously was then observed. Curiously, increasing the amount of BHT (from 2.5 eq. to 5 eq.) did not quite result in a doubling of this onset to the decay (Figure 3.25b).

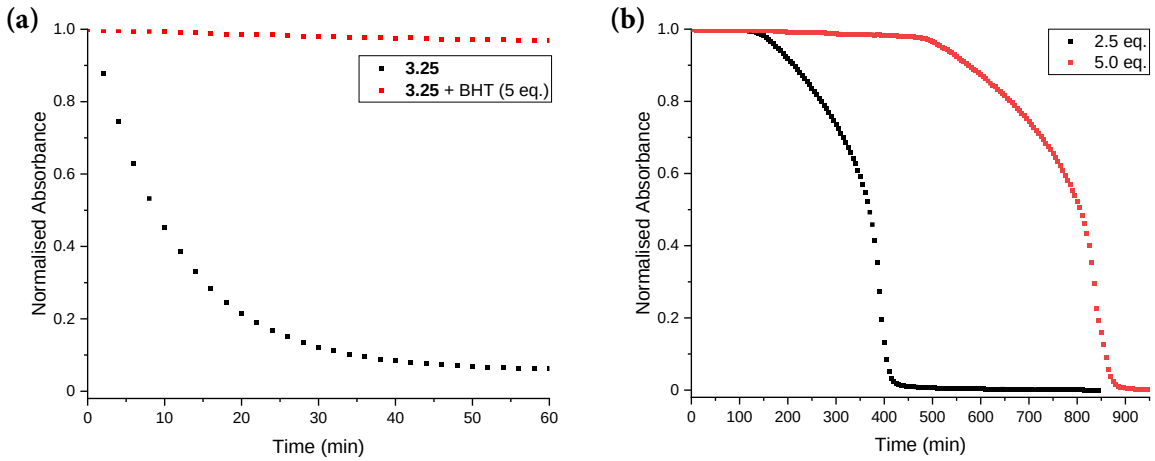

Figure 3.25: UV-vis decomposition comparison of 14-yne thread **3.25** (a) with (red) and without (black) BHT (5.0 eq.) present and; (b) with 2.5 eq. (black) and 5.0 eq. (red) of BHT inhibitor. Intensity of the lowest energy band was followed in each case. For (a) data was normalised following A/A_0 and (b) data have been normalised between 1 and 0 to aid comparison. All solutions in decalin at 80 °C.

Additional experiments would be required to confirm whether this is actually the case, or just an experimental anomaly. Nevertheless, the fact that the presence of BHT alters this process, suggests that the decomposition likely occurs via a radical-type process. Once all inhibitor had been consumed, the reaction then proceeded as normal. It is worth noting that these experiments were performed in a standard cuvette that was not particularly air-tight, thus the 'slow' period is observed as expected. Repeating this under rigorously degassed conditions appeared to result only in a very slow decrease in absorbance, but additional experiments (where this sample is monitored for a longer time period) would be required to confirm whether we may observe a transition directly into the exponential decay once the inhibitor is consumed. Even so, Figure 3.25 suggests that in the absence of O_2, there is still likely a radical process causing the degradation of the thread, which can be effectively inhibited by adding a free-radical inhibitor.

3.5 Conclusions

A new synthetic route towards polyyne [3]rotaxanes has been demonstrated. By incorporating a bulky dicobalt alkyne masking group to act both as a temporary, cleavable stopper for rotaxane synthesis, as well as for stabilising the synthetic intermediates, two masked [3]rotaxanes bearing different macrocycles have been prepared by an active metal template approach. Unmasking by oxidative decomplexation of the dicobalt group was successful in returning two polyyne [3]rotaxanes with the same C_{28} polyyne dumbbell component. Thermal stability measurements

have shown that the size and shape of the macrocycle influence its ability to alter the thermal stability of a threaded polyyne. A polyyne rotaxane bearing a large, flexible macrocycle only showed a modest 1.2 fold stability enhancement, but switching to a smaller, more rigid nanohoop macrocycle was found to show a 4.5 fold stability enhancement compared with that of the naked polyyne dumbbell in degassed decalin at 80 °C.

The supertrityl stoppering group provided excellent stability for these compounds, but the permanent nature of it limits the size of polyyne rotaxanes that can be prepared by this approach. While it should be possible to prepare larger polyynes through coupling of longer stoppering and masking group components in the AMT step, the gains to length would be marginal and soon a limit would be reached due to the instability of these components. A more useful approach would be one that first prepares a stable [2]rotaxane species bearing two temporary MAE stoppers and cleavable alkyne capping groups at each end. Through careful oligomerisation reactions with itself and a permanent, bulky stoppering group, this approach could be used to build up significantly longer masked polyyne [*n*]rotaxanes than currently possible.

3.6 References

1 K. M. Nicholas and R. Pettit, *Tetrahedron Lett.*, 1971, **12**, 3475–3478.

2 R. F. Lockwood and K. M. Nicholas, *Tetrahedron Lett.*, 1977, **18**, 4163–4165.

3 M. I. Bruce, M. E. Smith, N. N. Zaitseva, B. W. Skelton and A. H. White, *J. Organomet. Chem.*, 2003, **670**, 170–177.

4 M. J. Macazaga, M. L. Marcos, C. Moreno, F. Benito-Lopez, J. Gomez-González, J. González-Velasco and R. M. Medina, *J. Organomet. Chem.*, 2006, **691**, 138–149.

5 P. J. Low, K. A. Udachin, G. D. Enright and A. J. Carty, *J. Organomet. Chem.*, 1999, **578**, 103–114.

6 P. J. Low, R. Rousseau, P. Lam, K. A. Udachin, G. D. Enright, J. S. Tse, D. D. M. Wayner and A. J. Carty, *Organometallics*, 1999, **18**, 3885–3897.

7 H. Greenfield, H. W. Sternberg, R. A. Friedel, J. H. Wotiz, R. Markby and I. Wender, *J. Am. Chem. Soc.*, 1956, **78**, 120–124.

8 R. G. Pearson and W. R. Muir, *J. Am. Chem. Soc.*, 1970, **92**, 5519–5520.

9 T. R. Hoye, B. Baire, D. Niu, P. H. Willoughby and B. P. Woods, *Nature*, 2012, **490**, 208–212.

10 G. Cetini, O. Gambino, R. Rossetti and E. Sappa, *J. Organomet. Chem.*, 1967, **8**, 149–154.

11 N. T. Allison, J. R. Fritch, K. P. C. Vollhardt and E. C. Walborsky, *J. Am. Chem. Soc.*, 1983, **105**, 1384–1386.

12 Y. Shvo and E. Hazum, *J. Chem. Soc. Chem. Commun.*, 1974, 336.

13 A. Meyer, A. Gorgues, Y. Le Floc'h, Y. Pineau, J. Guillevic and J. Le Marouille, *Tetrahedron Lett.*, 1981, **22**, 5181–5182.

14 B. E. Hanson and J. S. Mancini, *Organometallics*, 1983, **2**, 126–128.

15 Y. Rubin, C. B. Knobler and F. Diederich, *J. Am. Chem. Soc.*, 1990, **112**, 4966–4968.

16 F. Diederich, Y. Rubin, O. L. Chapman and N. S. Goroff, *Helv. Chim. Acta*, 1994, **77**, 1441–1457.

17 M. M. Haley and B. L. Langsdorf, *Chem. Commun.*, 1997, **2**, 1121–1122.

18 D. R. Kohn, P. Gawel, Y. Xiong, K. E. Christensen and H. L. Anderson, *J. Org. Chem.*, 2018, **83**, 2077–2086.

19 W. A. Chalifoux and R. R. Tykwinski, *Nat. Chem.*, 2010, **2**, 967–971.

20 Y. Gao, Y. Hou, F. Gordillo Gámez, M. J. Ferguson, J. Casado and R. R. Tykwinski, *Nat. Chem.*, 2020, **12**, 1143–1149.

21 D. R. Kohn, *DPhil Thesis*, University of Oxford, 2017.

22 J. F. Woods, *Part II Thesis*, University of Oxford, 2019.

23 P. D. Bartlett, M. Roha and R. M. Stiles, *J. Am. Chem. Soc.*, 1954, **76**, 2349–2353.

24 L. D. Movsisyan, M. Franz, F. Hampel, A. L. Thompson, R. R. Tykwinski and H. L. Anderson, *J. Am. Chem. Soc.*, 2016, **138**, 1366–1376.

25 S. Eisler, N. Chahal, R. McDonald and R. R. Tykwinski, *Chem. Eur. J.*, 2003, **9**, 2542–2550.

26 F. A. Cotton and J. M. Troup, *J. Chem. Soc. Dalt. Trans.*, 1974, 800.

27 M. Denis and S. M. Goldup, *Nat. Rev. Chem.*, 2017, **1**, 0061.

28 S. Saito, K. Nakazono and E. Takahashi, *J. Org. Chem.*, 2006, **71**, 7477–7480.

29 S. Saito, E. Takahashi and K. Nakazono, *Org. Lett.*, 2006, **8**, 5133–5136.

30 M. J. Langton, J. D. Matichak, A. L. Thompson and H. L. Anderson, *Chem. Sci.*, 2011, **2**, 1897.

31 H. Sahnoune, Z. Baranová, N. Bhuvanesh, J. A. Gladysz and J.-F. Halet, *Organometallics*, 2013, **32**, 6360–6367.

32 Z. Baranová, H. Amini, N. Bhuvanesh and J. A. Gladysz, *Organometallics*, 2014, **33**, 6746–6749.

33 L. D. Movsisyan, M. D. Peeks, G. M. Greetham, M. Towrie, A. L. Thompson, A. W. Parker and H. L. Anderson, *J. Am. Chem. Soc.*, 2014, **136**, 17996–18008.

34 M. Franz, J. A. Januszewski, F. Hampel and R. R. Tykwinski, *Eur. J. Org. Chem.*, 2019, **2019**, 3503–3512.

35 S. L. Woltering, P. Gawel, K. E. Christensen, A. L. Thompson and H. L. Anderson, *J. Am. Chem. Soc.*, 2020, **142**, 13523–13532.

36 C. O. Dietrich-Buchecker and J.-P. Sauvage, *Tetrahedron Lett.*, 1983, **24**, 5091–5094.

37 C. Roche, *PhD Thesis*, Université de Strasbourg & University of Sydney, 2012.

38 P. Gawel, S. L. Woltering, Y. Xiong, K. E. Christensen and H. L. Anderson, *Angew. Chem. Int. Ed.*, 2021, **60**, 5941–5947.

39 R. Volpe, L. Aurelio, M. G. Gillin, E. H. Krenske and B. L. Flynn, *Chem. Eur. J.*, 2015, **21**, 10191–10199.

40 J. Lewis, B. Lin, M. S. Khan, M. R. A. Al-Mandhary and P. R. Raithby, *J. Organomet. Chem.*, 1994, **484**, 161–167.

41 L. Adamska, I. Nayyar, H. Chen, A. K. Swan, N. Oldani, S. Fernandez-Alberti, M. R. Golder, R. Jasti, S. K. Doorn and S. Tretiak, *Nano Lett.*, 2014, **14**, 6539–6546.

42 V. Coropceanu, J. Cornil, D. A. da Silva Filho, Y. Olivier, R. Silbey and J.-L. Brédas, *Chem. Rev.*, 2007, **107**, 926–952.

43 Y. Xu, M. Delius, M. von Delius and M. Delius, *Angew. Chem. Int. Ed.*, 2020, **59**, 559–573.

44 C. Zhao, F. Liu, L. Feng, M. Nie, Y. Lu, J. Zhang, C. Wang and T. Wang, *Nanoscale*, 2021, **13**, 4880–4886.

45 J. M. Van Raden, B. M. White, L. N. Zakharov and R. Jasti, *Angew. Chem. Int. Ed.*, 2019,

58, 7341–7345.

46 P. Li, T. J. Sisto, E. R. Darzi and R. Jasti, *Org. Lett.*, 2014, **16**, 182–185.

47 E. R. Darzi, B. M. White, L. K. Loventhal, L. N. Zakharov and R. Jasti, *J. Am. Chem. Soc.*, 2017, **139**, 3106–3114.

48 T. C. Lovell, C. E. Colwell, L. N. Zakharov and R. Jasti, *Chem. Sci.*, 2019, **10**, 3786–3790.

49 J. M. Van Raden, N. N. Jarenwattananon, L. N. Zakharov and R. Jasti, *Chem. Eur. J.*, 2020, **26**, 10205–10209.

50 A. S. Hay, *J. Org. Chem.*, 1962, **27**, 3320–3321.

51 N. Naveen, S. A. Babu, G. Kaur, N. A. Aslam and M. Karanam, *RSC Adv.*, 2014, **4**, 18904–18916.

52 G. Eglinton and R. Galbraith, A., *Chem. Ind. (London)*, 1956, 737.

53 H. L. Anderson, *Chem. Commun.*, 1999, 2323–2330.

54 M. Hoffmann, C. J. Wilson, B. Odell and H. L. Anderson, *Angew. Chem. Int. Ed.*, 2007, **46**, 3122–3125.

55 C. Roche, Q. Luo, G. Gil-Ramírez, H.-W. Jiang, D. R. Kohn, Y. Xiong, A. L. Thompson and H. L. Anderson, *J. Org. Chem.*, 2017, **82**, 7446–7462.

56 W. Yin, C. He, M. Chen, H. Zhang and A. Lei, *Org. Lett.*, 2009, **11**, 709–712.

57 X. Fan, N. Li, T. Shen, X.-M. Cui, H. Lv, H.-B. Zhu and Y.-H. Guan, *Tetrahedron*, 2014, **70**, 256–261.

58 A. F. Hill and R. A. Manzano, *Angew. Chem. Int. Ed.*, 2019, **58**, 15354–15357.

59 R. D. Dewhurst, A. F. Hill and A. C. Willis, *Chem. Commun.*, 2004, **2**, 2826–2827.

60 R. D. Dewhurst, A. F. Hill and A. C. Willis, *Organometallics*, 2005, **24**, 3043–3046.

61 M. J. Bartlett, B. J. Frogley, A. F. Hill, M. Sharma, M. K. Smith and J. S. Ward, *Dalt. Trans.*, 2019, **48**, 16534–16554.

62 M. I. Bruce, N. N. Zaitseva, B. K. Nicholson, B. W. Skelton and A. H. White, *J. Organomet. Chem.*, 2008, **693**, 2887–2897.

63 D. R. Kohn, L. D. Movsisyan, A. L. Thompson and H. L. Anderson, *Org. Lett.*, 2017, **19**, 348–351.

64 J. Zirzlmeier, S. Schrettl, J. C. Brauer, E. Contal, L. Vannay, É. Brémond, E. Jahnke, D. M. Guldi, C. Corminboeuf, R. R. Tykwinski and H. Frauenrath, *Nat. Commun.*, 2020, **11**, 4797.

3.7 Experimental

Contents

General Methods

Commercially available reagents were used as received. Dry solvents (THF, CH_2Cl_2, $CHCl_3$, pentane, DMF) for reactions were purified by a MBraun MB-SPS-5 bench-top SPS system under nitrogen (H_2O content < 20 ppm). All other solvents used were HPLC grade and dried over appropriate drying agents when required. Petroleum ether (petrol) had a boiling point range of 40–60 °C. *N,N,N′,N′*-Tetramethylethylenediamine (TMEDA) was dried with 3 Å molecular sieves (Linde-type) and then distilled over KOH under an Ar atmosphere prior to each use. EDTA/NH_3 solution was prepared by saturating a 1:1 solution of water/aqueous 35% NH_3 solution with tetrasodium EDTA. All solutions used during workups (NH_4Cl, $Na_2S_2O_3$ and brine) were saturated aqueous solutions, unless otherwise specified. Copper(I) chloride was freshly prepared.[1]

Reactions, unless otherwise stated, were carried out in oven-dried glassware under an Ar atmosphere. Thin layer chromatography (TLC) was carried out on aluminum-backed silica gel plates with 0.2 mm thick silica gel 60 F254 (Merck) and visualised by UV irradiation at either 254 nm or 366 nm. Preparative flash column chromatography was either carried out using flash silica gel 60 (230-400 mesh) obtained from Sigma-Aldrich, or on a Biotage Isolera One with a 200–400 nm UV detector. Size exclusion chromatography (SEC) was carried out using Bio-Beads S-X3, 40-80 μm (Bio Rad). Evaporation of solvents was performed at 20–50 °C and 5–1010 mbar. Analytical GPC was carried out using JAIGEL-3H-A (8 × 500 mm) and JAIGEL-4H-A (8 × 500 mm) columns in THF + 1% pyridine as eluent with a flow rate of 1.0 mL/min. Evaporation of solvents was performed at 20–50 °C and 5–1010 mbar. Reported yields refer to pure compounds dried under high vacuum (< 0.1 mbar).

^1H and ^{13}C nuclear magnetic resonance (NMR) spectra were recorded on Bruker Avance NEO 400, AVIII HD 500, Bruker AVIII HD 600 (Prodigy broadband cryoprobe), Avance NEO 600 (broadband helium cryoprobe), and AVIII 700 (1H/13C/15N TCI cryoprobe) spectrometers at 400 MHz, 500 MHz, 600 MHz, 600 MHz and 700 MHz (^1H) and 101 MHz, 126 MHz, 151 MHz, 151 MHz and 175 MHz (^{13}C), respectively at 298 K unless stated otherwise. NMR chemical shifts were reported in ppm relative to $SiMe_4$ ($\delta = 0$) and were referenced internally with respect to residual solvent protons using the reported values. Coupling constants are reported in Hz and ^1H multiplicities are reported in accordance with the following: br =

broad; s = singlet; d = doublet; t = triplet; q = quartet; and m = multiplet. ^{1}H assignments were made using 2D NMR methods (COSY, NOESY, HSQC, HMBC).

^{13}C NMR spectra of cobalt carbonyl complex of alkynes often show fewer than the expected number of peaks due to the broadness and low intensity (from the slow relaxation) of the carbons bound to cobalt and the overlap between the signals from the many carbon environments.

Electrospray mass spectrometry was carried out on a Waters Micromass LCT Premier XE spectrometer using 90:10 MeOH:H_2O (+0.1% formic acid) as the mobile phase. High-resolution ESI mass spectrometry (HR-MS) measurements were performed either by the mass spectrometry service at the University of Oxford on a Waters GTC classic or at the NMSF at Swansea University on a Bruker ultrafleXtreme.

UV-vis spectra were recorded in solution on a Perkin-Elmer Lambda 20 or Perkin-Elmer Lambda 25 spectrometer at 25 °C (unless otherwise noted), in fused silica cuvettes with a pathlength of 1 cm. Elevated temperature UV-vis experiments were run using a heated cuvette holder connected to a Perkin Elmer PTP-1 Peltier System.

Fluorescence spectra were acquired in solution in fused silica cuvettes at 298 K using an Edinburgh Instruments FS5 spectrofluorometer operating Fluoracle software and equipped with a xenon arc lamp (providing 230–1000 nm excitation range), a thermostatic sample holder (SC-20) and both an R13456 PMT detector (200–950 nm spectral coverage, Hamamatsu) and an InGaAs analogue NIR detector (850–1650 nm spectral coverage).

Differential scanning calorimetry (DSC) measurements were performed on a PerkinElmer DSC 4000 instrument using an aluminum plate as a reference. In cases when the sample decomposed, the onset temperature of the decomposition exothermic peak is reported, as well as the exothermic maxima corresponding to the decomposition.

Determination of Kinetic Parameters from VT NMR Spectra

Rate constants k at the corresponding temperatures T were determined using line shape fitting performed using the MestReNova software package. The Eyring equation relates the rate of a chemical reaction to the Gibbs energy of activation $G^{\ddagger}$ following Equation 1.

$$k = \frac{k_B T}{h} e^{\frac{-\Delta G^{\ddagger}}{RT}} \quad (1)$$

Since $\Delta G^{\ddagger} = \Delta H^{\ddagger} - T\Delta S^{\ddagger}$, it can be rewritten as Equation 2

$$\ln\left(\frac{k}{T}\right) = -\frac{\Delta H^{\ddagger}}{R}\left(\frac{1}{T}\right) + \frac{\Delta S^{\ddagger}}{R} + \ln\left(\frac{k_B}{h}\right) \quad (2)$$

where k_B, h and R are the Boltzmann constant, Planck constant and gas constant, respectively.

Plotting $\ln(k/T)$ *vs* T^{-1}, then linear regression (weighted by errors in k), gave a slope q and intercept c.

$$q = -\frac{\Delta H^{\ddagger}}{R} \qquad c = \frac{\Delta S^{\ddagger}}{R} + \ln\left(\frac{k_B}{h}\right)$$

Activation enthalpy $\Delta H^{\ddagger}$ and entropy $\Delta S^{\ddagger}$ for this process were determined from this slope q and intercept c, then the Gibbs energy of activation at 298 K ($G^{\ddagger}_{298\ K}$) was then determined (Figure S3.1).

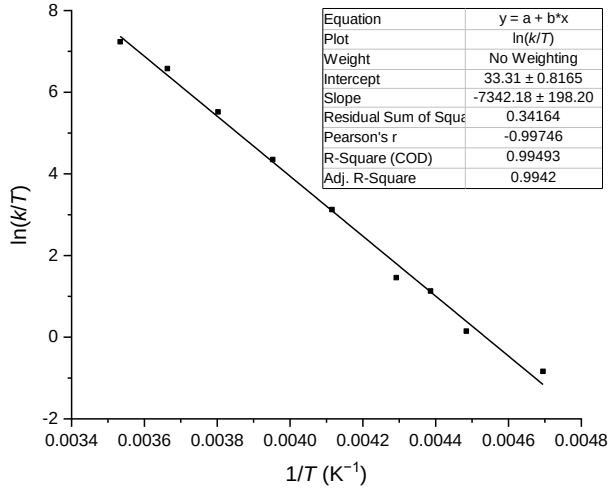

$\Delta H^{\ddagger}$ = 61 ± 9 kJ mol^{-1}

$\Delta S^{\ddagger}$ = 0.08 ± 0.01 kJ mol^{-1}

$\Delta G^{\ddagger}$ = 37 ± 9 kJ mol^{-1}

Figure S3.1: Eyring plot used to determine $\Delta H^{\ddagger}$ and $\Delta S^{\ddagger}$ for the fluxional motion of a dicobalt-masked hexatriyne in CD_2Cl_2.

Synthesis of Known Compounds

1,3,5-Tri-*tert*-butylbenzene 3.1[2]

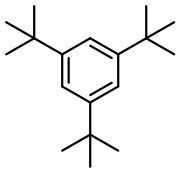

To a mixture of *tert*-butyl chloride (610 mL, 5.60 mol) and benzene (50.0 mL, 0.560 mol) cooled to –40 °C, $AlCl_3$ (37.1 g, 0.280 mol) was added in small portions and the reaction mixture was slowly warmed to –20 °C and stirred for 2 h while keeping the temperature below –10 °C. The reaction was quenched via slow addition of a water/ice-mixture (200 mL) at –20 °C. The mixture was warmed to 20 °C and the layers were separated, the organic phase washed with $NaHCO_{3(aq)}$ (3 x 100 mL), brine (3 × 100 mL), dried over Na_2SO_4 and filtered. The solvent was removed under reduced pressure and the crude material was recrystallised from hot EtOH to yield 1,3,5-tri-*tert*-butylbenzene **3.1** as a white solid (105 g, 0.426 mol, 76%).

^{1}H NMR (400 MHz, $CDCl_3$) δ_H 7.27 (s, 3H), 1.35 (s, 27H).

Analytical data as in lit.[2]

1-Bromo-3,5-di-*tert*-butylbenzene 3.2[2]

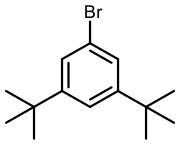

To a solution of 1,3,5-tri-*tert*-butylbenzene **3.1** (103 g, 0.416 mol) in dry $CHCl_3$ (480 mL), Fe powder (27.8 g, 0.499 mol) was added at 0 °C. A solution of Br_2 (45.0 mL, 0.873 mol) in dry $CHCl_3$ (30 mL) was added over 30 min through a dropping funnel, and the mixture was stirred for 4 h at 0 °C. The reaction was quenched by addition of $NaOH_{(aq)}$ (10%, 150 mL). The mixture was warmed to 20 °C, filtered through a filter paper, and the layers were separated. The organic phase was washed with sat. aqueous Na_2SO_3 (300 mL), sat. aqueous $NaHCO_3$ (300 mL), brine (300 mL) and dried over Na_2SO_4. The solvent was removed under reduced pressure and the crude product purified by fractional distillation (124–130 °C at $P \approx 8$ mbar) to yield 1-bromo-3,5-di-*tert*-butylbenzene **3.2** as a white solid (106 g, 0.395 mol, 95%).

^{1}H NMR (400 MHz, $CDCl_3$) δ_H 7.33 (s, 3H), 1.31 (s, 18H).

Analytical data as in lit.[2]

Supertrityl alcohol 3.3[3]

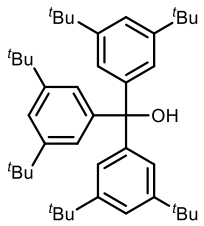

An I_2 crystal was added to activated (HCl/IPA-washed, then stirred overnight under high-vacuum) Mg turnings (3.46 g, 142 mmol) and heated under Ar for 5 min. Dry THF (10 mL) was added, and the mixture stirred until colourless. 1-Bromo-3,5-di-*tert*-butylbenzene **3.2** (35.5 g, 124 mmol) in dry THF (40 mL) was added and the reaction refluxed vigorously under N_2 overnight. After cooling to 20 °C, diethyl carbonate (4.30 mL, 35.6 mmol) in Na-dried THF (40 mL) was added, and the mixture stirred at 20 °C under N_2 for 2 d. The reaction mixture was filtered through celite. Sat. aqueous NH_4Cl solution (150 mL) and Et_2O (200 mL) were added and the organic layer extracted. The organic layer was washed with water (150 mL) then brine (150 mL). The organic layer was dried over Na_2SO_4 before evaporating solvent under reduced pressure. The crude material was purified first by SiO_2 chromatography (pet. ether/EtOAc, gradient elution from 0 to 5%), then recrystallisation from CH_2Cl_2/MeOH to yield alcohol **3.3** (17.1 g, 100 mmol, 81%) as a white solid.

^{1}H NMR (400 MHz, $CDCl_3$) δ_H 7.28 (t, *J* = 1.8 Hz, 3H, Ar-H), 7.04 (d, *J* = 1.8 Hz, 6H, Ar-H), 2.78 (s, 1H, OH), 1.23 (s, 54H, ^{t}Bu).

Analytical data as in lit.[3]

Supertrityl monoyne 3.4[3]

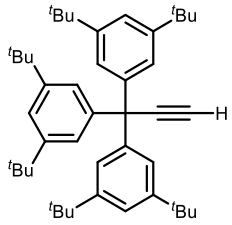

Oxalyl chloride (5.6 mL, 67 mmol, 5.2 eq.) was added dropwise to a solution of tris(3,5-di-*tert*-butylphenyl)methanol **3.3** (8.0 g, 13 mmol, 1.0 eq.) in dry THF (28 mL). The reaction was stirred under N_2 for 4 h before removing solvent under reduced pressure. The residual solid was dried under high-vacuum overnight. Dry THF (12 mL) was added to suspend the solid before slow addition of ethynylmagnesium bromide (135 mL, 67 mmol, 5.2 eq., 0.5 M in THF). The reaction stirred under N_2 for 3 d. Sat. aqueous NH_4Cl solution (80 mL) was added to quench the reaction, followed by Et_2O (80 mL). The organic layer was extracted, washed with water (80 mL), then brine (80 mL). The organic extracts were dried over Na_2SO_4 and the solvent removed under reduced pressure. The crude material was purified first by SiO_2 chromatography (pet. ether/CH_2Cl_2, gradient elution from 0 to 10%) followed by recrystallisation from CH_2Cl_2/MeOH to yield supertrityl monoyne **3.4** (7.2 g, 11.6 mmol, 89%) as a pale yellow solid.

^{1}H NMR (400 MHz, $CDCl_3$) δ_H 7.25 (t, J = 1.8 Hz, 3H, Ar-H), 7.00 (d, J = 1.8 Hz, 6H, Ar-H), 2.61 (s, 1H, C≡CH), 1.20 (s, 54H, ^{t}Bu).

Analytical data as in lit.[3]

Supertrityl alcohol 3.5[3]

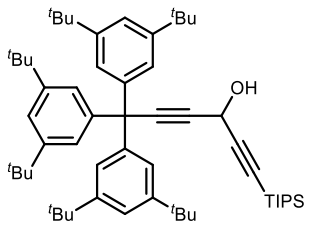

Supertrityl monoyne **3.4** (8.57 g, 14.2 mmol) was dissolved in dry THF (550 mL). The solution was cooled to −78 °C and sparged with Ar for 15 min. *n*-BuLi (9.30 mL, 14.9 mmol, 1.6 M in hexanes) was added dropwise via syringe and the reaction was stirred at −78 °C for 15 min. Neat (triisopropylsilyl)propiolaldehyde (3.28 g, 15.6 mmol) was added to the mixture over 5 min,

then the reaction warmed to 20 °C over 1 h. The reaction was quenched by addition of sat. aqueous NH_4Cl solution (150 mL) before addition of Et_2O (200 mL). The organic phase was extracted, washed with further sat. NH_4Cl solution (200 mL), H_2O (200 mL), then brine (200 mL) before drying over Na_2SO_4 and removal of the solvent under reduced pressure. The crude material was purified by SiO_2 chromatography (pet. ether/CH_2Cl_2, gradient elution from 1:0 to 3:1) to yield alcohol **3.5** (9.97 g, 12.2 mmol, 86%) as a white solid.

^{1}H NMR (400 MHz, $CDCl_3$) δ_H 7.25 (t, *J* = 1.8 Hz, 3H, Ar-H), 6.97 (d, *J* = 1.7 Hz, 6H, Ar-H), 5.32 (d, *J* = 8.1 Hz, 1H, CHOH), 2.11 (d, *J* = 8.1 Hz, 1H, CHOH), 1.20 (s, 54H, ^{t}Bu), 1.05 (s, 21H, Si^{i}Pr$_3$).

Analytical data as in lit.[3]

Supertrityl ketone 3.6[3]

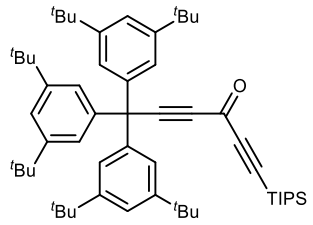

Molecular sieves (4 Å, 12 g) and Celite (12 g) were added to a solution of supertrityl alcohol **3.5** (9.97 g, 12.2 mmol) in dry CH_2Cl_2 (600 mL). The mixture was sparged with Ar for 15 min before addition of PCC (5.30 g, 24.6 mmol). The reaction was stirred under Ar at 20 °C for 24 h. After complete reaction, the mixture was passed through a short SiO_2 plug (CH_2Cl_2) and the solvent removed under reduced pressure to yield ketone **3.6** (9.24 g, 11.3 mmol, 93%) as a white solid.

^{1}H NMR (400 MHz, $CDCl_3$) δ_H 7.28 (t, *J* = 1.8 Hz, 3H, Ar-H), 6.96 (d, *J* = 1.7 Hz, 6H, Ar-H), 1.21 (s, 54H, ^{t}Bu), 1.12 – 1.05 (m, 21H, Si^{i}Pr$_3$).

Analytical data as in lit.[3]

Supertrityl dibromoolefin 3.7[3]

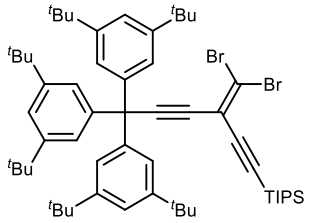

PPh_3 (12.7 g, 48.4 mmol) was added to a solution of CBr_4 (7.65 g, 23.1 mmol) dissolved in dry CH_2Cl_2 (600 mL) under Ar, and the mixture was left to stir for 1 h. Supertrityl ketone **3.6** (9.24 g, 11.4 mmol) dissolved in dry CH_2Cl_2 (150 mL) was added and the reaction stirred for 24 h at 20 °C. Once complete, the reaction mixture was concentrated to ~50 mL under reduced pressure. Pet. ether (250 mL) was added and a white precipitate of phosphine salts, in addition to an oily residue, was formed. The supernatant was decanted and passed through a celite plug. CH_2Cl_2 (50 mL) was added to dissolve the remaining oily residue, then pet. ether (250 mL) was added to precipitate, and the supernatant again decanted and passed through a celite plug (this process was repeated a further two times). The filtrate was concentrated under reduced pressure before purification of the crude material by SiO_2 chromatography (pet. ether/CH_2Cl_2, gradient elution from 0 to 2%) to yield dibromo olefin **3.7** (11.0 g, 11.1 mmol, 98%) as a white solid.

^{1}H NMR (400 MHz, $CDCl_3$) δ_H 7.23 (t, J = 1.8 Hz, 3H, Ar-H), 6.99 (d, J = 1.8 Hz, 6H, Ar-H), 1.19 (s, 54H, ^{t}Bu), 1.09–1.05 (m, 21H, Si^{i}Pr$_3$).

Analytical data as in lit.[3]

TIPS-protected supertrityl triyne 3.8[3]

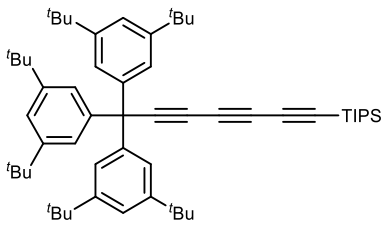

Supertrityl dibromo olefin **3.7** (11.0 g, 11.4 mmol) was dissolved in dry pentane (500 mL), cooled to −78 °C and sparged with Ar for 15 min. *n*-BuLi (8.50 mL, 13.6 mmol, 1.6 M in hexanes) was added dropwise, and the reaction stirred at −78 °C for 10 min, before warming to 20 °C over 1 h. The reaction was quenched with sat. aqueous NH_4Cl solution (150 mL) and the

organic layer separated then washed with brine (150 mL). The extracts were dried over Na_2SO_4 before removing the solvent under reduced pressure. The crude material was purified by SiO_2 chromatography (pet. ether/CH_2Cl_2, gradient elution from 0 to 5%) to yield TIPS-protected triyne **3.8** (7.80 g, 9.69 mmol, 85%) as a white solid.

^{1}H NMR (400 MHz, $CDCl_3$) δ_H 7.28 (t, *J* = 1.7 Hz, 3H, Ar-H), 6.95 (d, *J* = 1.7 Hz, 6H, Ar-H), 1.23 (s, 54H, ^{t}Bu), 1.11 (s, 21H, Si^{i}Pr$_3$).

Analytical data as in lit.[3]

Supertrityl triyne 3.9[3]

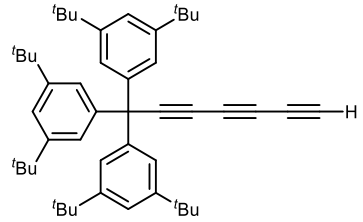

TIPS-protected supertrityl triyne **3.8** (3.0 g, 3.7 mmol, 1.0 eq.) was dissolved in dry THF (100 mL). Water (1 mL) and TBAF (4.1 mL, 4.1 mmol, 1.1 eq., 1.0 M in THF) was added dropwise. The reaction was stirred at 20 °C under N_2 for 15 min before quenching with sat. aqueous NH_4Cl solution (50 mL). Pet. ether (100 mL) was added and the organic layer extracted, washed with water (100 mL), then brine (100 mL). The organic extracts were dried over Na_2SO_4 and the solvent removed under reduced pressure. The crude material was suspended in Et_2O, centrifuged and the supernatant discarded. This process was repeated twice more to yield supertrityl triyne **3.9** (2.4 g, 3.7 mmol, 98%) as a white solid.

^{1}H NMR (400 MHz, $CDCl_3$) δ_H 7.27 (t, *J* = 1.8 Hz, 3H, ^{t}BuCCHC^{t}Bu), 6.92 (d, *J* = 1.8 Hz, 6H, ^{t}BuCHCC), 2.09 (s, 1H, C≡CH), 1.20 (s, 54H, ^{t}Bu).

Analytical data as in lit.[3]

Supertrityl triyne bromide 3.10[4]

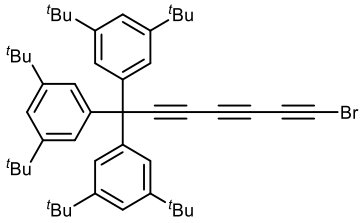

Supertrityl triyne **3.9** (1.5 g, 2.3 mmol), *N*-bromosuccinimide (610 mg, 3.5 mmol) and $AgNO_3$ (78 mg, 0.46 mmol) were suspended in dry acetone (150 mL) and stirred under N_2 for 5 h. The solvent was reduced to ~20 mL and pet. ether (180 mL) was added. The solution as passed through a SiO_2 plug (petrol) and concentrated under reduced pressure. The crude material was purified by SiO_2 chromatography (pet. ether) then precipitated into MeOH and filtered to yield supertrityl triyne bromide **3.10** (1.6 g, 2.16 mmol, 94%) as an off-white solid.

^{1}H NMR (400 MHz, $CDCl_3$) δ_H 7.27 (t, J = 1.7 Hz, 3H, ^{t}BuCCHC^{t}Bu), 6.91 (d, J = 1.8 Hz, 6H, ^{t}BuCCHC), 1.20 (s, 54H, ^{t}Bu).

Analytical data as in lit.[4]

(Triisopropylsilyl)propiolaldehyde 3.11[5]

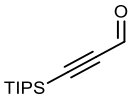

TIPS-acetylene (20 mL, 89 mmol) was dissolved in dry Et_2O (80 mL) under Ar and cooled to 0 °C. *n*-BuLi (78 mL, 130 mmol, 1.6 M in hexanes) was added over a period of 5 min. The reaction was stirred for 30 min, then cooled to −78 °C. Further dry Et_2O (80 mL) was added before a dropwise addition of dry DMF (21 mL, 270 mmol). The reaction was stirred under Ar at −78 °C for 3 h. A solution of 10% H_2SO_4 in H_2O (200 mL) was added to the reaction at 0 °C. The organic layer was extracted then the aqueous layer washed with Et_2O (2 × 20 mL). The combined organic extracts were dried over Na_2SO_4 and the solvent removed under reduced pressure to yield aldehyde **3.11** (18.6 g, 89 mmol, 100%) as a colourless oil.

^{1}H NMR (400 MHz, $CDCl_3$) δ_H 9.21 (s, 1H, CO-H), 1.11 (d, J = 4.7 Hz, 21H, Si^{i}Pr$_3$).

Analytical data as in lit.[5]

TIPS-TMS alcohol 3.12[5]

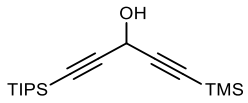

TMS-acetylene (13 mL, 98 mmol) was dissolved in dry Et_2O (280 mL) under Ar and cooled to −40 °C. *n*-BuLi (60 mL, 98 mmol, 1.6 M in hexanes) was added over a period of 5 min, then stirred (between −40 and −30 °C) for a period of 10 min. The reaction was cooled to −78 °C before addition of TIPS-aldehyde **3.11** (18.6 g, 89 mmol) in dry Et_2O (80 mL) over a period of 5 min. The mixture was allowed to warm to 20 °C and left to stir for 3 h. The reaction was quenched by addition of sat. aqueous NH_4Cl solution (80 mL), the organic layer separated, washed with H_2O (100 mL) and then brine (100 mL). The organic extract was dried over Na_2SO_4 and the solvent removed under reduced pressure to yield TIPS-TMS alcohol **3.12** (23 g, 76 mmol, 85%) as a colourless oil.

^{1}H NMR (400 MHz, $CDCl_3$) δ_H 5.08 (d, *J* = 4.1 Hz, 1H, OH), 2.14 (d, *J* = 6.2 Hz, 1H, CHOH), 1.08 (s, 21H, Si^{i}Pr$_3$), 0.18 (s, 9H, $SiMe_3$).

Analytical data as in lit.[5]

TIPS-TMS ketone 3.13[5]

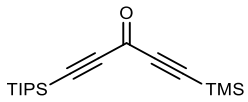

TIPS-TMS alcohol **3.12** (23 g, 32 mmol) was dissolved in dry CH_2Cl_2 (850 mL) and was sparged with Ar for 10 min. Activated MnO_2 (97 g, 87 mmol) was added in one portion and the reaction stirred at 20 °C under Ar for 20 h. The reaction was filtered through a pad of Celite to remove MnO_2 and the solvent removed under reduced pressure. The crude material was purified by SiO_2 chromatography (pet. ether/CH_2Cl_2, gradient elution from 0 to 10%) to yield TIPS-TMS ketone **3.13** (20 g, 28 mmol, 88%) as a pale-yellow oil.

^{1}H NMR (200 MHz, $CDCl_3$) δ_H 1.11 (d, *J* = 3.3 Hz, 21H, Si^{i}Pr$_3$), 0.26 (s, 9H, $SiMe_3$).

Analytical data as in lit.[5]

TIPS-TMS dibromoolefin 3.14[5]

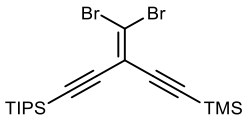

A solution of CBr_4 (39 g, 120 mmol) in dry CH_2Cl_2 (80 mL) was added to a solution of PPh_3 (62 g) dissolved in dry CH_2Cl_2 (160 mL) over a period of 10 min. The mixture was stirred at 20 °C under Ar for 1 h before addition of TIPS-TMS ketone **3.13** (18 g, 59 mmol) in dry CH_2Cl_2 (400 mL). The reaction was allowed to stir for 20 h under Ar. The mixture was concentrated under reduced pressure and pet. ether (~200 mL) was added to precipitate Ph_3PO as a white solid along with an oily residue. The supernatant was decanted and passed through a silica plug (pet. ether). The oily residue remaining in the flask was dissolved in minimal CH_2Cl_2 and pet. ether (~200 mL) was added. The heterogeneous mixture was then decanted and the supernatant passed through a silica plug (this procedure was repeated three times). The solvent was removed under reduced pressure to yield TIPS-TMS dibromo olefin **3.14** (26 g, 57 mmol, 96%) as a yellow solid.

^{1}H NMR (200 MHz, $CDCl_3$) δ_H 1.10 (d, J = 1.4 Hz, 21H, Si^{i}Pr$_3$), 0.22 (s, 9H, $SiMe_3$).

Analytical data as in lit.[5]

TIPS-TMS triyne 3.15[5]

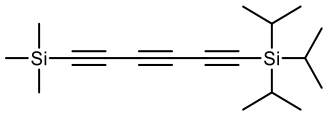

n-BuLi (41 mL, 64 mmol, 1.6 M in hexanes) was added to a solution of TIPS-TMS dibromo olefin **3.14** (24.5 g, 53 mmol) in pentane (550 mL) at −78 °C under Ar, over a period of 5 min. The reaction mixture was warmed to 20 °C over 1 h, then quenched by addition of a solution of sat. aqueous NH_4Cl (200 mL). The organic layer was extracted, washed with H_2O (200 mL), then brine (200 mL). The organic extract was dried over Na_2SO_4 and the solvent removed under reduced pressure. The crude material was purified by SiO_2 chromatography (pet. ether) to afford TIPS-TMS triyne **3.15** (16 g, 53 mmol, 100%) as an orange oil.

^{1}H NMR (400 MHz, $CDCl_3$) δ_H 1.08 (s, 21H, Si^{i}Pr$_3$), 0.20 (s, 9H, $SiMe_3$).

Analytical data as in lit.[5]

Dicobalt-masked triyne 3.16[6]

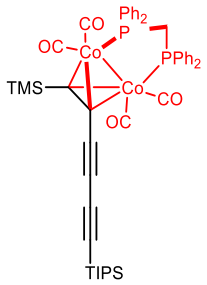

A solution of TIPS-TMS triyne **3.15** (4.5 g, 1.0 eq., 15 mmol) in dry pentane (250 mL) was sparged with Ar for 15 min, before addition of $Co_2(CO)_8$ (6.2 g, 90% w/w, 1.1 eq., 16 mmol). The mixture was stirred at 20 °C under Ar for 18 h. The pentane was removed under reduced pressure and the solid dissolved in dry toluene (100 mL). Bis(diphenylphosphino)methane (6.0 g, 1.1 eq., 16 mmol) was added and the mixture refluxed for 30 min. After cooling the solvent was removed under reduced pressure and the crude material purified by SiO_2 chromatography (pet. ether/CH_2Cl_2, gradient elution from 0 to 25%) to afford two regioisomers which where recrystallised from CH_2Cl_2/MeOH to yield compounds **3.16** (5.6 g, 6.1 mmol, 41%) and **3.17** (4.4 g, 4.8 mmol, 32%) as dark red crystals.

^{1}H NMR (400 MHz, $CDCl_3$) δ_H 7.45 – 7.37 (m, 4H, Ar–H), 7.34 – 7.26 (m, 10H, Ar–H), 7.22 (d, *J* = 7.2 Hz, 2H, Ar–H), 7.13 (t, *J* = 7.5 Hz, 4H, Ar–H), 3.98 (q, *J* = 11.1 Hz, 1H, PCHP), 3.34 – 3.21 (m, 1H, PCH'P), 1.17 (s, 21H, Si^{i}Pr$_3$), 0.36 (s, 9H, $SiMe_3$).

Analytical data as in lit.[6]

Dicobalt-masked triyne 3.17[6]

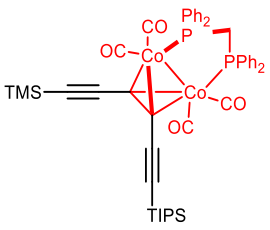

Procedure as above

^{1}H NMR (400 MHz, $CDCl_3$) δ_H 7.29 – 7.39 (m, 8H, Ar–H), 7.18 – 7.25 (m, 8H, Ar–H), 7.12 – 7.18 (m, 4H, Ar–H), 3.49 (ddd, 1H, PCHP), 3.33 (ddd, 1H, PCH'P), 1.12 (s, 21H, Si^{i}Pr$_3$), 0.24 (s, 9H, $SiMe_3$).

Analytical data as in lit.[6]

Cobalt monoyne 3.18[6]

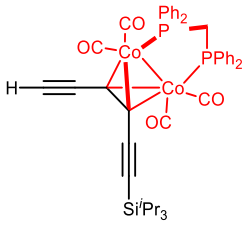

TIPS-TMS cobalt monoyne **3.17** (0.91 g, 0.99 mmol) and K_2CO_3 (1.38 g, 9.9 mmol) were dissolved in a 1:1 solution of MeOH/THF (total volume 80 mL). Water (0.1 mL) was added and the solution stirred at 20 °C for 30 min before removing the solvent under reduced pressure. The residual solid was suspended in a 1:1 solution of pet. ether/CH_2Cl_2 and passed through a SiO_2 plug, before evaporating the solvent under reduced pressure to yield cobalt monoyne **3.18** (0.80 g, 0.95 mmol, 95%) as a red solid.

^{1}H NMR (400 MHz, $CDCl_3$) δ_H 7.39 (tdd, J = 7.1, 5.3, 2.9 Hz, 4H, Ar–H), 7.19 – 7.32 (m, 12H, Ar–H), 7.13 (t, J = 7.4 Hz, 4H, Ar–H), 3.70 (t, J = 2.3 Hz, 1H, C≡CH), 3.41 (qt, J = 13.3, 10.4 Hz, 2H, PCH_2P), 1.09 – 1.11 (m, 21H, Si^{i}Pr$_3$).

Analytical data as in lit.[6]

TMS-protected cobalt diyne 3.19[6]

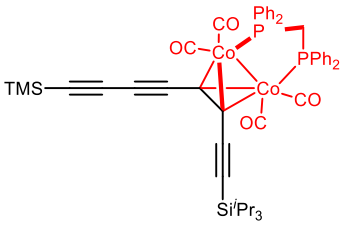

Deprotected cobalt monoyne **3.18** (840 mg, 1.0 mmol) was dissolved in dry CH_2Cl_2 (300 mL). Trimethylsilyl acetylene (4.1 mL, 30 mmol) and CuCl (2.46 g, 25 mmol) were added and O_2 bubbled through the vigorously-stirred solution. Freshly distilled *N,N,N,N*-

tetramethylethylenediamine (4.9 mL, 33 mmol) was added to the reaction mixture. Additional trimethylsilyl acetylene (4.1 mL, 30 mmol) was added over a period of 30 min via syringe pump. The reaction was monitored by TLC and, upon completion, was quenched with water (200 mL). The organic layer was extracted and washed with water (2 × 100 mL), then brine (100 mL) before drying over Na_2SO_4. The solvent was removed under reduced pressure and the crude material purified by SiO_2 chromatography (pet. ether/CH_2Cl_2, 4:1) to yield TMS-protected cobalt diyne **3.19** (0.80 g, 0.85 mmol, 90%) as a red solid.

^{1}H NMR (400 MHz, $CDCl_3$) δ_H 7.37 – 7.43 (m, 4H, Ar–H), 7.19 – 7.32 (m, 12H, Ar–H), 7.08 – 7.14 (m, 4H, Ar–H), 3.31 – 3.50 (m, 2H, PCH_2P), 1.08 – 1.11 (m, 21H, Si^iPr_3), 0.24 (s, 9H, $SiMe_3$).

Analytical data as in lit.[6]

Cobalt diyne 3.20[6]

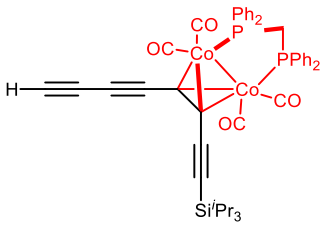

TMS cobalt diyne **3.19** (0.20 g, 0.21 mmol) and K_2CO_3 (0.29 g, 2.1 mmol) were suspended in a 1:1 solution of MeOH/THF (total volume 20 mL). Water (0.1 mL) was added and the solution stirred at 20 °C for 30 min before removing the solvent under reduced pressure. The residual solid was dissolved in a 1:1 solution of pet. ether/CH_2Cl_2 and passed through a SiO_2 plug, before evaporating the solvent under reduced pressure to yield cobalt monoyne **3.20** (0.18 g, 0.20 mmol, 96%) as a red solid.

^{1}H NMR (400 MHz, $CDCl_3$) δ_H 7.37 – 7.42 (m, 4H, Ar–H), 7.21 – 7.32 (m, 12H, Ar–H), 7.11 – 7.16 (m, 4H, Ar–H), 3.35 – 3.48 (m, 2H, PCH_2P), 2.78 (t, J = 1.2 Hz, 1H, C≡CH), 1.09 – 1.12 (m, 21H, Si^iPr).

Analytical data as in lit.[6]

1,3-Bis((6-bromohexyl)oxy)benzene 3.21[7]

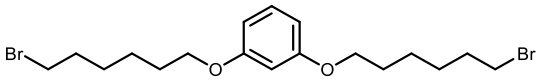

Dry acetone (1.6 L) was added to a mixture of resorcinol (5.00 g, 45.4 mmol) and K_2CO_3 (31.4 g, 227 mmol). 1,6-Dibromohexane (42.0 mL, 272 mmol) was added and the mixture stirred at 70 °C under N_2 for 3 d. The solvent of the cooled reaction mixture was evaporated under reduced pressure, the solid dissolved in minimal pet. ether/CH_2Cl_2 (3:2) and passed through a SiO_2 plug. The solvent was evaporated under reduced pressure and the crude material purified by SiO_2 chromatography (pet. ether/CH_2Cl_2, gradient elution from 1:0 to 0:1) to yield 1,3-bis((6-bromohexyl)oxy)benzene **3.21** (13.7 g, 31.3 mmol, 69%).

^{1}H NMR (400 MHz, $CDCl_3$) δ 7.15 (t, *J* = 8.2 Hz, 1H), 6.51 – 6.43 (m, 3H), 3.94 (t, *J* = 6.4 Hz, 4H), 3.42 (t, *J* = 6.8 Hz, 4H), 1.95 – 1.74 (m, 8H), 1.52-1.48 (m, 8H).

Analytical data as in lit.[7]

Saito Macrocycle M4[7]

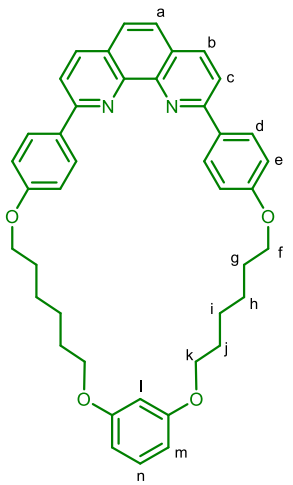

Dry DMF (1 L) was added to a mixture of diphenol phenanthroline (2.37 g, 6.49 mmol), 1,3-bis((6-bromohexyl)oxy)benzene **3.21** (2.83 g, 6.49 mmol) and K_2CO_3 (12.6 g, 90.9 mmol). A drying tube was fitted, and the mixture heated to 60 °C for 5 h. The solvent was removed under reduced pressure. The residual solid was dissolved in CH_2Cl_2 (300 mL) and washed with H_2O (300 mL). The aqueous layer was extracted with CH_2Cl_2 (2 × 150 mL) and the combined organic extracts washed with brine (300 mL), dried over Na_2SO_4 and the solvent removed under

reduced pressure. The crude material was purified by SiO_2 chromatography (pet. ether/EtOAc, 99:1) to yield the macrocycle **M4** (2.03 g, 3.18 mmol, 49%) as a white solid.

^{1}H NMR (400 MHz, $CDCl_3$) δ_H 8.45 (d, J = 8.9 Hz, 4H, H_d), 8.25 (d, J = 8.4 Hz, 2H, H_b), 8.08 (d, J = 8.4 Hz, 2H, H_c), 7.74 (s, 2H, H_a), 7.18 (t, J = 8.2 Hz, 1H, H_n), 7.12 (d, J = 8.9 Hz, 4H, H_e), 6.57 (t, J = 2.3 Hz, 1H, H_l), 6.52 (dd, J = 8.2, 2.3 Hz, 2H, H_n), 4.11 (t, J = 6.9 Hz, 4H, H_f), 4.02 (t, J = 6.2 Hz, 4H, H_k), 1.92 (t, J = 6.7 Hz, 4H, H_g), 1.87 (t, J = 6.3 Hz, 4H, H_j), 1.62 (p, J = 3.7 Hz, 8H, $H_{h,i}$).

^{13}C NMR (151 MHz, $CDCl_3$) δ_C 160.60, 160.59, 156.41, 146.16, 136.82, 132.16, 129.98, 129.09, 127.59, 125.66, 119.25, 114.94, 107.05, 101.28, 68.23, 67.93, 29.65, 29.24, 26.12, 26.07.

Analytical data as in lit.[7]

4,4-Dimethoxycyclohexa-2,5-dien-1-one 3.26[8]

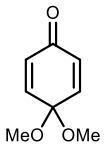

4-Methoxyphenol (84.0 g, 680 mmol, 1.00 eq.) and dry methanol (750 mL) was added to a 1L flame-dried Schlenk flask equipped with a magnetic stir bar. The reaction was kept under N_2 and cooled to 0 °C at which point solid (diacetoxyiodo)benzene (240 g, 740 mmol, 1.10 eq.) was added portion-wise over 2 h. The reaction was allowed to stir overnight, after which point it was neutralised with sodium bicarbonate solution. This solution was diluted with H_2O (500 mL) and extracted Et_2O (3 × 200 mL). The organic fractions were then washed with H_2O (3 × 500 mL), brine (500 mL), and then was dried over Na_2SO_4. Et_2O was removed under reduced pressure to give a yellow oil containing iodobenzene and the desired quinone monoketal. Iodobenzene was removed via distillation at 40 °C (P = 3 mbar) at which point the desired quinone monoketal was distilled at 60 °C (P = 3 mbar) to give ketone **3.26** as a faint yellow oil (57.4 g, 374 mmol, 55%).

^{1}H NMR (400 MHz, $CDCl_3$) δ_H 6.86 – 6.79 (m, 2H), 6.31 – 6.24 (m, 2H), 3.37 (s, 6H).

Analytical data as in lit.[8]

Chloroketone 3.27[9]

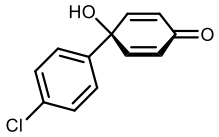

1-Bromo-4-chlorobenzene (130 g, 681 mmol, 1.50 eq.) was dissolved in dry THF (700 mL), cooled to −78 °C and sparged with Ar for 30 min. *n*-BuLi (2.5 M in hexanes, 200 mL, 499 mmol, 1.10 eq.) was added via a thin cannula to limit the rate of addition. The reaction was stirred for 30 min at −78 °C to give the lithiated species as a milky white solution. After this time, 4,4-dimethoxycyclohexa-2,5-dien-1-one **3.26** (70.0 g, 454 mmol, 1.00 eq.) was injected neat over a period of 15 min. The reaction was stirred for 90 min at −78 °C before being quenched with H_2O (300 mL) and allowed to warm to room temperature. The mixture was extracted with CH_2Cl_2 (600 mL). After separation of the phases, the aqueous layer was washed with CH_2Cl_2 (2 × 600 mL). The combined organic layers were washed with brine and dried over Na_2SO_4 and the solvent removed under reduced pressure. The solid was dissolved in acetone (350 mL). 10% AcOH/H_2O (330 mL) was added and the solution was stirred at room temperature for 1 h. The reaction was quenched with Na_2CO_3. The acetone was removed by rotary evaporation and the remaining aqueous layer was extracted with CH_2Cl_2 (3 × 200 mL). The combined organic layers were washed with brine (200 mL) and dried over Na_2SO_4 before removing the solvent under reduced pressure. The yellow solid was then recrystallised from hot EtOH to yield the chloroketone **3.27** as a faint yellow crystalline solid (85.0 g, 386 mmol, 85% yield).

^{1}H NMR (400 MHz, $CDCl_3$) δ_H 7.44 – 7.39 (m, 2H), 7.38 – 7.32 (m, 2H), 6.88 – 6.83 (m, 2H), 6.27 – 6.21 (m, 2H), 2.59 (s, 1H).

Analytical data as in lit.[9]

TES-protected chloroketone 3.28[10]

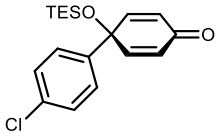

Chloroketone **3.27** (30.0 g, 136 mmol, 1.00 eq.) and imidazole (18.5 g, 272 mmol, 2.00 eq.) were dissolved in dry DMF (675 mL). Triethylchlorosilane (29.7 mL, 177 mmol, 1.30 eq.) was added

and the mixture sparged with Ar for 15 min. The mixture was heated to 50 °C and stirred under Ar for 90 min. H_2O (1.2 L) was added to the cooled reaction mixture, which was subsequently extracted with CH_2Cl_2 (3 × 300 mL). The combined organic extracts were washed with 5% LiCl solution (3 × 300mL), H_2O (300 mL) then brine (300 mL), before drying over Na_2SO_4 and evaporating solvent under reduced pressure. The crude material was purified by SiO_2 chromatography (pet. ether/CH_2Cl_2, gradient elution from 0 to 5%) to yield the TES-protected chloroketone **3.28** (42.2 g, 126 mmol, 93%) as a colourless oil.

^{1}H NMR (400 MHz, $CDCl_3$) δ_H 7.36 – 7.30 (m, 2H), 7.30 – 7.25 (m, 2H), 6.78 – 6.72 (m, 2H), 6.22 – 6.16 (m, 2H), 0.93 (t, *J* = 7.8 Hz, 9H), 0.62 (q, *J* = 7.9 Hz, 6H).

Analytical data as in lit.[10]

Chloro-bromo alcohol 3.29[10]

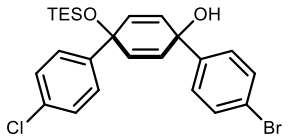

1,4-Dibromobenzene (3.9 g, 17 mmol, 1.1 eq.) was dissolved in dry THF (23 mL) and cooled to −78 °C under Ar. *n*-BuLi (9.8 mL, 1.6 M in hexanes, 16 mmol, 1.05 eq.) was added slowly, and the reaction stirred at −78 °C for 1 h. TES-protected chloroketone **3.28** (5.0 g, 15, 1.0 eq.) was added neat to the reaction over 5 min then the mixture stirred for 1 h. The reaction was quenched with H_2O (40 mL) at −78 °C, then warmed to 20 °C. The mixture was extracted with EtOAc (3 × 40 mL), then the combined organic extracts washed with brine (2 × 60 mL) before being dried over Na_2SO_4 and removal of the solvent under reduced pressure. The material was used directly in the next step without further purification.

Analytical data as in lit.[10]

TES-protected chloro-bromo compound 3.30[10]

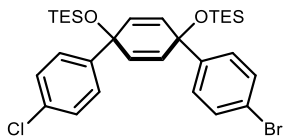

Chloro-bromo alcohol **3.29** (7.3 g, 15 mmol, 1.0 eq.) and imidazole (2.4 g, 30 mmol, 2.0 eq.) were dissolved in dry DMF (75 mL). Triethylchlorosilane (3.0 mL, 18 mmol, 1.2 eq.) was added and the mixture sparged with Ar for 10 min. The mixture was heated to 45 °C and stirred under Ar overnight. $NaHCO_3$ solution (40 mL) was added to the cooled reaction mixture, which was subsequently extracted with EtOAc (3 × 60 mL). The combined organic extracts were washed with 5% LiCl solution (50 mL), H_2O (50 mL) then brine (50 mL), before drying over Na_2SO_4 and evaporating solvent under reduced pressure. The crude material was purified by SiO_2 chromatography (pet. ether/CH_2Cl_2, gradient elution from 0 to 5%) to yield compound **3.30** (8.6 g, 14 mmol, 95%) as a colourless oil that solidifies to a white solid upon cooling.

^{1}H NMR (400 MHz, $CDCl_3$) δ_H 7.41 – 7.36 (m, 2H), 7.23 (s, 4H), 7.19 – 7.15 (m, 2H), 5.96 (s, 4H), 0.93 (td, *J* = 7.8, 1.0 Hz, 18H), 0.60 (qd, *J* = 7.6, 1.0 Hz, 12H).

Analytical data as in lit.[10]

Dichloro alcohol 3.31[10]

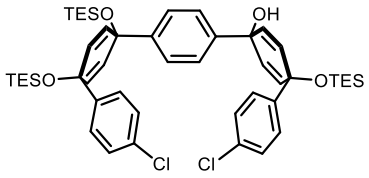

Compound **3.30** (8.6 g, 14 mmol, 1.1 eq.) was dissolved in dry THF (25 mL), cooled to −78 °C and sparged with Ar for 5 min. *n*-BuLi (8.4 mL, 1.6 M in hexanes, 14 mmol, 1.05 eq.) was added slowly, and the reaction stirred at −78 °C for 30 min. TES-protected chloroketone (4.3 g, 13 mmol, 1.0 eq.) was added neat to the reaction over 5 min then the mixture stirred for 1 h. The reaction was quenched with H_2O (20 mL) at −78 °C, then warmed to 20 °C. The mixture was extracted with EtOAc (3 × 40 mL), then the combined organic extracts washed with brine (50 mL) before being dried over Na_2SO_4 and removal of the solvent under reduced pressure. The material was used directly in the next step without further purification.

Analytical data as in lit.[10]

TES-protected dichloro compound 3.32[10]

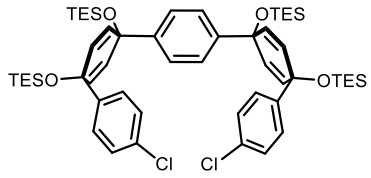

Dichloro alcohol **3.31** (11 g, 13 mmol, 1.0 eq.) and imidazole (2.2 g, 32 mmol, 2.5 eq.) were dissolved in dry DMF (75 mL). Triethylchlorosilane (2.6 mL, 15 mmol, 1.2 eq.) was added and the mixture sparged with Ar for 10 min. The mixture was heated to 45 °C and stirred under Ar for 18 h. $NaHCO_3$ solution (40 mL) was added to the cooled reaction mixture, which was subsequently extracted with EtOAc (3 × 100 mL). The combined organic extracts were washed with 5% LiCl solution (3 × 100 mL), H_2O (100 mL) then brine (100 mL), before drying over Na_2SO_4 and evaporating solvent under reduced pressure. The crude material was purified by SiO_2 chromatography (pet. ether/CH_2Cl_2, gradient elution from 0 to 15%) to yield compound **3.32** (12 g, 13 mmol, 97%) as a colourless oil that solidifies to a white solid upon cooling.

^{1}H NMR (400 MHz, $CDCl_3$) δ_H 7.24 (s, 4H), 7.23 – 7.17 (m, 8H), 6.04 – 5.99 (m, 4H), 5.93 – 5.88 (m, 4H), 0.93 (dt, J = 12.6, 7.9 Hz, 36H), 0.67 – 0.52 (m, 24H).

Analytical data as in lit.[10]

Di-BPin 3.33[11]

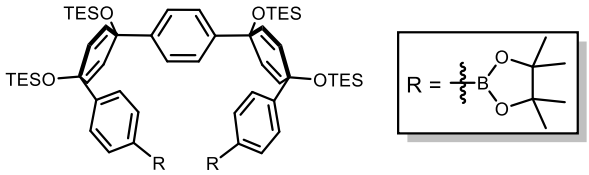

Anhydrous potassium acetate (3.32 g, 33.8 mmol, 6.60 eq.) was thoroughly dried by heating under high vacuum until all apparent moisture was removed. Compound **3.32** (5.00 g, 5.12 mmol, 1.00 eq.), $Pd(OAc)_2$ (57.5 mg, 256 μmol, 0.0500 eq.), bis(pinacolato)diboron (5.20 g, 20.5 mmol, 4.00 eq.) and SPhos (273 mg, 666 μmol, 0.13 eq.) were added to the flask and stirred under high vacuum for 1 h, during which time dry 1,4-dixoane (18 mL) was sparged with Ar for 1h. The flask was evacuated and flushed with Ar 5 times, then heated to 90 °C and stirred under Ar for 2 d. The mixture turned dark red in colour over the course of the reaction. EtOAc (30 mL) was added to the cooled reaction mixture, then the mixture filtered through a Celite

pad. The reaction flask was rinsed several times with EtOAc and aided by sonication. The filtrate was concentrated under reduced pressure yield a white waxy solid, which was rinsed with ethanol and filtered to yield di-BPin **3.33** as a white solid (3.91 g, 3.38 mmol, 66%).

^{1}H NMR (400 MHz, $CDCl_3$) δ_H 7.72 – 7.67 (m, 4H), 7.35 – 7.30 (m, 4H), 7.23 (s, 4H), 6.04 – 5.88 (m, 8H), 1.33 (s, 18H), 0.92 (td, *J* = 7.9, 3.6 Hz, 36H), 0.63 – 0.56 (m, 24H).

Analytical data as in lit.[11]

TES-protected macrocycle 3.34[12]

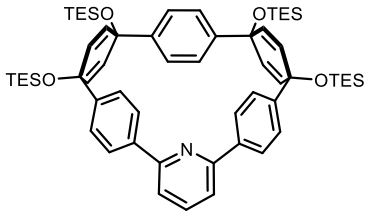

Di-BPin **3.33** (2.50 g, 2.16 mmol, 1.00 eq.), 2,6-dibromopyridine (766 mg, 3.23 mmol, 1.50 eq.) and Pd SPhos G2 (155 mg, 216 µmol, 0.10 eq.) were combined in a 1 L Schlenk flask. The flask was evacuated and flushed with Ar 5 times before addition of dry 1,4-dixoane (450 mL). The mixture was sparged with Ar for 30 min, during which time a 2.0 M solution of K_3PO_4 (19.2 g, 90.6 mmol, 42 eq.) in H_2O (45 mL) was sparged for at least 1 h. The reaction mixture was heated to 80 °C under Ar and stirred for 30 min. The degassed 2M K_3PO_4 solution was added to the reaction mixture, quickly turning the reaction from colourless to bright yellow in colour. The reaction was monitored until all starting material was consumed (~15 min), at which point the solution was allowed to cool to room temperature. The solvent was evaporated under reduced pressure and the residual oil extracted with CH_2Cl_2 (3 × 100 mL). The combined organic extracts were washed with H_2O (3 × 100 mL), then brine (100 mL), before drying over Na_2SO_4 and evaporating the solvent under reduced pressure. The crude material was purified by SiO_2 chromatography (pet. ether/CH_2Cl_2, gradient elution from 0 to 40%) to yield TES-protected macrocycle **3.34** (1.48 g, 1.51 mmol, 70%) as a white solid.

^{1}H NMR (400 MHz, $CDCl_3$) δ_H 7.77 (d, *J* = 8.1 Hz, 5H), 7.54 (d, *J* = 7.7 Hz, 2H), 7.52 – 7.47 (m, 4H), 6.99 (s, 4H), 6.09 – 6.02 (m, 4H), 5.76 – 5.69 (m, 4H), 0.95 (td, *J* = 7.9, 6.0 Hz, 36H), 0.70 – 0.57 (m, 24H).

Analytical data as in lit.[12]

Nanohoop M5[12]

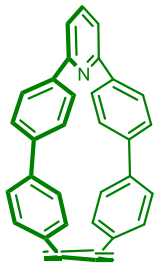

Preparation of H_2SnCl_4: To a solution of $SnCl_2{\cdot}2H_2O$ (1.7 g, 7.5 mmol, 1.0 eq.) in THF (100 mL) was added conc. HCl (1.3 mL, 15 mmol, 2.0 eq.). The resulting solution was then stirred for 15 min under Ar and used as needed.

TES-protected macrocycle **3.34** (1.5 g, 1.5 mmol, 1.0 eq.) was dissolved in THF (20 mL) and sparged with Ar for 10 min. TBAF (12 mL, 12 mmol, 8.0 eq.) was added slowly, then the mixture stirred for 1 h under Ar. The solvent was removed under reduced pressure, then H_2O (20 mL) was added, resulting in a white precipitate that was subsequently filtered. The solid was washed with H_2O (50 mL), then CH_2Cl_2 (15 mL) before being dried under high vacuum. The solid was suspended in dry THF (20 mL) to which the previously prepared H_2SnCl_4 solution (100 mL) was added, rapidly turning the mixture bright orange in colour. The reaction was stirred at 20 °C under Ar for 1 h. The mixture was neutralised by addition of NaOH solution (1.0 M, ~12 mL) at which point the mixture turned bright yellow in colour. The THF was removed under reduced pressure and the suspension extracted with CH_2Cl_2 (3 × 100 mL). The combined organic extracts were washed with H_2O (3 × 50 mL), then brine (50 mL) before being dried over Na_2SO_4 and removal of the solvent under reduced pressure. The crude material was run through a short alumina plug (CH_2Cl_2) to yield the nanohoop **M5** as a bright yellow solid (490 mg, 1.1 mmol, 71%).

^{1}H NMR (400 MHz, $CDCl_3$) δ_H 7.66 (t, J = 7.6 Hz, 1H), 7.47 – 7.44 (m, 4H), 7.44 (s, 4H), 7.43 – 7.38 (m, 6H), 7.37 – 7.34 (m, 4H), 7.33 – 7.30 (m, 4H).

^{13}C NMR (126 MHz, $CDCl_3$) δ_C 159.60, 141.56, 140.76, 137.63, 137.54, 137.16, 136.42, 130.18, 128.42, 128.10, 127.93, 127.81, 116.33.

Analytical data as in lit.[12]

Butadiyne-linked MAE 3.36[7]

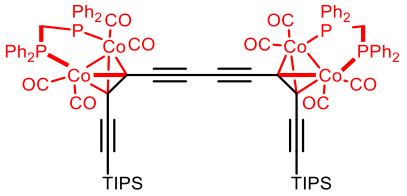

Method A: To Hg-linked MAE **3.35** (10 mg, 5.3 μmol, 1.0 eq.) was added bis(triphenylphosphine)rhodium(I) carbonyl chloride (0.44 mg, 0.64 μmol, 0.12 eq.) in thoroughly degassed tetrachloroethane-d_2 (0.7 mL). The mixture was added to a Young's tap NMR tube and the mixture then degassed with a further two freeze-pump-thaw cycles. The reaction was monitored by fixed time NMR experiments and was deemed complete after 10 h. After complete reaction, the solvent was removed under reduced pressure and purified by silica chromatography (petrol/CH_2Cl_2, gradient elution from 0 to 40%) to yield the butadiyne-linked MAE **3.36** (8.2 mg, 4.9 mmol, 92%) as a red solid.

Method B: CuCl (190 mg, 1.9 mmol, 25 eq.) was added to a solution of cobalt monoyne **3.18** (65 mg, 77 μmol, 1 eq.) in dry CH_2Cl_2 (50 mL). The mixture was vigorously stirred under O_2 for 5 minutes. TMEDA (220 mg, 29 μL, 1.9 mmol, 25 eq.) was added to the solution, and was stirred vigorously under an O_2 atmosphere for 30 min. The reaction was quenched by addition of water (50 mL), then the organic layer was extracted, and washed until there was no evidence of Cu ions in the aqueous phase. The extracts were washed with brine (50 mL), then dried over Na_2SO_4 before removing the solvent under reduced pressure. The crude material was purified by SiO_2 chromatography (pet. ether/CH_2Cl_2, gradient elution from 0 to 33%) to yield the butadiyne-linked MAE **3.36** (74 mg, 57%) as a red solid.

^{1}H NMR (500 MHz, C_6D_6) δ_H 7.35 – 7.28 (m, 16H, Ar-H), 7.08 – 6.98 (m, 12H, Ar-H), 6.93 – 6.87 (m, 12H, Ar-H), 3.48 – 2.98 (m, 4H, PCH_2P), 1.25 (d, J = 6.6 Hz, 42H, Si-^{i}Pr).

^{13}C NMR (126 MHz, C_6D_6) δ_C 132.22 (br, P-C), 130.16 (P-C-CH), 129.90 (P-C-CH-CH-CH), 128.72 (t, J = 4.9 Hz, P-C-CH-CH), 128.52 (t, J = 4.8 Hz), 110.03, 100.83, 87.79, 85.60, 30.23 (P-CH_2-P), 19.16 (CH_2-CH_3), 11.95 (CH_2-CH_3).

HRMS m/z = 1709.1998 $[M+Na]^+$ ($C_{88}H_{86}Co_4O_8P_4Si_2Na^+$ requires 1709.20319).

Analytical data as in lit.[7]

Synthesis of Novel Compounds

Cobalt [2]rotaxane 3.22·M4

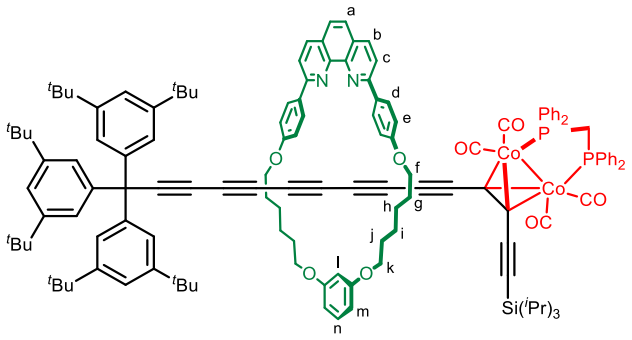

Macrocycle **M4** (212 mg, 1.05 eq., 332 μmol) and copper(I) iodide (60.3 mg, 1.00 eq., 317 μmol) were combined and dissolved in a solution of dry MeCN (10.5 mL) and dry CH_2Cl_2 (15.0 mL), then stirred for 1 h under argon at 20 °C. The solvent was removed under reduced pressure and the residual solid dissolved in dry THF (25 mL). Cobalt diyne **3.20** (275 mg, 1.00 eq., 317 μmol), supertrityl triyne bromide **3.10** (232 mg, 1.00 eq., 317 μmol) and potassium carbonate (219 mg, 5.00 eq., 1.58 mmol) were combined and evacuated of air and flushed with argon three times. The solids were cooled in liquid nitrogen, before adding the Cu-macrocycle complex, along with additional THF (25 mL). The reaction mixture was thoroughly degassed (3 freeze-pump-thaw cycles) before warming to 60 °C and stirring under Ar for 18 h. EDTA/NH_3 solution (50 mL) was added to the cooled reaction mixture and left to stir for 1 h. Et_2O (50 mL) was added and the organic layer extracted. The aqueous layer was washed with Et_2O (2 × 20 mL) and the combined organic extracts dried over Na_2SO_4 before removing the solvent under reduced pressure. The crude product was subject to SiO_2 chromatography (pet. ether/EtOAc, gradient elution from 0 to 33%) then size-exclusion chromatography (S-X3, toluene) and then recrystallised from CH_2Cl_2/hexane to yield [2]rotaxane **3.22·M4** (240 mg, 110 μmol, 35%) as a red-brown crystalline solid.

^{1}H NMR (500 MHz, $CDCl_3$) δ_H 8.49 (d, J = 8.8 Hz, 4H, H_d), 8.22 (d, J = 8.5 Hz, 2H, H_b), 8.06 (d, J = 8.4 Hz, 2H, H_c), 7.70 (s, 2H, H_a), 7.31 (d, J = 5.5 Hz, 4H, Co Ar-H), 7.25 (s, 3H, Tr* Ar-H), 7.22 – 7.16 (m, 12H, Co Ar-H), 7.15 – 7.12 (m, 4H, Co Ar-H), 7.08 (d, J = 8.2 Hz, 1H, H_n), 7.01 (t, J = 7.5 Hz, 4H, H_e), 6.86 (d, J = 1.8 Hz, 6H, Tr* Ar-H), 6.65 (t, J = 2.4 Hz, 1H, H_l), 6.49 (dd, J = 8.1, 2.3 Hz, 2H, H_m), 4.24 – 4.14 (m, 4H, H_f), 4.07 (t, J = 6.6 Hz, 4H, H_k), 3.43 – 3.26 (m, 2H,

PC$\underline{H}_2$P), 1.99 – 1.91 (m, 4H, H_g), 1.87 (q, J = 6.6 Hz, 4H, H_j), 1.64 (d, J = 5.8 Hz, 8H, $H_{h,i}$), 1.13 (s, 54H, ^{t}Bu), 1.03 (s, 21H, ^{i}Pr).

^{13}C NMR (126 MHz, $CDCl_3$) δ_C 160.82, 160.69, 156.55, 150.13, 146.18, 143.56, 136.51, 132.21 (br), 131.86, 131.37 (br), 130.28, 129.90, 129.66, 129.13, 128.55 (t, $J_{C\text{-}P}$ = 4.9 Hz), 128.41 (t, $J_{C\text{-}P}$ = 4.8 Hz), 127.36, 125.42, 123.78, 120.40, 118.99, 115.02, 108.38, 107.91, 101.71, 99.75, 86.66, 82.67, 80.91, 69.47, 69.40, 68.25, 67.83, 66.37, 64.68, 64.16, 63.63, 63.45, 57.46, 34.90, 31.46, 29.68, 29.28, 25.90, 25.87, 18.85, 11.55. *(7 carbons not distinguished)*

HRMS m/z = 2157.91431 $[M+H]^+$ ($C_{137}H_{149}Co_2N_2O_8P_2Si^+$ requires 2157.92170).

IR (ATR) (only selected signals) 2959.67 (C-H), 2924.67 (C-H), 2159.71 (s, C≡C), 2015.05 (s, C=O), 1990.65 (s, C=O) cm^{-1}.

Deprotected cobalt [2]rotaxane 3.23·M4

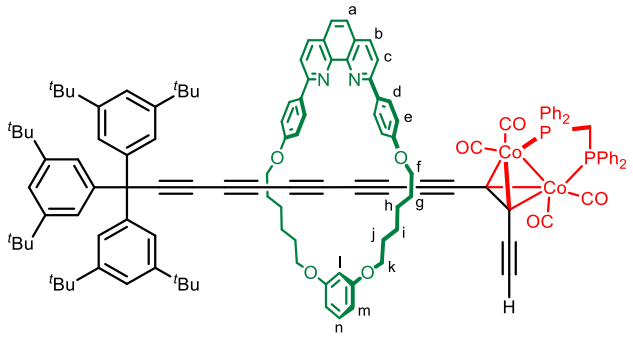

[2]Rotaxane **3.22·M4** (230 mg, 1.0 eq., 90 µmol) was dissolved in THF (35 mL) containing water (0.35 mL, 1% v/v). Tetrabutylammonium fluoride solution (0.53 mL, 5.0 eq., 0.53 mmol, 1.0 M in THF) was added dropwise and the mixture stirred for 30 min. The reaction was quenched with addition of aqueous NH_4Cl solution (30 mL), then Et_2O (30 mL) was added, and the organic layer extracted. The sat. aqueous layer was washed with Et_2O (2 × 15 mL) and the combined extracts washed with brine (40 mL), then dried over Na_2SO_4. The solvent was removed under reduced pressure and the crude material purified by silica chromatography (pet. ether/EtOAc, gradient elution from 0 to 25%) to yield the deprotected **3.23·M4** [2]rotaxane (170 mg, 86 µmol, 81%) as a red-brown solid.

^{1}H NMR (500 MHz, $CDCl_3$) δ_H 8.45 – 8.54 (m, 4H, H_d), 8.22 (d, J = 8.4 Hz, 2H, H_b), 8.07 (d, J = 8.5 Hz, 2H, H_c), 7.71 (s, 2H, H_a), 7.23 – 7.28 (m, 4H, Co Ar–$\underline{H}$), 7.19 – 7.21 (m, 3H, Tr* Ar–$\underline{H}$),

7.12 – 7.24 (m, 16H, Co Ar–H), 7.09 (t, 1H, H_n), 7.04 (t, J = 7.5 Hz, 4H, H_e), 6.85 (d, J = 1.8 Hz, 6H, Tr* Ar–H), 6.65 (t, J = 2.4 Hz, 1H, H_l), 6.49 (dd, J = 8.2, 2.3 Hz, 2H, H_m), 4.15 – 4.23 (m, 4H, H_f), 4.07 (t, J = 6.6 Hz, 4H, H_k), 3.75 (s, 1H, C≡C–H), 3.29 (br. s, 2H, PCH$_2$P), 1.94 (q, J = 6.8 Hz, 4H, H_g), 1.86 (q, J = 6.6, 6.1 Hz, 4H, H_j), 1.60 – 1.66 (m, 8H, $H_{h,i}$), 1.12 (s, 54H, ^{t}Bu).

^{13}C NMR (126 MHz, $CDCl_3$) δ_C 201.80 (br, C≡O), 160.80, 160.67, 156.51, 150.14, 146.16, 143.53, 136.54, 135.43 (t, $J_{C\text{-}P}$ = 26.5 Hz), 133.95 (t, $J_{C\text{-}P}$ = 21.0 Hz), 131.84 (t, $J_{C\text{-}P}$ = 5.5 Hz), 131.59 (t, $J_{C\text{-}P}$ = 6.2 Hz), 130.31, 130.04, 129.64, 129.15, 128.51 (dt, $J_{C\text{-}P}$ = 5.0, 5.0 Hz), 127.37, 125.43, 123.78, 120.40, 118.98, 115.00, 107.93, 99.81, 86.75, 86.16, 85.43, 82.59, 81.03, 69.38, 69.33, 68.24, 67.89, 66.44, 64.73, 63.87, 63.48, 63.36, 57.45, 36.82 (t, J = 20.7 Hz), 34.89, 31.44, 29.69, 29.27, 25.91, 25.85. *(4 carbons not distinguished)*

^{31}P{H} NMR (202 MHz, $CDCl_3$) δ_P 39.56.

HRMS m/z = 2002.7985 $[M+H]^+$ ($C_{128}H_{129}Co_2N_2O_8P_2^+$ requires 2002.7992).

Saito-protected masked [3]rotaxane 3.24·(M4)$_2$

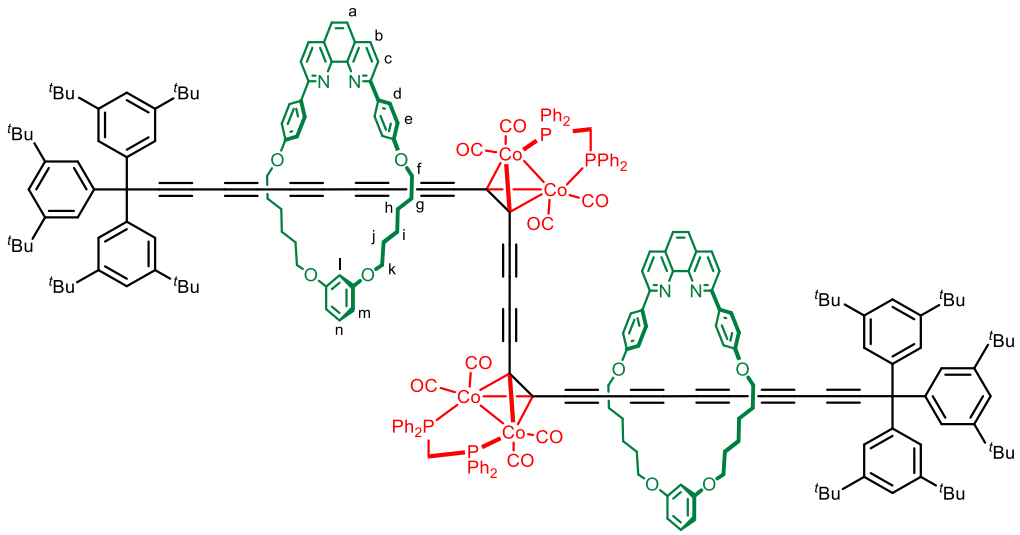

Copper(I) chloride (420 mg, 50 eq., 4.3 mmol) was added to a solution of deprotected [2]rotaxane **3.23·M4** (170 mg, 1.0 eq., 85 μmol) in dry CH_2Cl_2 (150 mL). The mixture was vigorously stirred under O_2 for 5 min. Freshly-distilled TMEDA (440 mg, 570 μL, 45 eq., 3.8 mmol) was added to the solution, and was stirred vigorously under an O_2 atmosphere for 30 min. Aqueous EDTA/NH_3 solution (150 mL) was added to the mixture, and was stirred for 1 h. The organic layer was extracted, and the aqueous layer washed with CH_2Cl_2 (2 × 50 mL).

The combined extracts were washed with brine (200 mL), then dried over Na_2SO_4 before removing the solvent under reduced pressure. The crude material was purified by SiO_2 chromatography (pet. ether/EtOAc, gradient elution from 0 to 40%), then recrystallised from CH_2Cl_2/hexane to yield [3]rotaxane **3.24**·(**M4**)$_2$ (150 mg, 38 μmol, 90%) as a red-brown crystalline solid.

^{1}H NMR (500 MHz, $CDCl_3$) δ_H 8.46 (d, *J* = 8.6 Hz, 8H, H_d), 8.17 (d, *J* = 8.4 Hz, 4H, H_b), 8.00 (d, *J* = 8.4 Hz, 4H, H_c), 7.67 (s, 4H, H_a), 7.20 (d, *J* = 1.8 Hz, 6H, Tr* Ar–H), 7.19 – 7.13 (m, 28H, Co Ar–H), 7.05-7.11 (m, 20H, Co Ar–H), 7.04 (t, *J* = 8.1 Hz, 2H, H_n), 6.85 (d, *J* = 1.8 Hz, 12H, Tr* Ar–H), 6.62 (t, *J* = 2.4 Hz, 2H, H_l), 6.44 (dd, *J* = 8.2, 2.3 Hz, 4H, H_m), 4.12 – 4.18 (m, 8H, H_f), 4.03 (q, *J* = 6.8 Hz, 8H, H_k), 3.73 – 2.82 (m, 4H, PPh_2CH_2), 1.89 (dd, *J* = 12.2, 5.4 Hz, 8H, $H_{g,k}$), 1.83 (q, *J* = 6.9 Hz, 8H, $H_{h,i}$), 1.12 (s, 108H, ^{t}Bu).

^{13}C NMR (126 MHz, $CDCl_3$) δ_C 160.68, 160.55, 156.32, 150.02, 146.03, 143.43, 136.37, 134.15, 131.82, 131.69, 131.37, 130.18, 130.12, 129.51, 128.97, 128.61, 128.42, 127.21, 125.29, 123.66, 120.29, 118.81, 114.88, 114.82, 107.70, 99.80, 87.74, 86.65, 82.87, 77.30, 77.05, 76.80, 69.85, 69.26, 68.12, 67.73, 66.56, 64.73, 63.96, 63.49, 63.31, 57.35, 53.44, 37.79 (d, *J* = 21.4 Hz), 34.78, 31.33, 29.56, 29.15, 25.79. *(3 carbons not distinguished)*

HRMS *m/z* = 2001.7829 $[M+2H]^{2+}$ ($C_{256}H_{256}Co_4N_4O_{16}P_4^{2+}$ requires 2001.7838).

IR (ATR) (only selected signals) 2961.43 (C-H), 2906.40 (C-H), 2866.26 (C-H), 2360.18, 2197.60 (w, C≡C), 2153.42 (w, C≡C), 2121.36 (w, C≡C), 2016.43 (s, C=O), 1991.75 (s, C=O), 1588.55, 1487.22, 1435.23, 1249.82, 1174.11, 738.98, 321.27, 692.96 cm^{-1}.

UV-vis (CH_2Cl_2) λ_{max} (ε) 414 (105000), 321 (224000), 312 (121000), 290 (256000) nm.

Saito-protected polyyne [3]rotaxane 3.25·(M4)$_2$

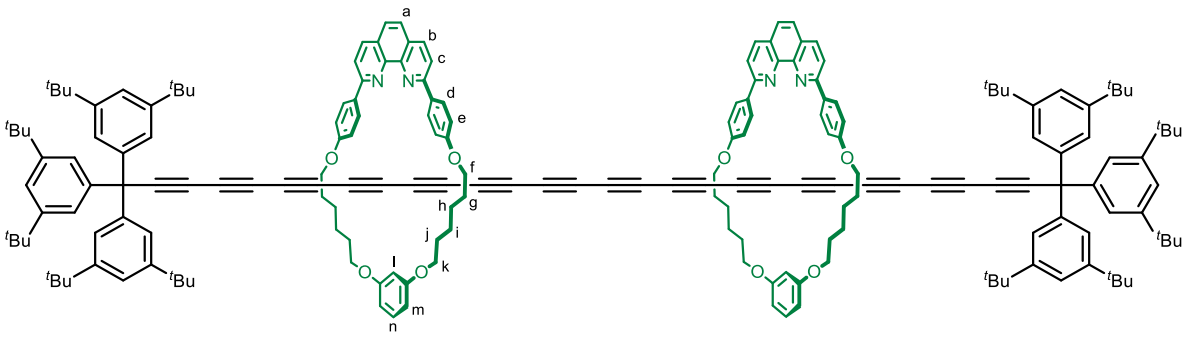

Iodine (25 mg, 20 eq., 0.10 mmol) was added to a solution of **M4**-protected masked [3]rotaxane **3.24**·(**M4**)$_2$ (20 mg, 1.0 eq., 5.0 μmol) in dry THF (3 mL). The reaction was monitored by TLC and stopped upon reaching completion after 3 h. Sat. aqueous sodium sulfite solution (3 mL) was added and the mixture stirred for 10 min. The organic layer was extracted, and the aqueous layer washed with CH_2Cl_2 (2 × 3 mL), the organic extracts combined and then dried over Na_2SO_4. The solvent was removed under reduced pressure and the crude material purified by SiO_2 chromatography (pet. ether/EtOAc, gradient elution from 0 to 15%) to yield polyyne [3]rotaxane **3.25**·(**M4**)$_2$ (4.9 mg, 1.8 μmol, 36%) as a light brown solid.

^{1}H NMR (400 MHz, $CDCl_3$) δ_H 8.38 (d, J = 8.8 Hz, 8H, H_d), 8.15 (d, J = 8.5 Hz, 4H, H_b), 7.98 (dd, J = 8.5, 2.5 Hz, 4H, H_c), 7.64 (s, 4H, H_a), 7.06 (t, 2H, H_n), 7.01 – 7.03 (m, 8H, H_e), 7.00 (s, 6H, Tr* Ar–H), 6.86 (d, J = 1.8 Hz, 12H, Tr* Ar–H), 6.42 (d, J = 2.2 Hz, 2H, H_l), 6.40 (s, 4H, H_m), 3.98 (t, J = 7.4 Hz, 8H, H_f), 3.80 – 3.89 (m, 8H, H_k), 2.08 (m, 8H, H_g), 1.97 – 2.06 (m, 8H, H_j), 1.44 – 1.51 (m, 16H, $H_{h,i}$), 1.17 (d, J = 0.9 Hz, 108H, ^{t}Bu).

HRMS m/z = 2772.62256 $[M+H]^+$ ($C_{198}H_{210}N_4O_8^+$ requires 2772.62215).

UV-vis (hexane) λ_{max} (ε) 423 (43900), 393 (44700), 368 (37300), 348 (32100), 330 (31300), 313 (31200), 283 (43700) nm.

Nanohoop-protected [2]rotaxane 3.22·M5

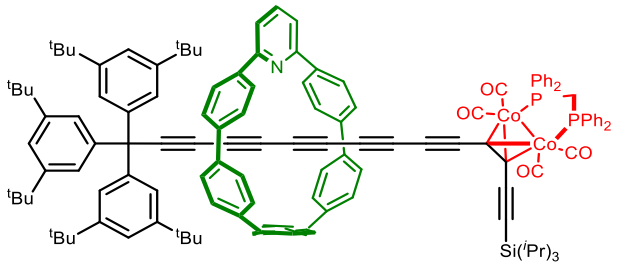

Cobalt diyne **3.20** (185 mg, 1.00 eq., 213 μmol), supertrityltriyne bromide **3.10** (156 mg, 1.00 eq., 213 μmol) macrocycle **M5** (107 mg, 1.10 eq., 234 μmol) and $[Cu(MeCN)_4][PF_6]$ (79.4 mg, 1.00 eq., 213 μmol) were combined, evacuated of air and flushed with Ar three times. The solids were cooled in liquid nitrogen, before addition of freshly-distilled diisopropylethyl amine (185 μL, 5.00 eq., 1.06 mmol) in dry $CHCl_3$ (22 mL). The reaction mixture was thoroughly degassed (3 freeze-pump-thaw cycles) before warming to 60 °C and stirred under Ar for 18 h. EDTA/NH_3 solution (22 mL) was added to the cooled reaction mixture and left to stir for 15 min. The organic layer was extracted, and the aqueous layer was washed with CH_2Cl_2 (2 × 20 mL). The combined organic extracts were dried over Na_2SO_4 before removing the solvent under reduced pressure. The crude product was subject to SiO_2 chromatography (pet. ether/EtOAc, gradient elution from 0 to 15%) to yield the nanohoop [2]rotaxane **3.22·M5** (179 mg, 91.6 μmol, 43%) as a dark brown solid; R_f (Petrol/EtOAc, 9/1) = 0.40.

^{1}H NMR (500 MHz, $CDCl_3$) δ_H 7.59 (t, J = 7.7 Hz, 1H, CPP-H), 7.51 – 7.44 (m, 12H), 7.41 (dd, J = 8.8, 2.2 Hz, 2H), 7.37 – 7.31 (m, 19H), 7.26 – 7.19 (m, 8H), 7.09 (t, J = 7.5 Hz, 4H), 7.01 (d, J = 1.7 Hz, 6H, Tr* Ar-H), 3.67 – 3.25 (m, 2H, P-CH_2), 1.26 (s, 54H, ^{t}Bu), 1.14 (d, J = 5.9 Hz, 21H, Si^{i}Pr$_3$).

^{13}C NMR (126 MHz, $CDCl_3$) δ_C 205.15 (C≡O), 200.20 (C≡O), 159.89, 150.27, 143.96, 141.91, 140.81, 138.11, 137.64, 137.49, 137.29, 137.06, 132.83 (t, $J_{C\text{-}P}$ = 6.4 Hz), 131.00 (t, $J_{C\text{-}P}$ = 6.0 Hz), 130.46, 130.43, 129.91, 129.29, 129.03, 129.00, 128.77, 128.73, 128.69, 128.42, 128.38, 128.33, 128.18, 127.82, 127.18, 123.88, 120.51, 115.94, 108.60, 100.66, 85.87, 83.10, 79.28, 70.02, 69.02, 64.32, 64.25, 63.78, 62.92, 57.55, 35.05, 31.57, 29.85, 19.07, 11.72. *(3 carbons not distinguished)*

HRMS *m/z* = 1976.7884 $[M+H]^+$ ($C_{130}H_{129}Co_2NO_4P_2Si^+$ requires 1976.7903).

IR (ATR) (only selected signals) 2980.12 (C-H), 2966.07 (C-H), 2161.82 (w, C≡C), 2012.46 (s, C=O), 1987.49 (s, C=O) cm^{-1}.

UV-vis (CH_2Cl_2) λ_{max} (ε) 372 (81400), 332 (109000), 312 (121000), 297 (121000) nm.

Deprotected cobalt [2]rotaxane 3.23·M5

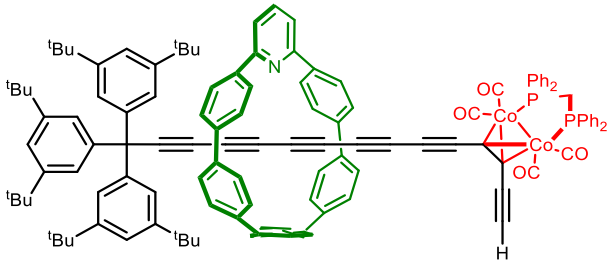

Nanohoop rotaxane **3.22·M5** (0.25 g, 1.0 eq., 0.13 mmol) was dissolved in THF (35 mL) containing water (0.35 mL, 1% v/v). TBAF (0.63 mL, 5.0 eq., 0.63 mmol, 1.0 M in THF) was added dropwise and the mixture stirred for 30 min. The reaction was quenched with addition of sat. aqueous NH_4Cl solution (20 mL), then pet. ether (10 mL) was added and the organic layer extracted. The aqueous layer was washed with pet. ether (2 × 10 mL) and the combined extracts washed with brine (20 mL), then dried over Na_2SO_4. The solvent was removed under reduced pressure and the crude material purified by silica chromatography (pet. ether/EtOAc, gradient elution from 15 to 20%) to give the deprotected [2]rotaxane **3.23·M5** (0.20 g, 0.11 mmol, 87%) as a dark brown solid; R_f (Petrol/EtOAc, 9/1) = 0.33.

^{1}H NMR (500 MHz, $CDCl_3$) δ_C 7.53 (t, J = 7.7 Hz, 1H, CPP-H), 7.44 – 7.36 (m, 12H), 7.33 (dd, J = 8.8, 2.1 Hz, 2H), 7.30 – 7.27 (m, 13H), 7.26 – 7.24 (m, 8H), 7.23 (d, J = 1.8 Hz, 2H), 7.20 (d, J = 2.0 Hz, 2H), 7.17 – 7.13 (m, 2H), 7.11 (t, J = 7.6 Hz, 4H), 6.95 (d, J = 1.8 Hz, 6H, Tr* Ar–H), 3.83 (s, 1H, C≡C–H), 3.59 (q, J = 10.5 Hz, 1H, P-CH_2), 3.20 (q, J = 10.5 Hz, 1H, P-CH_2), 1.19 (s, 54H, ^{t}Bu).

^{13}C NMR (126 MHz, $CDCl_3$) δ_C 159.90, 150.29, 143.97, 141.93, 140.81, 138.11, 137.62, 137.11, 137.07, 132.42 (t, $J_{C\text{-}P}$ = 6.2 Hz), 131.99 (t, $J_{C\text{-}P}$ = 6.3 Hz), 131.78 (t, $J_{C\text{-}P}$ = 6.3 Hz), 131.36 (t, $J_{C\text{-}P}$ = 6.2 Hz), 130.45, 130.38, 130.17, 130.09, 130.01, 128.90, 128.84, 128.79, 128.71, 128.67, 128.62, 128.57, 128.53, 128.39, 128.05, 127.67, 123.88, 120.53, 116.01, 85.78, 85.70, 85.66, 83.10, 79.16,

72.93, 70.05, 69.26, 64.31, 63.50, 62.96, 62.06, 57.57, 37.20, 35.06, 31.58. *(2 carbons not distinguished)*

^{31}P{H} NMR (202 MHz, $CDCl_3$) δ_P 39.09.

HRMS *m/z* = 1820.6546 $[M+H]^+$ ($C_{122}H_{109}Co_2NO_4P_2^+$ requires 1820.6569).

IR (ATR) (only selected signals) 2961.80 (C-H), 2904.91 (C-H), 2866.56 (C-H), 2196.23 (w, C≡C), 2160.27 (w, C≡C), 2011.48 (s, C=O), 1987.10 (s, C=O), 1591.05, 1434.97, 814.30, 738.13, 722.46, 694.88 cm^{-1}.

Cobalt [3]rotaxane 3.24·(M5)$_2$

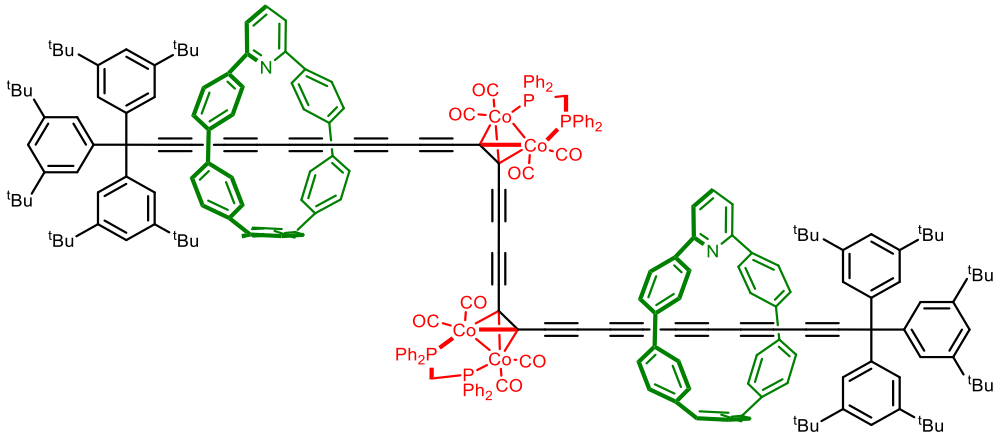

To a 100 mL round bottom flask was added deprotected nanohoop [2]rotaxane **3.23·M5** (125 mg, 2.00 eq., 68.6 µmol), 4,4'-di-*tert*-butyl-2,2'-bipyridine (92.1 mg, 10.0 eq., 343 µmol) and copper(I) chloride (40.8 mg, 12.0 eq., 412 µmol). Dry CH_2Cl_2 (20 mL) was sparged with O_2 for 10 min before addition to the solids. The reaction was stirred vigorously under O_2 at 30 °C for 20 h. Upon complete reaction, the mixture was evaporated to dryness under reduced pressure. The crude material was purified first by silica chromatography (pet. ether/EtOAc, gradient elution from 10 to 25%), then SEC (S-X3, toluene) to give the nanohoop [3]rotaxane **3.24·(M5)**$_2$ (95.7 mg, 26.3 µmol, 77%) as a brown solid.

^{1}H NMR (600 MHz, $CDCl_3$) δ_H 7.56 (t, *J* = 7.7 Hz, 2H, CPP-H), 7.46 – 7.40 (m, 24H), 7.38 – 7.35 (m, 8H), 7.35 – 7.27 (m, 34H), 7.24 (dt, *J* = 9.1, 5.1 Hz, 16H), 7.16 (t, *J* = 7.5 Hz, 8H), 7.02 (d, *J* = 1.8 Hz, 12H, Tr* Ar–H), 3.71 (q, *J* = 11.4 Hz, 2H, P-CH_2), 3.17 (q, *J* = 11.4 Hz, 2H, P-CH_2), 1.26 (s, 108H, ^{t}Bu).

^{13}C NMR (151 MHz, $CDCl_3$) δ_C 204.99 (C≡O), 200.17 (C≡O), 159.84, 150.31, 143.97, 141.91, 140.85, 138.12, 137.64, 137.08, 135.85 (t, $J_{C\text{-}P}$ = 24.0 Hz), 133.53 (t, $J_{C\text{-}P}$ = 22.0 Hz), 132.58 (t, $J_{C\text{-}P}$ = 5.9 Hz), 131.14 (t, $J_{C\text{-}P}$ = 5.9 Hz), 130.48, 130.43, 130.33, 130.01, 128.99 (t, $J_{C\text{-}P}$ = 5.0 Hz), 128.87, 128.57, 128.55 (t, $J_{C\text{-}P}$ = 5.1 Hz), 128.36, 128.03, 127.61, 123.88, 87.84, 87.79, 85.90, 85.36, 83.31, 79.77, 79.69, 70.03, 69.73 (br), 64.61, 64.29, 63.45 (br), 63.09, 62.14 (br), 57.58, 36.63 (br), 35.07, 31.59. *(6 carbons not distinguished)*

IR (ATR) (only selected signals) 2962.23 (C-H), 2905.46 (C-H), 2866.71 (C-H), 2198.35 (w, C≡C), 2161.59 (w, C≡C), 2124.39 (w, C≡C), 2032.82 (s, C=O), 2013.40 (s, C=O), 1989.14 (s, C=O), 1591.67, 1435.03, 813.91, 738.29, 722.56, 697.82 cm^{-1}.

UV-vis (CH_2Cl_2) λ_{max} (ε) 572 (7980), 410 (147000), 383 (137000), 318 (277000) nm.

Polyyne [3]rotaxane 3.25·(M5)$_2$

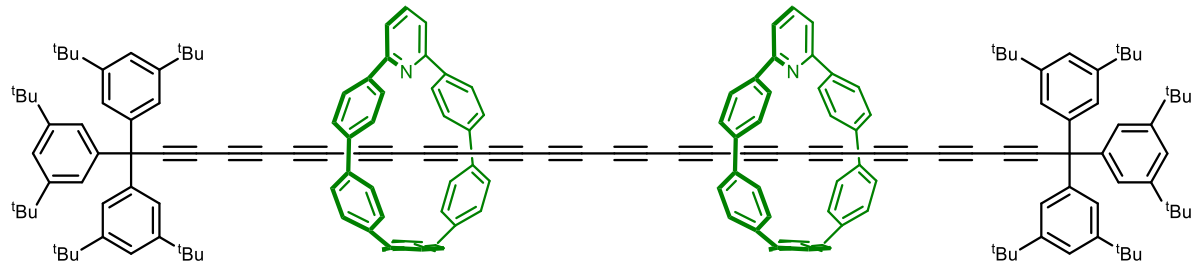

Masked nanohoop [3]rotaxane **3.24·(M5)$_2$** (40.0 mg, 1.00 eq., 11.0 μmol) was suspended in dry MeCN (5 mL) under Ar. A solution of iodine (27.9 mg, 10.0 eq., 110 μmol) in dry THF (5 mL) was then added and the mixture stirred at 25 °C for 5 min, until complete conversion was indicated by TLC. $Na_2S_2O_3$ (4 mL) was added to quench the reaction, then the organic layer extracted, dried over Na_2SO_4 and the solvent removed under reduced pressure. The crude material purified by a silica plug (pet. ether/EtOAc, gradient elution from 0 to 15%) then preparative TLC (pet. ether/EtOAc, 6%) to give nanohoop polyyne [3]rotaxane **3.25·(M5)$_2$** (8.6 mg, 3.6 μmol, 32%) as a yellow-orange solid; R_f (pet. ether/EtOAc, 6%) = 0.70.

^{1}H NMR (600 MHz, $CDCl_3$) δ_H 7.72 (t, J = 7.7 Hz, 2H, CPP-H), 7.47 (d, J = 7.7 Hz, 4H, CPP-H), 7.46 – 7.44 (m, 6H, CPP-H), 7.43 (d, J = 2.1 Hz, 4H, CPP-H), 7.43 – 7.42 (m, 6H, CPP-H), 7.40 (dd, J = 8.3, 1.9 Hz, 4H, CPP-H), 7.37 (dd, J = 8.8, 2.1 Hz, 4H, CPP-H), 7.35 (dd, J = 8.9, 2.2 Hz, 4H, CPP-H), 7.32 (t, J = 1.8 Hz, 6H, Tr* Ar-H), 7.30 (dd, J = 8.3, 2.0 Hz, 4H, CPP-H),

7.28 (d, *J* = 1.8 Hz, 2H, CPP-H), 7.28 – 7.26 (m, 4H, overlapping CPP-H), 7.25 (d, *J* = 2.1 Hz, 2H, CPP-H), 6.96 (d, *J* = 1.7 Hz, 12H, Tr* Ar-H), 1.24 (s, 108H, ^{t}Bu).

Note that the asymmetry of the nanohoop results in a series of doublet of doublets (confirmed by high-resolution HSQC experiments). Assignments were made using a combination of HSQC and diffusion-edited ^{1}H experiments.

^{13}C NMR (151 MHz, $CDCl_3$) δ_C 159.79, 150.46, 143.43, 142.01, 140.73, 137.95, 137.64, 137.48, 136.94, 130.42, 129.97, 128.87, 128.76, 128.63, 128.39, 128.32, 128.25, 127.94, 127.45, 123.86, 120.71, 116.22, 87.06, 68.91, 68.32, 63.61, 63.54, 63.17, 62.88, 62.66, 62.47, 62.26, 62.06, 61.94, 61.87, 61.80, 57.56, 35.05, 31.54.

MS (MALDI-TOF, DCTB matrix) 2409.5 $[M+H]^+$ ($C_{184}H_{172}N_2$ requires 2409.4).

UV-vis (*n*-hexane) λ_{max} (ε) 425 (80700), 395 (78300), 371 (46000), 350 (24600), 331 (19700), 316 (20600), 294 (25700), 283 (24100), 272 (19700), 259 (16200), 248 (16800) nm.

IR (ATR) (only selected signals) 2961.22, 2926.82, 2866.55, 2199.69, 2129.29, 2080.81, 2013.60, 1934.64, 1591.84, 814.84, 722.72, 699.87 cm^{-1}.

Cobalt [2]rotaxane thread 3.23

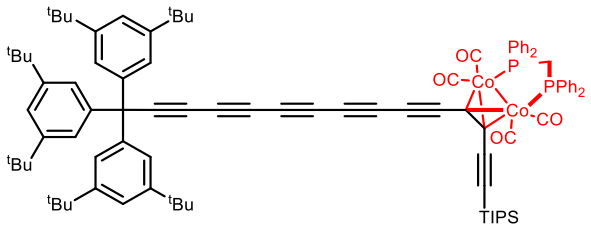

Supertrityltriyne bromide **3.10** (77 mg, 1.0 eq., 110 µmol), deprotected cobalt diyne **3.20** (110 mg, 1.2 eq., 13 µmol), bis(triphenylphosphine)palladium(II) dichloride (7.4 mg, 0.10 eq., 11 µmol) and copper(I) iodide (2.0 mg, 0.10 eq., 11 µmol) were cooled in liquid nitrogen before addition of dry THF (10 mL) and freshly-distilled diisopropylamine (32 mg, 45 µL, 3.0 eq., 320 µmol). The mixture was degassed by three freeze-pump-thaw cycles before being left to stir under Ar for 18 h at 25 °C. The reaction was quenched by addition of sat. aqueous NH_4Cl solution (10 mL). The mixture was diluted with pet. ether (10 mL), extracted then the organic layer washed with water (20 mL), then brine (20 mL). The organic layer was dried over Na_2SO_4, filtered, and concentrated under reduced pressure. The crude material was purified by silica

chromatography (pet. ether/CH_2Cl_2, gradient elution from 0 to 33%) to give dumbbell **3.22** (79 mg, 52 μmol, 50%) as a red solid.

^{1}H NMR (500 MHz, $CDCl_3$) δ_H 7.39 (q, J = 7.5 Hz, 4H, Co Ar-H), 7.34 – 7.26 (m, 10H), 7.26 – 7.22 (m, 5H), 7.15 (t, J = 7.5 Hz, 4H, Co Ar-H), 6.94 (d, J = 1.8 Hz, 6H, Tr* Ar-H), 3.42 (t, J = 9.9 Hz, 2H, P-CH_2), 1.22 (s, 54H, ^{t}Bu), 1.11 (d, J = 4.6 Hz, 21H, ^{i}Pr$_3$).

^{13}C NMR (151 MHz, $CDCl_3$) δ_C 202.87 (br, C≡O), 201.62 (br, C≡O), 150.25, 143.69, 136.33 (br), 133.69 (br), 132.30 (t, $J_{C\text{-}P}$ = 6.4 Hz), 131.47 (t, $J_{C\text{-}P}$ = 6.2 Hz), 130.31, 130.02, 128.65 (t, $J_{C\text{-}P}$ = 4.9 Hz), 128.50 (t, $J_{C\text{-}P}$ = 4.9 Hz), 123.88, 120.48, 108.53, 101.52, 86.66, 82.45, 81.17, 69.57, 69.45, 66.15, 64.37, 63.93, 63.69, 63.61, 57.51, 36.51 (br), 35.00, 31.53, 18.92, 11.62. *(2 carbons not distinguished)*

^{31}P{H} NMR (202 MHz, $CDCl_3$) δ_P 39.03.

HRMS m/z = 1519.6073 $[M+H]^+$ ($C_{95}H_{107}Co_2O_4P_2Si^+$ requires 1519.6072).

Deprotected cobalt [2]rotaxane thread 3.23

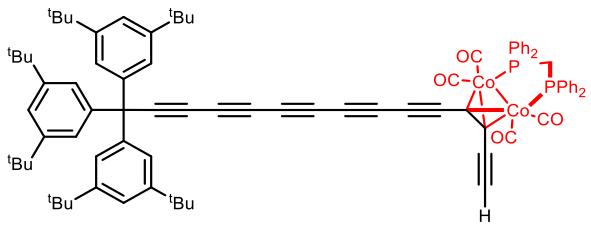

TIPS-protected [2]rotaxane thread **3.22** (89 mg, 1.0 eq., 59 μmol) was dissolved in THF (10 mL) containing water (0.10 mL). TBAF (0.29 mL, 1.0 M in THF, 5.0 eq., 0.29 mmol) was added dropwise and the mixture stirred for 90 min. The reaction was quenched with addition of sat. aqueous NH_4Cl solution (10 mL), then Et_2O (10 mL) was added and the organic layer extracted. The aqueous layer was washed with Et_2O (2 × 10 mL) and the combined extracts washed with brine (20 mL), then dried over Na_2SO_4. The solvent was removed under reduced pressure and the crude material purified by silica chromatography (pet. ether/EtOAc, gradient elution from 0 to 25%) to afford the deprotected [2]rotaxane thread **3.23** (66 mg, 48 μmol, 83%) as a red-brown solid.

^{1}H NMR (500 MHz, $CDCl_3$) δ_H 7.36 – 7.31 (m, 4H, Co Ar-H), 7.30 – 7.26 (m, 8H), 7.25 (m, 2H), 7.24 – 7.17 (m, 9H), 6.91 (d, J = 1.8 Hz, 6H, Tr* Ar-H), 3.78 (t, J = 1.7 Hz, 1H, C≡C–H), 3.38 (q, J = 12.7 Hz, 2H, P-CH_2), 1.19 (s, 54H, ^{t}Bu).

^{13}C NMR (126 MHz, $CDCl_3$) δ_C 201.80 (br, C≡O), 150.25, 143.65, 135.40 (br), 134.24 (br), 131.98 (t, $J_{C\text{-}P}$ = 6.2 Hz), 131.70 (t, $J_{C\text{-}P}$ = 6.2 Hz), 130.35, 130.21, 128.64 (td, $J_{C\text{-}P}$ = 4.9, 2.1 Hz), 123.87, 120.49, 86.71, 85.65, 85.62, 81.97, 81.65, 69.64, 69.37, 66.22, 64.44, 63.62, 63.54, 63.50, 57.49, 37.37, 35.00, 31.52. *(4 carbons not distinguished)*

^{31}P{H} NMR (203 MHz, $CDCl_3$) δ_P 39.71.

HRMS m/z = 1363.4744 $[M+H]^+$ ($C_{86}H_{87}Co_2O_4P_2^+$ requires 1363.4738).

Cobalt [3]rotaxane thread 3.24

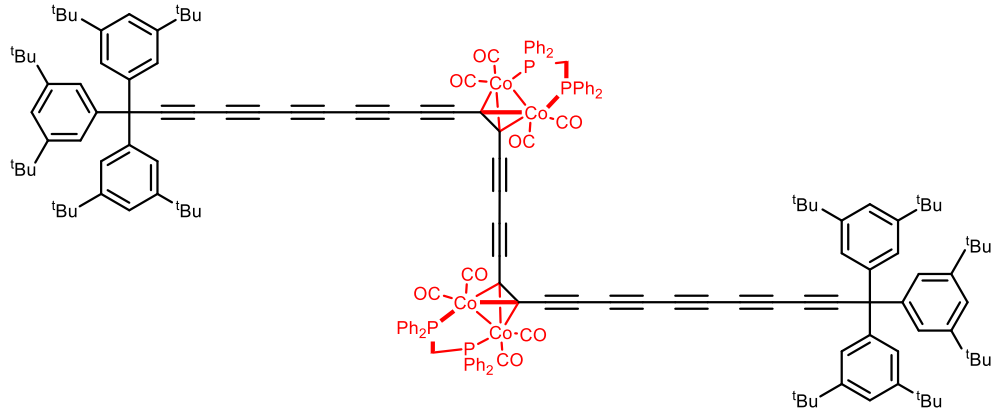

Deprotected [2]rotaxane thread **3.23** (65 mg, 2.0 eq., 48 μmol) and copper(I) chloride (120 mg, 50 eq., 1.2 mmol) were dissolved in dry CH_2Cl_2 (20 mL). Freshly-distilled TMEDA (140 mg, 180 μL, 50 eq., 1.2 mmol) was added, and the mixture stirred vigorously at 25 °C for 30 min under an O_2 atmosphere. Upon complete reaction, water (20 mL) was added, and the organic layer extracted, washed with water (2 × 20 mL), then brine (20 mL). The combined organic extracts were dried over Na_2SO_4 and the solvent removed under reduced pressure. The crude material was purified by silica chromatography (pet. ether/CH_2Cl_2, gradient elution from 0 to 33%) to yield the masked [3]rotaxane dumbbell **3.24** (46 mg, 17 μmol, 71%) as a brown solid.

^{1}H NMR (600 MHz, $CDCl_3$) δ_H 7.37 – 7.26 (m, 26H), 7.26 – 7.18 (m, 20H), 6.91 (d, J = 1.8 Hz, 12H, Tr* Ar-H), 3.56 (s, 2H, P-CH_2), 3.34 (s, 2H, P-CH_2), 1.19 (s, 108H, ^{t}Bu).

^{13}C NMR (151 MHz, $CDCl_3$) δ_C 202.86 (br, C≡O), 201.15 (br, C≡O), 150.25, 143.67, 134.98 – 134.28 (m), 132.00 (t, *J* = 6.1 Hz), 131.69 (t, *J* = 6.0 Hz), 130.43, 130.37, 128.84 (t, *J* = 4.9 Hz), 128.69 (t, *J* = 4.9 Hz), 123.88, 120.48, 88.04, 86.77, 85.63, 82.52, 81.90, 80.26, 78.30, 70.15, 69.43, 66.48, 64.55, 63.79, 63.65, 63.59, 57.51, 38.37 (t, *J* = 21.7 Hz), 35.00, 31.53. *(1 carbon not distinguished)*

^{31}P{H} NMR (243 MHz, $CDCl_3$) δ_P 40.06.

Supertrityl-stoppered 14-yne thread 3.25

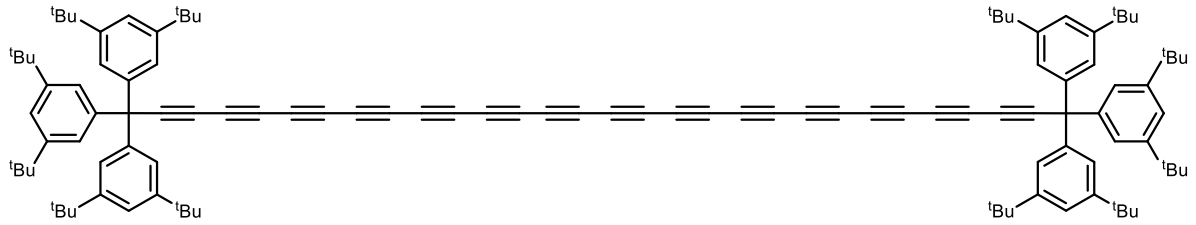

Masked [3]rotaxane thread **3.24** (45 mg, 1.0 eq., 17 μmol) was charged into a flask and flushed with Ar. A solution of iodine (84 mg, 20 eq., 0.33 mmol) in dry THF (20 mL) was added and the mixture was stirred at 25 °C for 5 min, until complete conversion by TLC. Sat. aqueous $Na_2S_2O_3$ (20 mL) was added, the organic layer extracted, dried over Na_2SO_4 and the solvent was removed under reduced pressure. The crude material purified by a silica plug (pet. ether/CH_2Cl_2, 15%) to give the supertrityl-stoppered 14-yne **3.25** (1.8 mg, 1.2 μmol, 7.3%).

^{1}H NMR (600 MHz, $CDCl_3$) δ_H 7.28 (t, *J* = 1.8 Hz, 6H, Tr* Ar-H), 6.89 (d, *J* = 1.8 Hz, 12H, Tr* Ar-H), 1.20 (s, 108H, ^{t}Bu).

^{13}C NMR (151 MHz, $CDCl_3$) δ_C 150.41, 143.29, 123.84, 120.67, 87.38, 68.71, 64.43, 64.15, 64.08, 63.85, 63.61, 63.39, 63.16, 62.89, 62.64, 62.60, 62.27, 62.12, 57.52, 35.01, 31.50.

MS (MALDI-TOF, DCTB matrix) 1495.2 $[M-H]^-$ ($C_{114}H_{126}$ requires 1495.0).

Analytical data as lit.[4]

Bis(masked triyne) mercury acetylide 3.35

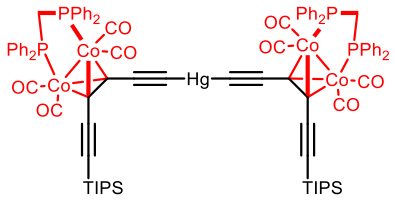

Co-masked TIPS-TMS triyne **3.17** (350 mg, 380 μmol, 2.1 eq.), potassium carbonate (500 mg, 3.6 mmol, 20 eq.) and mercury(II) acetate (58 mg, 180 μmol, 1 eq.) were dissolved in THF (20 mL) and MeOH (30 mL). The mixture was stirred at 20 °C for 2 h until complete by TLC. The solvent was removed under reduced pressure, then the crude material purified by silica chromatography (petrol/CH_2Cl_2, gradient elution from 0 to 33%) to yield the bis-MAE mercurial **3.35** (180 mg, 96 μmol, 53%) as a red solid, that appears stable indefinitely when stored at −18 °C.

^{1}H NMR (500 MHz, $CDCl_3$) δ_H 7.42 – 7.32 (m, 16H, Ar-H), 7.28 (dd, *J* = 8.4, 6.3 Hz, 6H, Ar-H), 7.25 – 7.15 (m, 18H, Ar-H), 3.56 – 3.33 (m, 4H, P-CH_2-P), 1.13 (s, 42H, Si-^{i}Pr).

^{13}C NMR (126 MHz, C_6D_{12}) δ_C 203.46 (br, C≡O) 137.20 (br), 136.58 (br), 132.74 (d, *J* = 26.3 Hz), 130.26, 129.99, 128.73 (m), 110.30, 108.61, 99.23, 77.59, 36.86 (br, P-CH_2), 19.28 (CH-CH_3), 12.43 (CH-CH_3). (1 signal not observed due to overlap, 2 Co-C signals not observed due to broadening)

^{31}P NMR (202 MHz, C_6D_{12}) δ_P 41.42.

^{199}Hg NMR (89 MHz, $CDCl_3$) δ_{Hg} -828.32.

TES-protected phenanthroline macrocycle

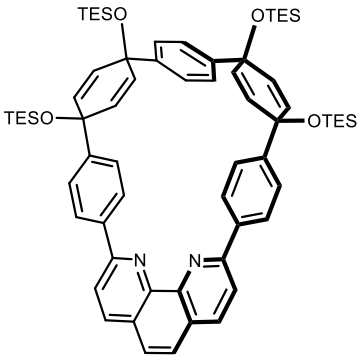

Di-BPin **3.33** (500 mg, 1.0 eq., 0.43 mmol), 2,9-dibromo-1,10-phenanthroline (220 mg, 1.5 eq., 0.65 mmol) and Pd SPhos G2 (31 mg, 0.10 eq., 43 μmol) were combined in a Schlenk flask. The flask was evacuated and flushed with Ar 5 times before addition of dry 1,4-dioxane (90 mL). The mixture was sparged with Ar for 30 min, during which time a 2.0 M solution of potassium phosphate, tribasic (3.8 g, 18 mmol) in water (9 mL) was sparged for at least 1 h. The reaction mixture was heated to 90 °C under Ar and stirred for 30 min. The degassed 2M K_3PO_4 solution was added to the reaction mixture, quickly turning the reaction from colourless to bright yellow/orange in colour. The reaction was monitored until all starting material was consumed (~15 min), at which point the solution was allowed to cool to room temperature. The solvent was evaporated under reduced pressure and the residual oil extracted with CH_2Cl_2 (3 × 20 mL). The combined organic extracts were washed with H_2O (3 × 20 mL), then brine (50 mL), before drying over Na_2SO_4 and evaporating the solvent under reduced pressure. The crude material was purified by SiO_2 chromatography (pet. ether/EtOAc, gradient elution from 0 to 33%) to yield TES-protected phenanthroline nanohoop (110 mg, 100 μmol, 24%) as a white solid.

^{1}H NMR (500 MHz, $CDCl_3$) δ_H 8.53 (d, *J* = 8.6 Hz, 4H), 8.24 (d, *J* = 8.4 Hz, 2H), 8.12 (d, *J* = 8.4 Hz, 2H), 7.72 (s, 2H), 7.53 (s, 4H), 6.17 – 6.11 (m, 4H), 5.97 – 5.91 (m, 4H), 1.07 (t, *J* = 7.9 Hz, 18H), 0.94 (t, *J* = 8.0 Hz, 18H), 0.79 (q, *J* = 7.9 Hz, 12H), 0.53 (q, *J* = 7.9 Hz, 12H).

^{13}C NMR (126 MHz, $CDCl_3$) δ_C 155.44, 147.68, 146.19, 145.84, 137.77, 136.53, 132.27, 130.89, 127.47, 127.26, 126.29, 126.08, 125.64, 118.68, 72.02, 70.95, 7.31, 7.27, 6.69, 6.53.

HRMS *m/z* = 1083.5731 $[M+H]^+$ ($C_{66}H_{86}N_2O_4Si_4^+$ requires 1083.5737)

Selected NMR Spectra

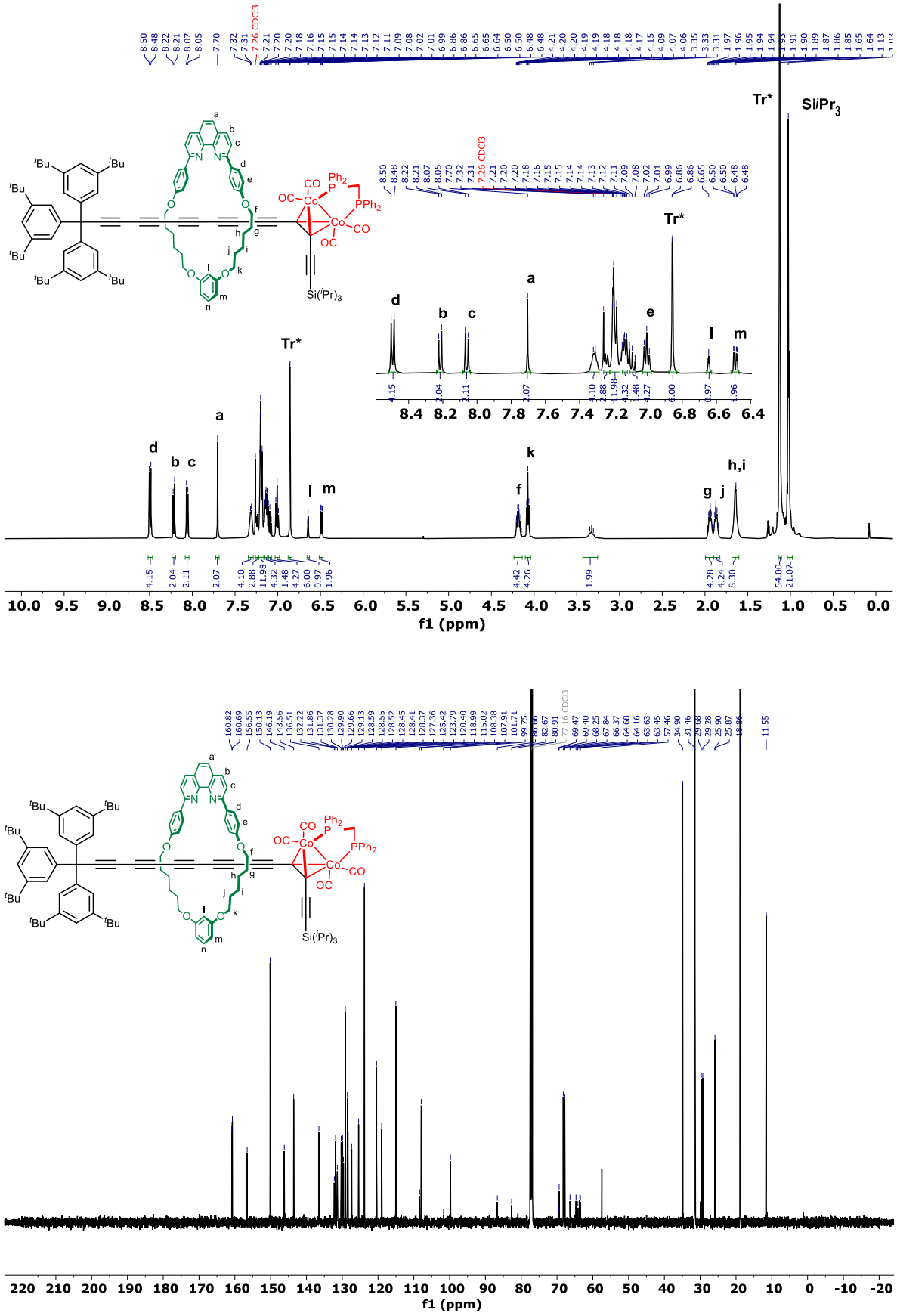

Figure S3.2: (top) ^{1}H NMR (500 MHz) and (bottom) ^{13}C NMR (126 MHz) spectra of [2]rotaxane **3.22·M4** ($CDCl_3$, 298 K).

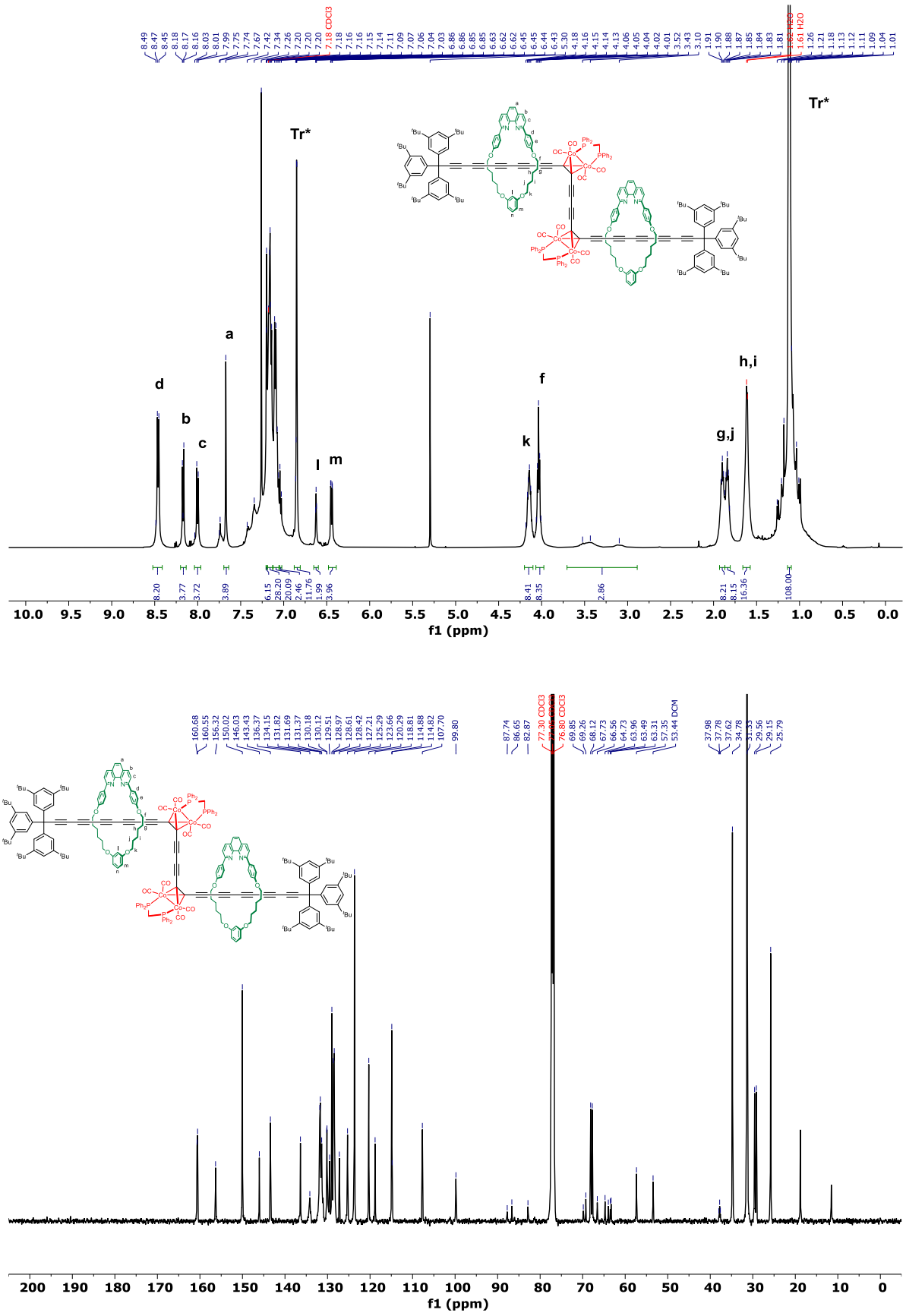

Figure S3.3: (top) ^{1}H NMR (500 MHz) and (bottom) ^{13}C NMR (126 MHz) spectra of supertrityl-cobalt [3]rotaxane **3.24**·(**M4**)$_2$ ($CDCl_3$, 298 K).

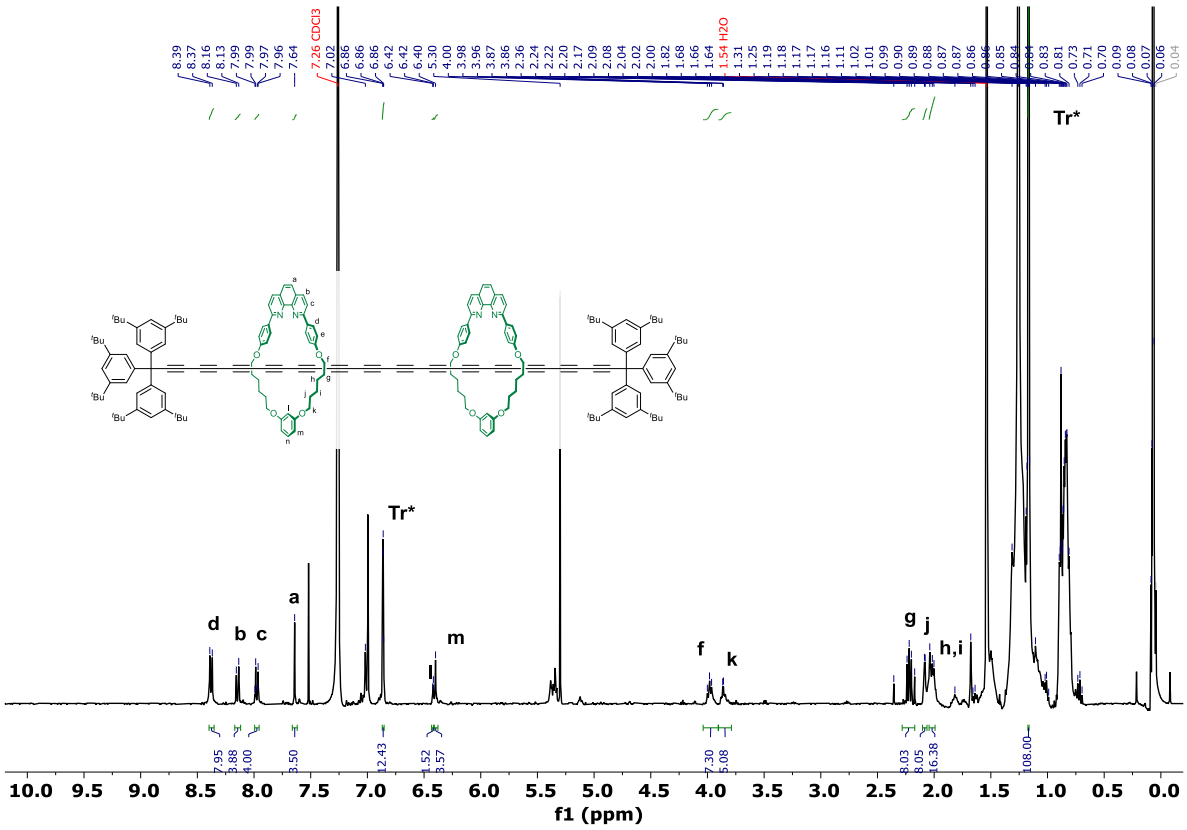

Figure S3.4: (top) ^{1}H NMR (500 MHz) spectrum of supertrityl polyyne [3]rotaxane **3.25**·(**M4**)$_2$ ($CDCl_3$, 298 K).

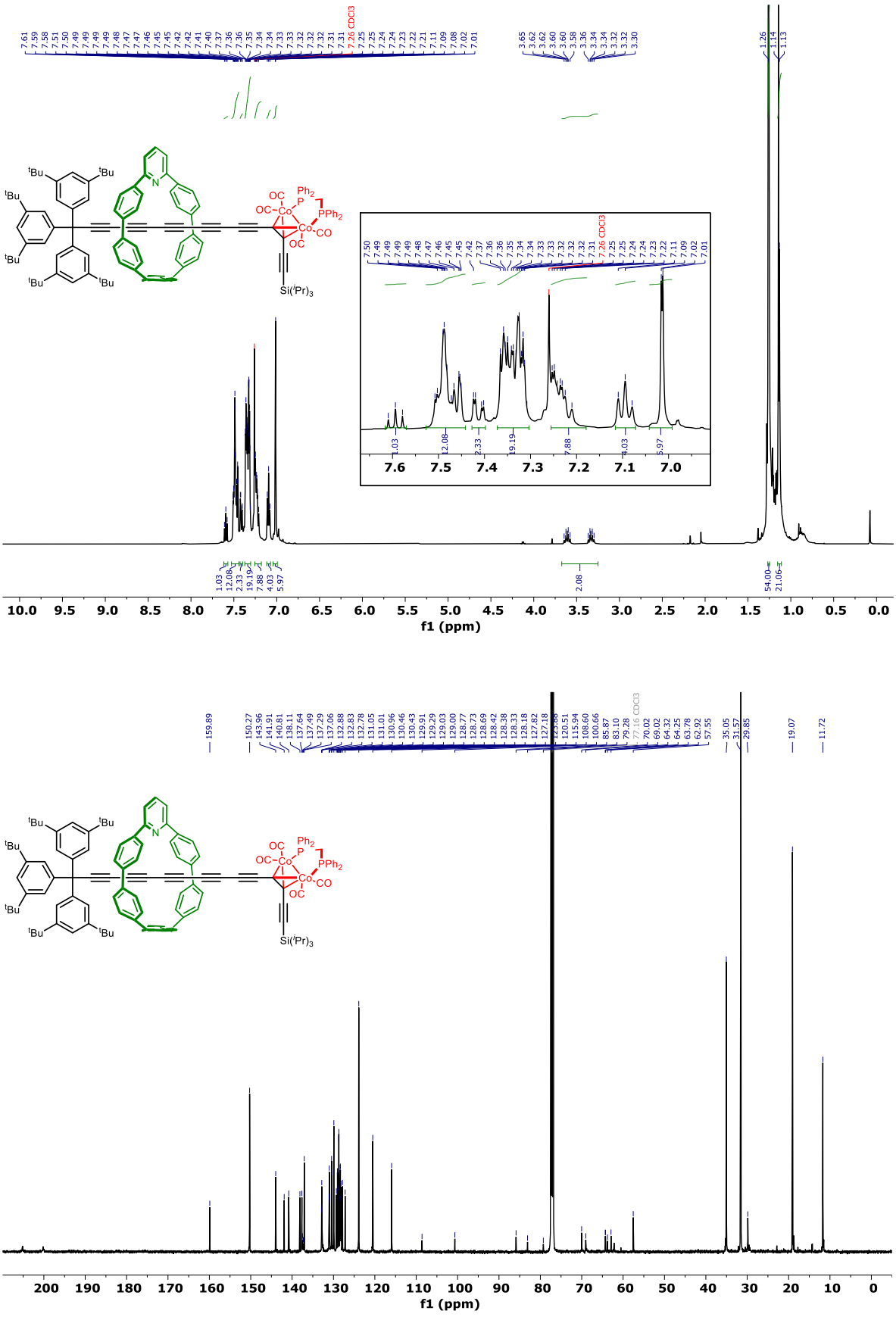

Figure S3.5: (top) ^{1}H NMR (500 MHz) and (bottom) ^{13}C NMR (126 MHz) spectra of supertrityl-cobalt [3]rotaxane **3.22·M5** ($CDCl_3$, 298 K).

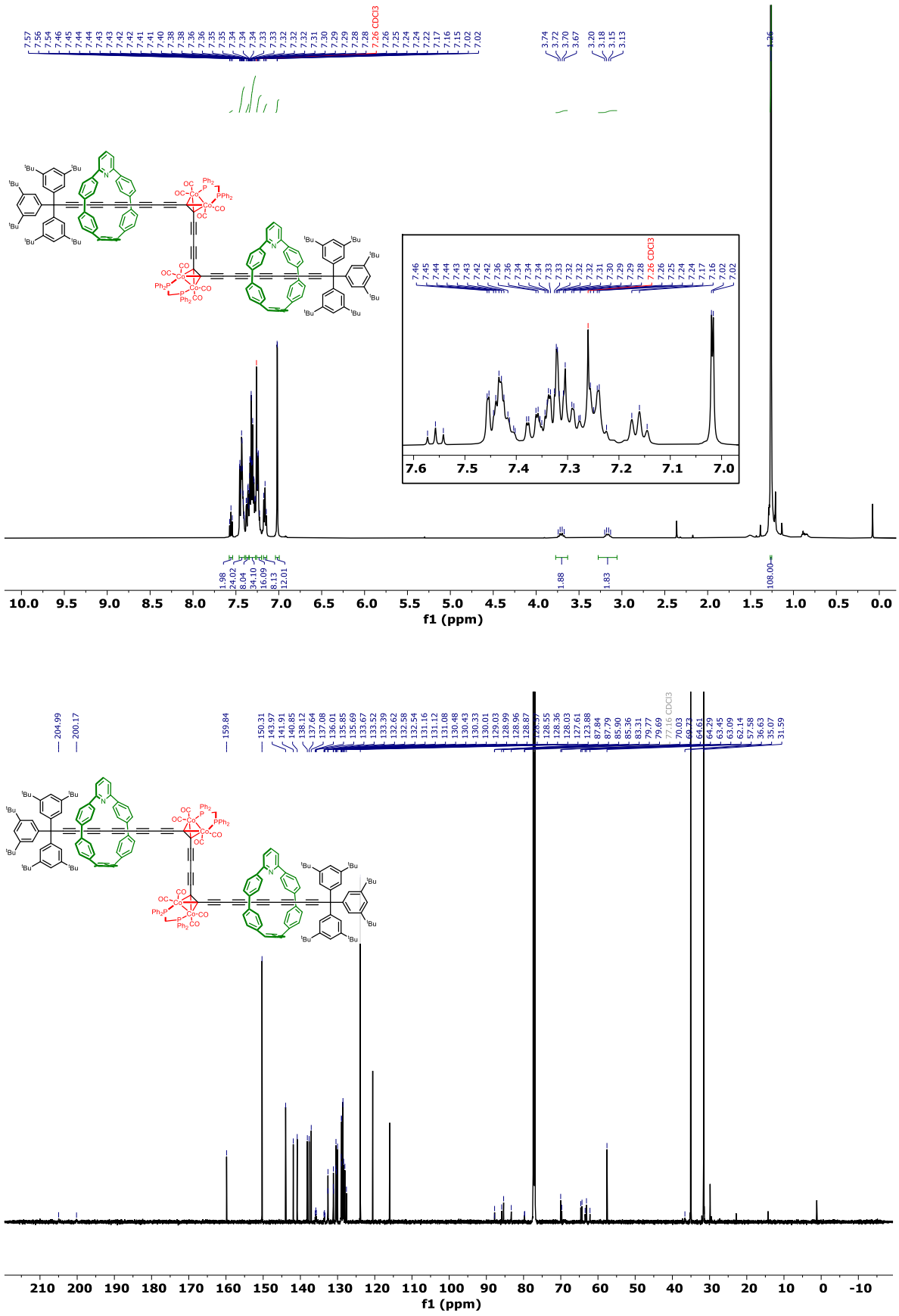

Figure S3.6: (top) ^{1}H NMR (600 MHz) and (bottom) ^{13}C NMR (151 MHz) spectra of masked nanohoop [3]rotaxane **3.24**·(**M5**)$_2$ ($CDCl_3$, 298 K).

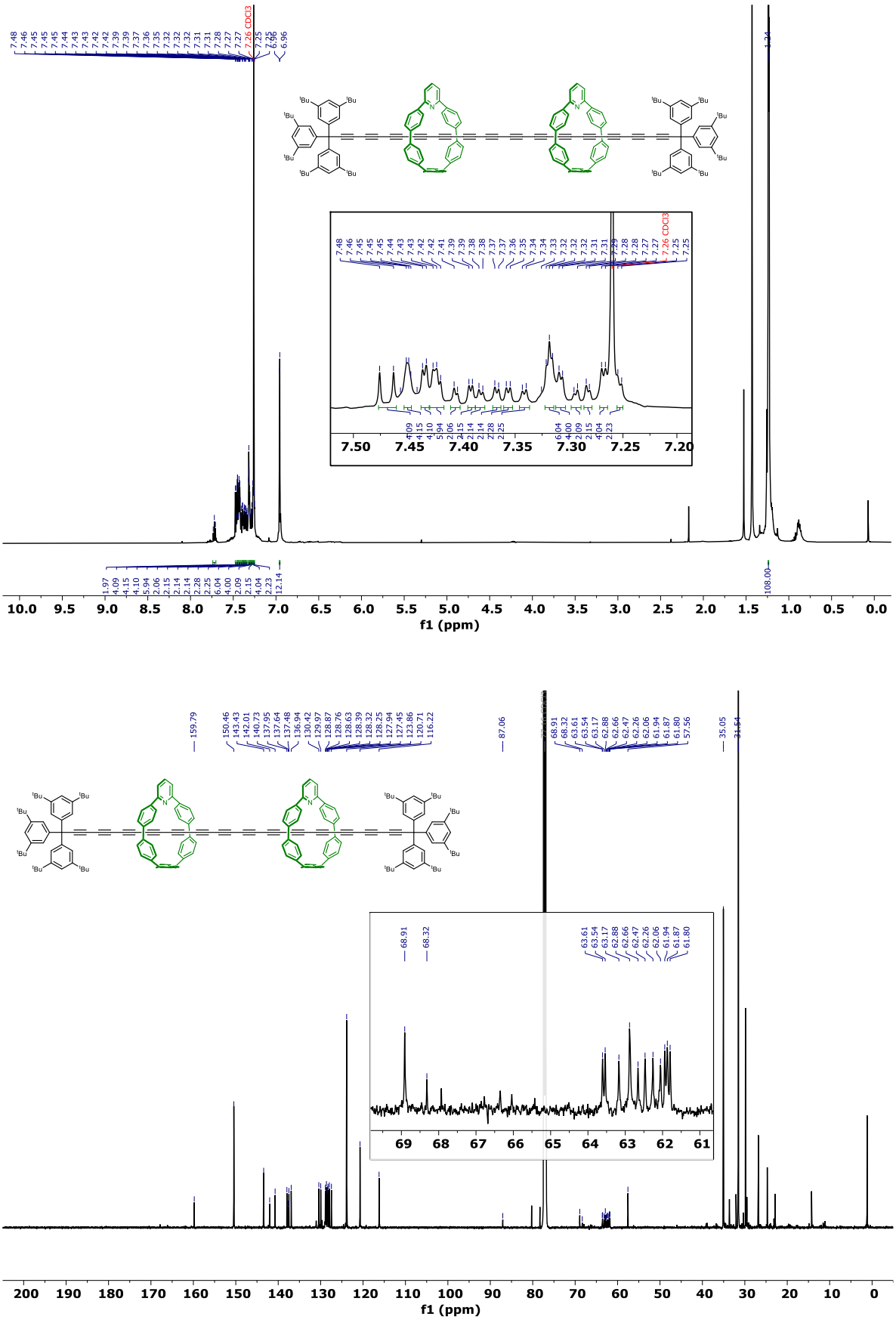

Figure S3.7: (top) ^{1}H NMR (600 MHz) and (bottom) ^{13}C NMR (151 MHz) spectra of nanohoop polyyne [3]rotaxane **3.25**·(**M5**)$_2$ ($CDCl_3$, 298 K).

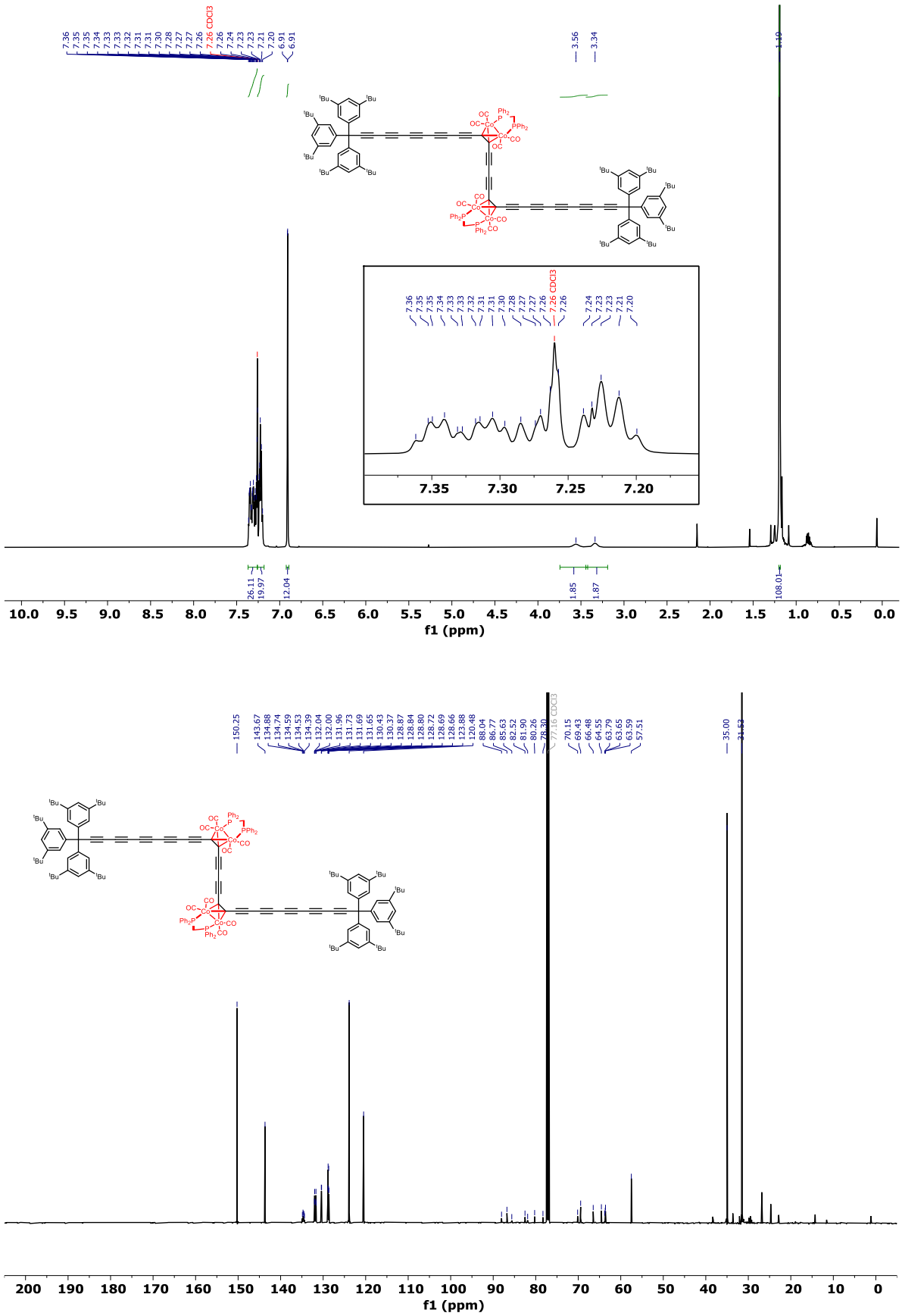

Figure S3.8: (top) ^{1}H NMR (500 MHz) and (bottom) ^{13}C NMR (126 MHz) spectra of masked [3]rotaxane thread **3.24** ($CDCl_3$, 298 K).

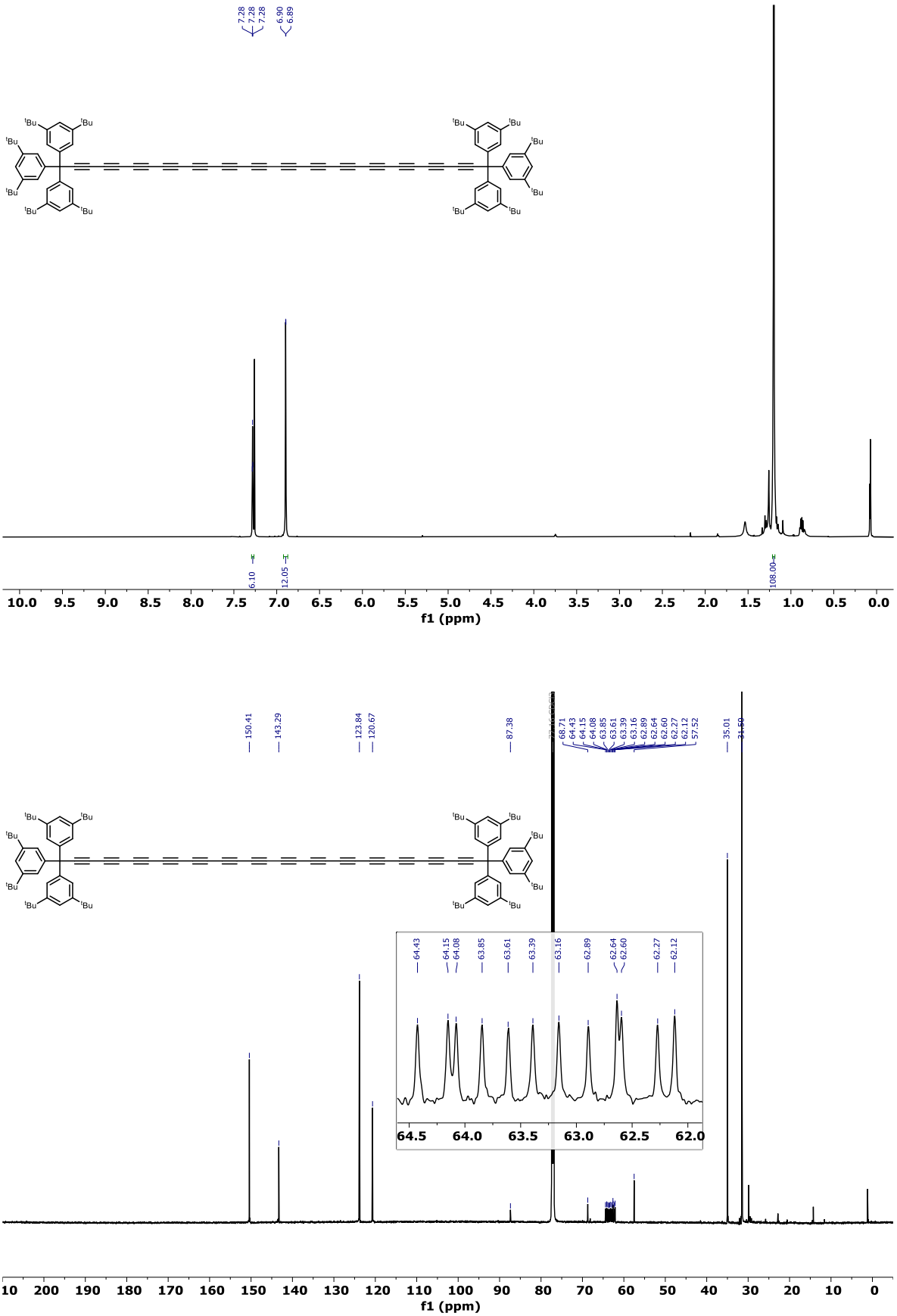

Figure S3.9: (top) ^{1}H NMR (600 MHz) and (bottom) ^{13}C NMR (151 MHz) spectra of polyyne dumbbell thread **3.25** ($CDCl_3$, 298 K).

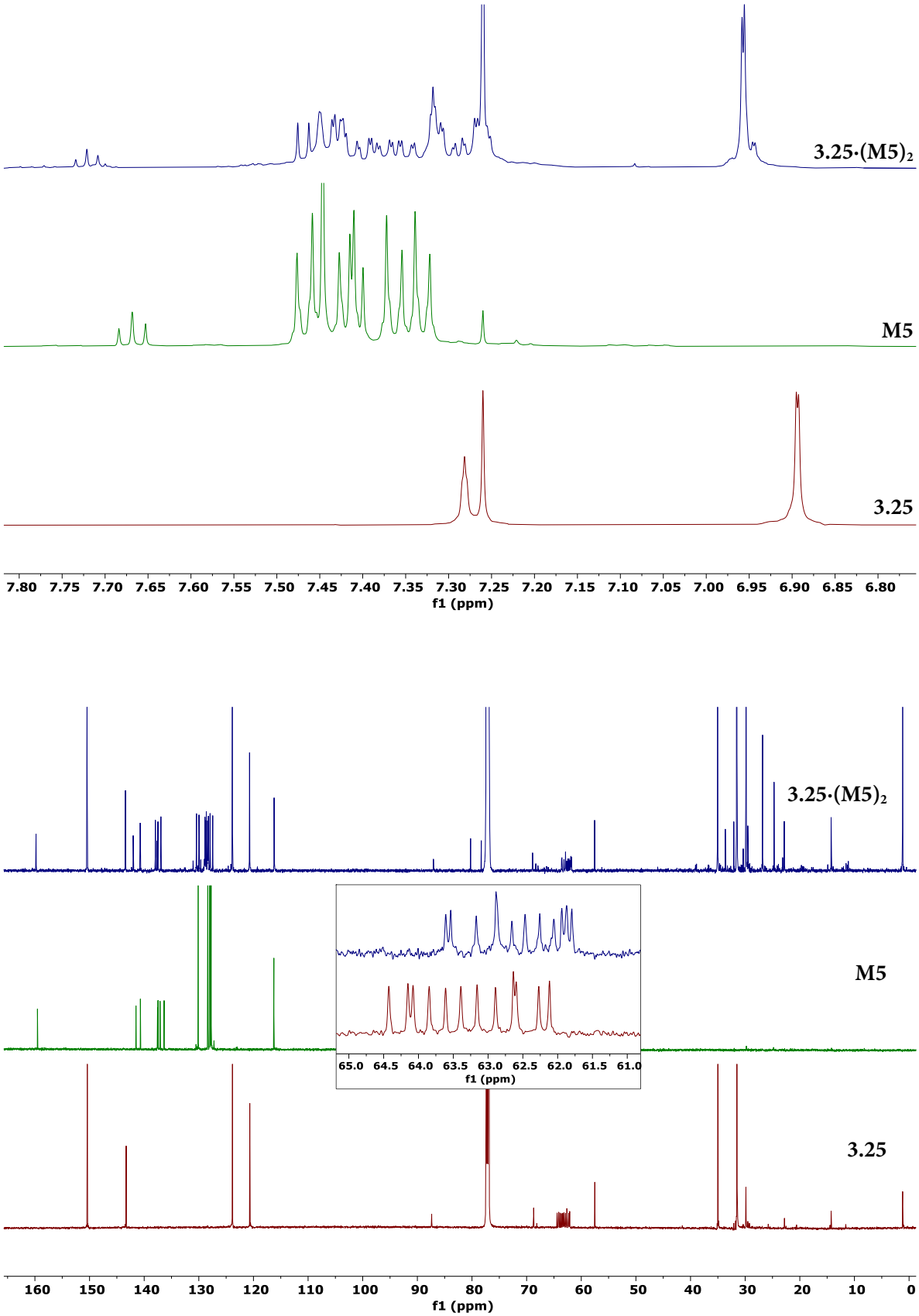

Figure S3.10: Stacked (top) ^{1}H NMR (600 MHz) and (bottom) ^{13}C NMR (151 MHz) spectra of (red) thread **3.25**, (green) nanohoop **M5** and (blue) [3]rotaxane **3.25·(M5)$_2$** ($CDCl_3$, 298 K).

Selected UV-vis Absorption Spectra

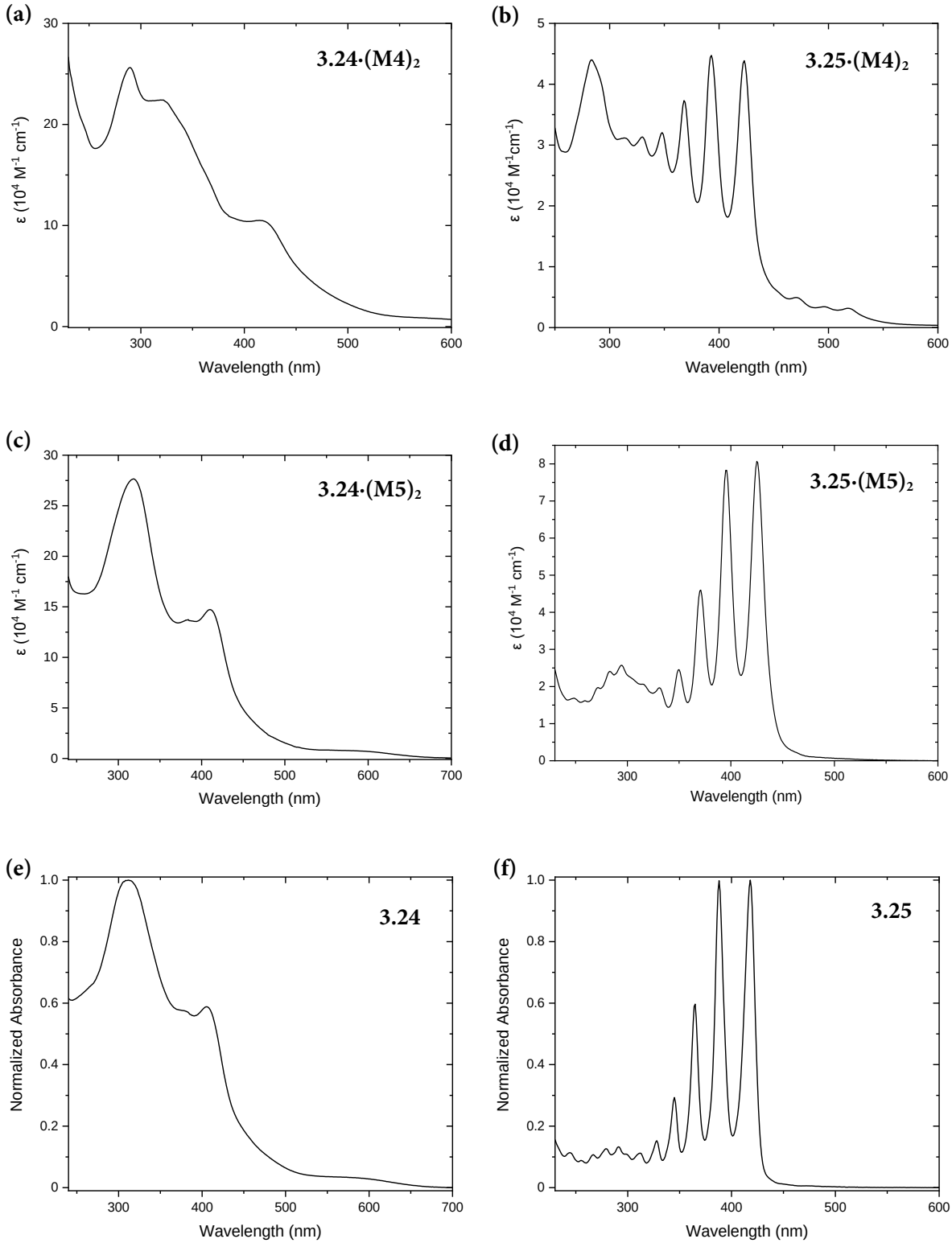

Figure S3.11: UV-vis spectra of (a) [3]rotaxane **3.24·(M4)**$_2$ ($CHCl_3$), (b) [3]rotaxane **3.25·(M4)**$_2$ (*n*-hexane), (c) [3]rotaxane **3.24·(M5)**$_2$ ($CHCl_3$), (d) [3]rotaxane **3.25·(M5)**$_2$ (*n*-hexane), (e) dumbbell **3.24** ($CHCl_3$) and (f) dumbbell **3.25** (*n*-hexane). All solutions at 25 °C.

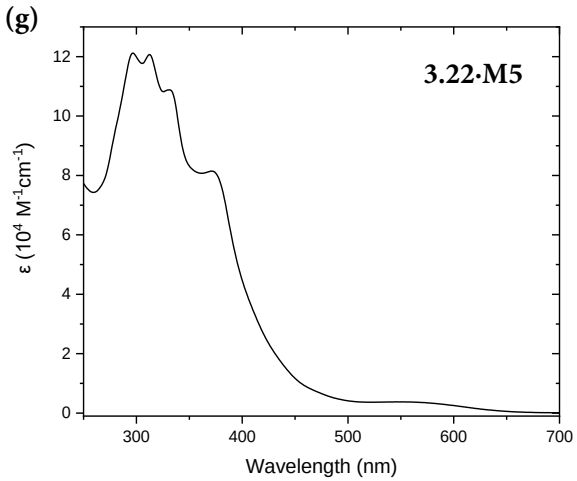

Figure S3.11 (*continued*)**:** UV-vis spectrum of (g) [2]rotaxane **3.22·M5** ($CHCl_3$, 25 °C).

Fluorescence Spectra

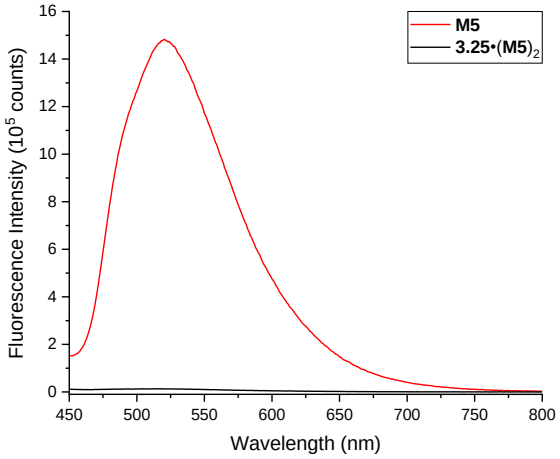

Figure S3.12: Emission spectra of (red) nanohoop **M5** and (black) nanohoop-shielded polyyne [3]rotaxane **3.25·(M5)**$_2$ (CH_2Cl_2, 298 K, λ_{ex} 320 nm, λ_{em} 520 nm). Sample concentrations of 4.31×10^{-7} M and 8.61×10^{-7} M for nanohoop **M5** and rotaxane **3.25·(M5)**$_2$, respectively. All solutions at 25 °C.

Selected Mass Spectra

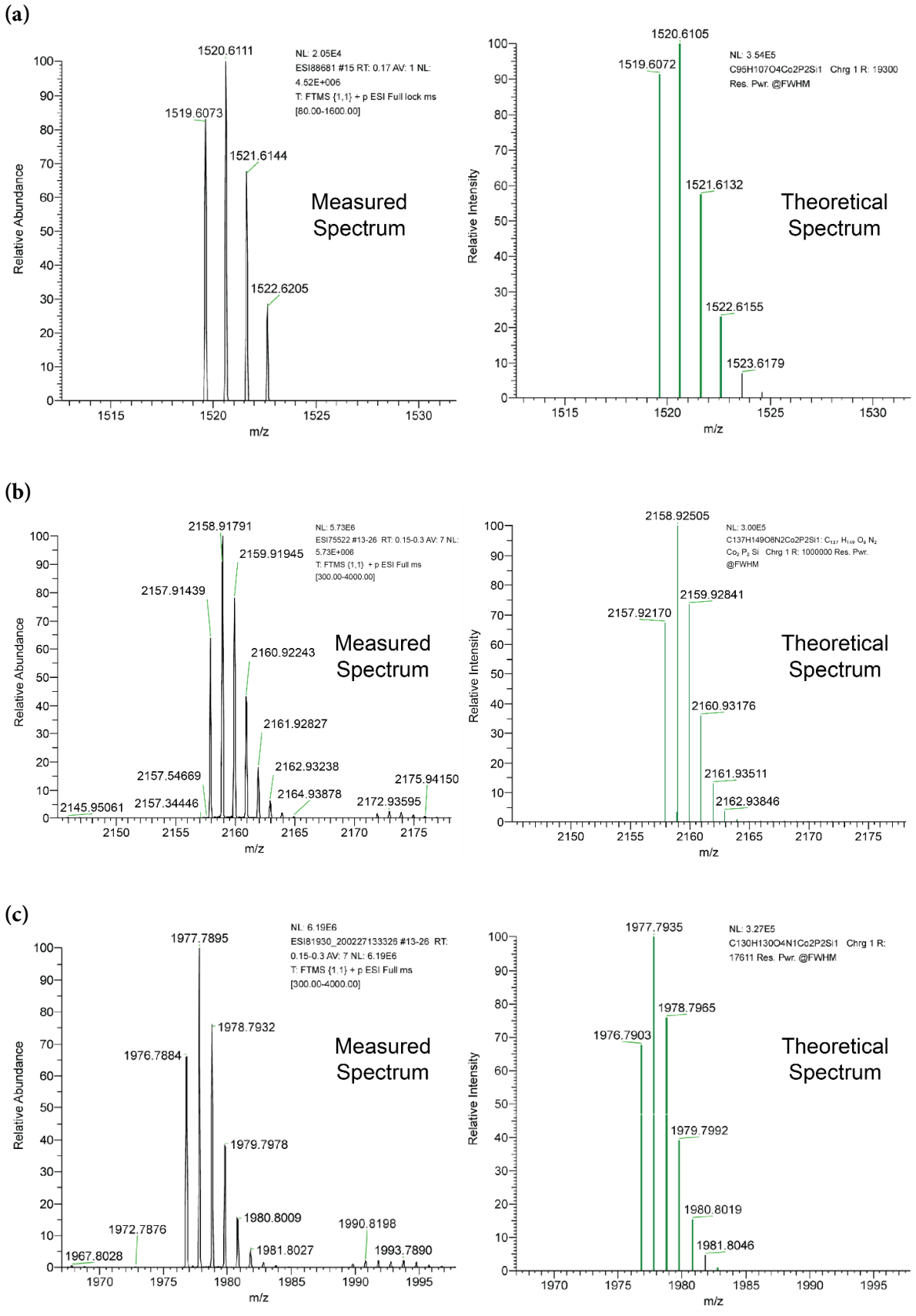

Figure S3.13: High-resolution mass spectra of (a) dumbbell **3.22**, (b) [2]rotaxane **3.22·M4** and (c) [2]rotaxane **3.22·M5**.

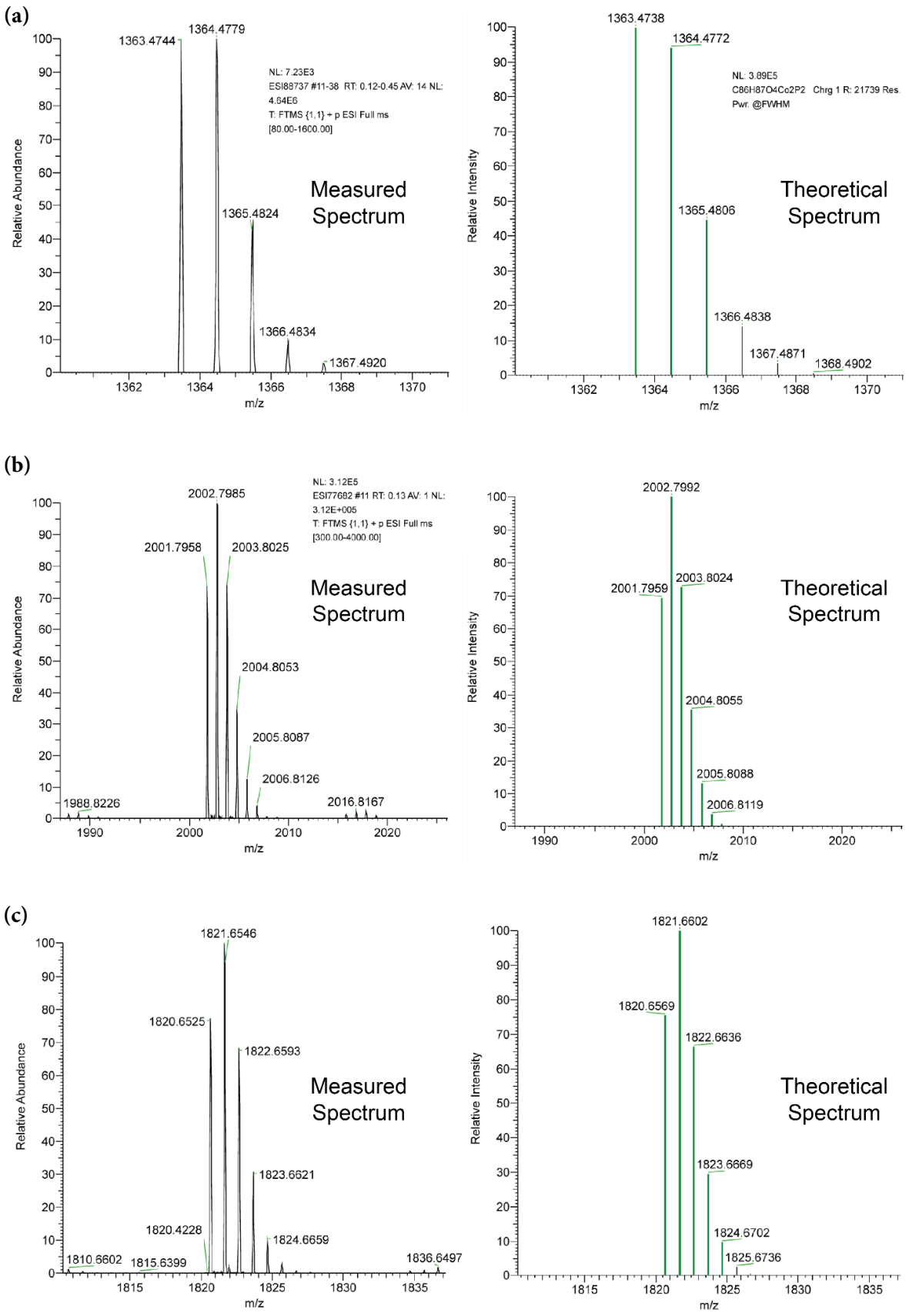

Figure S3.14: High-resolution mass spectra of (a) dumbbell **3.23**, (b) [2]rotaxane **3.23·M4** and (c) [2]rotaxane **3.23·M5**.

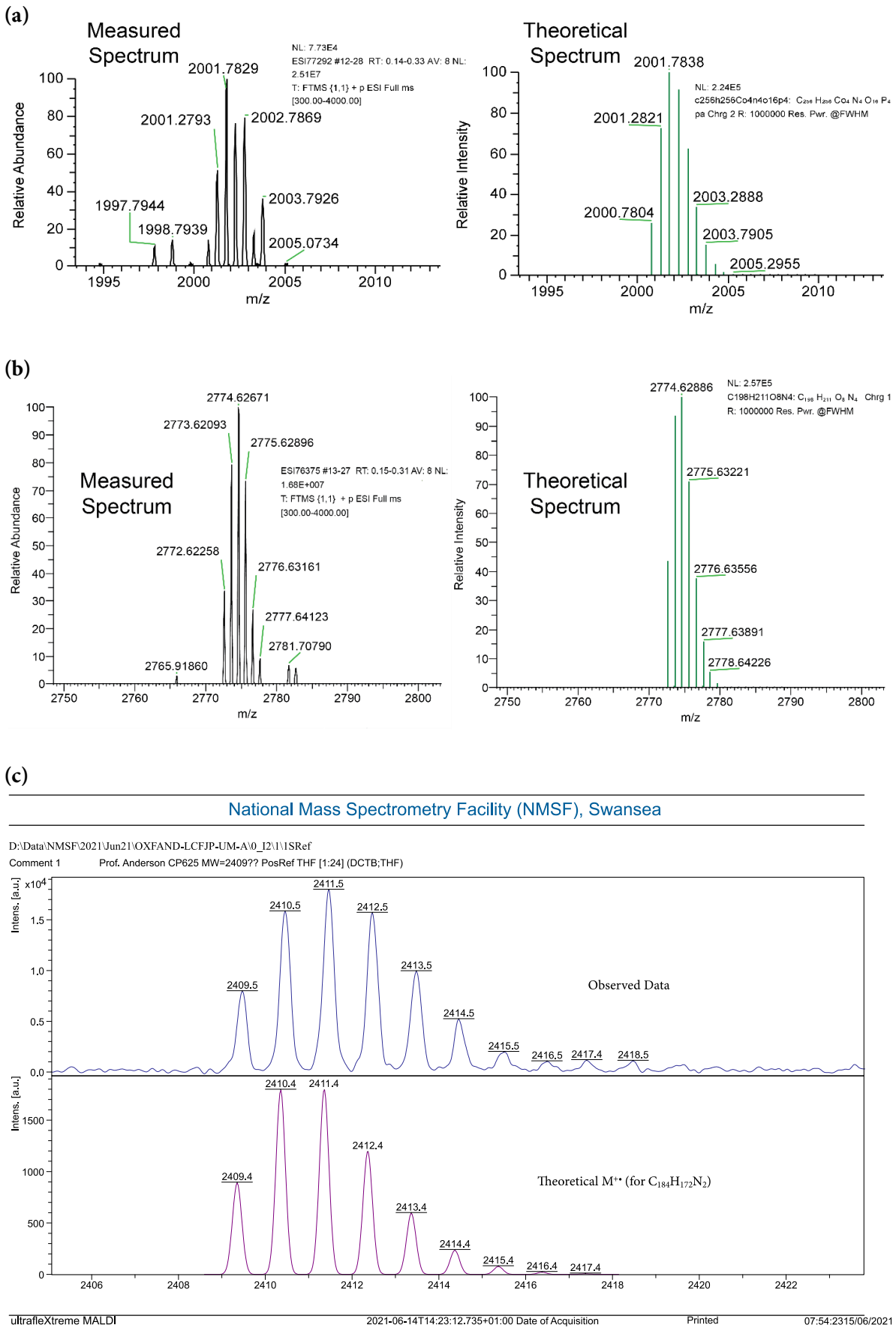

Figure S3.15: High-resolution (ESI) mass spectra of (a) [3]rotaxane **3.24**·(**M4**)$_2$, (b) polyyne [3]rotaxane **3.25**·(**M4**)$_2$ and (c) MALDI-TOF mass spectrum of polyyne [3]rotaxane **3.25**·(**M5**)$_2$ (DCTB matrix in THF used for MALDI-TOF).

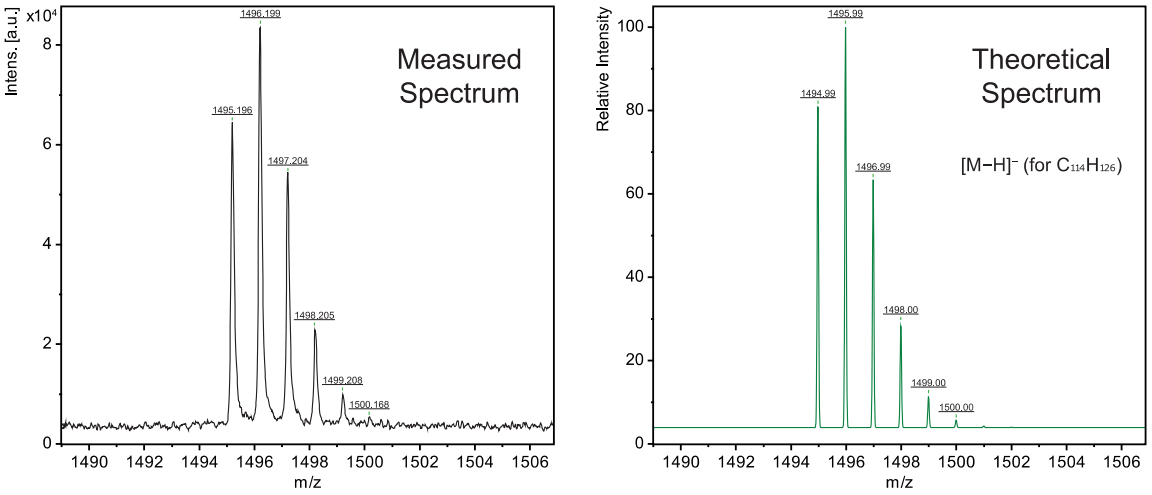

Figure S3.16: MALDI-TOF (DCTB matrix in THF) mass spectrum of polyyne thread **3.25**.

References

1 R. N. Keller and H. D. Wycoff, in *Inorg. Synth.*, 1946, pp. 1–4.

2 P. D. Bartlett, M. Roha and R. M. Stiles, *J. Am. Chem. Soc.*, 1954, **76**, 2349–2353.

3 W. A. Chalifoux and R. R. Tykwinski, *Nat. Chem.*, 2010, **2**, 967–971.

4 L. D. Movsisyan, M. Franz, F. Hampel, A. L. Thompson, R. R. Tykwinski and H. L. Anderson, *J. Am. Chem. Soc.*, 2016, **138**, 1366–1376.

5 S. Eisler, N. Chahal, R. McDonald and R. R. Tykwinski, *Chem. Eur. J.*, 2003, **9**, 2542–2550.

6 D. R. Kohn, P. Gawel, Y. Xiong, K. E. Christensen and H. L. Anderson, *J. Org. Chem.*, 2018, **83**, 2077–2086.

7 S. Saito, K. Nakazono and E. Takahashi, *J. Org. Chem.*, 2006, **71**, 7477–7480.

8 T. Dohi, T. Kamitanaka, S. Watanabe, Y. Hu, N. Washimi and Y. Kita, *Chem. Eur. J.*, 2012, **18**, 13614–13618.

9 P. Li, T. J. Sisto, E. R. Darzi and R. Jasti, *Org. Lett.*, 2014, **16**, 182–185.

10 E. R. Darzi, B. M. White, L. K. Loventhal, L. N. Zakharov and R. Jasti, *J. Am. Chem. Soc.*, 2017, **139**, 3106–3114.

11 T. C. Lovell, C. E. Colwell, L. N. Zakharov and R. Jasti, *Chem. Sci.*, 2019, **10**, 3786–3790.

12 J. M. Van Raden, B. M. White, L. N. Zakharov and R. Jasti, *Angew. Chem. Int. Ed.*, 2019, **58**, 7341–7345.

4

Towards Polyyne [*n*]Rotaxanes and Cyclocarbon [*n*]Catenanes

Contents

Chapter 4 - Towards Polyyne [*n*]Rotaxanes and Cyclocarbon [*n*]Catenanes

4.1 Introduction

Chapter 3 provided further evidence of the marked improvement in polyyne stability that is brought about by supramolecular encapsulation with shielding macrocycles. In that work, we noted that not all macrocycles are equally effective at shielding the polyyne axle, with the largest and most flexible macrocycle, **M4**, providing only a nominal stability enhancement. In contrast, the smallest and most rigid of the series, **M5**, provides a 4.5-fold enhancement. That work involved first building a stable [2]rotaxane, which was then homocoupled to give larger polyynes. This approach is fundamentally limited through use of a permanent, uncleavable polyyne end capping group. A limit to the stability, and thus length, of the [2]rotaxanes is quickly reached, and beyond this their stability becomes problematic. It therefore seems unlikely that much larger systems can feasibly be synthesised simply by incremental alkyne extension reactions of the [2]rotaxane precursors.

To address both the size and stability limitations of our previous approach, we next designed a 'polymerisable' masked [2]rotaxane that we anticipated would enable access to longer and, importantly, more stable polyynes than were previously possible. Chapter 3 demonstrated that stable [2]rotaxanes can be prepared with the bulky dicobalt masking group acting as a stopper. It should therefore be possible to prepare a [2]rotaxane using two dicobalt MAEs, one at each end of the axle. Unlike previous approaches, the important difference with this system is the inclusion of readily cleaved alkyne capping groups which can later be removed without trace to return the pristine polyyne. Additionally, each MAE bears a temporary silyl protecting group that, once removed, should allow for further chemical transformations to be made. In subsequent coupling steps, one could imagine that through careful control of reaction conditions (e.g. concentration, temperature), both cyclic and linear species made up of these constituent [2]rotaxane units could be prepared (Figure 4.1). In the case of the linear system, a final capping reaction with a permanent stoppering group could be made to prevent further reaction and to confer additional stability and improved solubility of these chains.

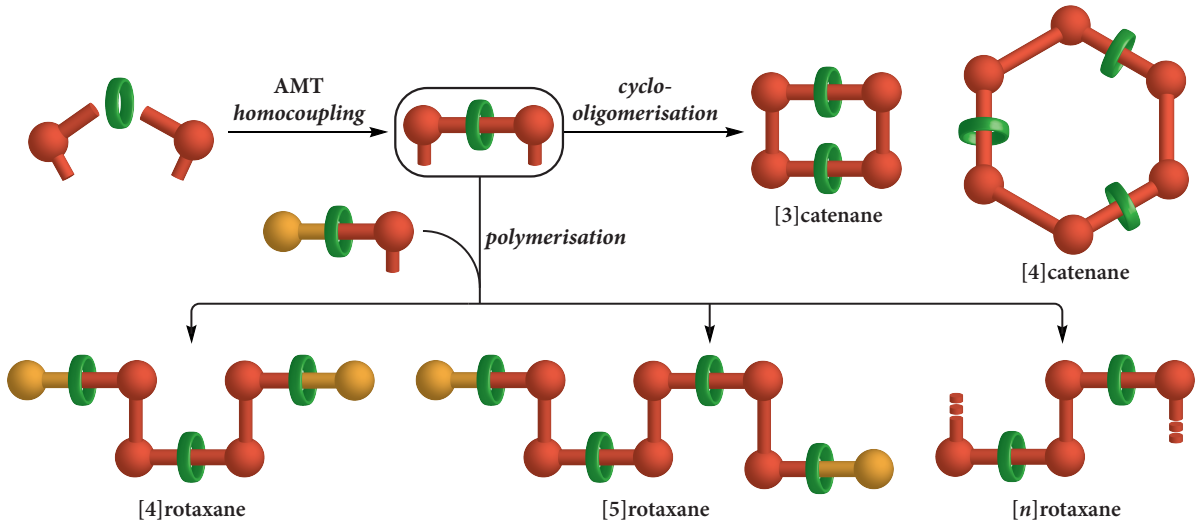

Figure 4.1: Pictorial representation of possible cyclic (catenanes) and linear (rotaxanes) species that can be prepared from a common [2]rotaxane precursor (see box).

4.2 Synthesis of a Tetracobalt [2]Rotaxane

In the previous chapter we demonstrated that a dicobalt masking group (complexed with a bulky phosphine ligand) offered sufficient bulk to yield highly-stable [2]rotaxanes that prevented large macrocycles from dethreading, but also allowed small macrocycles to participate in the key active metal template (AMT) reactions. We expected that it would be possible to prepare stable [2]rotaxanes employing this dicobalt masking group as a stopper at both ends of the thread. Computational models suggest that a tetrayne thread linking two dicobalt MAEs should offer sufficient space to permit the threading of a macrocycle, such as **M4** or **M5**. Construction of tetracobalt tetrayne **4.1** could be envisioned via a disconnection across the central bond in the tetracobalt linker to give two identical dicobalt components bearing a terminal diyne (Scheme 4.1). Active metal template alkyne homocoupling reactions are well-documented in the preparation of [2]rotaxanes (see Section 1.5.1). Unlike standard Glaser-type acetylene homocoupling reactions, which proceed simply in the presence of air, AMT couplings require additional oxidants for the reaction to proceed. This could be problematic, as we have previously shown (in Section 3.2.5) that oxidative decomplexation of

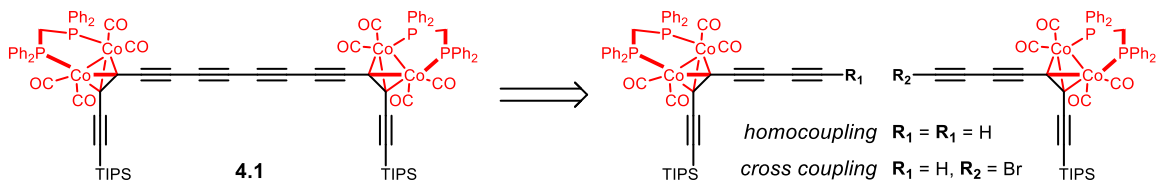

Scheme 4.1: A tetracobalt tetrayne can be formed by two possible approaches – a Glaser-like homocoupling, or a Cadiot-Chodkoweicz cross coupling.

these dicobalt groups can be induced in the presence of some oxidants. This is made worse in that all conditions reported to date for such AMT homocouplings employ the use of I_2 as the oxidant.[1] Thus, the use of I_2 as oxidant is perhaps the first challenge to address when exploring this approach.

As an alternative to the homocoupling approach, it may also be possible to generate the terminal haloalkyne on one of the dicobalt components. An AMT Cadiot-Chodkiewicz cross coupling approach could be used to generate the target tetracobalt [2]rotaxane. Importantly, the use of a haloalkyne means that that no additional oxidant is required for coupling under these conditions. We also know from work in Chapter 3 that these dicobalt-masked compounds show good stability under AMT Cadiot-Chodkiewicz conditions. One potential obstacle for this approach, however, is the preparation of the halogenated (typically brominated) dicobalt component. Common brominating agents for terminal acetylenes are often potent oxidising agents (e.g., NBS/$AgNO_3$, etc.) and could induce unmasking of the dicobalt group. A balance must therefore be struck in selecting conditions that successfully form the acetylene bromide yet are not too oxidising so as to unmask the dicobalt group.

As both the active metal template homocoupling and cross coupling approaches to these tetracobalt [2]rotaxanes appeared equally promising, investigations into both were made simultaneously.

4.2.1 Preparing Dicobalt-Masked Haloacetylenes

Previous work in the group has attempted the bromination of dicobalt-masked acetylenes but with little success. Typically, attempts either leave the starting material unchanged, induce unmasking of the dicobalt group, or result in decomposition. This observation is somewhat surprising since brominated alkynes are often more stable than their non-brominated analogues. Work by former Part II student Mr Joseph Woods explored a selection of common alkyne bromination conditions in an attempt to prepare compound **4.2** (Figure 4.2 and summarised in Table 4.1).[2] Perhaps one of the most obvious bromination conditions for terminal acetylenes is the use of *N*-bromosuccinimide (NBS) and $AgNO_3$ (entry **1**). Conditions similar to these have been frequently employed both in our group, and by others, with high levels of success. However, in

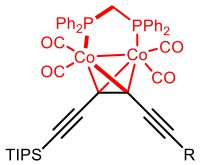

3.17 R = TMS
3.18 R = H
4.2 R = Br

Figure 4.2: TMS-protected (**3.17**), de-protected (**3.18**) and brominated (**4.2**) dicobalt-masked triyne.

Table 4.1: A summary of attempts made by former group member Mr Joseph Woods to prepare brominated dicobalt compound **4.2**.

Entry	Conditions	Outcome
1	NBS, $AgNO_3$, acetone	NBS unmasks dicobalt group, dicobalt group unstable with respect to $AgNO_3$
2	Br_2, KOH, Et_2O	Decomposition of **3.18**
3	*n*-BuLi *then* NBS, Et_2O	Decomposition of **3.18**
4[3]	PPh_3, CBr_4, CH_2Cl_2	Decomposition of **3.18**
5[4,5]	Chloramine-T, Br_2 *then* DBU, CH_2Cl_2	No reaction at −20 °C, slow decomposition at −10 °C

Chapter 3 we noted that rapid oxidative decomplexation of the dicobalt masking group was observed under these conditions. Additionally, it was noticed that the dicobalt masking group shows slight instability with respect to silver nitrate. Treating dicobalt-masked triyne **3.17** with $AgNO_3$ in acetone triggered the slow conversion to an unidentified species over a period of days. While the characteristic deep-red colour of the dicobalt masking group was not lost, the ^{1}H NMR spectrum displayed broad resonances, potentially indicating that oxidation of cobalt to a new paramagnetic species had occurred.

In contrast to the typical oxidative brominations, an alternative approach involves deprotonation of the acetylene followed by nucleophilic attack on an electrophilic bromine source. Two conditions (entries **2** and **3**) were trialled to investigate such an approach. The stability of the dicobalt species was first evaluated by treating **3.17** with Br_2 in the presence of KOH (entry **2**), or NBS after treatment with *n*-BuLi (entry **3**). Unfortunately, both led to the rapid unmasking of triyne **3.18**, rendering these conditions unsuitable. In a different approach (entry **4**), phosphorus ylids were used in an attempt to generate **4.2** through deprotonation of the acetylene by the ylid, then the subsequent attack onto a dibromophosphonium salt, which is formed *in situ* (Scheme 4.2a). The second (entry **5**) involved the bromination of **3.18** first by deprotonation using a non-nucleophilic base (1,8-diazabicyclo[5.4.0]undec-7-ene, DBU) then addition of a dibromo tosyl amide, which acts as a mild source of electrophilic bromine (Scheme 4.2b).[4,5] Despite **3.17** showing good stability under both conditions, when applying these to the terminal acetylene **3.18**, no evidence of the brominated compound **4.2** could be detected. The

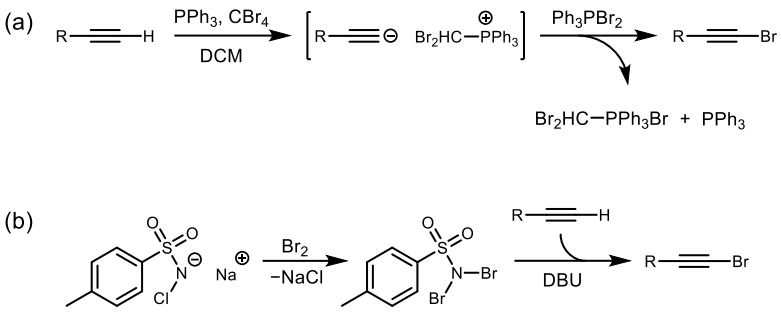

Scheme 4.2: Two possible approaches towards bromoacetylenes using a (a) phosphorus ylid and (b) mild brominating agent.

former resulted in complete degradation of **3.18**, while unreacted starting material was predominantly recovered in the latter. Based on this work, it seems that the bromination of these compounds is challenging; conditions that are typically successful are generally too oxidising for use on these compounds and result either in unmasking or decomposition of the material.

Driven by these difficulties, attempts were made towards the iodination of **3.18**. Iodoacetylenes can be prepared in a similar way to bromoacetylenes – by treating with *N*-iodosuccinimide (NIS) and $AgNO_3$. As with the analogous bromination reaction, the instability of **3.17** and **3.18** towards these reagents posed a potential problem. Fortunately, preliminary investigations showed that unmasking and decomposition of the dicobalt-masked compounds by NIS and $AgNO_3$ was slow in both cases. So, providing iodination could be achieved sufficiently quickly using this method, it may still prove a viable approach. Treating **3.18** with NIS (1.2 eq.) and $AgNO_3$ (0.1 eq.) resulted in the formation of a new species (visible by TLC), with a similar polarity to the starting material, and also accompanied by slight decomposition of **3.18** (Scheme 4.3). Separation of the two proved too difficult by silica chromatography, but ^{1}H NMR analysis of the mixture revealed an integration ratio between the acetylenic proton and the phosphine CH_2 bridge of 0.3:2, suggesting that partial iodination may have taken place to form **4.3a** in an estimated NMR yield of 60%. Attempts were made to optimise this reaction through systematic variation of solvent, as well as relative amounts of

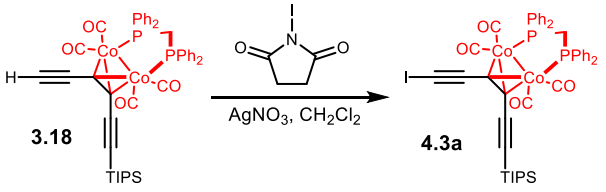

Scheme 4.3: Iodination of dicobalt compound **3.18** with *N*-iodosuccinide and $AgNO_3$.

NIS and $AgNO_3$, but unfortunately all attempts had little impact on the outcome. In all cases, some decomposition was observed, and full conversion could never be obtained – an inseparable mixture of **4.3a** contaminated by **3.18** was always formed.

In an alternative approach towards these iodinated species, the cross coupling of **3.18** with diiodoacetylenes was investigated (Scheme 4.4). We expected that through careful stoichiometric control of the two precursors, it may be possible to couple 1,2-diiodoethyne or 1,4-diiodobutadiyne with **3.18** just a single time to give the respective iodoacetylenes **4.3b** or **4.3c** (and minimal tetracobalt by-product **4.1**). The instability of these diiodoacetylene compounds I_2C_2 and I_2C_4 required a fresh batch to be prepared prior to each coupling. 1,2-Diiodoethyne was initially synthesised by the direct treatment of TMS-acetylene with NIS/$AgNO_3$ (Scheme 4.5a, top).[6] After 60 min, the diiodo compound could be identified by the characteristic ^{13}C NMR resonance at 0.56 ppm, but accompanied by an additional signal observed at 0.03 ppm – likely a TMS-containing by-product of the reaction. It should be possible to remove this by-product under reduced pressure, but the high volatility of the diiodo compound made this problematic. The similarly low polarity of the diiodo species and TMS-containing by-products rendered silica chromatography equally unsuitable. Homsi *et al.* reported an alternative approach towards 1,2-diiodoethyne that involved treating acetylenedicarboxylic acid with bis(collidine)iodine hexafluorophosphate in a CH_2Cl_2 solution (Scheme 4.5a, bottom)[7] but, after multiple attempts, the yields and purity of the product were generally too poor so no further exploration was made into this approach.

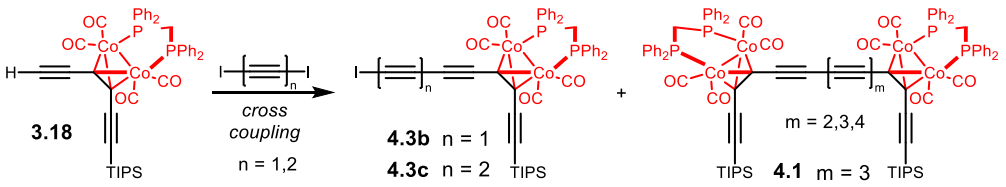

Scheme 4.4: Proposed route to dicobalt-masked iodoacetylenes **4.3b-c** and tetracobalt species **4.1** (and related compounds) via a cross coupling with a diiodoacetylene.

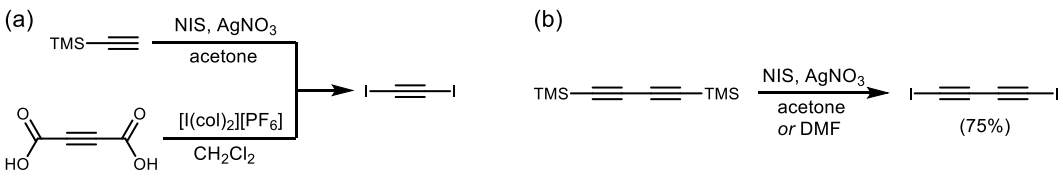

Scheme 4.5: Preparation of diiodoacetylenes. (a) 1,2-Diiodoaceylene through either: (*top*) treatment of TMS-acetylene with *N*-iodosuccinimide/$AgNO_3$[6] or; (*bottom*) treatment of acectylenedicarboxylic acid with bis(collidine)iodine hexafluorophosphate.[7] (b) 1,4-Diiodobutadiyne through treating bis-TMS butadiyne with *N*-iodosuccinimide/$AgNO_3$. (col = 2,4,6-trimethylpyridine).

Even though the treatment of TMS acetylene with NIS/$AgNO_3$ (Scheme 4.5a, top) appeared successful in affording the expected product, isolation of 1,2-diiodoethyne was challenging. We therefore instead aimed to prepare the next shortest diiodoacetylene, 1,4-diiodobutadiyne (n = 2), which is reported to be significantly less volatile, but at the expense of stability. Initial experiments involved treating bis-TMS butadiyne with NIS/$AgNO_3$ in acetone (Scheme 4.5b),[8] but it was found that simply by switching to DMF as the reaction solvent[9] led to a significant improvement in the yield of the diiodo compound. Purification of this compound was notably simpler, requiring only a silica plug (pentane), then removal of solvent and the TMS-containing impurities under reduced pressure (< 0.1 mbar) to give I_2C_4 as pale-yellow crystals in 75% yield.

With a reliable route to preparing the diiodobutadiyne identified, the cross coupling with dicobalt-masked triyne **3.18** was investigated. To simplify the reaction, we initially aimed to achieve the double coupling of diiodobutadiyne to give tetracobalt tetrayne **4.1** (Scheme 4.6). Should the reaction prove successful, optimisations could then be made to target the singly coupled species **4.3c**. Unfortunately, and despite screening various Cadiot-Chodkiewicz coupling conditions, we were unable to detect even traces of either dicobalt iodotriyne **4.3c** or tetracobalt tetrayne **4.1**. It is suspected that the iodoacetylene is simply too unstable under many of these conditions. In most cases a black, insoluble material could be found coating the reaction vessel, while in a few cases simply adding solvent to the diiodo compound was sufficient to trigger its explosive decomposition. It is possible that the diiodo species may be undergoing homocoupling at a much faster rate than the cross coupling reaction, and thus be forming an increasingly unstable oligo-/polyyne. While a more rigorous screening of reaction conditions may make it possible to prepare iodinated dicobalt species, it seemed likely that more effective approaches exist towards preparing the tetracobalt [2]rotaxane target.

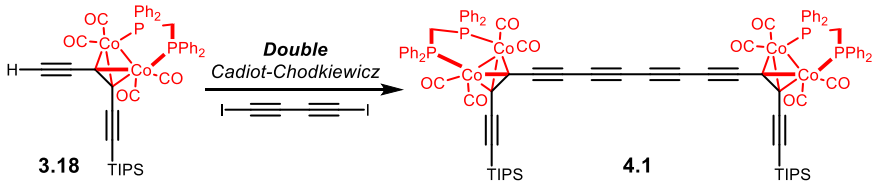

Scheme 4.6: A double Cadiot-Chodkoweicz cross coupling of dicobalt **3.18** with 1,4-diiodobutadiyne to generate tetracobalt tetrayne **4.1**.

4.2.2 Screening Oxidants for AMT Homocouplings

As discussed previously, the use of I_2 as an oxidant in AMT homocoupling reactions is incompatible with these dicobalt-masked compounds. During the many attempts to unmask the **M4**-protected [3]rotaxane **3.24**·(**M4**)$_2$ (described in detail in Section 3.2.5) a number of different oxidants were screened, however only a small handful proved successful at promoting the unmasking process. We therefore thought it would be sensible to test whether those oxidants that leave the dicobalt group untouched could be used in place of I_2 for the AMT homocoupling step.

Test reactions were run similarly to the AMT Cadiot-Chodkiewicz reaction previously used to prepare the supertrityl-stopped cobalt [2]rotaxanes in Chapter 3. As the phenanthroline-based macrocycle **M4** had previously shown the most success in forming interlocked compounds, it was also selected for these investigations. As before, **M4** was pre-complexed with Cu(I) first by stirring with CuI in a CH_2Cl_2/MeCN solvent mixture, then removal of the solvent prior to the reaction. The **M4**·Cu(I) complex was combined with the dicobalt diyne unit in a 1:2.5 ratio, using K_2CO_3 and THF as the base and solvent, respectively (Scheme 4.7). Five different oxidants were tested: (i) (diacetoxyiodo)benzene (PIDA); (ii) NIS; (iii) benzoquinone; (iv) H_2O_2 and; (v) ethyl 2,2-dibromo-3-oxobutanoate, all added to the reaction mixture at 1.0 eq. relative to **M4**·Cu(I). Unfortunately, no trace of [2]rotaxane could be observed in all cases. For (i), (ii) and (iii) the tetracobalt dumbbell was isolated, indicating that the oxidants were successfully promoting the coupling but was doing so outside of the macrocyclic cavity. In contrast, oxidants (iv) and (v) appear unable to promote coupling with only the starting cobalt diyne and macrocycle being recovered. Also problematic was that, while the dicobalt-masked triyne **3.17** appeared stable in the presence of PIDA and benzoquinone at room temperature, under the elevated temperature of the reaction (60 °C), decomposition was much more prevalent and only small quantities of the homocoupled thread could be isolated.

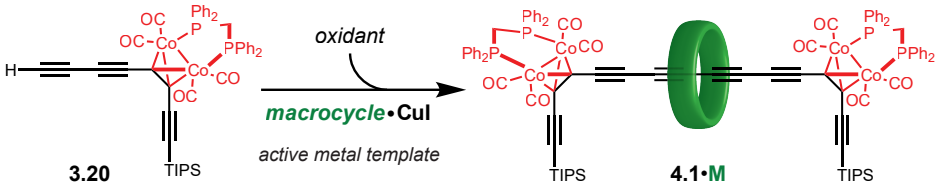

Scheme 4.7: AMT homocoupling of dicobalt diyne **3.20** to tetracobalt [2]rotaxanes **4.1**·**M**.

4.2.3 Unexpected Synthesis by Active Metal Template Cross-Coupling

When performing the AMT cross coupling to prepare [2]rotaxane **3.22·M4** (Scheme 3.4, Chapter 3) on a larger scale, we were surprised to observe the formation of two additional compounds bearing macrocycle **M4**, both formed in non-negligible quantities. Mass spectrometry analysis of these species revealed two intense signals at m/z = 1187 and 1862; the former displaying a mass and isotope pattern that perfectly matches what would be expected for the doubly-charged $[M+2H]^{2+}$ ion of the tetracobalt [2]rotaxane **4.1·M4** (Scheme 4.8). The latter species correlates well with the $[M+H]^{+}$ ion for a supertrityl-capped hexayne [2]rotaxane **4.4·M4** (formed by the AMT coupling of two stoppering units). In-depth NMR analysis on the suspected tetracobalt [2]rotaxane **4.1·M4** confirmed its identity – a species containing only dicobalt masking groups and macrocycle, and without signals from the supertrityl stopper. The ratio of integrals between TIPS and macrocycle resonances were particularly diagnostic; comparing the two revealed a 2:1 ratio of MAE to macrocycle, in agreement with that of the expected product. While these data provide strong evidence for the successful isolation of tetracobalt [2]rotaxane **4.1·M4**, final confirmation came from single crystal X-ray analysis (Figure 4.3). Single crystals of the [2]rotaxane were grown from slow diffusion of MeOH into a $CHCl_3$ solution containing the [2]rotaxane. Analysis of the X-ray data reveal the crystals are

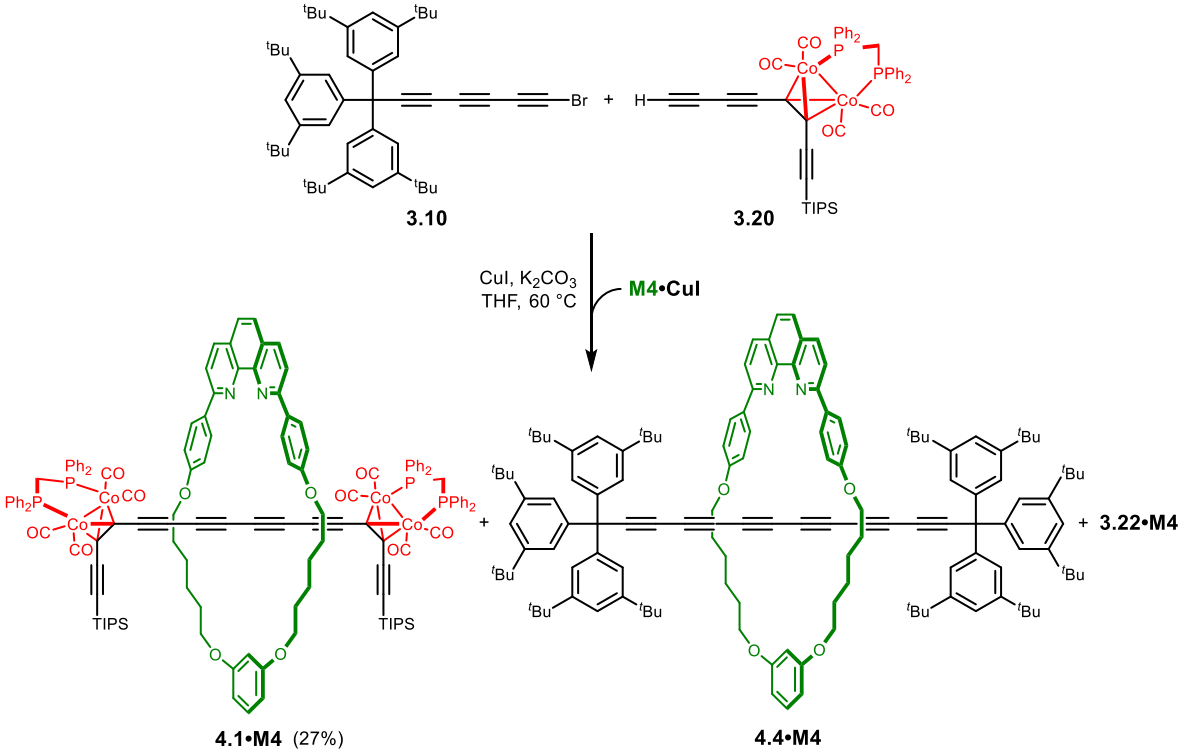

Scheme 4.8: Tetracobalt [2]rotaxane **4.1·M4** and supertrityl-capped hexayne [2]rotaxane **4.4·M4** unexpectedly formed in an AMT Cadiot-Chodkiewicz cross coupling originally used to prepare stoppered [2]rotaxane **3.22·M4**.

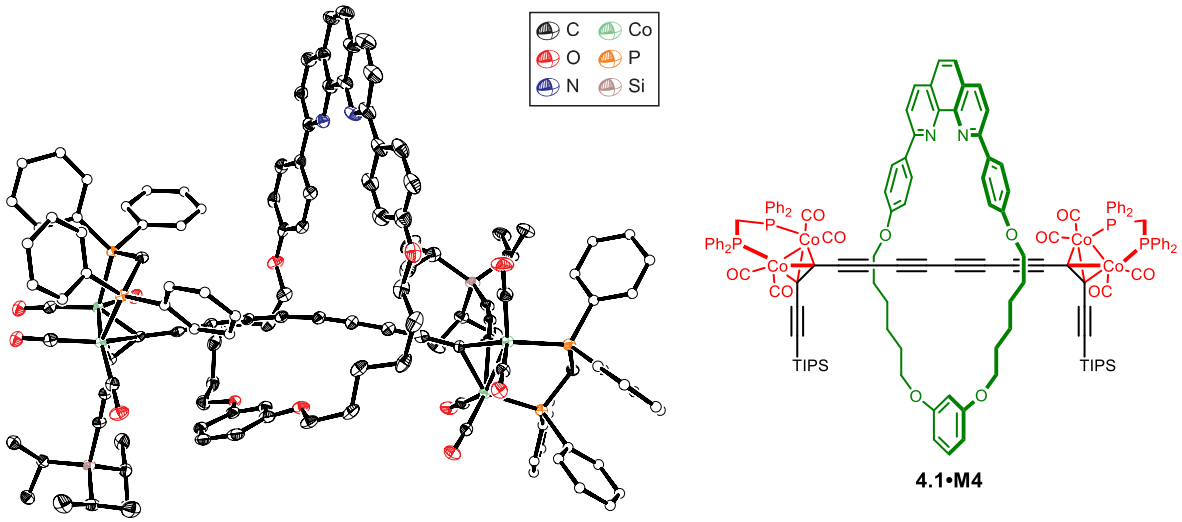

Figure 4.3: X-ray crystallographic structure of tetracobalt [2]rotaxane **4.1·M4**. (ellipsoids at 30% probability, hydrogen atoms omitted and dppm phenyl rings plotted as spheres for clarity)

monoclinic (*P*–1 space group) with two molecules per unit cell, and one molecule of [2]rotaxane **4.1·M4** in the asymmetric unit. The geometries of the dppm phenyl rings are oriented with one pointing towards the macrocycle and the other pointing away. Clear bond length alternation (BLA) can be observed along the C_{sp} chain with an average BLA calculated to be 0.131 Å – both smaller than ^{t}Bu- (0.151 Å)[10–12] and TIPS-capped (0.157 Å)[12,13] tetraynes reported by Tykwinski *et al.*

The formation of this rotaxane is a surprising result since all reported examples of active metal template homocouplings require addition of an oxidant. We initially believed that this observation was caused by small quantities of O_2 being present in the reaction mixture, originating from incomplete degassing. However, repeating the reaction without supertrityl stopper **3.10** (but in air, or under an O_2 atmosphere) only gave trace amounts of the tetracobalt [2]rotaxane (~5% yield). Curiously, when performing the reaction on a larger scale, the yield of tetracobalt rotaxane was significantly reduced (~1-2%), with only a small quantity of **4.1·M4** able to be isolated. While these results indicate that the presence of oxygen in the reaction may be a contributing factor, it is certainly not the sole cause for this unexpected observation.

Another possibility could be that the brominated stopper is acting as the oxidant for Cu(I) in this reaction. For example, once the bromoalkyne undergoes oxidative addition onto copper, some form of scrambling process (between different copper complexes) may be occurring before the subsequent reductive elimination step to return the tetracobalt species (Scheme 4.9). The observation of both possible homocoupled products – the tetracobalt

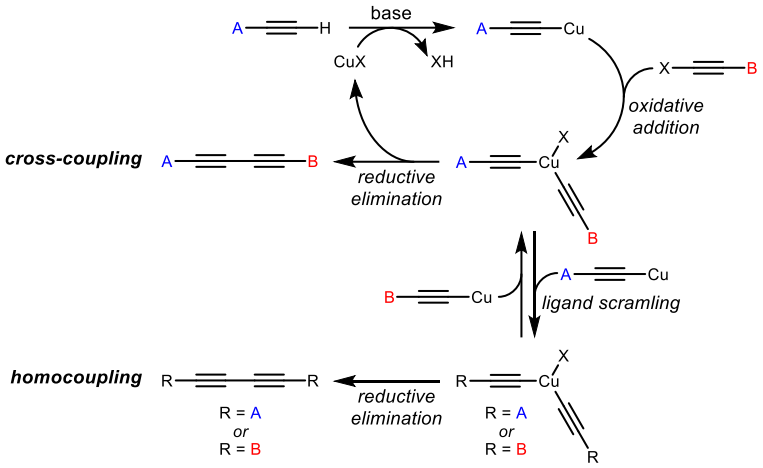

Scheme 4.9: Cadiot-Chodkiewicz alkyne cross coupling mechanism with an additional ligand scrambling process that may cause the unexpected formation of homocoupled products.

[2]rotaxane **4.1·M4** as well as the supertrityl-capped hexayne [2]rotaxane **4.4·M4** – rather than just the one, would support such a process. As no attempts were made to elucidate the mechanism of this ligand scrambling process, we will not speculate on exactly how this process may occur. The observation of significant homocoupling present in AMT Cadiot-Chodkiewicz cross couplings is not unique to this work. Competing homocoupling reactions are a frequent problem for the Cadiot-Chodkiewicz reaction under both AMT and non-AMT conditions.[14,15] Through careful screening of the AMT reaction conditions it is often possible to improve selectivity for the cross coupled product.[16]

To investigate whether the brominated stopper was giving rise to this interesting process, a single acetylene variant of the stopper (supertrityl monoyne bromide **4.5**, Figure 4.4) was prepared by bromination with NBS/$AgNO_3$. The high steric bulk of the supertrityl group combined with the short length of the single acetylene unit of **4.5** was expected to bring steric clashes with the macrocycle, rendering this compound unable form mechanically interlocked compounds. This compound should help us to elucidate any role the bromoacetylene may have on the outcome of the reaction. For example, should the bromoacetylenes be acting purely as an oxidant, we would expect the reaction to proceed as it did with the triyne bromide. However, the bulky nature of this compound should prevent the cross coupled [2]rotaxane from being formed. After a few experiments it quickly became apparent that **4.5** had little effect on the outcome of the reaction, with a similar ~5% yield being observed after the same time period. After further consideration of the scrambling

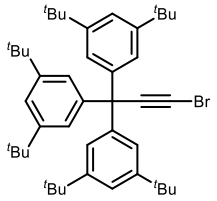

4.5

Figure 4.4: Supertrityl monoyne bromide **4.5**.

mechanism proposed previously (Scheme 4.9), we suspect that the high bulk of the supertrityl unit and limited extension of the single acetylene (versus a triyne in the previous case) would be causing significant steric congestion at the metal centre, perhaps any preventing oxidative addition process. With this unable to occur, there would no oxidant driving the reaction and thus proceeds similarly to that without any stopper present.

To confirm that this unexpected AMT homocoupling process was not unique to the supertrityl series of stoppers, an alternative stopper was prepared, based on the *para*-^{t}Bu functionalised trityl core from Chapter 2. Synthesis of the bromotriyne from the *p*-^{t}Bu monoyne **2.17** proceeded smoothly and analogously to the supertrityl series. Subjecting *p*-^{t}Bu bromotriyne **4.6** and dicobalt diyne **3.20** to the AMT conditions (Scheme 4.10) indeed resulted in both the stoppered [2]rotaxane **4.7·M4** and same tetracobalt [2]rotaxane **4.1·M4** being isolated in comparable yields to the supertrityl series.

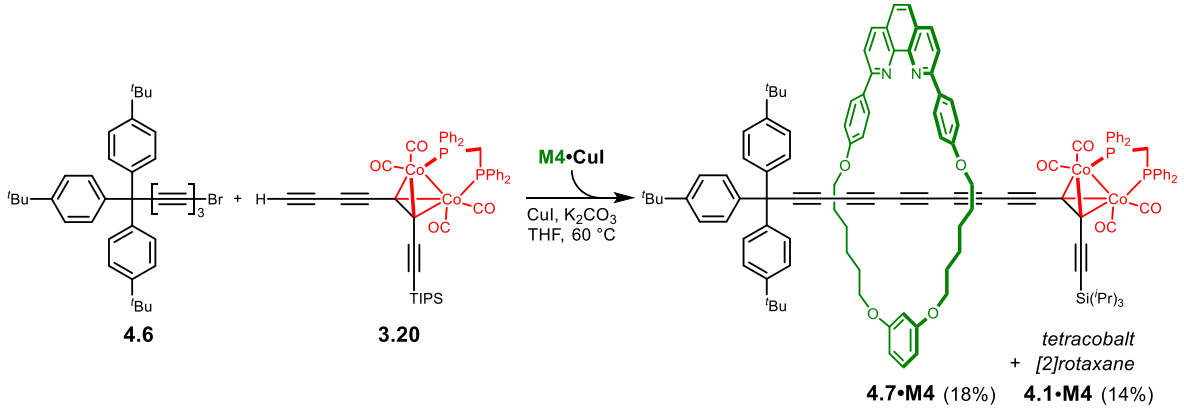

Scheme 4.10: Active metal template Cadiot-Chodkiewicz cross-coupling was successful with a *p*ara-^{t}Bu bromotriyne stopper **4.6** to give the respective stoppered [2]rotaxane **4.7·M4** and tetracobalt [2]rotaxane **4.1·M4**.

Strangely, but also rather fortunately, it seemed that simply by running the AMT Cadiot-Chodkiewicz coupling (with either supertrityl or *p*-^{t}Bu bromotriynes) on a larger (~300 mg) scale, a much-improved yield of tetracobalt [2]rotaxane **4.1·M4** could be obtained while also having little effect to the yield of stoppered [2]rotaxane **3.22·M4**. This observation has been confirmed by multiple repeat experiment, all of which reliably afforded the tetracobalt [2]rotaxane in an acceptable 25-30% yield. As there are many factors at work in this reaction, and with no mechanistic investigations made, it is difficult to draw any firm conclusions regarding why this process is observed.

4.3 Towards Cyclocarbon [*n*]Catenanes

With a synthetic route to the tetracobalt [2]rotaxane established, investigations then focussed on the coupling of this species. The indirect synthetic route to tetracobalt [2]rotaxane **4.1·M4** made it a synthetically costly compound to prepare and made access to large quantities rather difficult. With limited quantities of [2]rotaxane **4.1·M4** available, model reactions were carried out on the analogous dumbbell compound (**4.8**, Scheme 4.11) as it can be prepared in larger quantities. It was anticipated that this dumbbell should behave the same in nearly all respects to the [2]rotaxane given the complementary size and shape.

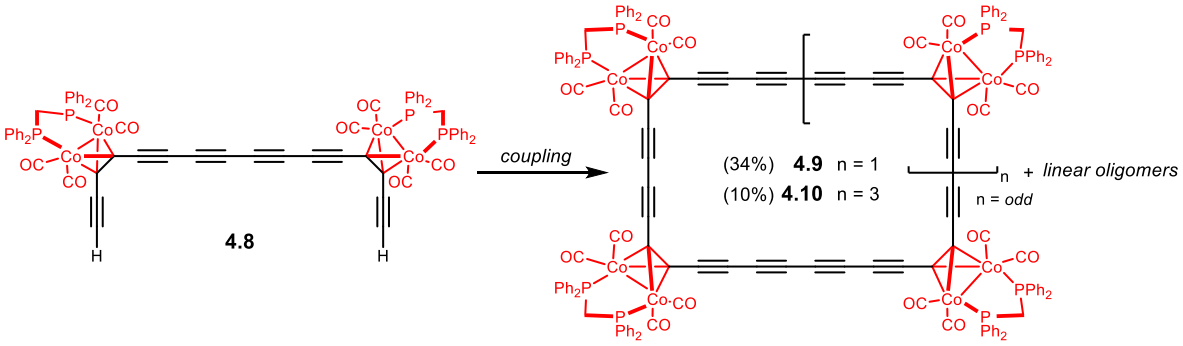

Scheme 4.11: Coupling of tetracobalt thread **4.8** to give cyclic and linear products.

Once suitable conditions have been identified, the coupling of [2]rotaxane **4.8·M4** would then be explored. The reaction was monitored using analytical gel permeation chromatography (GPC) as this technique allows for product detection based on molecular size – a feature that we anticipated would substantially different between each product. Initial cyclisation attempts were first made using standard Glaser-Hay conditions (CuCl, TMEDA, CH_2Cl_2, O_2), although it quickly became apparent from analytical GPC that these conditions were less ideal for forming rings; the chromatogram indicated that many larger, polymeric-like species were instead present. It was postulated that the high activity of the catalyst results in rapid coupling of the starting material, resulting predominantly in the formation of linear chains rather than the desired cyclic species. However, even when running the reaction under high-dilution conditions and carefully controlling the addition of tetracobalt thread **4.8** via syringe pump, only small quantities of the suspected cyclic products could be detected. It is possible that the formation of the (generally accepted) dimeric Cu(I) acetylide transition state in this copper-mediated reaction is simply too strained when forming the cyclic species, and would likely require a highly strained configuration to be adopted before homocoupling can

occur.[17,18] Identification of the reaction products was complicated by most products being undetectable by common mass spectrometry techniques (ESI and MALDI-TOF) and possessing very similar expected ^{1}H and ^{13}C NMR spectra.

Fortunately, using analytical GPC allowed us to screen a variety of coupling conditions and evaluate their product distributions (summarised in Table 4.2). Eglinton conditions (entry **2**) were successfully employed by Diederich *et al.* to prepare cyclic compounds with the dicobalt masking group (**1.12a** and **1.12b** from Section 1.4.2).[19,20] Unfortunately, when applied to this system, the reaction was found to proceed very slowly, forming 5 or 6 distinct species of different size over a period of days and was accompanied by notable decomposition. The slow reaction rate made a high-dilution approach less suitable and when trying to improve the rate by warming to 50 °C, rapid decomposition of the starting material was observed (entry **3**). Modified Glaser conditions (CuCl, pyridine, air, entry **4**) used with prior success in the group[21] were also found to be unsuccessful for this system and displayed rapid decomposition even at 20 °C. Unfortunately, the Glaser-like reaction using a *tert*-butyl bipyridine ligand (entry **5**),[22] which proved successful in preparing the nanohoop [3]rotaxane **4.24**·(**M5**)$_2$ in Chapter 3, was also found unsuitable for this cyclisation, and a distribution of products similar to entry **1** was observed.

Table 4.2: List of tetracobalt thread **4.8** coupling conditions and their respective outcomes.

Entry	Conditions	Outcome
1[23]	CuCl, TMEDA, CH_2Cl_2, 20 °C, O_2	Many linear species present (TLC and GPC)
2[24,25]	$Cu(OAc)_2$, pyridine, 20 °C, Ar	Very slow, never reached completion, formed 5-6 species (GPC), size suggests that all are linear
3[24,25]	$Cu(OAc)_2$, pyridine, 50 °C, Ar	Decomposition of **4.8**
4[21]	CuCl, pyridine, 20 °C, air	Decomposition of **4.8**
5[22]	CuCl, 4,4′-di-tert-butyl-2,2′-dipyridyl, CH_2Cl_2, 30 °C, O_2	Many species present, similar to entry **1**
6[26,27]	CuI, $Pd(PPh_3)_2Cl_2$, DIPA 1,4-benzoquinone, $CHCl_3$, air	Two species by TLC but mixture of 5 species (GPC), predominant signal is smallest size – possibly cyclic dimer **4.9**

Of all conditions investigated, it appeared that those using Cu/Pd/benzoquinone system (entry **6**) were the most promising at forming predominantly cyclic products, and corroborates findings by Haley *et al.*[18] After more in-depth studies into this reaction were made, it appeared that benzoquinone was not required in as high stoichiometry as previously reported.[28–32] Reducing the amount of benzoquinone (to 30 eq.) resulted in less decomposition (it appears there is a slight instability of the cobalt masking groups in the presence of benzoquinone) and seemed to have no impact on the reaction rate nor the ability to produce cyclic products. The suspected cyclic compounds were cleanly isolated using recycling GPC (THF) to afford both the cyclic dimer **4.9** and the cyclic trimer **4.10** in 34% and 10% yields, respectively (Scheme 4.11). While mass spectrometry evidence continues to be elusive for these compounds (likely due to the lack of any obvious acidic or basic residues and low redox activity), rigorous NMR analysis has been made and, when used in conjunction with GPC retention times and UV-vis molar extinction coefficients, can be used to distinguish the two cyclic species. The most notable indicators for the cyclic, rather than short oligomeric, products are the absence of any acetylenic proton resonance in the ^{1}H spectra of both compounds. Also promising were the relatively simple NMR spectra, which would be expected for these higher-symmetry cyclic species. Single crystals of **4.9** suitable for X-ray analysis were grown from slow diffusion of MeOH into a $CHCl_3$ solution of **4.9**. A preliminary solution confirms the connectivity of **4.9** is as expected (Figure S4.1, Section 4.8) and provides further evidence that the cyclisation had been successful.

With optimised conditions in hand, we then applied these conditions to prepare the desired catenanes (Scheme 4.12). Somewhat unexpectedly, subjecting the analogous [2]rotaxane **4.8·M4** to the same conditions did not yield the expected cyclic (or any oligomeric)

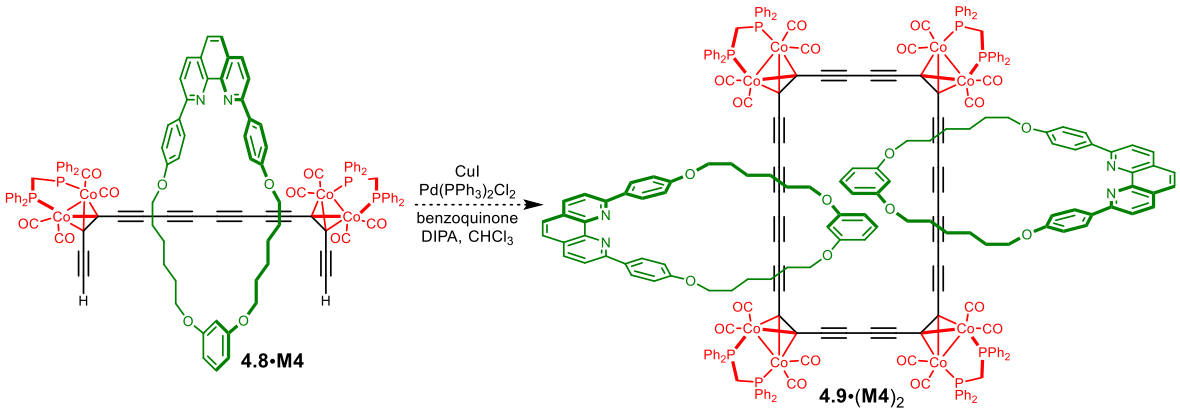

Scheme 4.12: Cu/Pd co-catalysed alkyne coupling of tetracobalt [2]rotaxane **4.8·M4** did not afford the expected [3]catenane **4.9·(M4)**$_2$.

products, but instead resulted in nearly complete decomposition of the [2]rotaxane starting material. While a small quantity of larger-sized species (likely linear, based on analytical GPC) appeared to have formed, the complicated NMR spectrum of these species suggested that they were not the expected product and further efforts to characterise these products were not pursued. Also noteworthy was the observation that these species formed significantly more slowly than for what was observed in the previously-described model reactions. As the macrocycle should have little influence on the chemical reactivity of the thread, this result came as a surprise. We attribute this reduced reactivity to the steric bulk of the (oversized) **M4** macrocycle, which may prevent two molecules from coming in sufficiently close proximity to couple.

To probe the impact of sterics on this reaction, we prepared a tetracobalt dumbbell with an additional acetylene unit at each end. We anticipated that this would move the reaction centre further away from the macrocyclic unit, limiting its ability to interfere with the key coupling event. In principle, this should allow for the coupling to proceed more readily. As before, the reaction was first trialled and optimised on the thread before being applied to the [2]rotaxane. The double extension of **4.8** was successfully achieved by a simple statistical Glaser-Hay cross coupling with excess TMS-acetylene (Scheme 4.13). Fortunately, the limited reactivity of both the thread and [2]rotaxane coupling with itself proved beneficial for the extension, with only minimal homocoupling being observed for two, and afforded the extended thread **4.11** and [2]rotaxane **4.11·M4** in yields of 66% and 69%, respectively (over 2 steps). TMS deprotection of both the thread **4.11** and [2]rotaxane **4.11·M4** proceeded cleanly and rapidly with K_2CO_3 in THF/MeOH, with complete deprotection observed after approximately 15 minutes to return the doubly-deprotected thread **4.12** (30%) and [2]rotaxane **4.12·M4** (97%), respectively.

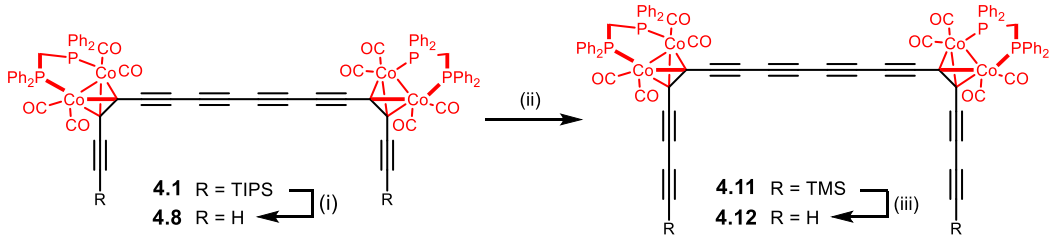

Scheme 4.13: Extension of tetracobalt thread **4.8** was made using a statistical Glaser-Hay coupling with TMS acetylene. (i) TBAF, THF/H_2O (1% v/v), 20 °C, 30 min, Ar, 94%; (ii) TMS-acetylene (100 eq.), CuCl, TMEDA, CH_2Cl_2, 20 °C, 30 min, O_2, 66%; (iii) K_2CO_3, THF/MeOH (1:1), 20 °C, 15 min, air, 30% or TBAF, THF/H_2O (1% v/v), 20 °C, 15 min, Ar. These conditions were also used to prepare the analagous [2]rotaxanes: (i) **4.8·M4** (88%), **4.11·M4** (69%) and **4.12·M4** (97%).

Particularly noteworthy was an observed difference in reactivity between deprotected thread **4.12** and [2]rotaxane **4.12·M4**. While **4.12·M4**, appeared indefinitely stable, both in solution and in the solid state under ambient conditions (20 °C, air, light), thread **4.12** seemed to decompose over a period of minutes-to-hours in the solid state under the same conditions. Thread **4.12** does not appear to show any sensitivity to light, and its stability appears much improved when stored at −18 °C. This is an elegant demonstration of the marked stability enhancement that can be brought about by supramolecular encapsulation. We expect that the **M4** macrocycle is sufficiently large such that it offers some degree of protection to the terminal diyne and also acts to disrupt close packing of **4.12·M4** in the solid state. Fortunately, extended thread **4.12** appears to only decompose in the solid state, with no decomposition observed even highly-concentrated solutions. To avoid MeOH from being carried over to the subsequent coupling step, a TBAF silyl deprotection (THF/H_2O 1% v/v) was instead used. Treating **4.11** with TBAF, followed by aqueous work up (organic extraction with $CHCl_3$) provided deprotected **4.12** as a solution in a THF/$CHCl_3$ mixture. The solvent was then replaced with $CHCl_3$ through successive removal of solvent to ~1-2 mL, then additions of $CHCl_3$ prior to the coupling reaction.

The Pd/Cu co-catalysed homocoupling of both the extended thread **4.12** and extended [2]rotaxane **4.12·M4** were then investigated. Pleasingly, both underwent successful coupling over a 2 hour period to give the corresponding cyclic dimers and cyclic trimers (Scheme 4.14) – [3]- and [4]catenanes, respectively, in the case of the interlocked compounds (Figure 4.5). Slow addition of **4.12** or **4.12·M4** to the reaction mixture (containing CuI, $Pd(PPh_3)_2Cl_2$, DIPA,

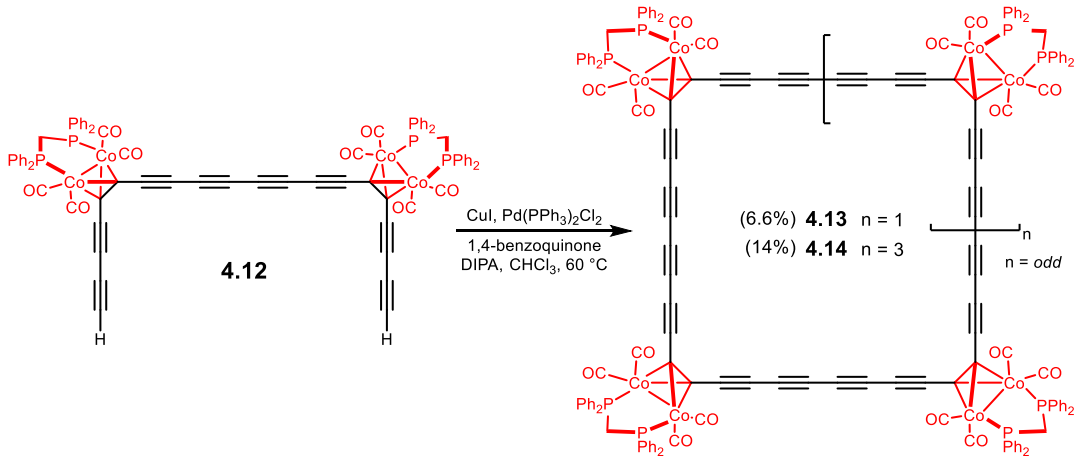

Scheme 4.14: Cu/Pd co-catalysed oxidative homocoupling of extended thread **4.12** to give the cyclic dimer **4.13** and cyclic trimer **4.14**. An analagous coupling was used with **M4** protected compound **4.12·M4** to yield [3]catenane **4.13·(M4)**$_2$ (20%) and [4]catenane **4.14·(M4)**$_3$ (4.3%), respectively.

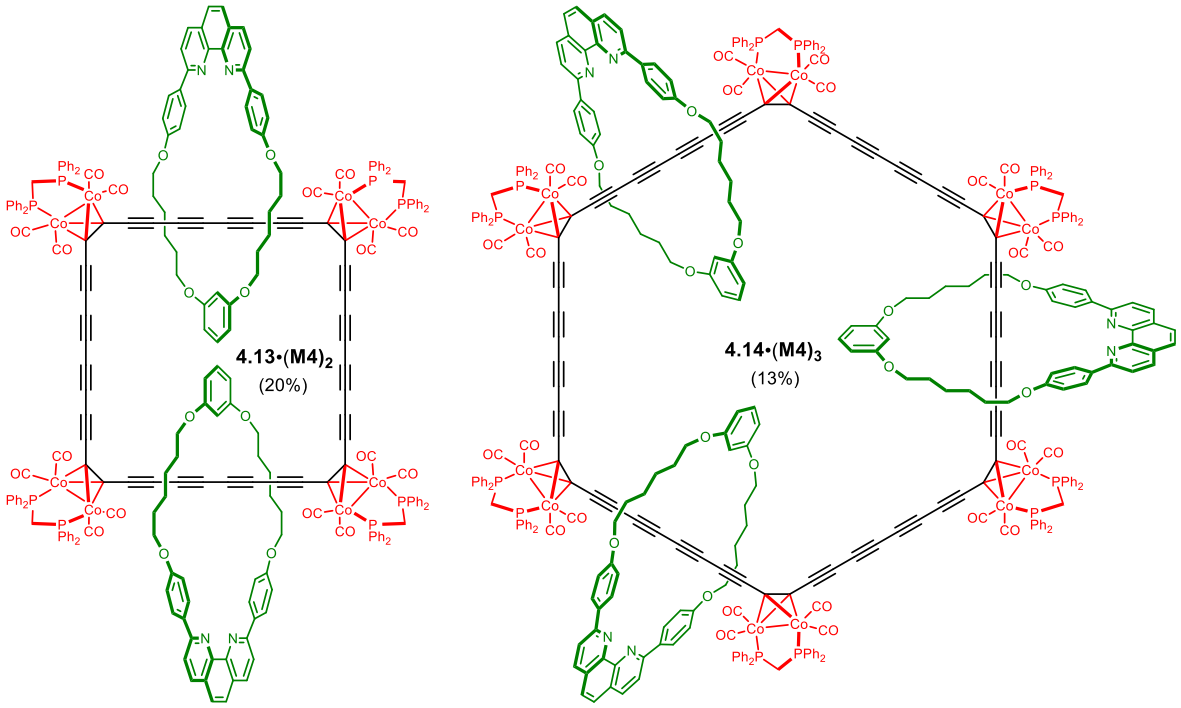

Figure 4.5: Respective [3]- and [4] catenanes **4.13**·(**M4**)$_2$ and **4.14**·(**M4**)$_3$ obtained from the oxidative homocoupling of extended [2]rotaxane **4.12**·**M4**.

$CHCl_3$ and benzoquinone) via syringe pump was found to favour formation of cyclic species, monitored by analytical GPC (Figure 4.6a). While the non-interlocked rings can be separated by silica chromatography using a petroleum ether/CH_2Cl_2 eluent system, the [3]- and [4]catenanes (**4.13**·(**M4**)$_2$ and **4.14**·(**M4**)$_3$, respectively) displayed nearly identical retention factors in a range of different solvent conditions, rending silica chromatography unsuitable. By exploiting the difference in their relative size, these species could be easily separated by recycling GPC (Figure 4.6b), allowing isolation of both in yields of 20% and 13%, respectively.

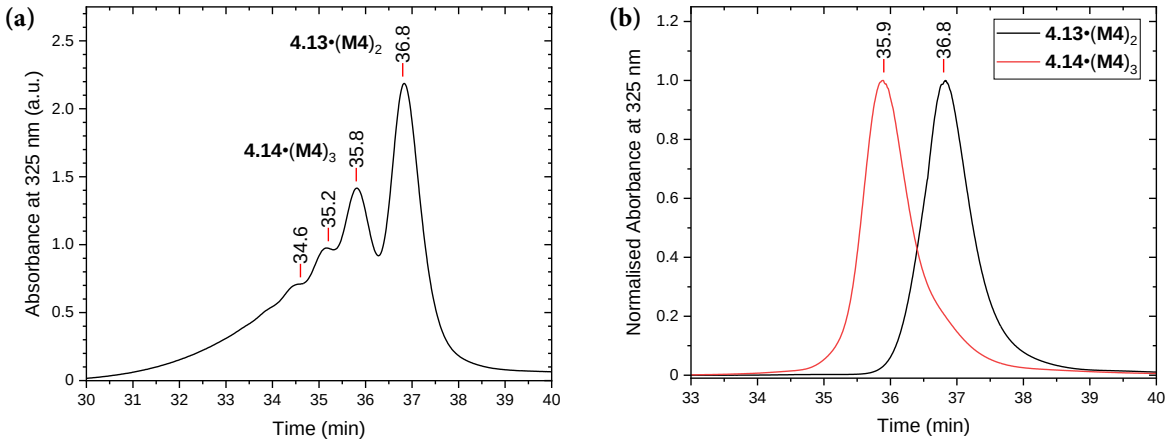

Figure 4.6: (a) Analytical GPC trace indicating multiple potential [*n*]catenanes are present after the Cu/Pd co-catalysed cyclisation of **4.12**; (b) normalised analytical GPC traces confirming successful separation of the two most prominent catenanes, **4.13**·(**M4**)$_2$ and **4.14**·(**M4**)$_3$. Analytical GPC was carried out using JAIGEL-3H-A (8 × 500 mm) and JAIGEL-4H-A (8 × 500 mm) columns in THF + 1% pyridine as eluent with a flow rate of 1.0 mL/min.

GPC retention times, combined with NMR, mass spectrometry and IR data all provided strong evidence for the formation of the [3]- and [4]catenanes, along with the corresponding non-interlocked dicobalt-masked rings. Final confirmation of the formation of [3]catenane **4.13**·(**M4**)$_2$ came after single crystals suitable for X-ray analysis were grown by vapour diffusion of cyclohexane into a solution of **4.13**·(**M4**)$_2$ in THF. Despite intense efforts, single crystals suitable for X-ray analysis of the [4]catenane **4.14**·(**M4**)$_3$ and dicobalt rings **4.13** and **4.14** have yet to be obtained.

Analysis of the X-ray data reveal the crystals are monoclinic ($P2_1/c$ space group) with two molecules per unit cell, and half a molecule of [3]catenane **4.13**·(**M4**)$_2$ in the asymmetric unit (Figure 4.7). It is interesting that the geometries of the dppm phenyl rings are all pointing towards the macrocycle (Figure 4.7), in stark contrast to both tetracobalt [2]rotaxane **4.1**·**M4** and supertrityl-stoppered [2]rotaxane **3.22**·**M4** in Chapter 3. Perhaps such an arrangement in this case is driven by favourable non-covalent interactions between the rings on the cobalt MAE and the phenanthroline macrocycle. As with **4.1**·**M4**, clear bond length alternation (BLA) can be observed along the tetrayne chain of both sides of the asymmetric unit. BLA was calculated to be 0.125 Å for the **M4**-shielded tetrayne and 0.148 Å for the unshielded one – the former slightly smaller than **4.1**·**M4**, while the latter being similar to previous reported tetraynes.[10–13]

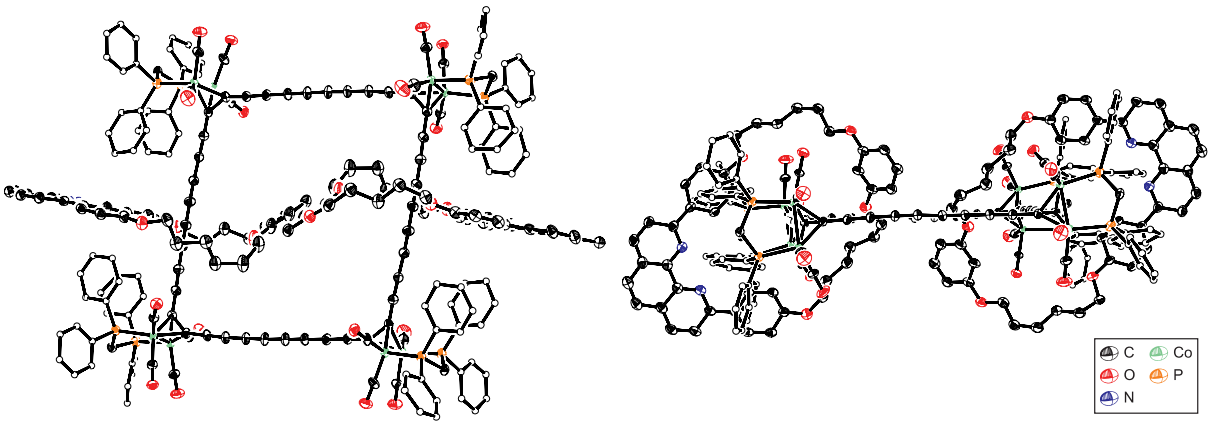

Figure 4.7: X-ray crystallographic structure of [3]catenane **4.13**·(**M4**)$_2$. (ellipsoids at 30% probability, hydrogen atoms omitted and dppm phenyl rings plotted as spheres for clarity)

The UV-vis spectra of both threads **4.13** and **4.14** and catenanes **4.13**·(**M4**)$_2$ and **4.14**·(**M4**)$_3$ appear very similar (Figure 4.8), with the exception of an additional peak at 292 nm observed for the catenanes that arises from the diaryl phenanthroline backbone of the macrocycle. As would be expected of mechanically interlocked compounds, in both cases the

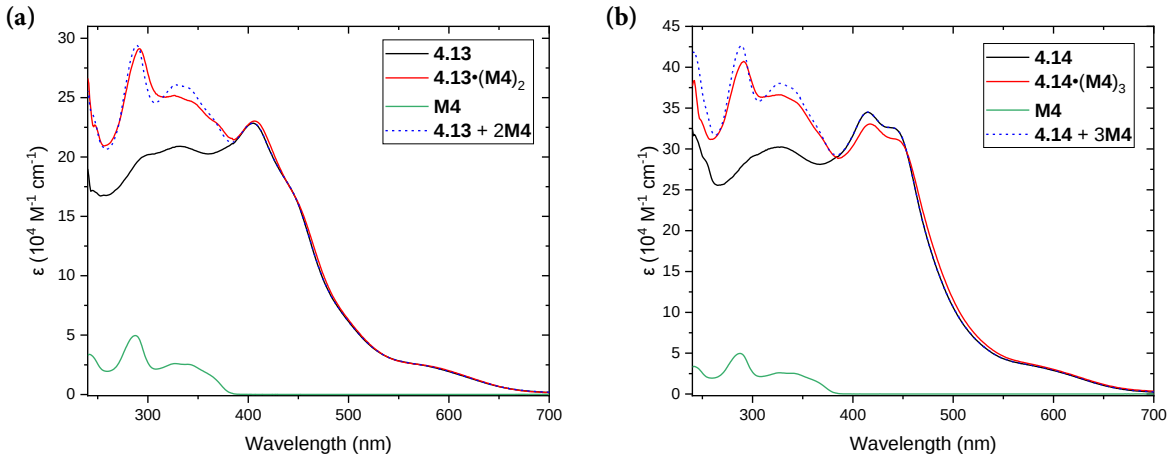

Figure 4.8: UV-vis spectra of (a) thread **4.13** and [3]catenane **4.13·(M4)**$_2$ and (b) thread **4.14** and [4]catenane **4.14·(M4)**$_3$. For each, the UV-vis spectrum of macrocycle **M4** is shown (green), along with the sum of **M4** and the thread (dotted blue), which matches well with the respective catenanes. All solutions in $CHCl_3$ at 25 °C.

[*n*]catenanes and corresponding dicobalt-masked backbones have comparable molar extinction coefficients, all in the order of 10^5 mol^{-1} dm^3 cm^{-1}. For the cyclic dimers **4.13** and **4.13·(M4)**$_2$, a strong absorption band is observed around 405 nm, while the cyclic trimers **4.14** and **4.14·(M4)**$_3$ show two closely spaced bands at approximately 415 nm and 445 nm. For all cyclic species, the absorption extends out to 700 nm. The sums of the UV-vis spectra for the threads (**4.13** and **4.14**) and macrocycle **M4** match well those of the respective catenanes (see dotted blue trace, Figure 4.8).

With robust synthetic routes to dicobalt-masked [3]- and [4]catenanes established, the next logical step was to investigate the unmasking ability of these compounds to form cyclo[40]carbon [3]catenane **4.15·(M4)**$_2$ and cyclo[60]carbon [4]catenane, respectively (Scheme 4.15). Treating both the free ring **4.13** and corresponding [3]catenanes **4.13·(M4)**$_2$ with I_2 (40 eq.) in either a THF or THF/MeCN (1:1) solvent system saw rapid consumption of the dicobalt-masked starting materials. Unfortunately, in all cases we were unable to detect any indication (by TLC, UV-vis spectroscopy or mass spectrometry) that the cyclocarbons **4.15** or **4.15·(M4)**$_2$ had been successfully generated. Unmasking attempts were also carried out at −78 °C to address any stability concerns with the resulting cyclo[40]carbon, however, we observed no evidence for the formation the desired products. In all cases, a dark-coloured high polarity species was formed, and further efforts to characterise this product were not made.

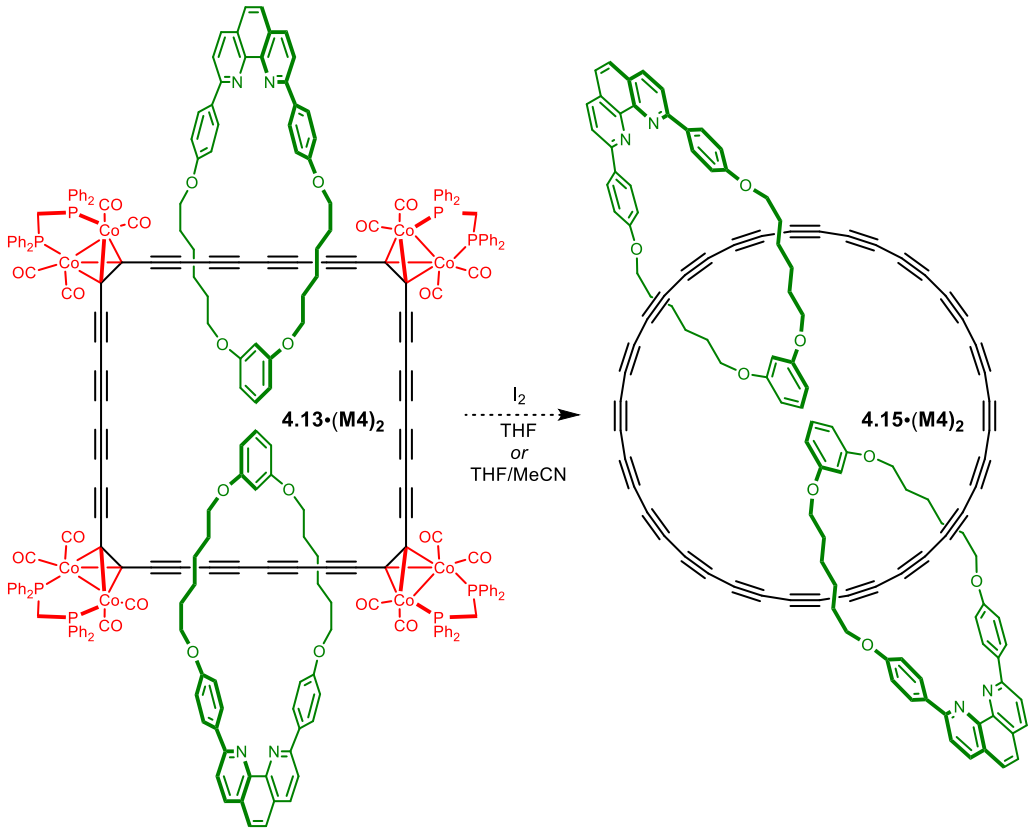

Scheme 4.15: Proposed dicobalt unmasking step to cyclo[40]carbon [3]catenane **4.15**·(**M4**)$_2$.

While these dicobalt-masked [*n*]catenanes are fascinating compounds, it seems likely that unmasking these particular catenanes will prove challenging. In Chapter 3, we noted the unmasking ability for these Saito-protected dicobalt-masked compounds is generally poor; **M4**-protected polyyne [3]rotaxane could seldom be obtained through unmasking of just two dicobalt units, due to presumed interference of the dicobalt group by the macrocycle. For these catenanes, we would require the successful unmasking of four or six dicobalt groups – something that we suspect would be very inefficient with the current unmasking conditions.

These results ultimately provide a robust blueprint for generating masked cyclocarbon precursors using dicobalt-masked units. It should be noted that unmasking these current derivatives would result in cyclo[40] and cyclo[60]carbons which we anticipate to be antiaromatic – a feature that would likely render these targets even more prone to degradation. Since the synthetic pathway presented in this chapter involves the AMT coupling of two identical fragments (**3.20**), the resulting [2]rotaxanes will always contain an even number of acetylene units. Cyclo-oligomerisation of these are therefore only able to prepare catenanes that unmask to antiaromatic cyclocarbons with $(4n)\pi$ electrons. Should [2]rotaxanes bearing an odd

number of acetylene units be prepared, it should then be possible to generate a mixture of anti-aromatic and aromatic cyclocarbon catenanes, with $(4n+2)\pi$ electrons.

In spite of this, we expect that the energy difference between aromatic and antiaromatic compounds decreases as the rings become larger. This effect is readily apparent from a Frost-Musulin diagram where, as the ring size increases, the energy levels move closer together, and the energy difference between aromatic and antiaromatic species becomes smaller.[32] Thus, it may be possible to isolate large cyclo[*n*]carbon catenanes with $(4n)\pi$ electrons that show similar stability to their similarly-sized aromatic counterparts. It is therefore difficult justify the more complex synthesis towards cyclocarbon catenanes with $(4n+2)\pi$ electrons. A more promising avenue to improve the stability of these cyclocarbons would be to prepare variants of this [2]rotaxane bearing different macrocycles. By using smaller phenanthroline-based macrocycles, or even the 2,6-pyridyl cycloparaphenylene **M5** from Chapter 3, it is probable that enhanced protection of the cyclocarbon can be obtained.

While our initial target was to prepare cyclocarbons, we were highly encouraged by the ability of these rotaxanes to polymerise. We hypothesised that by simple modifications to the coupling conditions, this work may lead to a route towards encapsulated polyynes of unprecedented length.

4.4 Towards Polyyne [*n*]Rotaxanes

4.4.1 Synthesis of Dicobalt-Masked [*n*]Rotaxanes

As an alternative to forming catenanes it should be possible to use the same tetracobalt [2]rotaxane **4.12·M4** building block to rapidly prepare much longer encapsulated linear systems as models for the infinitely-long polyyne, carbyne, than those previously reported. A final coupling reaction with a permanent stoppering group could then be used to prevent any further extension or cyclisation reaction. An interesting feature of this type of approach is that it would provide a very fast and relatively efficient means to build up long masked polyyne [*n*]rotaxanes. A statistical cross coupling reaction was envisaged between [2]rotaxane **4.8·M4** and supertrityl-capped [2]rotaxane **3.23·M4** from Chapter 3. This should result in a series of supertrityl-capped [*n*]rotaxanes, differing only by the number of tetracobalt [2]rotaxanes units (linkers) between the two capping [2]rotaxanes (stoppers) (Figure 4.1, bottom). It was hoped that by carefully

controlling the relative stoichiometries of stoppering and linking rotaxanes, we could tune the length distribution towards longer or shorter masked [*n*]rotaxanes as desired.

Initial experiments were made on the non-extended tetracobalt [2]rotaxane **4.8·M4**, but the same general observations were made as in Section 4.3; the reactivity of the monoyne is either generally too poor or that, due to steric constraints imposed by the macrocycle, the desired coupling reaction proceeds too slowly, if at all. As with the cyclic system, extending the tetracobalt component by one acetylene unit (**4.12** and **4.12·M4)** immediately showed more promise. Subjecting a 1:4 mixture of extended tetracobalt [2]rotaxane **4.12·M4** and deprotected supertrityl-stoppered [2]rotaxane **3.23·M4** to the same Pd co-catalysed reaction conditions (Scheme 4.16) produced multiple species of larger size (at GPC retention time < 35.3 min), as seen identified by analytical GPC (Figure 4.9). Since the size difference between each

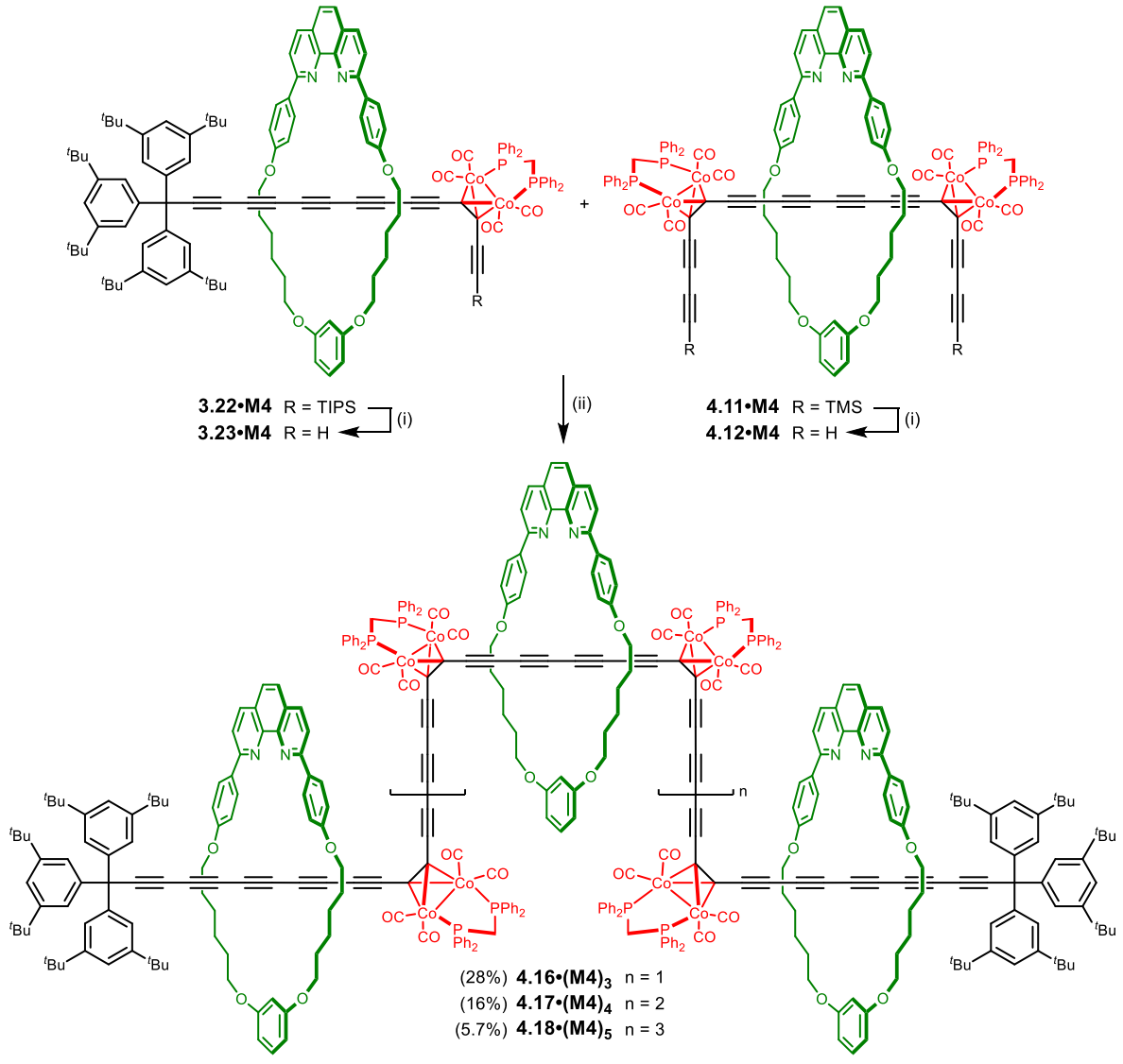

Scheme 4.16: A statistical coupling to dicobalt-masked polyyne [*n*]rotaxanes. (i) TBAF, THF/H_2O (1% v/v), 20 °C, 30 min, Ar; (ii) CuI, $Pd(PPh_3)_2Cl_2$, 1,4-benzoquinone, DIPA, $CHCl_3$, 20 °C, 2 h, air.

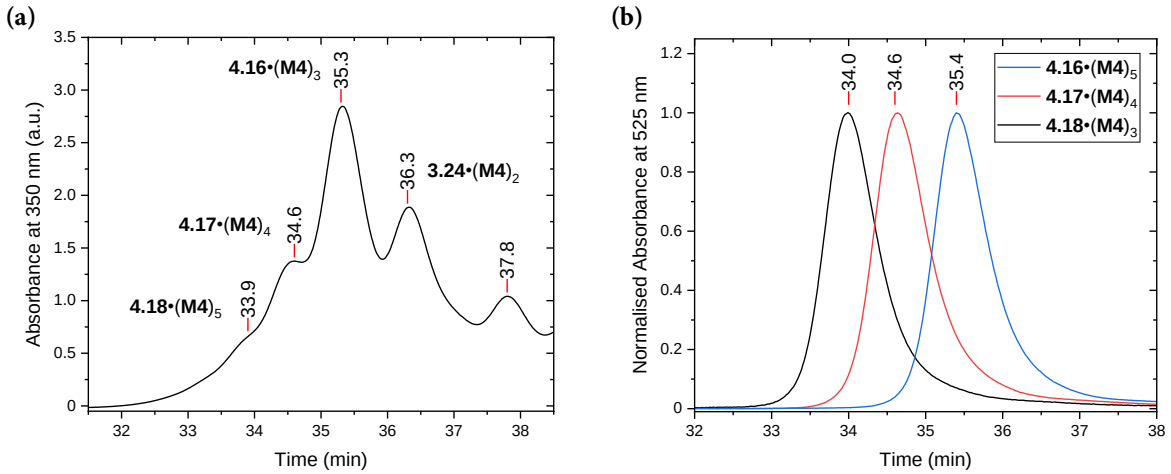

Figure 4.9: (a) Analytical GPC trace indicating multiple polyyne [*n*]rotaxanes are present after the statistical coupling of linker and stopper [2]rotaxanes; (b) normalised analytical GPC traces confirming successful separation of the three most prominent [*n*]rotaxanes by recycling GPC. Analytical GPC was carried out using JAIGEL-3H-A (8 × 500 mm) and JAIGEL-4H-A (8 × 500 mm) columns in THF + 1% pyridine as eluent with a flow rate of 1.0 mL/min.

[*n*]rotaxane is not particularly large, recycling GPC was required to separate the three largest species.

The smallest of these (GPC retention time of 35.3 min, Figure 4.9) was identified as the stoppered [4]rotaxane **4.16**·(**M4**)$_3$, while the larger two species being the respective stoppered [5]- (**4.17**·(**M4**)$_4$) and [6]rotaxanes (**4.18**·(**M4**)$_5$), obtained in 28%, 16% and 5.7% yields, respectively. While larger species, suspected to be the [7]rotaxanes and beyond, can be observed by recycling GPC, their limited quantities and large size restricted characterisation by mass spectrometry and NMR. For the three rotaxanes isolated, ^{1}H and ^{13}C NMR spectra appear as expected, and the presence of the phenanthroline macrocycle in these compounds generally means that they ionise well and can observed by ESI mass spectrometry. Accurate mass data has been obtained for the [4]- (Figure 4.10) and [5]rotaxanes, but due to the large size of

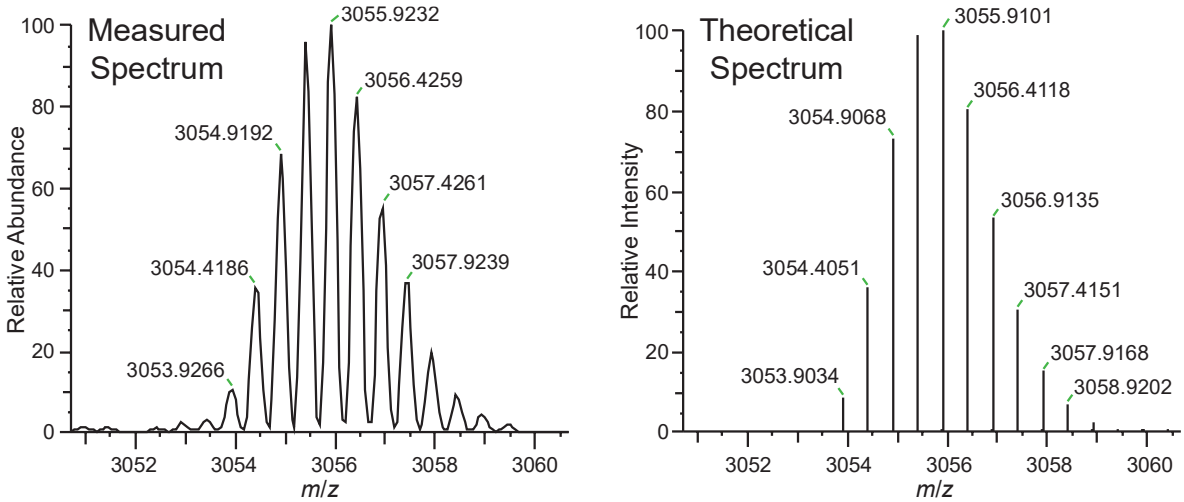

Figure 4.10: High-resolution mass spectrum of octacobalt [4]rotaxane **4.16**·(**M4**)$_3$.

[6]rotaxane **4.18**·(**M4**)$_5$ and limitations with the mass spectrometer, only low-resolution mass data could be obtained for this compound. We had hoped that MALDI-TOF (DCTB, DHB, CHCA matrices) would prove useful for these larger species, but we were unable to observe any signals in the mass spectrum.

^{1}H NMR has proven to be a particularly useful technique in rapidly determining the identity of these [*n*]rotaxanes. For example, simple comparison of the integration ratio between the supertrityl stopper ^{t}Bu signal and the phosphine bridge (or cobalt Ar-H) resonances, quickly identifies the number of linking tetracobalt units. Additionally, the fact that the macrocycles of the stoppering rotaxanes are in different chemical environments to those in the tetracobalt units, the ratio of integrals between the two can also be used for a similar purpose, as exemplified in Figure 4.11.

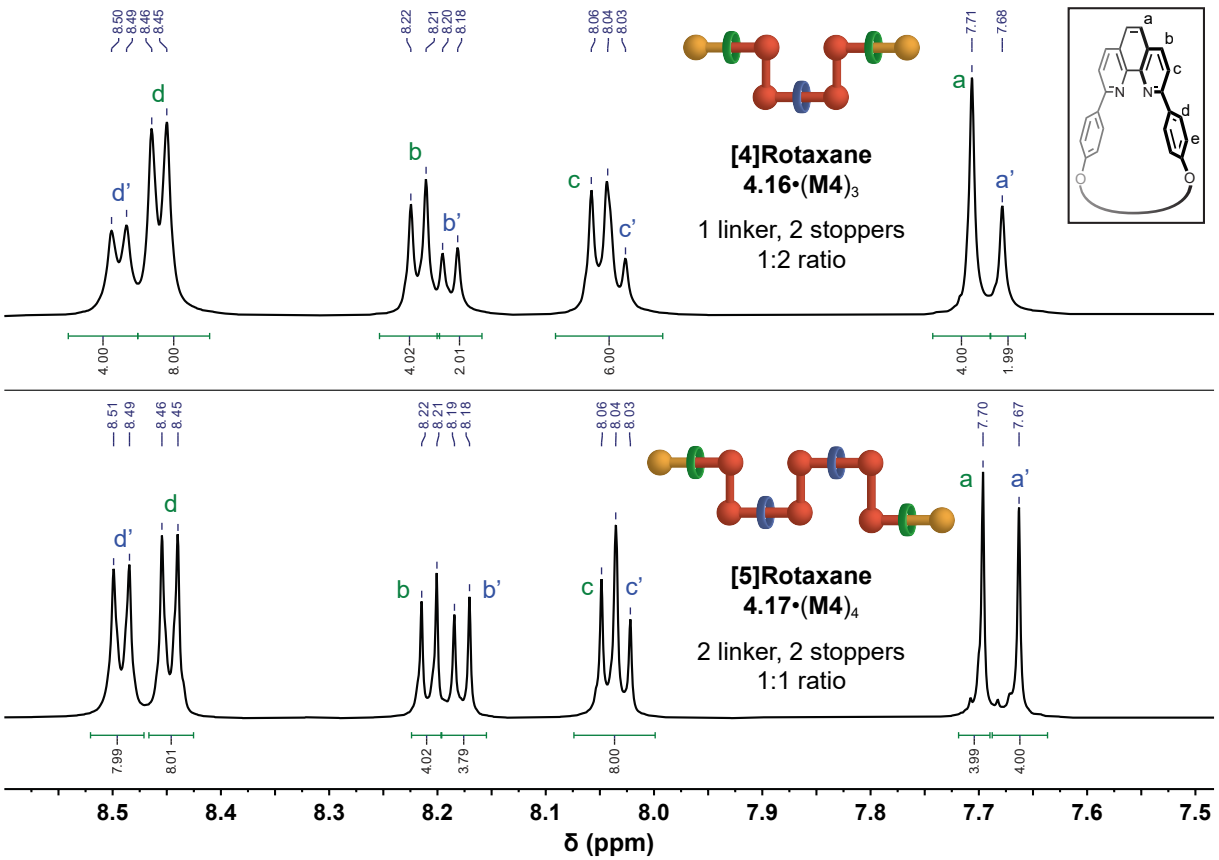

Figure 4.11: ^{1}H NMR (600 MHz, CD_2Cl_2, 298 K) comparison of masked polyyne [4]rotaxane **4.16**·(**M4**)$_3$ and [5]rotaxane **4.17**·(**M4**)$_4$. The ratio of integrals of macrocycle resonances can be used to deduce the number of constituent linker and stoppering rotaxanes. Assignments (shown in box) are coloured green and blue for stoppering and linking [2]rotaxane units, respectively.

It is expected that by carefully adjusting the ratio of stoppering rotaxane **3.23**·**M4** to tetracobalt rotaxane **4.12**·**M4**, the mass distribution could be shifted to favour longer or shorter

[*n*]rotaxanes. For example, switching to a 1:3 or even 1:2 ratio should result in longer polyynes, potentially allowing isolation of [7]rotaxanes and beyond.

UV-vis spectra for the [4]-, [5]- and [6]rotaxanes **4.16**·(**M4**)$_3$, **4.17**·(**M4**)$_4$, and **4.18**·(**M4**)$_5$, respectively, were obtained. In a similar manner to the cyclic compounds discussed earlier, the spectral forms of these dicobalt-masked compounds are comparable (Figure 4.12). In all cases, a strong absorption band due to the dicobalt masking group (located around 420-455 nm) is observed, along with a peak at 292 nm arising from the **M4** diaryl phenanthroline macrocyclic backbone. Absorption extends out to 700 nm for all and becomes more intense as the systems become larger. Molar extinction coefficients for all are in the order of 10^5 mol^{-1} dm^3 cm^{-1}. From a quick comparison it appears that with successive additions of each tetracobalt (linking) [2]rotaxane, a linear increase in molar extinction coefficients is brought about for these molecules.

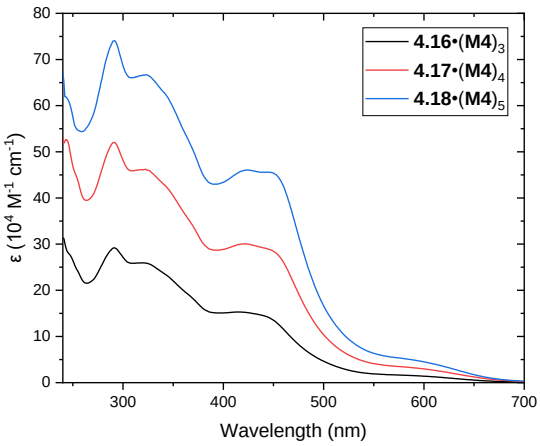

Figure 4.12: UV-vis spectra of dicobalt-masked (black) [4]-, (red) [5]- and (blue) [6]rotaxanes **4.16**·(**M4**)$_3$, **4.17**·(**M4**)$_4$, and **4.18**·(**M4**)$_5$, respectively. All solutions in $CHCl_3$ at 25 °C.

4.4.2 Unmasking to Polyyne [*n*]Rotaxanes

Following the successful isolation of these dicobalt-masked [4]-, [5]- and [6]rotaxanes, attempts were made to unmask the dicobalt group to give the corresponding polyyne (Scheme 4.17). Based on the many unmasking attempts of dicobalt-masked [3]rotaxane **3.24**·(**M4**)$_2$, also bearing the same phenanthroline macrocycle **M4** (and discussed in depth in Chapter 3), it seemed unlikely that the unmasking step would be efficient. Despite this, we would expect the resulting polyyne [*n*]rotaxanes to be very strongly absorbing, on account of their presumed high molar absorption coefficients arising from an extended, highly conjugated polyyne backbone.

It was hoped that due to these high molar extinction coefficients, we may be able to observe the unmasked compounds by UV-vis spectroscopy, which would require only a very small amount of material. We also expected that, due to the good compatibility of the **M4** macrocycle with ESI-MS, it should at least be possible to obtain accurate mass data for the unmasked species. Having only sub-milligram quantities of material does, however, restrict characterisation by NMR methods, especially regarding ^{13}C NMR data.

Unmasking attempts were made on the smallest [4]rotaxane that, if successfully unmasked, would return a polyyne [4]rotaxane with 24 contiguous acetylene units (Scheme 4.17). This compound was selected first due to its higher abundance from the coupling reaction, allowing for multiple unmasking attempts to be made. Another consideration made was regarding the efficiency of the unmasking reaction, which depends heavily on the number of dicobalt groups to be unmasked. [4]Rotaxane **4.16**·(**M4**)$_3$ requires the removal of the fewest

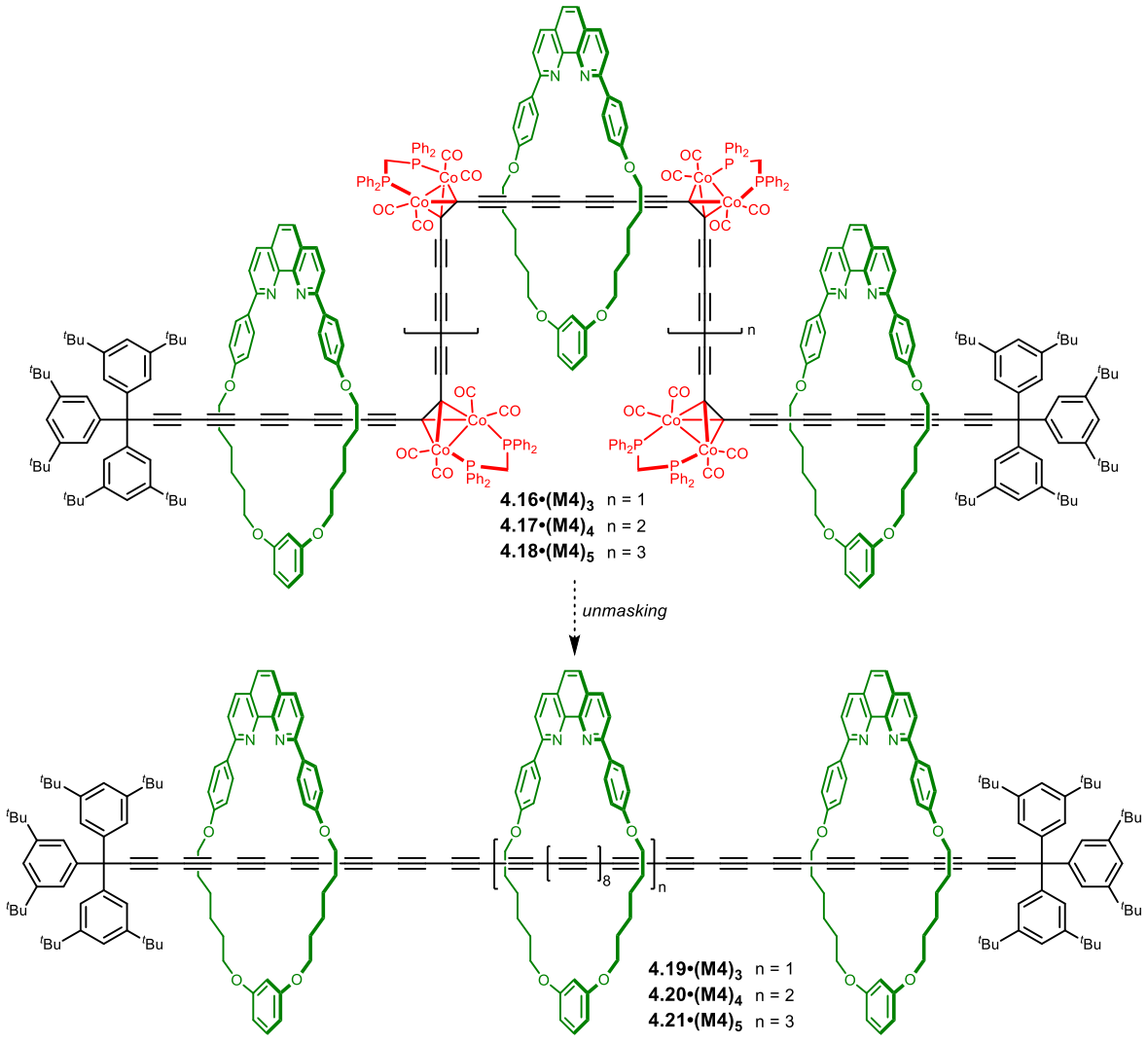

Scheme 4.17: Dicobalt unmasking to give polyyne [4]-, [5]- and [6]rotaxanes bearing 24 (**4.19**·(**M4**)$_3$), 34 (**4.20**·(**M4**)$_4$) and 44 (**4.21**·(**M4**)$_5$) contiguous acetylene units.

dicobalt groups (four), compared to the [5]- and [6]rotaxanes which require removal of six and eight dicobalt groups, respectively. We hoped that this would give us the best chance at detecting and isolating sufficient product for further studies.

The dicobalt-masked [4]rotaxane **4.16·(M4)**$_3$ was first treated with I_2 (40 eq.) in THF. After approximately 5 minutes it was apparent that all starting material had been consumed but, unfortunately, it also appears that the reaction was unsuccessful. No evidence of the unmasked compound could be detected by TLC or ESI-MS, nor were there any species that displayed the characteristic UV-vis vibronic signature of polyynes. Multiple repeat experiments were made due to the unpredictable nature of the unmasking process but, despite this, no evidence of the product could be detected. The unmasking was also investigated in two other solvents – MeCN and THF/MeCN (1:1), both using the same I_2 oxidant. Even under these conditions we were unable to detect formation of any polyyne-containing species.

As with [3]rotaxane **3.24·(M4)**$_2$ from Chapter 3, it is difficult to pinpoint exactly why the unmasking was unsuccessful with I_2. The absence of **4.19·(M4)**$_3$ in these attempts could be rationalised by considering the unmasking efficiency of these dicobalt groups. The unmasking of one dicobalt group (bearing the same **M4** macrocycle) occurs at best in 70% yield, while two groups in a tentative 20-30% yield (based on polyyne **3.25·(M4)**$_2$ from Chapter 3). Following this pattern, the unmasking of four cobalt groups could be expected to occur in sub-1% yields. It is also entirely possible that the product of this reaction – the 24-yne – is simply too unstable under either the reaction conditions, or during the brief workup step prior to UV-vis analysis. The 24-yne [4]rotaxane **4.19·(M4)**$_3$ is on par with longest isolated polyyne in literature (the pyridyl-capped 24-yne **1.10** from Section 1.2.1), which was reported to discolour in solution over a period of days and only in a matter of hours in the solid state.[22] We have demonstrated in previous work that this phenanthroline macrocycle offers little in the way of protection for the dumbbell, so it is entirely reasonable to expect only a nominal enhancement in stability compared 24-yne **1.10**.

Very recent and preliminary unmasking conditions employing a *meta*-chloroperoxybenzoic acid (*m*CPBA) oxidant have been developed by group members Mr Prakhar Gupta and Dr Yueze Gao. Initial attempts at treating [4]rotaxane **4.16·(M4)**$_3$ to these unmasking conditions were followed by *in-situ* UV-vis experiments. *m*CPBA (30 eq.) was

added to a solution of [4]rotaxane **4.16**·(**M4**)$_3$ in CH_2Cl_2. An immediate colour change to red-orange was observed after addition of the oxidant, suggesting that unmasking had been successful. Pleasingly, the UV-vis spectrum of the reaction mixture displayed a very similar spectral form to the pyridyl-capped 24-yne **1.10** previously reported by Tykwinski *et al*,[22] albeit with some other species contaminating the mixture. The unmasking reaction has since been repeated on a larger (2.0 mg) scale, which allowed for purification by silica chromatography (CH_2Cl_2/EtOAc, 9:1). It appears that polyyne [4]rotaxane **4.19**·(**M4**)$_3$ is stable during a brief workup step and also during silica chromatography.

The UV-vis spectra of both masked and unmasked [4]rotaxanes **4.16**·(**M4**)$_3$ and **4.19**·(**M4**)$_3$, respectively, are presented in Figure 4.13. The UV-vis spectrum of **4.19**·(**M4**)$_3$ displays several intense maxima, λ_{main}, with the lowest energy band extending out to 475 nm. Due to a 2 nm slit width on the spectrometer, it is difficult to attribute the slight (2 nm) bathochromic shift in the spectrum of **4.19**·(**M4**)$_3$ compared to the pyridyl-capped 24-yne **1.10** is due to a different solvation environment of the [4]rotaxane or due to variations between spectrometers. High-resolution mass spectrometry (ESI) reveals a weak signal around m/z = 1826, with an isotopic distribution corresponding to the $[M+2H]^{2+}$ ion of **4.19**·(**M4**)$_3$. While these results are still preliminary, unmasking by treatment with *m*CPBA appears much more promising than with I_2, at least with the **M4**-protected series of compounds. While [5]- and [6]rotaxanes **4.17**·(**M4**)$_3$ and **4.18**·(**M4**)$_3$ are yet to be unmasked, these promising findings suggest that it will soon be possible.

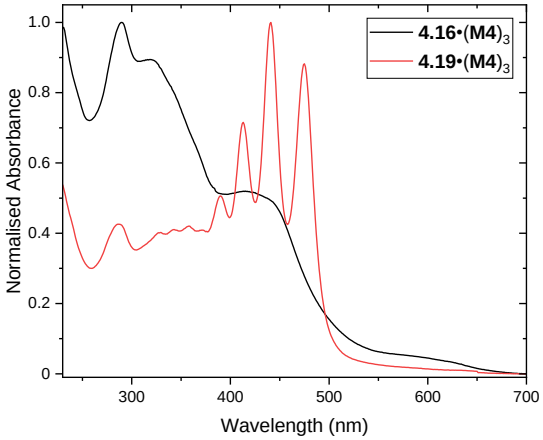

Figure 4.13: UV-vis spectra of (black) octacobalt [4]rotaxane **4.16**·(**M4**)$_3$ and (red) polyyne [4]rotaxane **4.19**·(**M4**)$_3$. All solutions in CH_2Cl_2 at 25 °C.

4.5 Using Alternative Macrocycles

As mentioned in Section 4.1, not all macrocycles offer the same level of protection to the polyyne. With this in mind, we turned our attention toward developing a rotaxane that would have superior protection ability for the longest polyynes in our series. In addition to the **M4**-protected [*n*]catenanes and [*n*]rotaxanes described in this chapter, it should also be possible to prepare variants of the tetracobalt [2]rotaxane with alternative shielding macrocycles. We have previously shown that 2,6-pyridyl nanohoop **M5** offers the best protection to the polyyne and most reliable unmasking chemistry (documented in Chapter 3), making this macrocycle an obvious choice. Unfortunately, and despite our best efforts, we have been unable to successfully prepare tetracobalt [2]rotaxane **4.1·M5** by the same approaches used for the phenanthroline macrocycles (discussed in Sections 4.2.2 and 4.2.3). Additionally, this macrocycle may have compatibility issues with the later Pd/Cu/benzoquinone coupling step. In Chapter 3 we reported unexpected reactivity of [2]rotaxane **3.23·M5** under these conditions, although in that case the reaction time was significantly longer and with a large excess of benzoquinone present.

4.5.1 Synthesis of a Smaller Phenanthroline Macrocycle

Since the AMT Cadiot-Chodkiewicz cross coupling with phenanthroline-bearing macrocycles has proven itself as a reliable approach in constructing interlocked compounds with these dicobalt-masked precursors, we therefore decided to explore alternative macrocycles bearing the diaryl phenanthroline core. Based on previous work (in Chapter 3), we know that macrocycle **M4** is much larger than necessary, and that we would likely see improved stability of the resulting polyynes should we switch to a smaller one. Thus, we turned our attention toward a smaller, more rigid phenanthroline-based macrocycle.

Diaryl ether phenanthroline macrocycle **M6** (Scheme 4.18) was synthesised from diphenol phenanthroline **2.12** following procedures reported in literature[33] as well as by former group members.[34,35] This macrocycle not only possess a much smaller cavity than the Saito macrocycle **M4**, but it is also significantly more rigid. These two properties render **M6** a strong candidate for both improved polyyne stability and efficient AMT reaction.

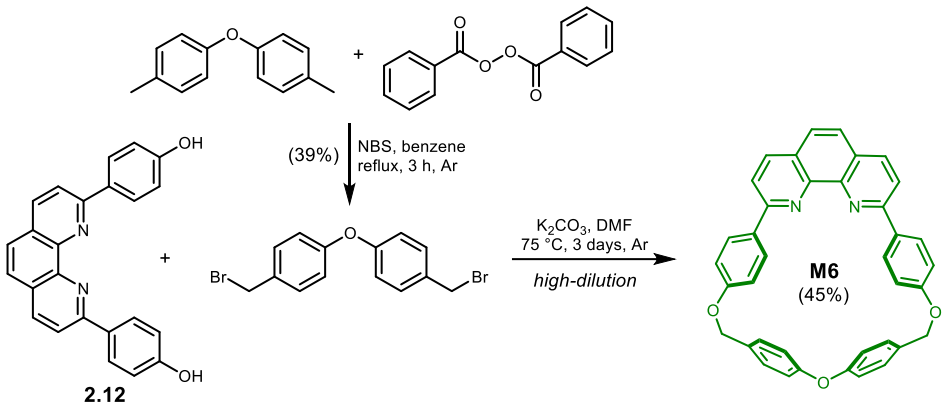

Scheme 4.18: Synthetic route to diaryl ether macrocycle **M6** from diphenol phenanthroline **2.12**.[33]

4.5.2 Preparing Alternative Tetracobalt [2]Rotaxanes

Rotaxanes with **M6** were then investigated using the same AMT Cadiot-Chodkiewicz cross-coupling conditions employed throughout Chapter 3. Supertrityl triyne bromide **3.10**, cobalt diyne **3.20** and **M6**·CuI complex were treated with the same AMT coupling conditions. After 18 hours, both supertrityl-stoppered [2]rotaxane **3.22·M6** and tetracobalt [2]rotaxane **4.1·M6** (Figure 4.14) were detected by high resolution (ESI) mass spectrometry. To our surprise, the stoppered [2]rotaxane bearing this **M6** macrocycle (**3.22·M6**) proved notably more challenging to purify than for the **M4** analogue. Initial purification by silica chromatography (petroleum ether/EtOAc) appeared to give a single species by TLC, but NMR analysis indicated that [2]rotaxane **3.22·M6** was contaminated by an impurity with ^{1}H resonances matching those of the tetracobalt tetrayne thread **4.1**. Further silica chromatography (now using a CH_2Cl_2/EtOAc solvent system) proved highly successful in separating the two, with tetracobalt tetrayne **4.1** eluting in neat CH_2Cl_2, then the [2]rotaxane **3.22·M6** eluting after addition of EtOAc. We suspect that the relatively poor solubility of the tetracobalt species in the petrol/EtOAc solvent system of the first purification resulted in this compound eluting later than might be expected.

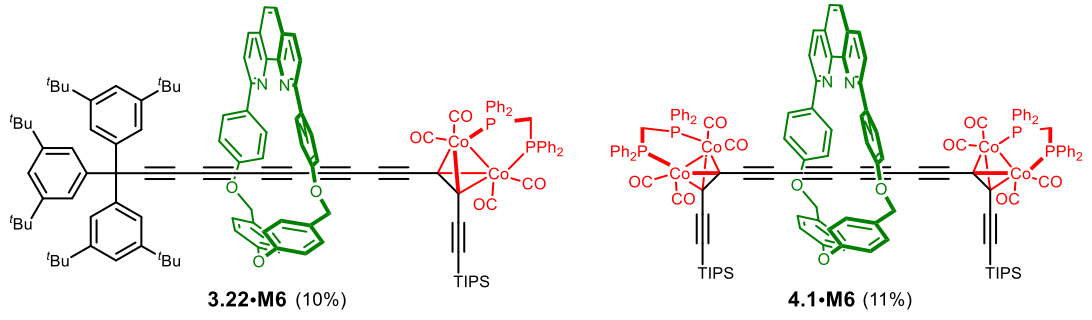

Figure 4.14: Supertrityl stoppered [2]rotaxane **3.22·M6** and tetracobalt [2]rotaxane **4.1·M6**, both bearing the tighter diaryl ether macrocycle **M6**.

NMR analysis of both **M6**-protected [2]rotaxanes revealed the expected resonances in both ^{1}H and ^{13}C spectra. For the supertrityl-stoppered [2]rotaxane **3.22·M6**, the ^{1}H NMR spectrum shows a splitting of the macrocyclic CH_2 resonance as they become diastereotopic. This is arising from a loss of symmetry made by the two different stoppering groups on this [2]rotaxane. By comparison, in the tetracobalt [2]rotaxane **4.1·M6**, which bears two identical dicobalt-based stoppers, these protons appear as the expected singlet resonance. In contrast to **M5**-based rotaxanes, the unhindered rotation of the *para*-phenylene units of **M6** mean that the Ar C-H signals do not show any splitting. Based on these initial experiments, it appears that yields of the stoppered [2]rotaxane **3.22·M6** were somewhat comparable (~20%) to those obtained using the Saito macrocycle **M4**, but were slightly reduced (~11%) for tetracobalt [2]rotaxane **4.1·M6**. Curiously, ongoing work by Dr Yueze Gao suggests that repeating this step with only minimal degassing (i.e. no specific freeze-pump-thaw step) appears to favour tetracobalt [2]rotaxane **4.1·M6** (~20%) at the expense of the stoppered [2]rotaxane **3.22·M6** (~11%). As with the **M4** system, we expect that by simple optimisation and scale-up of the reaction, it should be possible to improve yield of both [2]rotaxanes.

Single crystals of [2]rotaxane **4.1·M6** were grown from slow diffusion of MeOH into a $CHCl_3$ solution containing the [2]rotaxane. Analysis of the X-ray data (Figure 4.15) reveal the expected connectivity of **4.1·M6**. The crystals are monoclinic (*P*−1 space group) with two molecules per unit cell, and one molecule of [2]rotaxane **4.1·M6** in the asymmetric unit. In contrast to **4.1·M4** and **4.13·(M4)$_2$**, the geometry of the dppm phenyl rings is such that both are oriented away from the macrocycle. The conformational variation of the dppm group between

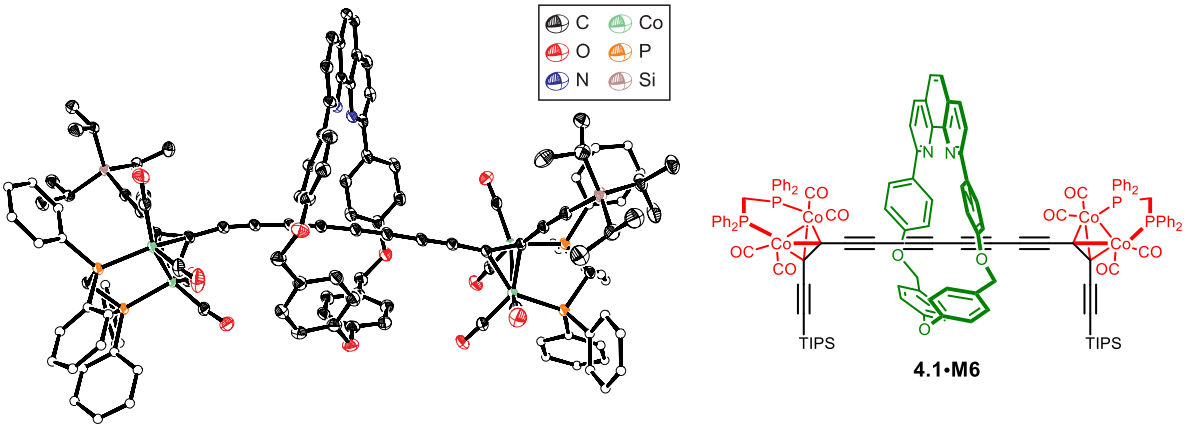

Figure 4.15: X-ray crystallographic structure of tetracobalt [2]rotaxane **4.1·M6**. (ellipsoids at 30% probability, hydrogen atoms omitted and dppm phenyl rings plotted as spheres for clarity)

X-ray structures highlights the dynamic nature of the dicobalt masking group (discussed further in Section 3.2.2.1, Chapter 3). As would be expected, bond length alternation (BLA) can be observed along the C_{sp} chain with an average BLA calculated to be 0.144 Å, a value that is more in line with the ^{t}Bu-capped tetraynes (0.151 Å) reported by Tykwinski *et al.*[10–12]

These results ultimately demonstrate a modular approach to generate the key rotaxanes for our targeted polyynes. While not explored, we anticipate that this methodology is general and would be amenable to a range of different macrocyclic geometries.

4.5.3 Towards Alternative Polyyne [*n*]Rotaxanes

Investigations by Dr Yueze Gao were made into preparing dicobalt-masked polyyne [*n*]rotaxanes bearing the **M6** macrocycle. Tetracobalt [2]rotaxane **4.1·M6** was extended to the TMS-protected diyne **4.11·M6** following the procedure for the analogous **M4**-protected [2]rotaxane described in Section 4.3. The oxidative homocoupling between the extended tetracobalt [2]rotaxane **4.12·M6** and supertrityl-stoppered [2]rotaxane **3.23·M6** was then investigated using the same Pd/Cu/benzoquinone for the analogous **M4**-protected compounds (Scheme 4.19). Through GPC analysis, it was found that the reaction was complete after 2 hours, with no further conversion observed after this point. Preliminary experiments indicate that the coupling of stoppered [2]rotaxane **3.23·M6** occurs much more quickly than for the **M4** series of compounds. As such, using the same 1:4 ratio of tetracobalt [2]rotaxane **4.12·M6** to stoppered [2]rotaxane **3.23·M6** (as for the **M4** series of compounds) instead appeared to predominantly form [3]rotaxane **3.24·(M6)**$_2$. Fortunately, switching to a 1:2 ratio allowed the product distribution to be shifted towards longer species, allowing isolation of [4]- and [5]rotaxanes **4.16·(M6)**$_3$ and **4.17·(M6)**$_4$, respectively. Rotaxane **4.16·(M6)**$_3$ has been characterised by NMR methods. While we were unable to isolate [6]rotaxane **4.18·(M6)**$_5$, we expect that it will be possible to prepare **4.18·(M6)**$_5$ (or larger [*n*]rotaxanes) simply by altering the stopper to linker ratio to 1:1 or higher.

The relative ease with which this chemistry can be applied to prepare rotaxanes with different macrocycles make this a very promising approach to preparing long, insulated polyynes. The concept of coupling stable linking and stoppering components, makes this approach highly tuneable. Simply by modulating the ratio of linker and stopper [2]rotaxanes,

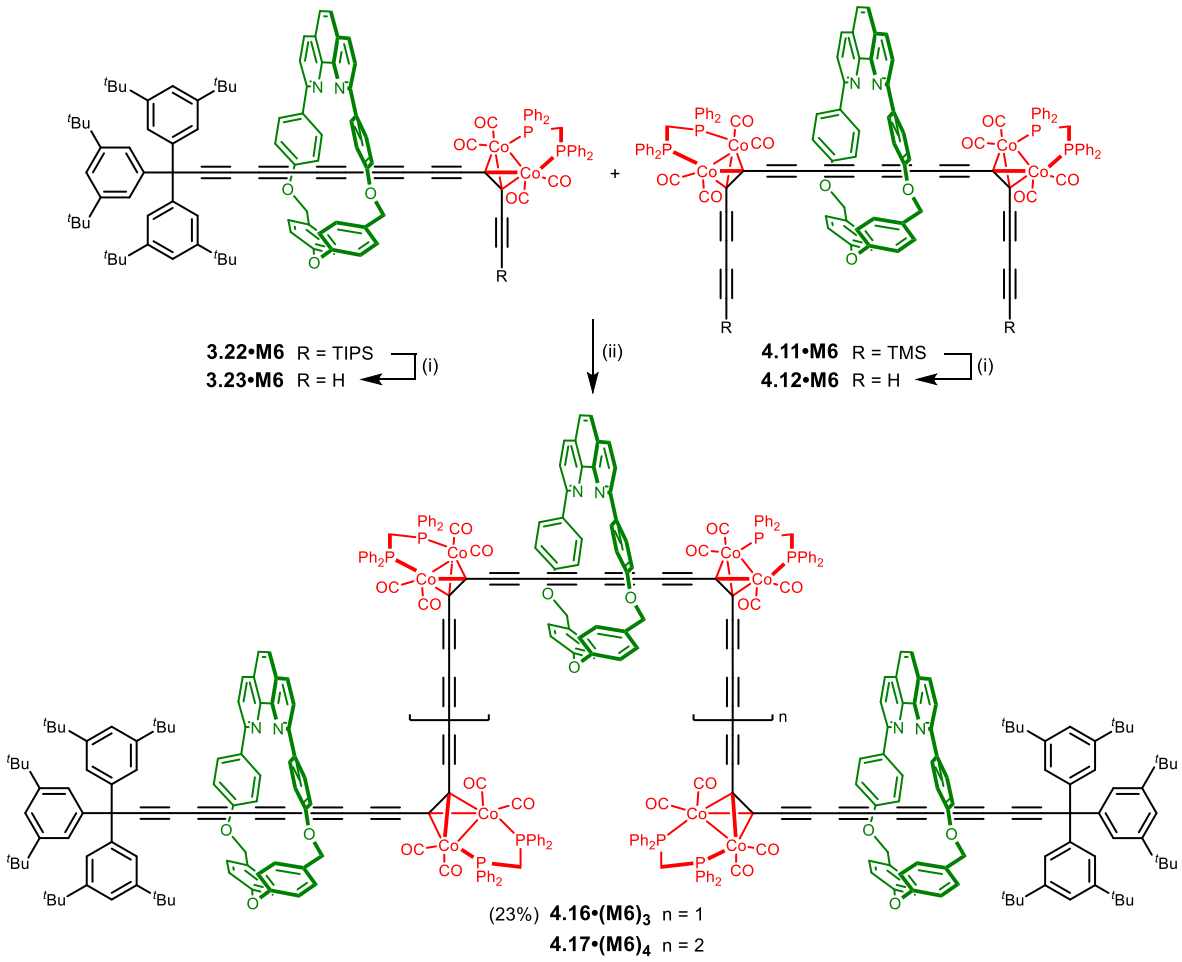

Scheme 4.19: A statistical coupling to **M6**-protected dicobalt-masked polyyne [*n*]rotaxanes. (i) TBAF, THF/H_2O (1% v/v), 20 °C, 30 min, Ar; (ii) CuI, $Pd(PPh_3)_2Cl_2$, 1,4-benzoquinone, DIPA, $CHCl_3$, 20 °C, 2 h, air.

the size distribution of resulting [*n*]rotaxanes can be adjusted. The success shown by initial unmasking experiments of [4]rotaxane **4.19**·(**M4**)$_3$ are very promising. There is still much room for optimisation, which we expect will push unmasking efficiency up further. Promising ongoing work in our group is currently screening suitable unmasking conditions. With this chemistry finessed, it will prove a novel and highly-modular approach to polyyne [*n*]rotaxanes.

4.6 Conclusions

This chapter has documented approaches to both masked cyclocarbon [*n*]catenanes and polyyne [*n*]rotaxanes. For the first time, a tetracobalt [2]rotaxane was prepared that contains two readily-cleavable silyl protecting groups, allowing for chemical transformations to be performed at both ends of the rotaxane. The tetracobalt [2]rotaxane was prepared as an unexpected but high-yielding by-product in an active metal template cross coupling reaction.

Even though the mechanism for its formation is still elusive, it can be reliably repeated both with the supertrityl and *para*-^{t}Bu bromotriyne stoppers.

Using Cu/Pd co-catalysed conditions, the oxidative homocoupling of a tetracobalt thread was used to prepare cyclic compounds but, due to suspected steric constraints imposed by the macrocycle, the coupling of the tetracobalt [2]rotaxane was not observed. Extending the tetracobalt species by one acetylene unit at each end permitted coupling of the [2]rotaxane to give [3]- and [4]catenanes – both masked precursors to cyclocarbon catenanes. Using similar coupling chemistry, but in the presence of a stoppering [2]rotaxane, we have demonstrated this approach as a simple route to dicobalt-masked [4]-, [5]- and [6]rotaxanes – precursors to polyyne [*n*]rotaxanes. We have also demonstrated good compatibility of this chemistry in preparing rotaxanes with alternative macrocycles.

Brief attempts were made to unmask [3]catenane **4.13**·(**M4**)$_2$ and [4]rotaxane **4.16**·(**M4**)$_3$ to prepare cyclo[40]carbon [3]catenane and 24-yne [4]rotaxane, respectively. Using optimised conditions from Chapter 3, we were unable to detect successful unmasking to return either the cyclocarbon or polyyne, likely due to an inefficient unmasking reaction combined with potential instability of the unmasked species. Promising preliminary experiments have demonstrated the successful *m*CPBA-mediated unmasking of octacobalt [4]rotaxane **4.16**·(**M4**)$_3$ to prepare a respective polyyne [4]rotaxane with 24 contiguous acetylene units. We expect that with careful optimisation of these conditions, it should be possible to prepare larger polyyne [*n*]rotaxanes on our journey towards insulated carbyne.

4.7 References

1 S. Saito, E. Takahashi and K. Nakazono, *Org. Lett.*, 2006, **8**, 5133–5136.

2 J. F. Woods, *Part II Thesis*, University of Oxford, 2019.

3 A. Wagner, M. . Heitz and C. Mioskowski, *Tetrahedron Lett.*, 1990, **31**, 3141–3144.

4 Puttaswamy and S. Dakshayani, *J. Chem. Sci.*, 2014, **126**, 1655–1664.

5 K. K. Rajbongshi, D. Hazarika and P. Phukan, *Tetrahedron*, 2016, **72**, 4151–4158.

6 C. Perkins, S. Libri, H. Adams and L. Brammer, *CrystEngComm*, 2012, **14**, 3033.

7 F. Homsi and G. Rousseau, *Tetrahedron Lett.*, 1999, **40**, 1495–1498.

8 L. Luo, C. Wilhelm, A. Sun, C. P. Grey, J. W. Lauher and N. S. Goroff, *J. Am. Chem. Soc.*, 2008, **130**, 7702–7709.

9 M. J. Langton, Y. Xiong and P. D. Beer, *Chem. Eur. J.*, 2015, **21**, 18910–18914.

10 R. J. Lagow, J. J. Kampa, H.-C. Wei, S. L. Battle, J. W. Genge, D. A. Laude, C. J. Harper, R. Bau, R. C. Stevens, J. F. Haw and E. Munson, *Science*, 1995, **267**, 362–367.

11 W. A. Chalifoux, R. McDonald, M. J. Ferguson and R. R. Tykwinski, *Angew. Chem. Int. Ed.*, 2009, **48**, 7915–7919.

12 R. R. Tykwinski, W. Chalifoux, S. Eisler, A. Lucotti, M. Tommasini, D. Fazzi, M. Del Zoppo and G. Zerbi, *Pure Appl. Chem.*, 2010, **82**, 891–904.

13 S. Eisler, A. D. Slepkov, E. Elliott, T. Luu, R. McDonald, F. A. Hegmann and R. R. Tykwinski, *J. Am. Chem. Soc.*, 2005, **127**, 2666–2676.

14 E. Negishi and L. Anastasia, *Chem. Rev.*, 2003, **103**, 1979–2018.

15 K. S. Sindhu, A. P. Thankachan, P. S. Sajitha and G. Anilkumar, *Org. Biomol. Chem.*, 2015, **13**, 6891–6905.

16 J. Berná, S. M. Goldup, A.-L. Lee, D. A. Leigh, M. D. Symes, G. Teobaldi and F. Zerbetto, *Angew. Chem. Int. Ed.*, 2008, **47**, 4392–4396.

17 F. Bohlmann, H. Schönowsky, E. Inhoffen and G. Grau, *Chem. Ber.*, 1964, **97**, 794–800.

18 J. A. Marsden, J. J. Miller and M. M. Haley, *Angew. Chem. Int. Ed.*, 2004, **43**, 1694–1697.

19 Y. Rubin, C. B. Knobler and F. Diederich, *J. Am. Chem. Soc.*, 1990, **112**, 4966–4968.

20 F. Diederich, Y. Rubin, O. L. Chapman and N. S. Goroff, *Helv. Chim. Acta*, 1994, **77**, 1441–1457.

21 H. L. Anderson, *Chem. Commun.*, 1999, 2323–2330.

22 Y. Gao, Y. Hou, F. Gordillo Gámez, M. J. Ferguson, J. Casado and R. R. Tykwinski, *Nat. Chem.*, 2020, **12**, 1143–1149.

23 A. S. Hay, *J. Org. Chem.*, 1962, **27**, 3320–3321.

24 N. Naveen, S. A. Babu, G. Kaur, N. A. Aslam and M. Karanam, *RSC Adv.*, 2014, **4**, 18904–18916.

25 G. Eglinton and R. Galbraith, A., *Chem. Ind. (London)*, 1956, 737.

26 M. Hoffmann, C. J. Wilson, B. Odell and H. L. Anderson, *Angew. Chem. Int. Ed.*, 2007, **46**, 3122–3125.

27 C. Roche, Q. Luo, G. Gil-Ramírez, H.-W. Jiang, D. R. Kohn, Y. Xiong, A. L. Thompson and H. L. Anderson, *J. Org. Chem.*, 2017, **82**, 7446–7462.

28 R. Rossi, A. Carpita and C. Bigelli, *Tetrahedron Lett.*, 1985, **26**, 523–526.

29 C. Ma, A. Lo, A. Abdolmaleki and M. J. MacLachlan, *Org. Lett.*, 2004, **6**, 3841–3844.

30 M. Balaz, H. A. Collins, E. Dahlstedt and H. L. Anderson, *Org. Biomol. Chem.*, 2009, **7**, 874.

31 M. C. O'Sullivan, J. K. Sprafke, D. V. Kondratuk, C. Rinfray, T. D. W. Claridge, A. Saywell, M. O. Blunt, J. N. O'Shea, P. H. Beton, M. Malfois and H. L. Anderson, *Nature*, 2011, **469**, 72–75.

32 M. Jirásek, M. Rickhaus, L. Tejerina and H. L. Anderson, *J. Am. Chem. Soc.*, 2021, **143**, 2403–2412.

33 M. Franz, J. A. Januszewski, D. Wendinger, C. Neiss, L. D. Movsisyan, F. Hampel, H. L. Anderson, A. Görling and R. R. Tykwinski, *Angew. Chem. Int. Ed.*, 2015, **54**, 6645–6649.

34 L. D. Movsisyan, M. Franz, F. Hampel, A. L. Thompson, R. R. Tykwinski and H. L. Anderson, *J. Am. Chem. Soc.*, 2016, **138**, 1366–1376.

35 P. Gawel, S. L. Woltering, Y. Xiong, K. E. Christensen and H. L. Anderson, *Angew. Chem. Int. Ed.*, 2021, **60**, 5941–5947.

4.8 Experimental

Contents

General Methods

Commercially available reagents were used as received. Dry solvents (Et_2O, THF, CH_2Cl_2, $CHCl_3$, pentane, DMF) for reactions were purified by a MBraun MB-SPS-5 bench-top SPS system under nitrogen (H_2O content < 20 ppm). All other solvents used were HPLC grade and dried over appropriate drying agents when required. Petroleum ether (petrol) had a boiling point range of 40–60 °C. *N,N,N′,N′*-Tetramethylethylenediamine (TMEDA) was dried with 3 Å molecular sieves (Linde-type) and then distilled over KOH under an Ar atmosphere prior to each use. EDTA/NH_3 solution was prepared by saturating a 1:1 solution of water/aqueous 35% NH_3 solution with tetrasodium EDTA. All solutions used during workups (NH_4Cl, $Na_2S_2O_3$ and brine) were saturated aqueous solutions, unless otherwise specified. Copper(I) chloride was freshly prepared.[1]

Reactions, unless otherwise stated, were carried out in oven-dried glassware under an Ar atmosphere. Thin layer chromatography (TLC) was carried out on aluminum-backed silica gel plates with 0.2 mm thick silica gel 60 F254 (Merck) and visualised by UV irradiation at either 254 nm or 366 nm. Preparative flash column chromatography was either carried out using flash silica gel 60 (230-400 mesh) obtained from Sigma-Aldrich, or on a Biotage Isolera One with a 200–400 nm UV detector. Size exclusion chromatography (SEC) was carried out using Bio-Beads S-X1 or S-X3, 40-80 μm (Bio Rad). Analytical GPC was carried out using JAIGEL-3H-A (8 × 500 mm) and JAIGEL-4H-A (8 × 500 mm) columns in THF + 1% pyridine as eluent with a flow rate of 1.0 mL/min. Semipreparative GPC was carried out on a Shimadzu recycling GPC system equipped with a LC-20 AD pump, SPD-20A UV detector and a set of JAIGEL 3H (20 × 600 mm) and JAIGEL 4H (20 × 600 mm) columns in THF as the eluent at a flow rate of 3.5 mL/min. Evaporation of solvents was performed at 20–50 °C and 5–1010 mbar. Reported yields refer to pure compounds dried under high vacuum (< 0.1 mbar).

^1H and ^{13}C nuclear magnetic resonance (NMR) spectra were recorded on Bruker AVIII HD 500, Bruker AVIII HD 600 (Prodigy broadband cryoprobe), Avance NEO 600 (broadband helium cryoprobe), and AVIII 700 (1H/13C/15N TCI cryoprobe) spectrometers at 500 MHz, 600 MHz, 600 MHz and 700 MHz (^1H) and 126 MHz, 151 MHz, 151 MHz and 175 MHz (^{13}C), respectively at 298 K unless stated otherwise. NMR chemical shifts were reported in ppm relative to $SiMe_4$ ($\delta = 0$) and were referenced internally with respect to residual solvent protons

using the reported values. Coupling constants are reported in Hz and ^{1}H multiplicities are reported in accordance with the following: br = broad; s = singlet; d = doublet; t = triplet; q = quartet; and m = multiplet. ^{1}H assignments were made using 2D NMR methods (COSY, NOESY, HSQC, HMBC).

^{13}C NMR spectra of cobalt carbonyl complex of alkynes often show fewer than the expected number of peaks due to the broadness and low intensity (from the slow relaxation) of the carbons bound to cobalt and the overlap between the signals from the many carbon environments.

Electrospray mass spectrometry was carried out on a Waters Micromass LCT Premier XE spectrometer using 90:10 MeOH:H_2O (+0.1% formic acid) as the mobile phase. High-resolution ESI mass spectrometry (HR-MS) measurements were performed by the mass spectrometry service at the University of Oxford on a Waters GTC classic.

UV-vis spectra were recorded in solution on a Perkin-Elmer Lambda 20 or Perkin-Elmer Lambda 25 spectrometer at 25 °C (unless otherwise noted), in fused silica cuvettes with a pathlength of 1 cm.

Raman spectra were recorded in CH_2Cl_2 solutions using a Bruker MultiRAM FT-Raman spectrometer. A continuous-wave Nd:YAG laser working at 1064 nm was employed for excitation. Raman scattering radiation was collected in a back-scattering configuration with a spectral resolution of 4 cm^{-1}.

Synthesis of Known Compounds

Bis[4-(bromomethyl)phenyl] ether[2]

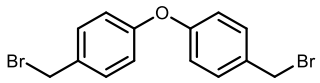

A mixture of *N*-bromosuccinimide (30 g, 2.2 eq., 17 mmol) and benzoyl peroxide (0.49 g, 75 wt%, 0.02 eq., 1.5 mmol) was added in portions over 20 min to a refluxing solution of di-*para*-tolyl ether (15 g, 1.0 eq., 76 mmol) and benzoyl peroxide (0.24 mg, 75 wt%, 0.01 eq., 760 µmol) in benzene (30.0 mL). The mixture was refluxed for 3 h. The cooled solution was filtered to remove succinimide, then washed with aqueous sodium hydroxide (1.0 M, 60 mL), water (60 mL) and then brine (60 mL). The organic extracts were dried over Na_2SO_4 and the solvent removed under reduced pressure. The solid residue was recrystallised from cyclohexanol, then from hexane to yield bis(4-bromomethylphenyl) (10 g, 29 mmol, 39%) as a white solid.

^{1}H NMR (400 MHz, $CDCl_3$) δ_H 7.37 (d, J = 8.6 Hz, 4H), 6.97 (d, J = 8.6 Hz, 4H), 4.51 (s, 4H).

Analytical data as in lit[2]

Diaryl ether phenanthroline macrocycle M6[3,4]

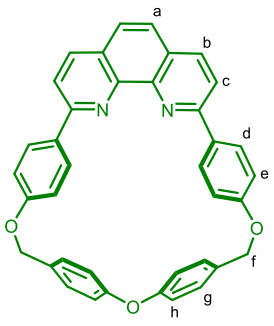

A mixture of diphenol phenanthroline **2.12** (2.00 g, 1.00 eq., 5.49 mmol) and bis(4-bromomethylphenyl) (1.95 g, 1.00 eq., 5.49 mmol) was suspended in dry DMF (400 mL) and added dropwise over a 6 h period to a stirred suspension of potassium carbonate (26.5 g, 35.0 eq., 192 mmol) in dry DMF (600 mL) at 75 °C. The reaction was stirred under Ar for 3 d. After cooling to 20 °C, the solvent was removed under reduced pressure. The residue was washed with water (excess), filtered, and purified by silica chromatography (CH_2Cl_2/EtOAc,

2%) followed by recrystallisation (CH_2Cl_2/MeOH) to yield diaryl ether macrocycle **M6** (1.39 g, 2.49 mmol, 45%) as a colourless solid.

^{1}H NMR (500 MHz, CD_2Cl_2) δ_H 8.30 (d, J = 8.3 Hz, 2H, H_b), 7.94 (d, J = 8.3 Hz, 2H, H_c), 7.88 (d, J = 8.7 Hz, 4H, H_d), 7.80 (s, 2H, H_a), 7.27 (d, J = 8.5 Hz, 4H, H_g), 7.08 (d, J = 8.6 Hz, 4H, H_h), 6.95 (d, J = 8.7 Hz, 4H, H_e), 5.31 (s, 4H, H_f).

^{13}C NMR (126 MHz, CD_2Cl_2) δ_C 159.61 (C_c-C-N), 158.20, 158.19, 146.62, 137.02 (C_b), 134.47 (C_e-C), 133.22 (C_f-C), 129.79 (C_d), 128.22 (C_h), 127.89, 126.19 (C_a), 121.24 (C_c), 121.05 (C_g), 117.28 (C_e), 70.81 (C_f).

Analytical data as in lit[3,4]

Tetracobalt tetrayne thread 4.1[5]

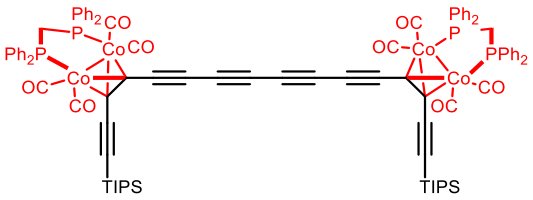

CuCl (2.6 g, 25 eq., 26 mmol) was added to a solution of deprotected cobalt diyne (0.90 g, 1.0 eq., 1.04 mmol) in dry CH_2Cl_2 (350 mL). The mixture was vigorously stirred under O_2 for 5 min. TMEDA (2.7 g, 3.5 mL, 23 eq., 23 mmol) was added to the solution, and was stirred vigorously under an O_2 atmosphere for 30 min). Pet. ether (150 mL) was added and the mixture passed through a short silica plug. The material was recrystallised from CH_2Cl_2/MeOH to yield tetracobalt tetrayne thread (0.70 g, 0.40 mmol, 78%) as a dark red crystalline solid.

^{1}H NMR (400 MHz, $CDCl_3$) δ_H 7.42 (dt, J = 8.8, 5.7 Hz, 8H, Ar-H), 7.33 – 7.24 (m, 24H, Ar-H), 7.19 (t, J = 7.1 Hz, 8H, Ar-H), 3.44 (q, J = 11.1 Hz, 4H, PCH_2P), 1.14 (s, 42H, Si^iPr_3).

^{31}P{H} NMR (162 MHz, $CDCl_3$) δ_P 38.96.

Analytical data as in lit[5]

1,4-Diiodobuta-1,3-diyne[6]

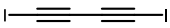

Silver nitrate (26 mg, 0.15 eq., 0.15 mmol) and *N*-iodosuccinimide (480 mg, 2.1 eq., 2.2 mmol) were added to a solution of bis-TMS-butadiyne (200 mg, 1.0 eq., 1.0 mmol) in dry DMF (20 mL). A drying tube was fitted, and the reaction vessel wrapped in aluminum foil. The reaction mixture was stirred at 20 °C for 4.5 h. Upon complete reaction (TLC), the mixture was treated with 5% LiCl solution (75 mL) and Et_2O (50 mL). The organic layer was extracted, then the aqueous later washed with Et_2O (2 × 25 mL) and dried over Na_2SO_4. Silica chromatography (pet. ether) was used to obtain 1,4-diiodobuta-1,3-diyne (230 mg, 0.77 mmol, 75%) as pale-yellow crystals. This material should be stored at −18 °C prior to use.

^{13}C NMR (126 MHz, $CDCl_3$) δ_C 79.98, -2.70.

Analytical data as in lit[6]

Synthesis of Novel Compounds

Supertrityl monoyne bromide 4.5

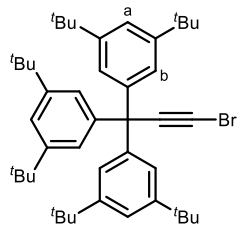

Tris(3,5-di-*tert*-butylphenyl)methyl acetylene (200 mg, 0.33 mmol) was dissolved in dry Et_2O (10 mL) under an N_2 atmosphere and the solution cooled to −78 °C. *n*-BuLi (0.25 mL, 0.36 mmol, 1.6 M in hexanes) was added dropwise before slowly warming the mixture to −30 °C. *N*-Bromosuccinimide (71 mg, 0.40 mmol) was quickly added and the reaction stirred at −25 °C for 4 h. The reaction was quenched with Na_2SO_3 solution (10 mL), the organic extracted, washed with H_2O (10 mL) and then brine (10 mL). The organic extracts were dried over Na_2SO_4 before evaporating solvent under reduced pressure. The crude material was purified by SiO_2 chromatography (pet. ether/CH_2Cl_2, gradient elution from 0 to 10%) to yield the monoyne bromide (150 mg, 65%) as a pale yellow solid.

^{1}H NMR (500 MHz, $CDCl_3$) δ_H 7.27 (t, J = 1.8 Hz, 3H, H_a), 6.96 (d, J = 1.8 Hz, 6H, H_b), 1.22 (s, 54H, ^{t}Bu).

^{13}C NMR (126 MHz, $CDCl_3$) δ_C 149.94 (C_a-C-^{t}Bu), 144.71 (C_b-C), 123.92 (C_b), 120.11 (C_a), 86.96 (C≡C-Br), 57.47 (C-Ar_3), 42.37 (C≡C-Br), 34.96 (C-$(CH_3)_3$), 31.54 (C-$(CH_3)_3$).

p-^{t}Bu alcohol

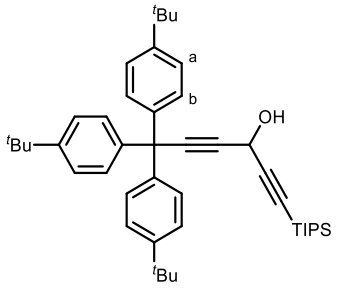

Tris(4-(*tert*-butyl)phenyl)prop-2-yne (2.4 g, 1.0 eq., 5.5 mmol) was dissolved in dry THF (250 mL). The solution was cooled to −40 °C and sparged with Ar for 15 min. *n*-BuLi (370 mg,

2.3 mL, 2.5 M in hexanes, 1.1 eq., 5.8 mmol) was added dropwise via syringe and the reaction was stirred at −40 °C for 15 mins before cooling to −78 °C. Neat (triisopropylsilyl)propiolaldehyde (1.3 g, 1.1 eq., 6.1 mmol) was added to the mixture over 5 min, then the reaction warmed to 20 °C over 1 h. The reaction was quenched by addition of sat. aqueous NH_4Cl solution (75 mL) before addition of Et_2O (100 mL). The organic phase was extracted, washed with further sat. aqueous NH_4Cl solution (100 mL), H_2O (100 mL), then brine (100 mL) before drying over Na_2SO_4 and removal of solvent under reduced pressure. The crude material was purified by silica chromatography (pet. ether/CH_2Cl_2, gradient elution from 0 to 25%) to yield *p*-^{t}Bu alcohol (2.6 g, 4.0 mmol, 73%) as a white solid.

^{1}H NMR (500 MHz, $CDCl_3$) δ_H 7.28 (d, J = 8.5 Hz, 6H, H_b), 7.16 (d, J = 8.7 Hz, 6H, H_a), 5.27 (d, J = 8.1 Hz, 1H, O<u>H</u>), 2.22 (d, J = 8.1 Hz, 1H, C<u>H</u>OH), 1.31 (s, 27H, ^{t}Bu), 1.10 (s, 21H, Si^{i}Pr$_3$).

^{13}C NMR (126 MHz, $CDCl_3$) δ_C 149.55 (C_a-<u>C</u>), 142.15 (C_b-<u>C</u>), 128.79 (C_a), 124.94 (C_b), 104.57 (C≡C), 91.16 (C≡<u>C</u>-Si^{i}Pr$_3$), 85.72 (C≡C), 81.86 (C≡C), 54.39 (<u>C</u>-Ar$_3$), 53.26 (<u>C</u>-OH), 34.53 (<u>C</u>-(CH$_3$)$_3$), 31.51 (C-(<u>C</u>H$_3$)$_3$), 18.73 (CH(<u>C</u>H$_3$)$_2$), 11.28 (<u>C</u>H(CH$_3$)$_2$).

HRMS m/z = 669.4456 $[M+Na]^+$ ($C_{45}H_{62}OSiNa^+$ requires 669.4462).

***p*-^{t}Bu ketone**

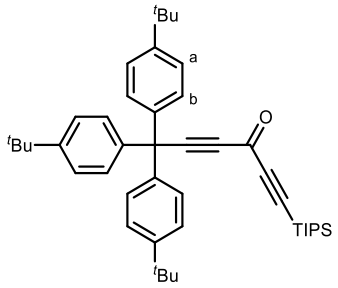

p-^{t}Bu alcohol (2.6 g, 1.0 eq., 4.0 mmol) was dissolved in dry CH_2Cl_2 (40 mL) and was sparged with Ar for 10 min. Celite (3 g) and mol. sieves (3 Å, 3 g) were added before addition of pyridinium chlorochromate (1.6 g, 1.8 eq., 7.2 mmol). The reaction stirred at 20 °C under Ar for 20 h. The reaction was filtered through a short silica plug and the solvent removed under reduced pressure. The crude material was purified by silica chromatography (pet. ether/CH_2Cl_2, gradient elution from 0 to 33%) to yield *p*-^{t}Bu ketone (2.2 g, 3.3 mmol, 83%) as a white solid.

^{1}H NMR (500 MHz, $CDCl_3$) δ_H 7.30 (d, J = 8.7 Hz, 6H, H_b), 7.14 (d, J = 8.5 Hz, 6H, H_a), 1.31 (s, 27H, ^{t}Bu), 1.12 (d, J = 5.2 Hz, 21H, Si^{i}Pr$_3$).

^{13}C NMR (126 MHz, $CDCl_3$) δ_H 160.77 (C=O), 150.18 (C_a-C), 140.57 (C_b-C), 128.81 (C_a), 125.22 (C_b), 105.40 (C≡C), 100.12 (C≡C-Si^{i}Pr$_3$), 97.07 (C≡C), 85.57 (C≡C), 55.07 (C-Ar$_3$), 34.59 (C-(CH$_3$)$_3$), 31.47 (C-(CH$_3$)$_3$), 18.64 (CH(CH$_3$)$_2$), 11.18 (CH(CH$_3$)$_2$).

HRMS m/z = 645.4476 $[M+H]^+$ ($C_{45}H_{61}OSi^+$ requires 645.4486).

***p*-^{t}Bu dibromoolefin**

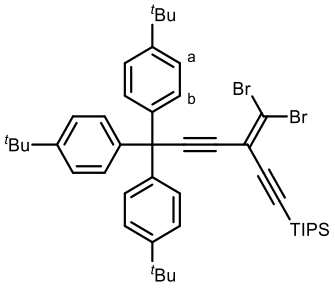

To a solution of triphenylphosphine (4.91 g, 2.50 eq., 18.7 mmol) in dry CH_2Cl_2 (150 mL) was added a solution of carbon tetrabromide (3.10 g, 1.25 eq., 9.36 mmol) in dry CH_2Cl_2 (100 mL) under Ar at 0 °C over a period of 10 min. The mixture warmed to 20 °C then stirred for 1 h. *p*-^{t}Bu ketone (4.83 g, 1.00 eq., 7.49 mmol) dissolved in dry CH_2Cl_2 (75 mL) was added and the reaction stirred for 24 h at 20 °C. Once complete, the reaction mixture was concentrated to ~50 mL under reduced pressure. Pet. ether (150 mL) was added and a white precipitate of phosphine salts, in addition to an oily residue, was formed. The supernatant was decanted and passed through a celite plug. CH_2Cl_2 (25 mL) was added to dissolve the remaining oily residue, then pet. ether (150 mL) was added to precipitate, and the supernatant again decanted and passed through a celite plug (this process was repeated a further two times). The filtrate was concentrated under reduced pressure before purification of the crude material by silica chromatography (pet. ether/CH_2Cl_2, gradient elution from 0 to 20%) to yield the *p*-^{t}Bu dibromoolefin (5.1 g, 6.4 mmol, 85%) as a white solid.

^{1}H NMR (500 MHz, $CDCl_3$) δ_H 7.28 (d, J = 8.7 Hz, 6H, H_b), 7.19 (d, J = 8.5 Hz, 6H, H_a), 1.31 (s, 27H, ^{t}Bu), 1.12 – 1.09 (m, 21H, Si^{i}Pr$_3$).

^{13}C NMR (126 MHz, $CDCl_3$) δ_C 149.63 (C_a-C), 141.72 (C_b-C), 128.84 (C_a), 124.96 (C_b), 115.10 (C=CBr_2), 107.55 (C≡C), 102.92 (C≡C), 102.67 (C=CBr_2), 99.27 (C≡C), 82.03 (C≡C), 55.48 (C-Ar_3), 34.54 (C-$(CH_3)_3$), 31.51 (C-(CH_3)$_3$), 18.76 (CH(CH_3)$_2$), 11.29 (CH$(CH_3)_2$).

HRMS *m/z* = 799.2903 $[M+H]^+$ ($C_{46}H_{61}{}^{79}Br_2Si^+$ requires 799.2904).

***p*-^{t}Bu TIPS-protected triyne**

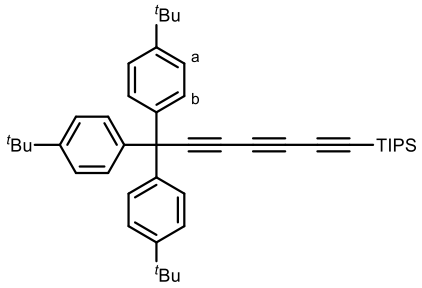

n-BuLi (490 mg, 3.0 mL, 2.5 M in hexanes, 1.2 eq., 7.6 mmol) was added to a solution of *p*-^{t}Bu dibromoolefin (5.1 g, 1.0 eq., 6.3 mmol) in pentane (250 mL) at −78 °C under Ar [Note: the dibromoolefin is not fully soluble], over a period of 10 min. The reaction mixture was warmed to 25 °C over 1 h, then quenched by addition of a solution of sat. aqueous NH_4Cl (70 mL). The organic layer was extracted, washed with H_2O (50 mL), then brine (50 mL). The organic extract was dried over Na_2SO_4 and the solvent removed under reduced pressure. The crude material was purified by silica chromatography (pet. ether/CH_2Cl_2, 2%) to afford *p*-^{t}Bu triyne (3.8 g, 6.0 mmol, 95%) as an off-white solid.

^{1}H NMR (500 MHz, $CDCl_3$) δ_H 7.28 (d, *J* = 8.5 Hz, 6H, H_b), 7.10 (d, *J* = 8.5 Hz, 6H, H_a), 1.30 (s, 27H, ^{t}Bu), 1.07 (d, *J* = 1.9 Hz, 21H, Si^{i}Pr$_3$).

^{13}C NMR (126 MHz, $CDCl_3$) δ_C 149.97 (C_a-C), 141.19 (C_b-C), 128.73 (C_a), 125.13 (C_b), 90.07 (C≡C), 84.69 (C≡C-Si^{i}Pr$_3$), 84.61 (C≡C), 69.72 (C≡C), 63.52 (C≡C), 61.39 (C≡C), 55.41 (CAr_3), 34.58 (C-$(CH_3)_3$), 31.48 (C-(CH_3)$_3$), 18.66 (CH(CH_3)$_2$), 11.41 (CH$(CH_3)_2$).

HRMS *m/z* = 641.4537 $[M+H]^+$ ($C_{46}H_{61}Si^+$ requires 641.4537).

***p*-^{t}Bu triyne**

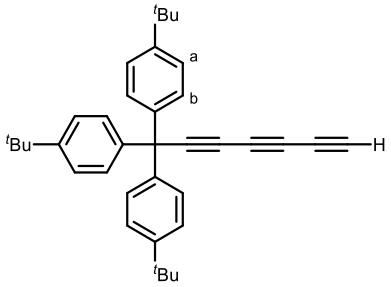

p-^{t}Bu TIPS-protected triyne (38 mg, 1.0 eq., 60 μmol) was dissolved in dry THF (5 mL). Water (1 mL) and TBAF (20 mg, 75 μL, 1.0 M, 1.3 eq., 75 μmol) was added dropwise. The reaction was stirred at 20 °C under Ar for 15 min before quenching with NH_4Cl solution (5 mL). Pet. ether (10 mL) was added and the organic layer extracted, washed with water (10 mL), then brine (10 mL). The organic extracts were dried over Na_2SO_4 and the solvent removed under reduced pressure. The crude material was purified by silica chromatography (pet. ether) to yield *p*-^{t}Bu triyne (27 mg, 56 μmol, 93%) as a white solid.

^{1}H NMR (500 MHz, $CDCl_3$) δ_H 7.30 (d, J = 8.5 Hz, 6H, H_b), 7.11 (d, J = 8.7 Hz, 6H, H_a), 2.10 (s, 1H, C≡C<u>H</u>), 1.31 (s, 27H, ^{t}Bu).

^{13}C NMR (126 MHz, $CDCl_3$) δ_C 150.07 (C_a-<u>C</u>), 141.04 (C_b-<u>C</u>), 128.75 (C_a), 125.18 (C_b), 84.24 (C≡C), 69.29 (C≡C), 68.75 (C≡C), 67.17 (C≡<u>C</u>H), 62.61 (C≡C), 61.13 (C≡C), 55.35 (C-Ar_3), 34.60 (<u>C</u>-$(CH_3)_3$), 31.49 (C-(<u>C</u>$H_3)_3$).

***p*-^{t}Bu bromotriyne 4.6**

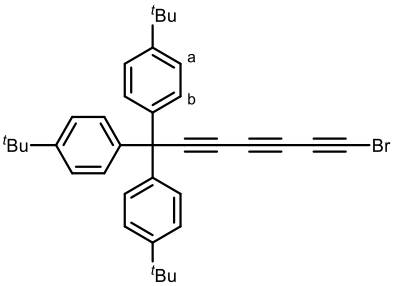

p-^{t}Bu triyne (2.9 g, 1.0 eq., 5.9 mmol), *N*-bromosuccinimide (1.6 g, 1.5 eq., 8.8 mmol) and silver(I) nitrate (200 mg, 0.20 eq., 1.2 mmol) were suspended in dry acetone (350 mL) and stirred under Ar for 4 h. The solvent was reduced to ~20 mL and pet. ether/CH_2Cl_2 (1:1, 200 mL) was added. The solution as passed through a SiO_2 plug (petrol/CH_2Cl_2, 1:1) and

concentrated under reduced pressure. The crude material was dissolved in minimal CH_2Cl_2, then precipitated into MeOH and filtered to yield *p*-^{t}Bu bromotriyne **4.6** (3.1 g, 5.5 mmol, 93%) as a pale yellow solid.

^{1}H NMR (500 MHz, $CDCl_3$) δ_C 7.30 (d, J = 8.6 Hz, 6H, H_a), 7.10 (d, J = 8.5 Hz, 6H, H_b), 1.31 (s, 27H, ^{t}Bu).

^{13}C NMR (126 MHz, $CDCl_3$) δ_C 150.07 (C_a-C), 141.07 (C_b-C), 128.75 (C_a), 125.17 (C_b), 83.93 (C≡C), 69.40 (C≡C), 66.28 (C≡C), 63.32 (C≡C), 59.81 (C≡C), 55.39 (CAr_3), 40.68 (C≡C-Br), 34.60 (C$(CH_3)_3$), 31.48 (C(CH_3)$_3$).

Deprotected tetracobalt tetrayne thread 4.8

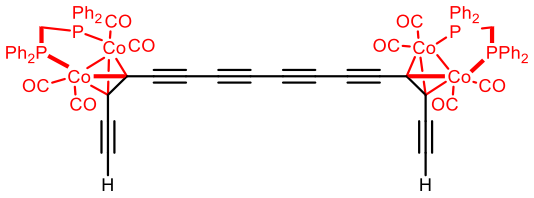

Tetracobalt tetrayne thread (0.18 g, 1.0 eq., 0.10 mmol) was dissolved in dry THF (30 mL) containing water (0.30 mL). TBAF (1.0 M in THF, 0.27 g, 1.0 mL, 10 eq., 1.0 mmol) was added dropwise and the mixture stirred at 20 °C for 30 min. The reaction was quenched with addition of sat. aqueous NH_4Cl solution (20 mL), then Et_2O (20 mL) was added, and the organic layer extracted. The aqueous layer was washed with Et_2O (2 × 10 mL) and the combined extracts washed with brine (20 mL), then dried over Na_2SO_4. The solvent was removed under reduced pressure and the crude material purified by silica chromatography (pet. ether/CH_2Cl_2, gradient elution from 0 to 100%) to yield deprotected tetracobalt tetrayne thread **4.8** (0.14 g, 0.98 mmol, 94%) as a red-brown solid.

^{1}H NMR (500 MHz, CD_2Cl_2) δ_H 7.42 – 7.37 (m, 8H, Ar-H), 7.37 – 7.30 (m, 16H, Ar-H), 7.30 – 7.22 (m, 16H, Ar-H), 3.89 (t, J = 1.8 Hz, 2H, C≡CH), 3.47 (t, J = 10.5 Hz, 4H, P-CH_2).

^{13}C NMR (126 MHz, CD_2Cl_2) δ_C 202.79 (C≡O), 135.68 (t, $J_{C\text{-}P}$ = 21.1 Hz, Ar-C), 134.50 (t, $J_{C\text{-}P}$ = 20.4 Hz, Ar-C), 132.29 (t, $J_{C\text{-}P}$ = 6.4 Hz, Ar-C), 131.95 (t, $J_{C\text{-}P}$ = 6.1 Hz, Ar-C), 130.58 (d, $J_{C\text{-}P}$ = 20.9 Hz, Ar-C), 128.88 (t, $J_{C\text{-}P}$ = 6.4 Hz, Ar-C), 85.81 (C≡CH), 85.69, 83.41, 82.28, 72.07 (Co-C), 70.66, 66.92, 65.24 (Co-C), 37.43 (t, $J_{C\text{-}P}$ = 21.3 Hz, P-CH_2).

^{31}P{H} NMR (203 MHz, CD_2Cl_2) δ_P 39.24.

HRMS *m/z* = 1420.9410 $[M+H]^+$ ($C_{74}H_{46}Co_4O_8P_4^+$ requires 1420.9398)

Cobalt 4-ring 4.9

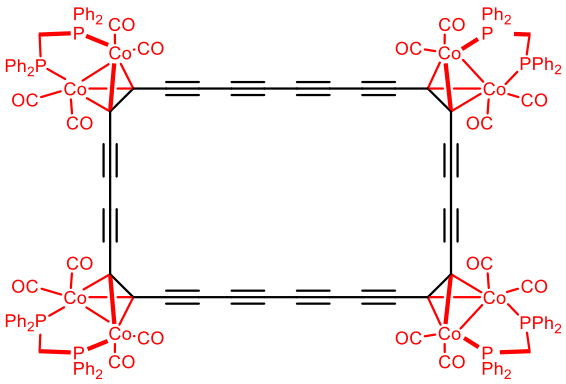

Dry $CHCl_3$ (100 mL) and freshly-distilled diisopropylamine (130 mg, 180 µL, 20 eq., 1.3 mmol) were added to deprotected tetracobalt tetrayne thread (90 mg, 1.0 eq., 63 µmol), bis(triphenylphosphine)palladium(II) dichloride (30 mg, 0.67 eq., 42 µmol), copper(I) iodide (40 mg, 3.3 eq., 21 µmol) and benzoquinone (93 mg, 14 eq., 0.86 mmol). A drying tube was fitted, and reaction stirred at 20 °C in air for 24 h. The mixture was passed through a short silica plug ($CHCl_3$) before removing the solvent under reduced pressure. The crude material was purified by recycling GPC, then recrystallised from $CHCl_3$/pentane to give the cyclic dimer **4.9** (30 mg, 11 µmol, 34%) and cyclic trimer **4.10** (9.1 mg, 2.1 µmol, 10%) as dark red crystalline solids.

^{1}H NMR (600 MHz, CD_2Cl_2) δ_H 7.59 – 7.36 (br m, 32H, Ar-H), 7.36 – 7.11 (br m, 48H, Ar-H), 3.72 – 3.25 (br m, 8H, P-CH_2).

^{13}C NMR (151 MHz, CD_2Cl_2) δ_C 202.67 (C≡O), 135.09 (br, Ar-C), 132.21, 130.63 (Ar-C), 128.97 (Ar-C), 88.34, 84.55 (br) 84.02, 82.62 (br), 70.58, 66.92, 38.52 (br, P-CH_2). *(2 carbons not distinguished)*

^{31}P{H} NMR (243 MHz, CD_2Cl_2) δ_P 40.25.

UV-vis (CH_2Cl_2) λ_{max} (ε) 557 (20900), 384 (180000), 326 (175000), 274 (181000) nm.

GPC (analytical, THF/pyridine 1% v/v) retention time = 43.02 min.

IR (ATR) (only selected signals) 2922.75 (C-H), 2852.28 (C-H), 2148.20 (w, C≡C), 2035.06 (s, C=O), 2015.34 (s, C=O), 1990.42 (s, C=O) cm^{-1}.

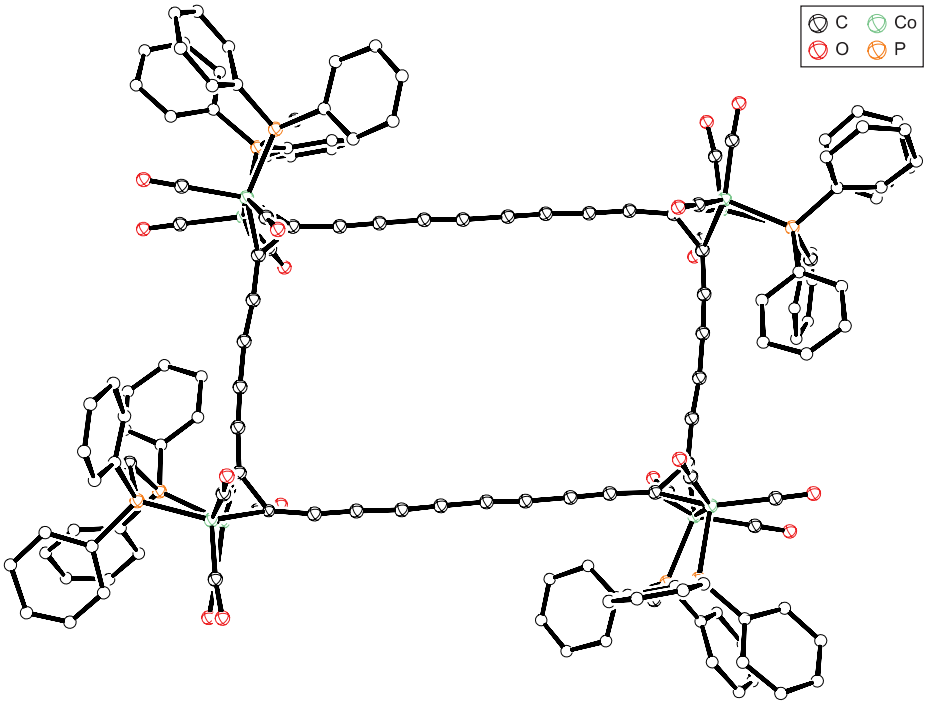

Figure S4.1: Preliminary X-ray crystallographic structure of cobalt 4-ring **4.9**. (all atoms are depicted as spheres of arbitrary radius, hydrogen atoms omitted)

Cobalt 6-ring 4.10

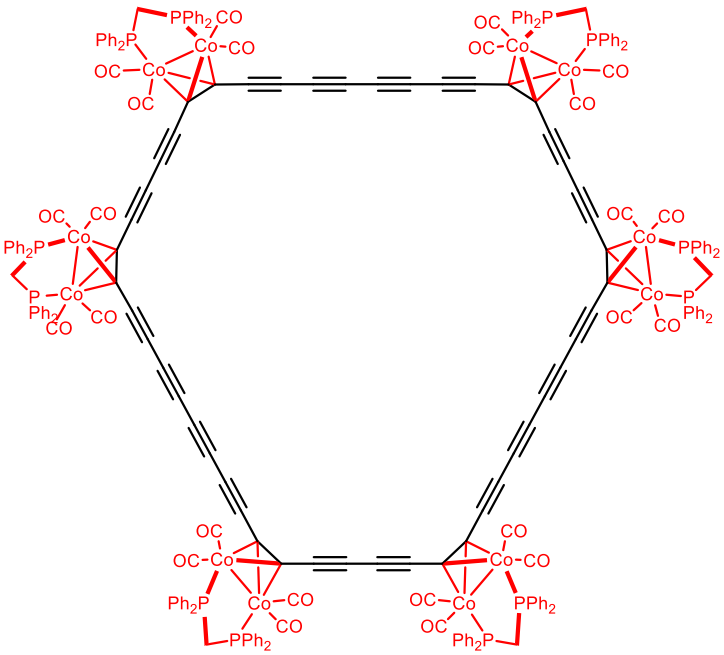

Procedure as above

^{1}H NMR (600 MHz, CD_2Cl_2) δ_H 7.38 – 7.25 (m, 62H, Ar-H), 7.22 (dd, J = 7.5, 4.8 Hz, 34H, Ar-H), 7.17 (t, J = 7.5 Hz, 24H, Ar-H), 3.44 (br s, 12H, P-CH_2).

^{31}P{H} NMR (243 MHz, CD_2Cl_2) δ_P 39.72.

^{13}C NMR (151 MHz, CD_2Cl_2) δ_C 202.74 (C≡O), 135.45 – 134.63 (m), 132.27 (t, $J_{C\text{-}P}$ = 6.1 Hz, Ar-C), 132.09 (t, $J_{C\text{-}P}$ = 6.2 Hz, Ar-C), 130.62 (Ar-C), 129.19 – 128.84 (m, Ar-C), 88.60, 85.37 (Co-C), 83.69, 83.40 (Co-C), 80.39, 78.44, 71.26, 67.26, 38.80 (t, $J_{C\text{-}P}$ = 21.9 Hz, P-CH_2).

GPC (analytical, THF/pyridine 1% v/v) retention time = 42.35 min.

Extended tetracobalt tetrayne thread 4.11

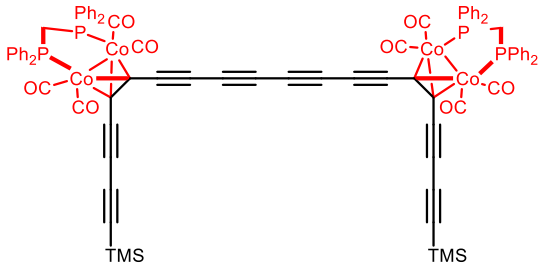

Deprotected tetracobalt thread (240 mg, 1.0 eq., 0.17 mmol) was dissolved in dry CH_2Cl_2 (250 mL). Trimethylsilyl acetylene (1.7 g, 1.2 mL, 50 eq., 8.5 mmol) and copper(I) chloride (0.75 g, 45 eq., 76 mmol) were added and O_2 bubbled through the vigorously-stirred solution. Freshly distilled TMEDA (0.78 mg, 1.0 mL, 40 eq., 6.8 mmol) was added to the reaction mixture. Additional trimethylsilyl acetylene (1.7 g, 1.2 mL, 50 eq., 8.5 mmol) was added over a period of 30 min via syringe pump. The reaction was monitored by TLC and, upon completion, was quenched by addition of water (100 mL). The organic layer was extracted and washed with water (2 x 150 mL), then brine (150 mL) before drying over Na_2SO_4. The solvent was removed under reduced pressure and the crude material initially purified by a SiO_2 plug, flushing first with petrol to remove the bis-TMS butadiyne, then 1:1 pet. ether/CH_2Cl_2. The crude material was then subject to SiO_2 chromatography (pet. ether/EtOAc, gradient elution from 0 to 40%), to yield the TMS-protected extended thread **4.11** (0.18 g, 0.11 mmol, 66%) as a red solid. R_f (pet. ether/EtOAc, 33%) = 0.60.

^{1}H NMR (600 MHz, CD_2Cl_2) δ_H 7.39 – 7.31 (m, 24H, Ar-H), 7.31 – 7.25 (m, 16H, Ar-H), 3.59 – 3.39 (m, 4H, P-CH_2), 0.26 (s, 18H, $SiMe_3$).

^{13}C NMR (151 MHz, CD_2Cl_2) δ_C 202.78 (C≡O), 202.12 (C≡O), 134.87 (q, $J_{C\text{-}P}$ = 23.0 Hz, Ar-C), 132.13 (t, $J_{C\text{-}P}$ = 6.2 Hz, Ar-C), 130.68 (d, $J_{C\text{-}P}$ = 9.5 Hz, Ar-C), 129.01 (dt, $J_{C\text{-}P}$ = 6.7, 3.2 Hz, Ar-C), 93.86, 89.85, 83.40, 83.09, 82.75, 80.30, 71.04, 69.84 (br, Co-C), 67.07, 66.36 (br, Co-C), 38.50 (t, $J_{C\text{-}P}$ = 22.0 Hz, P-CH_2), -0.21 ($SiMe_3$).

^{31}P{H} NMR (243 MHz, CD_2Cl_2) δ_P 39.63.

HRMS *m/z* = 1615.0386 $[M+H]^+$ ($C_{84}H_{63}Co_4O_8P_4Si_2^+$ requires 1615.0335)

Deprotected extended tetracobalt tetrayne thread 4.12

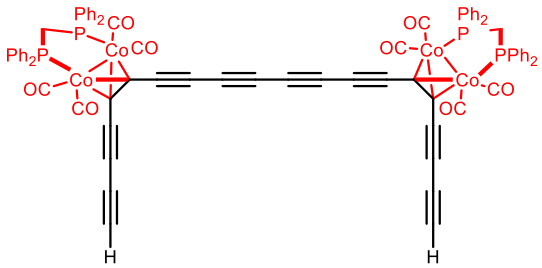

Method 1: Extended tetracobalt thread **4.11** (30 mg, 1.0 eq., 19 μmol) and K_2CO_3 (39 mg, 15 eq., 0.28 mmol) were dissolved in a 1:1 solution of THF (5 mL) and MeOH (5 mL). Water (0.1 mL) was added and the solution stirred at 20 °C for 20 min before addition of water (15 mL) and Et_2O (15 mL). The organic layer was separated, washed with water (10 mL) then brine (10 mL). The organic extract was dried over Na_2SO_4 and the solvent removed under reduced pressure to yield deprotected extended tetracobalt thread **4.12** (8.3 mg, 5.6 μmol, 30%) as a red-brown solid. R_f (pet. ether/EtOAc, 33%) = 0.45.

Method 2: Extended tetracobalt thread **4.11** (65 mg, 1.0 eq., 40 μmol) was dissolved in THF (25 mL) and water (0.25 mL, 1% v/v). TBAF solution (1.0 M in THF, 11 mg, 40 μL, 1.0 eq., 40 μmol) solution was added and the mixture stirred at 20 °C for 5 min before addition of aqueous sat. aqueous NH_4Cl (25 mL). Et_2O (10 mL) was added and the organic layer extracted, washed with water (20 mL), then brine (20 mL). The combined organic extracts were dried over Na_2SO_4 and the solvent reduced to minimal volume (~1-2 mL) under reduced pressure. $CHCl_3$ (25 mL) was added, then the solvent reduced to minimal volume under reduced pressure (this process was repeated twice more). The solution of deprotected extended tetracobalt tetrayne thread **4.12** in $CHCl_3$ was used directly in the next step.

Note: This compound is unstable as a dry solid, but stable both in solution and on silica. This compound should be handled in solution containing a minimal amount of solvent. Method 2 allows a solution of thread **4.12** in $CHCl_3$ to be obtained prior to the coupling step.

^{1}H NMR (600 MHz, CD_2Cl_2) δ_H 7.40 – 7.32 (m, 24H, Ar-H), 7.31 – 7.25 (m, 16H, Ar-H), 3.55 – 3.42 (m, 4H, P-CH_2), 2.93 (s, 2H, C≡CH).

^{13}C NMR (151 MHz, CD_2Cl_2) δ_C 202.86 (C≡O), 134.77 (br, Ar-C), 132.12 (t, $J_{C\text{-}P}$ = 6.2 Hz, Ar-C), 130.71 (d, $J_{C\text{-}P}$ = 7.7 Hz, Ar-C), 129.01 (q, $J_{C\text{-}P}$ = 3.8 Hz, Ar-C), 83.32, 81.71, 78.88, 74.14 (C≡CH), 71.06, 70.09, 67.05, 38.55 (br, P-CH_2).

^{31}P{H} NMR (243 MHz, CD_2Cl_2) δ_P 39.68.

HRMS *m/z* = 1468.9429 $[M\text{-}H]^-$ ($C_{78}H_{45}Co_4O_8P_4^-$ requires 1468.9425)

Extended cobalt 4-ring 4.13

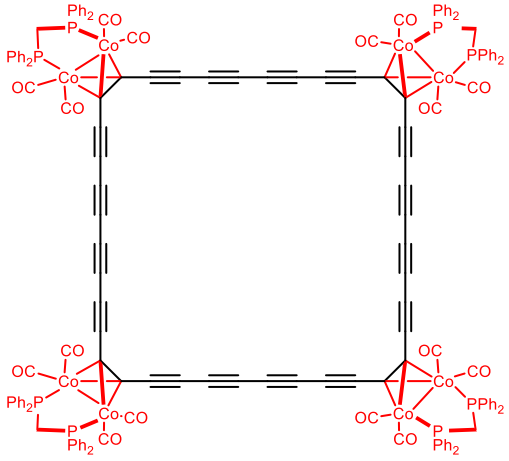

Dry $CHCl_3$ (60 mL) and freshly-distilled diisopropylamine (0.15 g, 0.21 mL, 40 eq., 1.5 mmol) were added to bis(triphenylphosphine)palladium(II) dichloride (35 mg, 1.3 eq., 50 μmol), copper(I) iodide (47 mg, 6.7 eq., 0.25 mmol) and benzoquinone (61 mg, 15 eq., 0.56 mmol). The mixture was stirred in air before addition of deprotected extended tetracobalt tetrayne thread **4.12** (55 mg, 1.0 eq., 37 μmol) in $CHCl_3$ (15 mL) over 1 h via syringe pump. After complete addition, the reaction was stirred at 20 °C in air for a further 1 h. Water (75 mL) was added and the organic layer was extracted, washed with additional water (50 mL) then brine (50 mL), before being dried over Na_2SO_4 and the solvent removed under reduced pressure. The crude material was subject to silica chromatography (pet. ether/CH_2Cl_2, gradient elution from

30 to 40%) to yield cobalt 4-ring **4.13** (3.6 mg, 1.2 µmol, 6.6%) and cobalt 6-ring **4.14** (7.6 mg, 1.7 µmol, 14%) as dark brown solids.

^{1}H NMR (600 MHz, CD_2Cl_2) δ_H 7.43 – 7.33 (m, 48H, Ar-H), 7.33 – 7.26 (m, 32H, Ar-H), 3.47 (br s, 8H, P-CH_2).

^{13}C NMR (151 MHz, CD_2Cl_2) δ_C 202.14 (C≡O), 134.72 (t, $J_{C\text{-}P}$ = 22.2 Hz, Ar-C), 132.14 (t, $J_{C\text{-}P}$ = 6.2 Hz, Ar-C), 130.7 (Ar-C), 129.04 (t, $J_{C\text{-}P}$ = 4.9 Hz, Ar-C), 83.62, 83.18, 71.07, 67.05, 38.94 (t, $J_{C\text{-}P}$ = 21.1 Hz, P-CH_2). *(2 carbons not distinguished)*

^{31}P{H} NMR (243 MHz, CD_2Cl_2) δ_P 40.38.

IR (ATR) (only selected signals) 2918.91 (C-H), 2850.61 (C-H), 2146.76 (C≡C), 2018.14 (s, C=O), 1994.85 (s, C=O) cm^{-1}.

UV-vis ($CHCl_3$) λ_{max} (ε) 569 (25400), 445 (169000), 405 (228000), 345 (246000), 335 (209000), 299 (202000) nm.

GPC (analytical, THF/pyridine 1% v/v) retention time = 36.83 min.

Extended cobalt 6-ring 4.14

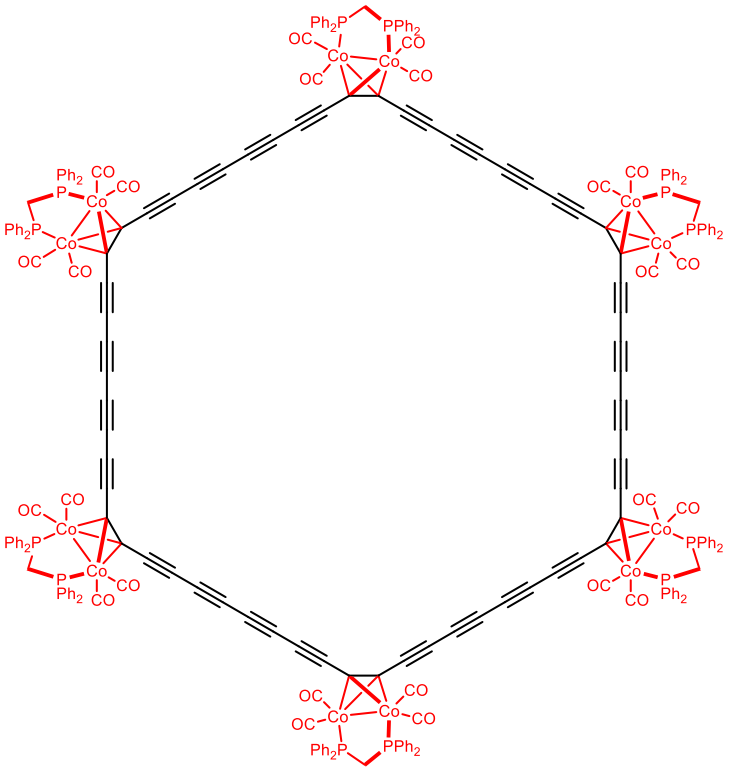

Procedure as above

^{1}H NMR (600 MHz, CD_2Cl_2) δ_C 7.42 – 7.33 (m, 72H, Ar-H), 7.32 – 7.26 (m, 48H, Ar-H), 3.50 (br s, 12H, Ar-H).

^{13}C NMR (151 MHz, CD_2Cl_2) δ_C 202.28 (C≡O), 134.71 (t, $J_{C\text{-}P}$ = 21.8 Hz, Ar-C), 132.13 (t, $J_{C\text{-}P}$ = 6.2 Hz, Ar-C), 130.78 (br, Ar-C), 129.06 (t, $J_{C\text{-}P}$ = 5.1 Hz, Ar-C), 83.63, 83.42, 71.48, 67.26, 38.82 (t, $J_{C\text{-}P}$ = 22.0 Hz, P-CH_2). *(2 carbons not distinguished)*

^{31}P{H} NMR (243 MHz, CD_2Cl_2) δ_P 39.90.

IR (ATR) (only selected signals) 2924.26 (C-H), 2853.82 (C-H), 2146.84 (C≡C), 2018.22 (s, C=O), 1994.94 (s, C=O) cm^{-1}.

UV-vis ($CHCl_3$) λ_{max} (ε) 590 (32000), 444 (323000), 415 (345000), 328 (302000), 300 (291000) nm.

GPC (analytical, THF/pyridine 1% v/v) retention time = 35.87 min.

Tetracobalt [2]rotaxane 4.1·M4

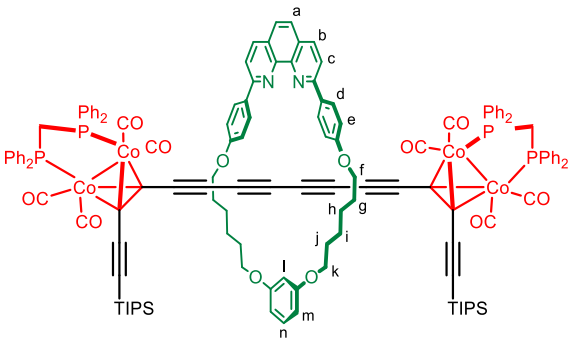

Saito macrocycle **M4** (212 mg, 1.05 eq., 332 µmol) and copper(I) iodide (60.3 mg, 1.00 eq., 317 µmol) were combined and dissolved in a solution of dry MeCN (10.5 mL) and dry CH_2Cl_2 (15.0 mL) and stirred for 1 h under Ar at 20 °C. The solvent was removed under reduced pressure and the residual solid dissolved in dry THF (25 mL). Deprotected cobalt diyne **3.20** (275 mg, 1.00 eq., 317 µmol), supertrityl triyne bromide **3.10** (232 mg, 1.00 eq., 317 µmol) and potassium carbonate (219 mg, 5.00 eq., 1.58 mmol) were combined and evacuated of air and flushed with Ar three times. The solids were cooled in liquid nitrogen, before adding the Cu-macrocycle complex, along with additional dry THF (25 mL). The reaction mixture was thoroughly degassed (3 freeze-pump-thaw cycles) before warming to 60 °C and stirring under

Ar for 18 h. EDTA/NH_3 solution (40 mL) was added to the cooled reaction mixture and left to stir for 1 h. Et_2O (50 mL) was added and the organic layer extracted. The aqueous layer was washed with Et_2O (2 × 20 mL) and the combined organic extracts dried over Na_2SO_4 before removing the solvent under reduced pressure. The crude product was subject to SiO_2 chromatography (pet. ether/EtOAc, gradient elution from 0 to 33%), then size-exclusion chromatography (Bio-Rad S-X3, toluene) to yield Tr* [2]rotaxane **3.22·M4** (240 mg, 110 μmol, 35%) and tetracobalt [2]rotaxane **4.1·M4** (101 mg, 42.5 μmol, 27%) as red-brown crystalline solids.

^{1}H NMR (700 MHz, $CDCl_3$) δ_H 8.52 (d, *J* = 8.5 Hz, 4H, H_d), 8.20 (d, *J* = 8.4 Hz, 2H, H_b), 8.05 (d, *J* = 8.4 Hz, 2H, H_c), 7.69 (s, 2H, H_a), 7.31 (s, 8H, Co Ar–H), 7.26 – 7.21 (m, 8H, Co Ar–H), 7.21 – 7.07 (m, 20H, Co Ar–H), 7.01 (t, *J* = 7.6 Hz, 8H, H_e & Co Ar–H), 6.73 (t, *J* = 2.4 Hz, 1H, H_l), 6.51 (dd, *J* = 8.1, 2.3 Hz, 2H, H_m), 4.26 (t, *J* = 7.4 Hz, 4H, $H_{f/k}$), 4.14 (t, *J* = 6.7 Hz, 4H, $H_{k/f}$), 3.34 (s, 4H, P-CH_2), 1.98 (p, *J* = 6.7 Hz, 4H, $H_{g/j}$), 1.90 (p, *J* = 6.7 Hz, 4H, $H_{j/g}$), 1.69 (d, *J* = 3.9 Hz, 8H, $H_{h,i}$), 1.01 (s, 42H, Si-^{i}Pr).

^{13}C NMR (176 MHz, $CDCl_3$) δ_C 160.93 (O-C-C_e), 160.77, 156.61 (N-C-C-N), 146.22 (C_a-C-C_b), 136.41 (C_b), 133.56 (br, Ar-C), 132.20 (br, Ar-C), 131.82, 131.43 (br, Ar-C), 130.21, 129.83 (C_n), 129.62 (C_d), 129.20, 128.51 (t, $J_{C\text{-}P}$ = 4.8 Hz, Ar-C), 128.39 (t, $J_{C\text{-}P}$ = 4.8 Hz, Ar-C), 127.29, 125.36 (C_a), 118.94 (C_c), 115.08 (C_e), 108.57 (C≡C), 108.13 (C_m), 101.35 (C≡C), 99.44 (C_l), 83.49 (C≡C), 82.08 (C≡C), 70.80 (C≡C), 68.35 ($C_{f/k}$), 67.87 ($C_{k/f}$), 67.30 (C≡C), 35.81 (P-CH_2), 29.74 ($C_{j/g}$), 29.39 ($C_{g/j}$), 25.89 ($C_{h/i}$), 25.84 ($C_{i/h}$), 18.86 (CH(CH_3)$_3$), 11.56(CH(CH_3)$_3$). *(3 carbons not distinguished)*

HRMS *m/z* = 1187.27101 $[M+2H]^{2+}$ ($C_{134}H_{130}Co_4N_2O_{12}P_4Si_2^{2+}$ requires 2374.54298).

Deprotected tetracobalt [2]rotaxane 4.8·M4

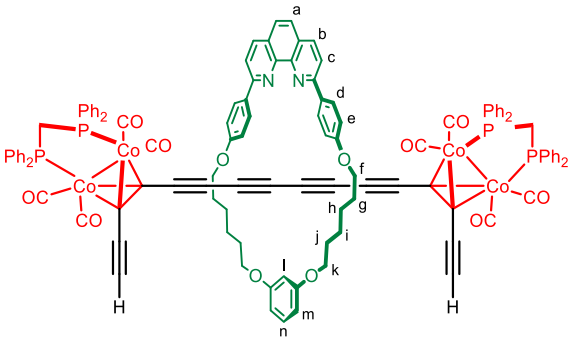

Tetracobalt [2]rotaxane **4.1·M4** (35 mg, 1.0 eq., 15 μmol) was dissolved in THF (15 mL) containing water (0.15 mL). TBAF solution (1.0 M in THF, 39 mg, 0.15 mL, 10 eq., 0.15 mmol) was added dropwise and the mixture stirred at 20 °C for 30 min. The reaction was quenched with addition of sat. aqueous NH_4Cl solution (15 mL), then Et_2O (10 mL) was added, and the organic layer extracted. The aqueous layer was washed with Et_2O (2 × 5 mL) and the combined extracts washed with brine (10 mL), then dried over Na_2SO_4. The solvent was removed under reduced pressure and the crude material purified by silica chromatography (pet. ether/EtOAc, gradient elution from 0 to 40%) to yield deprotected tetracobalt [2]rotaxane **4.8·M4** (27 mg, 13 μmol, 88%) as a dark brown solid.

^{1}H NMR (500 MHz, CD_2Cl_2) δ_H 8.52 (d, J = 8.9 Hz, 4H, H_d), 8.26 (d, J = 8.4 Hz, 2H, H_b), 8.10 (d, J = 8.5 Hz, 2H, H_c), 7.74 (s, 2H, H_a), 7.35 – 7.29 (m, 8H, Co Ar–H), 7.28 – 7.23 (m, 8H, H_e & Co Ar–H), 7.23 – 7.18 (m, 16H, Co Ar–H), 7.17 – 7.13 (m, 4H, Co Ar–H), 7.11 – 7.05 (m, 9H, H_n & Co Ar–H), 6.74 (t, J = 2.4 Hz, 1H, H_l), 6.48 (dd, J = 8.2, 2.4 Hz, 2H, H_m), 4.26 (t, J = 7.4 Hz, 4H, $H_{f/k}$), 4.14 (t, J = 6.8 Hz, 4H, $H_{k/f}$), 3.84 (s, 2H, C≡CH), 3.37 (dt, J = 22.4, 11.8 Hz, 4H, P-CH_2), 1.98 (t, J = 7.2 Hz, 4H, $H_{g/j}$), 1.91 (t, J = 6.8 Hz, 4H, $H_{j/g}$), 1.74 – 1.66 (m, 8H, $H_{h,i}$).

^{13}C NMR (126 MHz, CD_2Cl_2) δ_C 161.18 (O-C-C_e), 161.14, 156.40 (N-C-C-N), 146.51 (C_a-C-C_b), 136.82 (C_b), 135.91 (t, $J_{C\text{-}P}$ = 25.5 Hz, Ar-C), 134.12 (t, $J_{C\text{-}P}$ = 20.3 Hz, Ar-C), 132.25 (t, $J_{C\text{-}P}$ = 6.5 Hz, Ar-C), 131.99, 131.79 (t, $J_{C\text{-}P}$ = 5.9 Hz, Ar-C), 130.63 (Ar-C), 130.32 (Ar-C), 129.82 (C_n), 129.32 (C_d), 128.77 (t, $J_{C\text{-}P}$ = 5.2 Hz, Ar-C), 127.75, 125.76 (C_a), 119.17 (C_c), 115.36 (C_e), 108.13 (C_m), 99.90 (C_l), 86.28 (C≡CH), 85.61 (C≡C), 83.81 (C≡C), 82.21 (C≡C), 70.93 (C≡C), 68.68 ($C_{k/f}$), 68.30 ($C_{f/k}$), 67.38 (C≡C), 37.14 (t, $J_{C\text{-}P}$ = 21.1 Hz, P-CH_2), 30.10 ($C_{j/g}$), 29.67 ($C_{g/j}$), 26.29 ($C_{h/i}$), 26.19 ($C_{i/h}$). *(3 carbons not distinguished)*

^{31}P{H} NMR (202 MHz, CD_2Cl_2) δ_P 39.20.

HRMS *m/z* = 2061.2693 $[M+H]^+$ ($C_{116}H_{89}Co_4N_2O_{12}P_4^+$ requires 2061.2688).

***p*-^{t}Bu [2]rotaxane 4.7·M4**

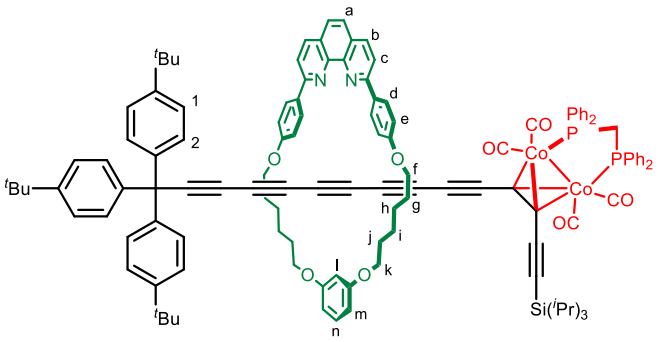

Saito macrocycle **M4** (139 mg, 1.05 eq., 218 μmol) and copper(I) iodide (39.5 mg, 1.00 eq., 207 μmol) were combined, dissolved in a solution of dry MeCN (7.00 mL) and dry CH_2Cl_2 (10.0 mL) and stirred for 1 h under Ar at 20 °C. The solvent was removed under reduced pressure and the residual solid dissolved in dry THF (15 mL). Deprotected cobalt diyne **3.20** (180 mg, 1.00 eq., 207 μmol), *p*-^{t}Bu triyne bromide **4.6** (117 mg, 1.00 eq., 207 μmol) and potassium carbonate (143 mg, 5.00 eq., 1.04 mmol) were combined and evacuated of air and flushed with Ar three times. The solids were cooled in liquid nitrogen, before adding the Cu-macrocycle complex, along with additional THF (15 mL). The reaction mixture was thoroughly degassed (3 freeze-pump-thaw cycles) before warming to 60 °C and stirring under Ar for 18 h. EDTA/NH_3 solution (30 mL) was added to the cooled reaction mixture and left to stir for 1 h. Et_2O (30 mL) was added and the organic layer extracted. The aqueous layer was washed with Et_2O (2 × 20 mL) and the combined organic extracts dried over Na_2SO_4 before removing the solvent under reduced pressure. The crude product was subject to SiO_2 chromatography (pet. ether/CH_2Cl_2, gradient elution from 0 to 100%, then pet. ether/EtOAc, 2:1) then size-exclusion chromatography (Bio-Rad S-X3, toluene) to yield *p*-^{t}Bu [2]rotaxane **4.7·M4** (73.9 mg, 37.1 μmol, 18%) and tetracobalt [2]rotaxane **4.1·M4** (32.9 mg, 27.8 μmol, 13%) as a red-brown crystalline solids.

^{1}H NMR (500 MHz, CD_2Cl_2) δ_H 8.53 (d, *J* = 8.9 Hz, 4H, H_d), 8.27 (d, *J* = 8.4 Hz, 2H, H_b), 8.10 (d, *J* = 8.4 Hz, 2H, H_c), 7.75 (s, 2H, H_a), 7.41 – 7.36 (m, 4H, Co Ar-H), 7.31 (d, *J* = 7.2 Hz, 2H, Co Ar-H), 7.27 (t, *J* = 7.2 Hz, 4H, Co Ar-H), 7.22 – 7.18 (m, 10H, Co Ar-H, H_2), 7.16 – 7.14 (m,

6H, Co Ar-H, H_l), 7.11 – 7.06 (m, 5H, Co Ar-H, H_n), 7.04 – 7.00 (m, 6H, Co Ar-H, H_e), 6.65 (t, J = 2.4 Hz, 1H, H_l), 6.48 (dd, J = 8.2, 2.4 Hz, 2H, H_m), 4.18 – 4.13 (m, 4H, H_f), 4.04 (t, J = 6.6 Hz, 4H, H_k), 3.48 – 3.35 (m, 2H, PCH_2P), 1.94 – 1.83 (m, 8H, $H_{g,j}$), 1.63 (dq, J = 7.5, 3.9 Hz, 8H, $H_{h,i}$), 1.20 (s, 27H, ^{t}Bu), 1.10 – 1.06 (m, 21H, ^{i}Pr).

^{13}C NMR (126 MHz, CD_2Cl_2) δ_C 203.43 (br, C≡O), 201.62 (br, C≡O), 161.12, 161.07, 156.26, 150.36, 146.56, 141.08, 136.88, 136.65 (t, $J_{C\text{-}P}$ = 29.1 Hz), 133.53 (t, $J_{C\text{-}P}$ = 22.2 Hz), 132.57 (t, $J_{C\text{-}P}$ = 6.6 Hz), 132.04, 131.62 (t, $J_{C\text{-}P}$ = 6.1 Hz), 130.69, 130.31, 129.91, 129.23, 128.91 (t, $J_{C\text{-}P}$ = 5.0 Hz), 128.80, 128.72 (d, $J_{C\text{-}P}$ = 4.9 Hz), 127.85, 125.84, 125.49, 125.43, 119.14, 115.35, 108.64, 107.80, 106.99, 100.45, 86.23, 83.43, 80.88, 70.84, 69.54, 68.59, 68.23, 66.20, 64.79, 64.75, 64.44, 55.89 (C-Ar$_3$), 36.44 (br, P-C-P), 34.64, 31.38, 30.04, 29.57, 26.33, 26.26, 18.96, 11.87. *(2 carbons not distinguished)*

^{31}P{H} NMR (202 MHz, CD_2Cl_2) δ_P 38.64.

HRMS *m/z* = 1989.7316 $[M+H]^+$ ($C_{125}H_{125}Co_2N_2O_8P_2Si^+$ requires 1989.7339).

Extended tetracobalt [2]rotaxane 4.11·M4

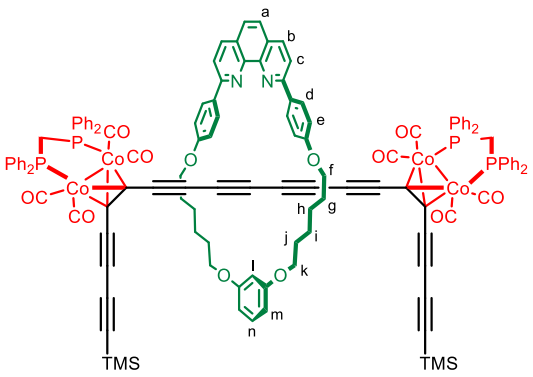

Deprotected tetracobalt [2]rotaxane **4.8·M4** (30 mg, 1.0 eq., 15 μmol) was dissolved in dry CH_2Cl_2 (20 mL). TMS-acetylene (73 mg, 0.10 mL, 50 eq., 0.72 mmol) and copper(I) chloride (65 mg, 45 eq., 0.68 mmol) were added and the solution stirred vigorously in air for 2 min. Freshly distilled TMEDA (68 mg, 87 μL, 40 eq., 0.74 mmol) was added to the reaction mixture. The remaining TMS-acetylene (72 mg, 0.10 mL, 50 eq., 1.46 mmol) was added over a period of 30 min via syringe pump. The reaction was monitored by TLC and, upon completion, was quenched by addition of water (50 mL). The organic layer was extracted and washed with water (2 × 20 mL), then brine (20 mL) before drying over Na_2SO_4. The solvent was removed under

reduced pressure and the crude material purified by SiO_2 chromatography (pet. ether/EtOAc, gradient elution from 0 to 33%), to yield the extended tetracobalt [2]rotaxane **4.11·M4** (23 mg, 10 μmol, 69% over 2 steps) as a red-brown solid; R_f (petrol/EtOAc, 50%) = 0.68.

^{1}H NMR (500 MHz, CD_2Cl_2) δ_H 8.52 (d, *J* = 8.8 Hz, 4H, H_d), 8.25 (d, *J* = 8.5 Hz, 2H, H_b), 8.09 (d, *J* = 8.5 Hz, 2H, H_c), 7.73 (s, 2H, H_a), 7.30 – 7.24 (m, 16H, H_e & Ar-H), 7.24 – 7.18 (m, 16H, Ar-H), 7.18 – 7.14 (m, 4H, Ar-H), 7.13 – 7.08 (m, 9H, H_n & Ar-H), 6.71 (t, *J* = 2.4 Hz, 1H, H_l), 6.49 (dd, *J* = 8.1, 2.3 Hz, 2H, H_m), 4.28 (t, *J* = 7.3 Hz, 4H, $H_{f/k}$), 4.13 (t, *J* = 6.6 Hz, 4H, $H_{k/f}$), 3.38 (s, 4H, P-CH_2), 2.01 (dd, *J* = 10.6, 3.8 Hz, 4H, $H_{g/j}$), 1.93 (dd, *J* = 8.2, 4.7 Hz, 4H, $H_{j/g}$), 1.73 (t, *J* = 3.5 Hz, 8H, $H_{h,i}$), 0.25 (s, 18H, $SiMe_3$).

^{13}C NMR (126 MHz, CD_2Cl_2) δ_C 202.31 (C≡O, br), 161.24 (O-C-C_e), 161.12, 156.36 (N-C-C-N), 146.50 (C_a-C-C_b), 136.80 (C_b), 135.04 (t, $J_{C\text{-}P}$ = 22.3 Hz, Ar-C), 134.41 (t, $J_{C\text{-}P}$ = 21.4 Hz, Ar-C), 131.99 (t, $J_{C\text{-}P}$ = 6.1 Hz, Ar-C), 130.68 (Ar-C), 130.49 (C_n), 129.85 (Ar-C), 129.26 (C_d), 128.89 (t, $J_{C\text{-}P}$ = 5.0 Hz, Ar-C), 127.75, 125.76 (C_a), 119.17 (C_c), 115.39 (C_e), 107.93 (C_m), 100.16 (C_l), 93.62, 89.95, 83.62, 83.10, 80.29, 71.29, 68.76 ($C_{k/f}$), 68.26 ($C_{f/k}$), 67.48, 60.63, 38.36 (t, $J_{C\text{-}P}$ = 22.0 Hz, P-CH_2), 30.11 ($C_{j/g}$), 29.70 ($C_{g/j}$), 26.35 ($C_{h/i}$), 26.29 ($C_{i/h}$), 14.41, -0.20 ($SiMe_3$). (*2 carbons not distinguished*)

^{31}P{H} NMR (202 MHz, CD_2Cl_2) δ_P 39.61.

HRMS *m/z* = 2253.3412 $[M+H]^+$ ($C_{126}H_{105}Co_4N_2O_{12}P_4Si_2^+$ requires 2253.3479)

Deprotected extended tetracobalt [2]rotaxane 4.12·M4

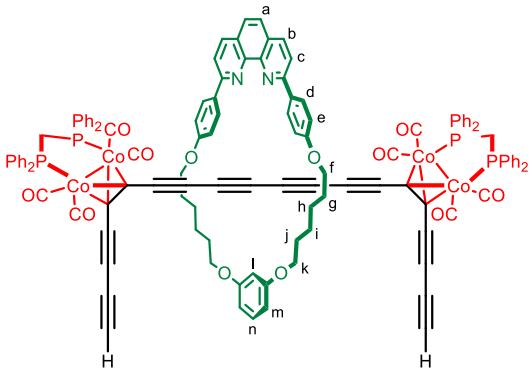

Extended tetracobalt [2]rotaxane **4.11·M4** (22 mg, 1.0 eq., 9.8 μmol) and potassium carbonate (20 mg, 15 eq., 0.15 mmol) were dissolved in a 1:1 solution of THF (5 mL) and MeOH (5 mL).

Water (0.05 mL) was added and the solution stirred at 20 °C for 20 min. The solvent was evaporated under reduced pressure and the crude material purified by SiO_2 chromatography (pet. ether/EtOAc, gradient elution from 0 to 50%) to yield deprotected extended tetracobalt [2]rotaxane **4.12·M4** (20 mg, 9.5 μmol, 97%) as a red-brown solid; R_f (petrol/EtOAc, 50%) = 0.49.

^{1}H NMR (600 MHz, CD_2Cl_2) δ_H 8.52 (d, *J* = 8.8 Hz, 4H, H_d), 8.25 (d, *J* = 8.4 Hz, 2H, H_b), 8.09 (d, *J* = 8.4 Hz, 2H, H_c), 7.73 (s, 2H, H_a), 7.30 – 7.26 (m, 14H, H_e & Ar-H), 7.25 – 7.20 (m, 17H, Ar-H), 7.19 – 7.16 (m, 4H, Ar-H), 7.14 – 7.10 (m, 10H, H_n & Ar-H), 6.72 (t, *J* = 2.3 Hz, 1H, H_l), 6.49 (dd, *J* = 8.1, 2.3 Hz, 2H, H_m), 4.27 (t, *J* = 7.3 Hz, 4H, $H_{f/k}$), 4.13 (t, *J* = 6.7 Hz, 4H, $H_{k/f}$), 3.38 (s, 4H, P-CH_2), 2.87 (s, 2H, C≡CH), 2.00 (t, *J* = 9.1 Hz, 4H, $H_{g/j}$), 1.93 (t, *J* = 6.6 Hz, 4H, $H_{j/g}$), 1.73 (p, *J* = 3.5 Hz, 8H, $H_{h,i}$).

^{13}C NMR (151 MHz, CD_2Cl_2) δ_C 202.55 (C≡O, br), 161.24 (O-C-C_e), 161.15, 156.39 (N-C-C-N), 146.53 (C_a-C-C_b), 136.81 (C_b), 135.01 (t, $J_{C\text{-}P}$ = 21.9 Hz, Ar-C), 134.40 (t, $J_{C\text{-}P}$ = 21.3 Hz, Ar-C), 132.00 (t, $J_{C\text{-}P}$ = 6.0 Hz, Ar-C), 130.72 (Ar-C), 130.54 (C_n), 129.86 (Ar-C), 129.28 (C_d), 128.91 (td, $J_{C\text{-}P}$ = 5.0, 2.3 Hz, Ar-C), 127.77, 125.77 (C_a), 119.18 (C_c), 115.40 (C_e), 107.97 (C_m), 100.18 (C_l), 83.59, 83.14, 82.02, 78.85, 74.03 (C≡CH), 71.35, 70.12, 68.77 ($C_{k/f}$), 68.29 ($C_{f/k}$), 67.51, 38.43 (t, $J_{C\text{-}P}$ = 21.8 Hz, P-CH_2), 30.11 ($C_{j/g}$), 29.71 ($C_{g/j}$), 26.36 ($C_{i/h}$), 26.30 ($C_{h/i}$). (*Two C-Co resonances not seen due to extremely long relaxation times*)

^{31}P{H} NMR (243 MHz, CD_2Cl_2) δ_P 39.63.

HRMS *m/z* = 2109.2695 $[M+H]^+$ ($C_{120}H_{89}Co_4N_2O_{12}P_4^+$ requires 2109.2688)

Octacobalt [3]catenane 4.13·(M4)$_2$

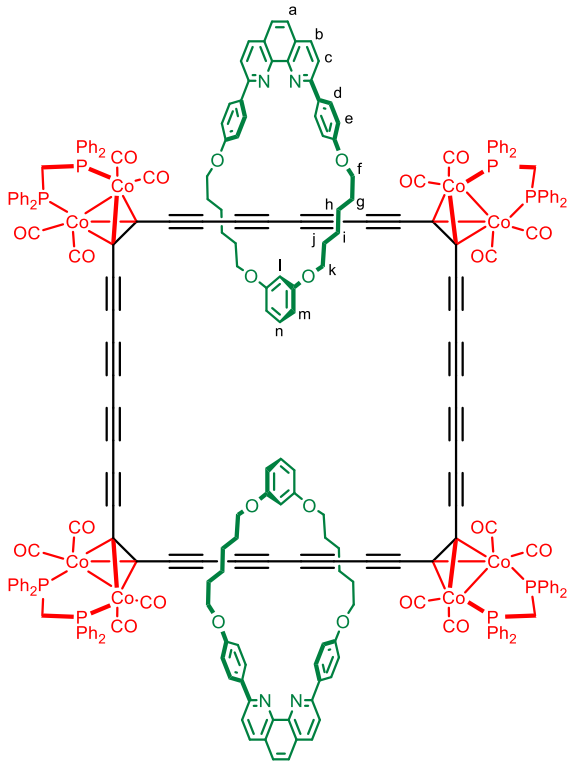

Dry $CHCl_3$ (40 mL) and freshly-distilled diisopropylamine (29 mg, 40 µL, 40 eq., 0.28 mmol) was added to bis(triphenylphosphine)palladium(II) dichloride (6.6 mg, 1.3 eq., 9.5 µmol), copper(I) iodide (9.0 mg, 6.7 eq., 47 µmol) and benzoquinone (12 mg, 15 eq., 0.11 mmol). The mixture was stirred in air before addition of extended tetracobalt [2]rotaxane **4.12·M4** (30 mg, 2.0 eq., 14 µmol) in dry $CHCl_3$ (10 mL) over 1 h via syringe pump. After complete addition, the reaction was stirred at 20 °C in air for a further 1 h. EDTA/NH_3 solution (25 mL) was then added, and the mixture stirred for 1 h. The organic layer was extracted, washed with water (20 mL). The crude material was purified by recycling GPC (THF) to yield the octacobalt [3]catenane **4.13·(M4)$_2$** (6.0 mg, 1.4 µmol, 20%) and dodecacobalt [4]catenane **4.14·(M4)$_3$** (3.9 mg, 0.62 µmol, 13%) as dark-brown solids.

^{1}H NMR (600 MHz, CD_2Cl_2) δ_H 8.54 (d, J = 8.3 Hz, 8H, H_d), 8.23 (d, J = 8.4 Hz, 4H, H_b), 8.08 (d, J = 8.6 Hz, 4H, H_c), 7.72 (s, 4H, H_a), 7.31 – 7.27 (m, 26H, H_e & Ar-H), 7.27 – 7.20 (m, 38H, Ar-H), 7.20 – 7.16 (m, 8H, Ar-H), 7.16 – 7.07 (m, 18H, H_n & Ar-H), 6.75 (s, 2H, H_l), 6.52 (dd, J = 8.2, 2.3 Hz, 4H, H_m), 4.26 (t, J = 7.3 Hz, 8H, $H_{f/k}$), 4.14 (d, J = 6.7 Hz, 8H, $H_{k/f}$), 3.55 – 3.24 (m, 8H, P-CH_2), 1.99 (t, J = 6.8 Hz, 8H, $H_{g/j}$), 1.93 (t, J = 6.5 Hz, 8H, $H_{j/g}$), 1.72 (br s, 16H, $H_{h,i}$).

^{13}C NMR (151 MHz, CD_2Cl_2) δ_C 202.14 (C≡O, br), 161.28 (O-C-C_e), 161.16, 156.31 (N-C-C-N), 146.51 (C_a-C-C_b), 136.82 (C_b), 134.84 (t, $J_{C\text{-}P}$ = 21.7 Hz, Ar-C), 134.35 (t, $J_{C\text{-}P}$ = 21.5 Hz, Ar-C), 132.03 (d, $J_{C\text{-}P}$ = 6.5 Hz, Ar-C), 130.78 (Ar-C), 130.64 (C_n), 129.96 (Ar-C), 129.28 (C_d), 128.96 (t, $J_{C\text{-}P}$ = 4.9 Hz, Ar-C), 127.78, 125.81 (C_a), 119.15 (C_c), 115.44 (C_e), 107.95 (C_m), 100.33 (C_l), 84.08, 83.71, 83.38, 83.21, 71.36, 71.11, 68.79 ($C_{k/f}$), 68.30 ($C_{f/k}$), 67.60, 66.97, 38.98 (t, $J_{C\text{-}P}$ = 21.5 Hz, P-CH_2), 30.11 ($C_{j/g}$), 29.70 ($C_{g/j}$), 26.38 ($C_{h/i}$), 26.37 ($C_{i/h}$).

^{31}P{H} NMR (243 MHz, CD_2Cl_2) δ_P 40.28.

HRMS *m/z* = 2107.2534 $[M+2H]^{2+}$ ($C_{240}H_{174}Co_8N_4O_{24}P_8^{2+}$ requires 2107.2532).

IR (ATR) (only selected signals) 2935.09 (C-H), 2145.45 (C≡C), 2018.51 (s, C=O), 1994.78 (s, C=O) cm^{-1}.

UV-vis ($CHCl_3$) λ_{max} (ε) 569 (24000), 406 (230000), 345 (246000), 327 (252000), 292 (291000) nm.

GPC (analytical, THF/pyridine 1% v/v) retention time = 36.83 min.

Dodecacobalt [4]catenane 4.14·(M4)$_3$

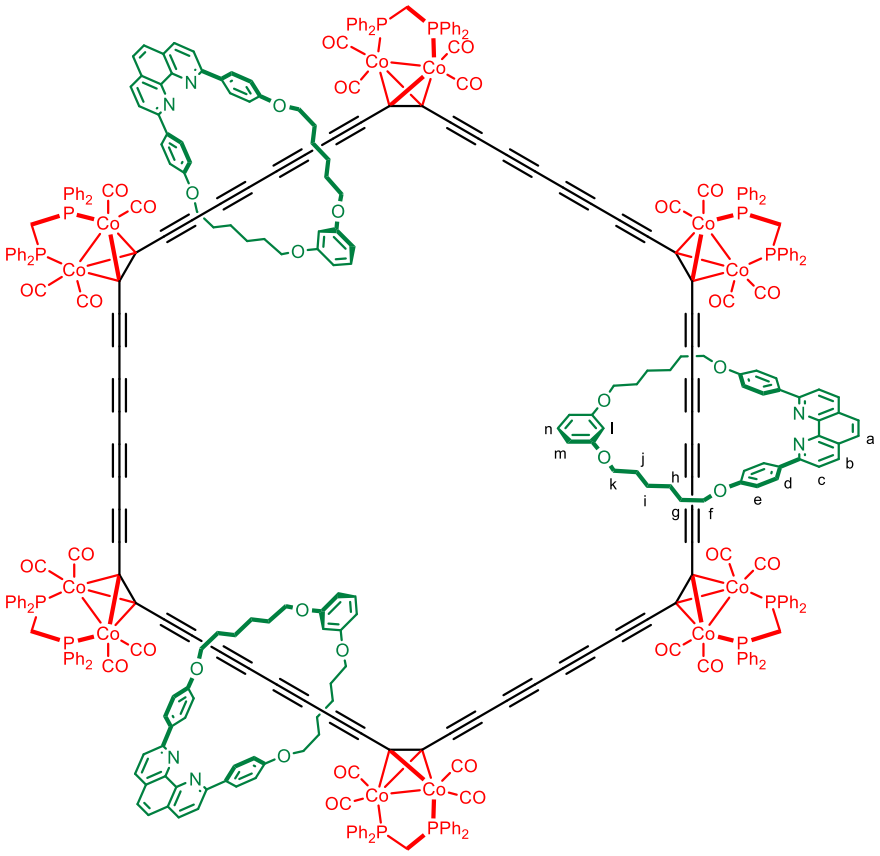

Procedure as above

^{1}H NMR (600 MHz, CD_2Cl_2) δ_H 8.51 (d, J = 8.3 Hz, 12H, H_d), 8.18 (d, J = 8.2 Hz, 6H, H_b), 8.04 (d, J = 8.3 Hz, 6H, H_c), 7.67 (s, 6H, H_a), 7.33 – 7.17 (m, 107H, H_e & Ar-H), 7.17 – 7.09 (m, 28H, Ar-H), 6.75 (s, 3H, H_l), 6.51 (d, J = 8.1 Hz, 6H, H_m), 4.27 (t, J = 7.3 Hz, 12H, $H_{f/k}$), 4.15 (t, J = 6.7 Hz, 12H, $H_{k/f}$), 3.68 – 3.10 (m, 12H, P-CH_2), 2.07 – 1.89 (m, 24H, $H_{j,g}$), 1.81 – 1.67 (m, 24H, $H_{h,i}$).

^{13}C NMR (151 MHz, CD_2Cl_2) δ_C 202.09 (C≡O, br), 161.26 (O-C-C_e), 161.16, 156.31 (N-C-C-N), 146.50 (C_a-C-C_b), 136.81 (C_b), 135.05 – 134.02 (m, Ar-C), 132.03 (d, $J_{C\text{-}P}$ = 7.3 Hz, Ar-C), 130.77 (Ar-C), 130.66 (C_n), 129.93 (Ar-C), 129.29 (C_d), 128.99 (t, $J_{C\text{-}P}$ = 5.2 Hz, Ar-C), 127.74, 125.79 (C_a), 119.17 (C_c), 115.41 (C_e), 108.00 (C_m), 100.23 (C_l), 83.78 (br), 83.32, 77.55, 71.76, 71.45, 68.77 ($C_{k/f}$), 68.32 ($C_{f/k}$), 67.77, 67.19, 38.75 (br, P-CH_2), 30.14 ($C_{j/g}$), 29.73 ($C_{g/j}$), 26.40 ($C_{i/h}$), 26.36 ($C_{h/i}$).

^{31}P{H} NMR (243 MHz, CD_2Cl_2) δ_P 39.84.

IR (ATR) (only selected signals) 2961.02 (C-H), 2860.92 (C-H), 2145.64 (C≡C), 2017.90 (s, C=O), 1994.86 (s, C=O) cm^{-1}.

UV-vis ($CHCl_3$) λ_{max} (ε) 592 (32700), 444 (312000), 417 (331000), 346 (354000), 328 (366000), 291 (407000) nm.

GPC (analytical, THF/pyridine 1% v/v) retention time = 35.89 min.

Octacobalt [4]rotaxane 4.16·(M4)$_3$

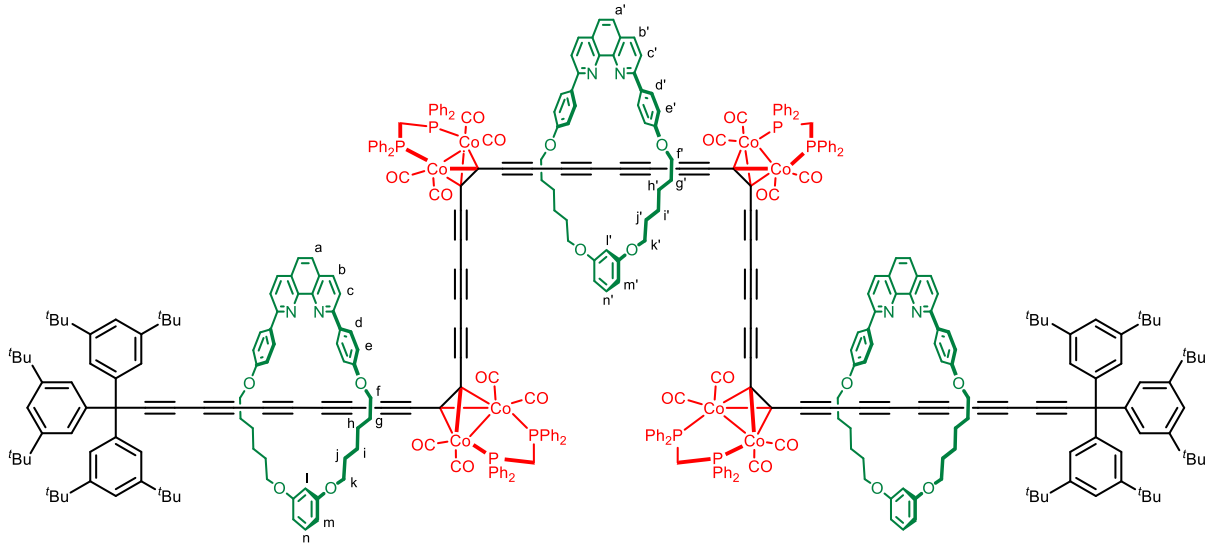

Dry $CHCl_3$ (75 mL) and freshly-distilled diisopropylamine (140 mg, 0.19 mL, 80 eq., 1.4 mmol) was added to bis(triphenylphosphine)palladium(II) dichloride (32 mg, 2.7 eq., 45 μmol), copper(I) iodide (43 mg, 13 eq., 0.22 mmol) and benzoquinone (55 mg, 30 eq., 0.51 mmol). The mixture was stirred in air before addition of a mixture of deprotected Tr* [2]rotaxane **3.23·M4** (140 mg, 4.0 eq., 67 μmol) and deprotected extended tetracobalt [2]rotaxane **4.12·M4** (36 mg, 1.0 eq., 17 μmol) in dry $CHCl_3$ (15 mL) over 1 hour via syringe pump. After complete addition, the reaction was stirred at 20 °C in air for a further 1 hour. EDTA/NH_3 solution (75 mL) was then added, and the mixture stirred for 1 h. The organic layer was extracted, washed with water (50 mL) then brine (50 mL), before being dried over Na_2SO_4 and the solvent removed under reduced pressure. The crude material was purified by recycling GPC (THF) to yield octacobalt [4]rotaxane **4.16·(M4)$_3$** (29.4 mg, 4.8 μmol, 28%), dodecacobalt [5]rotaxane **4.17·(M4)$_4$** (11.1 mg, 1.34 μmol, 16%) and hexadecacobalt [6]rotaxane **4.18·(M4)$_5$** (3.30 mg, 0.32 μmol, 5.7%) as dark-brown solids.

^{1}H NMR (600 MHz, CD_2Cl_2) δ_H 8.49 (d, *J* = 8.3 Hz, 4H, $H_{d'}$), 8.46 (d, *J* = 8.3 Hz, 8H, H_d), 8.22 (d, *J* = 8.5 Hz, 4H, H_b), 8.19 (d, *J* = 8.4 Hz, 2H, $H_{b'}$), 8.09 – 7.99 (m, 6H, $H_{c,c'}$), 7.71 (s, 4H, H_a), 7.68 (s, 2H, $H_{a'}$), 7.31 – 7.27 (m, 16H, Cr Ar-H), 7.26 – 7.17 (m, 65H, $H_{e,e'}$, Co & Tr* Ar-H), 7.15 – 7.10 (m, 17H, Co Ar-H), 7.09 – 7.05 (m, 3H, $H_{n,n'}$), 6.91 (d, *J* = 1.8 Hz, 12H, Tr* Ar-H), 6.73 (t, *J* = 2.4 Hz, 1H, $H_{l'}$), 6.64 (t, *J* = 2.4 Hz, 2H, H_l), 6.48 (dd, *J* = 8.1, 2.2 Hz, 2H, $H_{m'}$), 6.46 (dd, *J* = 8.1, 2.3 Hz, 4H, H_m), 4.29 – 4.11 (m, 16H, $H_{f,k}$), 4.07 (t, *J* = 6.6 Hz, 8H, $H_{f',k'}$), 3.64 – 3.16 (m, 8H, P-CH_2), 2.01 – 1.86 (m, 24H, $H_{g,j}$ & $H_{g',j'}$), 1.75 – 1.70 (m, 8H, $H_{h',i'}$), 1.66 (d, *J* = 5.5 Hz, 16H, $H_{h,i}$), 1.14 (s, 108H, ^{t}Bu).

^{13}C NMR (151 MHz, CD_2Cl_2) δ_C 201.65 (br, C≡O), 161.23, 161.16, 161.13, 161.07, 156.37, 150.70, 146.50, 143.81, 136.81, 134.97 (t, J_{C-P} = 22.3 Hz), 134.61 – 134.02 (m), 132.25 – 131.67 (m), 130.75, 130.64, 130.60, 129.90, 129.09 – 128.84 (m), 127.76, 127.73, 125.77, 123.93, 120.94, 119.21, 115.41, 115.32, 107.98, 107.89, 100.33, 100.26, 86.88, 85.14, 84.72, 84.25, 83.89, 83.54, 82.84, 82.26, 77.96, 77.75, 77.54, 74.51, 74.25, 71.77, 71.68, 71.38, 70.45, 69.98, 68.77, 68.63, 68.31, 68.22, 67.78, 66.92, 64.82, 64.29, 64.08, 63.83, 57.84, 38.34 (br), 31.47, 30.15, 30.05, 29.74, 29.64, 26.40, 26.32, 26.28. *(4 carbonyl resonances not distinguished due to overlap and broadening; 12 Ar-C resonances not observed due to overlap)*

^{31}P{H} NMR (243 MHz, CD_2Cl_2) δ_P 39.54.

HRMS *m/z* = 3053.9266 $[M+2H]^{2+}$ ($C_{376}H_{342}Co_8N_6O_{28}P_8^{2+}$ requires 3053.9034).

IR (ATR) (only selected signals) 2960.57 (C-H), 2866.07 (C-H), 2149.31 (C≡C), 2018.93 (s, C=O), 1995.46 (s, C=O) cm^{-1}.

UV-vis ($CHCl_3$) λ_{max} (ε) 589 (15200), 416 (153000), 319 (260000), 291 (292000) nm.

GPC (analytical, THF/pyridine 1% v/v) retention time = 35.40 min.

Dodecacobalt [5]rotaxane 4.17·(M4)$_4$

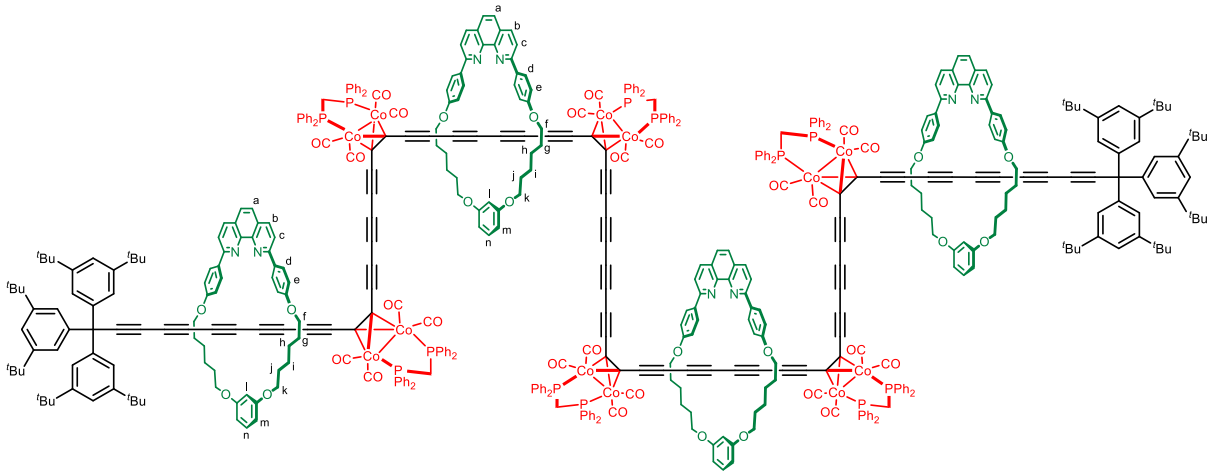

Procedure as above

^{1}H NMR (600 MHz, CD_2Cl_2) δ_H 8.50 (d, *J* = 8.8 Hz, 8H, H_d), 8.45 (d, *J* = 8.9 Hz, 8H, H_d), 8.21 (d, *J* = 8.4 Hz, 4H, H_b), 8.18 (d, *J* = 8.4 Hz, 4H, H_b), 8.04 (t, *J* = 8.0 Hz, 8H, H_c), 7.70 (s, 4H, H_a), 7.67 (s, 4H, H_a), 7.31 – 7.16 (m, 118H, H_e, Tr* Ar-H & Co Ar-H), 7.16 – 7.05 (m, 28H, H_n & Co Ar-H), 6.90 (d, *J* = 1.8 Hz, 12H, Tr* Ar-H), 6.73 (t, *J* = 2.4 Hz, 2H, H_l), 6.64 (t, *J* = 2.4 Hz, 2H, H_l), 6.49 (dd, *J* = 8.1, 2.3 Hz, 4H, H_m), 6.46 (dd, *J* = 8.1, 2.3 Hz, 4H, H_m), 4.27 (t, *J* = 7.3 Hz, 8H, $H_{f/k}$), 4.22 – 4.16 (m, 8H, $H_{f/k}$), 4.13 (t, *J* = 6.6 Hz, 8H, $H_{k/f}$), 4.06 (t, *J* = 6.6 Hz, 8H, $H_{k/f}$), 3.58 – 3.26 (m, 12H, P-CH_2), 2.03 – 1.84 (m, 32H, $H_{g,j}$), 1.78 – 1.61 (m, 32H, $H_{h,i}$), 1.13 (s, 108H, ^{t}Bu).

^{13}C NMR (151 MHz, CD_2Cl_2) δ_C 161.22, 161.16, 161.13, 161.06, 156.36, 150.69, 146.50, 143.80, 136.81, 135.15 – 134.72 (m), 134.63 – 134.16 (m), 132.36 – 131.67 (m), 131.03 – 130.48 (m), 129.90, 129.29, 129.23, 129.14 – 128.77 (m), 127.75, 125.77, 123.92, 120.93, 119.21, 115.40, 115.31, 107.97, 107.88, 100.31, 100.26, 86.86, 85.12, 84.71, 84.61, 84.25, 83.98, 83.70, 83.47, 83.31, 77.96, 77.75, 77.54, 73.97, 71.99, 71.85, 71.69, 71.48, 71.37, 70.99, 70.42, 69.97, 68.76, 68.62, 68.31, 68.21, 67.85, 67.22, 67.15, 66.91, 64.81, 64.30, 64.07, 63.83, 57.83, 38.35, 37.25, 35.10, 31.46, 30.15, 30.05, 29.73, 29.64, 26.41, 26.35, 26.31, 26.27, 25.99. *(9 Ar-C resonances not observed due to overlap; 6 Co-C resonances not observed due to their extremely long relaxation times)*

^{31}P{H} NMR (243 MHz, CD_2Cl_2) δ_P 39.60.

HRMS *m/z* = 2738.3529 $[M+3H]^{3+}$ ($C_{496}H_{429}Co_{12}N_8O_{40}P_{12}^{3+}$ requires 2738.3533).

IR (ATR) (only selected signals) 2951.28 (C-H), 2865.27 (C-H), 2147.78 (C≡C), 2019.19 (s, C=O), 1995.36 (s, C=O) cm^{-1}.

UV-vis ($CHCl_3$) λ_{max} (ε) 592 (31500), 449 (286000), 422 (301000), 346 (417000), 322 (462000), 291 (520000) nm.

GPC (analytical, THF/pyridine 1% v/v) retention time = 34.63 min.

Hexadecacobalt [6]rotaxane 4.18·(M4)$_5$

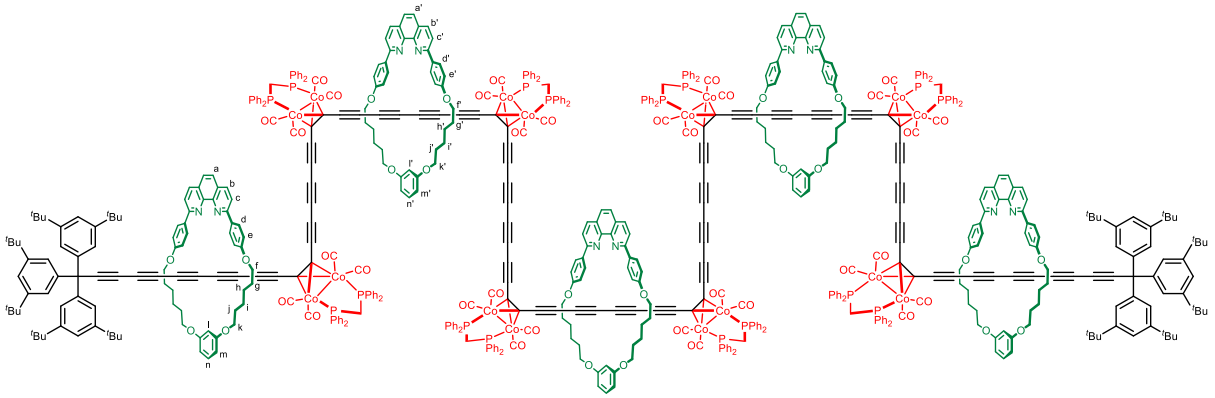

Procedure as above

^{1}H NMR (600 MHz, CD_2Cl_2) δ_H 8.59 – 8.48 (m, 12H, H_d), 8.45 (d, J = 8.6 Hz, 8H, H_d), 8.20 (dd, J = 18.8, 8.4 Hz, 10H, $H_{b,b'}$), 8.10 – 8.00 (m, 10H, $H_{c,c'}$), 7.70 (d, J = 2.4 Hz, 4H, H_a), 7.66 (d, J = 3.3 Hz, 6H, $H_{a'}$), 7.31 – 7.16 (m, 153H, $H_{e,e'}$, Tr* Ar-H & Co Ar-H), 7.10 (ddd, J = 31.4, 15.1, 7.8 Hz, 38H, $H_{n,n'}$ & Co Ar-H), 6.90 (d, J = 1.8 Hz, 12H, Tr* Ar-H), 6.77 – 6.71 (m, 3H, $H_{l'}$), 6.64 (t, J = 2.3 Hz, 2H, H_l), 6.49 (ddd, J = 8.3, 6.5, 2.3 Hz, 6H, $H_{m'}$), 6.46 (dd, J = 8.1, 2.3 Hz, 4H, H_m), 4.31 – 4.25 (m, 10H, $H_{f,k/f',k'}$), 4.24 – 4.16 (m, 10H, $H_{f,k/f',k'}$), 4.14 (td, J = 6.7, 3.7 Hz, 10H, $H_{k,f/k',f'}$), 4.06 (t, J = 6.6 Hz, 10H, $H_{k,f/k',f'}$), 3.69 – 3.16 (m, 16H, P-CH_2), 2.03 – 1.85 (m, 40H, $H_{g,j}$ & $H_{g'j'}$), 1.77 – 1.63 (m, 40H, $H_{h,i}$ & $H_{h'i'}$), 1.13 (s, 108H, ^{t}Bu).

^{13}C NMR (151 MHz, CD_2Cl_2) δ_C 201.89 (br, C≡O), 161.21, 161.16, 161.12, 161.06, 156.34, 150.69, 146.50, 143.80, 136.80, 135.12 – 134.63 (m), 134.61 – 134.04 (m), 132.10 – 131.96 (m), 131.91, 131.86, 130.76, 130.74, 130.67, 130.61, 129.90, 129.28, 129.23, 129.02 – 128.92 (m), 127.75, 125.76, 123.92, 120.93, 119.20, 115.40, 115.31, 107.96, 107.88, 100.31, 100.26, 86.97, 86.86, 85.33, 85.13, 84.72, 84.24, 83.97, 83.77, 83.70, 83.51, 83.37, 82.84, 82.23, 77.96, 77.75, 77.53, 71.98, 71.88, 71.78, 71.69, 71.48, 71.38, 70.43, 69.97, 68.76, 68.61, 68.31, 68.20, 67.86,

67.82, 67.77, 67.71, 67.68, 67.53, 67.24, 66.91, 64.81, 64.29, 64.07, 63.83, 57.83, 38.95 – 38.13 (m), 35.10, 31.46, 30.15, 30.05, 29.74, 29.64, 26.41, 26.35, 26.31, 26.28. *(carbonyl and 11 Ar-C resonances not distinguished due to overlap; 8 Co-C resonances not observed due to their extremely long relaxation times)*

^{31}P{H} NMR (243 MHz, CD_2Cl_2) δ_P 39.63.

IR (ATR) (only selected signals) 2952.42 (C-H), 2866.37 (C-H), 2147.24 (C≡C), 2018.48 (s, C=O), 1995.26 (s, C=O) cm^{-1}.

UV-vis ($CHCl_3$) λ_{max} (ε) 592 (48200), 450 (454000), 424 (461000), 344 (620000), 323 (667000), 291 (741000) nm.

GPC (analytical, THF/pyridine 1% v/v) retention time = 33.99 min.

24-yne [4]rotaxane 4.19·(M4)$_3$

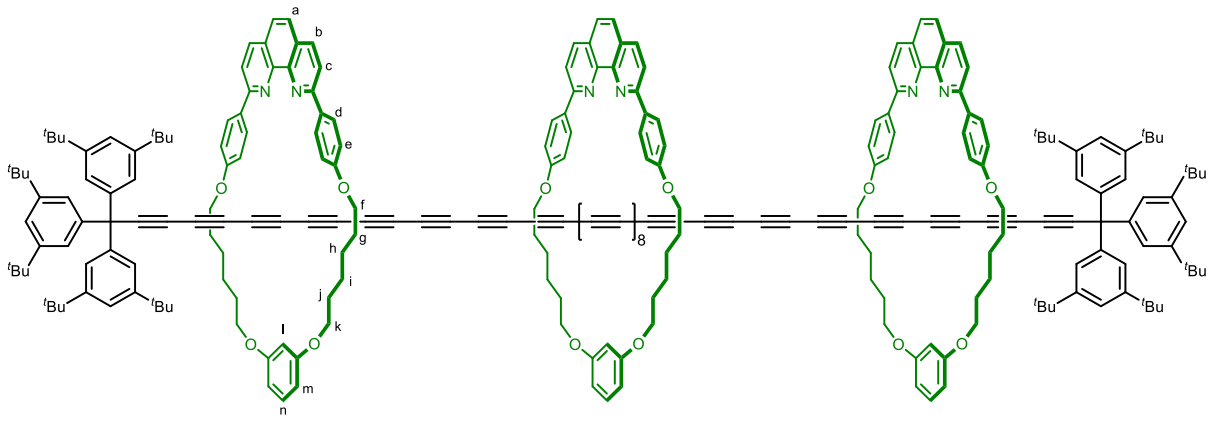

3-Chlorobenzoperoxoic acid (4.8 mg, 70 wt%, 30 eq., 20 μmol) was added in one portion to a solution of octacobalt [4]rotaxane **4.16·(M4)$_3$** (4.0 mg, 1.0 eq., 0.66 μmol) in CH_2Cl_2 (2.0 mL). The mixture was stirred for at 20 °C for 5 min. Water (5 mL) was added and the organic layer extracted. The aqueous layer was washed with CH_2Cl_2 (2 × 2.0 mL), then the combined organic extracts washed with brine (10 mL). The combined organic extracts were dried over Na_2SO_4 and the solvent removed under reduced pressure. The crude material was purified by silica chromatography (CH_2Cl_2/EtOAc, gradient elution from 0 to 33%) to yield 24-yne [4]rotaxane **4.19·(M4)$_3$** (1.5 mg, 0.42 μmol, 64%) as a deep red-orange solid.

Raman (CH_2Cl_2, only selected signals) 1909.87 (C≡C) cm^{-1}.

Tr* [2]rotaxane 3.22·M6

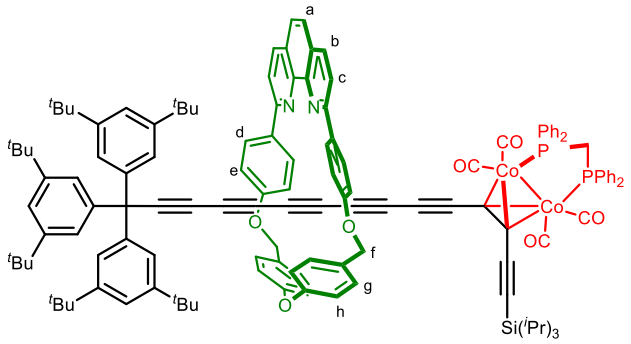

Diaryl ether phenanthroline macrocycle **M6** (40.1 mg, 1.05 eq., 71.7 μmol) and copper(I) iodide (13.0 mg, 1.00 eq., 68.3 μmol) were combined and dissolved in a solution of dry MeCN (2.00 mL) and dry CH_2Cl_2 (2.8 mL) and stirred for 1 h under Ar at 20 °C. The solvent was removed under reduced pressure and the residual solid dissolved in dry THF (5 mL). Deprotected cobalt diyne **3.20** (62.0 mg, 1.00 eq., 71.7 μmol), Tr* triyne bromide **3.10** (50.0 mg, 1.00 eq., 68.3 μmol) and potassium carbonate (47.2 mg, 5.00 eq., 342 μmol) were combined, evacuated of air and flushed with Ar three times. The solids were cooled in liquid nitrogen, before adding the Cu-macrocycle complex, along with additional dry THF (5 mL). The reaction mixture was thoroughly degassed (3 freeze-pump-thaw cycles) before warming to 60 °C and stirring under Ar for 18 h. EDTA/NH_3 solution (10 mL) was added to the cooled reaction mixture and left to stir for 1 h. Et_2O (10 mL) was added and the organic layer extracted. The aqueous layer was washed with Et_2O (2 × 5 mL) and the combined organic extracts dried over Na_2SO_4 before removing the solvent under reduced pressure. The crude product was subject to a SiO_2 chromatography (pet. ether/EtOAc, 1:1) then size-exclusion chromatography (Bio-Rad S-X3, toluene) then SiO_2 chromatography (pet. ether. EtOAc, gradient elution from 0 to 40%) to yield Tr* [2]rotaxane **3.22·M6** (14.0 mg, 6.74 μmol, 10%) and tetracobalt [2]rotaxane **4.1·M6** (14.0 mg, 7.51 μmol, 11%) as a red-brown crystalline solids.

^{1}H NMR (600 MHz, CD_2Cl_2) δ_H 8.22 (d, J = 8.3 Hz, 2H, H_b), 7.98 (d, J = 8.9 Hz, 4H, H_d), 7.90 (d, J = 8.3 Hz, 2H, H_c), 7.74 (s, 2H, H_a), 7.40 – 7.36 (m, 4H, Co Ar-H), 7.35 – 7.30 (m, 6H, H_g & Co Ar-H), 7.29 – 7.25 (m, 11H, H_h, Tr* Ar-H & Co Ar-H), 7.18 – 7.14 (m, 4H, Co Ar-H), 7.09 (dd, J = 9.5, 5.8 Hz, 2H, Co Ar-H), 7.02 (t, J = 7.3 Hz, 4H, Co Ar-H), 6.96 (d, J = 8.9 Hz, 4H, H_e), 6.93 (d, J = 1.7 Hz, 6H, Tr* Ar-H), 5.29 (d, J = 4.5 Hz, 4H), 3.46 – 3.31 (m, 2H), 1.18 (s, 54H), 1.06 – 1.01 (m, 21H).

^{13}C NMR (151 MHz, CD_2Cl_2) δ_C 204.26 (br, C≡O), 201.32 (br, C≡O), 159.81 (C_c-C-N), 158.52, 158.16, 150.70, 147.02 (C_a-C-C_b), 144.02, 137.11 (t, *J* = 25.4 Hz, Co Ar-C), 136.38 (C_b), 134.47 (C_f-C), 134.32 (C_e-C), 133.28 (t, *J* = 17.0 Hz, Co Ar-C), 132.71 (t, *J* = 6.3 Hz, Co Ar-C), 131.48 (t, *J* = 6.1 Hz, Co Ar-C), 130.62 (Co Ar-C), 130.19 (Co Ar-C), 130.06 (C_d), 128.90 (t, *J* = 5.0 Hz, Co Ar-C), 128.67 (t, *J* = 5.0 Hz, Co Ar-C), 127.66, 127.55 (C_h), 125.83 (C_a), 123.94 (Tr* Ar-C), 122.54 (C_g), 120.93 (Tr* Ar-C), 120.60 (C_c), 116.62 (C_e), 108.72 (C≡C), 101.64 (C≡C), 85.96 (C≡C), 81.97 (C≡C), 71.20 (C≡C), 70.71 (C_f), 70.34 (C≡C), 68.18 (C≡C), 66.92 (C≡C), 65.24 (C≡C), 64.64 (C≡C), 64.55 (C≡C), 63.82 (C≡C), 57.80 (CAr_3), 36.24 (br, P-CH_2-P), 35.15 ($C(CH_3)_3$), 31.52 ($C(CH_3)_3$), 18.99 ($CH(CH_3)_2$), 11.89 ($CH(CH_3)_2$). *(2 carbons not distinguished)*

^{31}P{H} NMR (202 MHz, CD_2Cl_2) δ_P 38.30.

HRMS *m/z* = 2077.7999 $[M+H]^+$ ($C_{133}H_{133}Co_2N_2O_7P_2Si^+$ requires 2077.8016)

Tetracobalt [2]rotaxane 4.1·M6

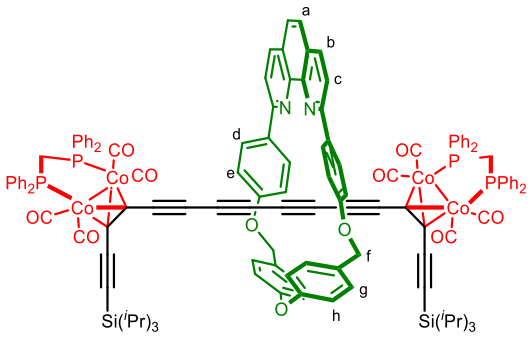

Procedure as above

^{1}H NMR (500 MHz, CD_2Cl_2) δ_H 8.21 (d, *J* = 8.3 Hz, 2H, H_b), 8.08 (d, *J* = 8.8 Hz, 4H, H_d), 7.92 (d, *J* = 8.3 Hz, 2H, H_c), 7.72 (s, 2H, H_a), 7.41 – 7.35 (m, 16H, H_g & Co Ar-H), 7.31 – 7.24 (m, 12H, H_h & Co Ar-H), 7.18 – 7.14 (m, 8H, Co Ar-H), 7.12 – 7.06 (m, 4H, H_e), 7.05 – 7.00 (m, 12H, Co Ar-H), 5.30 (s, 4H, H_f), 3.47 – 3.31 (m, 4H, P-CH_2), 1.04 (s, 42H, Si(^{i}Pr)$_3$).

^{13}C NMR (126 MHz, CD_2Cl_2) δ_C 160.01 (O-C-C_e), 158.53, 158.08 (N-C-C-N), 147.04 (C_a-C-C_b), 137.15 (br, C≡C-C-Co), 136.27 (C_b), 134.55, 134.22 (C_c-C-N), 133.46 (br, C≡C-C-Co), 132.66 (t, $J_{C\text{-}P}$ = 5.9 Hz, Ar-C), 131.51 (t, $J_{C\text{-}P}$ = 6.0 Hz, Ar-C), 130.54 (Ar-C), 130.11 (C_d), 129.37, 128.84 (t, $J_{C\text{-}P}$ = 4.9 Hz, Ar-C), 128.64 (t, $J_{C\text{-}P}$ = 4.9 Hz, Ar-CH), 127.54, 127.50, 125.74 (C_a), 122.77 (C_g), 120.37 (C_c), 116.82 (C_e), 108.90, 101.29, 83.27 (C≡C), 82.52 (C≡C), 72.56 (C≡C), 70.96 (C_f),

67.89 (C≡C), 35.97 (br, P-<u>C</u>H$_2$-P), 18.98 (CH(<u>C</u>H$_3$)$_2$), 11.88 (<u>C</u>H(CH$_3$)$_2$). *(2 carbons not distinguished)*

^{31}P{H} NMR (202 MHz, CD_2Cl_2) δ_P 38.20.

HRMS *m/z* = 2293.4133 $[M+H]^+$ ($C_{130}H_{113}Co_4N_2O_{11}P_4Si_2^+$ requires 2293.4156)

IR (ATR) (only selected signals) 2941.72 (C-H), 2863.82 (C-H), 2150.06 (C≡C), 2102.94 (C≡C), 2033.01 (s, C=O), 2012.58 (s, C=O), 1987.81 (s, C=O) cm^{-1}.

UV-vis ($CHCl_3$) λ_{max} (ε) 569 (9880), 409 (91100), 384 (85100), 357 (79000), 314 (85900), 282 (111000) nm.

Tr* heptayne [2]rotaxane

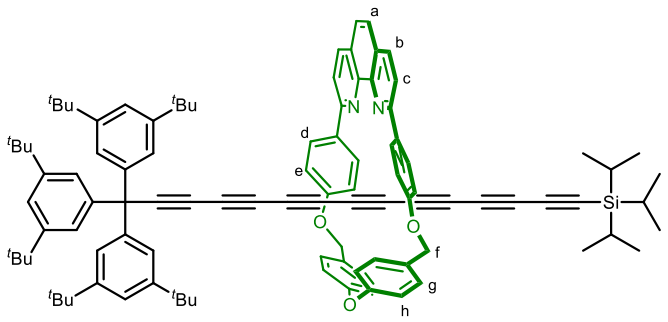

A solution of I_2 (20 mg, 8.0 eq., 77 µmol) in dry MeCN (2.0 mL) was added in one portion to a solution Tr* [2]rotaxane **3.22·M6** (20 mg, 1.0 eq., 9.6 µmol) dissolved in dry THF (4.0 mL). The mixture was stirred for 10 min at 20 °C before being quenched by addition of sat. aqueous $Na_2S_2O_3$ solution (10 mL). CH_2Cl_2 (20 mL) was added, the organic layer separated and then washed with brine (20 mL). The organic extract was dried over Na_2SO_4 and the solvent removed under reduced pressure. The crude material was purified by silica chromatography (pet. ether/EtOAc, gradient elution from 0 to 20%) to yield the heptayne [2]rotaxane (3.0 mg, 2.0 µmol, 21%) as a light brown solid.

^{1}H NMR (500 MHz, $CDCl_3$) δ_H 8.19 (d, *J* = 8.2 Hz, 2H, H_b), 7.93 – 7.90 (m, 4H, H_d), 7.88 (d, *J* = 8.4 Hz, 2H, H_c), 7.70 (s, 2H, H_a), 7.29 (d, *J* = 8.5 Hz, 4H, H_g), 7.26 (s, 3H, Tr* Ar-<u>H</u>), 7.22 (d, *J* = 8.7 Hz, 4H, H_h), 6.91 (d, *J* = 8.9 Hz, 4H, H_e), 6.88 (d, *J* = 1.8 Hz, 6H, Tr* Ar-<u>H</u>), 5.31 (s, 4H), 1.18 (s, 54H, ^{t}Bu), 0.97 (d, *J* = 2.6 Hz, 21H, Si^{i}Pr$_3$).

HRMS *m/z* = 1463.8346 $[M+H]^+$ ($C_{104}H_{111}N_2O_3Si^+$ requires 1463.8358)

Deprotected tetracobalt [2]rotaxane 4.8·M6

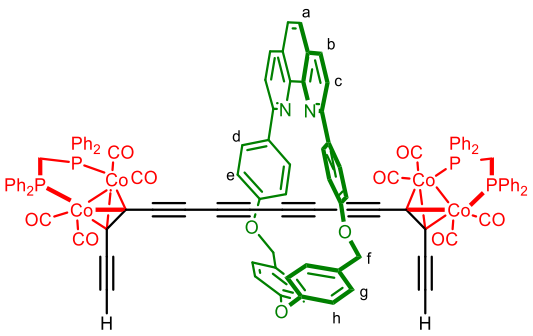

Tetracobalt [2]rotaxane **4.1·M6** (50 mg, 1.0 eq., 22 μmol) was dissolved in THF (10 mL) containing water (0.10 mL). TBAF solution (1.0 M in THF, 7.1 mg, 0.22 mL, 10 eq., 0.22 mmol) was added dropwise and the mixture stirred at 20 °C for 2.5 h. The reaction was quenched with addition of aqueous NH_4Cl solution (15 mL), then CH_2Cl_2 (10 mL) was added, and the organic layer extracted. The aqueous layer was washed with CH_2Cl_2 (2 × 5 mL) and the combined extracts washed with brine (10 mL), then dried over Na_2SO_4. The solvent was removed under reduced pressure and the crude material purified by silica chromatography (pet. ether/EtOAc, gradient elution from 0 to 40%) to yield deprotected tetracobalt [2]rotaxane **4.8·M6** (28 mg, 14 μmol, 65%) as a dark brown solid.

^{1}H NMR (500 MHz, CD_2Cl_2) δ_H 8.21 (d, *J* = 8.2 Hz, 2H, H_b), 8.10 (d, *J* = 8.9 Hz, 4H, H_d), 7.93 (d, *J* = 8.2 Hz, 2H, H_c), 7.72 (s, 2H, H_a), 7.43 – 7.33 (m, 16H, H_g & Co Ar-H), 7.33 – 7.24 (m, 13H, H_h & Co Ar-H), 7.23 – 7.18 (m, 8H, Co Ar-H), 7.14 – 7.07 (m, 10H, Co Ar-H), 7.05 (d, *J* = 9.3 Hz, 5H, H_e & Co Ar-H), 5.33 (d, *J* = 1.2 Hz, 4H, H_f), 3.40 (dq, *J* = 68.4, 11.0 Hz, 4H, P-CH_2).

Extended tetracobalt [2]rotaxane 4.11·M6

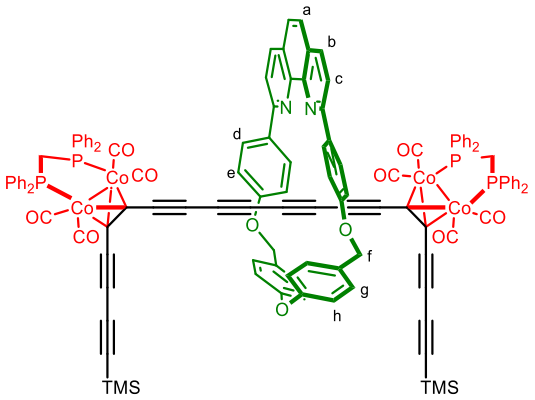

Deprotected tetracobalt [2]rotaxane **4.8·M6** (29 mg, 1.0 eq., 15 μmol) was dissolved in dry CH_2Cl_2 (20 mL). TMS-acetylene (73 mg, 0.10 mL, 50 eq., 0.74 mmol) and copper(I) chloride (15 mg, 10 eq., 0.15 mmol) were added and the solution stirred vigorously in air for 2 min. Freshly-distilled TMEDA (68 mg, 87 μL, 40 eq., 58 μmol) was added to the reaction mixture. The remaining TMS-acetylene (72 mg, 0.10 mL, 50 eq., 0.74 mmol) was added over a period of 30 min via syringe pump. The reaction was monitored by TLC and, upon completion, was quenched by addition of EDTA/NH_3 solution (50 mL) and stirred for 1 h. The organic layer was extracted and washed with water (2 × 20 mL), then brine (20 mL) before drying over Na_2SO_4. The solvent was removed under reduced pressure and the crude material purified by SiO_2 chromatography (pet. ether/EtOAc, gradient elution from 0 to 33%), to yield the extended tetracobalt [2]rotaxane **4.11·M6** (12 mg, 5.6 μmol, 37%) as a red-brown solid.

^{1}H NMR (500 MHz, CD_2Cl_2) δ_H 8.21 (d, J = 8.4 Hz, 2H, H_b), 8.09 (d, J = 8.7 Hz, 4H, H_d), 7.93 (d, J = 8.4 Hz, 2H, H_c), 7.72 (s, 2H, H_a), 7.40 (d, J = 8.7 Hz, 4H, H_g), 7.37 – 7.34 (m, 4H, H_h), 7.33 – 7.27 (m, 13H, Ar-H), 7.25 – 7.19 (m, 17H, Ar-H), 7.13 – 7.07 (m, 12H, Ar-H), 7.05 (d, J = 8.9 Hz, 4H, H_e), 5.35 (s, 4H, H_f), 3.50 – 3.29 (m, 4H, P-CH_2), 0.26 (s, 18H, $SiMe_3$).

^{13}C NMR (126 MHz, CD_2Cl_2) δ_C 202.95 (br, C≡O), 160.03 (O-C-C_e), 158.51, 158.04 (N-C-C-N), 147.01 (C_a-C-C_b), 136.98, 136.33 (C_b), 135.27 (t, J = 22.2 Hz, Co Ar-C), 134.54, 134.41 (t, J = 20.9 Hz, Co Ar-C), 134.21 (C_c-C-N), 132.08 (t, J = 6.4 Hz, Co Ar-C), 131.93 (t, J = 6.1 Hz, Co Ar-C), 130.58 (Ar-C), 130.44, 130.14 (C_k), 128.89 (q, J = 4.5 Hz, Co Ar-C), 127.55, 127.50, 125.78 (C_a), 122.65 (C_g), 120.41 (C_c), 116.86 (C_e), 93.56 (C≡C), 90.01 (C≡C), 84.23 (C≡C), 82.95 (C≡C), 82.31 (C≡C), 80.53 (C≡C), 72.67 (C≡C), 70.98 (C_f), 67.81 (C≡C), 38.78 (t, J = 21.3 Hz, P-CH_2), -0.17 (Si(CH_3)$_3$). *(3 carbons not distinguished)*

HRMS *m/z* = 2173.2286 $[M+H]^+$ ($C_{122}H_{89}Co_4N_2O_{11}P_4Si_2^+$ requires 2173.2278)

Octacobalt [4]rotaxane 4.16·(M6)$_3$

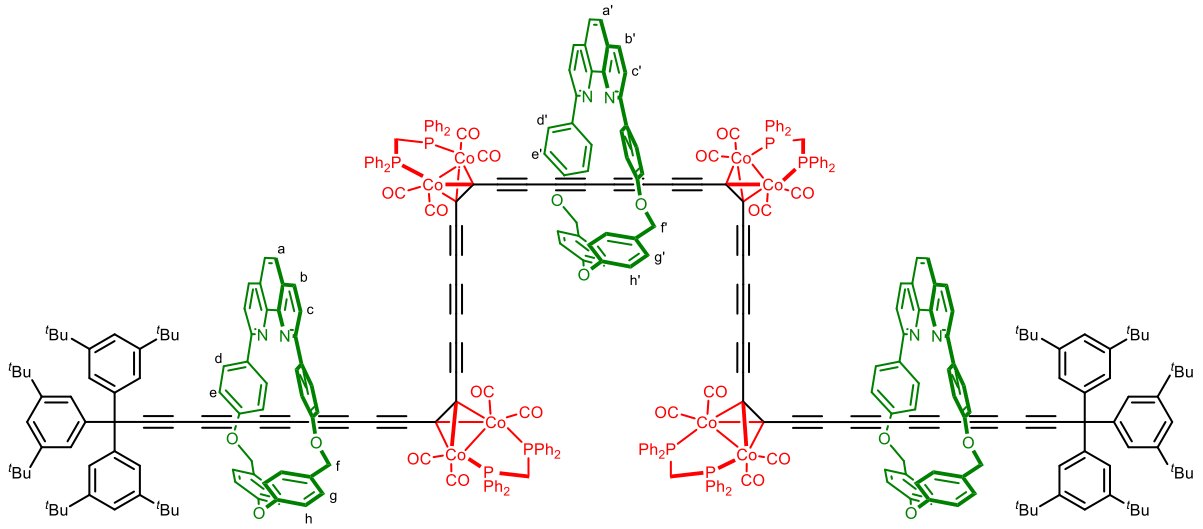

Dry $CHCl_3$ (30 mL) and freshly-distilled diisopropylamine (91 mg, 0.13 mL, 80 eq., 0.91 mmol) was added to bis(triphenylphosphine)palladium(II) dichloride (24 mg, 3.0 eq., 43 μmol), copper(I) iodide (32 mg, 15 eq., 0.17 mmol) and benzoquinone (25 mg, 20 eq., 0.23 mmol). The mixture was stirred in air before addition of a mixture of deprotected Tr* [2]rotaxane **3.23·M6** (44 mg, 2.0 eq., 23 μmol) and deprotected extended tetracobalt [2]rotaxane **4.12·M6** (23 mg, 1.0 eq., 11 μmol) in dry $CHCl_3$ (12 mL) over 1 hour via syringe pump. After complete addition, the reaction was stirred at 20 °C in air for a further 1 hour. EDTA/NH_3 solution (25 mL) was then added, and the mixture stirred for 1 h. The organic layer was extracted, washed with water (25 mL) then brine (25 mL), before being dried over Na_2SO_4 and the solvent removed under reduced pressure. The crude material was purified by recycling GPC (THF) then silica chromatography (CH_2Cl_2/EtOAc with Et_3N additive (5%), gradient elution from 0 to 20%) to yield octacobalt [4]rotaxane **4.16·(M6)$_3$** (15 mg, 2.6 μmol, 23%) and dodecacobalt [5]rotaxane **4.17·(M6)$_4$** (5.0 mg, 0.63 μmol, 5.6%) as dark-brown solids.

^{1}H NMR (600 MHz, CD_2Cl_2) δ_H 8.18 (dd, *J* = 10.6, 8.3 Hz, 6H, $H_{b,b'}$), 8.15 – 8.07 (m, 6H, $H_{d,d'}$), 8.00 – 7.97 (m, 6H, $H_{d,d'}$), 7.89 (dd, *J* = 10.1, 8.3 Hz, 6H, $H_{c,c'}$), 7.70 (s, 4H, H_a), 7.67 (s, 2H, $H_{a'}$), 7.43 – 7.40 (m, 6H, Ar-H), 7.35 – 7.30 (m, 32H, Ar-H), 7.29 – 7.27 (m, 12H, Ar-H), 7.25 – 7.21 (m, 42H, Ar-H), 7.16 – 7.10 (m, 24H, Ar-H), 7.08 – 7.04 (m, 6H, Ar-H), 7.02 (d, *J* = 8.8 Hz, 4H,

$H_{e'}$), 6.97 (d, *J* = 8.7 Hz, 8H, H_e), 6.93 (d, *J* = 1.7 Hz, 12H, Tr* Ar-H), 5.33 (br s, 12H, $H_{f,f'}$), 3.58 – 3.26 (m, 8H, P-CH_2), 1.17 (s, 108H, ^{t}Bu).

^{13}C NMR (151 MHz, CD_2Cl_2) δ 203.32 (br, C≡O), 201.24 (br, C≡O), 160.06, 159.81, 158.60, 158.52, 158.09, 158.00, 150.70, 147.01, 146.98, 143.98, 136.38, 136.33, 135.07 (t, *J* = 21.2 Hz, Co Ar-C), 134.63, 134.50, 134.31, 134.27, 132.15 (dt, *J* = 13.1, 6.0 Hz, Co Ar-C), 131.90 (dt, *J* = 12.4, 5.4 Hz, Co Ar-C), 131.72, 131.48, 130.64, 130.59, 130.16, 130.08, 129.18 – 128.80 (m, Co Ar-C), 128.64, 128.52, 127.63, 127.55, 125.83, 125.78, 123.93, 122.77, 122.53, 120.93, 120.59, 120.40, 116.86, 116.62, 116.30, 116.20, 86.16, 84.92, 84.83, 84.66, 84.42, 83.36, 82.64, 81.66, 73.06, 71.88, 71.49, 71.22, 70.98, 70.69, 70.27, 69.50, 69.35, 68.17, 68.05, 67.15, 65.07, 64.53, 64.46, 64.11, 64.06, 57.80, 38.93 (br, P-CH_2), 35.14 (C$(CH_3)_3$), 31.51 (C(CH_3)$_3$). *(12 carbons not distinguished)*

^{31}P{H} NMR (243 MHz, CD_2Cl_2) δ_P 39.36.

Selected NMR Spectra

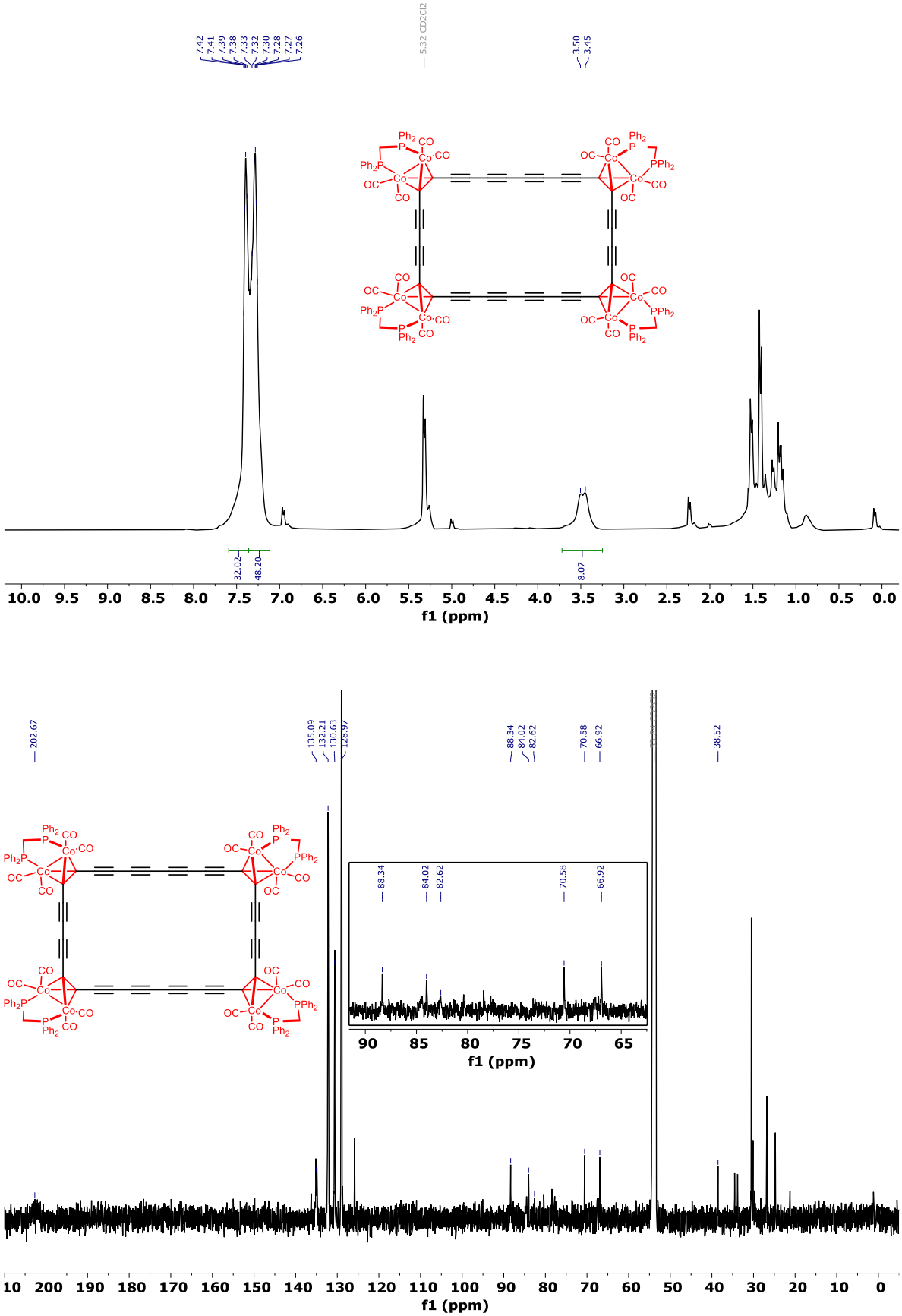

Figure S4.2: (top) ^{1}H NMR (600 MHz) and (bottom) ^{13}C NMR (151 MHz) spectra of cobalt 4-ring **4.9** (CD_2Cl_2, 298 K).

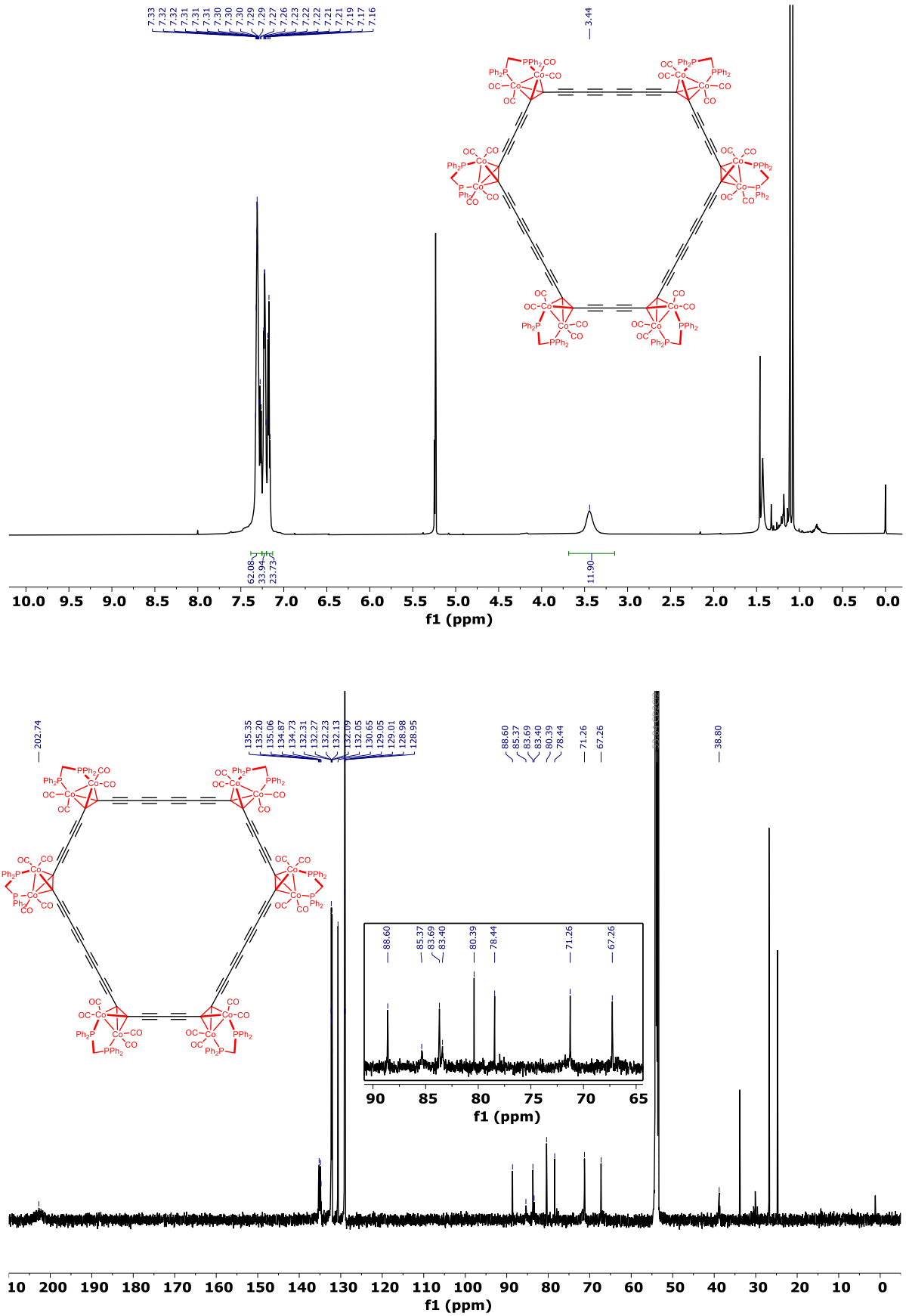

Figure S4.3: (top) ^{1}H NMR (600 MHz) and (bottom) ^{13}C NMR (151 MHz) spectra of cobalt 6-ring **4.10** (CD_2Cl_2, 298 K).

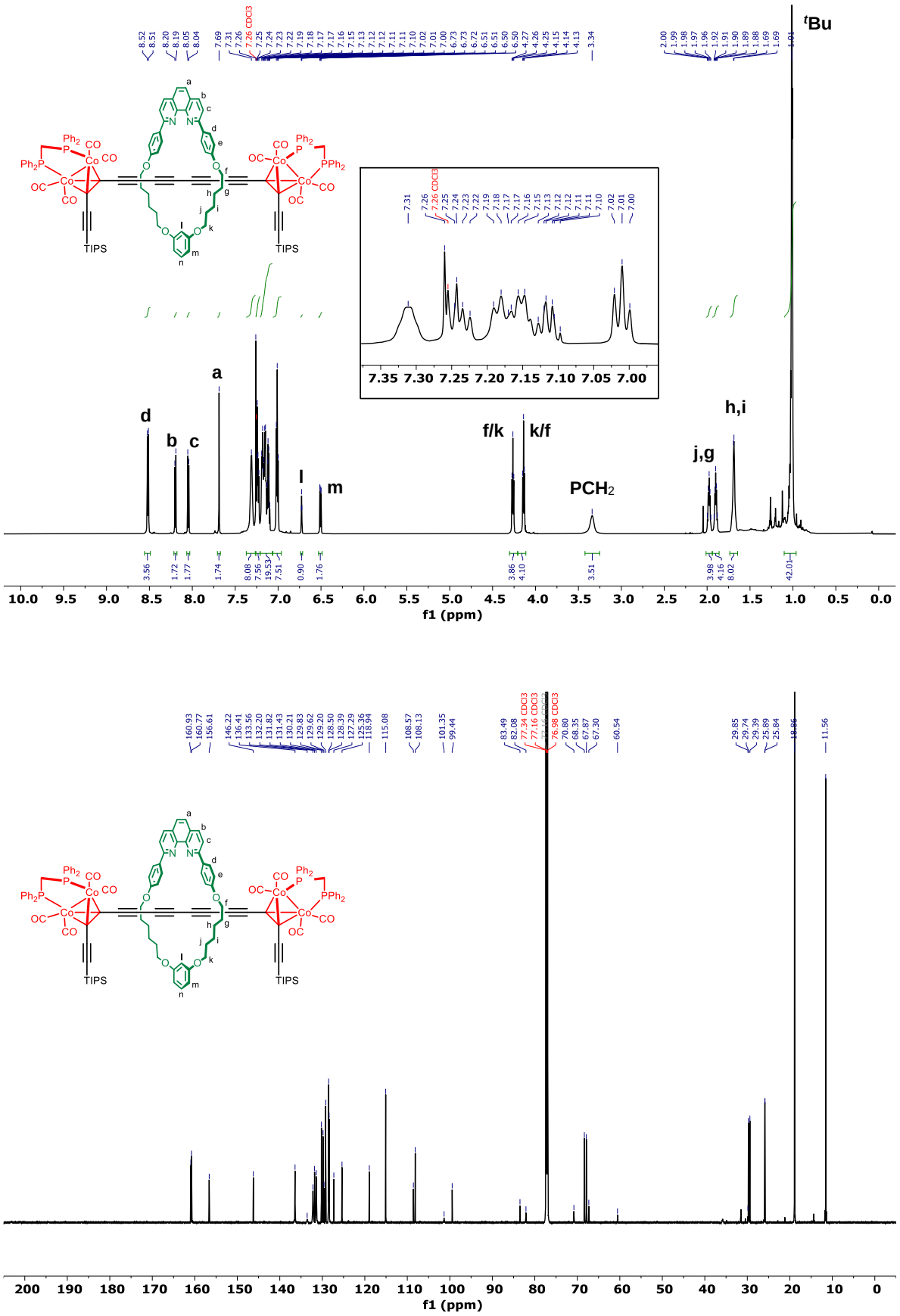

Figure S4.4: (top) ^{1}H NMR (700 MHz) and (bottom) ^{13}C NMR (176 MHz) spectra of tetracobalt [2]rotaxane **4.1·M4** ($CDCl_3$, 298 K).

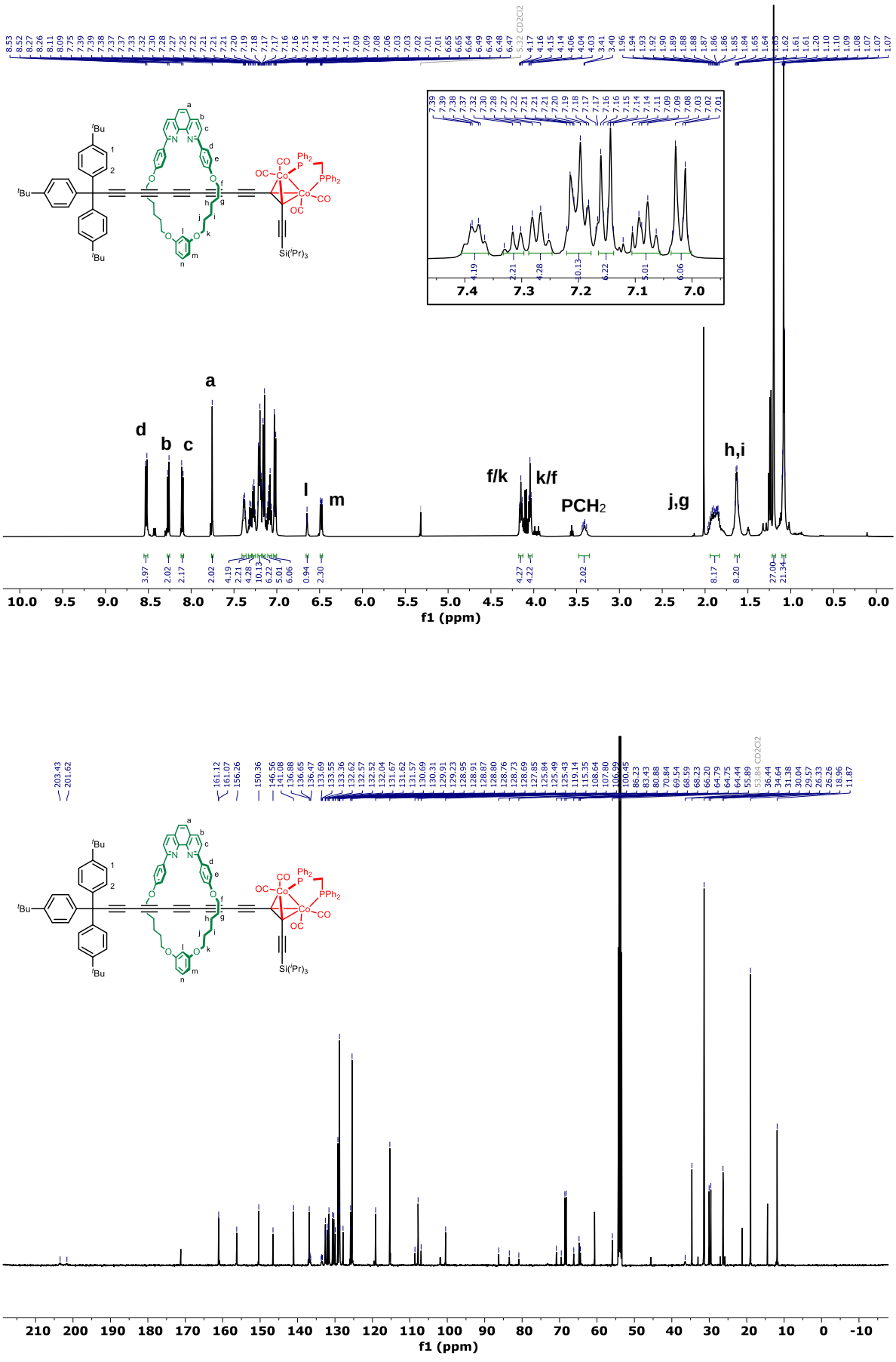

Figure S4.5: (top) ^{1}H NMR (500 MHz) and (bottom) ^{13}C NMR (126 MHz) spectra of *p*-^{t}Bu-stoppered [2]rotaxane **4.7·M4** (CD_2Cl_2, 298 K).

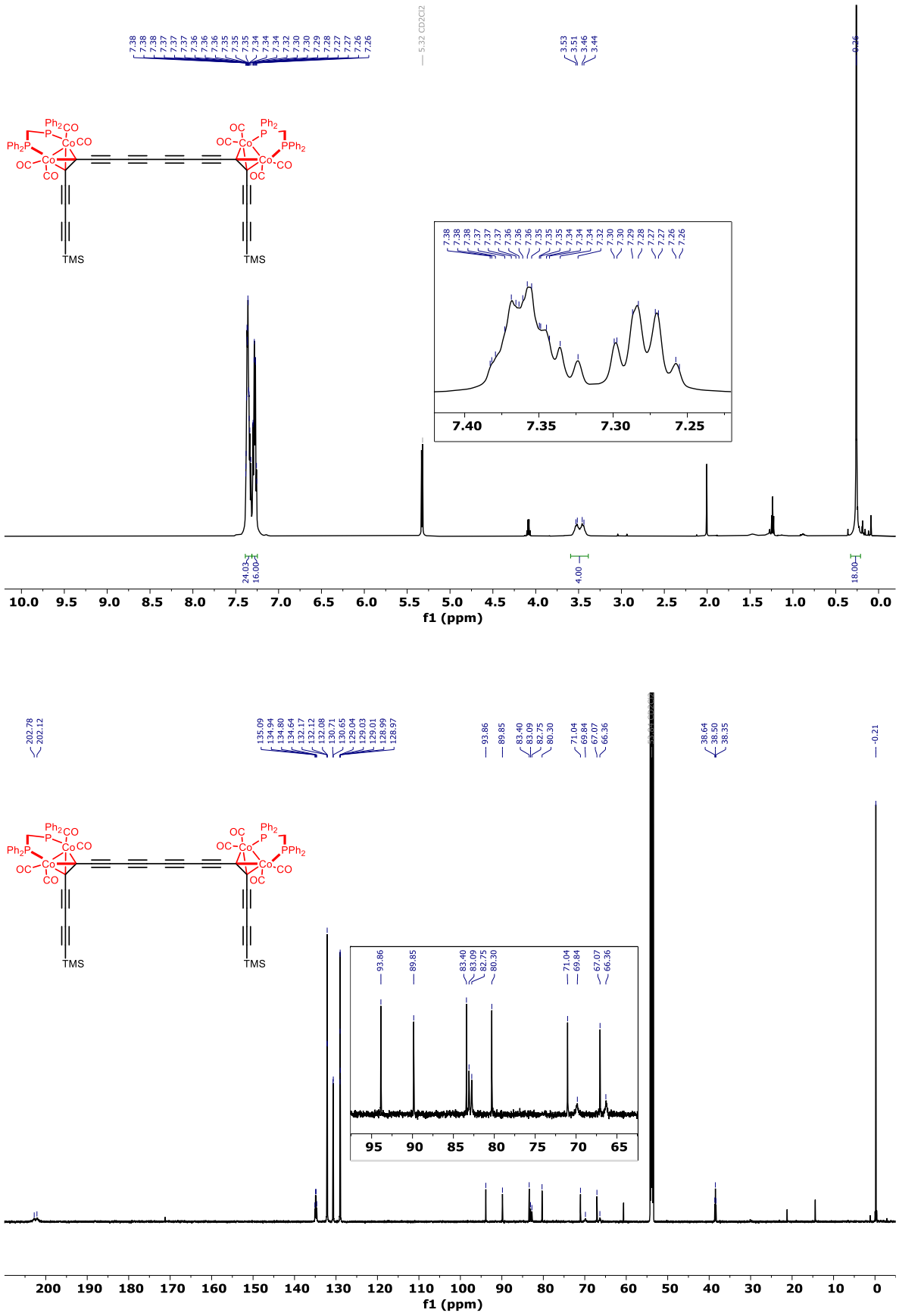

Figure S4.6: (top) ^{1}H NMR (600 MHz) and (bottom) ^{13}C NMR (151 MHz) spectra of extended tetracobalt thread **4.11** (CD_2Cl_2, 298 K).

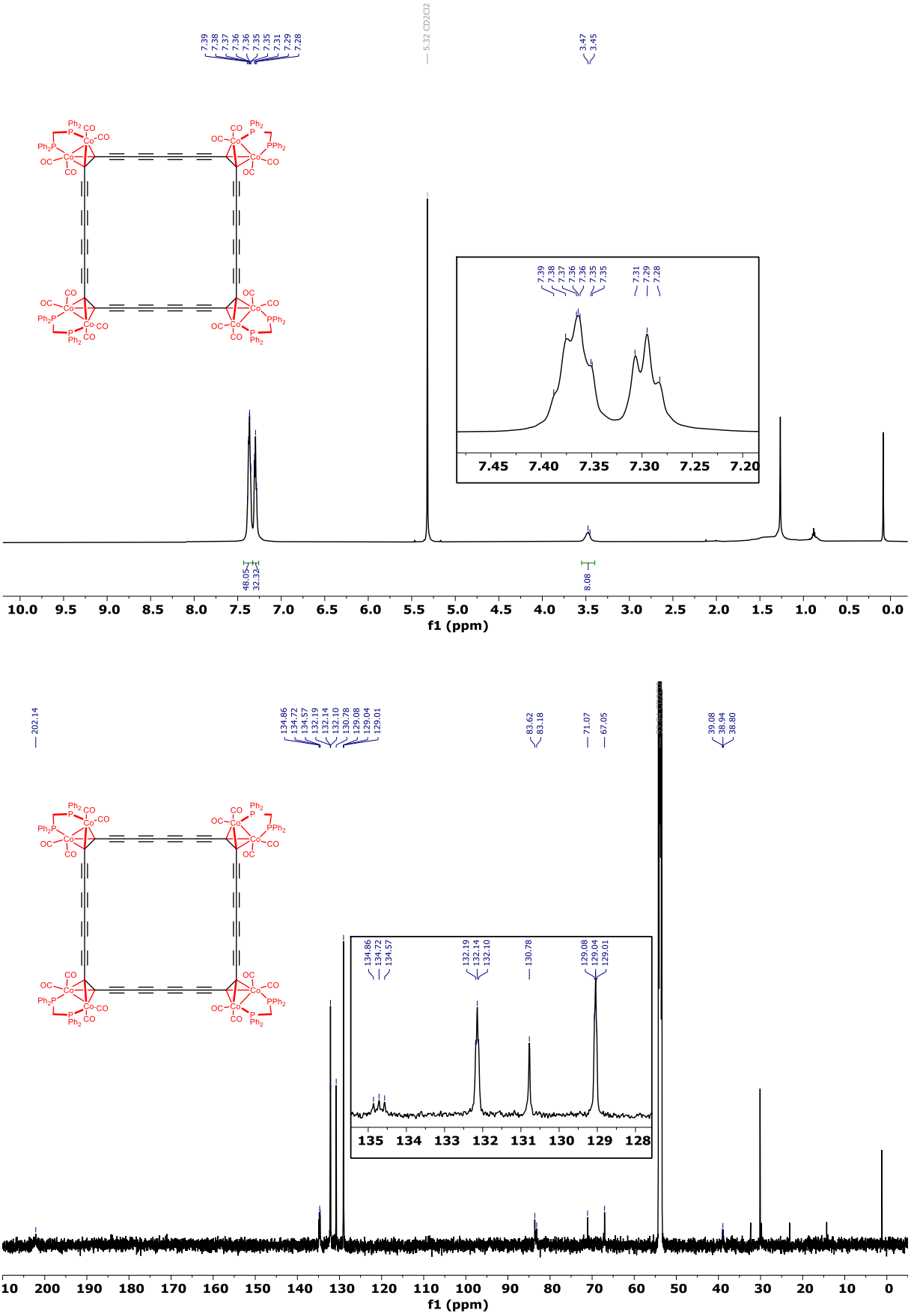

Figure S4.7: (top) ^{1}H NMR (600 MHz) and (bottom) ^{13}C NMR (151 MHz) spectra of extended cobalt 4-ring **4.13** (CD_2Cl_2, 298 K).

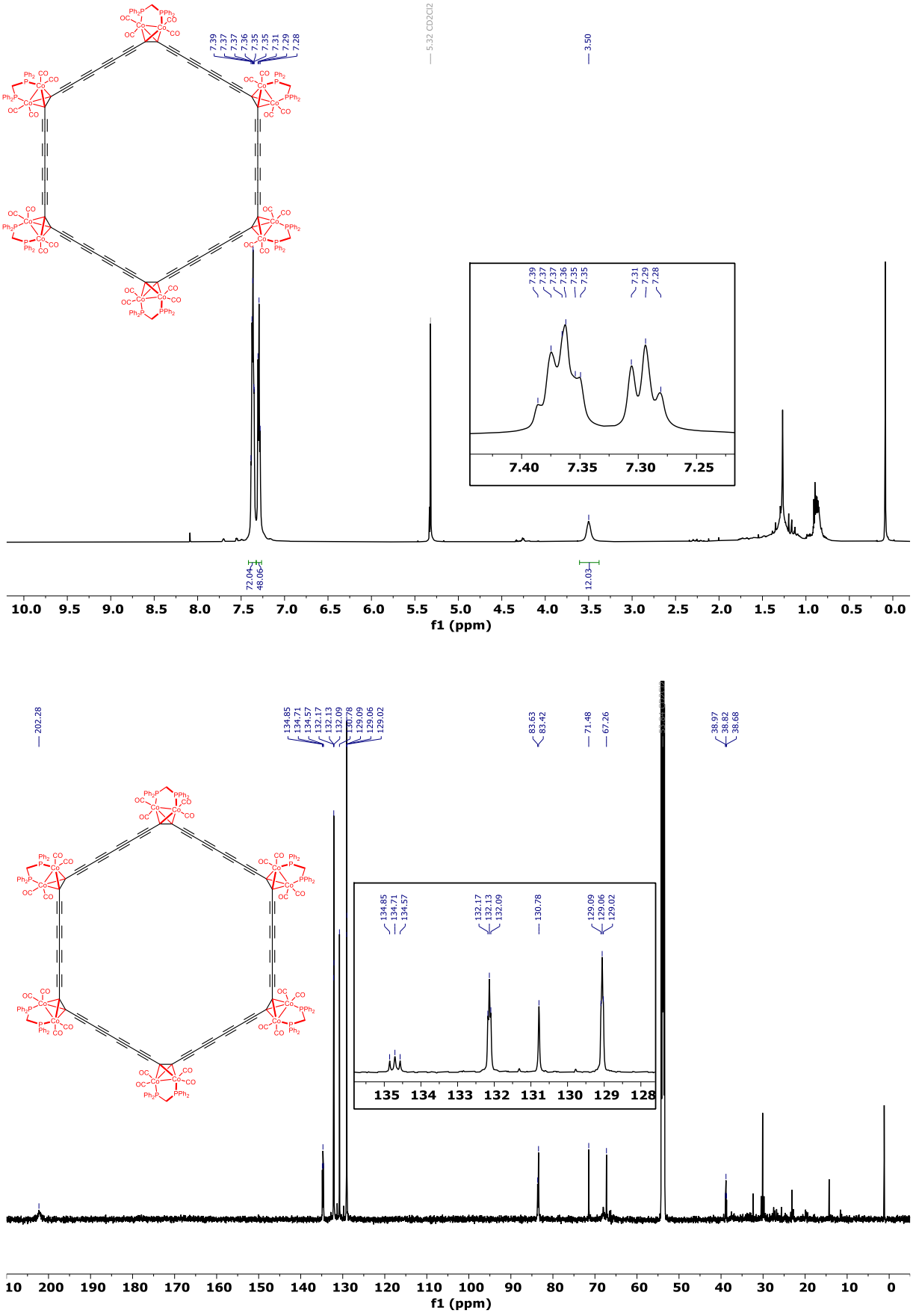

Figure S4.8: (top) ^{1}H NMR (600 MHz) and (bottom) ^{13}C NMR (151 MHz) spectra of extended cobalt 6-ring **4.14** (CD_2Cl_2, 298 K).

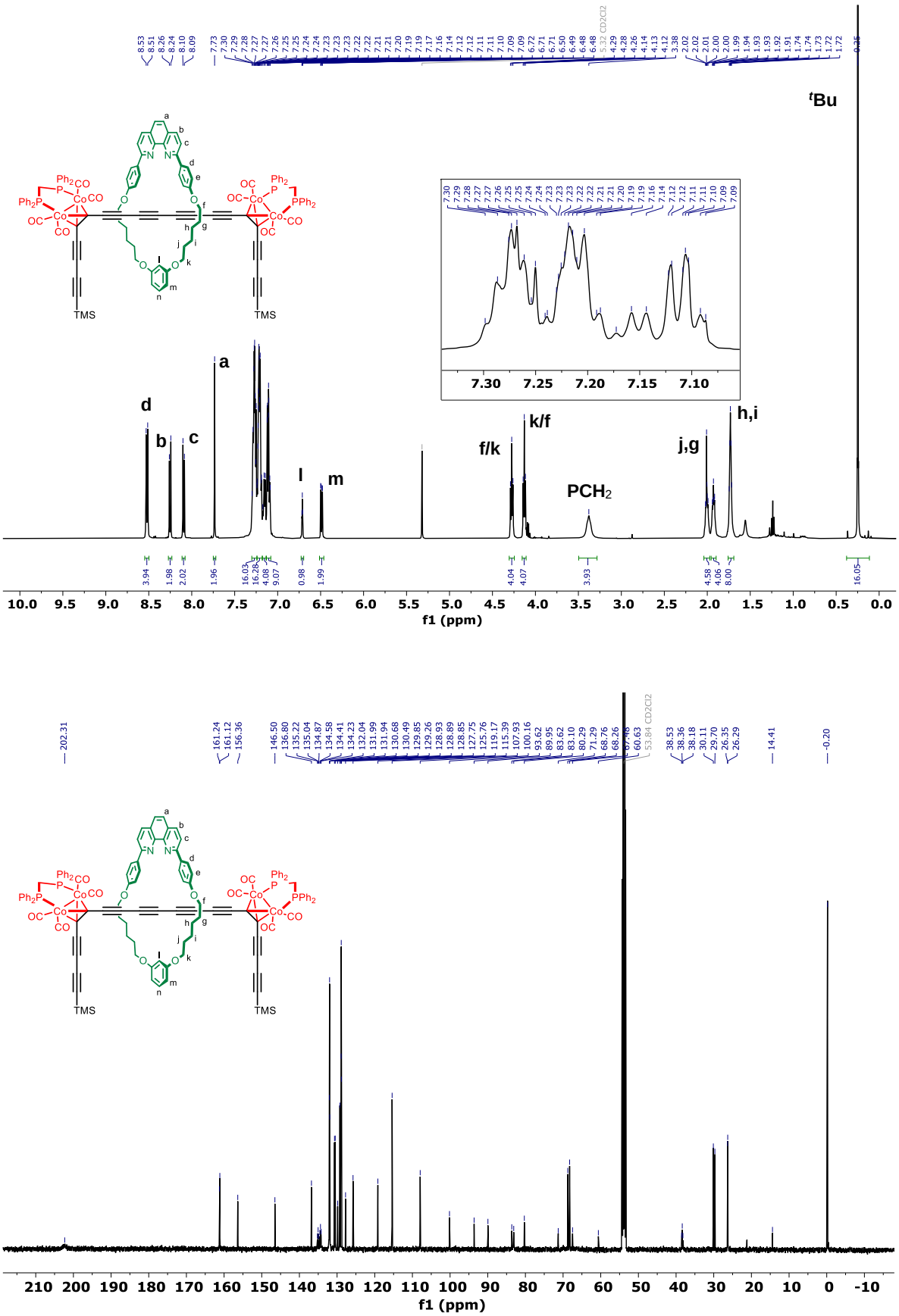

Figure S4.9: (top) ^{1}H NMR (500 MHz) and (bottom) ^{13}C NMR (126 MHz) spectra of extended tetracobalt [2]rotaxane **4.11·M4** (CD_2Cl_2, 298 K).

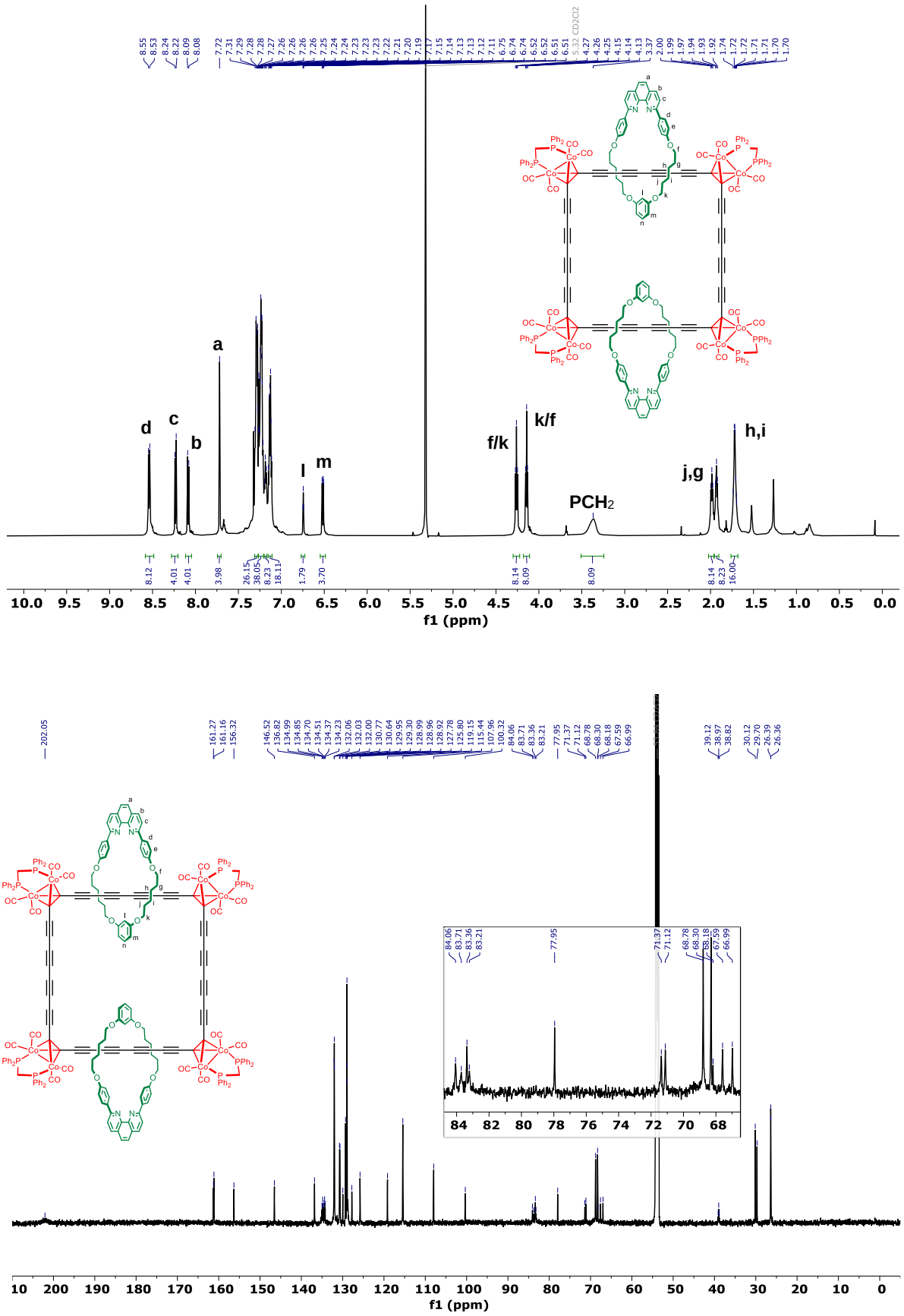

Figure S4.10: (top) ^{1}H NMR (600 MHz) and (bottom) ^{13}C NMR (151 MHz) spectra of octacobalt [3]catenane **4.13**·(**M4**)$_2$ (CD_2Cl_2, 298 K).

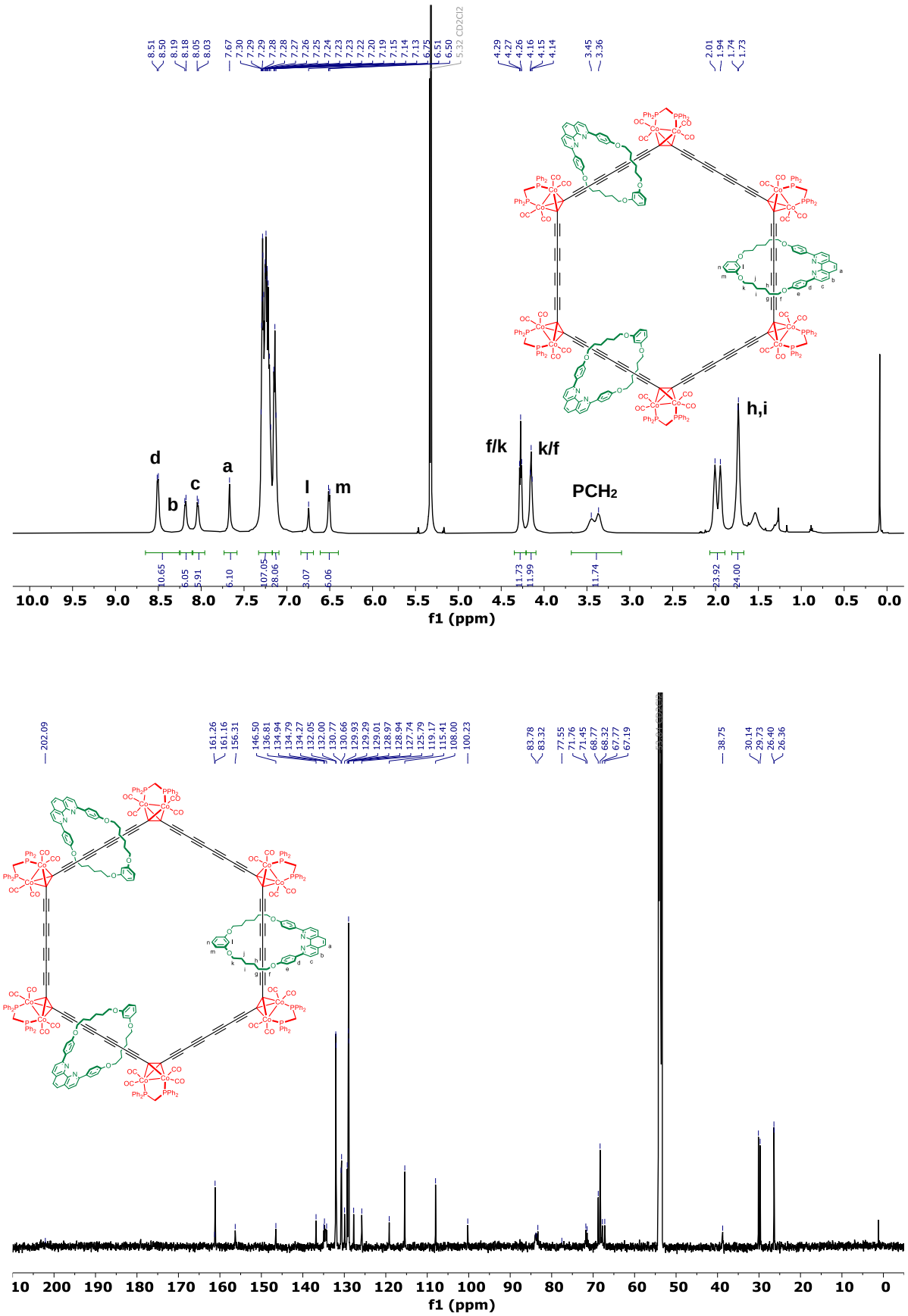

Figure S4.11: (top) ^{1}H NMR (600 MHz) and (bottom) ^{13}C NMR (151 MHz) spectra of dodecacobalt [4]catenane **4.14**·(**M4**)$_3$ (CD_2Cl_2, 298 K).

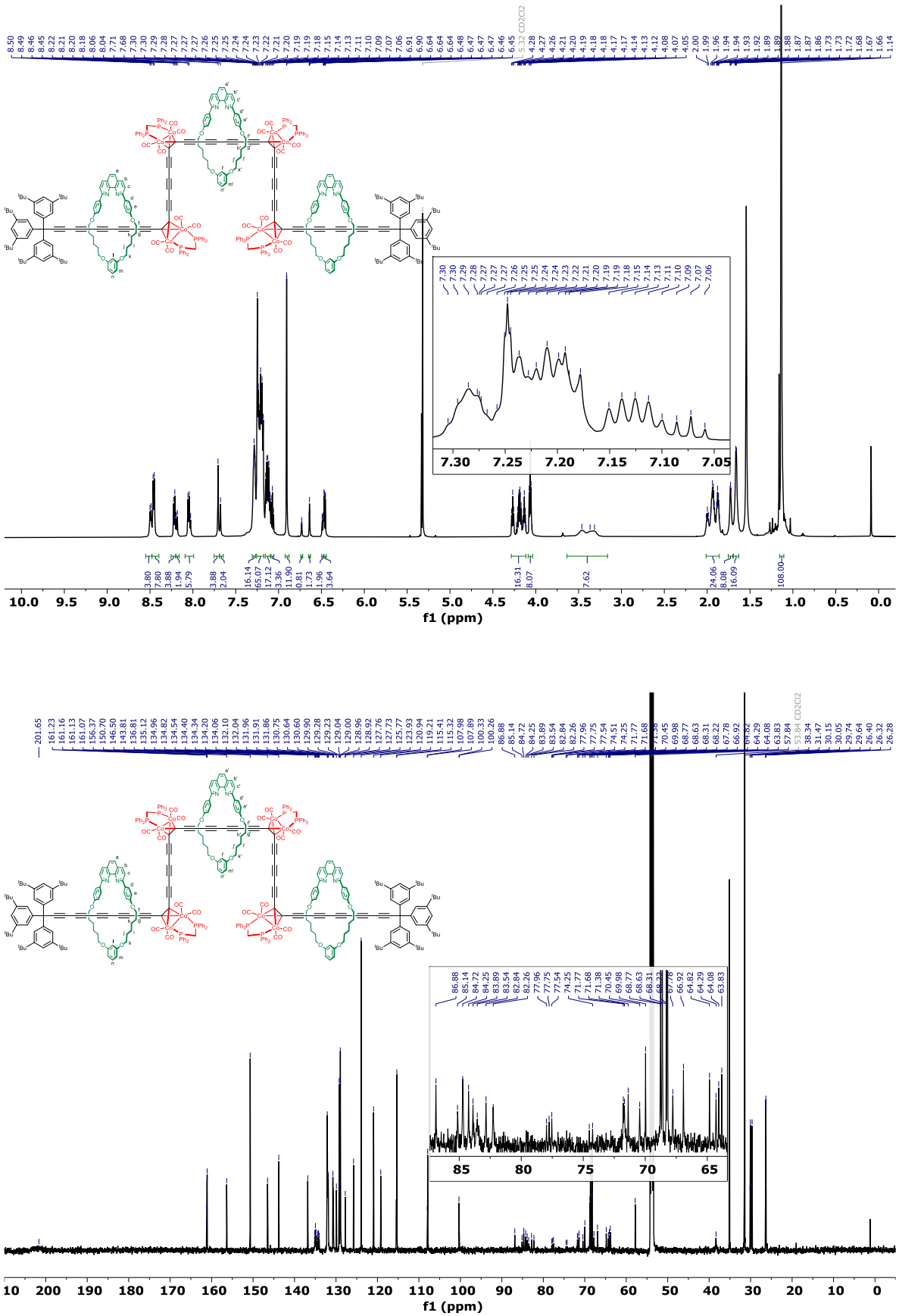

Figure S4.12: (top) ^{1}H NMR (600 MHz) and (bottom) ^{13}C NMR (151 MHz) spectra of octacobalt [4]rotaxane **4.16**·(**M4**)$_3$ (CD_2Cl_2, 298 K).

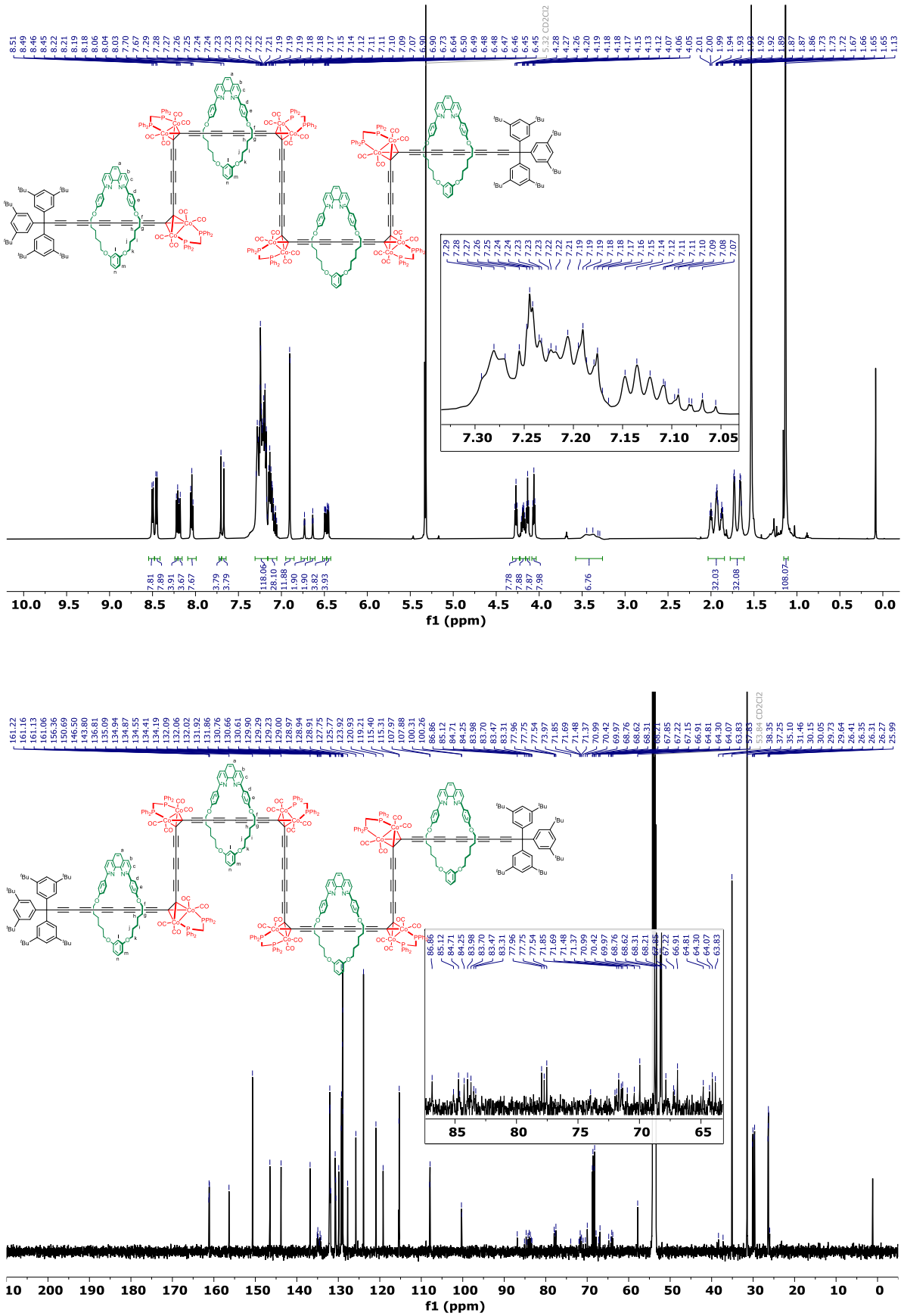

Figure S4.13: (top) ^{1}H NMR (600 MHz) and (bottom) ^{13}C NMR (151 MHz) spectra of dodecacobalt [5]rotaxane **4.17**·(**M4**)$_4$ (CD_2Cl_2, 298 K).

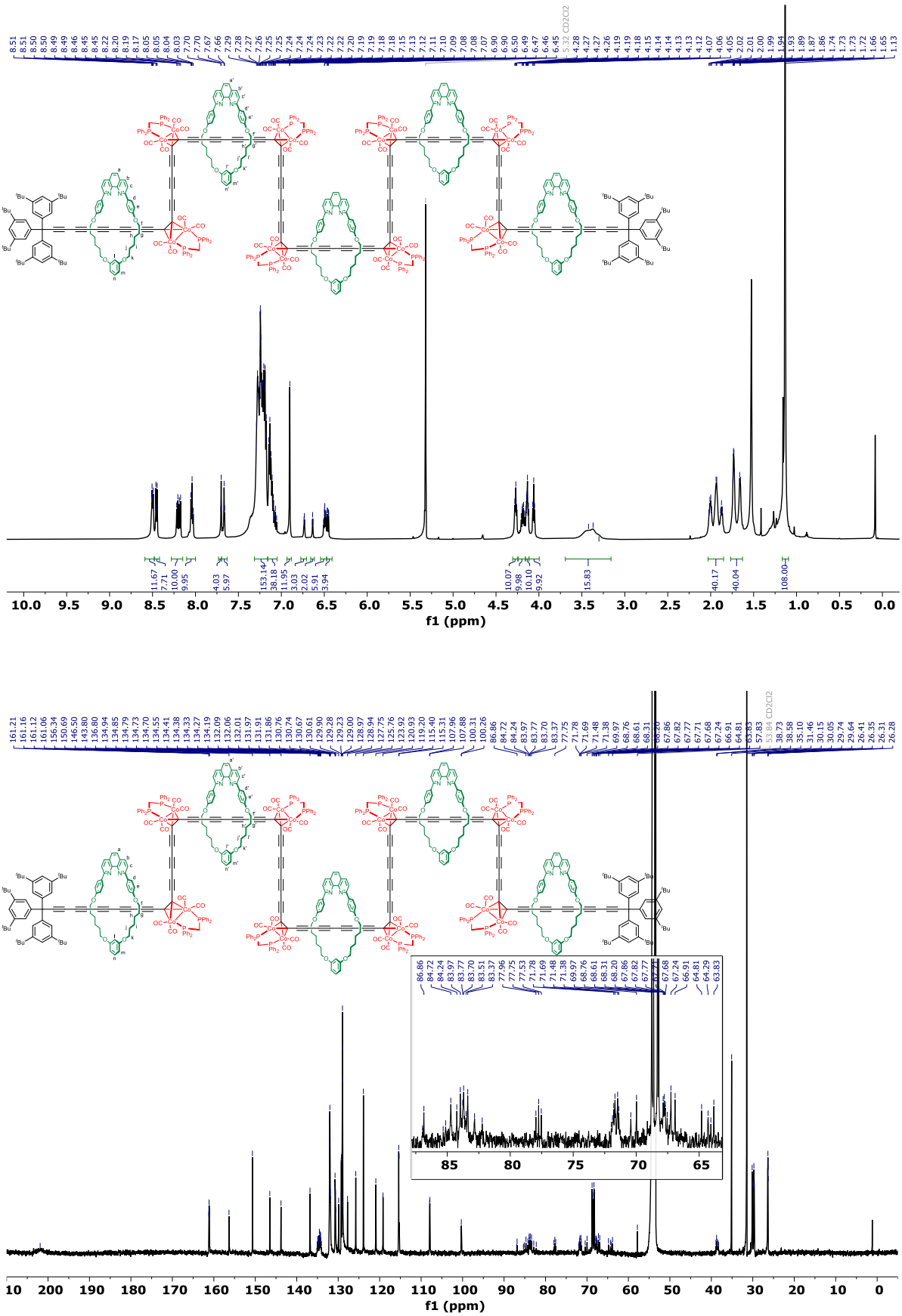

Figure S4.14: (top) ^{1}H NMR (600 MHz) and (bottom) ^{13}C NMR (151 MHz) spectra of hexadecacobalt [6]rotaxane **4.18**·(**M4**)$_5$ (CD_2Cl_2, 298 K).

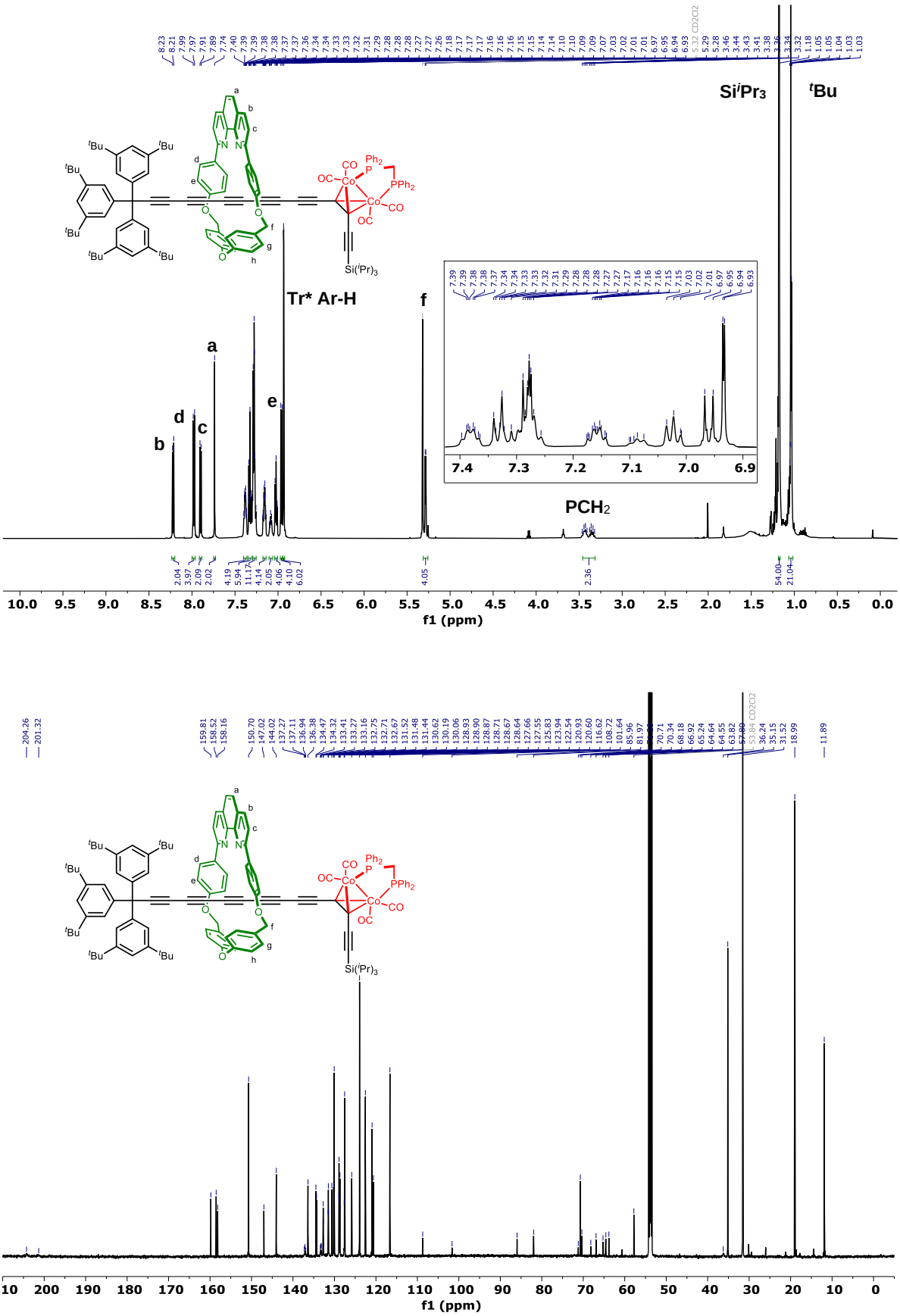

Figure S4.15: (top) ^{1}H NMR (600 MHz) and (bottom) ^{13}C NMR (151 MHz) spectra of supertrityl-stoppered [2]rotaxane **3.22·M6** (CD_2Cl_2, 298 K).

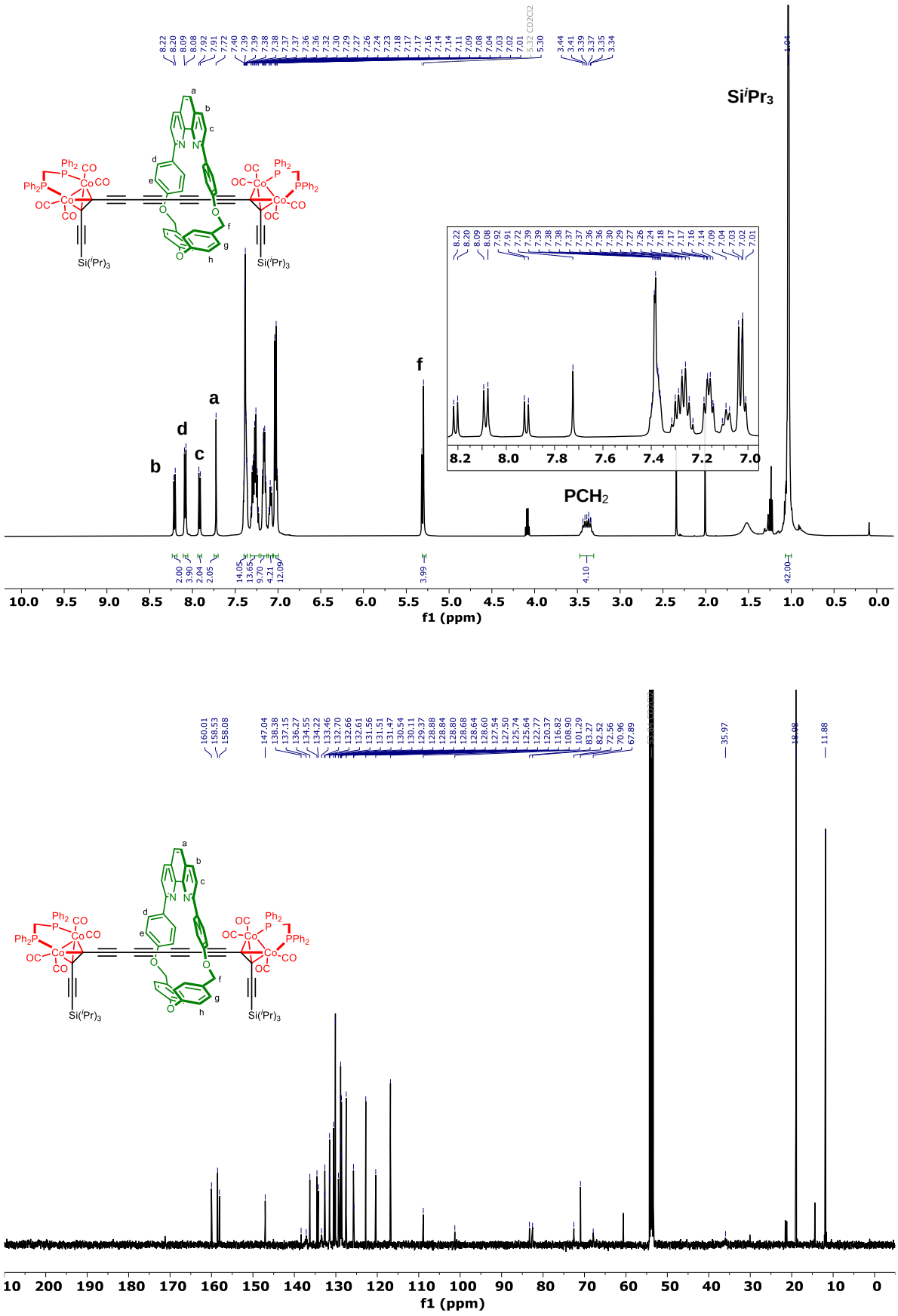

Figure S4.16: (top) ^{1}H NMR (500 MHz) and (bottom) ^{13}C NMR (126 MHz) spectra of tetracobalt [2]rotaxane **4.1·M6** (CD_2Cl_2, 298 K).

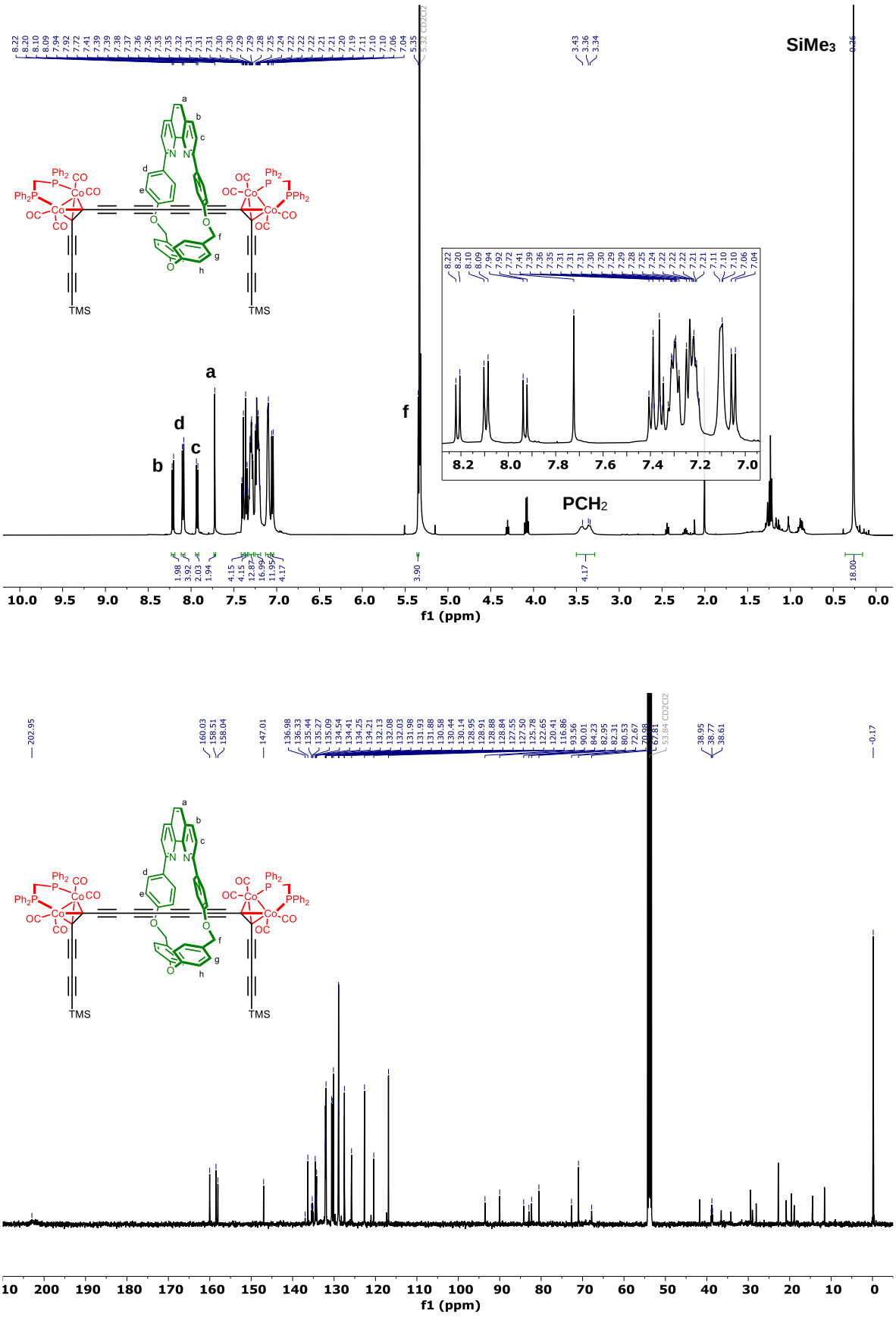

Figure S4.17: (top) ^{1}H NMR (500 MHz) and (bottom) ^{13}C NMR (126 MHz) spectra of extended tetracobalt [2]rotaxane **4.11·M6** (CD_2Cl_2, 298 K).

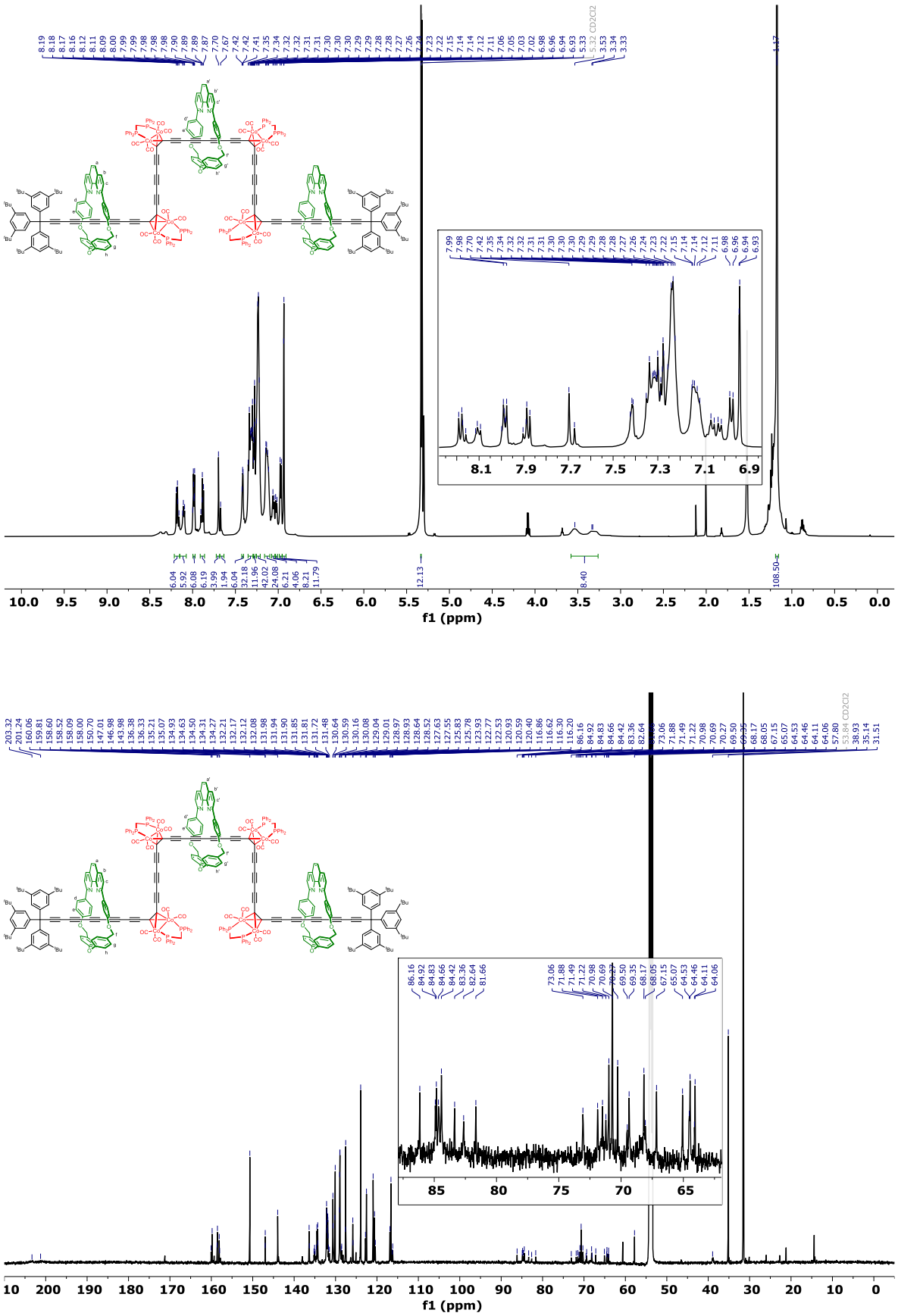

Figure S4.18: (top) ^{1}H NMR (600 MHz) and (bottom) ^{13}C NMR (151 MHz) spectra of octacobalt [4]rotaxane **4.16**·(**M6**)$_3$ (CD_2Cl_2, 298 K).

Selected UV-vis Spectra

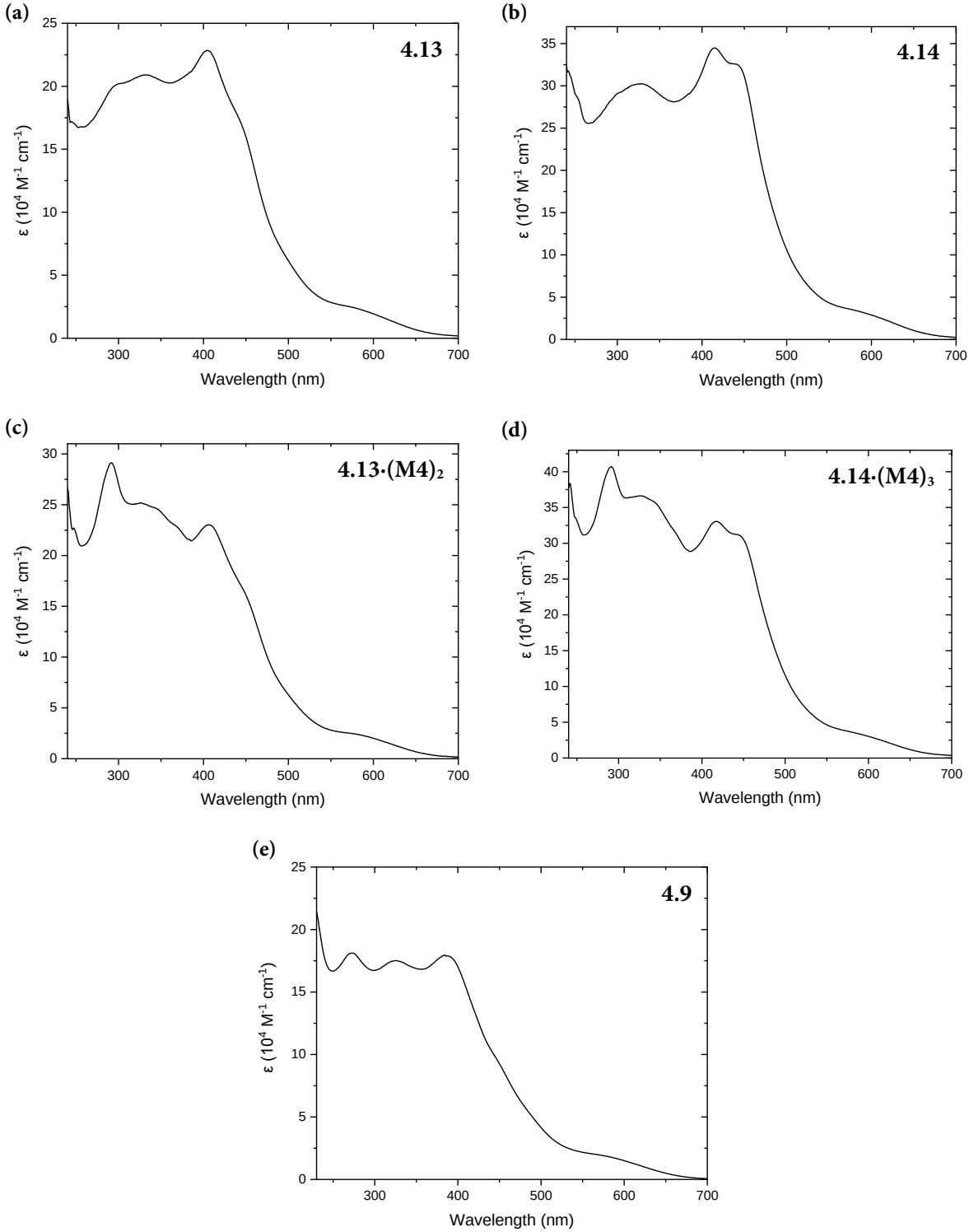

Figure S4.19: UV-vis spectra of (a) extended cobalt 4-ring **4.13**, (b) extended cobalt 6-ring **4.14**, (c) octacobalt [3]catenane **4.13**·(**M4**)$_2$, (d) dodecacobalt [4]catenane **4.14**·(**M4**)$_3$ and (e) cobalt 4-ring **4.9**. All samples recorded in $CHCl_3$ solutions at 25 °C.

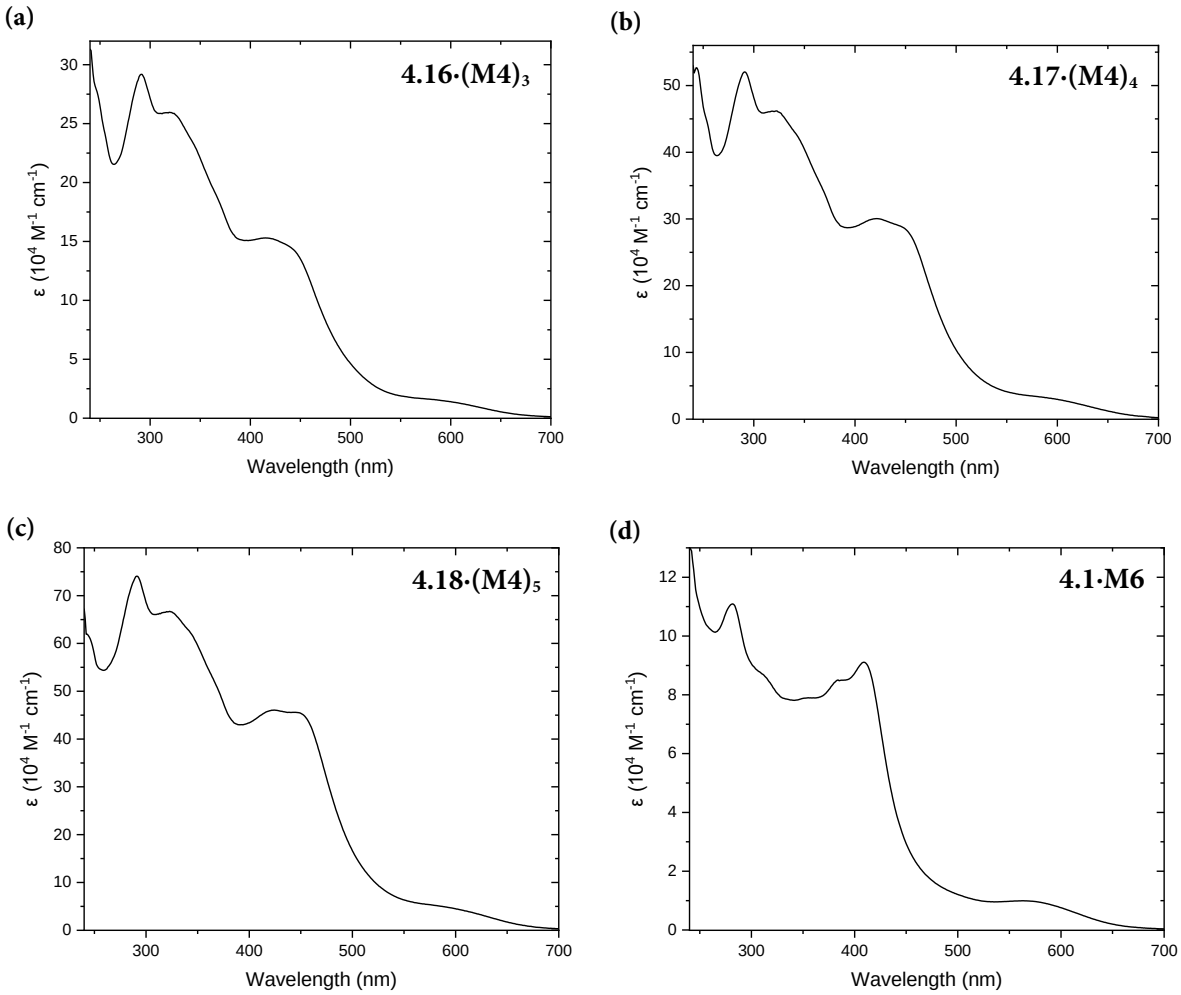

Figure S4.20: UV-vis spectra of (a) octacobalt [4]rotaxane **4.16·(M4)**$_3$, (b) dodecacobalt [5]rotaxane **4.17·(M4)**$_4$, (c) hexadecacobalt [6]rotaxane **4.18·(M4)**$_5$ and (d) tetracobalt [2]rotaxane **4.1·M6**. All samples recorded in $CHCl_3$ solutions at 25 °C.

Raman Spectra

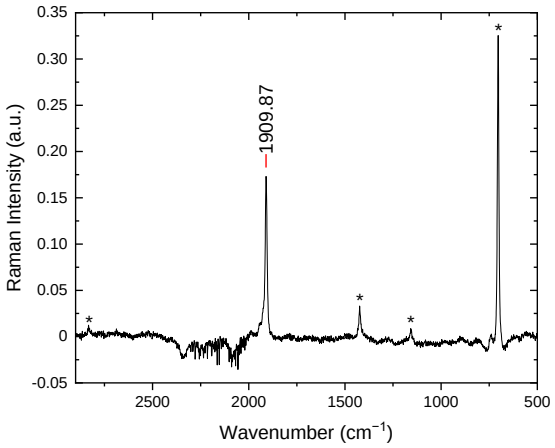

Figure S4.21: FT-Raman spectrum of 24-yne [4]rotaxane **4.19·(M4)**$_3$ (CH_2Cl_2, 298 K). Peaks marked with * denote signals arising from the CH_2Cl_2 solvent.

Selected Analytical GPC Traces

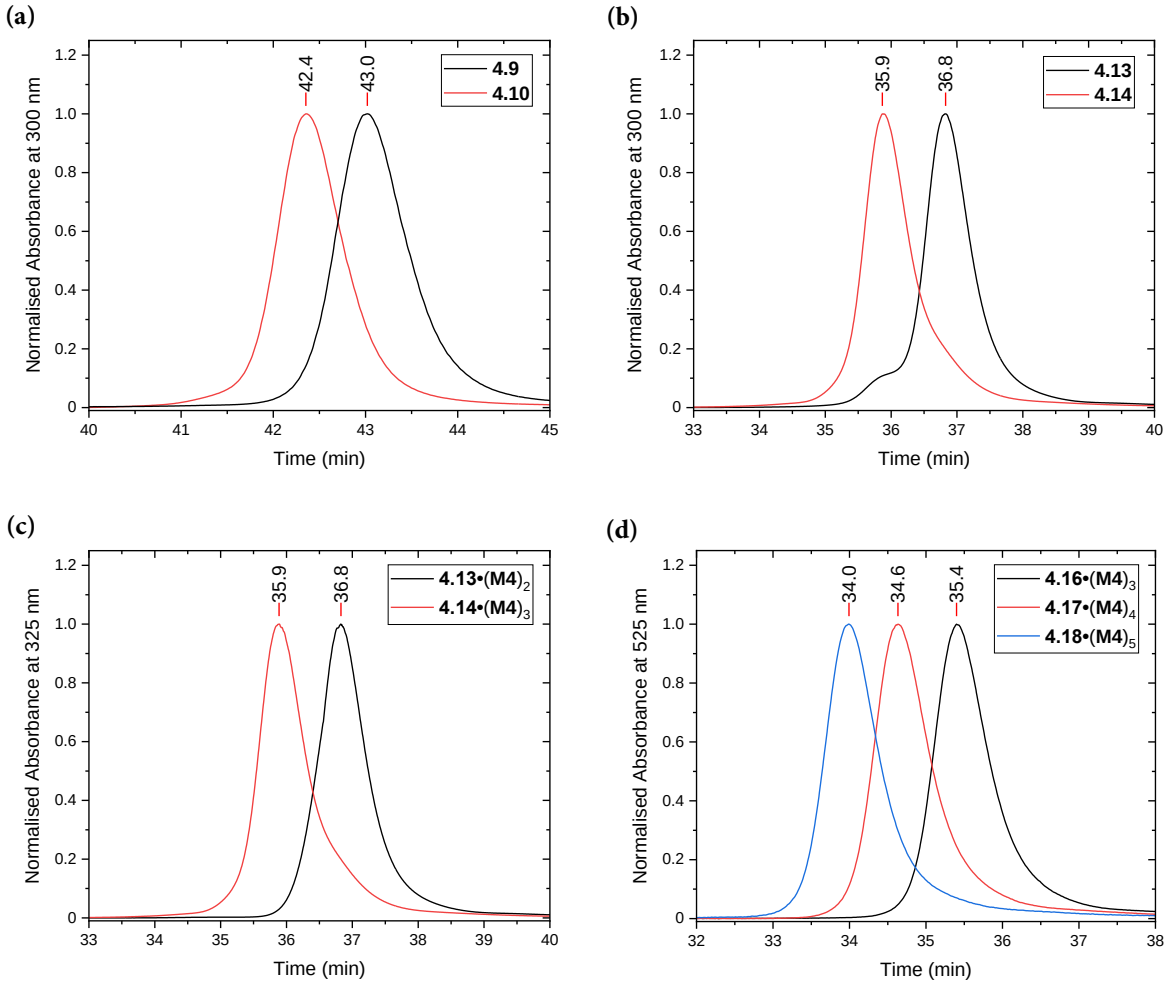

Figure S4.22: Analytical GPC traces of (a) cobalt 4-ring **4.9** (black) and cobalt 6-ring **4.10** (red), (b) extended cobalt 4-ring **4.13** (black) and extended cobalt 6-ring **4.14** (red), (c) octacobalt [3]catenane **4.13**·(**M4**)$_2$ (black) and dodecacobalt [4]catenane **4.14**·(**M4**)$_3$ (red) and (d) octacobalt [4]rotaxane **4.16**·(**M4**)$_3$ (black), dodecacobalt [5]rotaxane **4.17**·(**M4**)$_4$ (red) and hexadecacobalt [6]rotaxane **4.18**·(**M4**)$_5$ (blue). Analytical GPC was carried out using JAIGEL-3H-A (8 × 500 mm) and JAIGEL-4H-A (8 × 500 mm) columns in THF + 1% pyridine as eluent with a flow rate of 1.0 mL/min.

Selected Mass Spectra

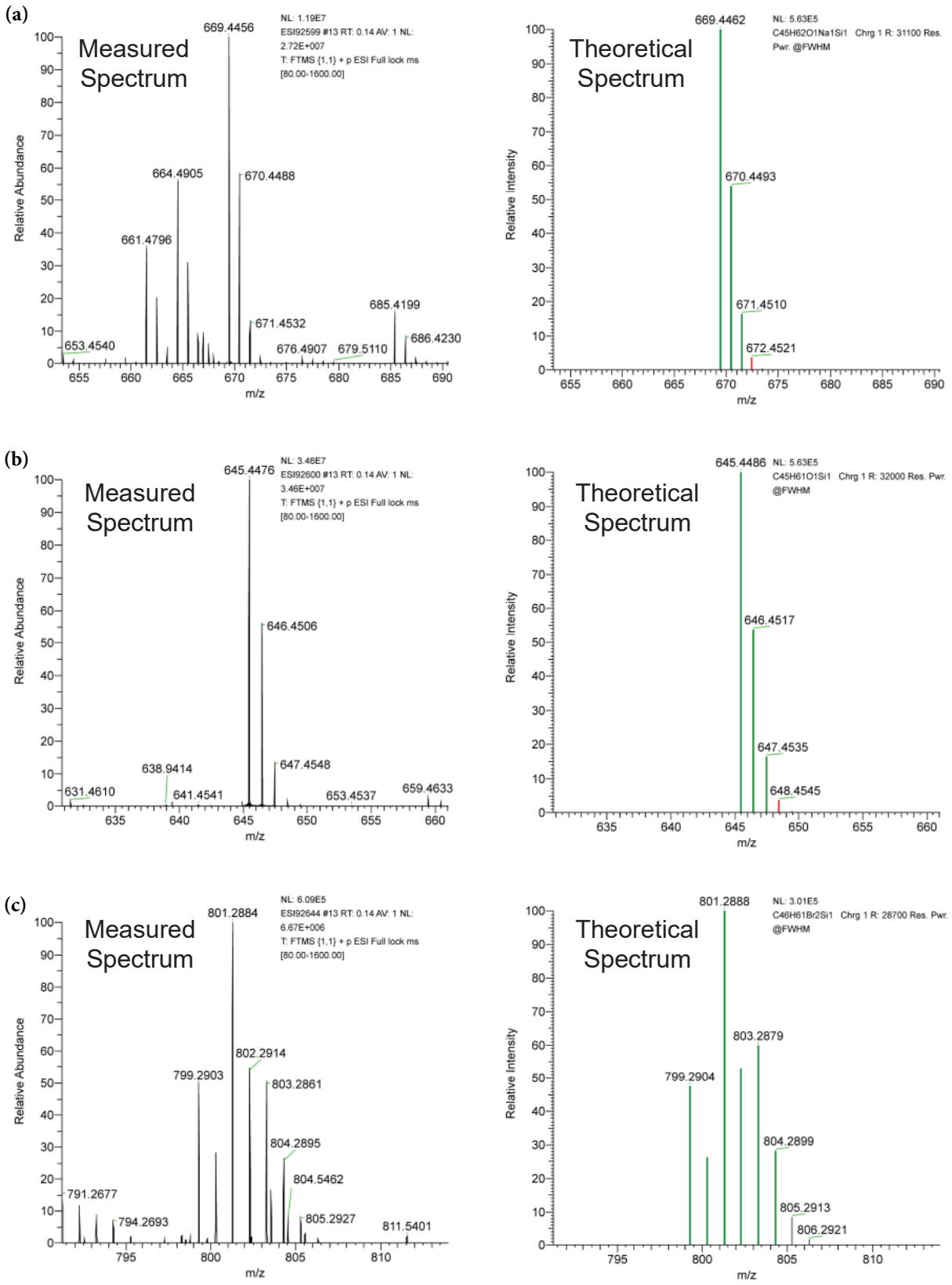

Figure S4.23: High-resolution mass spectra of (a) *p*-^{t}Bu alcohol, (b) *p*-^{t}Bu ketone and (c) *p*-^{t}Bu dibromoolefin.

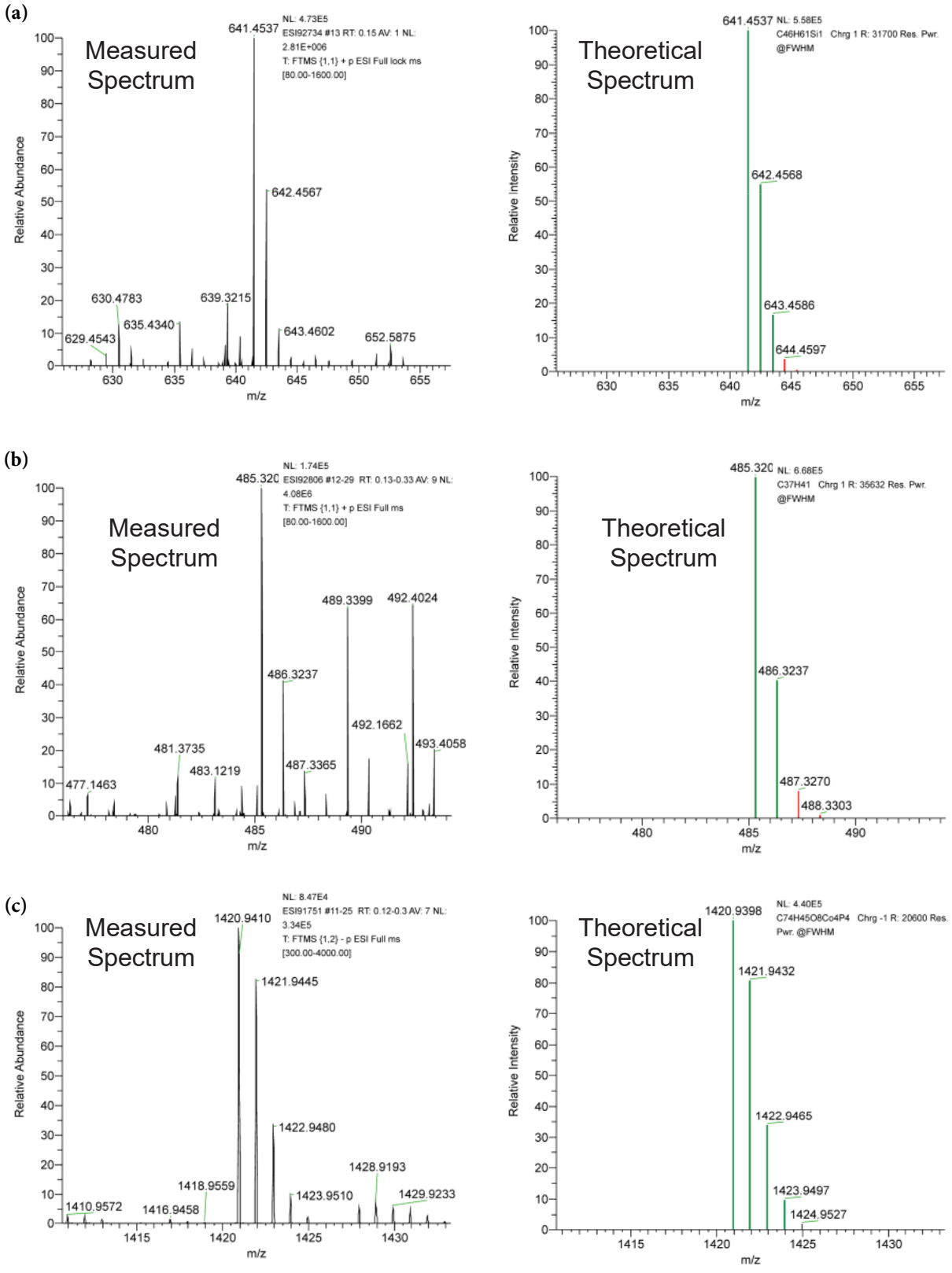

Figure S4.24: High-resolution mass spectra of (a) *p*-^{t}Bu TIPS-protected triyne, (b) *p*-^{t}Bu triyne and (c) deprotected tetracobalt tetrayne thread **4.8**.

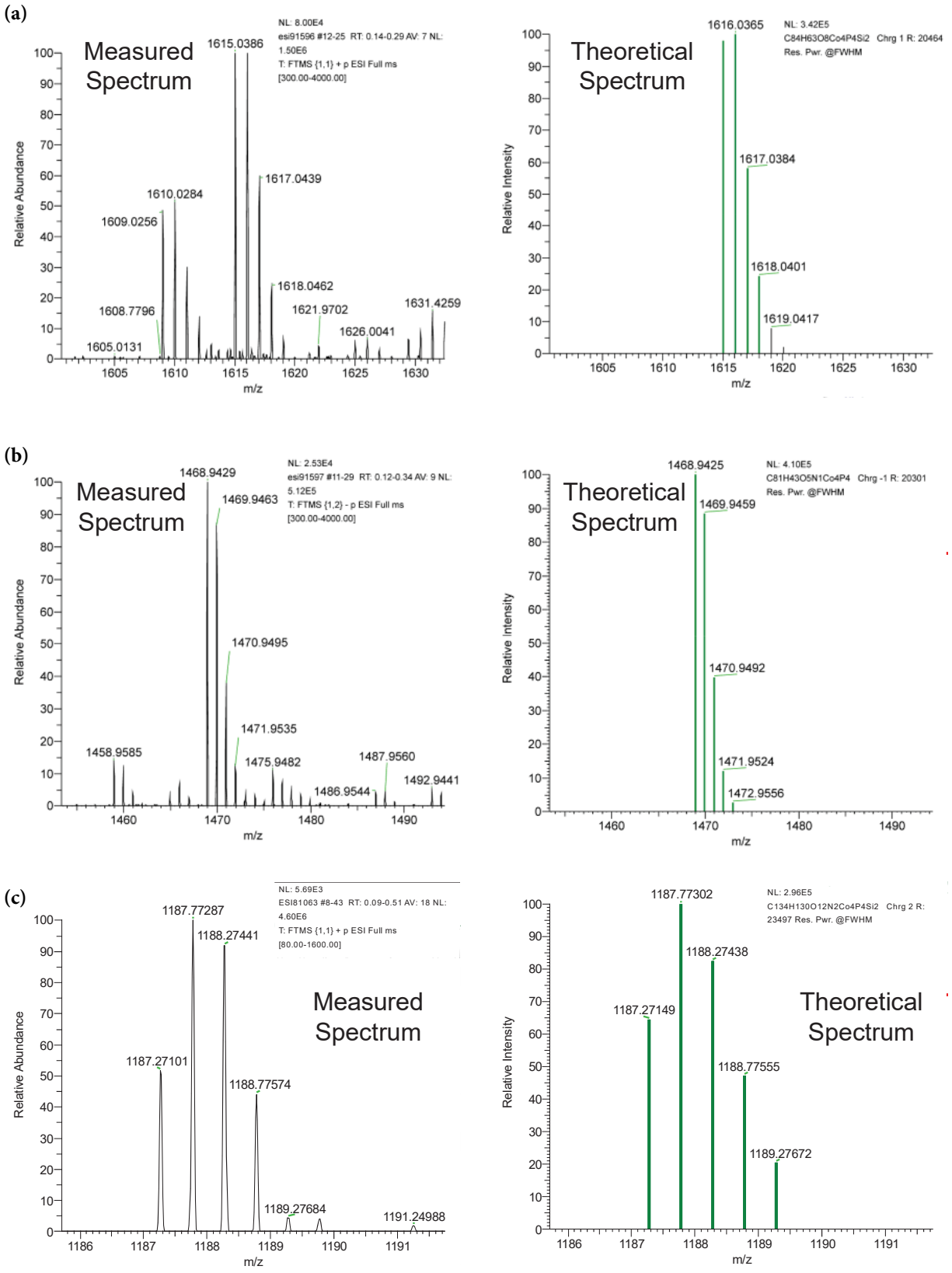

Figure S4.25: High-resolution mass spectra of (a) extended tetracobalt tetrayne thread **4.11**, (b) deprotected extended tetracobalt tetrayne thread **4.12** and (c) tetracobalt [2]rotaxane **4.1·M4**.

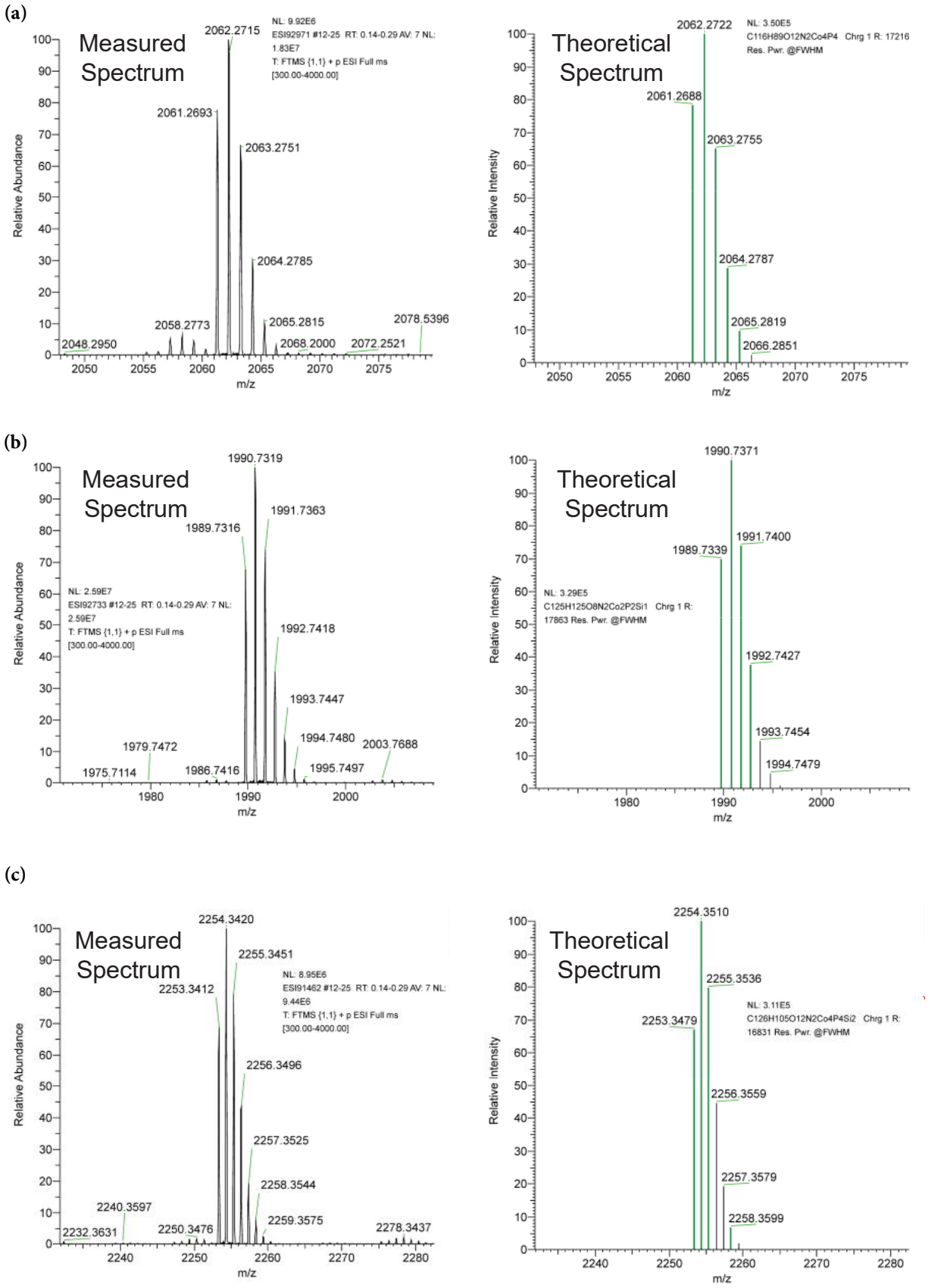

Figure S4.26: High-resolution mass spectra of (a) deprotected tetracobalt [2]rotaxane **4.8·M4**, (b) *p*-^{t}Bu [2]rotaxane **4.7·M4** and (c) extended tetracobalt [2]rotaxane **4.11·M4**.

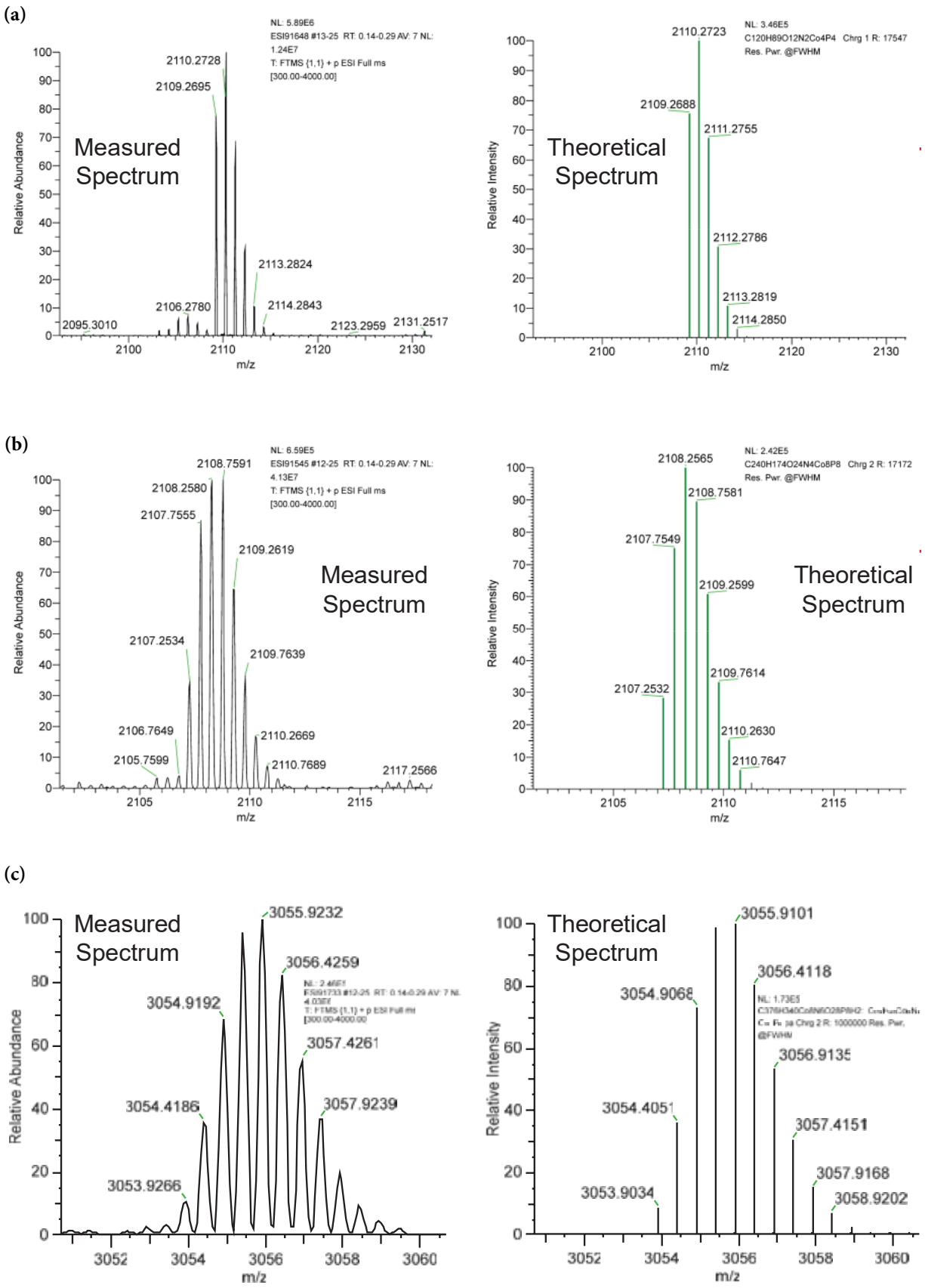

Figure S4.27: High-resolution mass spectra of (a) deprotected extended tetracobalt [2]rotaxane **4.12·M4**, (b) octacobalt [3]catenane **4.13·(M4)**$_2$ and (c) octacobalt [4]rotaxane **4.16·(M4)**$_3$.

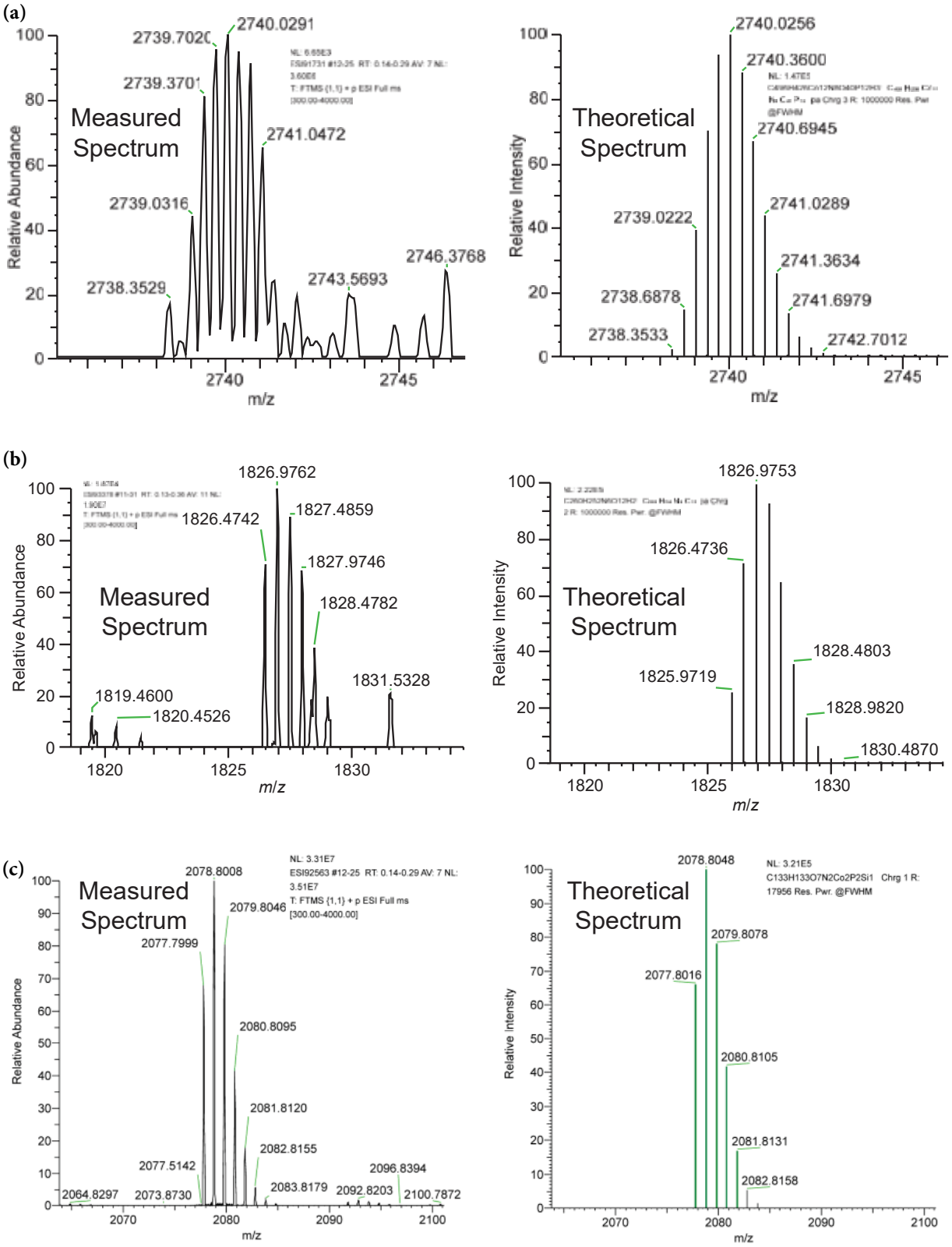

Figure S4.28: High-resolution mass spectra of (a) dodecacobalt [5]rotaxane **4.17·(M4)**$_4$, (b) 24-yne [4]rotaxane **4.19·(M4)**$_3$ and (c) Tr* [2]rotaxane **3.22·M6**.

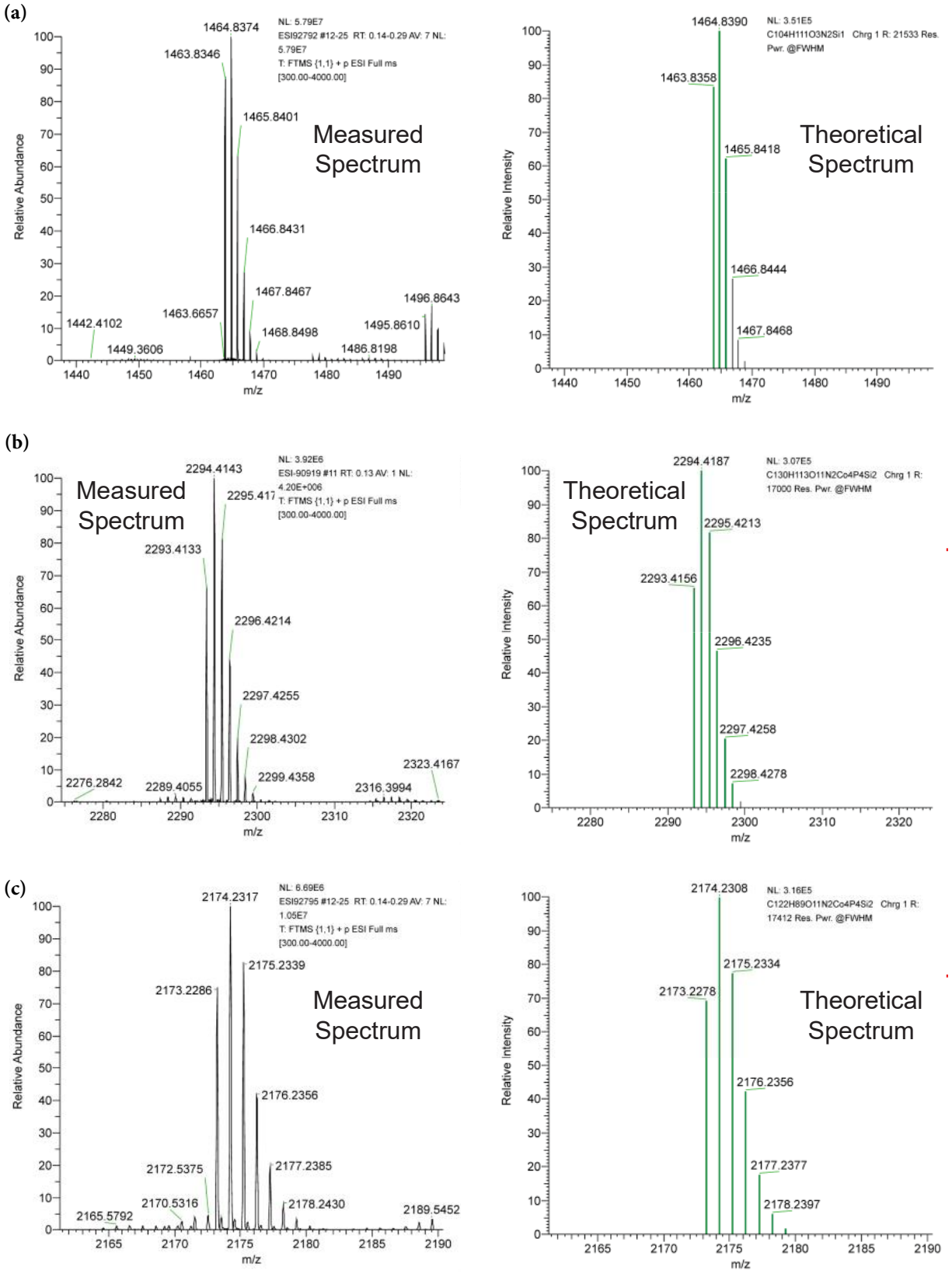

Figure S4.29: High-resolution mass spectra of (a) Tr* heptayne [2]rotaxane, (b) tetracobalt [2]rotaxane **4.1·M6** and (c) extended tetracobalt [2]rotaxane **4.11·M6**.

References

1 R. N. Keller and H. D. Wycoff, in *Inorg. Synth.*, 1946, pp. 1–4.

2 J. H. Golden, *J. Chem. Soc.*, 1961, 1604.

3 A. M. Blanco-Rodríguez, M. Towrie, J. Collin, S. Záliš and A. V. Jr., *Dalt. Trans.*, 2009, **53**, 3941.

4 M. Franz, J. A. Januszewski, D. Wendinger, C. Neiss, L. D. Movsisyan, F. Hampel, H. L. Anderson, A. Görling and R. R. Tykwinski, *Angew. Chem. Int. Ed.*, 2015, **54**, 6645–6649.

5 D. R. Kohn, P. Gawel, Y. Xiong, K. E. Christensen and H. L. Anderson, *J. Org. Chem.*, 2018, **83**, 2077–2086.

6 M. J. Langton, Y. Xiong and P. D. Beer, *Chem. Eur. J.*, 2015, **21**, 18910–18914.

5

Conclusions and Outlook

Contents

Chapter 5 - Conclusions and Outlook

5.1 Conclusions

Molecules consisting exclusively of *sp* carbon atoms – carbyne and cyclo[*n*]carbons – have long been theorised but have yet to be isolated in bulk. Despite their long-standing academic interest, their elusive nature has meant that many questions remain unanswered. The synthesis of pristine cyclo[*n*]carbons have been attempted by many research groups but, to date, only fleeting gas-phase observations,[1,2] or on-surface isolation[3] have been possible. It seems unlikely that carbyne and cyclocarbons can exist as pure carbon allotropes without some type of supramolecular encapsulation. New methods of stabilisation are probably the best approach towards their isolation. Bulky terminal groups stabilise polyynes with up to 24 contiguous alkyne units,[4] but the end group stabilisation effect is expected to diminish with increasing chain length. Supramolecular encapsulation (e.g. polyyrotaxane formation) could stabilise polyynes of any length, making it possible to study the properties of long carbyne chains in solution. This thesis summarises attempts towards polyyne [*n*]rotaxanes and cyclocarbon [*n*]catenanes by combining bulky stoppering groups with supramolecular encapsulation. Bulky masked alkyne equivalents (MAEs) have been employed to stabilise synthetic intermediates and prepare the first masked polyyne [2]rotaxane with temporary stoppering groups, which can later be removed without trace.

A review of previous research in carbon-rich chemistry is presented in **Chapter 1**. Previous synthetic efforts towards end-group stabilised oligo-/polyynes are presented, along with summaries of their UV-vis studies. A variety of MAEs were highlighted and their uses towards preparing pristine cyclocarbons evaluated. Finally, high-yielding approaches towards rotaxane and catenane synthesis are discussed to help guide our efforts towards preparing encapsulated *sp*-allotropes of carbon.

Chapter 2 documented efforts in preparing a novel masked alkyne equivalent with intrinsic metal binding abilities. The MAE was expected to form preorganised complexes in the presence of copper(I) cations that aid formation of mechanically interlocked products, then can then be later removed without trace to return the alkyne. Synthesis towards a masked triyne was achieved in three steps – significantly shorter than for many previous masking groups.[2,5–11]

Unfortunately, successful photochemical unmasking of a model triyne could not be realised due to an unexpected competing reaction between multiple MAE units dominating the outcome. To overcome this, attempts were made to prepare [2]rotaxanes using both threading-then-stoppering and clipping methodologies, but both approaches proved unsuccessful in yielding the expected mechanically interlocked compounds.

Chapter 3 presented a novel synthetic route to the first polyyne [3]rotaxane with two macrocycles on the same polyyne thread. A bulky dicobalt masking group was used both as a temporary, cleavable stopper but also to improve stability of the synthetic intermediates. Two polyyne [3]rotaxanes were prepared with different macrocycles – one oversized and flexible macrocycle, and one smaller, more rigid one. Thermal stability measurements have shown that the size and shape of the macrocycle influence its ability to enhance the thermal stability of a threaded polyyne. UV-vis decomposition experiments demonstrated a modest 1.2 fold stability enhancement (relative to the dumbbell) for the larger macrocycle, while the smaller and more rigid nanohoop displayed a 4.5 fold stability enhancement compared with that of the naked polyyne dumbbell.

Chapter 4 documented the synthesis of a novel masked [2]rotaxane with two temporary, cleavable dicobalt-based stoppers. The [2]rotaxane bears two readily-cleavable silyl protecting groups, allowing for chemical transformations to be made at both ends of the molecule. Through oxidative alkyne homocoupling reactions, both dicobalt-masked cyclocarbon [*n*]catenanes and polyyne [*n*]rotaxanes have been prepared for the first time. Early unmasking experiments have successfully afforded a polyyne bearing 24 contiguous acetylene units and suggest that larger polyynes should be viable using this route. The modular approach offered by this work makes it simple to prepare dicobalt-masked polyynes or cyclocarbons of a wide array of sizes and bearing a variety of macrocycles.

5.2 Future Work

This thesis has uncovered promising avenues for continued research in the pursuit of acetylene-rich molecules. We believe that the relative ease with which these dicobalt compounds can be unmasked justifies any synthetic difficulties presented by these compounds. The high bulk of the bis(diphenylphosphino)methane- (dppm) functionalised dicobalt carbonyl complexes presented in Chapters 3 and 4 make them ideal candidates for stable, temporary stoppers in

rotaxane formation. However, the high stability conferred by dppm also brings with it a notable decrease in unmasking ease. It should be possible to prepare analogous complexes with alternative phosphine ligands (e.g. bis(dimethylphosphino)methane or bis(dicyclohexylphosphino)methane). Current work in the group by DPhil student Mr Prakhar Gupta is investigating how changing the bulk and electron-donating ability of the phosphine ligand influences the efficiency of rotaxane formation and unmasking.

We believe that it would be valuable to reopen efforts towards brominating dicobalt-masked species. Promising preliminary results from Mr Prakhar Gupta indicate that bromination of dicobalt diyne **3.20** may be possible when treating with CBr_4, 18-crown-6 and K_2CO_3 in a 1:1 THF/MeOH solvent mixture. This fascinating result may provide a more efficient path to the tetracobalt [2]rotaxanes discussed in Chapter 4. Importantly, access to bromo compound **5.1** may also allow rotaxanes to be prepared using other macrocycles that were not previously possible, such as rotaxanes bearing nanohoop **M5** (Scheme 5.1). The ability to prepare **M5**-protected polyynes is exciting prospect, since work in Chapter 3 demonstrated the marked stability enhancement of a polyyne [3]rotaxane bearing this macrocycle compared to naked polyyne. These **M5**-protected compounds also displayed much improved unmasking ability compared to analogous compounds bearing phenanthroline-based macrocycle **M4**. A combination of these two factors would likely prove beneficial in helping access longer shielded polyynes.

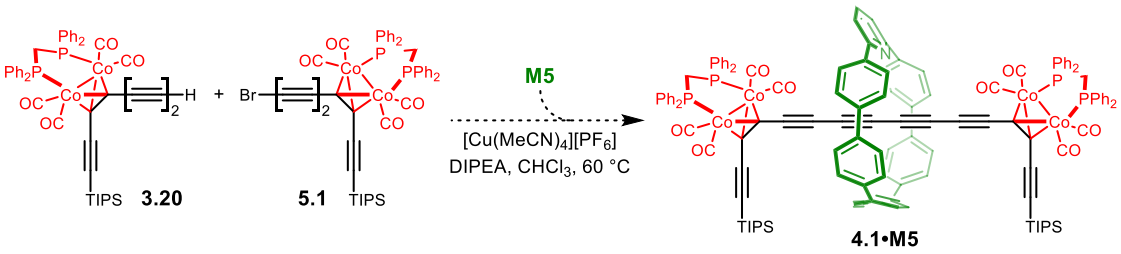

Scheme 5.1: Active metal template Cadiot-Chodkiewicz approach to dicobalt-masked [2]rotaxane **4.1·M5**.

One of the important factors affecting the stability of encapsulated cyclocarbons or polyynes is the ability for the macrocycles to move independently along the chain. In Chapter 3, we mentioned that 2,9-diarylphenanthroline tends to form stacked aggregates,[12] which would probably reduce the screening of the polyyne thread. One approach to overcome this could be to hold macrocycles distant from each other by means of a rigid linking group. Taking

nanohoop **M5** as an example, a functional handle could be installed at the pyridine 4-position that can later be used to prepare a macrobicycle. For example, it should be possible to prepare macrocycle **M7** (Scheme 5.2) from a cross coupling with 2,6-dibromo-4-chloropyridine (**5.2**), then reductive aromatisation following previously reported procedures.[13] Macrocycle **M7** is expected to participate in AMT coupling reactions similarly to **M5** (Scheme 5.3).

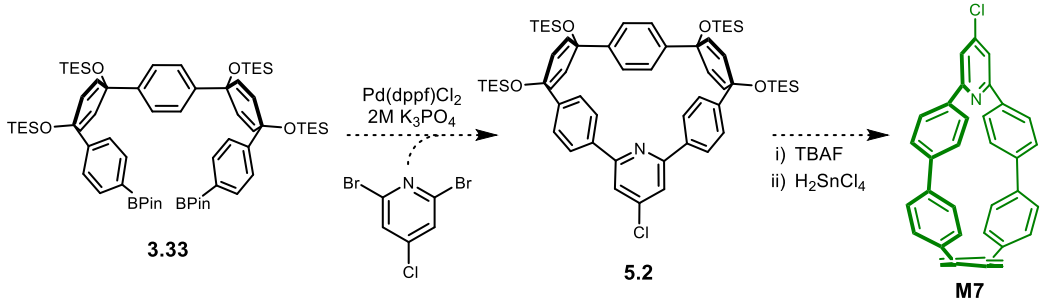

Scheme 5.2: Proposed synthetic route a functionalised nanohoop **M7** from synthetically accessible precursor **3.33**.

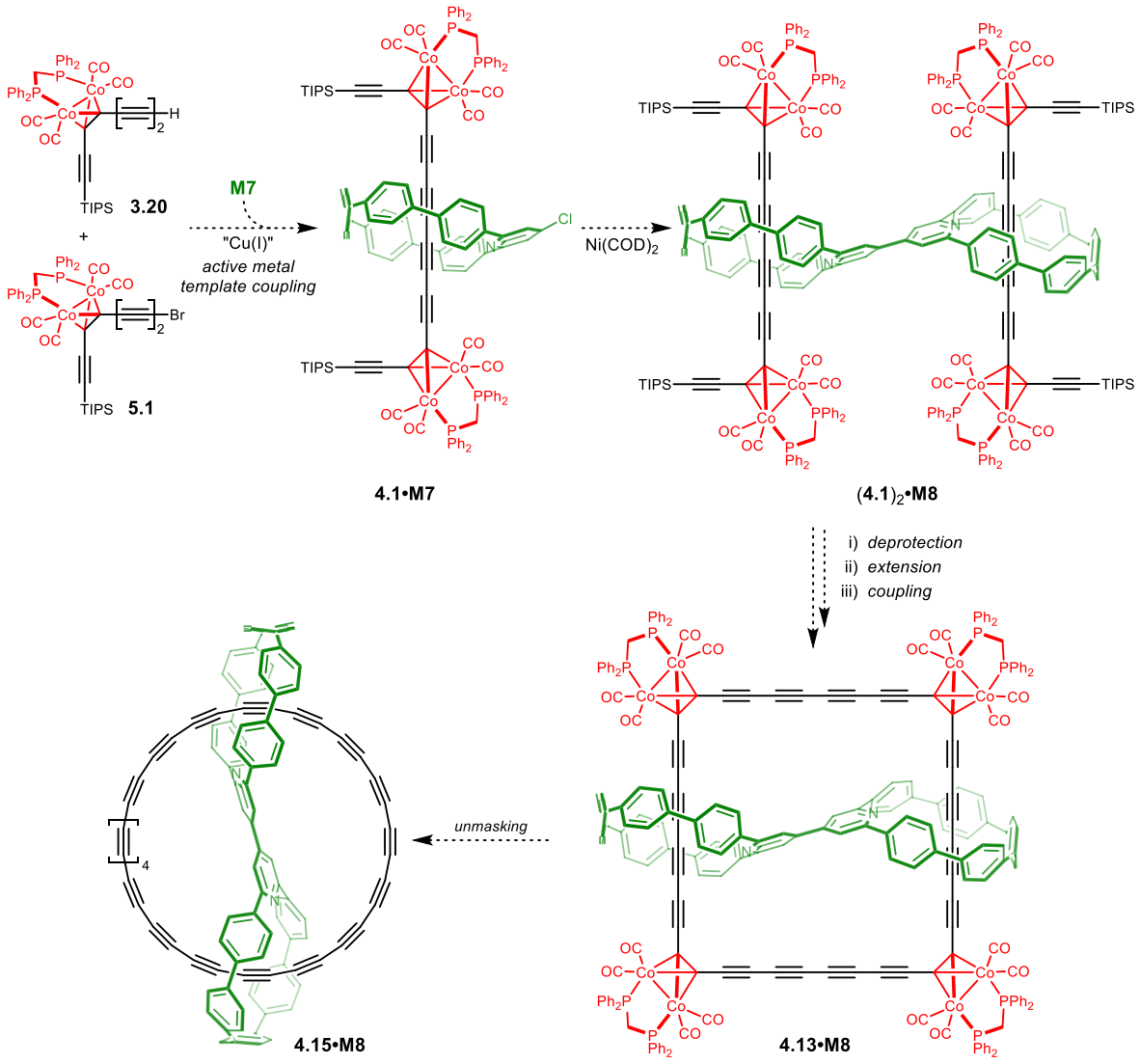

Scheme 5.3: Proposed route to cyclocarbon catenanes **4.15·M8** using nanohoop-based macrobicycle **M8**.

It should be possible to prepare a tetracobalt [2]rotaxane with the **M7** macrocycle using the brominated dicobalt species discussed previously. With the [2]rotaxane now assembled, a Yamamoto (or similar) coupling could be employed to link the two macrocycles together before oxidative homocoupling of the acetylene chain to assemble the masked cyclocarbon backbone. With the macrocycle holding the two tetracobalt threads in close proximity to each other, we would expect exceptional yields for the cyclisation step.

In this example, the macrocycles were held via an aryl-aryl linkage. There are, of course, many other possible linkages that can be envisaged. Each linker can be designed to hold the macrocycles in a specific orientation, and at specific separations from one another. Figure 5.1 presents some possible examples that demonstrates the flexibility of this approach. Many of

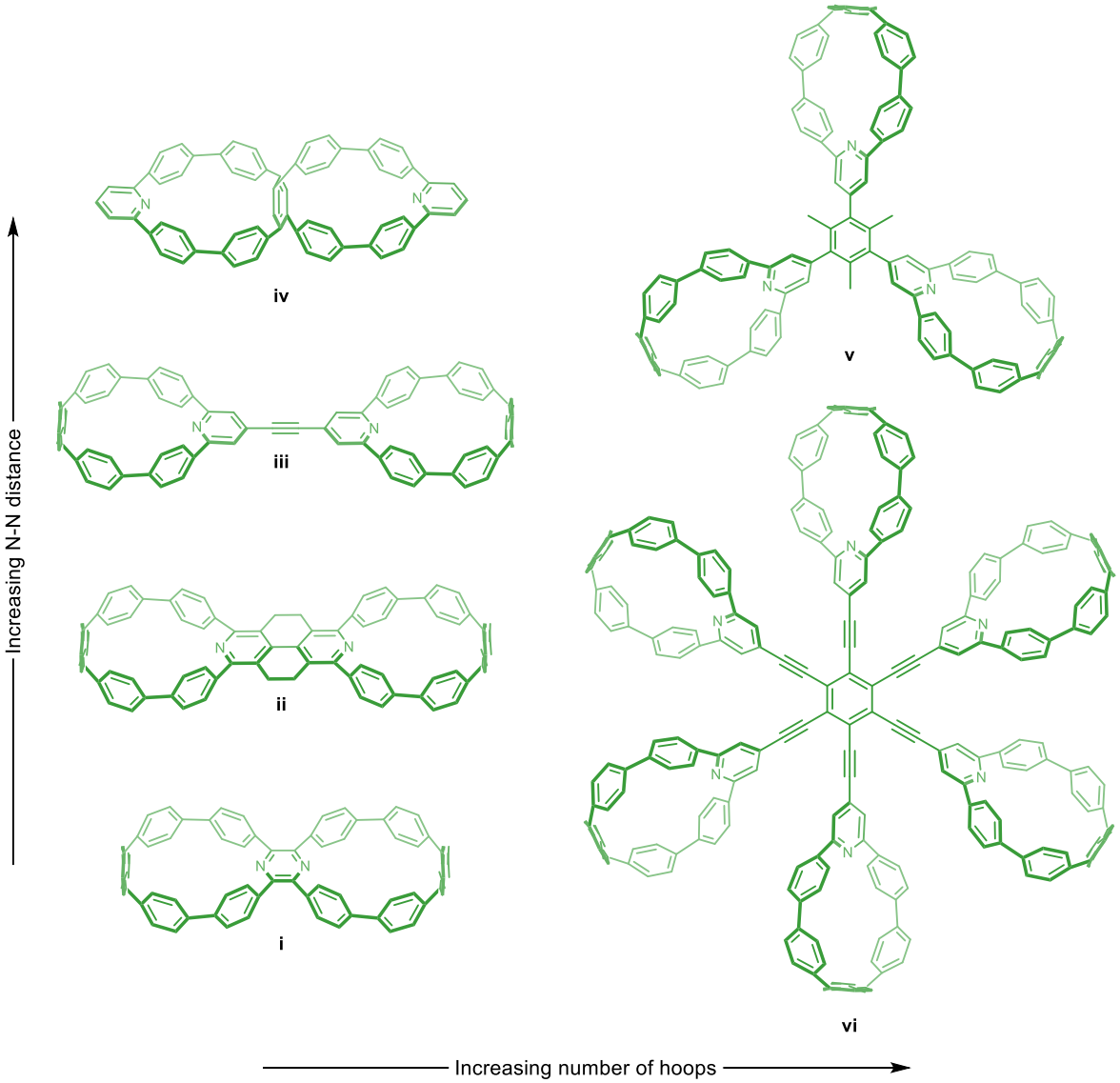

Figure 5.1: A variety of macro-multicycles based on nanohoop **M5** developed by Jasti *et al.*[13] All compounds have been computationally modelled to ensure a resonable gas-phase geometry that should allow threading through the cavity. Optimisation made using semi-emprical methods (PM7 level of theory with D2 dispersion corrections).

these macrocycles could be prepared with only minor modifications to reported synthetic procedures, and all from common building blocks. While variants of nanohoop **M5** were demonstrated in this example, a similar approach would be possible with a wide array of macrocycles. For example, the resorcinol unit in macrocycle **M4** would also offers opportunities for modification via a similar approach.

These novel approaches towards stabilising *sp*-carbon chains carry enormous promise for the ability to isolate encapsulated polyynes, cyclocarbons and other carbon-rich materials that are stable under ambient conditions. It is only a matter of time until this long-awaited milestone is reached.

5.3 References

1 F. Diederich, Y. Rubin, O. L. Chapman and N. S. Goroff, *Helv. Chim. Acta*, 1994, **77**, 1441–1457.

2 Y. Tobe, R. Umeda, N. Iwasa and M. Sonoda, *Chem. Eur. J.*, 2003, **9**, 5549–5559.

3 K. Kaiser, L. M. Scriven, F. Schulz, P. Gawel, L. Gross and H. L. Anderson, *Science*, 2019, **365**, 1299–1301.

4 Y. Gao, Y. Hou, F. Gordillo Gámez, M. J. Ferguson, J. Casado and R. R. Tykwinski, *Nat. Chem.*, 2020, **12**, 1143–1149.

5 F. Diederich, Y. Rubin, C. B. Knobler, R. L. Whetten, K. E. Schriver, K. N. Houk and Y. Li, *Science*, 1989, **245**, 1088–1090.

6 Y. Rubin, C. B. Knobler and F. Diederich, *J. Am. Chem. Soc.*, 1990, **112**, 4966–4968.

7 Y. Li, Y. Rubin, F. Diederich and K. N. Houk, *J. Am. Chem. Soc.*, 1990, **112**, 1618–1623.

8 Y. Rubin, M. Kahr, C. B. Knobler, F. Diederich and C. L. Wilkins, *J. Am. Chem. Soc.*, 1991, **113**, 495–500.

9 G. A. Adamson and C. W. Rees, *J. Chem. Soc. Perkin Trans. 1*, 1996, **2**, 1535–1543.

10 Y. Tobe, T. Fujii, H. Matsumoto, K. Naemura, Y. Achiba and T. Wakabayashi, *J. Am. Chem. Soc.*, 1996, **118**, 2758–2759.

11 Y. Tobe, H. Matsumoto, K. Naemura, Y. Achiba and T. Wakabayashi, *Angew. Chem. Int. Ed.*, 1996, **35**, 1800–1802.

12 M. J. Langton, J. D. Matichak, A. L. Thompson and H. L. Anderson, *Chem. Sci.*, 2011, **2**, 1897.

13 J. M. Van Raden, B. M. White, L. N. Zakharov and R. Jasti, *Angew. Chem. Int. Ed.*, 2019, **58**, 7341–7345.